24th Polish Conference of Chemical and Process Engineering

13–16 June 2023, Szczecin, Poland

Book of Abstracts

okichip24.zut.edu.pl

24th Polish Conference of Chemical and Process Engineering

13–16 June 2023, Szczecin, Poland

Book of Abstracts

Title
24th Polish Conference of Chemical and Process Engineering, Szczecin, 13–16 June 2023.
Book of abstracts.

Editors
Magdalena Cudak
Barbara Zakrzewska
Marta Major-Godlewska
Anna Kiełbus-Rąpała

English proofreading
Marek Stelmaszczyk

Design & typesetting
Barbara Zakrzewska

Published with the consent of the Rector of the West Pomeranian University of Technology in Szczecin.

ISBN 978-83-7663-359-6

The University Publishing House
of the West Pomeranian University of Technology in Szczecin

Piastów 48
70-311 Szczecin
Poland
tel. +48 91 449 47 60
e-mail: wydawnictwo@zut.edu.pl

Patronage

Patronat honorowy

Minister Edukacji i Nauki

Ministerstwo Rozwoju i Technologii

PATRONAT HONOROWY
WOJEWODA
ZACHODNIOPOMORSKI
ZBIGNIEW BOGUCKI

Patronat Honorowy
Prezydenta
Miasta Szczecin

PATRONAT HONOROWY
MARSZAŁKA WOJEWÓDZTWA
ZACHODNIOPOMORSKIEGO
OLGIERDA GEBLEWICZA

PATRONAT HONOROWY
JM REKTORA
ZACHODNIOPOMORSKIEGO UNIWERSYTETU
TECHNOLOGICZNEGO W SZCZECINIE

POWIAT
POLICKI

NCBR
National Centre for Research
and Development

MORSKIE
CENTRUM
NAUKI

Media patronage

RADIO SZCZECIN

Sponsors

Platinum

Grupa Azoty
POLYOLEFINS

Silver

Perlan
a member of Altium Group

Eurotek
International

ESC GLOBAL
LABORATORIUM
ANALIZ
FIZYKOCHEMICZNYCH

SITP
Chem
Oddział Police

gunt
HAMBURG

Bronze

CEMIS
TECH

shim-pol®

chem-Land®

Scientific Committee

Chair:
prof. dr hab. inż. Eugeniusz Molga, Politechnika Warszawska

Vice-Chairs:
prof. dr hab. inż. Dorota Antos, Politechnika Rzeszowska
prof. dr hab. inż. Joanna Karcz, Zachodniopomorski Uniwersytet Technologiczny w Szczecinie
prof. dr hab. inż. Władysław Kamiński, Politechnika Łódzka

Scientific Secretary:
dr hab. inż. Łukasz Makowski, profesor uczelni, Politechnika Warszawska

Members:
dr inż. Paweł Bielski, dyrektor Instytutu Chemii Przemysłowej
dr hab. inż. Katarzyna Bizon, profesor uczelni – Politechnika Krakowska
prof. dr hab. inż.Tomasz Ciach – Politechnika Warszawska
dr hab. inż. Magdalena Cudak, profesor uczelni – Zachodniopomorski Uniwersytet Technologiczny w Szczecinie
dr hab. inż. Grzegorz Dzido – Politechnika Śląska
prof. dr hab. inż. Marek Dziubiński – Politechnika Łódzka
dr hab. inż. Marta Gmurek, profesor uczelni – Politechnika Łódzka
prof. dr hab. inż. Leon Gradoń – Politechnika Warszawska
prof. dr hab. inż. Andrzej Górak, emerytowany profesor Uniwersytetu Technicznego w Dortmundzie (Niemcy)
dr hab. inż. Jerzy Hapanowicz, profesor uczelni – Politechnika Opolska
prof. dr hab. inż. Andrzej Heim – Politechnika Łódzka
prof. dr hab. inż. Marek Henczka – Politechnika Warszawska
prof. dr hab. inż. Andrzej Jarzębski – Politechnika Śląska
dr hab. inż. Małgorzata Jaworska, profesor uczelni – Politechnika Warszawska
prof. dr hab. inż. Zdzisław Jaworski – Zachodniopomorski Uniwersytet Technologiczny w Szczecinie
prof. dr hab. inż. Bożenna Kawalec-Pietrenko, emerytowany profesor Politechniki Gdańskiej
prof. dr hab. inż. Stanisław Ledakowicz – Politechnika Łódzka
prof. dr hab. inż. Janusz Magiera – Politechnika Krakowska
dr hab. inż. Julita Zofia Mrowiec-Białoń – Instytut Inżynierii Chemicznej PAN w Gliwicach
prof. dr hab. inż. Andrzej Noworyta – Politechnika Wrocławska
prof. dr hab. inż. Roman Petrus – Politechnika Rzeszowska
dr hab. inż. Paulina Pianko-Oprych – Zachodniopomorski Uniwersytet Technologiczny w Szczecinie
prof. dr hab. inż. Ryszard Pohorecki, czł. rzeczywisty PAN – Politechnika Warszawska
prof. dr hab. inż. Rafał Rakoczy – Zachodniopomorski Uniwersytet Technologiczny w Szczecinie
prof. dr hab. inż. Andrzej Sobkowiak, Politechnika Rzeszowska, Członek Zespołu II Nauk Inżynieryjno-Technicznych Rady Doskonałości Naukowe
prof. dr hab. inż. Tomasz Sosnowski – Politechnika Warszawska
prof. dr inż. Andrzej Stankiewicz – Politechnika Warszawska
prof. dr hab. inż. Piotr Synowiec – Politechnika Śląska
dr hab. inż. Marek Tańczyk – Instytut Inżynierii Chemicznej PAN w Gliwicach
prof. dr hab. inż. Anna Trusek – Politechnika Wrocławska
prof. dr hab. inż. Kazimiera Wilk, Politechnika Wrocławska, Członek Zespołu II Nauk Inżynieryjno-Technicznych Rady Doskonałości Naukowej
prof. dr hab. inż. Ireneusz Zbiciński – Politechnika Łódzka

Organizing Committee

Conference Chair: prof. dr hab. inż. Rafał Rakoczy

Conference Vice-Chairs:
dr hab. inż. Agata Markowska-Szczupak, prof. ZUT
dr inż. Barbara Zakrzewska

Scientific Secretary: prof. dr hab. inż. Joanna Karcz

Financial Secretary: dr inż. Dorota Downarowicz

Secretariat:
dr inż. Halina Murasiewicz
dr inż. Anna Story

Members:
prof. dr hab. inż. Zdzisław Jaworski
dr hab. inż. Magdalena Cudak, prof. ZUT
dr hab. inż. Elżbieta Gabruś, prof. ZUT
dr hab. inż. Marian Kordas, prof. ZUT
dr hab. inż. Agnieszka Kowalczyk, prof. ZUT
dr hab. inż. Ewelina Kusiak-Nejman, prof. ZUT
dr hab. inż. Marta Major-Godlewska, prof. ZUT
dr hab. inż. Robert Pełech, prof. ZUT
dr hab. inż. Jolanta Szoplik, prof. ZUT
dr hab. inż. Konrad Witkiewicz, prof. ZUT
dr hab. inż. Elwira Wróblewska, prof. ZUT
dr hab. inż. Beata Zielińska, prof. ZUT
dr inż. Tomasz Aleksandrzak
dr inż. Adrian Augustyniak
dr inż. Marcin Gano
dr inż. Karolina Kiełbasa
dr inż. Anna Kiełbus-Rąpała
dr inż. Maciej Konopacki
dr inż. Edyta Kucharska
dr inż. Aleksander Orecki
dr inż. Paula Ossowicz-Rupniewska
dr inż. Marlena Musik
dr inż. Grzegorz Story
mgr inż. Tomasz Borowski
mgr Elżbieta Brodacka
mgr inż. Dorota Igras
mgr inż. Krzysztof Kowalski
mgr inż. Kamila Dubrowska
mgr inż. Joanna Jabłońska
mgr inż. Martyna Jurkiewicz
mgr inż. Agata Kraśkiewicz
mgr inż. Oliwia Paszkiewicz
mgr inż. Magdalena Siwoń
mgr inż. Dawid Sołoducha

Dean's Address

The greeting message from the Dean of the Faculty of Chemical Technology and Engineering, West Pomeranian University of Technology in Szczecin

As the Dean of the Faculty of Chemical Technology and Engineering and the Conference Chairman, on behalf of the Organizing Committee, I am delighted to welcome all participants to the 24th National Conference of Chemical and Process Engineering, scheduled to be held at the West Pomeranian University of Technology in Szczecin on June 13-16, 2023.

One of the main objectives of this conference will be to define the expectations of innovative companies in the chemical industry regarding scientists in the field of chemical engineering. This event will also provide an excellent opportunity to explore new avenues for the dissemination of knowledge and innovation resources.

I strongly believe that our conference will serve as an outstanding platform for establishing connections between scientists and industry representatives. Collaboration between academia and industry is essential for establishing industrial and scientific consortia capable of conducting research and development projects in the field of chemical industry.

The conference will bring together approximately 250 distinguished specialists from Poland and abroad, whose research focuses on chemical and process engineering. The topics discussed during the conference will include modern trends in chemical engineering and technology, circular economy and climate protection, chemical engineering and new energy sources, industrial process engineering, intensification of transport processes, chemical reaction engineering, process modeling and simulation, environmental chemical engineering, technological and process innovations, bioprocess engineering and medical applications, as well as green and sustainable chemical engineering. Additionally, a forum for young researchers will be organized during the conference, providing an opportunity to analyze the results of scientific work carried out by students and doctoral candidates.

Furthermore, I believe that the conference will provide an excellent opportunity to present a research offer related to the capabilities of the Center for Advanced Materials and Manufacturing Processes Engineering (CZMIMP), which can serve as a research base for the industry.

I would like to take this opportunity to express my gratitude to all those who will participate in our conference. The results of their scientific work constitute a valuable contribution to the advancement of chemical engineering, shaping the innovative directions of this scientific discipline.

Sincerely,

Professor Rafał Rakoczy
Dean of Faculty of Chemical Technology and Engineering

Table of contents

Lectures

Plenary lectures

MECHANOCHEMISTRY: A SUSTAINABLE AND DISRUPTIVE FORCE FOR PRODUCTION OF FUNCTIONAL NANOMATERIALS

Matej Baláž*

Institute of Geotechnics, Slovak Academy of Sciences, Watsonova 45, 04001 Košice
*corresponding author: balazm@saske.sk

Mechanochemistry represents an environmentally sound alternative to the traditional solution-based chemistry, as it offers the option to obtain desired compounds in a one-step solvent-free fashion without the need of supplying external heat or pressure. It is also recognized by International Union of Pure and Applied Chemistry (IUPAC), which considers a mechanochemical reaction as a chemical reaction that is induced by direct absorption of mechanical energy [1]. It is particularly interesting for the preparation of nanocrystalline materials, as instead of using organo-metallic compounds, products can be obtained through purely solid-state processing of elemental precursors, very common non-toxic compounds or even natural materials.

The present talk will focus mainly on two areas, namely on the mechanochemical synthesis of (i) bionanocomposites based on silver nanoparticles and (ii) metal chalcogenides.

Silver nanoparticles are well-known mainly due to their overwhelming antibacterial activity [2]. During the last couple of years, our research group has developed a biomechanochemical approach, where by one-step mechanochemical processing of $AgNO_3$ used as Ag precursor and natural material used as a reducing agent, antibacterially active Ag nanoparticles embedded in the residual matrix of the natural species were successfully prepared. The process was performed in a laboratory-scale planetary ball mill. The natural reducing agents encompassed common plants such as thyme, elderberry, lavender, or various lichen species [3-4]. The principle of bio-mechanochemical synthesis applying three common plants as reducing agents is shown in Fig. 1.

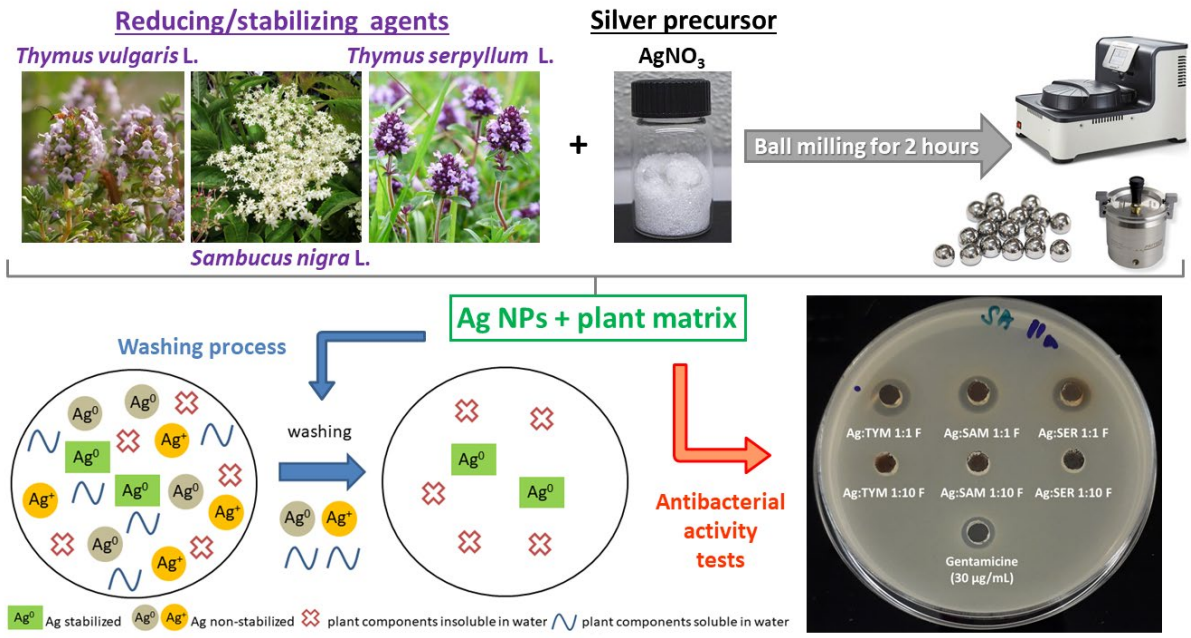

Fig. 1. Principle of bio-mechanochemical synthesis of Ag nanoparticle-based bionanocomposites [4]

Metal chalcogenides are currently among the most intensively studied materials in various areas of materials science, namely in the field of energy conversion. Among the most common groups of metal chalcogenides, metal sulfides are very interesting, because they contain abundant

sulfur and are applicable in various fields [5]. By just co-grinding sulfur with corresponding metals, it is possible to obtain nanocrystaline metal chalcogenides in a very convenient way [6]. Recently, we published a study describing the mechanochemical synthesis of 12 ternary and quaternary Cu-based sulfides in a scalable fashion (100 g batch) using eccentric vibratory milling from their elemental precursors and revealing their great potential as antibacterial agents [7].

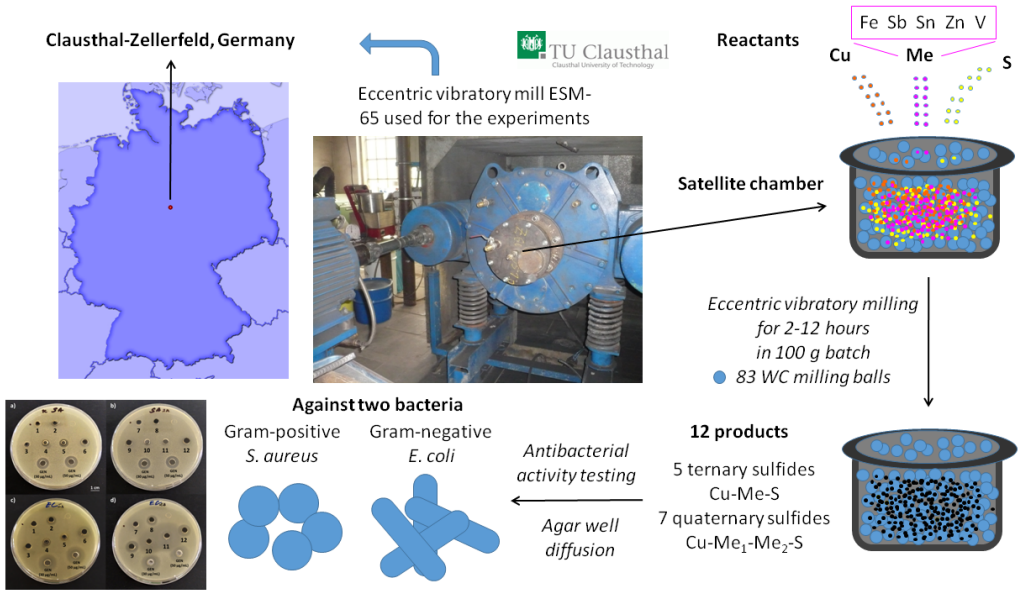

Fig. 2. Scalable mechanochemical synthesis of various copper-based ternary and quaternary metal chalcogenides as prospective antibacterial agents [7]

At the end, the possibility to recycle a rich plethora of waste materials via mechanochemistry will be shown. This topic was comprehensively summarized in a monograph published in 2021, where more than 1000 studies dealing with the recycling strategies of consumer, technogenic, and agricultural waste were reviewed [8].

This work was supported by the projects of the Slovak Grant Agency VEGA (2/0112/22) and the Slovak Research and Development Agency APVV (VV 18-0357).

References

[1] McNaught A.D., Wilkinson, A., *IUPAC Compendium of Chemical Terminology („The Golden Book"). 2nd ed.*, Oxford, Blackwell Scientific Publication 1997.

[2] Kim J.S., Kuk E., Yu K.N., Kim J.-H., Park S.J., Lee H.J., Kim S.H., Park Y.K., Park Y.H., Hwang Ch.-Y., Kim Y.-K., Lee Y.-S., Jeong D.H., Cho M.-H., Antimicrobial effects of silver nanoparticles, *Nanomed. - Nanotechnol. Biol. Medicine*, 2007, 3(1), 95-101.

[3] Baláž M., Goga M., Hegedüs M., Daneu N., Kováčová M., Tkáčiková L., Balážová L., Bačkor M., Biomechanochemical solid-state synthesis of silver nanoparticles with antibacterial activity using lichens, *ACS Sust. Chem. Eng.* 2020, 8, 13945-13955.

[4] Kováčová M., Daneu N., Tkáčiková L., Búreš R., Dutková E., Stahorský M., Lukáčová Bujňáková Z., Baláž M., Sustainable one-step solid-state synthesis of antibacterially active silver nanoparticles using mechanochemistry, *Nanomaterials* 2020, 10(11), 2119.

[5] Yin J., Jin J., Lin H., Yin Z., Li J., Lu M., Guo L., Xi P., Tang Y., Yan Ch.-H., Optimized Metal Chalcogenides for Boosting Water Splitting, *Adv. Sci.* 2020, 7(10), 1903070.

[6] Baláž P., Baláž M., Achimovičová M.,Bujňáková Z., Dutková E., Chalcogenide mechanochemistry in materials science: insight into synthesis and applications (a review), *J. Mater. Sci.*, 2017, 52, 11851-11890.

[7] Baláž M., Tkáčiková L., Stahorský M., Casas-Luna M., Dutková E., Čelko L., Kováčová M., Achimovičová M., Baláž P., Ternary and quaternary nanocrystalline Cu-based sulfides as perspective antibacterial materials mechanochemcially synthesized in a scalable fashion, *ACS Omega* 2022, 7(31), 27164–27171.

[8] Baláž, M., *Environmental Mechanochemistry: Recycling Waste into Materials Using High-Energy Ball Milling*. Cham, Springer 2021.

THE JOURNEY FROM MECHANISTIC TO DATA-DRIVEN MODELS IN PROCESS ENGINEERING: DIMENSIONALITY REDUCTION, SURROGATE AND HYBRID APPROACHES AND DIGITAL TWINS

Katarzyna Bizon*

Faculty of Chemical Engineering and Technology, Cracow University and Technology,
Warszawska 24, 31-155 Kraków, Poland
*corresponding author: katarzyna.bizon@pk.edu.pl

The design, optimization and control of chemical engineering problems, including fundamental phenomena, unit operations as well as complex industrial processes, involves the need for the formulation and subsequent implementation of mathematical models characterized by a range of levels of complexity. Although at the design phase of new processes and equipment it seems to be economically justified (e.g., to avoid time- and cost-consuming experiments) to employ detailed models accounting for many constituent phenomena and based on first principles, the use of such tools for process optimization or control, especially when dealing with multiscale problems or complex process plants, is virtually impossible. However, the computational burden inherent to the numerical solution of mechanistic models can be substantially reduced by replacing the entire model or even just some of its elements with a data-driven submodel (Fig. 1a). Over the last decades, a number of techniques emerged, and related publications (Fig. 1b), that make it possible to use directly the information extracted from the so-called full numerical model as well as the real physical object aimed at developing computationally efficient numerical simulations.

The study analyzes different approaches through which data of both simulation and experimental origin can be used to construct light yet robust numerical models [1-3]. In addition to an overview of various methodologies and possible applications in chemical engineering, including industrial process engineering, related problems and challenges are outlined that are likely to boost future research.

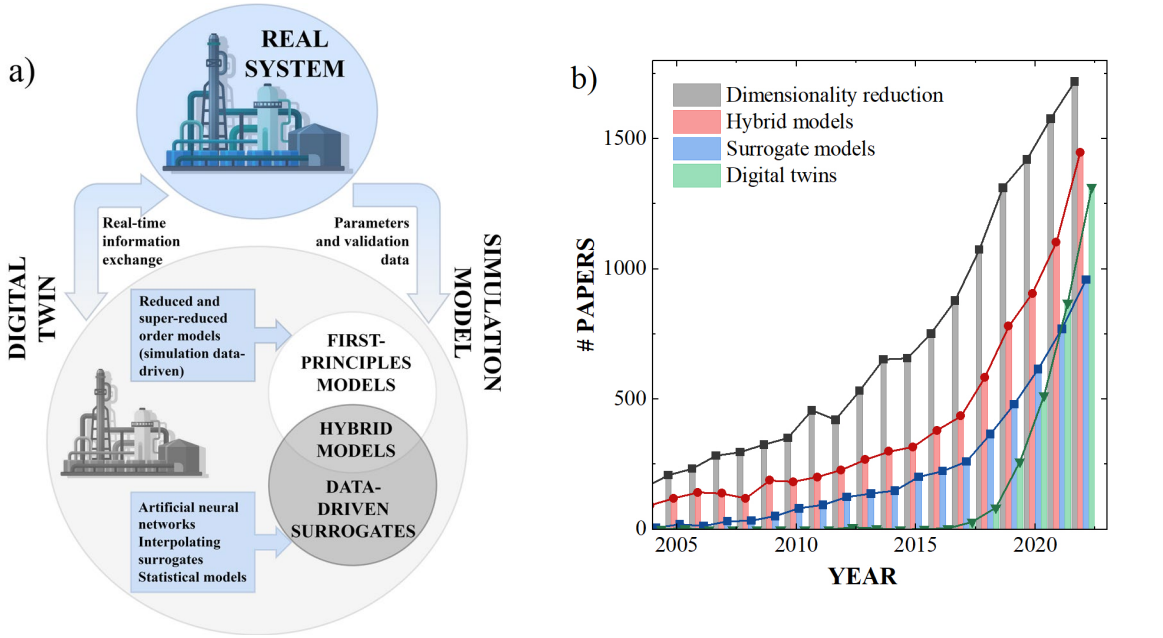

Fig. 1. Illustration of the classification of data-driven models (a) and the number of publications (in Scopus indexed journals) over the years on dimensionality reduction, hybrid and surrogate models, and digital twins addressing issues in chemical engineering, chemistry, material and environmental science, and energy (b)

It is necessary to recognize that data-driven models are not an invention of recent years, yet due to lack of computing power, in research works they began to appear only in the 1950s [1], and in practical industrial applications well beyond that. Speaking of data-driven models, also referred to as empirical, it is necessary to distinguish between two basic categories of such objects, that is, models reduced by methods exploiting knowledge of the behavior of the object, but fully preserving its mechanistic character, and so-called surrogate models.

As for the first group, also categorized as white-box models, one of the most widely used and powerful methodologies today is dimensionality reduction via the Galerkin projection combined with an empirical basis, determined from numerical (or very rarely experimental) observations obtained from the non-reduced model using the Proper Orthogonal Decomposition [1, 4]. The method has been intensively researched and used since the 1990s in chemical reactors, engineering applications and study of turbulent flows. Today it can also be coupled with solvers for Computational Fluid Dynamics. The latter fact strongly confirms its significant applicative and not just theoretical character in process engineering. Anyhow, some issues such as appropriate reduction of non-linear terms (via so-called super-reduction), which are ubiquitous in engineering problems, or selection of "most informative" data to create an optimal basis are still the subject of intensive research [4].

On the other hand, surrogate (or surrogative) models [2], which are simply black-box models, encompass a huge group of methods that allow to handle complex problems in an equation-free manner. These methods can be divided into interpolation (e.g. Krigging [2]) and non-interpolation methods, with the last group primarily including a wide range of techniques based on Machine Learning (e.g. Artificial Neural Networks [2, 5]). The latter, apart from predictive modeling, can also be successfully used in engineering applications as virtual (soft) sensors [5]. The use of Machine Learning to simulate chemical and physical processes seems to be extremely attractive nowadays and research on the development on entirely data-driven models for the description of multiscale and multiphysics systems are intensively conducted. Preserving at least a fragment of the model in a mechanistic form is more adequate for process optimization applications, which involves the exploration of a wide parameter space. In this context semi-empirical hybrid (or grey-box) models [2, 3, 6] combining first-principles models with data-driven surrogates developed using feature extraction, regression/interpolation and Machine Learning methodologies appear to be the best solution. Hybrid models are also an excellent solution for simulating integrated processes, e.g. Combined Heat and Power systems [6]. Indeed, some elements of complex process installations can often be described using relatively simple models based on first principles, while others are almost impossible to describe without data-driven methodologies.

Eventually, the extremely rapid development of hardware and computing power over the last decade allowed to combine simulation models of different nature with their constant updating and real-time interaction with the simulated real world asset. This brought about the birth of a whole novel group of computational tools: the so-called Digital Twins [3], which are an important element of the age of Industry 4.0 and, closely allied to it, widespread digitalization. They can profit from all available techniques (Fig. 1a): starting from white- through grey- to black-box modeling, and without a doubt they are a tool that will be of great importance in industrial applications in the near future.

References

[1] Holmes P., Lumley J.L., Berkooz G., *Turbulence, coherent structures, dynamical systems and symmetry*, Cambridge, Cambridge University Press 1996.

[2] Hou C.K.J.., Behdinan. K., Dimensionality reduction in surrogate modeling: A review of combined methods, *Data Sci. Eng.*, 2022, 7, 402-427.

[3] Wright L., Davidson S., How to tell the difference between a model and a digital twin, *Adv. Model. and Simul. in Eng. Sci.*, 2020, 7, 13.

[4] Cutillo E.A., Petito G., Bizon K., Continillo G., Analysis of an innovating sampling strategy based on k-means clustering algorithm for POD and POD-DEIM reduced order models of 2-D reaction-diffusion system, *Combust. Theor. Model.*, 2023.

[5] Bizon K., Continillo G., Mancaruso E., Vaglieco B.M., Towards on-line prediction of the in-cylinder pressure in diesel engines from engine vibration using artificial neural networks, *SAE Tech. Pap*, 2013, 2013-24-0137.

[6] Marra F.S., Bizon K., Continillo G., Fast predictive model for design and optimization of a low emission biomass fueled CHP system, 23rd EUBCE, 2015, Vienna, Austria.

DESIGN OF ADVANCED NANOMATERIALS FOR CHEMICAL ENGINEERING PROCESSES

Kamil Czelej*, Leon Gradoń

Faculty of Chemical and Process Engineering, Warsaw University of Technology,
Waryńskiego 1, 00-645 Warsaw, Poland
*corresponding author: kamil.czelej@pw.edu.pl

Over the past few decades, mankind has experienced an enormous growth leading to the introduction of many cutting-edge technologies that significantly increased our living standards and longevity. With this rate of progress, however, comes massive responsibility for our future and the safety of natural environment. In fact, to fuel the ever-growing consumerism of our modern society and satisfy an enormous energy demand, we are burning more and more fossil fuels, and extracting precious natural resources that eventually disturb the environmental equilibrium. This, in turn, leads to extreme natural phenomena, high levels of air and drinking water pollution, hostile climate and the accelerated extinction of various fauna and flora species. To reverse or at least mitigate this trend, two fundamental concepts of 1) zero waste, and 2) circular economy were introduced, and subsequently an international effort has been undertaken to put it into action. The goal of zero waste is to design and manage the manufacturing and consumption of products in a way that minimizes waste and recovers as many resources as possible, while keeping toxic substances out of the environment. The ultimate goal of the circular economy, however, is a system of a global scale, where we can primarily rely on resources we have already harvested, rather than ignoring recyclables and exploiting raw materials. A successful implementation of these two concepts would not be possible without novel sophisticated nanomaterials that constitute a foundation for the next generation sustainable and green processes.

The design of novel nanomaterials for green chemical engineering processes is frequently a very complex and multidimensional procedure because it requires thorough understanding of physics and chemistry of materials at nanoscale, and how the physics and chemistry change upon external stimuli such as light, temperature, electric field etc. In addition, the target nanostructures must be long-term stable, nontoxic, and synthesized from easily available and cheap precursors to make the process economically viable. In an ideal scenario, the newly designed nanomaterials should outperform their conventional and unsustainable counterparts. All the aforementioned requirements have to be taken into account simultaneously making the design process very challenging. To speed up the design procedure, we often involve high power supercomputers together with modern computational simulation packages that allow us to screen through large possible configuration space and narrow down the number of promising nanomaterials.

Although advanced nanomaterials can be regarded as a heart of green and sustainable technologies, chemical engineering is a body, and they both cannot be disentangled. In fact, chemical engineering plays a major role prior and after production of nanomaterials. The synthesis protocol which has to be properly tuned to reproduce the designed properties of nanomaterials for a given process application, and the process application itself has to be optimized to reach the highest possible efficiency.

We are going to provide a general perspective on the design procedure of advanced nanomaterials that can be successfully implemented in sustainable and green chemical processes. For the sake of clarity, particular attention is given to nanostructures for light-driven processes. First, we introduce some intrinsic properties of a nanostructure and their relationships with photocatalytic properties that can be tuned via chemical and phase compositions. We emphasize the role of the state-of-the-art quantum chemistry methods in designing efficient nanostructured catalysts [1]. Next, we discuss the concept of quantum efficiency as a direct indicator of nanocatalyst performance and how to control and increase its value. In this case, we focus our

attention on the localized surface plasmonic resonance (LSPR) phenomenon and its benefit in efficient light harvesting [2, 3]. We discuss a few possible strategies to control the LSPR by changing the chemical composition, size, and shape of plasmonic nanostructure [2]. Finally, we demonstrate several examples of designed and synthesized nanomaterials in their respective applications [2, 3].

References

[1] Czelej K., Ćwieka K., Colmenares J.C., Xu Y.J., Kurzydłowski K.J., Toward a Comprehensive Understanding of Enhanced Photocatalytic Activity of the Bimetallic PdAu/TiO_2 Catalyst for Selective Oxidation of Methanol to Methyl Formate, *ACS Appl. Mater. Interfaces*, 2017, 9(37), 31825–31833.

[2] Czelej K., Colmenares J.C., Ćwieka K., Jabłczyńska K., Werner Ł., Gradoń L., Sustainable hydrogen production by plasmonic thermophotocatalysis, *Catal. Today*, 2021, 380, 156–186.

[3] Ćwieka K., Czelej K., Colmenares J.C., Jabłczyńska K., Werner Ł., Gradoń L., Supported plasmonic nanocatalysts for hydrogen production by wet and dry photoreforming of biomass and biogas derived compounds: Recent progress and future perspectives, *ChemCatChem*, 2021, 13, 21, 4458–4496.

FABRICATION AND PRACTICAL UTILITY OF HYBRID MATERIALS

Teofil Jesionowski*

Poznan University of Technology, Faculty of Chemical Technology,
Berdychowo 4, 60-965 Poznan, Poland
Corresponding author: Teofil.Jesionowski@put.poznan.pl

Intensive technological development and performance requirements for modern materials with defined properties determine new challenges towards the design of advanced, functional hybrid systems. By combining two or more components (mainly inorganic and of natural origin), materials with improved properties and great practical relevance are produced.

The lecture will focus on current trends in the fabrication and development of advanced hybrid materials. Additionally, practical utilities of those materials will be also emphasized. Methods of their production, characteristics, how and above all the most important areas of their use will be indicated, e.g. in such areas as: disposal of organic compounds or metals harmful to the environment, production of materials for medical applications, formation of advanced sensors, immobilization of enzymes, electrochemistry, catalysis, functional membranes etc.

An extremely important element of research is work devoted to neutralization of contaminants with metals harmful to the environment or substances of organic origin (dyes, pesticides, pharmaceuticals, estrogens, etc.). Although there are many methods and techniques used for this purpose, adsorption and photocatalysis seem to be unusually useful [1, 2].

Currently, materials of natural origin, obtained from biomass or other sources, are of great interest among scientists. Lignin and its derivatives are becoming increasingly important in this respect. Lignin is chemically modified/activated to give its surface or structure appropriate chemical functionality. Hybrid materials produced with lignin and selected oxides (e.g. SiO_2, Al_2O_3, Fe_3O_4) can serve as advanced fillers, eco-friendly components of abrasives or biosensors as well as cement additives (Fig. 1) [3, 4].

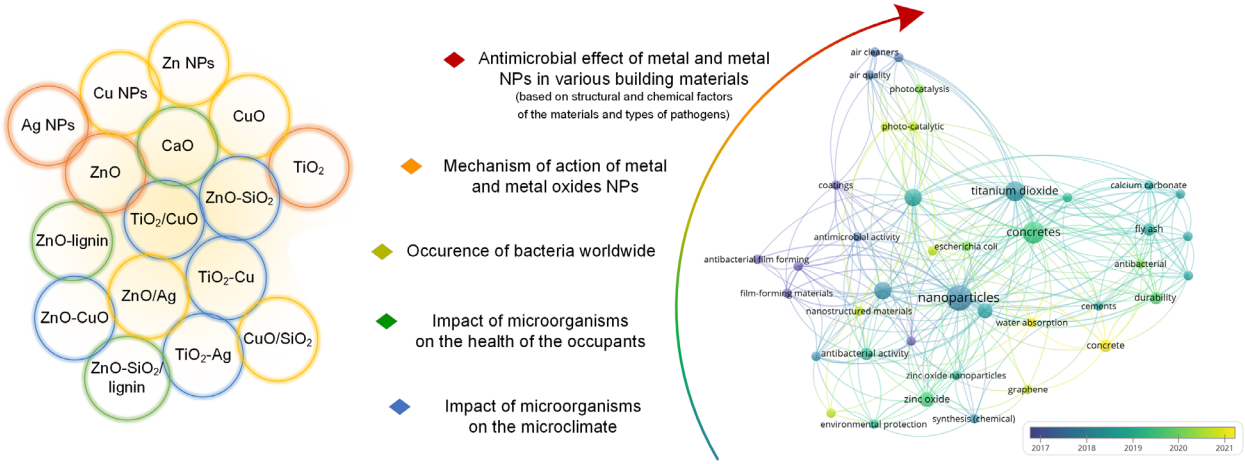

Fig. 1. Design and fabrication of functional cement composites

Chitin, a polysaccharide with unique properties, is also very popular. An interesting field of research concerns the mineralization of chitin under extreme environmental conditions (Fig. 2a). Sea sponges or their derivatives (skeletons, including carbonized forms), due to their unique spatial structure and properties, are also the subject of numerous studies. They are used as adsorbents of harmful metals and carriers in the immobilization of enzymes. Together with dyes, both natural and synthetic, adsorbed on their surface, they form hybrid systems with antioxidant, antibacterial

and catalytic properties [5-7]. Recently, the use of deep eutectic solvents in the design of materials for tissue engineering has also become very important.

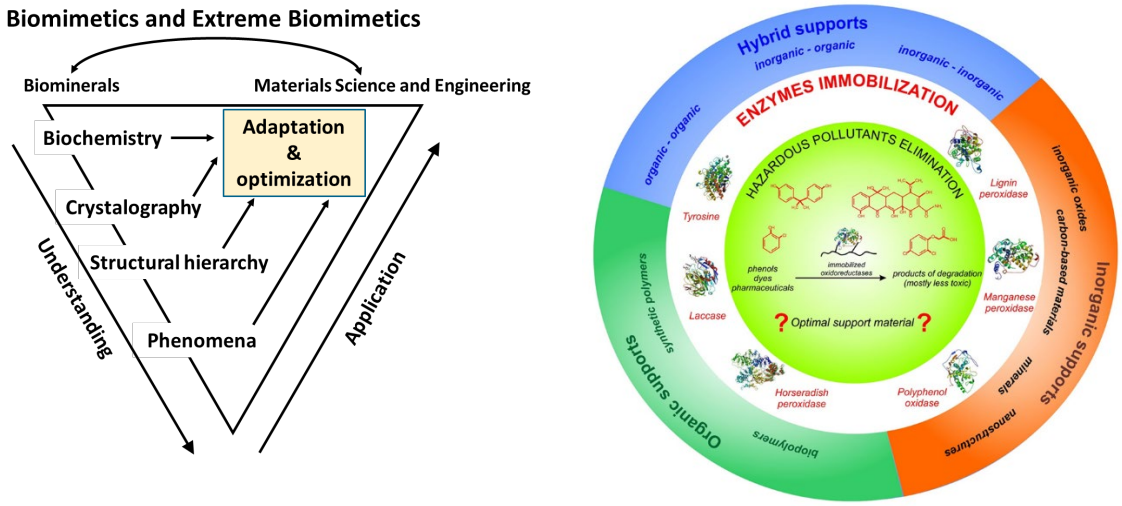

Fig. 2. Bioinspired hybrid material fabrication strategy (a) and exemplary supports in enzyme immobilization (b) [5-7]

Another direction of development of hybrid materials is their use as carriers in the immobilization of enzymes (Fig. 2b), followed by the production of enzymatic biosensors. For this purpose, nanomagnetite, lignin, polydopamine, poly(caffeic acid), etc. are used as components, as well as suitable enzymes dedicated to environmental or medical applications. Additionally, functional hybrid materials can be used to produce unique non-enzymatic sensors as well as advanced membranes [8].

Acknowledgements

This work was supported by National Science Center Poland under the research grant no. 2021/43/B/ST8/01854. The author would like to thank all those who participate in the research in the area included in this paper.

References

[1] Kubiak A., Bielan Z., Bartkowiak A., Gabała E., Frankowski M., Zalas M., Siwińska-Ciesielczyk K., Janczarek M., Jesionowski T., A novel microwave-assisted strategy to fabricate multifunctional photoactive titania-based heterostructures with enhanced activity, *Mater. Res. Bull.*, 2022, 147, 111633-1-111633-15.
[2] Weidner E., Wójcik G., Kołodyńska D., Jesionowski T., Ciesielczyk F., Insight into the removal of vanadium ions from model and real wastewaters using surface grafted zirconia-based adsorbents: Batch experiments, equilibrium and mechanism study, *J. Environ. Manag.*, 2022, 324, 116306-1-116306-19.
[3] Klapiszewska I., Parus A., Ławniczak Ł., Jesionowski T., Klapiszewski Ł., Ślosarczyk A., Production of antibacterial cement composites containing ZnO/lignin and ZnO–SiO2/lignin hybrid admixtures, *Cement Concrete Comp.*, 2021, 124, 104250-1-104250-17.
[4] Janczarek M., Klapiszewski Ł., Jędrzejczak P., Klapiszewska I., Ślosarczyk A., Jesionowski T., Progress of functionalized TiO_2-based nanomaterials in the construction industry: A comprehensive review, *Chem. Eng. J.*, 2022, 430, 132062-1-132062-28.
[5] Ehrlich H., Wysokowski M., Jesionowski T., The philosophy of extreme biomimetics, *Sust. Mater. Tech.*, 2022, 32, e00447-1-e00447-27.
[6] Jesionowski T., Zdarta J., Krajewska B., Enzyme immobilization by adsorption: A review, *Adsorption*, 2014, 20, 801-821.
[7] Zdarta J., Jesionowski T., Pinelo M., Meyer A.S., Iqbal H.M.N., Bilal M., Nguyen L.N., Nghiem L.D., Free and immobilized biocatalysts for removing micropollutants from water and wastewater: Recent progress and challenges, *Biores. Technol.*, 2022, 344, 126201-1-126201-14.
[8] Kuznowicz M., Rębiś T., Jędrzak A., Nowaczyk G., Szybowicz M., Jesionowski T., Glucose determination using amperometric non enzymatic sensor based on electroactive poly(caffeic acid)@MWCNT decorated with CuO nanoparticles, *Microchim. Acta*, 2022, 159, 159-1-159-14.

ENVIRONMENTAL APPLICATIONS OF HETEROGENEOUS PHOTOCATALYSIS

Ewa Kowalska[1,2,*], Zhishun Wei[2,3], Maya Endo-Kimura[2], Zuzanna Bielan[1], Kunlei Wang[2], Tamer M. Khedr[2,4], Marcin Janczarek[2,5], Agata Markowska-Szczupak[2,6]

[1]Faculty of Chemistry, Jagiellonian University, Gronostajowa 2, 30-387 Krakow, Poland
[2]Institute for Catalysis (ICAT), Hokkaido University, N21, W9, 001-0021 Sapporo, Japan
[3]Hubei Provincial Key Laboratory of Green Materials for Light Industry, Hubei University of Technology, Wuhan 430068, China
[4]Institute of Advanced Materials, Central Metallurgical research and Development Institute (CMRDI), 87 Helwan, Cairo 11421, Egypt
[5]Institute of Chemical Technology and Engineering, Faculty of Chemical Technology, Poznan University of Technology, Berdychowo 4, 60-965 Poznan, Poland
[6]Faculty of Chemical Technology and Engineering, West Pomeranian University of Technology in Szczecin, Piastow Ave. 42, 71-065 Szczecin, Poland
*corresponding author: ewa.k.kowalska@uj.edu.pl

Clean environment, pure water and green energy are the major challenges that the world humanity is facing. It is thought that heterogeneous photocatalysis under solar radiation might solve (at least in part) these tasks. Under irradiation with energy equal and/or larger than semiconductor bandgap, the semiconductor photocatalyst is excited, and thus formed charge carriers (electrons and holes) might initiate various redox reactions, including the formation of reactive oxygen species (e.g., hydroxyl radicals and superoxide ions) that could efficiently purify water and decompose various pollutants. Moreover, photo-conversion of solar energy on the surface of irradiated photocatalysts could be used for both photocurrent generation and fuel production.

In our study, various photocatalysts have been synthesized, characterized and tested for different environmental applications, especially for hydrogen generation, and decomposition of organic and microbiological pollutants [1-6]. Either commercial or self-synthesized photocatalysts, mainly based on titanium(IV) oxide (titania), have been applied. Although nanoparticulate titania is very efficient, its three shortcomings should be overcome for efficient applications, i.e., (i) charge carriers' recombination (typical for all semiconductors), (ii) inactivity under vis irradiation (due to its wide bandgap), and (iii) expensive recovery after reactions. Accordingly, different methods have been applied (e.g., surface modification, doping, and nanoarchitecture design, resulting in the preparation of novel structures, such as faceted nanoparticles, nanotubes, nanowires, core@shells and inverse opals [7-10]) to achieve vis-responsive photocatalysts with high quantum yields of photocatalytic reactions and feasible recovery (e.g., by magnetic separation [11]). Additionally, other materials have also been examined, such as bismuth tungstate, bismuth vanadate, graphitic carbon nitride (e.g., [12]).

During this talk, several examples of vis-responsive materials will be presented, including the aspects of property-dependent activity and probable mechanisms of photocatalysis reactions (e.g., Figure 1 [13]). Both advantages and disadvantages, as well as still existing challenges (with possible solutions) for the further development of solar heterogeneous photocatalysis will be discussed.

Acknowledgements

The project is co-financed by the Polish National Agency for Academic Exchange within Polish Returns Program (BPN/PPO/2021/1/00037) and The National Science Centre (2022/01/1/ST4/00026).

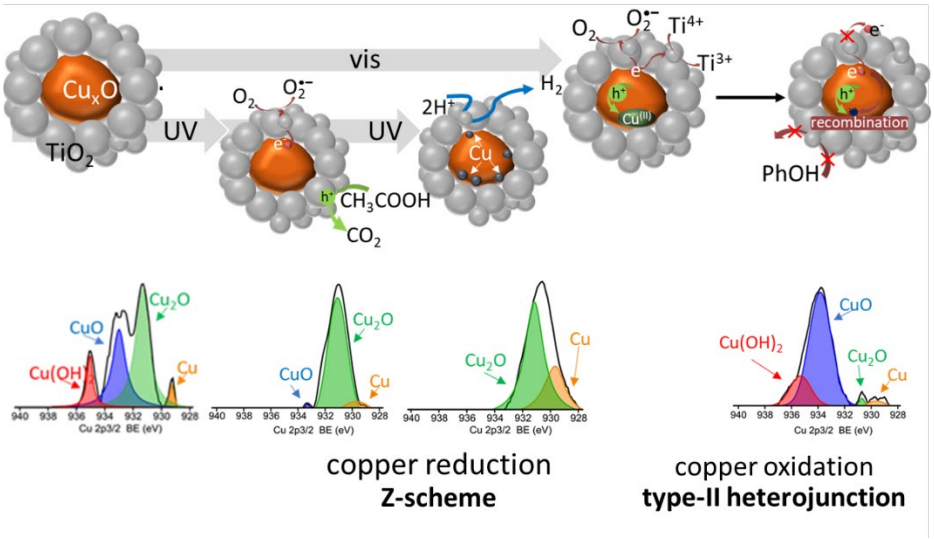

Fig. 1. The schematic drawing of the photocatalysis mechanism on $Cu_xO@TiO_2$ photocatalyst under vis or UV irradiation in anaerobic (H_2 evolution) or aerobic (oxidation of organic compounds) conditions [13]

References

[1] Kowalska E., Abe R., Ohtani B., Visible light-induced photocatalytic reaction of gold-modified titanium(IV) oxide particles: action spectrum analysis, *Chem. Commun.* 2009, 2, 241–243.

[2] Kowalska E., Yoshiiri K., Wei Z., Zheng S., Kastl E., Remita H., Ohtani B., Rau S., Hybrid photocatalysts composed of titania modified with plasmonic nanoparticles and ruthenium complexes for decomposition of organic compounds, *Appl. Catal. B-Environ*., 2015, 178, 133–143.

[3] Markowska-Szczupak A., Wang K., Rokicka P., Endo M., Wei Z., Ohtani B., Morawski A.W., Kowalska E., The effect of anatase and rutile isolated from titania P25 on pathogenic fungi, *J. Photochem. Photobiol. B*, 2015, 151, 54–62.

[4] Wei Z., Endo M., Wang K., Charbit E., Markowska-Szczupak A., Ohtani B., Kowalska E., Noble metal-modified octahedral anatase titania particles with enhanced activity for decomposition of chemical and mi-crobiological pollutants, *Chem. Eng. J*., 2017, 318, 121–134.

[5] Kowalska E., Remita H., Colbeau-Justin C., Hupka J., Belloni J., Modification of titanium dioxide with platinum ions and clusters: Application in photocatalysis, *J. Phys. Chem. C*., 2008, 112(4), 1124–1131.

[6] Endo M., Wei Z., Wang K., Karabiyik B., Yoshiiri K., Rokicka P., Ohtani B., Markowska-Szczupak A., Kowalska E., Noble metal-modified titania with visible-light activity for the decomposition of microorganisms, *Beilstein J. Nanotechnol*., 2018, 9, 829–841.

[7] Wei Z., Janczarek M., Endo M., Balčytis A., Nitta A., Mendez Medrano M.G., Colbeau-Justin C., Juodkazis S., Ohtani B., Kowalska E., Noble metal-modified facetted anatase titania photocatalysts: Octahedron versus Decahedron, *Appl. Catal. B-Environ*., 2018, 237, 574–587.

[8] Raja-Mogan T., Lehoux A., Takashima M., Kowalska E., Ohtani B., Slow Photon-induced enhancement of photocatalytic activity of gold nanoparticle-incorporated titania inverse opal, *Chem. Lett*., 2021, 50(4), 711–713.

[9] Kowalska E., Juodkazis, S., Henkiel P., Kowalski D. Site-Selective Au+ Electroreduction in Titania Nanotubes for Electrochemical and Plasmonic Applications, *ACS Appl. Nano Mater.*, 2022, 5, 6, 7696–7703.

[10] Mohagheghab N., Endo-Kimura M., Wang K., Wei Z., Najafabadi A. H., Zehtabi F., Kouchehbaghi N.H., Sharma S., Markowska-Szczupak A., Kowalska E., Apatite-coated Ag/AgBr/TiO_2 nanocomposites: Insights into the antimicrobial mechanism in the dark and under visible-light irradiation, Appl. Surf. Sci., 2023, 156574.

[11] Bielan Z., Kowalska E., Dudziak S., Wang K., Ohtani B., Zielinska-Jurek A., Mono- and bimetallic (Pt/Cu) titanium(IV) oxide core-shell photocatalysts with UV/vis response and magnetic separability, *Catal. Today*, 2021, 361, 198–209.

[12] Khedr T. M., El-Sheikh S. M., Endo-Kimura M., Wang K., Ohtani B., Kowalska E., Facile gas-templating synthesis of 2D porous S-doped g-C_3N_4 photocatalyst for enhanced photocatalytic H_2 evolution under visible light, *Nanomaterials*, 2023, 13(1), 62.

[13] Wang K., Bielan Z., Endo-Kimura M., Janczarek M., Zhang D., Kowalski D., Zielinska-Jurek A., Markowska-Szczupak A., Ohtani B., Kowalska E., On the mechanism of photocatalytic reactions on $Cu_xO@TiO_2$ core-shell photocatalyst, *J. Mat. Chem. A*, 2021, 9, 10135-10145.

THE ROLE OF LIFE CYCLE ASSESSMENT IN THE IMPLEMENTATION OF CIRCULAR ECONOMY IN SUSTAINABLE FUTURE

Stanisław Ledakowicz* Aleksandra Ziemińska-Stolarska*

Faculty of Process and Environmental Engineering, Lodz University of Technology
Wólczańska 213, 90-924 Lodz, Poland *

corresponding authors: stanislaw.ledakowicz@p.lodz.pl; aleksandra.zieminska-stolarska@p.lodz.pl

The most commonly quoted definition of sustainability: "Sustainable development is development that meets the needs of the present generation without compromising the ability of future generations to meet their own needs" comes from a report by Gro Harlem Brundtland, Prime Minister of Norway [1]. Sustainability was explained in depth in this 300-page document through the discussion of climate change, economic development and global goals that should be implemented. It is based on three fundamental pillars: social, economic and environmental. To gain an understanding of sustainability and its implication it is essential to mention 17 Sustainability Development Goals (SDGs) and the 2030 Agenda [2]. The United Nation publishes an annual report analysing how each goal is progressing and in March 2022 UN Secretary-General Antonio Guterres warned that humanity is moving backwards in relation to the majority of the SDGs.

In 2021, the UN's International Energy Agency (IEA) estimated that a global energy transition off fossil fuels would increase demand for key minerals such as lithium, graphite, nickel, and rare earth metals by 4200%, 2500%, 1900%, and 700%, respectively, by 2040 [3]. However, there is no capacity to reach such a demand. Critical raw materials are the backbone of modern economies and are key components of future development. Their use has serious environmental and social consequences, from extraction to disposal. Therefore, resource conservation aims to establish a circular economy that keeps products and raw materials in economically valuable loops, moving from waste to resource.

The circular economy (CE) stands for an economy, which maintains the value of materials for as long as possible while minimizing waste generation and emissions by closing material loops along life cycles of products and services. The CE concept's life-cycle thinking helps to implement the waste hierarchy laid down by focusing on waste prevention. Implementing the CE concept systemically requires a shift from linear to circular systems, thus calling for system transformation in production, consumption and governance systems as well as in society. It is necessary to develop promising interventions in order to facilitate this transformation. While circular economy strategies can be implemented in various sectors such as industry, waste, energy and transportation, life cycle assessment is required to optimize new systems [4].

A quantitative measure of sustainability is needed. The only necessary evaluation method is provided by Life Cycle Engineering (LCE), which is a sustainability-oriented methodology , which takes into account the complex technical, environmental and economic impacts of life cycle decisions. The definition of LCE is "an engineering activity that involves the application of technological and scientific principles to the manufacture of products in order to protect the environment, conserve resources, promote economic progress, keeping in mind social concerns and the need for sustainability, while optimizing the life cycle of the product and minimizing pollution and waste."[4]. As you can see from this definition, however, LCE includes, in addition, social aspects that are difficult for us engineers to quantify. Therefore, in this article we will limit ourselves only to the basic LCE tool of life cycle assessment (LCA).

Life cycle assessment (LCA) is a standardized tool to evaluate the environmental impacts associated with all the stages of a product's life, which is from raw material extraction through materials processing, manufacture, distribution, use and disposal. Nowadays, LCA analysis is

particularly important for emerging technologies that have not been tested in real operating conditions. The results of the analysis, which allow drawing conclusions at the design stage, are also of great importance. Consequently, LCA analysis is becoming an integral part of projects developing new technologies with market implementation potential.

After a short presentation of the LCA methodology (Goals and Scope, Inventory Analysis, Impact Assessment, Interpretation) and the methods used, as well as the software programs we apply, (e.g. IPCC 2021, ReCiPe) examples of specific applications will be presented.

For example, aviation industry works to achieve its goal of net-zero carbon emissions by 2050. The development of hybrid-electric regional aircraft is seen as one of the key issues to success; development of new high-voltage technologies will help pave the way for future hybrid-electric platforms and reduce carbon footprint [5].

The environmental consequences of a material substitution decision can be also successfully determined with life cycle assessment. Approximately 90% of the annual indium consumption accounts for transparent conducting oxide films (TCOs) in the form of indium tin oxides (ITOs). Today, ITOs are technologically entrenched in the commercial manufacture of components like flat panels displays, liquid crystal displays (LCDs), light emitting diodes (LEDs), touch screens and photovoltaic cells. Replacement of ITO by other materials like for example ZnO proved to be an optimal strategy towards minimization of the environmental impact of TCOs [6].

LCA methodology is widely applied as a decision making tool not only for support replacement of raw materials in different products but also for alternative synthesis methods. Comparative LCA was performed for the synthesis of 2'3'-cyclic GMP-AMP (2'3'-cGAMP) in an early development stage. The cyclic dinucleotide (CDN) is of interest for pharmaceutical applications such as cancer immunotherapy and can be synthesized either by enzymes or chemical catalysis. Comparison of chemical and enzymatic processes for the synthesis of the same compound by conducting LCA analysis can support further process improvement and help to determine possibilities of environmental impact minimization. Based on the LCA results, the biocatalytic 2'3'-cGAMP synthesis was identified as a significantly more environmentally friendly route [7].

It is hoped that this presentation will make you aware of the necessity of using the Life Cycle Assessment method in making decisions regarding the choice of development path for a new product or process under development, thus contributing to the fulfillment of at least some of the sustainable development goals.

References

[1] Brundtland G.H., *Our Common Future: The Report of the World Commission on Environment and Development*. Oxford University Press, Oxford & New York 1987.

[2] https://sdgs.un.org/2030agenda (accessed Feb. 28,.2023).

[3] IEA. The Role of Critical Minerals in Clean Energy Transitions; IEA: Paris, 2021;available on-line https://www.iea.org/reports/the-role-of-critical-minerals-in-clean-energy-transitions (accessed May 12 2022).

[4] Hauschild, M., *Life cycle assessment: theory and practice.* Springer International Publishing AG, 2018.

[5] Hybrid ElectriC regional Aircraft distribution Technologies, HECATE PROJECT, https://cordis.europa.eu/project/id/101101961.

[6] Zieminska-Stolarska A., Barecka M., Zbicinski I., *Effect of replacement of tin doped indium oxide (ITO) by ZnO: analysis of environmental impact categories,* January 2017, 19, E3S Web Conf..

[7] Becker M., Ziemińska-Stolarska A., Markowska D., Lütz S., Rosenthal K., Comparative Life Cycle Assessment of Chemical and Biocatalytic 2'3'-Cyclic GMP-AMP Synthesis, *ChemSusChem*, 2022, 16(5), e202201629.

NEW CHALLENGES OF THERMAL SEPARATION PROCESSES IN CHEMICAL ENGINEERING

Jerzy Maćkowiak[1,2]*

[1]ENVIMAC Engineering GmbH, Oberhausen, Germany
[2]ENVIMAC Polska Sp. z o.o., Ostrów Wlkp., Poland
*corresponding author: j.mackowiak@envimac.de

The rapidly increasing energy costs in the world nowadays, the shortage of raw materials, stricter authority requirements and regulations in environmental protection to decrease ecological impacts by reducing the emissions of substances into air and water require new and modern design of industrial processes, especially fluid separation plants. The emissions of hazardous gases like H_2S, SO_2, NO_x, CO_2, CH_4, and low-molecular chlorinated hydrocarbons from industrial processes into the atmosphere and emissions to the water body have to be reduced.

This also leads to the conclusion that today's plants have to be designed for higher production capacity, higher efficiency and with more accurate design without exceedingly high safety factors [1]. This is achieved with new components, more effective equipment and modern process control systems.

In the last decades, remarkable progress was achieved in all unit operation and also in thermal separation processes such as distillation, absorption and extraction processes [1]. Consequently, during the last 20 years the industrial world production increased by about 70% and at the same time energy consumption was significantly reduced by about 30%.

This worldwide progress in thermal separation processes was possible only owing to new developments in different parts of thermal separation processes such as optimization and design of new technology for separation processes with and without chemical reaction. Besides, progress has been made in modeling of fluid dynamics and mass transfer processes [1-9], in development of new column internals of active and non-active parts of columns and plants [1, 2], in more effective process automation, measurement of process parameter, in the development of new, high temperature resistant plastic materials that could be used for distillation and absorption processes. This is the main reason for a great reduction in investment and operation costs for process equipment during that time.

Because of the use of new simulation technics for flow measurements like Laser-Doppler-Anemometry (LDA) and Computational Fluid Dynamics (CFD), an effective and rapid optimization of existing internals as well as the development of new internals was possible and resulted in an increased separation efficiency of column internals. Also, column internals, which are not active parts for mass transfer like support grids, liquid and vapor distributors and droplet separators could be optimized with the previously mentioned tools (such as CFD) as inherent part of more highly efficient separation columns [5, 8].

New, generally valid models for column design such as suspended bed of droplets model (SBD) lead also to faster and effective development of new column internals using BPD- data (the basic performance data) of internals [9]. BPD-data is relevant data for design of distillation and absorption processes and comprise pressure drop, flooding point and operating range, hold-up and mass transfer parameters in the whole operating range. Thus, the development costs could be decreased and years of costly and extensive testing with different test systems avoided. Today, the progress in this field is so advanced that it is possible to determine and evaluate the BPD-data of structured and random packings within a very short time and with very low experimental effort using only an air-water simulator plant [9].

For the last 2-3 decades, a very important way to increase the effectiveness of chemical production plants has been the revamping of plants, e.g. changing internals of existing vacuum columns filled with trays into packed columns. This led to the rapid decrease of operation costs of

plants and increase of plant capacity. Revamping has not only improved the throughput of plants without the need for costly new investment but has also improved product quality. This has been done with a new generation of structured and random packings of the new generation: the so-called lattice type packing [2, 4, 6-8].

In this work, numerous examples from industrial practice are presented. They demonstrate and document progress made in the last decades. The future and the prosperity of all countries in the EU depends strongly on whether investments are made and how quickly the achievements of thermal separation technology are incorporated into different industrial processes. In this field, also the research area is open for new activities and for active cooperation with industrial companies.

The very important role of thermal separation technology today for science and industry is well recognized e.g. through numerous awards in the international scientific community. For example, in 2015 the three-volume book edited by Górak and Olujic [1] was awarded by the Association of American Publishers, where the new developments of the last years are presented by technical contributions of experts from individual subject areas. Distillation and absorption processes are the most important thermal separation processes and are not a marginal part of Chemical Engineering, but an essential element for all industrial applications and research and development in science and industry [3].

References:

[1] Górak A., Olujic Z., Distillation: Equipment and Processes, Amsterdam: Elsevier, 2015.
[2] Maćkowiak J., Fluid Dynamics of Packed Columns, Berlin: Springer, 2010.
[3] H. Z. Kister H.Z., Distillation Design, New York: McGraw-Hill, 1992.
[4] Billet R., Schultes M., Prediction of mass transfer columns with dumped and arranged packings: updated summary of the calculation method of Billet and Schultes, *Chem. Eng. Res. Des.,* 1999, 77(6), 498-504.
[5] Maćkowiak J., Maćkowiak J.F., Einsatz von Lamellen-Tropfenabscheidern in Trennkolonnen, *Chem. Ing. Tech.,* 2021, 93(7), 1178-1182.
[6] Maćkowiak J., Prediction of separation efficiency of structured and stacked packings, *Chem. Eng. Res. Des,* 2022, 186, 713-729.
[7] Maćkowiak J., Progress in design of random packing for gas-liquid systems, *Chem. Eng. Res. Des.,* 2015, 99, 28-42.
[8] Salten A.H., Maćkowiak J.F., Maćkowiak J., Kenig E. Y., A new hydrodynamic analogy model for the determination of transport phenomena in random packings, *Chem. Eng. Sci.,* 2021, 233, 11624.
[9] Maćkowiak J., Rapid Method for Prediction of Random Packing Performance (BPD) based on Minimized Experimental Effort, Presented at Distillation & Absorption, Toulouse, 2022.

FROM WASTES TO SUPERCAPACITORS

Ewa Mijowska*, Xiaodong Xu, Xin Wen, Xuecheng Chen

Faculty of Chemical Technology and Engineering, Department of Nanomaterials Physicochemistry, West Pomeranian University of Technology, Szczecin, Poland
*corresponding author: emijowska@zut.edu.pl

With the depletion of fossil fuels and the environmental crisis associated with their use, huge efforts are being made to provide efficient, clean and sustainable energy sources and technologies for energy storage and conversion. Development of electrical energy storage systems has attracted massive attention due to their widespread applications in hand-handle electronic devices, electronic vehicles, and renewable energy techniques. Supercapacitors (SCs) are devices which employ carbon materials with specific surface area as a key parameter influencing its capacity for carbon-based electrostatic double layer SCs (EDLC). A variety of carbon materials, such as activated carbon, carbon nanotubes, carbon aerogels, and graphene have been used as electrode materials. Among different electrode materials, hierarchical porous carbons (HCPs) have been deeply explored. Main attempts have been made to decrease the cost of their fabrication. Therefore, using solid wastes as their precursors seems to be most advantageous in terms of environment crisis allowing some materials to be reused, which will prevent rubbish from being deposited in landfills.

In this contribution, we focused on two groups of solid wastes: (i) biowastes and (ii) polymer wastes to demonstrate that they can be a source of well-designed HCPs serving as electrode material in EDLC.

The conducted research demonstrated that the physicochemical properties (2D/3D morphology, S_{BET}, micropore volume, meso-/macropore volume, doping with heteroatoms and combining metal oxides) play key roles in the electrochemical response of these porous carbons and composites. Tuning these properties of porous carbons boosts charge storage capacity, rate capability, pseudocapacitance contribution, energy density, long-cycle stability and reversible specific capacity. What is worth underlining is that the optimization of one of the physicochemical properties alone does not efficiently boost electrochemical properties. The synergy of these optimized physicochemical properties delivers: (i) increased charge storage capacity, (ii) a continuous electron pathway to benefit ion transport via short diffusion pathways for a high rate capability, (iii) charge storage sites to create a large electric double layer for great charge storage capacity, (iv) doping heteroatom into carbon matrix to enhance electronic conductivity and surface wettability for pseudocapacitance.

MODERN TRENDS IN CHEMICAL AND PROCESS ENGINEERING

Eugeniusz Molga*

Faculty of Chemical and Process Engineering, Warsaw University of Technology
Waryńskiego 1, 00-645 Warszawa, Poland
*corresponding author: eugeniusz.molga@pw.edu.pl

Chemical engineering is a science discipline, which enables a description and modelling matter transformation processes, including chemical, biochemical and physical ones. As a result, cost effective production of materials and chemicals can be designed and implemented. Modern chemical engineering has to satisfy the needs of chemical and related industries, meet market requirements and economy demands as well as the social and environmental constraints. Due to its interdisciplinary approach the chemical engineering is applicable not only in chemical industries but also plays a significant role in development of other branches of industry – e.g. in biotechnology, biochemical and biomedical engineering, production of nanomaterials, environment protection, green processes, decarbonization of energy systems etc. Therefore, chemical engineering is considered one of the few scientific disciplines, which will contribute significantly to implementation of sustainable development strategy and participate in technological development in 21th century.

Chemical engineering has been changing throughout the years – from the first "unit operations" paradigm initiated by Arthur D. Little and presented in the textbook by Walker et al. [1], through the second "transport phenomena" paradigm determined with publication of the famous textbook by Bird et al. [2], to further developments set with interest in bio-based processes, biomedical engineering and nanotechnologies. This last-mentioned period is even called the third "multiscale approach" paradigm [3], as now an understanding of how phenomena at molecular level influence system behaviour at the production scale is crucial for reasonable development of the considered processes. Therefore, an integrated system approach for description of all stage processes is required, in which complex, multidisciplinary, non-linear, non-equilibrium processes occurring at different length and time scales have to be taken into account.

Challenges humankind faces today include: prevention of climate change, improvement of energy transformation and storage, reasonable consumption of raw materials, intensification of recycling leading to a full circular economy, production and distribution of food, conservation and purification of water, production of new materials and medicines and many others. Chemical engineering has opportunities and tools to contribute significantly to solving these problems, therefore participation in these activities is crucial for its role and significance today and in the future.

Based on a comprehensive literature review – e.g. see [4-6] – the following most important directions for future development and applications of chemical engineering can be indicated:

Decarbonization of energy systems

Chemical engineering should intensively participate in elaboration of non-fossil-based energy sources and in modification of energy carriers. Particularly novel systems are required to improve solar energy capture and its conversion to energy carriers via reactions with water, nitrogen and CO_2 to produce hydrogen, ammonia and liquid fuels (e.g. methanol). Successful mitigation of climate change and transition to a low-carbon energy systems, will require closer collaboration of chemical engineering with other disciplines as chemistry, biology, economics and social science to ensure economic, competitive and scalable solutions.

Sustainable engineering for environmental systems

Chemical engineering should increase its contribution to solving environmental problems – especially with water, food and air quality. Due to its specific research opportunities, chemical engineering is able to support significantly development of membrane and other separation

methods at both - basic (fundamental) and application levels. Global problems concerning climate change and population growth require research on precision agriculture, non-animal-based and low-carbon-intensity food production as well as reduction or elimination of food waste. Chemical engineers have to continue and develop research on improvement of air quality, including reduction of CO_2 emissions and other greenhouse gases as well as their removal from atmosphere and conversion into useful chemicals. In this topic a more intensive collaboration and interdisciplinary approach including chemistry, physics, meteorology and climatology is also required.

Engineering approach to medicine

A contribution of chemical engineering in the area of biomedical and biomolecular engineering ranges from molecular to manufacturing level and includes: - development of novel bio- and cell-based processes, isolation of small molecules from biological systems, development of biologically derived products, designing of reactors and separation processes, drug formulation and manufacturing, vaccine design, cell engineering, production of bio-implants and scaffolds. Participation in modelling and designing of noninvasive methods for drug delivery as well as contribution to development of immunology – e.g. cancer immunotherapies and modelling of therapeutic treatments is also crucial.

Flexible manufacturing and circular economy

As chemical engineers play a critical role in manufacturing processes, they can significantly contribute to more sustainable production by increasing efficiency and applying improvements – e.g. process intensification. The implementation of sustainable development strategy requires a shift from linear to circular economy which reduces consumption of energy and raw materials as well as simultaneously limits waste generation. Therefore, the existing and novel production processes should be redesigned to be more efficient, environmentally friendly and cost-effective to reduce or eliminate pollution, utilize waste, improve products to be used longer and to be recyclable and also modify processes to use sustainable feedstocks.

Novel and improved materials

Chemical engineering intensively contributes to the development of new materials and their production processes in the full range from molecular to macroscopic scale. Investigations and modelling on molecular level assisted by thermodynamics, mass and heat transfer phenomena, rheology, catalysis and chemical kinetics enable advances in production and help to invent new materials both for industry and medicine. Here, manufacturing nanomaterials for biomedicine is of particulate importance, as they are applied in regenerative engineering and organ-on-a-chip technology. Tools attributed to chemical engineering – such as modelling and design of reactors and separation processes - are also very useful for materials in electronics.

It should be distinguished that although the indications listed above are defined as a vision for the future of chemical engineering, a lot of research is already carried out within indicated areas.

References

[1] Walker W.H., Lewis W.K., McAdams W.H., *Principles of chemical engineering*. McGraw-Hill Book Company, 1923.

[2] Bird R.B., Stewart W.E., Lightfoot E.N., *Transport phenomena*. J. Wiley and Sons Inc., New York, 1960.

[3] Charpentier J.C., Among the trends for a modern chemical engineering, the third paradigm: The time and length multiscale approach as an efficient tool for process intensification and product design and engineering, *Chem. Eng. Res. Des.,* 2010, 88, 248–254.

[4] *New Directions for Chemical Engineering*, National Academies of Sciences, Engineering, and Medicine. The National Academies Press, Washington, DC, 2022. https://doi.org/10.17226/26342.

[5] Haghi A.K. (Editor), *Modern trends in chemistry and chemical engineering*, Apple Academic Press, Toronto, New Jersey, 2020.

[6] Gani R., Bałdyga J., Biscans B., Brunazzi E., Charpentier J.-C., Drioli E., Feise H., Furlong A., Van Geem K.M., de Hemptinne J.-Ch., ten Kate A.J.B., Kantogeoris G.M., Manenti F., Marin G.B., Mansouri S.S. Piccione P.M., Povoa A., Rodrigo M.A., Sarup B., Sorensen E, Udugama I.A. Woodley J.M., A multi-layered view of chemical and biochemical engineering, *Chem. Eng. Res. Des.,* 2020, 155, A133-A145.

"GREEN AMMONIA" AS HYDROGEN STORAGE – TECHNOLOGICAL CHALLENGES AND APPLICATIONS

Antoni W. Morawski*

West Pomeranian University of Technology, Faculty of Chemical Technology and Engineering,
Department of Inorganic Chemical Technology and Environment Engineering,
70-322 Szczecin, Pułaskiego 10, Poland
*corresponding author: Antoni.Morawski@zut.edu.pl

The paper will present a critical analysis of the current ammonia production technology from the so-called "gray hydrogen". This technology is based on reforming methane with water:

$$CH_4 + H_2O \Leftrightarrow CO + 3H_2 \quad (1)$$

and next

$$CO + H_2O \Leftrightarrow CO_2 + H_2 \quad (2)$$

which finally emitted CO_2. The total CO_2 emission, including the energy needed to operate the compressors, is 1.6-2.5 tons of CO_2/1 tonne of NH_3. Therefore, the main problems of "gray ammonia" to be solved are: 1) Energy; 2) CO_2 and 3) catalyst.

The directions of development and changes of this technology will be indicated with the participation of the so-called "green hydrogen". These two reactions are decisive and critical to this new technology. The first is a 2-electron endothermic decomposition of water:

$$H_2O \rightarrow H_2 + O_2 \qquad + 285.8\ \mathrm{kJ/mol} \quad (3)$$

and the second is a 3-electron exothermic reaction producing ammonia:

$$^1/_2\,N_2 + {}^3/_2\,H_2 \Leftrightarrow\ -46.05\ \mathrm{kJ/mol} \quad (4)$$

Each of the production stages in the technological line will be discussed, starting from energy sources, water electrolysis, separation of nitrogen from the air, reactor and synthesis loop, storage and transport, as well as new applications, apart from the fertilizer industry.

Comparative considerations of the properties of "green ammonia" and "green hydrogen" as hydrogen storage methods will be also carried out. Some examples of the application of electricity production will be shown. An analysis of the advantages of "green ammonia" over other fuels and the actual trends in their use will be presented.

Industrial solutions for the use of "green ammonia" for the propulsion of vehicles and sea vessels will be discussed [1]. Possibilities of building and locating small installations for the synthesis of "green ammonia" in industries other than chemical will be pointed out. New requirements and critical points for production installations of "green ammonia" will be specified.

In addition, new solutions from the world literature regarding the production of "green ammonia" will be shown, including artificial photosynthesis, photocatalytic, electrochemical, etc. [2–4].

References

[1] Machaj K., Kupecki J., Malecha Z., Morawski A.W., Skrzypkiewicz M., Stanclik M., Chorowski M., Ammonia as a potential marine fuel: A review, *Energy Strategy Rev.*, 2022, 44, 100926.
[2] Morawski A.W., Ćmielewska K., Ekiert E., Kusiak-Nejman E., Pełech I., Staciwa P., Sibera D., Wanag A., Kapica-Kozar J., Gano M., Lendzion-Bieluń Z., Narkiewicz U., Effective green ammonia synthesis from gaseous nitrogen and CO2 saturated water vapour utilizing a novel photocatalytic reactor, *Chem. Eng. J.*, 2022, 446, Part3, 137030.

[3] Li R., Photocatalytic nitrogen fixation: An attractive approach for artificial photocatalysis, *Chinese J. Catal.*, 2018, 39, 1180-1188.
[4] Shen H., Yang M., Hao L., Wang J., Strunk J., Sun Z., Photocatalytic nitrogen reduction to ammonia: insights into the role of defect engineering in photocatalysts, *Nano Res.*, 2022, 15, 2773-2809.

CHALLENGES TOWARDS A SUSTAINABLE FUTURE

Emilia Nowak[1]*, Derek Kawiti[2]

[1]Massey University, College of Sciences, Palmerston North, Aotearoa New Zealand
[2]Victoria University of Wellington, School of Architecture, Wellington, Aotearoa New Zealand
*corresponding author: e.nowak@massey.ac.nz

Chemical engineering has the potential to tackle global challenges sustainably. Engaging in technical developments in various sectors requires collaborations with multiple disciplines. This opens perspectives and co-existing ways of thinking that may create a unique knowledge ecosystem benefitting Earth and humankind.

Dr E. Nowak will discuss multiphase (gas/liquid/solid) systems, where processing may be still inefficient and use redundant resources across separation processes, food processing, pharmaceutical, oil and gas industry. Capturing appropriate physics and chemistry at the interfaces across a wide range of lengths and time scales remains a challenge. Some applications and processes (e.g. chemical reactors) target higher precision and performance at small time and length scales, where interfacial phenomena dominate the bulk behaviour. Advancing fundamental knowledge of multiphase flows enables the reduction of (semi-)empiricism in the optimization of the mass and energy transfer in complex systems such as the processing of natural materials. To progress understanding of the dynamics at the interfaces, insights from miscible and immiscible liquid interfaces will be presented. Numerical simulations on the binary coalescence in the presence of surfactant provide a deeper understanding of the problem of setting boundary conditions and deformable interfaces for liquid flows.

Prof D. Kawiti will present revitalising lost knowledge on the complexities of Māori design and geometries, as genuinely inspired by nature, with modern technologies. These can offer approaches for optimisation beyond current science norms and for the preservation of ecosystem diversity towards more resilient communities. Selected aspects of the convergence of digital design technologies with indigenous customary knowledge and craft will be presented.

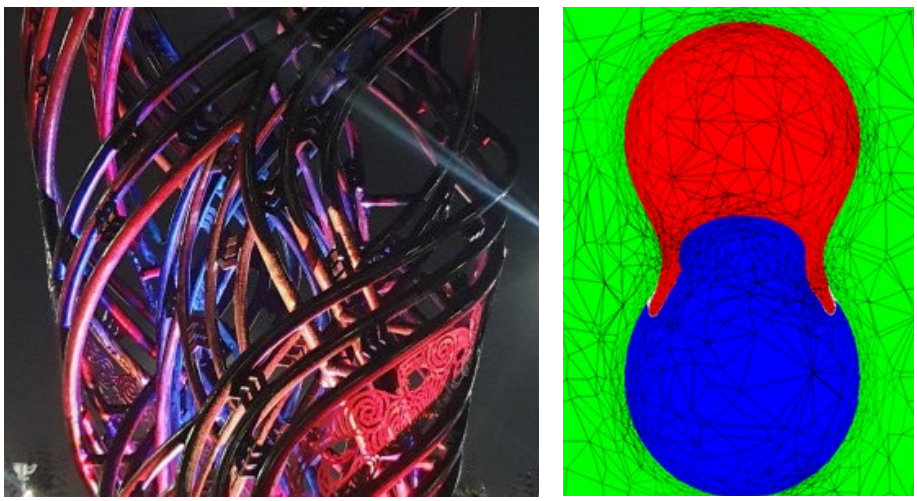

Fig. 1. Te Ahi Tupua, the largest 3D printed sculpture in the world [1], simulation of drop coalescence [2]

References

[1] ORNAMENTAL STRUCTURATION. Digital tool use with Māori geometries. Proceedings of the 22nd International Conference of the Associa-tion for Computer-Aided Architectural Design Research in Asia CAADRIA 2017.
[2] Kawiti D., Gordine S., Janssen P., Loh P., Raonic A., Schnabel M., Soft Matter, 2017,13, 4616-4628.

HOW TO GREEN THE BIG BAD WOLF? NOVEL CHEMICAL ENGINEERING APPROACHES TO DECARBONIZATION

Andrzej I. Stankiewicz[1,2,*]

[1]Delft University of Technology, Process & Energy Department, Leeghwaterstraat 39, 2628 CB Delft, The Netherlands
[2]Warsaw University of Technology, Faculty of Chemical and Process Engineering, Waryńskiego 1, 00-645 Warsaw, Poland
[*]corresponding author: andrzej.stankiewicz@pw.edu.pl

Decarbonization of energy-intensive industries presents arguably the most important technological challenge in the years to come. Among those industries, the chemical sector (including refineries) is by far the biggest energy consumer - according to the U.S. Energy Information Administration [1], in 2021 manufacturers of coal, petroleum and chemical products used 59% of the entire energy consumed by the American industry. On the other hand, the chemical industry is one of the biggest greenhouse gas emitters - in the U.K. second only to the steel sector [2].

The aim of the present lecture is to examine the role that novel chemical engineering approaches already play or will play in achieving the decarbonization of chemical and related industries. The four basic pathways leading to that goal include:

- energy-lean processing;
- renewable electricity-based processing;
- manufacturing of zero-carbon fuels, hydrogen and ammonia in particular;
- chemical valorization of the greenhouse gases, carbon dioxide and methane in particular.

Latest developments in each of the above areas are briefly discussed in the lecture and are illustrated with relevant examples from both the academia and the industry.

References

[1] U.S. Energy Information Administration, Use of energy explained. Energy use in industry; (https://www.eia.gov/energyexplained/use-of-energy/industry.php).
[2] Griffin, P.W., Hammond G.P., Norman J.B., Industrial energy use and carbon emissions reduction: a UK perspective, *WIREs Energy Environ*, 2016, 5(6), 684–714.

PHOTOCATALYTIC FUNCTIONAL MATERIALS FOR SOLAR-DRIVEN ENVIRONMENTAL REMEDIATION

Anna Zielińska-Jurek*

Gdańsk University of Technology, Faculty of Chemistry, Department of Process Engineering and Chemical Technology, Narutowicza 11/12, 80-233 Gdańsk, Poland

*corresponding author: annjurek@pg.edu.pl

One of the primary challenges that societies will face during 21st century is improvement of water and air quality by reducing pollution according to the European Green Deal and 2050 climate-neutrality goal in synergy with clean and circular economy using the fundamentals of green chemistry and green engineering processes. Current and future environmental challenges related to increased body burdens of various micropollutants, their bioaccumulation, and biomagnification require understanding the nature of the problems and their relationships to other phenomena.

The occurrence of some pharmaceuticals in aqueous environments worldwide results from an increase in their consumption in the last few decades and no susceptibility to degradation by conventional wastewater treatment processes. For example, carbamazepine is found at one of the highest levels in wastewater influents and effluents (after treatment) due to its low sorption properties on activated sludge microorganisms (less than 10%) and, as a consequence, low removal efficiency from municipal wastewater treatment plants (WWTPs). Furthermore, undegraded carbamazepine in aquatic systems can form more toxic by-products, mostly acridine and acridone, when exposed to sunlight during photolysis. Therefore, carbamazepine has been identified as an anthropogenic chemical marker of water contamination. Besides carbamazepine, ibuprofen, diclofenac and acetaminophen are examples of poorly degraded drugs by WWTPs being detected in surface waters, groundwater, and occasionally in drinking water in Europe, America, and Asia.

Considering the contamination of water with pharmaceutical residues, there is a need for the development of advanced treatment technologies to efficiently remove these pollutants from wastewater before their discharge into the receiving environment. In this regard, improving water treatment technologies is a proactive approach of high importance to increase water quality and ensure the sustainability of water cycle management.

Advanced oxidation processes (AOP), based on the in-situ generation of the strongest oxidants - hydroxyl radicals and sulfate radicals - have been recognized as a promising approach for wastewater treatment from residues of recalcitrant and emerging organic contaminants. In recent years, ozonation, Fenton process and UV irradiation have already been established and started at a technological scale for the treatment of drinking water and water reuse facilities. Nevertheless, ozonation is restricted by the high cost of ozone and low mineralization efficiency, while the Fenton reaction usually operates under a limited pH range (3-4) and generates $Fe(OH)_3$ precipitation. Therefore, among the various AOP processes, photocatalysis utilizing sunlight is a promising method for environmental remediation.

Although great progress has been achieved in the field of solar-driven photocatalytic degradation of persistent organic pollutants, there are still some challenges concerning (i) photocatalyst design for the particular application, (ii) separation of semiconductor particles from post-treatment suspension, (iii) low quantum efficiency associated with charge transfer, and (iv) reactor design enabling efficient light penetration and exposure of the photocatalyst to the light.

The mechanism of photocatalysis is dependent on the electrical structure of a semiconductor. Our recent studies on the relationships between crystal and surface structure, surface chemistry, and photocatalytic properties have advanced our understanding of the behavior of photocatalytic materials, thereby enabling improvements in their performance [1-4]. The results showed that for the non-modified photocatalyst exposing the majority of only one facet, the {1 0 1} crystal planes

exhibited the highest degradation rate and mineralization when compared to the {1 0 0} and {0 0 1} ones. It proved that the efficiency of such a process depended on the density of the surface trapping sites of the photocatalyst, which should be high for this facet rather than its surface energy [3]. Therefore, controlling the structure of synthesized materials enables designing the photocatalyst for desired environmental applications.

In this regard, the twofold strategy to optimize photocatalyst structure toward the degradation of selected pharmaceuticals not susceptible to biodegradation was proposed within our study, as presented in Figure 1. Firstly, the modification of surface chemistry and controlled growth of semiconductor nanocrystals with a higher proportion of oxidative or reductive facets result in improved charge separation of photogenerated carriers. The electron-donor cocatalyst loading on crystal facets with the preference of hole accumulation and electron-acceptor for reductive facets was proposed to improve charge carrier separation. Furthermore, the hybridization of semiconductor with graphene-related material and combining photocatalytic reaction with transition metal-based PMS acceleration properties allowed efficient degradation and mineralization of pharmaceutically active compounds in 5–30 min of photodegradation process under simulated solar light.

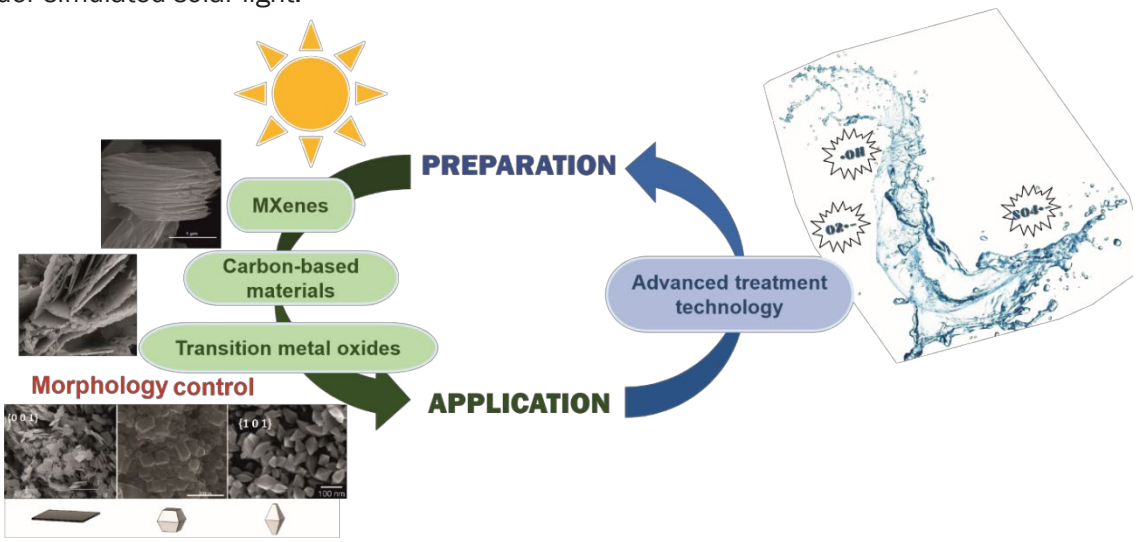

Fig. 1. Schematic illustration of different strategies to enhance activity and selectivity of the proposed photocatalytic materials in photooxidation(degradation of pharmaceuticals) and photoreduction (CO2 conversion) reactions under solar light irradiation

Acknowledgments

This research was financially supported by the Polish National Science Centre, grant no. NCN 2021/43/B/ST5/02983.

References

[1] Dudziak S., Kowalkińska M., Karczewski J., Pisarek M., Siuzdak K., Kubiak A., Siwińska-Ciesielczyk K., Zielińska-Jurek A., Solvothermal growth of {0 0 1} exposed anatase nanosheets and their ability to mineralize organic pollutants. The effect of alcohol type and content on the nucleation and growth of TiO_2 nanostructures, *Appl. Surf. Sci.*, 2021, 565, 150360.

[2] Dudziak S., Kowalkińska M., Karczewski J., Pisarek M., Gouveia J.D., Gomes J.R.B., Zielińska-Jurek A., Surface and trapping energies as predictors for the photocatalytic degradation of aromatic organic pollutants, *J. Phys. Chem. C*, 2022, 126, 4859-14877.

[3] Grzegórska A., Gajewicz-Skretna A., Trykowski G., Sikora K., Zielińska-Jurek A., Design and synthesis of TiO_2/Ti_3C_2 composites for highly efficient photocatalytic removal of acetaminophen: The relationships between synthesis parameters, physicochemical properties, and photocatalytic activity, *Catal. Today*, 2022 doi:10.1016/j.cattod.2022.12.011.

[4] Dudzika S., Fiszka Borzyszkowska A., Zielińska-Jurek A., Photocatalytic degradation and pollutant-oriented structure-activity analysis of carbamazepine, ibuprofen and acetaminophen over faceted TiO_2, *J. Environ. Chem. Eng.*, 2023, 11, 109553.

Lectures

S1. Intensification of transport processes

ROTATING PACKED BED TECHNOLOGY – AN INNOVATIVE APPARATUS IN PROCESS INTENSIFICATION

Michał Blatkiewicz*, Maciej Jaskulski, Marcin Piątkowski, Justyna Wojtasik-Malinowska, Dawid Zawadzki, Małgorzata Majdzik, Andrzej Górak

Department of Process and Environmental Engineering, Lodz University of Technology,
Wólczańska 213, 93-005 Łódź, Poland
*corresponding author: michal.blatkiewicz@p.lodz.pl

Rotating Packed Bed (RPB) is an innovative device designed for intensified mass transfer. It was first patented in 1981 by Ramshaw and Mallison [1]. RPB is an alternative to traditional, stationary bed processes, where it substitutes the gravitational force with centrifugal force. In the counter-current operation, the denser phase (liquid) is introduced in the eye of a rotor, flows through the annular packing, where it is subjected to high centrifugal force, and then leaves the packing in the form of fine spray that splashes onto the outer casing wall to be eventually collected at the bottom of the device. The lighter phase (gas or vapor) is introduced at the outer cavity zone and flows inward due to pressure gradient and is eventually collected in the eye of the rotor. Fine dispersion of the liquid phase and intensive micro-mixing of the phases lead to volumetric mass transfer coefficients up to three orders of magnitude higher than of analogous stationary packed bed processes [2].

In the last decades, RPBs have gained a lot of interest in academia and industry, due to their compact design, high responsivity, good mass transfer efficiency, as well as portability [3]. Although most research regarding the technology has been limited mostly to China and India, in the last years, several universities in Europe have taken interest in RPBs, including the ones in Dortmund, Berlin, Brno, Newcastle and Toulouse.

One of the pioneers of the rotating packed bed in Europe is the RPB team of Lodz university of Technology, who have been researching the technology for almost a decade.

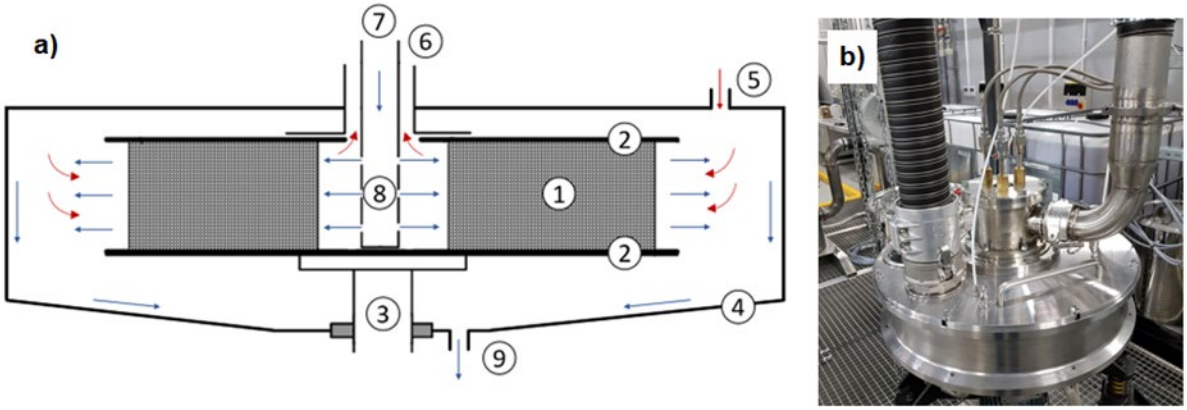

Fig. 1. a) Schematic representation of an RPB apparatus: internal (1), rotor plates (2), rotating shaft (3), stationary casing (4), gas inlet (5), gas outlet (6), liquid inlet (7), liquid distributor (8), liquid outlet (9); b) The RPB device owned by the RPB team

The RPB team is a part of the Chair of Environmental Engineering, Department of Process and Environmental Engineering, Lodz University of Technology. The team formed in 2016, as it implemented and delivered the INVITES project. Currently, the RPB owned by the team remains one of the most technologically advanced RPB research units in Europe.

The team has been awarded three research grants for the development of RPB technology:

1. **Innovative Equipment for Intensified Recovery of CO2 from Flue Gases (INVTES),** financed by the National Centre for Research and Development, and completed within the Polish-German cooperation for sustainable development STAIR, along with the industrial companies ENVIMAC and OMNIKON. The purpose of the project was development of RPB apparatus and thorough comparison of carbon capture processes in rotating and stationary beds. The project was carried out in 2016–2019.
2. **Innovative Method for Computer-Aided Process Design of Internals for Rotating Packed Beds**, financed by the National Science Centre within the OPUS 17 program. The project was based on a complex research system, which combined experimental studies, computational fluid dynamics simulations and rapid prototyping with the use of additive manufacturing. The goal of the project was to develop efficient structured internals for rotating packed bed equipment. The project was carried out in 2020–2023
3. **Holistic approach to rotating packed bed absorption process with the use of three-dimensional computational fluid dynamics, visual studies, and mass transfer experiments**, financed by the National Science Centre within the OPUS LAP 20 program, and conducted in cooperation with Brno University of Technology. The goal of the project is to develop a universal mass transfer model of the whole RPB apparatus, taking into account the rotor eye zone, packing zone, and outer cavity zone. Mass transfer experiments and kinetic modeling are intertwined with liquid structure visual studies and computational fluid dynamics.

Currently, the team is applying for another RPB-related project within the OPUS LAP WEAVE program by the National Science Centre.

The bulk of RPB research done by the team has been focused on development of innovative internals for RPB devices, regarding reduction of pressure drop and increasing effective mass transfer area. Additionally, the team has been researching absorption processes with the use of RPB, mostly using enzyme-enhanced tertiary amine solutions. Recently, the focus of the group has been shifted toward modeling of overall absorption process in an RPB device, taking into account mass transfer in the rotor eye zone, packing zone, and outer cavity zone.

References

[1] Ramshaw C., Mallinson R.H., "US 4,283,255, Mass transfer process," United States Patent, no. 19, p. 12, 1981, [Online]. Available: https://patents.google.com/patent/US4283255A/en.
[2] Rao D.P., The story of 'HIGEE, *Indian Chemical Engineer*, 2015, 57, 3–4, 282–299.
[3] Neumann K., Gladyszewski K., Groß K., Qammar H., Wenzel D., Górak A., Skiborowski M., A guide on the industrial application of rotating packed beds, *Chem. Eng. Res. Des.*, 2018, 134, 443–462.

SPECIATION OF ZINC IN ELECTRIC ARC FURNACE DUST BY PARTICLE SIZE

Christof Lanzerstorfer*

University of Applied Sciences Upper Austria, Process Engineering and Production,
Stelzhamerstraße 23, 4600 Wels, Austria
*corresponding author: c.lanzerstorfer@fh-wels.at

Electric arc furnace dust (EAFD) is a by-product in steelmaking from scrap and direct reduced iron in an electric arc furnace (EAF). The reported range of EAFD per ton of liquid steel is 10–30 kg [1]. EAFD consists mainly of Fe but other metals volatile at steelmaking conditions can also be found in EAFD. Zn is found in EAFD at higher concentrations because of its wide-spread use for galvanizing steel components for corrosion protection [2]. Zn enters the EAF with the scrap. Because of high temperature and reducing conditions all Zn is volatized in the furnace and leaves it with the off-gas. During cooling of the off-gas Zn is mostly deposited on dust particles. Zn concentration values in EAFD are in the range of 2–43% [1]. EAFD is classified as hazardous as it contains heavy metals and other hazardous components [3]. Although some part of EAFD is still sent to landfill, increasing shares of EAFD are utilized to recover Zn [4]. For Zn recovery several hydrometallurgical and pyrometallurgical process routes are available [4, 5]. Independent of the recycling route, a high Zn content makes recycling of EAFD more economical. Therefore, recycling of EAFD back into the EAF can be used to increase the Zn content of the discharged EAFD [6]. Since Zn is enriched in the finest size fractions of the EAFD, air classification can be applied to optimize dust recycling [7]. In the EAFD Zn is mainly present as zinc oxide (ZnO, zincite) and zinc ferrite ($ZnFe_2O_4$, franklinite) [6]. Especially for hydrometallurgical processes it is essential in which compound Zn is present since zinc oxide is much more accessible [8].

EAFD from four different steel mills was air classified into five size fractions. Details of such an air classification procedure and a description of the analytical methods can be found elsewhere [9]. The Zn concentration of EAFD A was 8.0%, for EAFD B it was 16.3%, for EAFD C it was 14.5% and for EAFD D it was 2.6%. Figure 1 shows the size dependence of Zn concentration in various EAFDs.

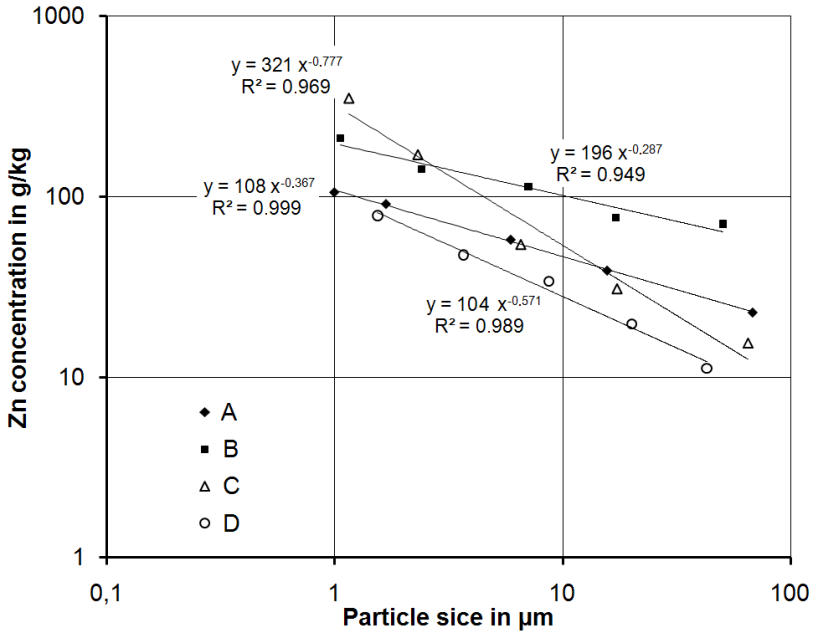

Fig. 1. Zn concentration in EAFD as a function of particle size

As expected, the Zn concentration was significantly higher in the fine size fractions and lower in the coarser size fractions. Power functions can be used to approximate the Zn concentration as a function of the particle size. However, the exponents vary from -0.29 to -0.78. There is no correlation between the exponent and the Zn concentration of the EAFD. Further investigations including the off-gas conditions at the EAF are needed to identify the reason for the considerable variation of the exponent.

To distinguish between zinc oxide and zinc ferrite in various size-fractionated EAFDs the samples were leached for 3h in 1 M sodium acetate in acetic acid at pH 5. After leaching, the samples were centrifuged and diluted prior to analysis with ICP-OES. Leaching of pure zinc oxide (from Fluka) and zinc ferrite (from Alfa Aesar) under the same conditions showed that 72% of the zinc oxide was dissolved while zinc ferrite was not dissolved under these conditions. Thus, the fraction of Zn leached can be used as an indication for the fraction of Zn present as zinc oxide. Figure 2 shows the fraction of Zn leached for various size fractions. A significant difference was found for the different EAFDs. Generally, the fraction of leached Zn was somewhat higher in the coarse size fractions compared to the fine size fractions.

To find the reason for the differences in the fractions of Zn in zinc oxide and zinc ferrite further investigations should include the operation conditions at the EAF.

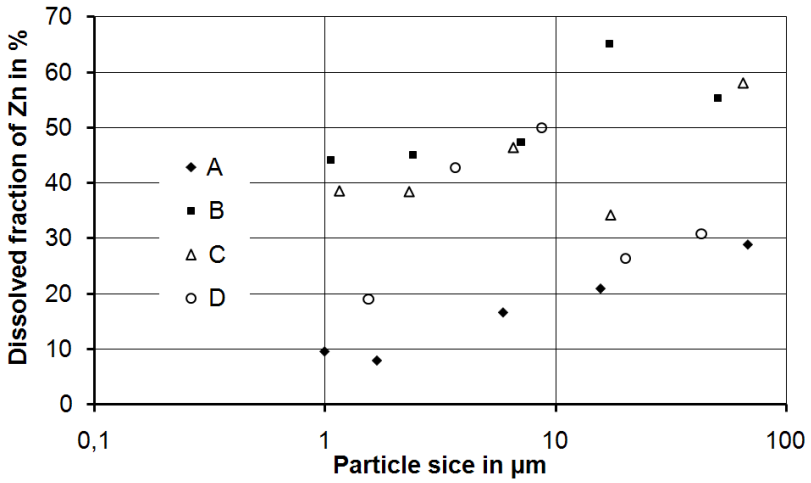

Fig. 2. Zn concentration in EAFD as a function of particle size

References

[1] Remus R., Aguado-Monsonet M.A., Roudier S., Sancho L.D., *Best Available Techniques (BAT) Reference Document for Iron and Steel Production, Industrial Emissions Directive 2010/75/EU, Integrated Pollution Prevention and Control.* Luxembourg, Publications Office of the European Union 2013.

[2] de Buzin P.J.W.K., Heck N.C., Vilela A.C.F., EAF dust: An overview on the influences of physical, chemical and mineral features in its recycling and waste incorporation routes, *J. Mater. Res. Technol.*, 2017, 6(2), 194–202.

[3] Nair A.T., Mathew A., Archana R.A., Akbar M.A., Use of hazardous electric arc furnace dust in the construction industry: A cleaner production approach, *J. Clean. Prod.,* 2022, 377, 134282.

[4] Antrekowitsch J., Rösler G., Steinacker S., State of the Art in Steel Mill Dust Recycling, *Chem. Ing. Tech.,* 2015, 87(11), 1498–1503.

[5] Jha M.K., Kumar V., Singh R. J., Review of hydrometallurgical recovery of zinc from industrial wastes, *Resour. Conserv. Recy.,* 2001, 33(1), 1–22.

[6] Lopez F.A., Lopez-Delgado A., Enhancement of Electric Arc Furnace Dust by Recycling to Electric Arc Furnace, *J. Environ. Eng.,* 2002, 128(12), 1169–1174.

[7] Lanzerstorfer C., Electric arc furnace (EAF) dust: application of air classification for improved zinc enrichment in in-plant recycling, *J. Clean. Prod.,* 2018, 174, 1–6.

[8] Yu B.-S., Wang Y.-R., Tien-Chin Chang T.-C., Hydrothermal treatment of electric arc furnace dust, *J. Hazard. Mater.,* 2011, 190(1-3), 397–402.

[9] Lanzerstorfer C., Kröppl M., Air classification of blast furnace dust collected in a fabric filter for recycling to the sinter process, *Resour. Conserv. Recy.,* 2014. 86, 132–137.

EXPERIMENTAL INVESTIGATIONS OF THE INFLUENCE OF RADIAL GAS MIXING IN AN INERT BED IN THERMAL COMBUSTION OF LEAN METHANE-AIR MIXTURES

Anna Pawlaczyk-Kurek*, Aleksandra Janusz-Cygan

Institute of Chemical Engineering Polish Academy of Sciences, Baltycka 5, 44-100 Gliwice, Poland
*corresponding author: ania.pawlaczyk@iich.gliwice.pl

The paper discussed the possibility of applying ceramic foam in thermal combustion of a lean methane-air mixture. The mixture is produced by the mining industry, wherever coal is extracted from methane mines. For many years the mixture, known as VAM (Ventilation Air Methane), was treated as a production waste. Nowadays, it is pollution unfriendly to the environment which should be destroyed. The issue of VAM utilization became physically tangible because of the announced inclusion of methane in the EU ETS system. However, it is difficult to use VAM as a fuel in industrial practice because of a very low methane concentration (often below 0.4 vol.%), a huge flow rate, massive pollution in the form of dust, high humidity and other gases that might contain sulfur. The most advanced utilization technology dedicated to mitigation VAM is combustion in thermal flow reversal reactors. Those reactors are filled with ceramic honeycomb monoliths. Due to a large number of parallel channels, monoliths are characterized by low flow resistance, which is essential, especially when the reactor is in the final sections of the technological line, where the pressures are not too high. The biggest disadvantage of the monolith structure is that it is not possible to mix reactants in the reactor cross-section, which in the case of an industrial scale reactor may contribute to uneven spreading of the stream in the bed [1]. In a high-temperature process, the phenomenon directly affects distribution of temperature in the cross-section, forming some space without reaction, and without generating heat. In such a space the accumulation of heat is also limited. The goal of the work was to show the impact of the implementation of ceramic foam in the reactor on the thermal combustion process. Open solid foams are widely discussed in the literature. They are usually used in catalytic processes as a support of the catalyst [2]. The foam structure (Fig. 1) ensures good reactant mixing with enhanced radial heat and mass transfer which is significant in highly endo- and exothermic reactions.

Fig. 1. Ceramic foam

The experiments of thermal combustion of lean methane-air mixtures were done using the experimental setup described elsewhere [3]. The difference is that another bed was previously studied, a monolith honeycomb, in place of the foam currently being investigated. A tubular reactor filled with foam samples was symmetrically placed in a three-zone laboratory furnace with separate temperature control for each zone. Due to the high temperatures in the reaction environment, a foam made of Al_2O_3 was used. The decision about choosing the right size of foams was made based on the size of the surface area of tested samples. It was assumed that this value in the case of ceramic foams should be similar to the monolith B (870 $m^2 \cdot m^{-3}$), tested in [3]. The pore density of investigated foam sample was 10 PPI, with a specific surface of 860 $m^2 \cdot m^{-3}$. The experiments were carried out with stable flow of the gas mixture of 800 $dm^3 \cdot h^{-1}$ through the

foam bed. The methane concentrations were within a range of 0.51-0.76 vol.%. The change in methane conversion was obtained by changing the temperature set. The temperature in the combustion zone was measured with thermocouples, enabling the appointment of a temperature profile along the bed. The composition of the gas mixture at the inlet and outlet of the reactor was measured with precision gas analyzers (IR).

The results showed a dependence of the composition of the post-reaction mixture on the temperature in the reaction zone. Similar to studies in [3], the presence of CH_4, CO, and CO_2 was observed in the stream flowing out of the reactor. The experimentally determined ignition temperature of diluted methane in the air was close to the value obtained in the case of the monolith. It was noticed that in certain temperature ranges, methane conversion and the shape of measured temperature profile was dependent on the concentration of the combustible component, which was not observed in the case of monolith tests. Moreover, a favorable effect of foam geometry on methane conversion was found, as shown in Fig. 2, which shows the dependence of methane conversion on the average temperature value in the combustion zone for the foam bed and monolith (MB). The difference in total conversion is around 15 pp for 720 °C and increases even to 60 pp for 760 °C.

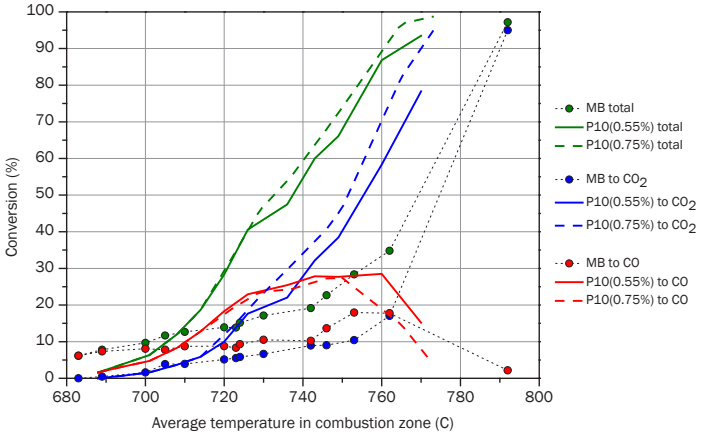

Fig. 2. Dependence of methane conversion (total - green color, to CO - red color, to CO_2 - navy blue color) on the average temperature in the combustion zone for monolithic filling (MB) and foam 10 PPI and inlet CH_4 concentration 0.55% vol. - P10 (0.55%) and 0.75% vol. - P10 (0.75%)

It was also observed that the length of the combustion zone was longer for the same temperature set point than in the case test of MB. Comparing data for the practically identical average temperature in the combustion zones for the foam and the monolith shows the length of the combustion zone is shorter in the case of foam and the total conversion of methane determined in the combustion zone is much higher.

The investigations confirmed that the structure characteristic of the foam provides the conditions for good mixing of mixture components, which influence the temperatures measured in the bed axis, and these in turn the average temperatures in the reaction zone and the length of the combustion zone. Higher temperatures in the foam filling with the same set parameters as for the monolithic filling confirm that the use of foam fillings may be advantageous and improve the uniformity of temperature distribution in the cross-section of the reactor.

Acknowledgments: Financial support by the National Science Centre is gratefully acknowledged (grant: MINIATURA 4 No. DEC-2020/04/X/ST8/00585).

References

[1] Gosiewski K., Pawlaczyk-Kurek A., Aerodynamic CFD simulations of experimental and industrial thermal flow reversal reactors, *Chem. Eng. J.*, 2019, 373, 1367–1379.

[2] Gancarczyk A., Sindera K., Iwaniszyn M., Piątek M., Macek W., Jodłowski P.J., Wroński S., Sitarz M., Łojewska J., Kołodziej A., Metal Foams as Novel Catalyst Support in Environmental Processes, *Catalysts*, 2019, 9, 587.

[3] Pawlaczyk A., Gosiewski K., Combustion of lean methane–air mixtures in monolith beds: Kinetic studies in low and high temperatures, *Chem. Eng. J.*, 2015, 282, 29–36.

CHEMICAL ENGINEERING TOOLS IN THE DEVELOPMENT OF GAS NANOBUBBLE GENERATION AND STABILITY

Paweł Sobieszuk*, Karol Ulatowski

Warsaw University of Technology, Faculty of Chemical and Process Engineering, Waryńskiego 1, 00-645 Warsaw, Poland
*corresponding author: Pawel.Sobieszuk@pw.edu.pl

Nanobubbles are referred to in this work as gas structures in a liquid whose diameter is less than 1 μm, which is the most commonly used definition [1-3] due to the fact that around this limit, the rising velocity of gas bubbles becomes less than the Brownian motion velocity. Due to surface tension forces, nanobubbles do not deform and assume a spherical shape when they are in a free state deep within the liquid. One of the most surprising facts about nanobubbles is their long residence time in a liquid unchanged in size. This can exceed even a month in distilled water, without the addition of any surfactants in a static system. Dispersions of gas nanobubbles and nanobubbles themselves have many properties that are not observed for bubbles at larger scales. This allows them to be used in processes where larger gas objects are not applicable, or to intensify those where a reduction in bubble size results in improved efficiency. This work concerns the subjects connected to the design of nanobubble generation and their stability models using tools commonly applied in chemical engineering research.

The usual methods for nanobubble dispersion generation are hydrodynamic methods, especially membrane methods with tangential shear forces. In such methods, a gas is pressurized through a membrane and it is cut off from its surface by induction of shear forces. The need to generate nanobubbles in small volumes pushed us to design a method of nanobubble generation incorporating high shear impellers which are able to induce shear stress locally near the membrane surface. Additionally, generation in smaller volumes allowed us to carry out the investigation of minimal shear stress needed to generate stable gas nanodispersion in liquids.

Two different gases (carbon dioxide, nitrogen) and two liquids (water and ethanol 98%) were used. These fluids were chosen to check how gas solubility and presence of liquids of different physicochemical properties affect nanobubble generation. It was assumed that there was a minimum shear stress limit in the system that would shear nanobubbles from the membrane. Thus, experiments were performed for different stirrer speeds for both liquids, followed by DLS measurements for obtaining the Sauter diameter. After finding the minimum rotational speed at which nanobubbles are generated reproducibly, the shear stress (τ) and three criterion numbers were calculated: the Reynolds number (Re), the capillary number (Ca) and the Weber number (We). The characteristic velocity in the system was set as the linear velocity of the edge of the stirrer. We observed that lower shear stresses were needed for ethanol solutions than for water, similarly when comparing the generation of nitrogen and carbon dioxide bubbles.

However, we could not find a single criterial number which would allow to predict the minimum value of velocity at the stirrer edge for different gas-liquid pairs. It is connected to the fact that neither of the chosen criterial numbers takes into account the properties of gas phase, especially its solubility in liquid phase. For that reason, one must include gas solubility in liquid in such an approach in addition to the combination of criterial numbers.

Other interesting phenomena are the reasons for nanobubble stability in liquids. Literature presents multiple theories of the reasons for such prolonged existence of nanobubbles in liquids [4], including: skin model [5], armored bubble model [6], charged surface models [1, 3] and dynamic equilibrium model [7]. In our studies, we have used the equation proposed by Lord Rayleigh (Equation 1), which describes the change of surface tension between droplet and surrounding air, when the surface is charged. We have proposed that a similar effect would be encountered for a nanobubble with charged surface surrounded by the aqueous phase.

$$\sigma = \sigma_0 - \frac{\left(\frac{q}{8\pi}\right)^2}{\varepsilon\left(\frac{d_{32}}{2}\right)^3} \quad (1)$$

We assumed that the pressure inside the nanobubble cannot exceed the operational pressure used during nanobubble generation. Based on the analysis of the charge required for appropriate surface tension reduction, we proved that the number of ions from the auto dissociation of water is sufficient with an appropriate margin. Therefore, it shows that nanobubbles can be stable even in pure water.

Acknowledgement
This work was supported by National Science Centre, Poland, grant number 2018/29/B/ST8/00365.

References

[1] Ulatowski K., Sobieszuk P., Mróz A., Ciach T., Stability of nanobubbles generated in water using porous membrane system, *Chem. Eng. Process*., 2019, 136, 62–71.
[2] Ulatowski K., Sobieszuk P., Influence of liquid flowrate on size of nanobubbles generated by porous-membrane modules, *Chem. Proc. Eng*., 2018, 39, 335–345.
[3] Ahmed A.K.A., Sun C., Hua L., Zhang Z., Zhang Y., Zhang W., Marshaba T., Generation of Nanobubbles by Ceramic Membrane Filters: The Dependence of Bubble Size and Zeta Potential on Surface Coating, Pore Size and Injected Gas Pressure, *Chemosphere*, 2018, 203, 327–335.
[4] Tan B.H., An H., Ohl C.D., Stability of Surface and Bulk Nanobubbles, *Curr. Opin. Colloid Interface Sci*., 2021, 53, 101428.
[5] Yasui K., Tuziuti T., Kanematsu W., Mysteries of Bulk Nanobubbles (Ultrafine Bubbles); Stability and Radical Formation, *Ultrason. Sonochem*., 2018, 48, 259–266.
[6] Mohamedi G., Azmin M., Pastoriza-Santos I., Huang V., Perez-Juste J., Liz-Marzan L. Edirisinghe M., Stride E., Effects of Gold Nanoparticles on the Stability of Microbubbles, *Langmuir*, 2012, 28, 13808–13815.
[7] Yasui K., Tuziuti T., Kanematsu W., Kato K., Dynamic Equilibrium Model for a Bulk Nanobubble and a Microbubble Partly Covered with Hydrophobic Material, *Langmuir*, 2016, 32, 11101–11110.

Lectures

S2. Environmental chemical engineering

RIGOROUS MODELING AND OPERATION OF NITROUS GAS ABSORPTION FOR INDUSTRIAL APPLICATIONS

Jan F. Maćkowiak[1,2]*, Reiner Chromik[1], Jerzy Maćkowiak[1,2]

[1]ENVIMAC Engineering GmbH, Oberhausen, Germany
[2]ENVIMAC Polska Sp. z o.o., Ostrów Wlkp., Poland
*corresponding author: jan.mackowiak@envimac.de

The class of nitrous gases (NOx) can also be assigned to common air pollutants, which are produced, for example, in incineration plants and various industrial processes. The term NOx describes a gas mixture, which mainly consists of nitrogen monoxide (NO), nitrogen dioxide (NO_2) and higher oxides like nitrous oxide (N_2O_3) and nitrous tetroxide (N_2O_4). While the transport sector is one of the main emitters of NOx, industry is nevertheless a relevant one.

In this work, the absorption process for the removal of nitrogen oxides using aqueous solutions from industrial gas streams is examined in detail. The description of such an absorption process is difficult because of the complex chemical reaction system, which consists of various instantaneous and kinetically controlled gas- and liquid phase reactions. Mass transfer performance is highly affected by the chemical reaction system. The analysis of literature data reveals an inconsistent presentation of the reaction mechanism, which can lead to great inaccuracies in column design. Separation capacities are underestimated or overestimated by factors depending on the model used.

Thus, there is a need to take a deep look into the reaction system. The focus of this work is therefore the development of a rigorous simulation model taking into account the gas and liquid phase reactions as well as the reaction kinetics and the heat and mass transfer.

Our own extensive experimental investigations of industrial processes in DN300 packed column and aqueous solutions adding e.g. NaOH, H_2O_2 as well as a detailed analysis of literature data lead to new findings regarding the reaction and mass transfer mechanism of NOx absorption in aqueous solutions. This, finally, enables the safe design of separation processes over a very wide concentration range of NOx.

In this work, a rate-based model has been developed which accounts for chemical reactions in the gas- and liquid phase. It has been shown that kinetics as well as the considered reaction route can play a decisive role for the description of the NOx absorption process and that the correct route depends on the composition and the concentration of nitrous gases. The model has been validated with literature data and with a large number of our own experiments, performed in an industrial scale pilot plant.

INCREASING SELF-CONSUMPTION OF ENERGY IN HYBRID RES INSTALLATIONS WITH PV PANELS

Sebastian Pater*

Cracow University of Technology, Faculty of Chemical Engineering and Technology,
Warszawska 24, 31-155 Cracow, Poland
*corresponding author: sebastian.pater@pk.edu.pl

In recent years, due to political and economic events in the world that have largely hit European countries, interest in technologies based on renewable energy sources (RES) has increased significantly. Residential installations with photovoltaic (PV) panels and heat pumps (HP) of various types are the most dynamically developing sectors. Currently, the interest in increasing self-consumption (SC) of electrical energy produced by PV array in grid-connected installation is growing among owners of such systems. Improved SC can increase the profit associated with the operation of PV systems [1]. It also brings other positive aspects, which include the reduction of energy losses in the network, or the smaller need to modernize the electrical infrastructure resulting from distributed generation of energy from RES in the power systems [2].

SC of electrical energy can be defined as the share of the directly consumed energy E_c in total energy generated E_{gen} in the PV system which is represented by Equation (1):

$$SC = \frac{E_c}{E_{gen}} \tag{1}$$

The value of SC is calculated over an assumed period of time, usually during a given day, month or year. SC can be a value between 0% and 100%, where 100% means that all E_{gen} is consumed by the loads. According to the research presented elsewhere [3] PV system in grid-connected installation without a storage system or special energy management systems can obtain SC from around 15% to 40% in one-year period. Similar values are confirmed by my own research on a 3.3 kW PV on-grid installation in a residential building located near Brzesko in the Lesser Poland operating under real conditions. In the installation with 9 monocrystalline panels (each with a capacity of 365 kWp, inclination of 35°, facing south) in 2022 the SC value of 25% was obtained with the annual electricity consumption of 3,800 kWh.

An increase in the SC value can be achieved by skillfully combining PV installations with electrical devices using RES to produce heat and/or cold in hybrid installations. The idea behind the operation of hybrid energy installations is based on the mutual compensation of the advantages and disadvantages of using individual energy sources. This allows reduction in the overall electrical energy drawn from the grid for the operation of devices, which contributes to cheaper operational costs of the installation.

This short paper presents the results of one year-round analysis of a PV array grid-connected in hybrid installations with air-source HP in a residential building in Cracow. Operational simulations of various installation configurations were carried out in the Transient System Simulation Tool (TRNSYS). The results obtained from the simulation of only one of several considered installations are briefly presented below.

The most important elements of the installation shown in Fig. 1 are: component type103b simulating the operation of a 6.84 kWp PV installation (18 monocrystalline 380 Wp PV panels with, inclination of 35°, facing south); component type917 simulating an air-to-water HP with rated heating capacity 2 kW and power 0.49 kW; weather data processor (type15-6) processing annual weather data for Cracow (such as dry bulb temperature, beam and diffuse radiation, air humidity ratio) taken from the Meteonorm database for other TRNSYS components; type156 being a 300l cylindrical storage tank with immersed coiled-tube heat exchanger. The efficiency of the inverter was set to 90%. It was assumed in the calculations that electricity consumption in the building is equal to 4,380 kWh per year, i.e. 12 kWh/day and the corresponding hourly consumption profile,

which is identical on each day of the year. The daily consumption of domestic hot water was set at 250l. HP operation is controlled by a differential controller type165 processing input signals from the type156 tank and time dependent forcing function type 14h.

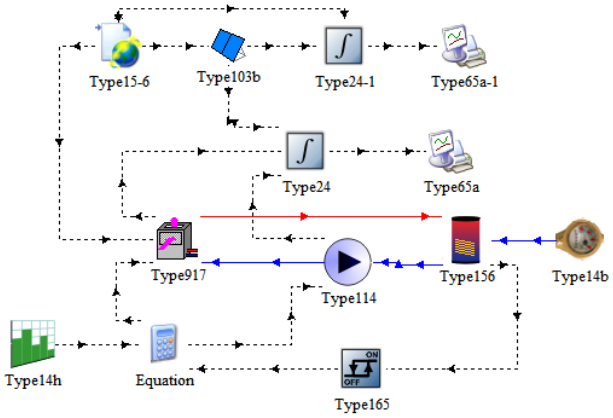

Fig. 1. One of the TRNSYS models of analyzed HYBRID systems with PV panels and air-source HP

Fig. 2 presents the results of the installation operation simulation during the year regarding the daily values of the SC coefficient for PV installations with and without HP, as well as solar insulation and PV energy generation. In the case of PV panels cooperating with HP, a 13.3% increase in the annual value of SC was obtained to the level of 56%. During the year, the PV installation generated 6,585 kWh of electricity, achieving a solar radiation conversion efficiency of 18.3%.

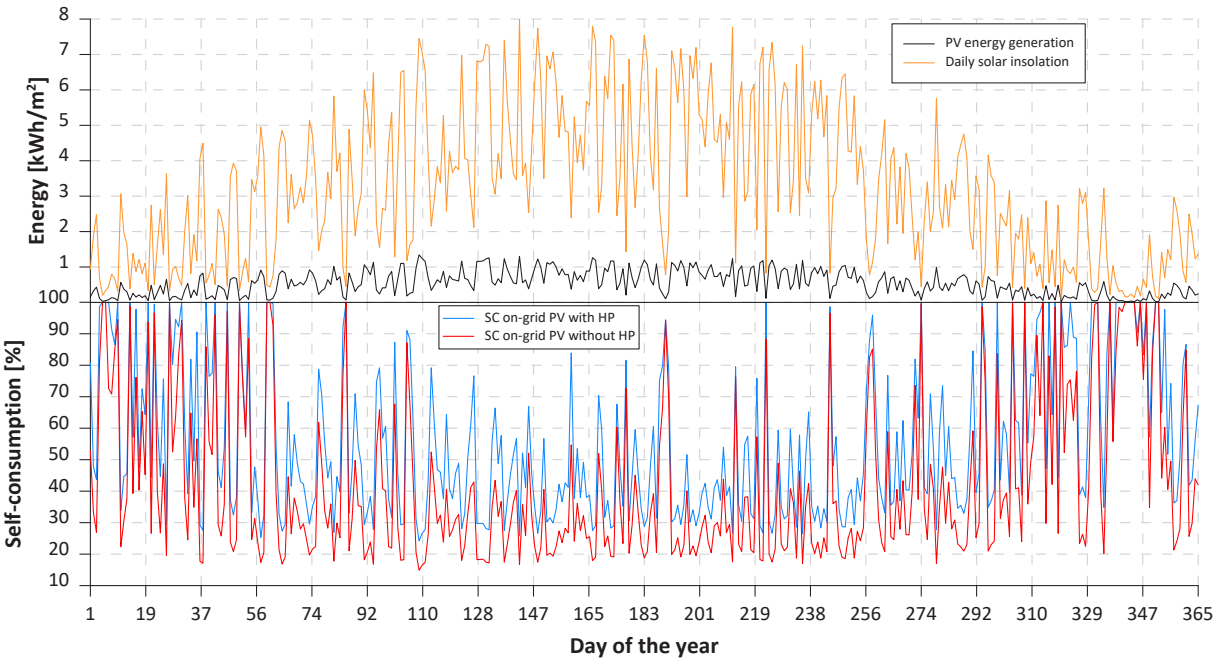

Fig. 2. The daily values of the SC coefficient for PV installations with and without HP, solar insulation and PV energy generation

References

[1] Luthander R., Widén J., Nilsson D., Palm J., Photovoltaic self-consumption in buildings: A review, *Appl. Energy*, 2015, 142, 80–94.

[2] Ciocia A., Amato A., Di Leo P., Fichera S., Malgaroli G., Spertino F., Tzanova S., Self-Consumption and Self-Sufficiency in Photovoltaic Systems: Effect of Grid Limitation and Storage Installation, *Energies*, 2021, 14(6), 1591.

[3] Hassan Q., Evaluate the adequacy of self-consumption for sizing photovoltaic system, *Energy Reports*, 2022, 8, 239–254.

INFLUENCE OF INOCULUM THERMAL PRETREATMENT ON HYDROGEN PRODUCTION IN DARK FERMENTATION PROCESS

Radosław Ślęzak*, Marlena Domińska, Justyna Świątkiewicz, Katarzyna Paździor, Stanisław Ledakowicz

Department of Bioprocess Engineering, Faculty of Process and Environmental Engineering, Lodz University of Technology, Wolczanska 213, 90-924 Lodz, Poland
*corresponding author: radoslaw.slezak@p.lodz.pl

A growing proportion of the organic fraction of municipal solid waste (OFMSW) poses serious environmental and economic problems. One method of using OFMSW to produce useful energy and materials is through a partial methane fermentation process called dark fermentation (DF). The process produces H_2 + CO_2 and volatile fatty acids (VFAs): acetic, propionic and butyric. The amount and composition of the resulting products are strictly dependent on the conditions of the process, as well as the type of inoculum (bacterial consortium). The process can be carried out using either pure culture or mixed culture (MC). The use of MC as inoculum has a primary advantage because the bioreactor can operate under non-sterile conditions. MC contains methanogenic bacteria, which can be inhibited by heat pretreatment, but too high temperature and treatment time can also destroy the bacteria. The aim of the study was to investigate the effect of thermal pretreatment of inoculum on H_2 and VFAs production in the DF process.

Kitchen waste from households in the city of Lodz (Poland) was selected as the substrate for the DF process. The inoculum for the process was taken from an anaerobic digestion plant at a group wastewater treatment plant in Lodz. The study was carried out in four batch bioreactors with volume of 1 dm^3 each, without pH adjustment during the process. The volume ratio of inoculum to organic waste was 7:3. To each bioreactor, 13 g volatile solid (VS) of KW was added. In the 1st bioreactor, water was used instead of inoculum to check the biodegradation of KW. In bioreactor 2, inoculum was placed without thermal treatment. Meanwhile, in bioreactors 3 and 4, the inoculum was heated at 70°C for 15 and 30 minutes, respectively. Volume of gas formed by DF process was measured with a water displacement method. The composition of produced gas (CO_2, CH_4 and O_2) was determined with 8610C gas chromatography (SRI Instruments). The quality and quantity of produced volatile fatty acids (VFAs) were measured with a VARIAN CP4800 gas chromatograph.

At the beginning of the process pH was in the range from 7.30 to 7.63. After 4 days of dark fermentation process a decrease of pH was observed in all bioreactors, which was due to the production of VFA (Fig. 1). The highest decrease of pH was noticed in bioreactor no. 1, which was caused by lack of inoculum. In addition to the bacterial consortium, the inoculum contains ammonium nitrogen, which buffers the system, so the pH does not change much. The observed slight decrease of pH in bioreactor no. 2, was caused by the VFAs produced, which were partially used by methanogenic bacteria to produce CH_4. Thermal pretreatment of inoculum did not have any significant impact on the final value of pH.

The lowest production of VFAs was observed in bioreactors 1 and 2 (Fig. 2). Increasing the thermal treatment time of inoculum in the bioreactor resulted in a 15% increase in VFA production. The main dominant acids produced were acetic, propionic and butyric acids. The production of acetic and butyric acid was linked to the production of H_2 in biochemical pathways of dark fermentation process.

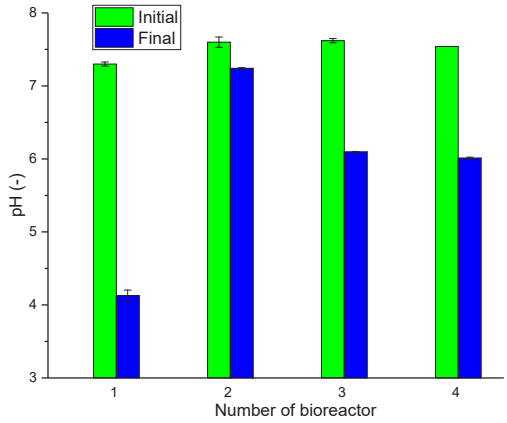

Fig. 1. Changes of pH at the beginning and the end of process

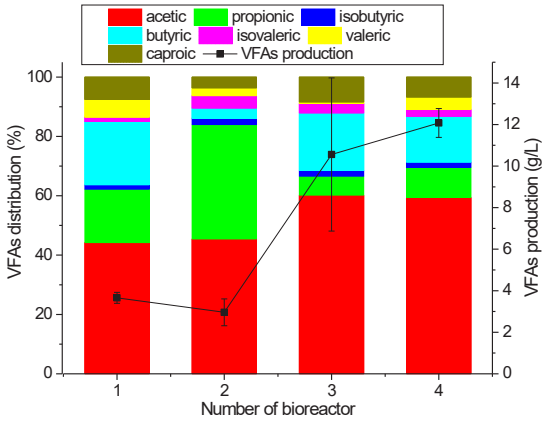

Fig. 2. Production of VFA

During 4 days of the process the lowest CO_2 production yield was observed in bioreactor no. 1 without inoculum. In bioreactor no. 2, which contained inoculum without thermal pretreatment, the highest CO_2 production was observed. CH_4 production was also recorded in this bioreactor (Fig. 3). The time of thermal pretreatment of the inoculum (bioreactors 3 and 4) had no significant effect on CO_2 and H_2 production yields.

The highest yield and rate of H_2 production were observed in bioreactors 3 and 4 in which inoculum was thermally pretreated (Fig. 4). The lowest production of H_2 was observed in bioreactor 2 without thermal pretreatment. A delay in H_2 production was evident in bioreactor 1. H_2 production in this bioreactor confirmed that the bacterial consortia contained in KW can carry out dark fermentation process.

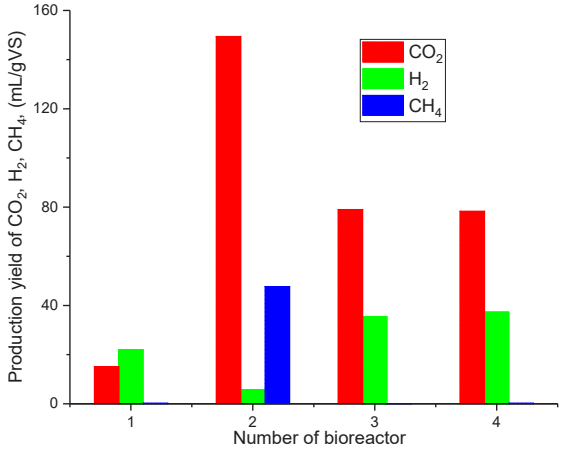

Fig. 3. Production yield of CO_2, H_2 and CH_4

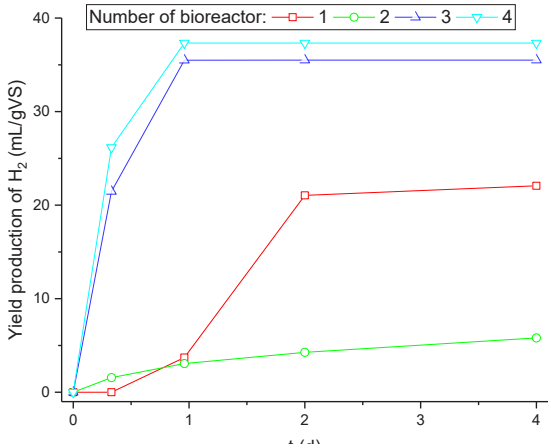

Fig. 4. Changes in production of H_2

Acknowledgment

The study under project no. 2021/43/B/ST8/00298 was financially supported by the National Science Center (Poland).

Lectures

S3. Engineering of chemical reactions

3D PRINTED TRIPLY PERIODIC MINIMAL SURFACES AS INTERNALS IN CATALYTIC REACTORS

Marzena Iwaniszyn[1,*], Joanna Maszybrocka[2], Przemysław J. Jodłowski[3]

[1]Institute of Chemical Engineering, Polish Academy of Sciences, Bałtycka 5, 44-100 Gliwice, Poland
[2]Faculty of Science and Technology, Institute of Materials Engineering, University of Silesia, 75 Pułku Piechoty 1A, 41-500 Chorzów, Poland
[3]Faculty of Chemical Engineering and Technology, Cracow University of Technology, Warszawska 24, 31-155 Kraków, Poland
*corresponding author: miwaniszyn@iich.gliwice.pl

Recently, 3D-printed periodic cellular structures have become popular due to the ease and speed of their design and manufacturing. Triply periodic minimal surface (TPMS) structures, called also porous scaffolds, are periodic three-dimensional cellular lattices with mathematically defined topology: solid or sheet [1-3]. Depending on the mathematical formulas, unit cell shapes can be generated, for instance, primitive (P), gyroid (G), diamond (D), i-graph and wrapped package (IWP) [1, 2, 4-6]. TPMS architectures provide low weight, high strength and surface area, optimal thermal and electrical conductivities, energy absorption, heat and sound insulation, and optimized fluid permeability [1, 5]. Therefore, they are applied in many engineering disciplines, such as tissue engineering, heat exchange, and noise control [1, 4].

In order to use TPMS structures in catalytic processes, e.g. catalytic oxidation of volatile organic compounds (VOCs) or selective catalytic reduction of nitrogen oxides, the knowledge of heat/mass transfer and fluid flow characteristics is crucial. The morphological parameters, such as specific surface area, void volume, unit cell size and wall thickness, affect transport and hydraulic characteristics. The larger the porosity of the solid-G structure, the more intense mass transfer and the lower pressure drop [7]. The impact of wall thickness and unit cell size was considered only for sheet-based TPMS structures [7]. Therefore, the aim of this work was to study the impact of unit cell size of skeletal-gyroid structures on their fluid flow and heat transfer in relation to their potential application as catalyst support.

Five solid-G architectures differing in unit cell size (2, 2.5, 3, 3.5 and 4 mm) were mathematically modeled with constant porosity of 81%. The modelling area was a cuboid with dimensions 35 x 45 x 10 mm (Fig. 1). The ANSYS Fluent software package was applied to numerically evaluate the hydraulic and transport properties of the designed 3D models. Two samples, with the smallest and the highest unit cells, were manufactured using the selective laser melting (SLM) technique from 316 stainless steel. These samples were tested experimentally in order to verify the results of computational simulations.

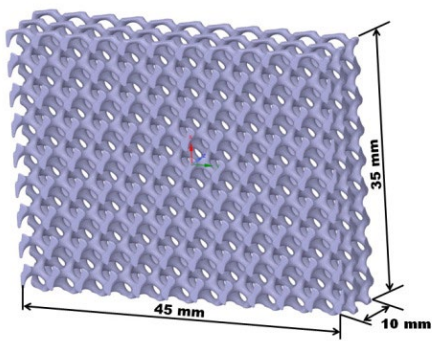

Fig. 1. Geometry of solid-G with 4 mm unit cell size

The results show that the effect of unit cell size on heat transfer is insignificant (Fig. 2). However, the pressure drop increased with a smaller unit cell size due to the lower wall thickness. Solid-G structures ensure enhanced heat transfer in comparison with monolith of 100 cpsi (channels per square inch) and 0.2 m long. Unfortunately, their flow resistance also increased but was lower than that of the packed bed of 3 mm grains.

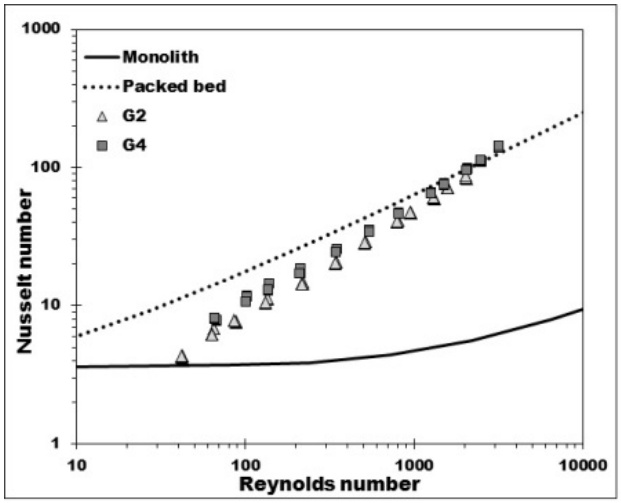

Fig. 2. Comparison of heat transfer for different reactor internals

Acknowledgements
This work was supported by the research grants from The National Centre for Research and Development (Project LIDER/204/L-6/14/NCBR/2015).

References

[1] Al-Ketan O., Rowshan R., Abu Al-Rub R.K., Topology-mechanical property relationship of 3D printed strut, skeletal, and sheet based periodic metallic cellular materials, *Addit. Manuf.*, 2018, 19, 167–183.
[2] Benedetti M., du Plessis A., Ritchie R.O., Dallago M., Razavi S.M.J., Berto F., Architected cellular materials: A review on their mechanical properties towards fatigue-tolerant design and fabrication. *Mater. Sci. Eng. R Rep.*, 2021, 144, 100606.
[3] Montemurro M., Refai K., Catapano A., Thermal design of graded architected cellular materials through a CAD-compatible topology optimisation method, *Compos. Struct.*, 2022, 280, 114862.
[4] Zhang X., Zhang K., Zhang L., Wang W., Li Y., He R., Additive manufacturing of cellular ceramic structures: From structure to structure-function integration. *Mater. Des.*, 2022, 215, 110470.
[5] Pan C., Han Y., Lu J., Design and Optimization of Lattice Structures: A Review, *Appl. Sci.*, 2020, 10, 6374.
[6] Yeranee K., Rao Y., A Review of Recent Investigations on Flow and Heat Transfer Enhancement in Cooling Channels Embedded with Triply Periodic Minimal Surfaces (TPMS), *Energies*, 2022, 15, 8994.
[7] Sreedhar N., Thomas N., Al-Ketan O., Rowshan R., Hernandez H.H., Abu Al-Rub R.K., Arafat H.A., Mass transfer analysis of ultrafiltration using spacers based on triply periodic minimal surfaces: Effect of spacer design, directionality and voidage, *J. Membr. Sci.*, 2018, 561, 89–98.

COLD PLASMA AS A VERSATILE TOOL FOR THE PREPARATION OF NANOSTRUCTURED THIN FILMS FOR CATALYTIC APPLICATIONS

Hanna Kierzkowska-Pawlak*, Jacek Tyczkowski

Department of Molecular Engineering, Faculty of Process and Environmental Engineering,
Lodz University of Technology, Wólczańska 213, 93-005 Łódź, Poland
*corresponding author: hanna.kierzkowska-pawlak@p.lodz.pl

The use of cold plasma in the development and production of new materials with unique properties that cannot be obtained by other methods favors its wider application in green catalysis [1, 2]. Among existing plasma technologies, the plasma deposition method known as PECVD (*plasma enhanced chemical vapor deposition*) from organometallic volatile precursors deserves special attention. It allows the bottom-up fabrication of a new material in the form of a thin film (<<1 μm) with a specific nanostructure that exhibits catalytic properties. A thin-film catalyst deposited on a metallic structured packing, for example on a fine mesh, while maintaining its original geometry, opens up new possibilities in the design of heterogeneous structured reactors. In turn, compared to typical packed beds of particle catalysts, such catalytic structured packings allow a lower pressure drop, better mass and heat transfer and a vast array of possibilities for customizing their design to a specific application [3]. These features, coupled with a tailored nanostructure of the active phase, are key points for achieving remarkable process intensification in numerous applications, such as chemical technology and solving environmental issues [4].

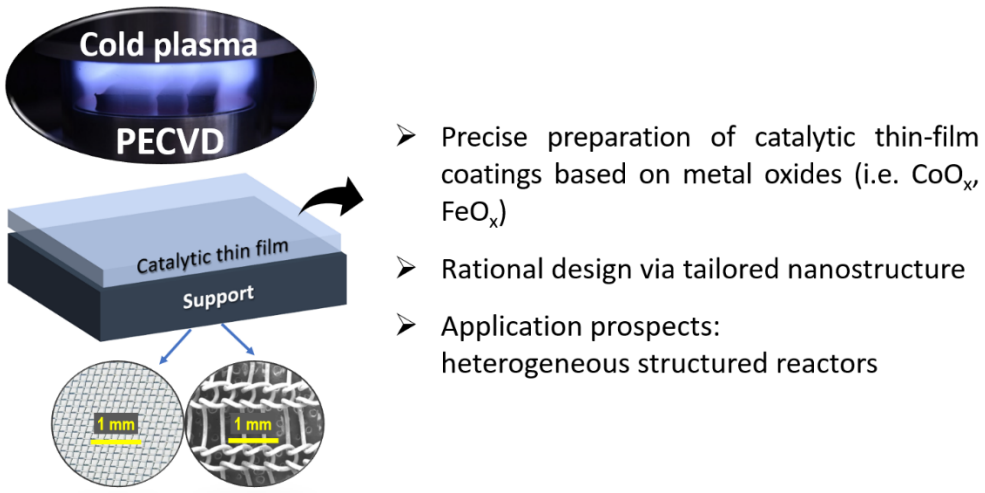

Fig. 1. Cold plasma approach for the preparation of catalytic thin films on structured packings

Here, we present and discuss our findings on the development of the cold plasma deposition method for preparation of thin films based on transition metal oxides of the desired chemical composition and nanostructure and linking them to catalytic activity. The thin film catalysts were characterized using different techniques such as XPS, XRD, SEM/EDX and Raman spectroscopy. Given the example of the fabrication process of CoO_x-based films deposited on a metallic fine mesh, the influence of plasma operation parameters and the calcination step on the resulting nanostructure was discussed. It has been shown that for a given discharge power, increasing the flow rate of precursor vapor allows to create larger Co_3O_4 nanocrystallites while keeping the same

concentration of the active phase (Co_3O_4) [5]. The effect of the Co_3O_4 nanocrystallite size on catalytic activity was demonstrated using the oxidation of n-nonane as an illustration.

We also include recent advancements in producing nanohybrid structures composed of nanoparticles of different oxides. Using the plasma co-deposition process, a series of nanocomposites based on iron and cobalt oxides (FeO_x/CoO) was fabricated with varied composition [6]. In the process of CO_2 hydrogenation, these nanocomposites favored the production of CO and revealed much higher activity towards CO than that obtained for pure FeO_x and CoO-based structures. It was tentatively explained by changes in the electronic structure of the mixed catalyst resulting from the formation of p-n heterojunctions between nanoparticles of cobalt and iron oxides. This finding provides better understanding of the fundamental concept in terms of 'structure sensitivity' of heterogeneous catalysts [7] and offers practical opportunities of preparing sophisticated catalytic nanostructures tailored for purpose under full control.

This research has confirmed that cold plasma technology is a powerful and versatile tool for preparing highly active thin films with a rationally designed nanostructure, which is difficult with the conventional approaches of catalyst preparation. Additionally, these nano-engineered thin film coatings possess the desirable performance characteristics, such as excellent durability and adhesion to metallic packings, making them highly suitable for further use in new designs of heterogeneous structured reactors. Furthermore, the cold plasma deposition requires fewer chemicals, less energy and time-consuming steps than conventional wet coating methods.

References

[1] Wang Z., Zhang Y., Neyts E.C., Cao X., Zhang X., Jang B.W.L., Liu C.J., Catalyst preparation with plasmas: how does it work?, *ACS Catal.*, 2018, 8(3), 2093–2110.

[2] Liu C., Li M., Wang J., Zhou X., Guo Q., Yan J., Li Y., Plasma methods for preparing green catalysts: Current status and perspective. *Chinese J. .Catal.*, 2016, 37(3), 340–348.

[3] Landi G., Novel structured catalytic reactors. *Catalysts*, 2021, 11(12), 1472.

[4] Kapteijn F., Moulijn J.A., Structured catalysts and reactors – Perspectives for demanding applications. *Catal. Today,* 2022, 383, 5–14.

[5] Tyczkowski J., Kapica R., Kozanecki M., Kierzkowska-Pawlak H., Sielski J., Aoki T., Mimura H., Tailoring the nanostructure of plasma-deposited CoO_X-based thin films for catalytic applications–A step forward in designing nanocatalysts. *Mater. Des.*, 2022, 222, 111095.

[6] Kierzkowska-Pawlak H., Ryba M., Fronczak M., Kapica R., Sielski J., Sitarz M., Zając P., Łyszczarz K., Tyczkowski J., Enhancing CO_2 conversion to CO over plasma-deposited composites based on mixed Co and Fe oxides, *Catalysts*, 2021, 11, 883.

[7] Vogt C., Weckhuysen B.M., The concept of active site in heterogeneous catalysis. *Nat. Rev. Chem.*, 2022, *6*(2), 89–111.

DME PRODUCTION TECHNOLOGIES FOR SMALL HYDROCARBON DEPOSITS, PROGRESS AND PERSPECTIVES

Andrzej Rogala*, Izabela Wysocka

[1]Gdańsk University of Technology, Faculty of Chemistry, Department of Process Engineering and Chemical Technology, Narutowicza 11/12, 80-233 Gdansk, Poland
*corresponding author: andrzej.rogala@pg.edu.pl

Dimethyl ether (DME) is the simplest compound from the group of ethers, recognized as a multi-source, environmentally friendly medium for storing and distributing energy with a wide range of applications. Although it is currently used primarily as a propellant in aerosols, thanks to its properties it can also be used as a fuel for diesel engines, an intermediate product in the synthesis of many chemical compounds, including other synthetic fuels, as well as a source of energy in fuel cells.

Nowadays when environmental protection is becoming more and more important, and the problem of smog is becoming common, more stringent requirements are placed on energy resources. New transport fuels are therefore necessary to reduce harmful emissions in terms of both particulate matter and gaseous pollutants. In this regard, DME looks very promising. In addition to the excellent physical and chemical properties of DME (cetane number, liquefaction properties similar to LPG), its combustion in a diesel engine does not generate particulate matter. Adding to this a much higher combustion efficiency than in the case of diesel (despite almost twice lower combustion energy, engines burn up to 5% more DME), we can talk about a real substitute, not just a potential one. In addition to a number of experimental studies available in the scientific literature, Ford Company presented in 2019 a Ford Mondeo car model fully powered by DME, capable of being implemented in mass production, proving that scientific concepts are fully validated in practice. Therefore, DME is considered to be one of the most promising substitutes for diesel fuel. It is also a great fuel for powering marine engines, especially due to the amendment to the Act on the prevention of marine pollution by ships in force since January 1, 2015, regarding the introduction of Directive 2012/33/EU of the European Parliament and of the Council of November 21, 2012 regarding the reduction of emission limits sulfur in exhaust gases, Dz.U 2014 item 1554 - DME is a sulfur-free fuel.

In addition, dimethyl ether is a promising potential chemical hydrogen carrier. Steam reforming of dimethyl ether enables the production of hydrogen at a much lower temperature (approx. 350˚C) than from methane/natural gas (800˚C and more). This combination puts DME in the perfect position as a single fuel and hydrogen carrier to enable a smooth transition in the automotive industry – from moving away from conventional fuel cars to hydrogen and electric cars using hydrogen fuel cells.

The presentation will discuss the possibility of a wide use of DME on the Polish and EU markets, as well as present the results of research on the modification of the method of obtaining DME on a laboratory and model scale. Possibilities of catalyst modification, problems of scaling up and the most important problems of commercialization of the solution will be presented. In addition, the advantage of a slurry reactor over a plug flow reactor for the investigated process will be analyzed.

Acknowledgment

The research was financed by the National Center for Research and Development and Polish Oil and Gas Company (PGNiG) under the project "Development of DME production technology for small hydrocarbon deposits" No. POIR.04.01.01-00-0064/18-00.

OPTIMIZATION OF NANOPARTICLE DEPOSITION PROCESS ONTO POLYMERIC NON-WOVEN FRAMEWORK

Łukasz Werner*, Karol Ćwieka, Kamil Czelej, Zuzanna Bojarska, Katarzyna Jabłczyńska, Leon Gradoń

Faculty of Chemical and Process Engineering, Waryńskiego 1, 00-645 Warsaw, Poland
*corresponding author: lukasz.werner@pw.edu.pl

The investigation demonstrates the deposition and immobilization of photocatalyst nanoparticles (NPs) on polymeric porous non-woven. To commercialize photocatalytic hydrogen production, the issue of durable deposition of particles on a spatial framework seems to be of great importance due to the possibility of using such hybrid materials in flow systems, which, unlike batch solutions, can be scaled [1, 2]. Moreover, the easy recovery of polymer framework with NPs from the reactor chamber greatly facilitates their reuse and brings significant economic and environmental consequences.

In NP immobilization design, several important aspects should be considered. First, the selection of appropriate framework material, which should be chemically inert and stable under reaction conditions, but at the same time, should not limit the efficiency of the photocatalyst. The melt-blown technique can be used to design and manufacture polymeric non-wovens [3]. The great advantage of this method is the ability to produce non-woven materials with micro- and nanosize fiber diameters and high porosity. Thus, obtaining a framework with a highly developed surface is possible. Second, the uniform distribution of nanoparticles on the surface of the support material (fibers) and the strong adhesion of NPs to the polymer. NP deposition onto non-woven fibers can be obtained with various methods, e.g. spray-coating (e.g. with the methodology developed by our group [4]), dip-coating, and spin-coating methods. Herein, we combined the dip-coating and spin-coating techniques. The scheme of the developed non-woven covering procedure is shown in Fig. 1.

The process of particle deposition on fibers can be designed to increase the dispersion and adhesion of NPs to the polypropylene (PP) non-woven by electrostatic attraction between the fibers and NPs, due to induction of static charges with opposite signs. The induction of static charges on the surface can be controlled by zeta potential, which depends on the pH of the solution in which non-wovens and nanoparticles are immersed [5].

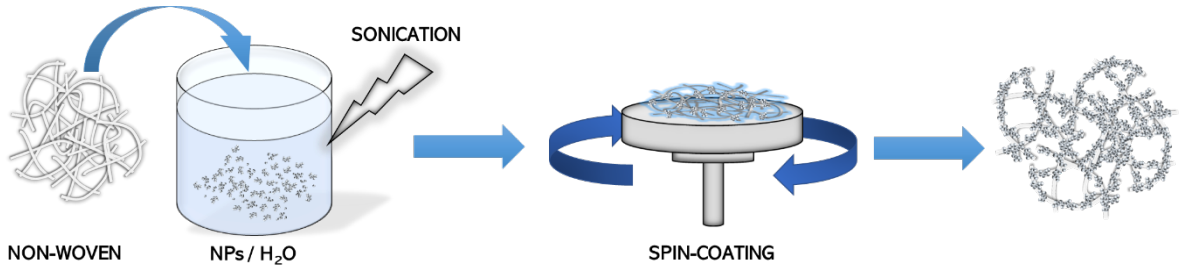

Fig. 1. Scheme of the developed method used to cover the non-wovens

Titanium dioxide (TiO_2) nanoparticles were used as a model catalyst. A few drops of isopropanol were added to NP powder to improve the wetting of TiO_2 and facilitate its dispersion in water. The prepared suspension was sonicated for 5 minutes to achieve the appropriate dispersion of particles. Next, the PP non-woven, which also was previously immersed in alcohol, was placed in the TiO_2/H_2O suspension and sonicated for 30 s. After this time, the PP-TiO_2 material was placed in a spin-coater with a special holder adapted to the sample. To prevent the formation of liquid bridges, which can transform into large particle agglomerates, excess water and particles that were not deposited directly on the fiber surface were removed by applying centrifugal force.

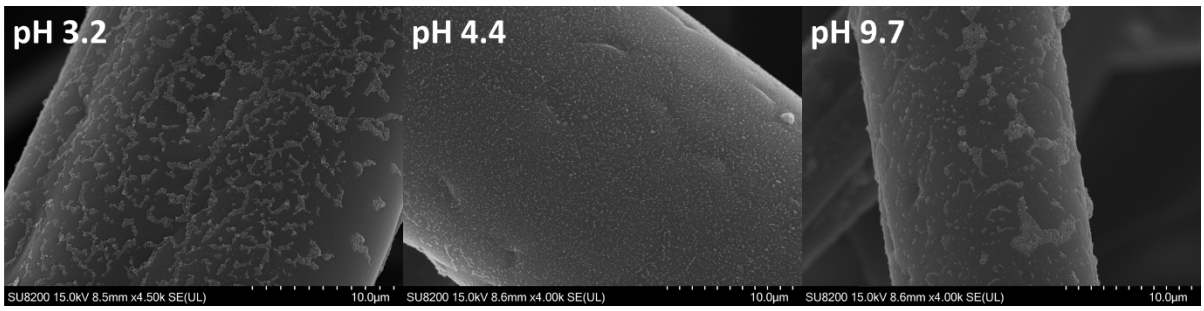

Fig. 2. The SEM images of TiO2 nanoparticles deposited on PP fibers from suspensions of different pH: 3.3, 4.4, 9.7

The scanning electron microscopy (SEM) analysis shows that for pH ~3.2 and pH ~9.7 (where the zeta potential was 12 mV and -30 mV, respectively) TiO_2 nanoparticles had a strong tendency to form large agglomerates on the fiber surface. Results indicate that the most favorable particle dispersion of NPs on the polypropylene non-woven was obtained in an acidic environment with a pH of ~4.4, where the zeta potential value for TiO_2 was close to zero.

References

[1] Alalm M.G., Djellabi R., Meroni D., Pirola C., Bianchi C.L., Boffito D.C., Toward scaling-up photocatalytic process for multiphase environmental applications, Catalysts, 2021, 11, 1–23.
[2] Rehm T.H., Reactor Technology Concepts for Flow Photochemistry, *ChemPhotoChem*, 2019, 235–254.
[3] Jackiewicz A., Werner L., Separation of nanoparticles from air using melt-blown filtering media, *Aerosol Air Qual. Res*., 2015, 15, 2422-2435.
[4] Czelej K., Ćwieka K., Jabłczyńska K., Werner Ł., Gradoń L., Colmenares J.C., Pat. 241804, Method of producing hybrid systems of non-woven fabric - composite nanoparticles, 2022., https://ewyszukiwarka.pue.uprp.gov.pl/search/pwp-details/P.432594
[5] Xu R., Progress in nanoparticles characterization: Sizing and zeta potential measurement, *Particuology*, 2008, 6, 112–115.

CONTROLLED PRODUCTION OF HYDROXYAPATITE NANOPARTICLES IN A SPHERE, PLATE, OR ROD SHAPE - THEIR MODIFICATION AND APPLICATIONS

Michał Wojasiński[1,*], Joanna Latocha[1], Jolanta Czerska-Duszak[1], Rafał Podgórski[1], Kornel Prystupiuk[1], Stanisław Gierlotka[2], Tomasz Ciach[1], Paweł Sobieszuk[1]

[1]Warsaw University of Technology, Faculty of Chemical and Process Engineering, Waryńskiego 1, 00-645 Warsaw, Poland
[2]Institute of High Pressure Physics, Polish Academy of Sciences, Laboratory of Nanostructures, Sokołowska 29/37, 01-142 Warsaw, Poland
*corresponding author: michal.wojasinski@pw.edu.pl

Synthetic hydroxyapatite nanoparticles (nHAp), the most popular form amongst synthetic calcium orthophosphates, find applications in the area of catalysis, as fertilizers and in medical applications as dental filling material, composite reinforcement for bone tissue regeneration or as a drug delivery system. Every application requires specific morphology of nHAp, from spherical to fiber-like whiskers, or specific surface modification. This study aimed to produce spherical, plate-like, and rod-like nHAp, their subsequent modification, and description of two specific applications: 1) a drug delivery system with increased cellular uptake, 2) polycaprolactone/nHAp 3D printed composites for bone tissue engineering with appropriate mechanical properties.

This work presents two methods of nHAp formation. First, the wet precipitation in a flow microreactor of nHAp from calcium and phosphate salts with the addition of lecithin (LE) for sphere-shaped nHAp-LE production [1, 2]. This process was used to produce drug-carrying particles for osteoporosis treatment. Second, the batch precipitation/remodeling of nHAp in pH- and temperature-controlled environment for the plate and rod-shaped particles [3]. The plate and rod-shaped nHAp was subsequently surface modified with sodium stearate (ss). The product quality was determined with spectroscopy (FTIR) and x-ray diffraction (XRD) analysis; the morphology of crystallites and particles was studied with XRD and scanning electron microscopy (SEM). The tendency of nanoparticles to agglomerate was also found and confirmed by zeta potential measurements. The drug release capabilities from spherical nHAp-LE were determined in controlled release experiments, and increased cellular uptake was tested in human cell culture *in vitro*. The applicability of nHAp-ss as a reinforcement of composite polymer/nHAp filaments [4] for 3D printing was determined by producing them and using them to 3D print a designed scaffolding material.

It was found that continuous precipitation always results in spherical particles, regardless of the amount of lecithin used. Such spherical particles find applications as a drug delivery system. When precipitated with alendronate – the osteoporosis treatment drug – nHAp-LE-AL becomes amorphous, releases the drug over about 30 days, and shows increased cellular uptake *in vitro* in human osteoblastic cells. However, in a controlled precipitation/remodeling batch process, the precipitation temperature affects the shape of the obtained nanoparticles. At 40 °C and 80 °C, the proposed precipitation/remodeling yields plate-shaped and rod-shaped nanoparticles, respectively. At the same time, the rate of pH change determines the size of precipitated particles. SEM images prove that all particles retain their shape upon surface modification with sodium stearate. Regardless of the morphology, nHAp-ss mixed well with polycaprolactone solutions in dichloromethane, yielding a properly mixed substrate for pressure-extrusion of filaments for commercial 3D printing. Printability results show that plate and rod-shaped nHAp-ss can be added to the polymer with a concentration reaching 50% by mass.

The originally proposed methods to control the morphology and the size during the precipitation and precipitation/remodeling of nHAp, with subsequent surface modification, allow not only the drug delivery system design and production but also the preparation of polymer/nHAp composites with properties.

Studies were funded by the BIOTECHMED-1 project granted by the Warsaw University of Technology under the Excellence Initiative: Research University (ID-UB) program.

The research was funded by (POB Biotechnology and Biomedical Engineering) of Warsaw University of Technology within the Excellence Initiative: Research University (IDUB) program.

References

[1] Latocha J., Wojasiński M., Jurczak K., Gierlotka S., Sobieszuk P., Ciach T., Precipitation of hydroxyapatite nanoparticles in 3D-printed reactors, *Chem. Eng. Process. – Process Intensif.*, 2018, 133, 221–233.

[2] Wojasiński M., Latocha J., Liszewska P., Makowski Ł., Sobieszuk P., Ciach T., Scaled-Up 3D-Printed Reactor for Precipitation of Lecithin-Modified Hydroxyapatite Nanoparticles, *Ind. Eng. Chem. Res.*, 2021, 60, 12944–12955.

[3] Latocha J., Wojasiński M., Janowska O., Chojnacka U., Gierlotka S., Ciach T., Sobieszuk P., Morphology-controlled precipitation/remodeling of plate and rod-shaped hydroxyapatite nanoparticles, *AIChE J.*, 2022, 68(12), e17897.

[4] Podgórski R., Wojasiński M., Trepkowska-Mejer E., Ciach T., A simple and fast method for screening production of polymer-ceramic filaments for bone implant printing using commercial fused deposition modelling 3D printers, *Biomaterials Adv.*, 2023, 146, 213317.

CATALYSTS FOR SYNGAS GENERATION OF H_2/CO RATIO CLOSE TO UNITY

Izabela Wysocka*, Andrzej Rogala

[1]Gdańsk University of Technology, Faculty of Chemistry, Department of Process Engineering and Chemical Technology, Narutowicza 11/12, 80-233 Gdansk, Poland
*corresponding author: izabela.wysocka@pg.edu.pl

Synthetic gas (syngas) is one of the most important substrates in the chemical industry. It is used in many processes such as methanol, dimethyl ether and formaldehyde synthesis. The method of production, and therefore, the composition of the obtained syngas, depends on its final use. For example, for the production of methanol, the preferred H_2/CO ratio is two, whereas for the single-stage synthesis of dimethyl ether, H_2/CO is equal to one. The required composition of the synthesis gas can be achieved by selecting appropriate process conditions and catalysts.

In recent years, special attention has been paid to processes involving the dry reforming of hydrocarbons (DRH). It may be a pro-environmental alternative to steam reforming owing to the use of carbon dioxide as a substrate. Among them, dry reforming of methane (DRM) allows the production of syngas with an H_2/CO ratio in the outlet stream close to unity. The application of dry methane reforming may be suitable as the first step in synthetic fuel production. The industrial use of DRM is limited mainly by the lack of a suitable catalyst characterized by high stability and activity under DRM conditions. Currently used catalysts based on nickel and metal oxide supports are rapidly deactivated owing to sintering and coking. Therefore, global research in this field is directed towards the development of DRM catalysts that are not susceptible to fast deactivation.

In this view, this presentation will analyze the properties of catalysts and process parameters in terms of the use of hydrocarbons in dry reforming for syngas generation with a H_2/CO ratio close to unity. The discussion will be based on the literature findings and our own research. Special attention will be paid to the differences in the properties of traditional nickel and nickel-carbide catalysts as well as differences in the influence of the source of hydrocarbons on the final decomposition of the process products.

Acknowledgment

The research was financed by the National Center for Research and Development and Polish Oil and Gas Company (PGNiG) under the project "Development of DME production technology for small hydrocarbon deposits" No. POIR.04.01.01-00-0064/18-00.

Lectures

S4. Modern trends in chemical engineering and technology

TOWARDS AUTOMATION OF TWO-PHASE PROCESS CONTROL USING VIDEOGRAMMETRY

Stanisław Anweiler*

Opole University of Technology, Mechanical Engineering Dept., Mikołajczyka 5, Opole, Poland
*corresponding author: s.anweiler@po.edu.pl

In the field of chemical and process engineering, two-phase processes, that is, processes in which two different states of matter (gas and liquid) are present simultaneously, are vital. For example, two-phase flow is often used in the drilling, energy, chemical and food industries to transfer media such as oil, gas, steam, ground solid fuels or food. One of the key challenges in these processes is controlling the flow, that is, maintaining the proper velocity and uniformity of two-phase fluids through pipelines and inside equipment. A special case of a two-phase process is fluidization, in which solid particles (such as powder) are driven into motion by a burst of gas, creating a behavior similar to that of a fluid. In industrial processes, fluidization is often used for mixing, drying, separation and chemical reactions in the chemical, food and energy industries. Control of the fluidization process is key to achieving the desired process parameters, such as uniform mixing, maintaining a stable fluid bed and minimizing pressure losses.

Videogrammetry is a field that deals with the use of video recordings to take measurements and gather information about objects and environments captured in the recordings, using dynamic image analysis, among other techniques. The technique is often used in engineering to accurately measure various physical properties of objects. The use of videogrammetry in the automation of two-phase process control involves using video recordings to gather data and information about a specific process, and then utilizing this information to control and regulate the process. This allows the process to be monitored and controlled in real time, helping to ensure that the process runs smoothly and efficiently, and that potential problems are quickly detected and resolved. Using videogrammetry in this way can lead to improved process control, increased accuracy and uniformity, and reduced downtime and maintenance costs. By automating the control of two-phase processes using videogrammetry, the entire process can be structured, making it more efficient and effective.

This article discusses the most important issues related to two-phase flow process control, paying particular attention to the latest research and technology. It also presents various measurement and control methods that are currently used in the industry to ensure effective and safe control of the two-phase flow process. In particular, phenomena such as pressure loss and flow regimes that affect the stability and performance of two-phase processes are discussed. The paper also presents a literature review on controlling two-phase flow to ensure that the information presented is complete and up-to-date.

The main objective of the conducted research was to develop a system for automatic regulation of two-phase gas-solid flow. The regulation process is based on the principle of feedback derived from the result of dynamic image gray level measurement. Dynamic image analysis is a process that uses digital technologies and computational algorithms to analyze images and visualize data in real time. In the context of two-phase flow process control, dynamic image analysis can be used to monitor gas flow parameters such as flow velocity, temperature, pressure, etc. In the context of gas flow process control, dynamic image analysis can be used to visualize images from cameras or image sensors mounted on pipelines or two-phase mixture devices. The system can analyze images to detect patterns of mixture movement, such as turbulence, bubbles, plugs or laminar flow, and detect possible problems in the flow process.

In the present study, a PLC (Programmable Logic Controller) was used to control the gas flow process and dynamic image analysis was used to measure the gray level of the image and monitor the process in real time by providing feedback to the electropneumatic gas flow valve control

system. If problems are detected (unstable or incorrect flow regime), the system can automatically take appropriate action, such as changing the flow rate to restore the assumed regime, sending notifications to personnel or stopping the process. The measurement system is shown in Figure 1.

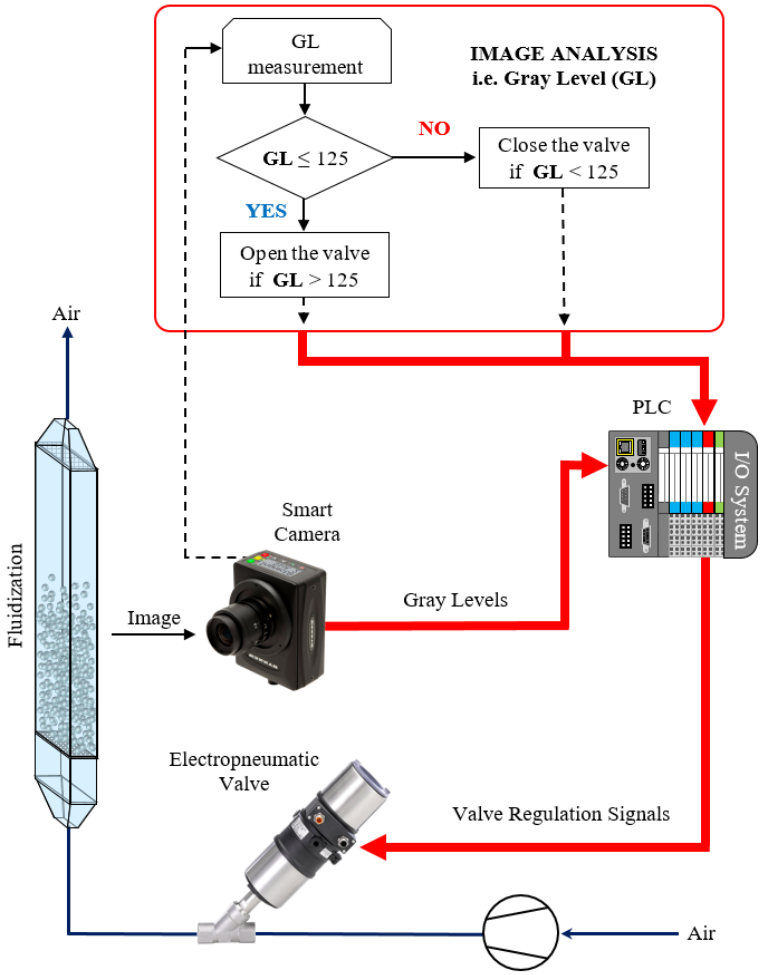

Fig. 1. The idea of automatic two-phase flow control system based on dynamic image analysis with outline of the decision-making system

The developed videogrammetry system with dynamic image analysis is a tool that makes it possible to monitor and control the gas flow process in real time, allowing quick response to problems and increasing the efficiency of the process.

OPTIMIZATION METHODS IN THE MANUFACTURE OF PROFESSIONAL PRODUCTS

Sebastian J. Balicki*

Department of Engineering and Technology of Chemical Processes, Faculty of Chemistry, Wrocław University of Science and Technology, Wybrzeże Wyspiańskiego 27, 50-370 Wrocław, Poland
*corresponding author: sebastian.balicki@pwr.edu.pl

The systematic and structured planning of experiments (the Design of Experiments, DoE) helps one to comprehend the cause-and-effect relationship in processes, making it the most effective approach to solution development. The DoE approach enables the chemical engineer to efficiently acquire information and use it to create innovation and high-quality products through careful planning and decision-making (Fig. 1). It is ideal for developing effective formulations for various chemicals or determining the optimal conditions for manufacturing professional products [1-4].

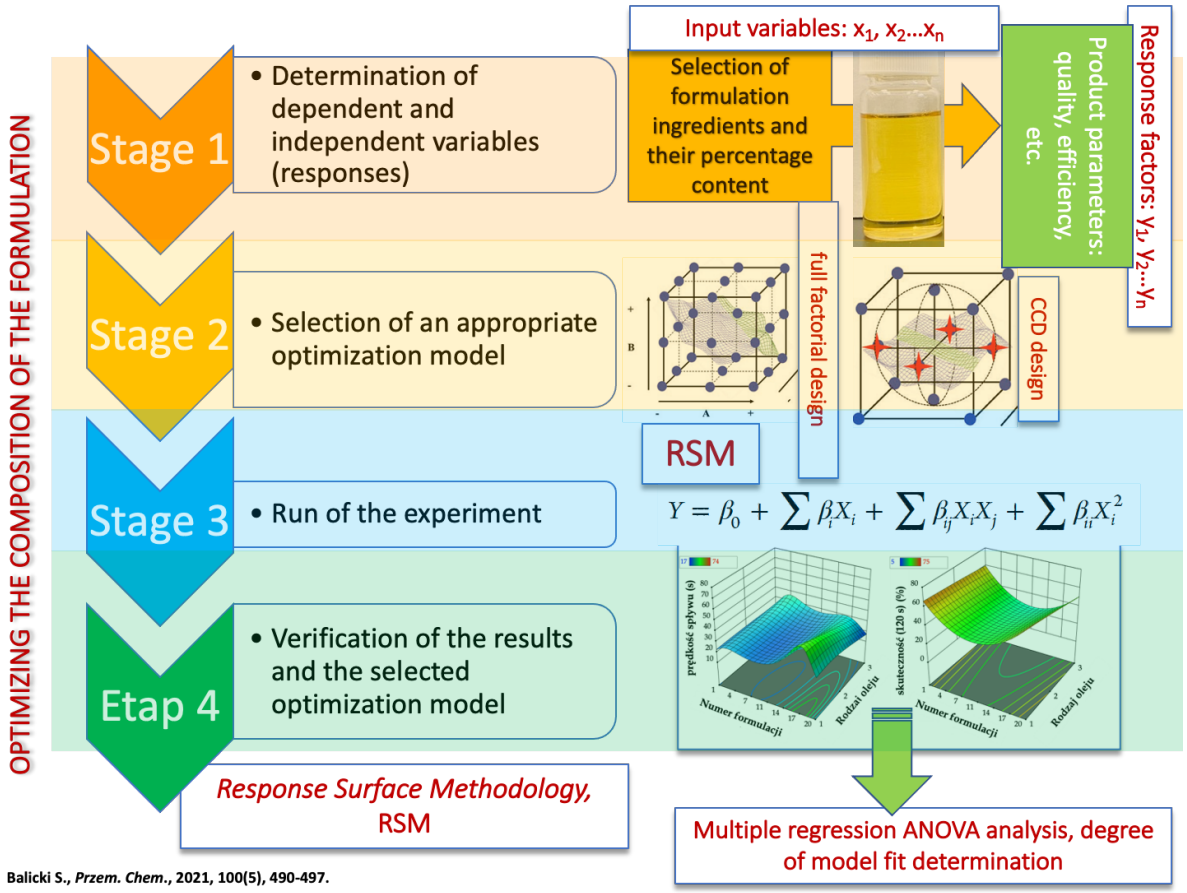

Fig. 1. Principal stages in the design of experiments (DoE) and optimization approach

Such a strategy is closely related to QbD (Quality by Design). The primary responsibility of manufacturers of novel formulations in the sectors of building chemicals, cosmetics, or fine chemicals (e.g., specialty surfactants, nanocarriers for drug delivery systems, bioactive compounds, etc.) is to supply customers with high-quality products. According to the QbD principle, this work must be completed by comprehending all elements and phases of the intended product's

manufacturing. In other words, the basis of this concept is that quality should be included in all stages of the process rather than simply at the end (quality control) to assure consistent quality of the final product. Statistical data analysis, as well as planning and design of experiments' (DoE) approaches, provide appropriate tools for implementing this idea in practice [1-4].

In the current contribution, a comparison of the various possibilities of DoE utilization was presented in order to express all attitudes required for Fine Chemicals manufacturing. Mainly, different operation units, processes of production, and professional product formulations were optimized [1-7]. First, the optimization of the solid-liquid extraction process of plant-derived bioactive food fiber, assisted by physical factors, was performed. The alkaline extraction of polyphenolic-polysaccharide conjugates from *Erigeron canadensis* L. under variable conditions of time, temperature, and power of utilized ultrasounds or microwaves was optimized by means of response surface methodology (RSM). The main goal of optimization was to maintain the yield, chemical character, and bioactivity at a similar or higher level than in conventional hot-alkaline extraction with noticeably reduced process time [5-6]. The second example of DoE implementation was the optimization of the production process of graffiti paint eco-removers. The concentration of different classes of sugar or amino-acid-based surfactants, high-pressure homogenization conditions, and biosolvent types were all considered independent variables in this case. The influence of the input variables on the quality and efficiency of graffiti removers was studied [2, 4, 7]. Finally, the last example of DoE was optimization of cementitious composite formulations. This study analyzed the influence of various forms of titanium dioxide additives on the performance of the resulting cement composites, with enhanced photocatalytic and antibacterial functions, for professional use in construction engineering. The optimization through RSM consisted of studying the influence of the type of TiO_2 and its concentration on the final characteristics of the cementitious samples [1].

References

[1] Jędrzeczjak P., Parus A., Balicki S., Kornaus K., Janczarek M., Wilk K.A., Jesionowski T., Ślosarczyk, A., Klapiszewski Ł., The influence of various forms of titanium dioxide on the performance of resultant cement composites with photocatalytic and antibacterial functions, *Mater. Res. Bull.*, 2023, 160, 112139.

[2] Bartman M., Balicki S., Wilk K.A., Formulation of Environmentally Safe Graffiti Remover Containing Esterified Plant Oils and Sugar Surfactant, *Molecules*, 2021, 26(15), 4706.

[3] Balicki S., Unit process optimization in the organic technology, *Przem. Chem.*, 2021, 100(5), 490–497.

[4] Bartman M., Balicki S., Hołysz L., Wilk K.A., Graffiti coating eco-remover developed for sensitive surfaces by using an optimized high-pressure homogenization process, *Colloid Surf. A-Physicochem. Eng. Asp.*, 2023, 659, 130792.

[5] Balicki S., doctoral thesis: *Preparation of the plant-derived polyphenolic-polysaccharide conjugates with the pro-health potential assisted by selected physical factors*, 2019, Wrocław University of Science and Technology.

[6] Balicki S., Pawlaczyk-Graja I., Gancarz R., Capek P., Wilk K.A., Optimization of Ultrasound-Assisted Extraction of Functional Food Fiber from Canadian Horseweed (*Erigeron canadensis* L.), *ACS Omega*, 2020, 5(33), 20854–20862.

[7] Bartman, M., Balicki S., Hołysz L., Wilk K.A., Surface Properties of Graffiti Coatings on Sensitive Surfaces Concerning Their Removal with Formulations Based on the Amino-Acid-Type Surfactants, *Molecules*, 2023, 28(4), 1986.

BULK POLYMERIZATION USING AN EXTRUDER

Czech Zbigniew[1,*], Kowalczyk Agnieszka[2],

[1]Faculty of Chemical Technology and Engineering, Department of Chemical Organic Technology and Polymerics Materials, 70-322 Szczecin, Poland
[2]Faculty of Chemical Technology and Engineering, Department of Chemical Organic Technology and Polymerics Materials, 70-322 Szczecin, Poland
*corresponding author: psa_czech@wp.pl

The present publication describes a problem to develop solvent-free acrylic pressure-sensitive adhesives (PSA). Solvent-free PSAs are established materials for the manufacturing of various self-adhesive products. Only by means of these acrylic PSA was it possible to succeed in drafting the present surprisingly efficient generation of double-sided pressure-sensitive adhesive tapes, medical products, protective masking films, films for the graphics market, and various specialty products [1].

The desire to use PSA without having to deal with an organic solvent has existed since self-adhesive products started to be mass produced [2]. Solvent-free PSAs achieved real practical significance in the 1970s with the appearance of thermoplastic rubber, the styrene-butadiene (SBS) and styrene-isoprene (SIS) block copolymers. These PSA based on synthesis rubbers show unacceptable temperature resistance, unacceptable temperature resistance or poor resistance to plasticizers.

The first development work on using an extruder as the chemical reactor for polymerization was done about 50 years ago. A patent publication [4] EP 0 160 394 from 3M describes a continuous process for the polymerization of acrylate monomers in a single or double screw extruder (Fig. 1).

Fig. 1. Twin-screw extruder Model LSM34GL from Leistritz Inc. (Germany)

The following experiments were conducted in order to study the diverse parameters such as acrylic acid content, radical starter concentration and screw speed during the polymerization in the extruder, viscosity, molecular mass, tack, peel adhesion, shear strength and other important properties of the polymerization process such as polymer yield and polymerization conversion.

References

[1] Czech Z., Wesołowska M., Development of solvent-free acrylic pressure-sensitive adhesives, *Eur. Polym. J.*, 2007, 43, 3604-3612.
[2] Czech Z., *Crosslinking of acrylic pressure-sensitive adhesives*, Szczecin: ed. at Szczecin University of Technology, 1999 (ISBN 83-87423-18-1).
[3] Benedek I., *Pressure-sensitive design and formulation, application*, Leiden Boston, ed. at Martinus Nijhoff Publishers and VSP, 2006.
[4] EP 0 160 394 from 3M (1995).

CONTROLLING THE DISTRIBUTION OF Pd DOPANT IN SnO_2 SYNTHESIZED WITH FLAME SPRAY METHOD

Katarzyna Jabłczyńska[1,2,*], Alexander Gogos[3], Christian Kubsch[1], Sotiris E. Pratsinis[1]

[1]Particle Technology Laboratory, Department of Mechanical and Process Engineering, Institute of Energy and Process Engineering, ETH Zurich, CH-8092 Zurich, Switzerland
[2]Faculty of Chemical and Process Engineering, Warsaw University of Technology, 00-645 Warsaw, Poland
[3]Particles-Biology Interactions, Swiss Federal Laboratories for Materials Science and Technology (Empa), Department of Materials Meet Life, CH-9014 St. Gallen, Switzerland
*corresponding author: katarzyna.jablczynska@pw.edu.pl

In recent years, the use of semiconducting nanoparticles has been widely investigated for various technological applications, including sensors, catalysts, solar cells, and electronic devices. Among the various types of nanoparticles, tin dioxide (SnO_2) nanoparticles have gained considerable attention due to their unique electrical, optical, and magnetic properties, which can be tailored by doping with various transition metal and rare-earth elements.

Flame spray pyrolysis (FSP) is one of methods that allows the embedding of noble metals into the semiconducting matrix. This method is widely used for the synthesis of nanomaterials due to its ability to produce particles with high purity, narrow size distribution, and unique morphologies. In FSP, a liquid precursor is atomized into fine droplets and injected into a flame, where it undergoes rapid pyrolysis and oxidation to form solid particles. By introducing a noble metal precursor into the flame, it is possible to incorporate the metal into the nucleating particle, resulting in a nanocomposite material with enhanced properties.

The high-temperature flame generated in FSP allows the incorporation of metal dopant atoms into the SnO_2 lattice, leading to the formation of solid solutions. In addition, the support particles used in FSP can be decorated with metal clusters, which can act as catalytic sites for various chemical reactions. But the distinctive feature of FSP lies in the ability to embed a fraction of metal clusters within the semiconducting matrix of nanoparticles, creating a composite structure that distributes dopants on both the atomic and cluster levels. Figure 1 shows (a) micrographs of palladium (Pd) containing SnO_2 nanoparticles produced with FSP and (b) their elemental mapping exhibiting Pd-rich spots.

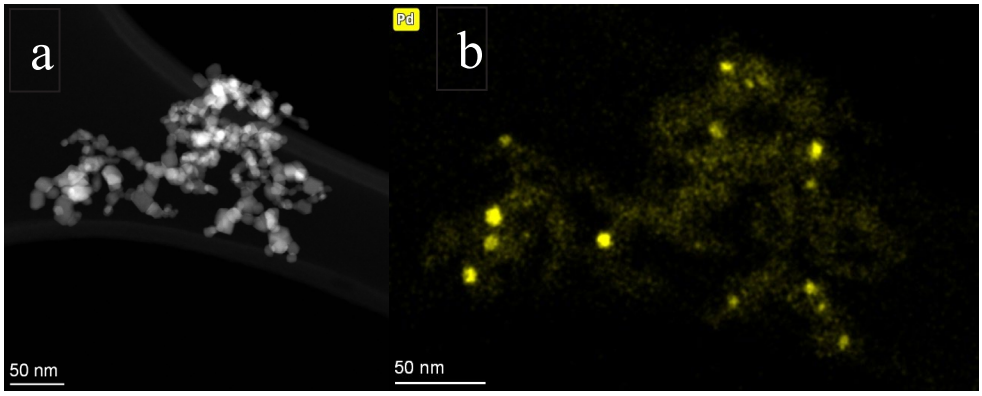

Fig. 1. 3% Pd/SnO_2 nanoparticles produced with FSP imaged with a) Scanning Transmission Electron Microscopy (STEM) and b) Energy Dispersive X-Ray Analysis (EDXS)

The inclusion of noble metal atoms or clusters exerts a substantial influence on the catalytic and electronic characteristics of nanoparticles, which hold significant relevance in various fields, e.g., gas sensing applications. A recent study demonstrated that the sensing capabilities of carbon

monoxide (CO), acetone and ethanol can be significantly improved by embedding Pd into SnO_2 instead of depositing it onto the surface [1].

The primary aim of this study was to investigate the impact of changing FSP process conditions on the SnO_2 crystal size, the partitioning of Pd between the surface and interior of the particle and the resulting particle characteristics. To demonstrate the significant differences in particle properties resulting from these modifications, the study conducted gas sensing experiments. Specifically, the sensors' response to CO and acetone was evaluated, and the results were compared to those obtained using particles with Pd deposited solely on the surface or particles with both surface and embedded Pd.

SnO_2 particles embedded with Pd or PdO were synthesized using FSP. The embedded fraction of Pd was varied by changing the FSP precursor solution concentration (PSC), Pd content and the ratio of precursor solution to dispersion oxygen flow rates (P/D). Synthesis was followed by annealing and nitric acid leaching to remove Pd from the particle surface. The Inductively Coupled Plasma – Optical Emission Spectrometry (ICP-OES) analysis of leaching solutions was performed to evaluate the amount of surface Pd. The sensors' response to 1 ppm of acetone and CO was tested, and the results were compared for Pd-containing and pure SnO_2 sensors.

The SnO_2 crystal size increased with increasing PSC and P/D ratio, while it decreased slightly with increasing palladium dopant content. Embedded Pd fraction decreased with increasing PSC, P/D and Pd content. As a result, the crystal size of SnO_2 particles ranged from 11 to 24 nm, and the fraction of Pd embedded within them varied from 30 to 80% of the initial Pd content. The FSP allowed simultaneous control on the embedded palladium fraction and the size of tin dioxide crystals by adjustment of all three process parameters.

The sensing measurements demonstrated that the sensors made with particles in which Pd was embedded solely within the SnO_2 matrix exhibited up to two orders of magnitude higher sensitivity to CO and acetone in comparison to other particles. This illustrates the significant impact of both FSP process conditions and particle post-treatment on the distribution of Pd within SnO_2 matrix and the sensor's overall performance.

References

[1] Pineau N.J., *Palladium embedded in SnO_2 enhances the sensitivity of flame-made chemoresistive gas sensors*, *Microchim. Acta*., 2020, 187, 96.

EXTRACTIVE DETOXIFICATION OF HYDROLYSATES WITH SIMULTANEOUS FORMATION OF DEEP EUTECTIC SOLVENTS

Patrycja Makoś-Chełstowska*, Karolina Kucharska, Edyta Słupek, Jacek Gębicki

Gdansk University of Technology, Faculty of Chemistry, Department of Process Engineering and Chemical Technology, 80-233 Gdansk, Poland
*corresponding author: patrycja.makos@pg.edu.pl

Biohydrogen is currently considered to be one of the most favorable alternatives to fossil fuels. The production of biohydrogen mainly involves processing of lignocellulosic biomass, which, as the first step, must be subjected to hydrolysis to convert the complex structures of hemicellulose and lignin into simple fermentable sugars. However, this process also produces other substances called fermentation inhibitors such as carboxylic and dicarboxylic acids, furans, phenols, and polyphenols. These substances inhibit cell growth, induce DNA damage, and inhibit several enzymes involved in glycolysis, thereby reducing the efficiency and production of biohydrogen. However, these are extremely valuable substances that can be extracted and used in other processes. Therefore, the use of a detoxification method before fermentation is crucial for the process efficiency [1].

Currently, adsorption, membrane extraction, membrane filtration, solvent extraction, and ion exchange are the main methods used for the detoxification of hydrolysates. However, most of these methods are relatively expensive, complicated, and result in the loss of large amounts of sugars [2-6]. Among the aforementioned methods, liquid-liquid extraction is very attractive due to its simple implementation, low-cost procedure, and the possibility of high removal of fermentation inhibitors without loss of sugars. In addition, a properly selected nontoxic solvent allows the selective capture of a targeted group of inhibitors, followed by their simple separation [7].

This paper presents a novel *in situ* liquid–liquid extraction approach, that involves the addition of a substance capable of forming specific non-covalent bonds with fermentation inhibitors, that is, hydrogen bonds, electrostatic, and van der Waals interactions. In this way, deep eutectic solvents (DES) are formed directly in an aqueous solution, which, in the next stage, can be easily separated and used for the purification of biohydrogen streams, for example, in the process of absorption. Examination of the hydrolysate composition enabled the identification of four major fermentation inhibitors: furfural, 4-hydroxymethylfurfural, vanillin, and 4-hydroxybenzoic acid. Among the identified fermentation inhibitors, furfural was found to be present at the highest concentration. Subsequently, the second component of DES, including 1-hexanol, 1-heptanol, 1-nonanol, 1-decanol, menthol, thymol, carvone, camphor, eugenol, eucalyptol, and α-terpineol, was added to the broth. As a result, the second DES phase occurred in selected samples. These were subjected to further analysis. To ensure the highest extraction efficiency for fermentation inhibitors, an optimization procedure was performed using the Box-Behnken design. In addition, structural studies using spectroscopic methods, including FT-IR and NMR, were performed for the formed DES, as well as studies of basic physicochemical properties, including melting point, density, viscosity, and surface tension.

These results indicate that it is possible to form deep eutectic solvents composed of furfural and monoterpenes, that is, eugenol, carvone, menthol, and thymol. Therefore, further studies were performed on the removal of furfural from a model aqueous solution (1 mg/mL). These results indicate that thymol forms the strongest non-covalent bonds with furfural bonds (Figure 1). Thymol contains an -OH active group in its structure that can act as a hydrogen bond donor. In contrast, furfural contains two hydrogen bond acceptor groups: =O and -O-. When combined, the active sites form strong hydrogen bonds between the molecules. As a result, a stable DES molecule is created. The furfural removal efficiency from aqueous solutions was equal to 82.5% with respect to its initial concentration. However, excess thymol must be used to achieve this high efficiency because of the competitiveness of the hydrogen bonds formed between water and furfural. Detoxification studies

of real hydrolysates showed only a slight reduction in furfural removal efficiency. This slight change is due to the attachment of other fermentation inhibitors to the active sites of thymol.

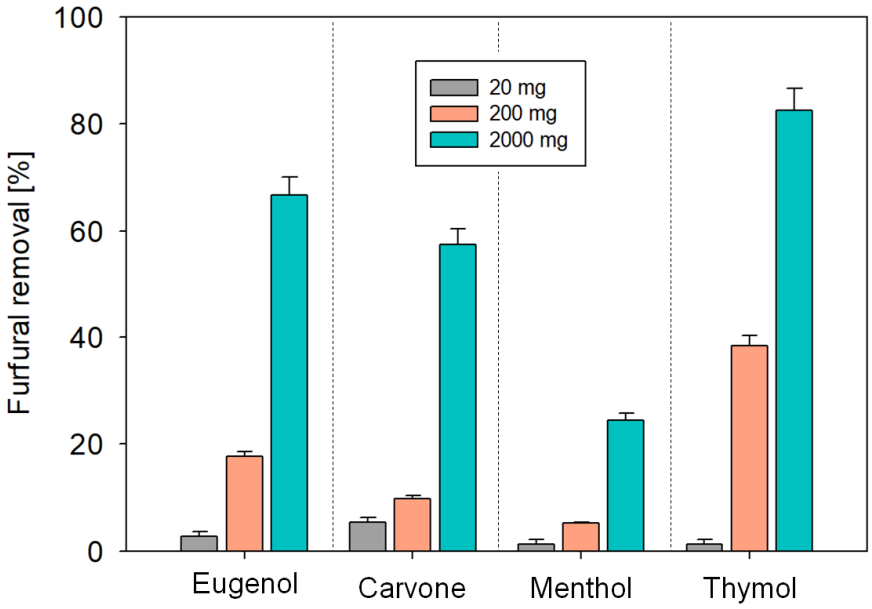

Fig. 1. Removal of furfural via in situ deep eutectic solvent formation method

This research was funded by the National Science Centre, Poland, under research project No. UMO-2021/41/B/ST8/02395

References

[1] Makoś P., Słupek E., Gębicki J., Extractive detoxification of feedstocks for the production of biofuels using new hydrophobic deep eutectic solvents – Experimental and theoretical studies, *J. Mol. Liq.*, 2020, 308, 113101–113112.

[2] Grzenia D.L., Schell D.J., Ranil Wickramasinghe S., Membrane extraction for detoxification of biomass hydrolysates," *Bioresour. Technol.*, 2012, 111, 248–254.

[3] Pan L., He M., Wu B., Wang Y., Hu G., Ma K., Simultaneous concentration and detoxification of lignocellulosic hydrolysates by novel membrane filtration system for bioethanol production, *J. Clean. Prod.*, 2019, 227, 1185–1194.

[4] Doddapaneni T.R.K.C., Jain R., Praveenkumar R., Rintala J., Romar H., Konttinen J., Adsorption of furfural from torrefaction condensate using torrefied biomass, *Chem. Eng. J.*, 2018, 334, 558–568.

[5] Carvalho G.B.M., Mussatto S.I., Cândido E.J., Almeida e Silva J.B., Comparison of different procedures for the detoxification of eucalyptus hemicellulosic hydrolysate for use in fermentative processes, *J. Chem. Technol. Biotechnol.*, 2006, 81(2), 152–157.

[6] Ludwig D., Amann M., Hirth T., Rupp S., Zibek S.,, Development and optimization of single and combined detoxification processes to improve the fermentability of lignocellulose hydrolyzates, *Bioresour. Technol.*, 2013, 133, 455–461.

[7] Makoś-Chełstowska P., Słupek E., Kucharska K., Kramarz A., Gębicki J., Efficient Extraction of Fermentation Inhibitors by Means of Green Hydrophobic Deep Eutectic Solvents, *Molecules*, 2022, 27, 57.

FORMULATION AND STABILISATION OF TWO- PHASE EMULSION USING TWEEN 40 AND 80 SURFACTANTS

Halina Murasiewicz*[1], Khrystyna Illienko[2]

[1]West Pomeranian University of Technology, Szczecin, Faculty of Chemical Technology and Engineering, Department of Chemical and Process Engineering
Piastów Ave. 42, 71-065 Szczecin, Poland
[2]National Technical University of Ukraine "Igor Sikorsky Kyiv Polytechnic Institute"
Prosp.Peremohy 37, Solomyanskyi district, Kyiv, Ukraine
*corresponding author: halina.murasiewicz@zut.edu.pl

Oil-in-water emulsions can be found in a range of food and beverage products, including creams, desserts, dressings, soft drinks, and others [1]. However, they are not only attractive to the food industry. Applications of emulsion as transport agents for vitamins, supplements, and other nutraceuticals [2] have attracted many researchers. Emulsions are widely present in our daily life, e.g. in personal and home care products [3]. Emulsions and microemulsions have been applied to environmental technologies such as subsurface remediation and biofuel production [4]. They facilitate transportation of heavy oil, storage of milk, synthesis of chemicals or materials but they can also lead to serious upgrading or environmental issues (e.g., pipeline plugging, corrosion to equipment, water pollution, soil pollution). However, the presence of emulsions in many cases is undesired and can cause serious problems.

Emulsions can be formed using either high-energy or low-energy methods [5]. High-energy approaches rely on specialized equipment to disrupt and intermingle the oil and water phases, thereby forming small droplets. In contrast, low-energy approaches require no specialized equipment and utilize the physicochemical properties of the surfactant, oil and water system to spontaneously generate emulsion droplets by simple mixing procedures or by changing environmental conditions such as temperature. High-energy methods are currently the most commonly used in the food industry because they are already well-established and capable of large production, while low-energy methods are of growing interest due to their low cost and ease of implementation [5].

The two-phase emulsions are generally formed by mixing two naturally immiscible fluids. Emulsifiers are added to enhance product stability to obtain a satisfactory shelf-life. The result of an emulsion of oil and water mix varies depending on the volume fraction of both phases and the kind of emulsifier utilized. Therefore, the impact of the type and concentration of emulsifier used on the emulsion stability and emulsifying properties of 5% by volume of liquid paraffin oil-in-water emulsion were discussed in this study. The emulsions were prepared by using a jacket stirred vessel fitted with the Rushton turbine at constant temperature. The complexes of Tween 40 (HLB = 15.6) and Tween 80 (HLB = 4) were selected as emulsifiers. Both surfactants are known as nonionic with the critical micelle concertation (CMC) estimated at T=298 K equals $CMC_{Tween40}$ = 0.033 mM and $CMC_{Tween80}$ = 0.015 mM [6], respectively. The concentration of emulsifiers used in the experiment corresponds to the following values: 0.01665 mM, 0.025 mM, 0.033 mM and 0.042 mM for Tween 80 and 0.0075 mM, 0.011m M, 0.015 mM, 0.019 mM for Tween 80. The emulsions were formed for four different impeller speeds at the above concentrations of surfactants. The density, interfacial tension and drop size and distribution of 5% of liquid paraffin oil-in-water emulsion were investigated and compared. The drop size distributions (DSD) were measured with a Mastersizer 3000 (Malvern Instruments, Malvern, UK) to obtain the mean Sauter diameter, d_{32}, skewness, width and homogeneity of DSD. The structure of emulsions was observed under the microscope and examples of captured images are shown in Figure 1.

a) 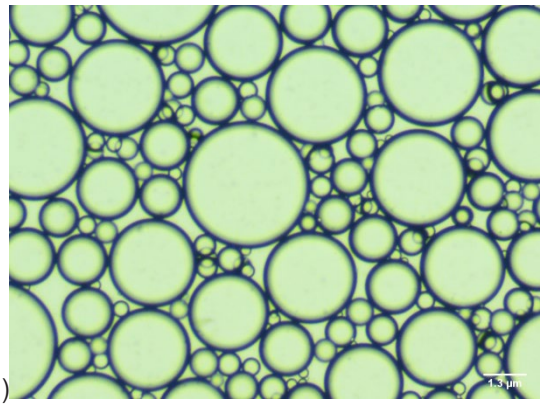 b) 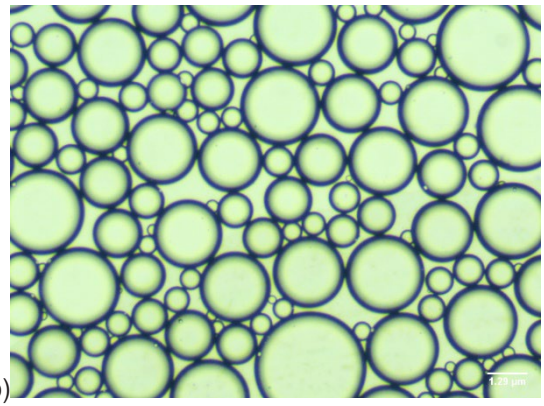

Fig. 1. Example of the system of paraffin and water supplemented with a) 0.033 mM of Tween 40 and b) 0.015 mM of Tween 80

The experimental results showed that DSDs were narrowed, which is typical for the system with an emulsifier when compared to those for a non-surfactant system. The mean Sauter diameter values were decreased as the concertation of emulsifier was increased. A similar trend was observed when the impeller speeds were increased. It was found that increasing concentration of Tween 40 and 80 effectively reduced the surface tension up to the CMC concentration. Above the CMC, the surface tension of the solution was constant because the interfacial surfactant concentration did not change any more. The observation of the stability of emulsions based on values of d_{32} revealed that they remained stable during 30 days of storage. Qualitatively similar values of mean Sauter diameter were found between fresh and aged emulsion. However, the following question should be addressed: how do the hydrodynamic conditions during emulsification at high emulsifier concentration influence the mean drop diameter?

In conclusion, this study helped to understand the effect of nonionic concentrations of emulsifiers on drop size distribution and mean Sauter diameter. Obtained experimental results of value of the interfacial area are important to control transport processes. Results and conclusions achieved in this work are beneficial for aforementioned industries as they may allow optimization of heat or mass transfer processes.

References

[1] McClements D.J., Emulsion design to improve the delivery of functional lipophilic components, *Annu Rev. Food Sci. Technol*., 2010, 1, 241–69.

[2] Okochi H., Nakano M., Preparation and evaluation of w/o/w type emulsions containing vancomycin, *Adv. Drug Deliv. Rev*., 2000, 45, 5–26.

[3] Lee J.S., Kim J.W., Han S.H.; Chang I.S., Kang H.H., Lee O.S., Oh S.G., Suh K.D., The stabilization of L-ascorbic acid in aqueous solution and water-in-oil-in-water double emulsion by controlling pH and electrolyte concentration, *J. Cosmet. Sci.,* 2004, 55, 217.

[4] Schramm L.L., Emulsions: *Fundamentals and Applications in the Petroleum Industry*. In Petroleum Emulsion; Schramm, L.L., Ed.; American Chemical Society: Washington, DC, USA, 1992

[5] Abbas S., Hayat K., Karangwa E., An Overview of Ultrasound-Assisted Food-Grade Nanoemulsions, *Food Eng. Rev*., 2013, 5, 139–157.

[6] Mahmood M. E., Al-Koofee D. A. F., Effect of Temperature Changes on Critical Micelle Concentration for Tween Series Surfactant, *Glob. J. Sci. Front. Res*., 2013, 13(4), 1–7.

CARBON DIOXIDE NANOBUBBLES IN AQUEOUS DISPERSIONS OF BIOCOMPATIBLE SURFACTANTS – STABILITY STUDIES

Karol Ulatowski*, Andrzej Cecuga, Paweł Sobieszuk

Warsaw University of Technology, Faculty of Chemical and Process Engineering, Waryńskiego 1, 00-645 Warsaw, Poland
*corresponding author: Karol.Ulatowski@pw.edu.pl

Nanobubbles proved to be a viable agent in multiple biomedical processes [1], where they are used as drug carriers [2], ultrasonographic contrasts [3], or in treatments of chronic wounds. In this last application, diabetic foot ulcers are treated in Japanese hospitals using carbon dioxide nanobubble dispersions, directly on site [4, 5]. However, it would be helpful for the patients if they were able to carry out the treatment at home. For that to happen, one has to determine whether it is possible to obtain stable nanodispersions of carbon dioxide in water and whether such stability is influenced by the presence of surfactants.

This work focuses on the answering of question whether it is possible to obtain stable gas nanobubbles in aqueous dispersions of biocompatible surfactants from the Pluronic group, namely Pluronic L121, Pluronic P123 and Pluronic F127. These three surfactants are biocompatible polymers which share the same monomers, being block-co-polymers of poly(ethylene glycol) and poly(propylene glycol). All polymers were dissolved in water to obtain solutions with concentrations corresponding to 0.2, 0.5, or 0.8 of critical micellar concentration (CMC). Then we generated nanobubbles in such aqueous solutions and in pure (deionized) water. The nanobubble membrane-stirrer generation setup (designed by us) consisted of a high-shear mechanical stirrer (diameter 20 mm) embedded in a polycarbonate cylinder (internal diameter 24 mm, capacity 50 mL) and placed directly above the flat silicon carbide ceramic membrane (pore size 0.2 μm) enclosed securely in the setup. Here, the shear stress is induced by the rotation of the stirrer. Gas is pressurized through the membrane and is cut off from the membrane surface in the form of nanobubbles. The rotation rate and gas flow rate are controlled and set at a constant value by the internal driver of the stirrer motor and mass flow controllers (Brooks, USA). All of the investigations were carried out for the flow rate of carbon dioxide of 10 mL/min.

After each generation, the liquid was transferred to the freshly cleaned glass vial with a glass cap to ensure minimalization of mass transfer with the environment. Samples from the liquid were analyzed using the DLS technique directly after generation and then after 7, 14, and 21 days after generation to check the stability of average size and density of number distribution in time of storage. Based on the densities of size distributions, we found the Sauter diameter describing each distribution.

We stated two research questions:

1) Does the duration of CO_2 bubble generation in our generation setup affect the stability of nanobubbles in the presence of different concentrations of P123 surfactant for the constant rotation rate of the impeller?

2) How does the change in the rotation rate of the impeller affect the stability of CO_2 nanobubbles for constant generation time for all three surfactants?

For finding the answer to the first question, we generated bubbles in our setup for a rotation rate of 900 rpm and a duration of generation of 15, 30, 45, 60, 90, and 120 minutes for each of the concentrations of P123 surfactant. Figure 1 presents the results obtained for this part of the study. One can see that the generation duration clearly affects the stability of nanobubble dispersions, as we observe the change in Sauter diameter of bubbles as function of generation duration. What is interesting is when the concentration of surfactant changes, we observe different responses of Sauter diameter to the change of generation duration. In most cases we see the monotonous change of initial diameter of nanobubbles (blue points in Figure 1) for the first 30-60

minutes which is followed by a drastic decrease of diameter. We suspect that after the first 60 minutes, during which bubbles mostly grow in size, the maximum concentration of bubbles is achieved and existing bubbles quickly coalesce to microbubbles which rise to the surface, causing new bubble origins to form and grow. Due to the fact that after initial bubble coalescence the liquid is still saturated, the following increase in size is more rapid, as there is less mass outflux from the bubble to the liquid.

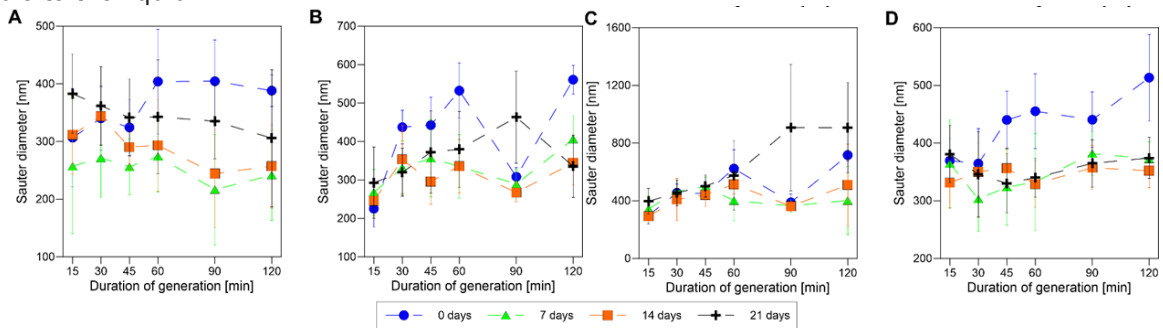

Fig. 1. The Sauter diameter of CO2 nanobubbles generated (900 rpm) in dispersions with different concentrations of Pluronic P123 surfactant during storage. The concentration of surfactant differs between plots: (A) 0.0 CMC of surfactant (pure water), (B) 0.2 CMC, (C) 0.5 CMC, (D) 0.8 CMC

To answer the second question, we generated nanobubbles for all three surfactants in all three concentrations with the rotation rate of the impeller set to 600, 900, or 1200 rpm. Pluronic P123 produced the maximum Sauter diameter in the function of the rotation rate of impeller and surfactant concentration in the investigated range of parameters, while for Pluronic L121 the minimum is visible. The heaviest of surfactants, Pluronic F127, was least affected by the change of rotation rate of the stirrer and fraction of CMC.

To sum up, this study has shown that all three biomedical surfactants can be used as stabilizers of nanobubble dispersion of carbon dioxide and therefore bubble dispersions can potentially be used as the medium for home applications for treatment. However, this requires further study, especially in cooperation with medical institutions.

Acknowledgement
This work was supported by National Science Centre, Poland, grant number 2018/29/B/ST8/00365.

References

[1] Odziomek M., Ulatowski K., Dobrowolska K., Górniak I., Sobieszuk P., Sosnowski T.R., Aqueous dispersions of oxygen nanobubbles for potential application in inhalation therapy, *Sci. Rep.,* 2022, 12, 12455..
[2] Argenziano M., Banche G., Luganini A., Finesso N., Allizond V., Gulino G.R., Khadjavi A., Spagnolo R., Tullio V., Giribaldi G., Guiot C., Cuffini A.M., Prato M., Cavalli R., Vancomycin-loaded nanobubbles: A new platform for controlled antibiotic delivery against methicillin-resistant Staphylococcus aureus infections, *Int. J. Pharm.,* 2017, 523, 176–188..
[3] Kim C., Qin R., Xu J.S., Wang L.V., Xu R., Multifunctional microbubbles and nanobubbles for photoacoustic and ultrasound imaging, *J. Biomed. Opt.,* 2010, 15, 010510.
[4] Shalan N., Al-Bazzaz A., Al-Ani I., Najem F., Al-Masri M., Effect of Carbon Dioxide Therapy on Diabetic Foot Ulcer, *J. Diabetes. Mellit.,* 2015, 05, 284–289. https://doi.org/10.4236/jdm.2015.54035.
[5] Riyad Abdulhamza G., Luay Al-Omary H., Physiological Effects of Carbon Dioxide Treatment on Diabetic Foot Ulcer Patients, *IOSR J. Pharm. Biol. Sci.* 2018, 13, 1–07.

APPLICATION OF COMPUTATIONAL FLUID DYNAMICS FOR PREDICTING HEMOLYSIS IN MITRAL PARAVALVULAR CHANNELS

Krzysztof Wojtas[1,*], Krzysztof Truchel[1], Michał Kozłowski[2], Łukasz Makowski[1], Wojciech Orciuch[1]

[1] Warsaw University of Technology, Faculty of Chemical and Process Engineering, Warynskiego 1, 00-645 Warsaw, Poland
[2] Medical University of Silesia, Department of Cardiology and Structural Heart Diseases, Ziolowa 45/47, 40-635 Katowice, Poland
*corresponding author: krzysztof.wojtas@pw.edu.pl

Paravalvular leaks (PVLs) are common pathologies which can occur after surgical valve replacement. Approximately 17% of patients with prosthetic aortic valves and 22% of patients with prosthetic mitral valves are affected at the time of discharge after surgery [1]. Moreover, the majority of PVLs develop during the first year after surgery [2]. Among other complications, PVLs can cause hemolysis, that is destruction of red blood cells. Hemolysis in patients with PVLs can have various levels of severity—at worst repeated blood transfusions and interventional treatment are required. Hemolysis is a quite common pathology in this setting—current data place hemolysis as the main indication for PVL closure in up to 20% of cases.

It appears that many factors correspond to pathogenesis of hemolysis, whereas shear stress seems to be one of the more important ones (suspected factors include also turbulent pattern of blood flow, interactions of erythrocytes with prosthetic material and others) [3, 4]. Shear stress and also other important flow parameters in the PVL channel can currently be relatively accurately predicted using specialized computer software and principles of computational fluid dynamics (CFD). Nowadays, CFD and other numerical techniques are being more and more often used in interdisciplinary science fields such as biomedical engineering [5-8]. Thanks to more modern medical equipment and a better understanding of the dynamics of human cardiovascular and respiratory systems and also the rheology of bodily fluids, it is becoming possible to run simulations of phenomena occurring in real patients. This is, of course, partly due to the fact that CFD (supplied with e.g. CT-scan models) allows non-invasive research into the nature of pathological conditions in e.g. blood flows in the cardiovascular system.

To study the hemodynamics inside the left heart affected by a mitral paravalvular leak, simulations were performed using computational fluid dynamics software. Simulations were focused on parameters characterizing the risk of hemolysis, which can occur due to high shear stress values. It was assumed that hemolysis occurs in areas with stresses above 300 Pa [3]. In this study, we tested the validity of the simplified approach to left heart modeling. In this case, a left heart affected by mitral paravalvular leak derived from computed tomography (CT) scan was investigated.

We compared two approaches to left ventricle contraction. First, using left ventricular motion, that is dynamic mesh, and real shape of the left heart. Second, using static mesh, where the mesh motion was ignored, and universal, simple shape of the left ventricle and atrium. The geometry of the PVL was not simplified in any way in both cases. Simulations were performed for the unsteady phase of cardiac contraction using a non-Newtonian viscosity model (Carreau-Yasuda). The main aim of this work was to investigate whether it is necessary to include full per-patient geometry data to accurately predict hemodynamics inside mitral paravalvular leaks.

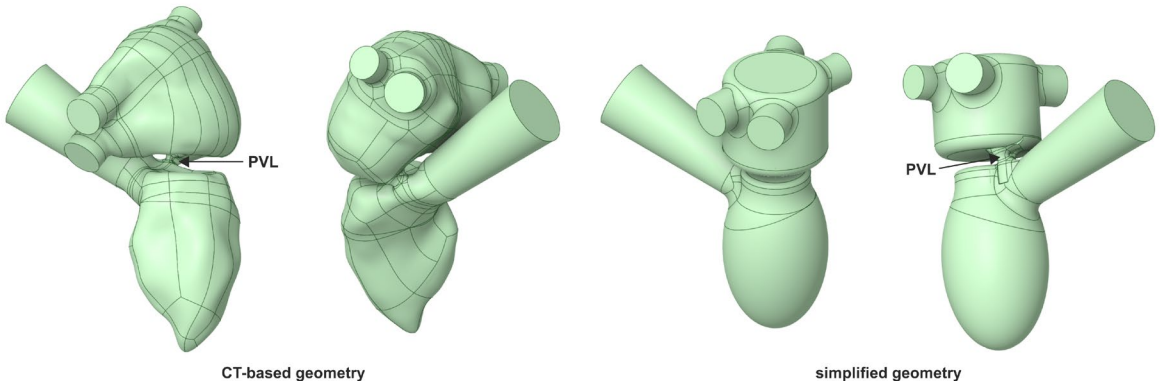

Fig. 1. Left heart geometries

The study showed that the differences between “simple” and “complex” approach are not significant, and the use of simple model and static mesh can be considered justified in the PVL setting. This means that simplification of left heart geometry can be used in further research and has potential in the future to be applied by clinicians in day-to-day medical diagnostics. Especially since it seems rather difficult (and very expensive) to model the whole patient's heart in a feasible time frame. Regarding the PVL, the area of high shear stress values occurs only near the walls of the PVL-ventricle junction. The shape of this connection (PVL entry) is considered to have a significant effect on the risk of hemolysis.

Acknowledgements

This study was funded by the BIOTECHMED-3 project granted by the Warsaw University of Technology under the program, Excellence Initiative: Research University.

References

[1] Ionescu A., Prevalence and Clinical Significance of Incidental Paraprosthetic Valvar Regurgitation: A Prospective Study Using Transoesophageal Echocardiography, *Heart*, 2003, *89*, 1316–1321.
[2] Cruz-Gonzalez I., Rama-Merchan J.C., Calvert P.A., Rodríguez-Collado J., Barreiro-Pérez M., Martín-Moreiras J., Diego-Nieto A., Hildick-Smith D., Sánchez P.L., Percutaneous Closure of Paravalvular Leaks: A Systematic Review, *J. Interv. Cardiol.*, 2016, *29*, 382–392.
[3] Nevaril C.G., Lynch E.C., Alfrey C.P., Hellums J.D., Erythrocyte Damage and Destruction Induced by Shearing Stress, *J. Lab. Clin. Med*. 1968, 71, 784–790.
[4] Garcia M.J., Vandervoort P., Stewart W.J., Lytle B.W., Cosgrove D.M., Thomas J.D., Griffin B.P., Mechanisms of Hemolysis with Mitral Prosthetic Regurgitation Study Using Transesophageal Echocardiography and Fluid Dynamic Simulation, *J. Am. Coll. Cardiol.*, 1996, 27, 399–406.
[5] Prather R., Seligson J., Ni M., Divo E., Kassab A., DeCampli W., Patient-Specific Multiscale Computational Fluid Dynamics Assessment of Embolization Rates in the Hybrid Norwood: Effects of Size and Placement of the Reverse Blalock–Taussig Shunt, *Can. J. Physiol. Pharmacol*. 2018, 96, 690–700.
[6] Wojtas K., Kozłowski M., Orciuch W., Makowski Ł., Computational Fluid Dynamics Simulations of Mitral Paravalvular Leaks in Human Heart, *Materials*, 2021, 14, 7354.
[7] Kozłowski M., Wojtas K., Orciuch W., Smolka G., Wojakowski W., Makowski Ł., Parameters of Flow through Paravalvular Leak Channels from Computational Fluid Dynamics Simulations—Data from Real-Life Cases and Comparison with a Simplified Model, *JCM*, 2022, 11, 5355.
[8] Jędrzejczak K., Makowski Ł., Orciuch W., Model of Blood Rheology Including Hemolysis Based on Population Balance, *Commun Nonlinear Sci Numer Simul*, 2023, 116, 106802.

Lectures

S5. Forum for young researchers

IS IT STILL NANO? STUDIES OF FINE POWDER IRON NITRIDING

Aleksander Albrecht[1,2], Marcin Sadłowski, Kasturi Narasimha Sasidhar[2,3]

[1]West Pomeranian University of Technology in Szczecin, Faculty of Chemical Technology and Engineering, Piastów 42, 71-065 Szczecin, Poland
[2]Max-Planck-Institut für Eisenforschung GmbH, Max-Planck Straße 1, Düsseldorf 40237, Germany
[3]Currently at: College of Engineering, University of Wisconsin-Madison, USA
*corresponding author: aleksander.albrecht@zut.edu.pl

Multiple records suggested that the to-date knowledge gathered on bulk Fe-N materials and technology of iron nitriding process is not directly applicable to nanometric systems [1–3]. It was proved, for example, that homogeneity ranges of crystalline phases differ between coarse materials and their nano-counterparts [4]. It was also observed that values of thermodynamic parameters of phase transformations between α-Fe, γ'-Fe_4N and ε-$Fe_{3-2}N$ deviate between bulk- and nanomaterials [5]. It was proposed that the size of crystallites is another degree of freedom that should be considered and that it allows the coexistence of two phases in this system in a wider range of nitriding potentials and temperatures [6]. Nanocrystalline iron nitrides, which owe their popularity to impressive magnetic properties, are expected to become especially useful for the production of sensors and markers for medicinal use [7]. Thus, further studies on the fine details of the nitriding process are necessary.

Fine powder iron samples, different in terms of morphology and crystallite size, were subjected to gaseous nitriding at 400 °C. In situ analyses performed in an Anton Paar XRK 900 reaction chamber attached to a PANalytical X'pert Pro MPD powder diffractometer were compared with results from thermogravimetric studies (Linseis STA PT1600). During reactions, the values of nitriding potential were stepwise increased after reaching quasi-stationary state in previous step. Additional electron microscopy studies (FEI Tecnai G2 F-20 S TWIN) were conducted to support the findings.

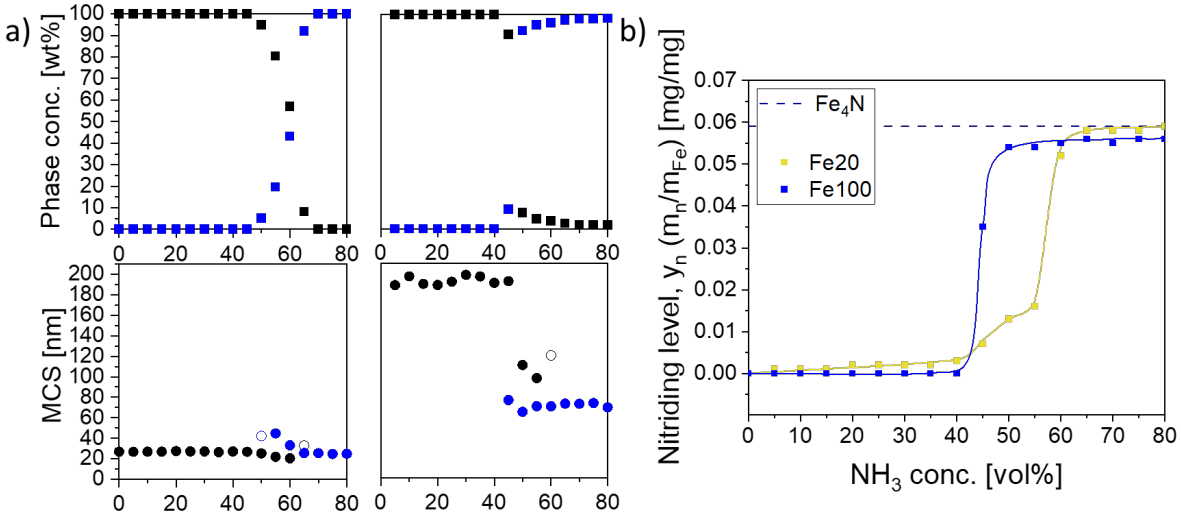

Fig. 1. The results of in situ a) XRPD and b) TG analyses of fine powder iron nitriding

The mean crystallite size, crystalline phase fraction, lattice parameter and nitriding level changes during α-Fe to γ'-Fe_4N phase transformation were determined (Figure 1). The dependence of the thermodynamics of the process on the crystallite size was experimentally proved. An explanation of different mechanisms of nitriding in bulk and nanometric systems is proposed in

analogy to the research done in a metal-hydrogen system [8]. Differences between elastic and plastic accommodation of transformation-related stress were pointed out. Experimental results and calculations allowed to estimate the critical value of the crystallite size, at which the material stops behaving like a bulk and shows phenomena observed for nanostructures.

Acknowledgements
This research was funded by the Polish Ministry of Education and Science, grant number DI2018003348. A. A. would like to thank NAWA Poland for the scholarship financed as a part of the NAWA Bekker Programme, project no. BPN/BEK/2021/1/00349. A. A. is thankful to Krzysztof Sielicki and Iwona Pełech from WPUT in Szczecin for aid with TEM measurements, and to Dariusz Moszyński for supervision.

References

[1] Nishimaki K., Ohmae S., Yamamoto T.A., Katsura M., Formation of iron-nitrides by the reaction of iron nanopartiecles with a stream of ammonia, *NanoStruct. Mater.*, 1999, 12, 527–530.
[2] Pelka R., Arabczyk W., Studies of the Kinetics of Reaction Between Iron Catalysts and Ammonia - Nitriding of Nanocrystalline Iron with Parallel Catalytic Ammonia Decomposition, *Top. Catal.*, 2009, 52, 1506–1516.
[3] Tong W., He C., He J., Zuo L., Tao N., Wang Z., Strongly enhanced nitriding kinetics by means of grain refinement, *Appl. Phys. Lett.*, 2006, 89, 021918.
[4] Wohlschlögel M., Welzel U., Mittemeijer E.J., Unexpected formation of e iron nitride by gas nitriding of nanocrystalline a-Fe films, *Appl. Phys. Lett.*, 2007, 91, 141901.
[5] Moszyński D., Moszyńska I., Arabczyk W., The transformation of a-Fe into γ'-Fe4N in nanocrystalline Fe-N system: Influence of Gibbs-Thomson effect, *Appl. Phys. Lett.*, 2013, 103, 253108.
[6] Arabczyk W., Ekiert E.A., Pelka R., Hysteresis phenomenon in a reaction system of nanocrystalline iron and a mixture of ammonia and hydrogen, *Phys. Chem. Chem. Phys.*, 2016, 18, 25796–25800.
[7] Rajaji U., Muthumariyappan A., Chen S.-M., Chen T.-W., Ramalingam R.J., A novel electrochemical sensor for the detection of oxidative stress and cancer biomarker (4-nitroquinoline N-oxide) based on iron nitride nanoparticles with multilayer reduced graphene nanosheets modified electrode, *Sensors and Actuators B: Chemical*, 2019, 291, 120–129.
[8] Syrenova S., Wadell C., Nugroho F.A.A., Gschneidtner T.A., Diaz Fernandez Y.A., Nalin G., Świtlik D., Westerlund F., Antosiewicz T.J., Zhdanov V.P., Moth-Poulsen K., Langhammer C., Hydride formation thermodynamics and hysteresis in individual Pd nanocrystals with different size and shape, *Nature Materials*, 2015, 14, 1236–1244.

PARTICLE IMAGE VELOCIMETRY OF 3D-PRINTED ANATOMICAL BLOOD VASCULAR MODELS AFFECTED BY ATHEROSCLEROSIS

Arkadiusz Antonowicz[1,2], Krzysztof Wojtas[3], Łukasz Makowski[4], Wojciech Orciuch[5], Michał Kozłowski[6]

[1]Eurotek International Sp. z o.o., Skrzetuskiego 6, 02-726 Warsaw, Poland
[2,3,4,5] Faculty of Chemical and Process Engineering, Warsaw University of Technology, Waryńskiego 1, 00-645 Warsaw, Poland
[6] Department of Cardiology and Structural Heart Diseases, Medical University of Silesia, Ziołowa 47, 40-635 Katowice, Poland
*corresponding author: lukasz.makowski.ichip@pw.edu.pl

ABSTRACT

The study of biomedical fluid dynamics in complex geometries with mechanical inaccessibility using non-intrusive visualizing methods on a micro-scale has become possible using a proper 3D printing process. The computed tomography scan of a patient with atherosclerosis was processed, and a 3D-printed artery with an inlet diameter of 4.2 mm was developed and measured using three different constant flow rates. In this work, the flow of glycerin and water solution was studied. Sodium iodide (NaI) was used to adjust the refractive index (RI) of the solution to that of the 3D printed object for reduction of optical distortions, and xanthan gum (XG) was added to the fluids to give them non-Newtonian properties. Results of Particle Image Velocimetry (PIV) are comparable with computational fluid dynamics (CFD) with the same conditions. This work presents the results of PIV as multi-stitched, color-coded vector maps from the axis cross-section along the whole 3D-printed biomedical model. Furthermore, the results of the stitched 16 base images of the artery and the 3D-printed model were included. The results of this study show that 3D prints allow the creation of any desired geometry.

1. Introduction

Particle Image Velocimetry is a well-known measurement technique that allows to obtain instantaneous velocity vector maps in a cross-section of the flow in a non-intrusive way. Studies of flows within the human body, especially those within the circulatory system, have attracted significant interest in recent years. New knowledge obtained from this research field may improve the prevention, detection, or even treatment of dangerous pathologies occurring in the human body. The main challenges of the use of PIV results for CFD validation in complex models are difficulties to fabricate transparent models, that are possible to be described numerically. One of the methods might be the silicone model [1], but 3D printing seems to be a more available technique [2]. Another challenge is to find a compromise between a right refractive index matched of a transparent resin and the transparent fluid with the required parameters [3]. The experimental results might be compared with CFD simulations for the same conditions.

2. Methodology

Geometries of printed models were obtained via Computer Tomography of a patient with atherosclerosis. The geometry was modified by adding a necking to simulate atherosclerosis. The considered geometry is that of one artery with a diameter of about 4 mm. The model was printed on a 3D-printer from FormLabs using transparent resin. After printing, the model was cleaned of residual resin using isopropanol and distilled water, dried, UV radiation cured, and polished on the outer walls. The refractive index of the prepared object was measured with a refractometer. A solution of distilled water and glycerin allows to obtain proper viscosity which substituted blood, adding sodium iodide allows to maintain appropriate refractive index as 3D-printed object, xanthan

gum makes the solution with non-Newtonian properties. In addition, the solution containing sodium iodide underwent oxidation which led to a yellowing of the solution. To prevent or undo this process sodium thiosulfate can be used. A fluorescent rhodamine-B-labeled poly(methyl methacrylate) particles with a mean diameter of 10 μm were used as seedling particles. Measurements with the solution were performed as a closed loop using a syringe pump with constant flow rate.

PIV experiments were conducted using a PIV system based on a double-pulsed 532 nm laser with a <10 ns pulse duration and a double-frame camera was used with a resolution of 2048 × 2048 pixels, a 7.4 μm pixel size, and a 12-bit pixel depth. For camera optics, a microscope with a view of 4.85 x 4.85 mm2 with a long-pass filter that blocked <550 nm light was used. Everything was managed using DynamicStudio v7 fluid measurement software and the synchronization unit. The 3D-printed object was placed horizontally on an XYZ translation stage with a micrometer screw that allowed the object to be accurately positioned in relation to a field-of-view (FOV) camera.

3. Results and conclusions

The results of 2D PIV measurements are presented in Fig. 1. Measurements were conducted for 3 Reynolds (Re) numbers on the inlet. The results show color-coded velocity vector maps of the entire 3D-printed vessel. The connections between consecutive images were seamless and consistent. We observed that the velocity values increased proportionally, while the structure changed typically and as expected. No boundary defects were noticed. Everything can be compared with CFD results.

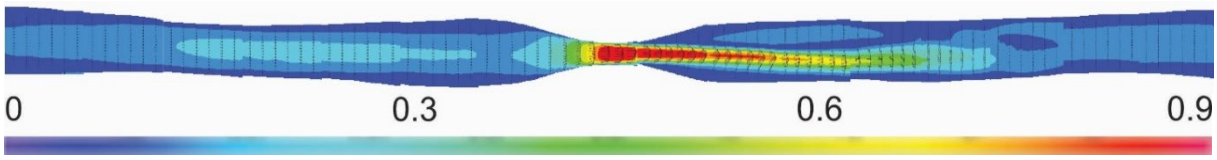

Fig. 1. Vector statistics and velocity magnitudes (m/s) along the whole blood vessel for Re = 72

This study aimed to find the best solution when using 3D printing technology to measure the geometry data of numerically indescribable objects. The methodology indicates the great potential of 3D printing technology and material for printing difficult geometries. The ability to obtain comparable refractive indices of the material and fluid is extremely important.

One of the disadvantages of using a resin material for 3D printing is the relatively high refractive index (which is approximately 1.5 and is impossible to obtain with only a glycerin and water solution). Sodium iodide or other similar additives are required to maintain the RI of 3D-printings. In addition, the calibration tool has to be custom-designed and, even better, certified.

Further work should aim to measure longer flow periods and flows for larger Re numbers for some geometries. We plan to apply our findings in future studies that will include measurements of paravalvular leaks in the human heart. Hence, future work with time-resolved PIV is planned to understand the true nature of the flow in natural heart pulse conditions and a stereoscopic microscope for Stereo μPIV analysis since 2D measurement cannot explain the behavior of 3D flows.

Acknowledgment

This study was funded by the BIOTECHMED-1 and BIOTECHMED-3 projects granted by the Warsaw University of Technology under the program Excellence Initiative: Research University.

References

[1] Triep M., Hess D., Chaves H., Brücker C., Balmert A., Westhoff G., Bleckmann H., 3D Flow in the Venom Channel of a Spitting Cobra: Do the Ridges in the Fangs Act as Fluid Guide Vanes?, *PLoS ONE*, 2015, 8, e61548

[2] Aycock K., Hariharan P., Craven B., Particle image velocimetry measurements in an anatomical vascular model fabricated using inkjet 3D printing, *Exp. Fluids*, 2017, 58, 11, article id.154, 8 pp

[3] Ho W.H., Tshimanga I.J., Ngoepe M.N., Jermy M.C., Geoghegan P.H., Evaluation of a Desktop 3D Printed Rigid Refractive-Indexed-Matched Flow Phantom for PIV Measurements on Cerebral Aneurysms. *Cardiovasc. Eng. Technol.*, 2020, 11, 14–23.

PRODUCTION, CHARACTERIZATION AND APPLICATIONS OF HYBRID NANOSTRUCTURES BASED ON MOLYBDENUM DISULFIDE AND CARBON NANOMATERIALS

Zuzanna Bojarska*, Marta Mazurkiewicz-Pawlicka, Łukasz Makowski

Faculty of Chemical and Process Engineering, Warsaw University of Technology, Warsaw, Poland
*corresponding author: zuzanna.bojarska@pw.edu.pl

Due to the changing climatic conditions that directly and indirectly affect human life, European Union (UE) has started the fight against greenhouse gas emissions. UE has an ambitious plan to achieve climate neutrality by 2050, along with an interim emission reduction target of 55% by 2030. For this purpose, investments in renewable energy, energy efficiency, or other clean, low-carbon technologies are made. Among renewable energy technologies, hydrogen has been distinguished as the fuel of the future. In the political and business environment, clean hydrogen is gaining unprecedented momentum. Nowadays, hydrogen is mainly produced from natural gas, obtaining grey and blue types. The new paradigm is to obtain hydrogen using renewable energy sources (RES), a green attempt. Accompanying water splitting with RES is a promising way to obtain a sustainable and balanced energy economy.

However, the high cost and/or insufficient efficiency of the aforementioned technologies limit the usability of green hydrogen. Meeting the market requirements, novel, low-cost, and accessible catalysts for hydrogen production are sought. Herein, molybdenum disulfide (MoS_2) can be distinguished as a promising option. MoS_2 is an exciting example of a two-dimensional material due to its low toxicity, relatively low cost, and electrochemical activity. In addition, MoS_2 nanoparticles (NPs) have been considered a noteworthy alternative for widely used but expensive platinum. The use of MoS_2-based catalyst for hydrogen evolution reaction (HER) in water splitting may be a way to lower the cost of green hydrogen production.

The transition period between the common usage of green hydrogen and the present time, which according to the EU, is approximately 20–30 years, requires focusing on current transportation issues, one of which is to limit engine exhaust emissions. Nowadays, specialists propose the use of electric and hybrid vehicles. Yet, their prices prevent their fast exchange with combustion engine cars. The solution for the above problem may be fuel and oil additives that extend engine lifetime and mitigate the negative effects on the environment. MoS_2 has also found its application for these purposes. Owing to its layered structure, MoS_2 is considered an excellent lubricant. The addition of MoS_2 to engine oil significantly enhanced its tribological and rheological properties, thus improving engine combustion conditions and reducing emissions.

Certainly, MoS_2 is a material with unique properties, with the potential to be used in many fields, not only for hydrogen production and lubricant additives. However, the obstacle to overcome is that MoS_2 changes its properties with the particle size. In both applications, better results are obtained for NPs. There are many methods to reduce the size of MoS_2. An interesting approach is adding carbon nanomaterials (CNMs) while synthesizing molybdenum disulfide forming hybrid nanostructures – MoS_2/CNMs. Adding carbon nanomaterials during MoS_2 precipitation results in decreased particle size and expanded surface area.

There are many methods to produce hybrid nanostructures. Nevertheless, most of them are not scalable and/or associated with high technological costs, which causes problems with the widespread use of these materials. Designing a scalable and low-cost production method would allow further development of these materials and their applications. Moreover, due to the variety of uses of these materials, which require different characteristics, their production method should make it possible to control the properties of the obtained particles. Therefore, one method would allow the preparation of hybrid nanostructures for advanced applications such as catalysis and more vast fields, such as lubricants.

In this study, wet chemical synthesis was used for preparing hybrid nanostructures based on MoS_2 and CNMs, such as graphene oxide, reduced graphene oxide, and carbon nanotubes. The foreign substance present in the supersaturated solution reduces the nucleation energy, so heterogeneous nucleation occurs earlier than homogeneous. In this way, the surface of CNMs is covered with MoS_2 NPs. Wet chemical synthesis can be carried out in commonly used tank reactors, but also in impinging jet reactors. The latter, in particular, are suitable for the controlled production of such particles. High mixing intensity is related to the formation of an area with a high energy dissipation rate in the contact zone of the inlet streams. This allows to obtain materials with the desired and repeatable properties in an inexpensive, continuous, and easy to scale way. The direct product of the synthesis is an amorphous MoS_2 deposited on the CNMs surface [1]. To remove by-products, further purification and annealing need to be performed. Two temperatures of annealing were applied [2]. The lower temperature maintains the amorphous form, and the second temperature gives MoS_2 crystals (Fig. 1). A comprehensive physicochemical analysis of the obtained materials was conducted, using various analytical techniques: particle size distribution, thermogravimetric analysis, X-ray diffraction, and scanning electron microscopy.

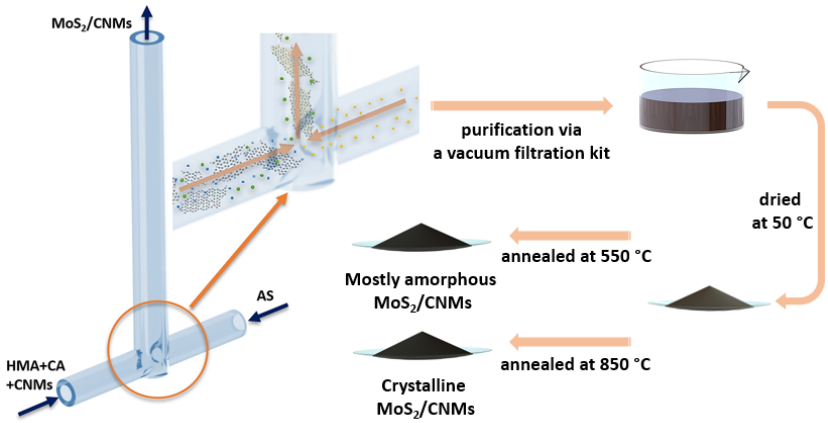

Fig. 1. Preparation of MoS_2/CNMs using the impinging jet reactor

Due to the potential application of materials based on MoS_2 in the HER catalysis and energy storage, linear sweep voltammetry and cyclic voltammetry of the synthesized materials were performed using a three-electrode system. The maximum current density obtained at a potential of 0.2 V vs. RHE for the best hybrid sample was 16 times higher than in the case of pure MoS_2 [3]. Furthermore, MoS_2 is commonly used as a lubricant. Therefore, it was checked how hybrid nanostructures affected the lubricating properties of engine oil [4]. Studies of the size distribution of particulate matter in the engine exhaust gas showed that the use of oil with the addition of MoS_2/CNMs allowed to reduce the total volume of particulate matter in the exhaust gas by 91% and 49% under idling conditions and with load compared to work with the base oil.

Acknowledgments: This work was supported by the National Science Centre [2021/41/N/ST8/03764]

References

[1] Bojarska Z., Mazurkiewicz-Pawlicka M., Gierlotka S., Makowski Ł., Production and properties of molybdenum disulfide/graphene oxide hybrid nanostructures for catalytic applications, *Nanomater.*, 2020, 10(9), 1865.
[2] Wojtalik M., Bojarska Z., Makowski Ł., Experimental studies on the chemical wet synthesis for obtaining high-quality MoS_2 nanoparticles using impinging jet reactor, *J. Solid State Chem.*, 2020, 285, 121254,
[3] Bojarska Z., Mazurkiewicz-Pawlicka M., Mierzwa B., Płociński T., Makowski Ł,. Effect of the carbon support on MoS_2 hybrid nanostructures prepared by an impinging jet reactor for hydrogen evolution reaction catalysis. *J. Environ. Chem. Eng.*, 2022, 10(4), 108038.
[4] Bojarska Z., Kopytowski J., Mazurkiewicz-Pawlicka M., Bazarnik P., Gierlotka S., Rożeń A., Makowski Ł., Molybdenum disulfide-based hybrid materials as new types of oil additives with enhanced tribological and rheological properties, *Tribol. Int.,* 2021, 160, 106999.

PREPARATION OF REDUCED GRAPHENE OXIDE USING SUPERCRITICAL CARBON DIOXIDE FOR APPLICATION IN OXYGEN REDUCTION CATALYSTS

Piotr Cendrowski, Marta Mazurkiewicz-Pawlicka, Zuzanna Bojarska, Monika Jałowiecka, Jan Krzysztoforski*

Faculty of Chemical and Process Engineering, Warsaw University of Technology, Waryńskiego 1, 00-645 Warsaw, Poland

*corresponding author: jan.krzysztoforski@pw.edu.pl

In recent years, the development of novel materials for construction of fuel cells has gained much interest due to rapidly evolving energy policies. One of the key challenges is to find a suitable support for oxygen reduction reaction (ORR) catalysts, which can be present in the form of metallic nanoparticles. The support should meet several specific requirements, such as high purity, specific surface area, electrical conductivity and hydrophobicity. For example, hydrophobicity promotes the removal of water, produced during fuel cell operation, from the surface of ORR catalysts, resulting in lower mass transfer resistance and increased electrode performance. One group of promising ORR catalyst support materials are carbon nanomaterials, e.g. reduced graphene oxide (rGO), which is obtained by oxidation of graphite – forming graphene oxide (GO) – and subsequent thermal or chemical reduction of GO to rGO. However, the performance of standard rGO as ORR catalyst support is lower than in the case of carbon nanotubes (CNTs). On the other hand, it has been demonstrated that treatment with supercritical fluids (SCFs), especially supercritical carbon dioxide ($scCO_2$), can modify the properties of various carbon nanomaterials. Therefore, the aim of this study was to investigate the effect of applying treatment with $scCO_2$ during preparation of rGO suitable as a material for ORR catalyst supports.

In the work, two rGO preparation methods were investigated: preparation of standard rGO through graphite oxidation and subsequent reduction of GO to rGO at ambient pressure, followed by treatment of rGO with $scCO_2$ (method I) or integration of the GO reduction step with the $scCO_2$ treatment (method II). For both methods, GO was synthetized using the modified Hummers' method. Thermal or chemical reduction (hydrazine or ascorbic acid in method I and ethanol or ascorbic acid in method II) of GO to rGO was considered. Different sets of $scCO_2$ treatment pressure, temperature and duration were tested using a lab-scale high pressure system. The resulting materials were investigated using various analytical procedures, including FTIR, TGA and elemental analysis. Standard, untreated rGO was used as the reference material.

The level of reduction of GO was tested in all applied methods. The most reduced material for method I was the hydrazine treated sample, and the ascorbic acid treated sample for method II. The value of pressure used in experiments visibly influenced the properties of obtained materials, including an increase in the specific surface area, while the effect of temperature and process time was significantly weaker. The samples which had undergone $scCO_2$ treatment showed transition from hydrophilic to hydrophobic. Another positive effect observed in the experiment was further purification of GO from residues of reduction agents (or even reagents from GO production), when exposed to $scCO_2$. The results obtained using method II confirmed that GO reduction to rGO and treatment with $scCO_2$ can be performed in one step, in an integrated manner.

The study proved that $scCO_2$ treatment of standard rGO (method I) or simultaneous GO reduction to rGO with $scCO_2$ treatment (method II) are effective processes for improving properties of rGO for its application as ORR catalyst support, especially in terms of development of the specific surface area, removal of impurities and increase in hydrophobicity. The $scCO_2$ treatment process can be fine-tuned for optimization of the properties of the resultant material. The obtained materials will undergo further examination by testing them as ORR catalyst supports.

ENZYME CO-IMMOBILIZATION WITH POST-IMMOBILIZATION TREATMENTS

Katarzyna Czyżewska, Anna Trusek*

Group of Micro, Nano and Bioengineering, Wroclaw University of Science and Technology,
Wybrzeze Wyspianskiego 27, 50-370 Wroclaw, Poland
*corresponding author: anna.trusek@pwr.edu.pl

Biocatalysis is considered an integral part of modern technological processes related to green chemistry. Current scientific trends are focused on multi-enzymatic cascades. One-pot systems are attractive due to the possibility of using multiple enzymes in a single reactor [1]. Nowadays, enzyme co-immobilization is still essential in industrial applications because of the high cost of enzymes and the possibility of improving enzyme stability under process conditions. Enzyme co-encapsulation, similar to individual encapsulation, can be subject to enzyme leakage from the hydrogel matrix [2]. To prevent enzyme leakage, strategies of post-immobilization treatments are proposed. One is related to chemical cross-linking, which leads to additional linkages between enzyme molecules and support, resulting from the increased strength of enzyme binding within the hydrogel matrix [3].

Glucose oxidase (GOX) and catalase (CAT) are popular enzymes utilized in food processes. The cooperation between glucose oxidase and catalase is classified as a two-enzymatic cascade. In this case, catalase decomposes hydrogen peroxide, which acts as an inhibitor relative to glucose oxidase. On the other hand, oxygen generated by catalase is consumed by glucose oxidase and used as a substrate during glucose oxidation, Equations (1) and (2).

$$glucose + O_2 \xrightarrow{GOX} gluconic\ acid + H_2O_2 \quad (1)$$

$$H_2O_2 \xrightarrow{CAT} O_2 + H_2O \quad (2)$$

The presented work refers to co-encapsulating glucose oxidase and catalase into the alginate matrix with additional cross-linking with glutaraldehyde (GA) or carbodiimide (EDC). The proposed preparation was characterized under low-temperature biocatalysis (12 °C), which corresponded to milk storage and transport temperature. It can be used to reduce the excessive sweetness of lactose-free milk.

The individual encapsulation of enzymes preceded the co-encapsulation of GOX and CAT. Encapsulation of glucose oxidase in alginate was running out with enzyme leakage, in contrast to catalase encapsulation, which was characterized by high efficiency [4]. These observations emphasize the importance of post-immobilization treatment during GOX-CAT co-encapsulation.

Comparing two cross-linking strategies, with glutaraldehyde (GA) and carbodiimide (EDC), indicates better results for carbodiimide modification, which was related to improved enzyme retention, Table 1. The subsequent experiments were performed based on EDC cross-linking.

Table 1. The enzyme leakage expressed as the enzymatic activity of the reaction mixture obtained after the incubation of capsules

Type of capsules	Alginate	Alginate + GA	Alginate + EDC
Time [hours]	Glucose conversion [%]		
0	0	0	0
5.3	63.84	32.35	16.13
22	98.6	77.31	35.89

To confirm good enzymes retention in co-encapsulated preparations with EDC cross-linking, the operational stability was determined. The half-life time was calculated at 12 days. Almost complete glucose decomposition (>90%) took place in 5–7 hours. To determine the reuse of enzymes, the batch process was conducted. Co-encapsulated glucose oxidase and catalase can be used in 9 cycles preserving approximately 40% of the initial activity, Fig. 1.

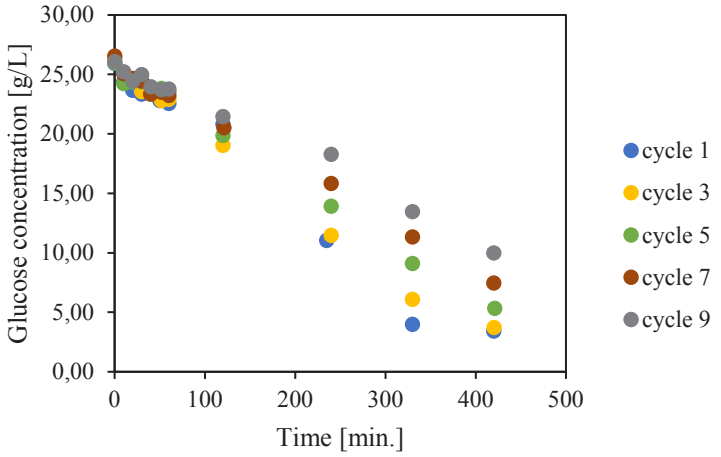

Fig. 1. The re-use of co-encapsulated glucose oxidase and catalase

Glucose decomposition catalyzed by co-encapsulated glucose oxidase and catalase at 12 °C runs according to first-order kinetics, Fig. 2 for a wide range of substrate concentrations.

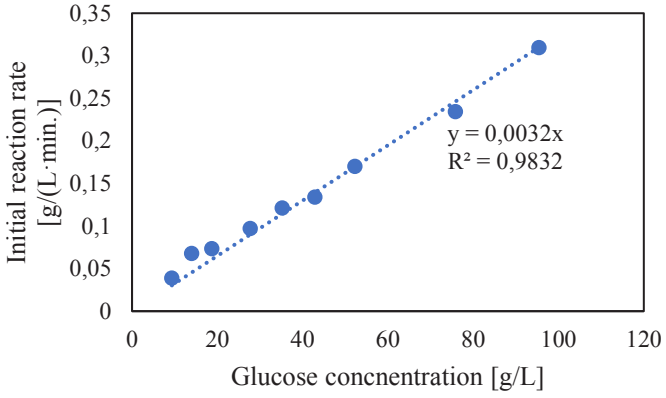

Fig. 2. The kinetics of co-immobilized glucose oxidase and catalase

The presented results show that co-encapsulated glucose oxidase and catalase in an alginate matrix with cross-linking with EDC can be considered a valuable tool in dairy biocatalysis, e.g., to produce lactose-free milk with the standard sweetness level.

References

[1] Velasco-Lozano S., Lopez-Gallego F. Wiring step-wise reactions with immobilized multienzyme systems, *Biocatal. Biotransformation*., 2017, 36(3), 184-194.
[2] Arana-Pena A., Carballares D., Morellon-Sterlling R., Berenguer-Murcia Á., Alcántara A.R., Rodrigues R.C., Fernandez-Lafuente R., Enzyme co-immobilization: Always the biocatalyst designers' choice...or not?, *Biotechnol. Adv*., 2021, 51, 107584.
[3] Labus K., Bryjak J., *Postimmobilization treatments before applications, in: Biocatalyst Immobilization. Foundations and Applications*, Ferreira M.L. (Ed.), Elsevier 2023, 55-71.
[4] Czyzewska K., Trusek A. Encapsulated Catalase from *Serratia* Genus for H_2O_2 decomposition in food applications, *Pol. J. Chem. Technol*., 2018, 20, 39-43.

EFFECT OF ELECTRONIC AND MAGNETIC INTERACTIONS BETWEEN BARIUM HEXAFERRITE AND FACETED TITANIUM DIOXIDE PARTICLES ON PHOTOCATALYTIC WATER TREATMENT

Szymon Dudziak*, Anna Zielińska-Jurek*

Department of Process Engineering and Chemical Technology, Gdansk University of Technology, G. Narutowicza 11/12, 80-233, Gdansk, Poland
*corresponding authors: dudziakszy@gmail.com, annjurek@pg.edu.pl

Photocatalytic processes present a promising but still challenging solution for water treatment from persistent organic micropollutants, such as pharmaceuticals. The main focus of the present study was the design of a suitable photocatalyst with improved degradation efficiency under solar light irradiation. Recent studies have shown that significant differences in photocatalytic activity can be achieved by alternating exposition of the specific crystal planes of TiO_2, which directly affect the behavior of photogenerated charge carriers at the surface [1–3]. Therefore, an increase in process efficiency might be achieved by controlling the morphology and nanostructure of the photocatalyst. Simultaneously, the post-separation of semiconductor nanoparticles after water treatment remains still challenging. As a possible solution, the development of magnetic photocatalysts, usually in the form of ferromagnet-photocatalyst composites, has been proposed in recent years. However, such composite materials present a rather complex case of possible electronic and magnetic interactions between both phases, which could be additionally affected by the anisotropic character of their properties. As the preparation of different nanostructured materials is progressing fast, it seems important to verify if the approach can be used to optimize ferromagnet-photocatalyst composites and to track down the source of possible effects.

In this regard, in the present study, faceted TiO_2 photocatalyst, exposing the majority of either {0 0 1}, {1 0 0} or {1 0 1} facets, combined with a suitable ferromagnetic phase, was designed and applied for degradation of organic pollutants. As the magnetic part of the composite, barium hexaferrite ($BaFe_{12}O_{19}$) was selected due to high remanent magnetization, uniaxial magnetic anisotropy, platelet character of the prepared microcrystals, and Curie temperature of approx. 450 °C [4]. This composition allowed us to achieve a relatively well-defined orientation between TiO_2 and $BaFe_{12}O_{19}$ structures and allowed easy changes between a magnetized and demagnetized state of the ferrite, with a minimal effect on crystal structure and morphology. Preparation of pure compounds was performed hydrothermally, and all materials were subject to a set of detailed structural and spectroscopic analyses. In particular, a detailed description of the magnetic and electronic properties of the $BaFe_{12}O_{19}$ sample was made before combining with TiO_2. Furthermore, 3 types of composites were prepared, depending on the TiO_2 facet exposition, by physically mixing suspensions of both materials in a solution. Combined powders were calcined at 500 °C to strengthen the connection between the phases and demagnetize $BaFe_{12}O_{19}$ particles by crossing the Curie point. Prepared composites were analyzed concerning their crystal structure and morphology, with exemplary scanning electron microscope (SEM) images shown in Figure 1, together with a scheme of idealized orientation between $BaFe_{12}O_{19}$ and faceted TiO_2. Furthermore, control samples were made by modifying the $BaFe_{12}O_{19}$ surface with an additional layer of SiO_2 in order to hinder electron transfer between the ferrite and TiO_2. The SiO_2 layer was obtained using tetraethyl orthosilicate as Si source, and the SiO_2 presence was confirmed with the combination of energy-dispersive X-ray spectroscopy (EDX), X-ray photoelectron spectroscopy (XPS) and Fourier transform infrared spectroscopy (FTIR) analyses.

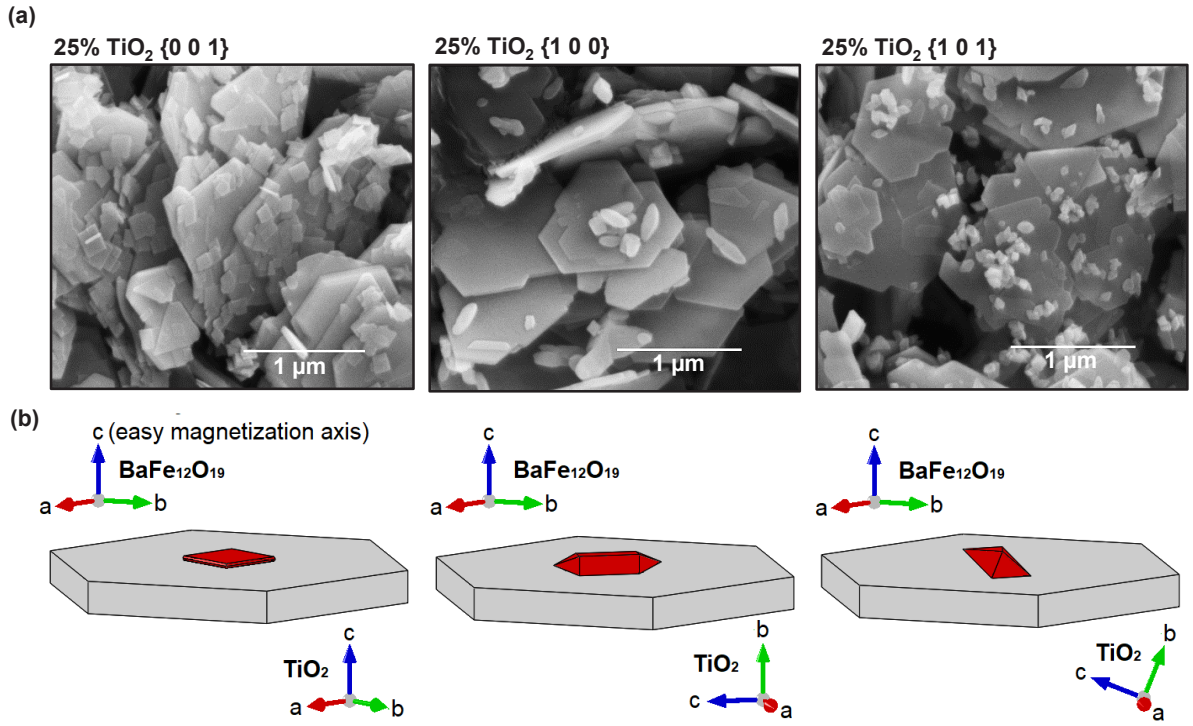

Fig. 1. (a) SEM images of the prepared $BaFe_{12}O_{19}$ composites TiO_2 nanocrystals exposing majority of different crystal facets and (b) scheme of their idealized relative orientation (TiO_2 in red)

The set of prepared composites was used for photocatalytic water treatment, using phenol as the model pollutant. All of the prepared materials showed the ability to remove phenol, together with the possible separation in the magnetic field, without significant changes in their crystalline structure. Moreover, a comparison of the results obtained using composite with magnetized $BaFe_{12}O_{19}$, demagnetized $BaFe_{12}O_{19}$, as well as $BaFe_{12}O_{19}$ covered with SiO_2 layer allowed us to separate the effect of the electronic and magnetic interactions between both phases. Remarkably, electron transfer between $BaFe_{12}O_{19}$ and TiO_2 was found to highly decrease the performance of the {1 0 1} exposing TiO_2, while the internal magnetic field of the ferrite highly promoted the activity of the {1 0 0} exposing nanostructures. Ultimately, both effects of electronic and magnetic interactions were found to depend on the exact $BaFe_{12}O_{19}$-TiO_2 combination. The overall highest activity was observed for the combination of $BaFe_{12}O_{19}$ with the {1 0 1} exposing TiO_2, when SiO_2 was introduced to prevent electron transfer.

Acknowledgments

This work was financially supported by the Polish National Science Center with grant no. NCN 2018/30/E/ST5/00845

References

[1] Kowalkińska M., Dudziak S., Karczewski J., Ryl J., Trykowski G., Zielińska-Jurek A., *Chem. Eng. J.*, 2021, 404, 126493.
[2] Dudziak S., Kowalkińska M., Karczewski J., Pisarek M., Gouveia J.D., Gomes J.R.B., Zielińska-Jurek A., *J. Phys. Chem. C*, 2022, 126, 14859-14877.
[3] Dudziak S., Kowalska E., Karczewski J., Wang K., Sawczak M., Ohtani B., Zielińska-Jurek A., *Appl. Catal. B: Environ.* 2023, 328, 122448.
[4] Pullar R.C., *Prog. Mater. Sci.* 2012, 57, 1191-1334.

DETERMINATION OF FLUID PHASE BEHAVIOUR IN LIQUID CHROMATOGRAPHY WITH CFD METHOD

B. Filip[1]*, R. Bochenek[2], D. Antos[2]

[1]Rzeszow University of Technology, Doctoral School of Engineering and Technical Sciences, Powstańców Warszawy 8, 35-959 Rzeszów, Poland
[2]Rzeszow University of Technology, The Faculty of Chemistry, Powstańców Warszawy 8, 35-959 Rzeszów, Poland
*corresponding author: d495@stud.prz.edu.pl

1. Introduction

In order to obtain elution data suitable for determining the operational window of the process and optimizing the operating variables for large-scale chromatographic purification, very small volume chromatographic columns are used in the development stage of protein chromatography. However, this technique has a downside, as the effect of extra-column volumes (ECV) enhances as the column size is reduced. It affects the shape and retention of eluted compounds and may lead to misinterpretation of retention data. This can be a cause of failure in scaling up the process from laboratory scale, in which the contribution of ECV is significant, to industrial scale, in which that contribution is negligible.

To quantify the ECV effect, both theoretical and experimental approaches were used [1]. As evidenced in previous studies, a simplified model that accounts for laminar flow distribution in a straight tube cannot reproduce correctly band shapes, particularly at higher mobile phase velocity and for elution of viscous solution. Therefore, the CFD method was used for this purpose, in which various models of the geometry of chromatographic systems were implemented; from the simplest 2D geometries to a 3D model that accounted for the curvatures of the flow paths.

2. Methods

Three model compounds were used in the experimental studies: bovine serum albumin, a monoclonal antibody as a representative of a macromolecular compound and acetone, i.e. a representative of low-molecular compounds. Phosphate buffer pH = 7 was used as the mobile phase and its flow rate was varied in the range of 0.0679-0.679 ms^{-1}.

Experiments were carried out using the Äkta chromatographic system, which consisted of a dosing loop, capillaries of various lengths connecting the UV detector and TRICORN column packed with POROS XS bed. The ANSYS software was used for formulating and discretizing the models of the system geometry. Different approximations of the ECV system were implemented, in which the geometry complexity subsequently increased as shown in Fig. 1. The number of mesh elements in the radial and axial directions was appropriately selected to control the numerical error. A non-stationary model was used for the laminar flow of multicomponent systems with typical boundary conditions such as: inlet, outlet and wall.

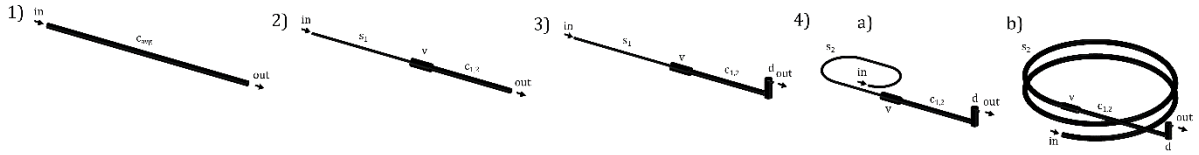

Fig. 1. An illustration of the increasing complexity of geometric systems (1, 2, 3, 4a and 4b)

3. Equations used in CFD model

The Ansys Fluent software transforms the general scalar transport equation into a numerically solvable algebraic equation using the control volume. To determine the flow behaviour of solutions in ECV, a mathematical model of the species transport, which accounted for laminar flow profile in the capillary system was used. By default, Ansys Fluent uses the dilute approximation (Fick's law)

to model mass diffusion due to concentration gradients. (1) The viscosity, density and diffusion coefficient of the protein solution were dependent on the mass fraction of the sample by means of UDFs.

$$J_i = -\rho D_{i,m} \nabla Y_i \tag{1}$$

where: $D_{i,m}$ is the mass diffusion coefficient for species i, Y_i is its mass fraction.

4. Results and discussion

4.1 Flow behaviour in ECV

2D and 3D numerical models were used to simulate band profiles of micro- and macromolecules in ECV. Typical results obtained for acetone and BSA are depicted in Figs. 2A and 2B.

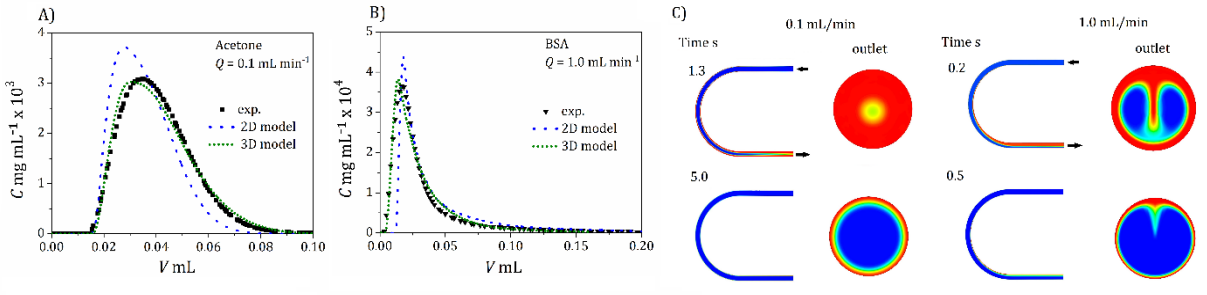

Fig. 2. Concentration profiles of acetone and BSA in ECV (A,B); flow through arc geometry (C)

The concentration profiles of the eluting compounds simulated indicate that the correct structure of the geometry of the system is of key importance for correct prediction of the retention and shape of the concentration profiles. The mass fraction contour clearly shows in curved parts of the ECV system characteristic fluid structures called as Dean vortices are formed at higher flow velocities, as shown in Fig. 2C. Those structures are induced by the secondary flows that are perpendicular to the main direction of movement of the fluid, and influence of the shape of band profiles.

4.2 Flow behaviour of viscous protein solution in the chromatographic system

Fig. 3 shows the simulations of the migration of a viscous protein solution in a chromatographic column packed with a porous bed. The viscosity of the solution is several times higher than the mobile phase, which causes the formation of finger-shaped structures. Those characteristic patterns arise in porous zones known as the Saffman-Taylor instabilities. They occur when the more viscous fluid is replaced with the less viscous one. The CFD model developed in this study allowed to reproduce the resulting band profiles of the model compounds.

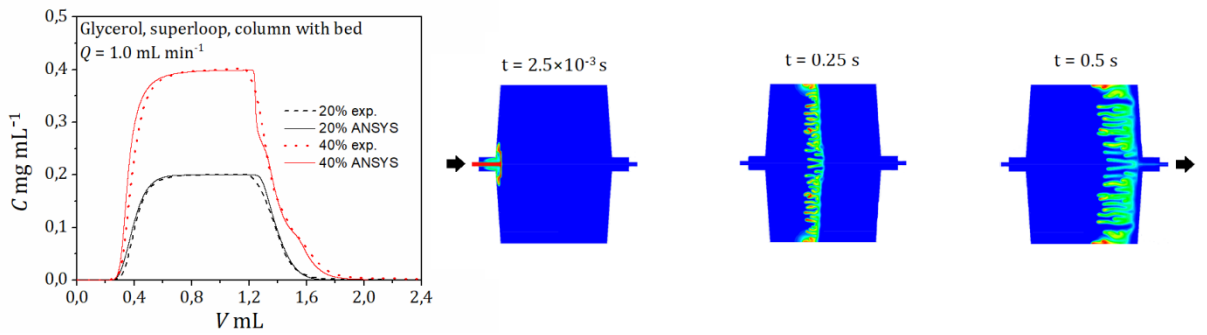

Fig. 3. Mass fraction band profiles and contours of viscous solution flowing through the column

References

[1] Baran K., Marek W.K., Piątkowski W., Antos D., *Effect of flow behavior in extra-column volumes on the retention pattern of proteins in a small column*, *J. Chromatogr. A*, 2019, 1598, 154–162.

IMPACT OF THERMAL WAVES ON CARBON DIOXIDE CAPTURE EFFICIENCY IN A HYBRID FIXED-BED REACTOR

Marcin Gunia*, Julia Ciećko, Katarzyna Bizon

Faculty of Chemical Engineering and Technology, Cracow University of Technology,
Warszawska 24, 31-155 Kraków, Poland
*corresponding author: marcin.gunia@doktorant.pk.edu.pl

Carbon dioxide capture and storage (CCS) using solid sorbents [1] is today not only a powerful measure to minimize anthropogenic CO_2 emissions, but can also be integrated with the concept of Power-to-Gas (PtG). Following the PtG idea, CO_2 can be converted to CH_4 by reaction with renewable H_2 derived from electrolysis [2]. One possibility is to conduct both processes, i.e. CO_2 capture and methanation, in a single, layered, apparatus, also referred to as a hybrid, fixed-bed reactor.

This study reports on the impact of bed structure and process thermal effects on the performance of adsorption stage. Analysis was conducted using a 1D model of a bed consisting of alternating layers of adsorbent and catalyst (Fig. 1). The main simplifying model assumptions were: negligible pressure drop, constant gas velocity, and gas-phase obeying the ideal gas law. Given these assumptions, the mass balance of component *i* in the gas phase is:

$$\left(\varepsilon_{t,ads}f_{ads} + \varepsilon_{t,cat}f_{cat}\right)\frac{\partial C_i}{\partial t} = \varepsilon_b D_{ax}\frac{\partial^2 C_i}{\partial x^2} - u\frac{\partial C_i}{\partial x} - \rho_{b,ads}f_{ads}\frac{\partial q_i}{\partial t} \tag{1}$$

with the mass transfer in the solid phase described by the linear driving force (LDF) model:

$$\frac{\partial q_i}{\partial t} = k_i(q_i^* - q_i) \tag{2}$$

and the equilibrium concentration q_i^* in the solid phase given by the Toth model for zeolite 13X [3]:

$$q_i^* = \frac{ap_i}{[1+(bp_i)^\tau]^{1/\tau}} \text{ where } a = a_0 exp\left(\frac{E}{T}\right),\ b = b_0 exp\left(\frac{E}{T}\right),\ \tau = \tau_0 + \frac{c}{T} \tag{3}$$

The energy balance for the gas and solid phases inside the column is expressed by the equation:

$$\begin{aligned}\left[\left(\varepsilon_{t,ads}f_{ads} + \varepsilon_{t,cat}f_{cat}\right)\rho_g c_g + \rho_{b,ads}f_{ads}\left(c_{s,ads} + c_{ads}\right) + \rho_{b,cat}f_{cat}c_{s,cat}\right]\frac{\partial T}{\partial t} = \\ = K_{ax}\frac{\partial^2 T}{\partial x^2} - u\rho_g c_g\frac{\partial T}{\partial x} - \rho_{b,ads}f_{ads}\sum\left(-\Delta H_{ads,i}\right)\frac{\partial q_i}{\partial t}\end{aligned} \tag{4}$$

For the sake of simplicity, constant average values of ρ_g and c_g were adopted. The same applies to the adsorbed phase heat capacity c_{ads} and the heat of adsorption $-\Delta H_{ads}$, with the latter determined using the Clausius-Clapeyron equation. The axial dispersion D_{ax} coefficient was calculated based on the expression proposed in Ref. [4], while the effective thermal conductivity K_{ax} was determined from the formula accounting both for solid, stagnant (film) and flowing gas contributions [5].

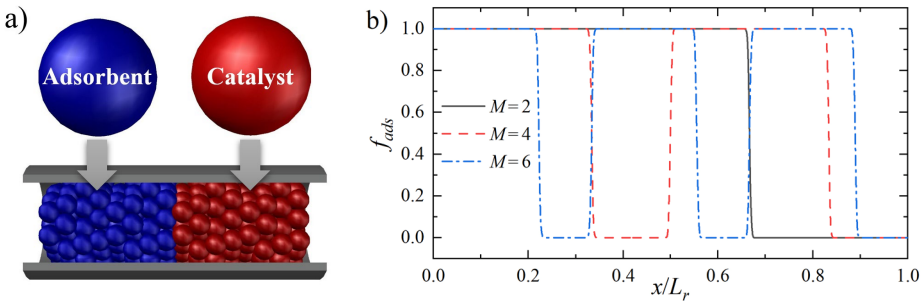

Fig. 1. Conceptual illustration of the hybrid fixed-bed with two layers (a) and distributions of adsorbent fractions (*M* denotes the total number of adsorbent and catalyst layers) used in simulations (b)

The model equations (1)–(4) were discretized using the method of lines and solved in MATLAB using the *ode23tb* solver. Simulations were conducted until the bed breakthrough time t_b defined as the instant at which $y_{CO2,out}/y_{CO2,in} = 0.01$. The main parameter values employed in the simulations are given in Table 1. Moreover, it was assumed that the volume ratio of adsorbent to catalyst particles was 2:1, and calculations were made for three bed configurations characterized by such a ratio and consisting, respectively, of $M = 2$, 4 and 6 total layers (Fig. 1b).

Table 1. Values of key parameters used in the simulations

Parameter	Value	Parameter	Value	Parameter	Value
L_r	1 m	d_p	10^{-3} m	a_0	$6.509 \cdot 10^{-3}$ mol/(kg·kPa)
u	0.2 m/s	$\rho_{p,ads}$	1085 kg/m^3	b_0	$4.884 \cdot 10^{-4}$ 1/kPa
$y_{CO2,in}$	0.05	$\rho_{p,cat}$	2355 kg/m^3	c	3.805·10 K
T_{in}	300 K	$-\Delta H_{ads,CO2}$	$3.898 \cdot 10^{-4}$ J/mol	τ	$7.487 \cdot 10^{-2}$

Fig. 2 shows results of numerical studies obtained for the bed consisting of two layers of the adsorbent and two layers of catalyst (treated as inert during the adsorption step) and corresponding values of adsorbed CO_2 (Fig. 2b). The catalyst sandwiched between the adsorbent (Fig. 2a) acts as a heat sink and is the source of the formation of characteristic temperature waves that have a beneficial effect on the process performance. This is confirmed by the global values of adsorbed CO_2 for different configurations and corresponding values of the breakthrough time: $Q_{CO2} = 1.014$ mol/kg and $t_b = 1486$ s for $M = 6$, $Q_{CO2} = 0.916$ mol/kg and $t_b = 1341$ s for $M = 4$, and $Q_{CO2} = 0.772$ mol/kg and $t_b = 1129$ s for $M = 2$. The results show that proper tailoring of the bed can be an excellent tool for controlling temperature profiles and, consequently, the performance of the apparatus and thus its optimization. It is expected that a similar synergistic effect resulting from an appropriate bed structure will also allow to control temperature profiles along the bed, and thus CO_2 desorption, at the following methanation stage. Such a tailor-made structure is particularly important from the viewpoint of running the flexible-load process.

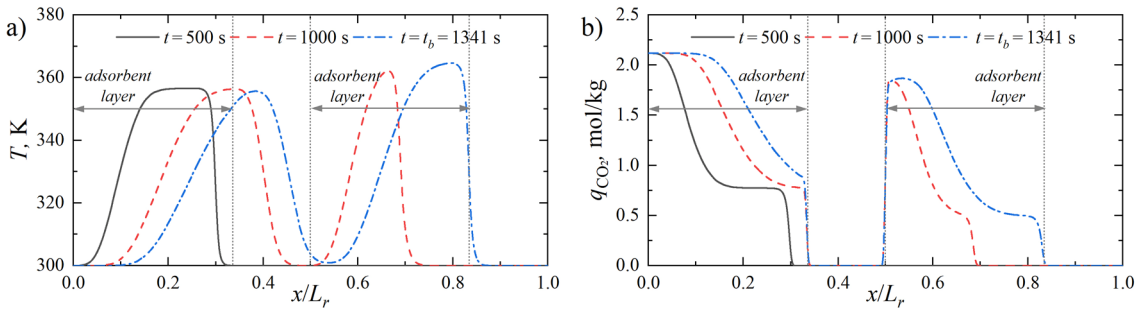

Fig. 2. Temperature profiles along the hybrid fixed-bed (a) and the adsorbed amount of CO_2 (b) for $M = 4$

Acknowledgements: The research was financed by the Polish National Science Centre, project no. UMO-2021/42/E/ST8/00313.

References

[1] Dhoke C., Zaabout A., Cloete S., Amini S., Review on reactor configurations for adsorption-based CO_2 capture, *Ind. Eng. Chem. Res.*, 2021, 60, 3779-3787.
[2] Herrmann F., Grünewald M., Meijer T., Gardemann U., Feierabend L., Riese J., Operating window and flexibility of a lab-scale methanation plant, *Chem. Eng. Sci.*, 2022, 254, 117632.
[3] Wang Y., LeVan M.D., Adsorption equilibrium of carbon dioxide and water vapor on zeolites 5A and 13X and silica gel: Pure components, *J. Chem. Eng. Data*, 2009, 54, 2839–2844.
[4] Wakao N., Funazkri T., Effect of fluid dispersion coefficient on particle-to-fluid mass transfer coefficients in packed beds, *Chem. Eng. Sci.*, 1978, 33, 1375–1384.
[5] Yagi S., Kunii D., Endo E., Heat transfer in packed beds through which water is flowing, *Int. J. Heat Mass Transfer*, 1964, 7, 333–339.

MASS TRANSFER INTENSIFICATION BY DEVELOPING NEW FLOW FIELD DESIGNS IN A DIRECT FORMIC ACID FUEL CELL

Monika Jałowiecka*, Zuzanna Bojarska, Artur Małolepszy, Łukasz Makowski

Warsaw University of Technology, Faculty of Chemical and Process Engineering, Waryńskiego 1, 00-645 Warsaw, Poland
*corresponding author: monika.jalowiecka.dokt@pw.edu.pl

Fuel cells are electrochemical devices that allow more efficient energy generation (with a 40–60% efficiency) while reducing harmful gas emissions. Direct liquid fuel cells are the subtype of polymer membrane fuel cells (PEMFCs) fed by liquid fuels, characterised by lower cost of storage and transportation than hydrogen. In this group of fuels, formic acid appears to be an environmentally friendly, non-toxic chemical of 26.4% higher volume energy density than hydrogen compressed to 700 bars [1]. Formic acid exhibits lower crossover through the nafion membrane [2] and oxidises effectively at 30 °C [3], leading to higher power densities and lower operational costs. However, mass transfer towards the reaction surface, placed at the bottom of the porous electrode structure, has to be intensified to take full advantage of the benefits of this liquid fuel. The flow regime encountered in fuel cells is laminar, characterised by a slow diffusion mechanism in the mass transport process, limiting the maximum power of the fuel cell. Increasing the contribution of a convection mechanism is crucial for increasing the reagent concentration at the reaction surface, consequently widening the range of attainable power densities. Mass transport intensification in fuel cells can be achieved by changing the geometry of the single flow channel or by modification of the whole channel arrangement of the distribution system, which is milled in graphite plates used as current collectors in fuel cells.

The following research combines these two strategies, aiming to i) enhance mass transport by the implementation of baffles to the flow channel structure and ii) propose a new flow pattern providing more uniform flow distribution across the system as well as better mixing conditions. Numerical modelling using computational fluid dynamics (CFD) was applied to prototype and predict the influence of geometrical modifications of the system on the mass transfer conditions.

In the first approach, right-angled trapezoidal baffles were introduced at the anode side of the DFAFC. Formic acid concentration distribution at the reaction surface was compared with that attained for the standard serpentine system without any baffles. Simulations revealed a significant improvement in the fuel supply to the reaction zone. Experimentally determined current-voltage characteristics for the DFAFC (Fig. 1) showed that the baffle implementation led to an even 8-fold increase of maximum power density compared to the standard serpentine system [4].

In further research, the serpentine flow pattern was replaced by a mesh of intermixing channels with a distinguished distributor and collector zone to provide uniform flow distribution. The proposed flow field is characterised by the greater contact area of the flow with the porous electrode, increasing the utilisation of the catalyst layer in the system. The most promising flow fields were selected for further experimental testing based on the CFD simulations predictions and residence time distribution analysis to evaluate the mixing conditions in the system.

The following study presents a complex approach to designing a reagent distribution system in DFAFC, considering baffle implementation in the channel and flow field assessment by 3D CFD simulations of the flow and reaction at the anode side, together with residence time distribution analysis and experiments performed on DFAFC.

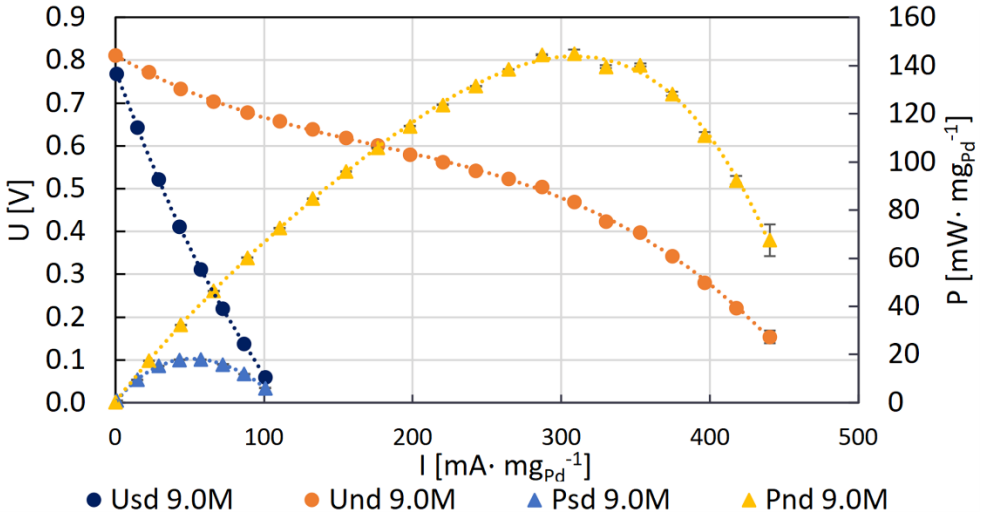

Fig. 1. Current-voltage characteristics for the standard system without baffles (sd) and with baffles (nd) [4]

References

[1] Eppinger J., Huang K.W., Formic Acid as a Hydrogen Energy Carrier, *ACS Energy Lett.*, 2017, 2, 188–195.

[2] Chiou Y.-J., Chen K.-Y., Lin H.-M., Liou W.-J., Liou H.-W., Wu S.-H., Mikolajczuk A., Mazurkiewicz M., Malolepszy A., Stobinski L., Borodzinski A., Kedzierzawski P., Kurzydlowski K., Chien S.-H., Chen W.-C., Electrocatalytic properties of hybrid palladium–gold/multi-walled carbon nanotube materials in fuel cell applications, *Phys. Status Solidi.*, 2011, 208, 1778–1782.

[3] Bieloshapka I., Jiricek P., Yakovlev Y., Hruska K., Tomsik E., Houdkova J., Malolepszy A., Mazurkiewicz M., Lobko Y., Lesiak B., Thermal and chemical activation methods applied to DFAFC anodes prepared by magnetron sputtering, *Int. J. Hydrogen Energy.*, 2020, 45, 14133–14144.

[4] Jałowiecka M., Bojarska Z., Małolepszy A., Makowski Ł., Mass transport enhancement in direct formic acid fuel cell with a novel channel design, *Chem. Eng. J.*, 2022, 451.

INFLUENCE OF BLOOD RHEOLOGY AND CHANGES IN THE DEGREE OF ATHEROSCLEROTIC STENOSIS IN ASSESSING THE RISK OF HEMOLYSIS

Krystian Jędrzejczak*, Łukasz Makowski, Wojciech Orciuch, Krzysztof Wojtas

Faculty of Chemical and Process Engineering, Warsaw University of Technology, Waryńskiego 1, 00-645 Warsaw, Poland
*corresponding author: krystian.jedrzejczak.dokt@pw.edu.pl

Introduction

Cardiovascular diseases, including atherosclerosis, are among the most common causes of death in 21st century [1]. One of the most common causes of atherosclerosis is an unhealthy diet and lack of physical activity [2]. As a consequence, cholesterol is deposited in the area of blood vessels [3], reducing the cross-sectional area of the vessel available for blood flow, increasing local blood velocity, and shear stresses to which red blood cells are exposed. An increase in shear stress increases the risk of hemolysis due to the disruption of the erythrocyte wall [4]. Determination of shear stresses to which erythrocytes are exposed requires adopting an appropriate blood rheological model [5], [6]. Blood consists mostly of water, which is the main component of plasma and red blood cells. Other minerals and cells make up the small remnant of the blood. Due to the complex composition of blood and the agglomeration and deagglomeration of red blood cells, the determination of viscosity and shear stress is complicated. There are many models of blood rheology in the literature that describe viscosity as a function of shear rate [5], [7]–[11]. Another approach is to reconstruct the physiological phenomena associated with agglomeration and deagglomeration of red blood cells based on population balance [6], [12]–[16].

Methodology

Hemolysis modelling was performed in the ANSYS Fluent software environment enriched with the user's own functions. As part of the simulation, a blood rheology model was used based on a population balance [6], which was compared with the Carreau-Yasuda model [5]. Geometric models of narrowed blood vessels were developed based on models provided by the Medical University of Silesia. CFD simulations were performed for blood flow in the range of 0.62 to 6.25 ml/s. As part of the study, blood hemolysis was modelled for stenosis diameters up to 30% to 60% of the diameter before the stenosis.

Results and conclusions

Results of the CFD simulation provided information about the maximum shear stresses. Hence, a correlation was developed linking the shape of the constriction and the speed before the constriction with the maximum shear stresses, which are key factors in assessing the risk of hemolysis. Based on that correlation, in the future, it may be possible to quickly analyze the risk of hemolysis in cardiac diagnostics without the need for complex numerical software.

Acknowledgments
This study was funded by the BIOTECHMED-3 project of the Warsaw University of Technology under the Excellence Initiative: Research University (IDUB) program.

References

[1] Amini M., Zayeri F., Salehi M., Trend analysis of cardiovascular disease mortality, incidence, and mortality-to-incidence ratio: results from global burden of disease study 2017, *BMC Public Health*, 2021, 21, 1.
[2] Henning R.J., *Obesity and obesity-induced inflammatory disease contribute to atherosclerosis: a review of the pathophysiology and treatment of obesity*," 2021. [Online]. Available: www.AJCD.us/ISSN:2160-200X/AJCD0135880.

[3] Bentzon J.F., Otsuka F., Virmani R., Falk E., Mechanisms of plaque formation and rupture, *Circ Res*, 2014, 114, 12, 1852–1866.
[4] Giersiepen M., Wurzinger L.J., Opitz R., Reul H., Estimation of shear stress-related blood damage in heart valve prostheses-in vitro comparison of 25 aortic valves, *Int J Artif Organs*, 1990, 13, 5, 300–306.
[5] Boyd J., Buick J. M., Green S., Analysis of the Casson and Carreau-Yasuda non-Newtonian blood models in steady and oscillatory flows using the lattice Boltzmann method, *Physics of Fluids*, 2007, 19, 9, 93103.
[6] Jędrzejczak K., Makowski Ł., Orciuch W., Model of blood rheology including hemolysis based on population balance, *Commun Nonlinear Sci Numer Simul*, 2023, 116, 106802.
[7] Siauw W.L, Ng E.Y.K., Mazumdar J., Unsteady stenosis flow prediction: a comparative study of non-Newtonian models with operator splitting scheme, *Med Eng Phys*, 2000, 22, 4, 65–277.
[8] Shibeshi S.S., Collins W.E., The rheology of blood flow in a branched arterial system, *Applied Rheology*, 2005, 15, 6, 398–405.
[9] Johnston B.M.,. Johnston P.R, Corney S., Kilpatrick D., Non-Newtonian blood flow in human right coronary arteries: Transient simulations, *J Biomech*, 2006, 39, 6, 1116–1128.
[10] Doost S.N., Zhong L., Su B., Morsi Y.S., The numerical analysis of non-Newtonian blood flow in human patient-specific left ventricle, *Comput Methods Programs Biomed*, 2016, 127, 232–247.
[11] Morbiducci U., et al., On the importance of blood rheology for bulk flow in hemodynamic models of the carotid bifurcation, *J Biomech*, 2011, 44, 13, 2427–2438.
[12] Jariwala S., Horner J.S., Wagner N.J., Beris A.N., Application of population balance-based thixotropic model to human blood, *J Nonnewton Fluid Mech*, 2020, 281, 104294.
[13] Owens R. G., A new microstructure-based constitutive model for human blood, *J Nonnewton Fluid Mech*, 2006, 140, 1–3, 57–70.
[14] Moyers-Gonzalez M., Owens R.G., Fang J., A non-homogeneous constitutive model for human blood. Part 1. Model derivation and steady flow, *J Fluid Mech*, 2008, 617, 327–354.
[15] Moyers-Gonzalez M.A., Owens R.G., A non-homogeneous constitutive model for human blood: Part II. Asymptotic solution for large Péclet numbers, *J Nonnewton Fluid Mech*, 2008, 155, 3, 146–16.
[16] Moyers-Gonzalez M.A., Owens R.G., Fang J., A non-homogeneous constitutive model for human blood: Part III. Oscillatory flow, *J Nonnewton Fluid Mech*, 2008, 155, 3, 161–173.

ADSORPTION OF A FOUR-COMPONENT GASEOUS MIXTURE OF VOCS ON ACTIVATED CARBON

Martyna Jurkiewicz*, Marlena Musik, Robert Pełech

Department of Chemical Organic Technology and Polymeric Materials, Faculty of Chemical Technology and Engineering, West Pomeranian University of Technology in Szczecin, 70-322 Szczecin, Poland
*corresponding author: martyna.jurkiewicz@zut.edu.pl

Both outdoors and in buildings, people are exposed to emissions of volatile organic compounds. This group of compounds includes, for example, aliphatic hydrocarbons, aromatic hydrocarbons, aldehydes, alcohols, and ketones. VOC emissions can come from various antecedent sources such as agriculture, combustion vehicles, industrial processes, or daily life. They can also be produced by plants under stressful conditions. Due to the harmfulness of VOCs, it is necessary to explore methods that enable air streams to be cleaned of these compounds [1–3].

In this work, we investigated the adsorption of a mixture of four VOCs from the air: acetone, ethyl acetate, toluene, and n-butyl acetate. WG-12 activated carbon (Grand Activated Sp. z o.o) was used as the adsorbent.

It was concluded that competitive adsorption takes place in the studied system. Moreover, the volatility of the adsorbate is a key factor influencing the adsorption affinity [3]. It was studied how the height of the adsorption bed influences the bed breakthrough time and gas purification efficiency. The study showed that the breakthrough time of the adsorption bed increased linearly with increasing bed height.

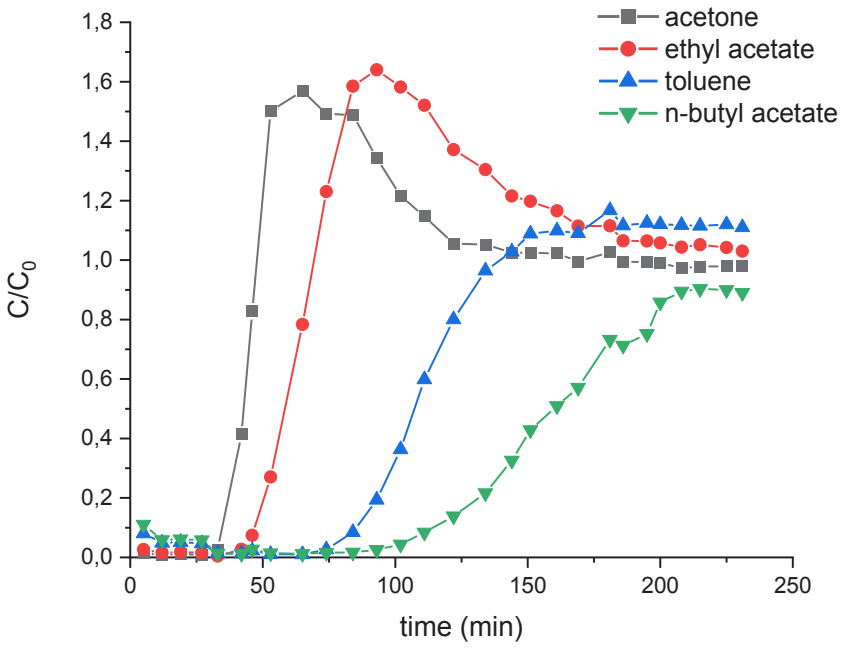

Fig. 1. Bed breakthrough curve showing the adsorption process of the gaseous mixture acetone, ethyl acetate, toluene, n-butyl acetate [3]

References

[1] Zhu L., Shen D., Luo K., A critical review on VOCs adsorption by different porous materials: Species, mechanisms and modification methods, *J. Hazard. Mater.*, 2020, 389, 122102.
[2] Niu H., Mo Z., Shao M. Lu S., Xie S., Screening the emission sources of volatile organic compounds (VOCs) in China by multi-effects evaluation, *Front. Environ. Sci. Eng.* 2016, 10(5), 01.
[3] Jurkiewicz M., Musik M., Pełech R., Adsorption of a Four-Component Mixture of Volatile Organic Compound Vapors on Modified Activated Carbons, *Ind. Eng. Chem. Res.*, 2023

CFD SIMULATION OF A JET PUMP MIXER HYDRODYNAMICS

Mateusz Krzemiński[1],*, Wojciech Ludwig[2]

[1]Wroclaw University of Science and Technology, Doctoral School, Wybrzeże Wyspianskiego 27, 50-370, Wroclaw, Poland
[2]Wroclaw University of Science and Technology, Department of Process Engineering and Technology of Polymer and Carbon Materials, Gdanska 7/9, 50-344, Wroclaw, Poland
*corresponding author: mateusz.krzeminski@pwr.edu.pl

Engineers cannot do without numerical simulations. Computer tools lower the costs of designing prototypes at each research stage. A properly created geometric model and appropriate computational methods eliminate the stages of interim prototypes, enabling the creation of the final prototype.

A jet pump mixer has a jet pump inside its tank in which stirring is done. Neither jet pumps nor jet pump mixers have moving parts. This feature alone should facilitate the use of CFD (Computational Fluid Dynamics) to simulate the fluid behaviour. Strangely, there are very few papers on this topic. This is a surprise because jet pump mixers are among the best in creating emulsions through multiphase mixing.

Dziak [1] carried out a study on crude oil desalination using a hybrid system consisting of a jet pump mixer and a microfilter. The results of the kinetics of this process and the destruction of water emulsions led to designing the desalination plant on a large scale.

Ludwig and Sawinski [2] published a study on CFD modelling for the jet pump mixer. The jet pump mixer was made by modifying a laboratory water pump. The suction chamber was drilled with holes, allowing the liquid to flow into the pump. The presented CFD model made it possible to determine the hydrodynamic factors in the jet pump mixer such as velocity and pressure fields.

The main goal of this study was to apply the CFD methods to model jet pump mixer hydrodynamics. During research one of the most important parameters – ejection coefficient – was calculated.

The laboratory apparatus was constructed for desalination of crude oil. It contained a thick-walled glass mixing tank and a round bottom with an outlet. The axis of the tank was fitted with a jet pump. The working principle of this mixer is as follows. First, it is filled up with water to 80% of its volume. Second, water is introduced under pressure through a jet pump nozzle into the jet pump mixing chamber. Water creates a pressure difference between the jet pump body and the inside of the tank, which is responsible for creating suction into the jet pump mixing chamber through the four inlets. The main mixing takes place in the zone located axially above the outlet of the mixing tank.

During research, the following parameters were tested taking into account the ejection coefficient: velocity of the liquid in the jet pump nozzle (1.33, 1.99, 2.65, 3.32, 3.98 m/s), the jet pump nozzle diameter (2,3,4,5,6 mm), distance between the nozzle outlet and the mixing chamber inlet (1.74,2.74,3.74,5.74 mm). The jet pump was located at the center as far and as close as possible to the outlet.

Ansys Fluent was chosen as the numerical solver with settings presented below:

- solver type - pressure-based,
- velocity formulation - absolute,
- time - steady,
- viscous model - sst-k-omega, low-re corrections, curvature correction.

The flowing liquid was water with constant physical properties: density: 998.2 [kg/m3], viscosity 0.001003 [kg/(m*s)].

The applied boundary conditions were:

- main nozzle inlet - velocity inlet, turbulent intensity 5%, hydraulic diameter set according to the nozzle diameter,
- all 4 inlets to the jet pump -interior,
- mixing chamber outlet -interior,
- mixing tank outlet - pressure outlet, turbulent intensity 5%, hydraulic diameter 0.0065m.

To experimentally validate the CFD model, jet velocities values were compared with those obtained by PIF (Particle Image Velocimetry). The expansion of the jet cone was studied at 20, 50, 80, 110, 140 and 170 mm distances from the tank outlet. When the lines covered each other within a +/- 5–10% error margin, the simulated expansion profile was treated as validated (Fig. 1.). The impact of the nozzle velocity on the ejection coefficient for different distances between the nozzle and mixing chamber is presented in Fig. 2.

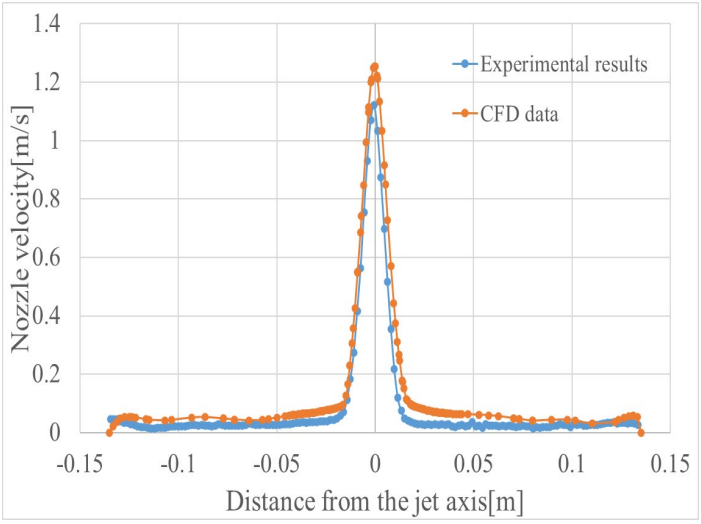

Fig. 1. Comparison between the simulation and experimental data of the jet velocity (nozzle diameter 4 mm, nozzle velocity 2.65 m/s, distance between nozzle and mixing chamber 3.74mm, jet pump located centrally in the mixing tank, distance from tank outlet 110 mm)

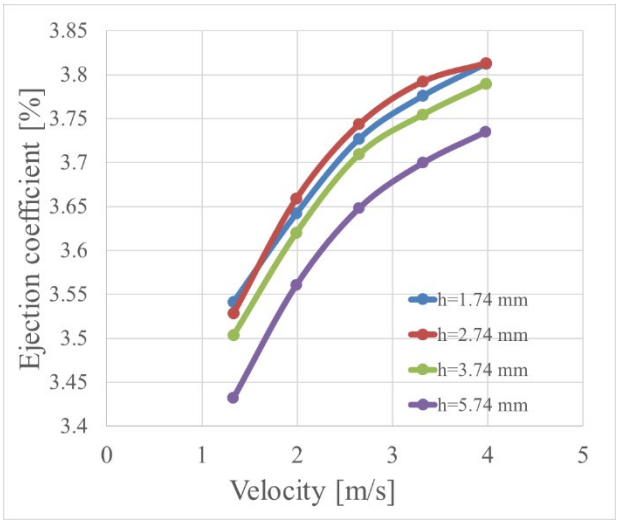

Fig. 2. Impact of the nozzle velocity on ejection coefficient for different distances between the nozzle and mixing chamber (nozzle diameter 2 mm, jet pump located centrally in the mixing tank)

The research results lead to the following conclusions:

- The ejection coefficient does not depend on the location of the jet pump in the mixing tank.
- The increase in the nozzle velocity augments the ejection coefficient.
- When the nozzle diameter increases, the ejection coefficient diminishes (at constant liquid velocity in the nozzle).
- The increase in the distance between the nozzle and the mixing chamber decreases the ejection coefficient.

References

[1] Dziak J., Odsalanie surowej ropy naftowej z użyciem układu hybrydowego: mieszalnik strumienicowy – mikrofiltr, *Inż. Ap. Chem*., 2013, 52, 4, 302-303.
[2] Ludwig W., Sawiński W., Modelowanie CFD mieszalnika strumienicowego, *Inż. Ap. Chem*., 2013, 52, 6, 543-544.

CHARACTERISATION OF COMMERCIAL TiO_2 POWDERS – INDUSTRIAL APPLICATION OF STRUCTURE ANALYSIS

Radosław Krzosa[1]*, Łukasz Makowski[1], Wojciech Orciuch[1], Radosław Adamek[2], Michał Wojasiński[1]

[1]Faculty of Chemical and Process Engineering, Warsaw University of Technology, Warsaw, Poland
[2]ICHEMAD – Profarb sp. z o. o., Gliwice, Poland
*corresponding author: 01113344@pw.edu.pl

Titanium dioxide powders used in the industry can vary between different manufacturers. The properties of the final product depend not only on the composition of the substance but also on its structure. The particle size affects the maximum light scattering. The largest value of refraction index for titanium dioxide is for a particle size of 200 nm [1]. Particle size distribution and particle porosity affect the suspension's rheological behavior. The differences between powders can affect the product properties and further processing.

The industry uses two methods of producing titanium dioxide powders: sulfite and chloride. In the sulfite method, primary particles of TiO_2 are precipitated in a water solution. Due to supersaturation, particles can stick to one other and form structures named aggregates. Primary particles are connected via solid bridges. This type of connection is rigid and difficult to break. Aggregates in specific conditions can form larger structures via weak van der Waals forces. Those structures are named agglomerates and can be easily broken by hydrodynamic stresses. To disintegrate aggregates more energy is needed. Similar structures are formed in the chloride process, but the reaction occurs in the gas phase.

Breakage of particles is conducted in many types of devices, such as ball mills, ultrasonic homogenizers or high-shear mixers. Prediction of particle size changes in time, using a specific type of device, can be achieved by applying a computational fluid dynamic method (CFD) combined with population balance, as shown in [2, 3]. To use this method, the properties of the powder are required. Those methods need to specify the particle fractal dimension to connect the particle size with its mass. This parameter is used to describe the fragment size distribution of particles obtained via breakage. Also, this parameter is used to specify the tensile strength of agglomerates. Tensile strength is a crucial parameter in the breakage process. It describes whether the agglomerate breakage occurs under a specific load. To model also the tensile strength, the interacting forces between particles are required to be specified. Also, the presence of a different substance can affect the particle size change over time.

In this work, six types of titanium dioxide powders were examined to find the parameters needed in population balance modelling and to characterize the tensile strength of the agglomerates using Tang model [4]. In this model, the tensile strength can be calculated using the equation:

$$\sigma_T = \frac{9}{8}\frac{(1-\varepsilon)}{\varepsilon}\frac{F}{L_a^2} \tag{1}$$

where F is an interacting force between particles, L_a is an aggregate size, and ε is an aggregate porosity.

The porosity of particles was calculated using the fractal dimension. To determine the fractal dimension of a particles, a small angle light scattering technique was used. An assumption was made that the intensity of scattering from two populations of particles: aggregates and agglomerates, is a sum of the scattering intensity from each population. This phenomenon is illustrated in Figure 1.

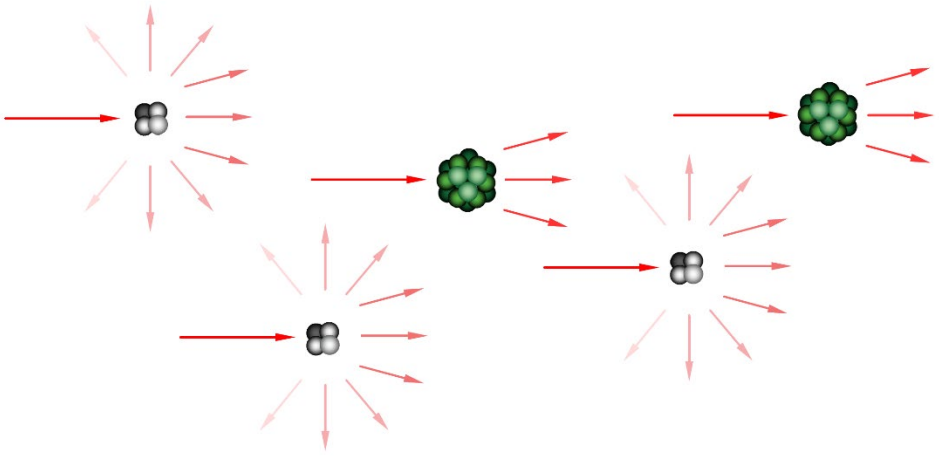

Fig. 1. Scattering intensity from two populations of particles

XRF and FTIR techniques were used to determine the composition of the powders. Based on that, the impurities in two types of powder were identified. Also, the composition of a coating layer of particles was confirmed.

The repulsive electrostatic and Born and attractive van der Waals potentials were calculated to determine the interacting forces. Based on that, the separation distance was found, and force was calculated. Zeta potential measurement was used to determine the electrostatic potential. Attractive van der Waals and repulsive Born potentials were calculated by integration of the Lennard-Jones potential over a volume of two interacting particles. This calculation needed particle size distribution and primary particle size distribution. Particle size distribution was obtained using a Beckmann&Coluter particle size analyzer. Primary particle size distribution was obtained by manually counting the particles from scanning electron microscope images.

The results of this analysis gave us a complete set of parameters required in population balance calculation. Based on this, in further work, we will construct the population balance model of particle breakage in high-energy devices and predict the process of particle breaking in time.

References

[1] Ohenoja, K., Illikainen, M., Niinimäki, J., Effect of operational parameters and stress energies on the particle size distribution of TiO2 pigment in stirred media milling. *Powder technology*, 2013, 234, 91–96.

[2] Krzosa, R., Makowski, Ł., Orciuch, W., Adamek, R., Population balance application in TiO2 particle deagglomeration process modeling. *Energies*, 2021, 14(12), 3523.

[3] Krzosa, R., Wojtas, K., Golec, J., Makowski, Ł., Orciuch, W., Adamek, R., Modelling particle deagglomeration in a batch homogeniser using full CFD and mechanistic models. *Chem. Process Eng. – Inż. Chem. Proces.*, 2021, 42(2), 105–118.

[4] Tang, S., Ma, Y., Shiu, C., Modelling the mechanical strength of fractal aggregates. *Colloids Surf. A: Physicochem. Eng. Asp.*, 2001, 180(1–2), 7–16.

INFLUENCE OF EXPERIMENTAL SETTING AND DATA PROCESSING METHODOLOGIES ON GAS BUBBLE HYDRODYNAMIC PROPERTIES

Przemysław Luty*, Mateusz Prończuk, Katarzyna Bizon

Faculty of Chemical Engineering and Technology, Cracow University of Technology,
Warszawska 24, Kraków 31-155, Poland
*corresponding author: przemyslaw.luty@doktorant.pk.edu.pl

A two-phase liquid-gas flow is of great importance in various branches of modern industry, including chemical, biochemical and petrochemical industries [1]. With the proper share of gas not exceeding a certain critical value, the flow of gas through a liquid layer occurs in the form of gas bubbles. Such flow has many advantages, e.g. good liquid mixing and aeration, and highly developed liquid-gas interface translating into intense mass and heat interfacial transfer.

To enable the use of these advantages, it is key to know the hydrodynamic properties of gas bubbles, mainly their number per volume unit, size and velocity. Investigation of these parameters is possible thanks to multidimensional measurement techniques, among which an important group of methods are optical shadowgraphy techniques [2]. The parameter that significantly affects the size of the interfacial liquid-gas area is bubble size, which can be expressed by its equivalent diameter. Although shadowgraphy methods are used often to investigate bubble properties and numerous models to predict them have been developed using these methods, there are few reports in the scientific literature as to the legitimacy of using individual procedures.

In this work, various procedures to determine bubble equivalent diameter were investigated. Based on the research, one procedure was selected and is recommended. Not only does it give results close to real, but also it is quite universal and convenient to use.

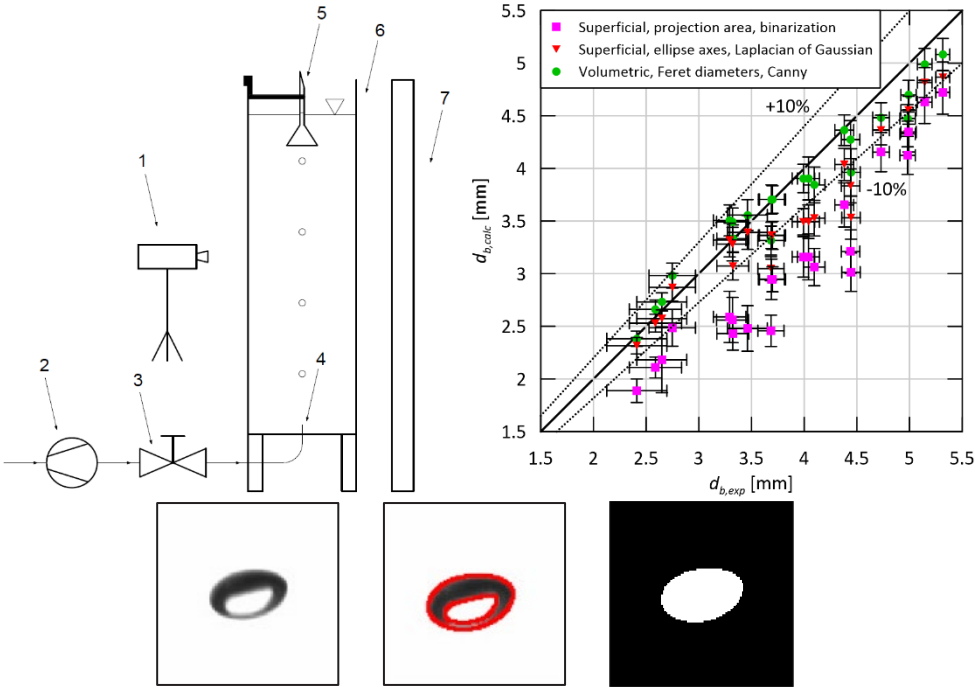

Fig. 1. The experimental setup: 1 – camera, 2 – compressor, 3 – valve, 4 – nozzle, 5 – funnel, 6 – bubble column, 7 – LED backlight (top left); experimental bubble equivalent diameters vs calculated bubble equivalent diameters for selected procedures of its determination (top right); selected stages of bubble image processing (bottom): unprocessed image (left), rims detected (middle), bubble detected (right)

The experimental setup is shown in Fig. 1. The main device of the stand was a bubble column of rectangular cross-section. It was almost fully filled with a stagnant liquid (water). The gas phase (air) was injected through a brass nozzle located at the bottom of the column. The gas flow was ensured by a compressor and was regulated using a valve. Gas flow rate was set to be low enough to allow the bubbles to flow one at a time. Then bubble formation was close to static. In one part of the studies, bubble diameters were measured experimentally – then the bubble entered the capillary of the funnel installed at the top of the column. On the basis of the volume of air between the liquid layers in the capillary, the volume of the bubble was measured, and then its equivalent diameter was determined. The videos of flowing bubbles were recorded using two fast cameras (CMOS IDS UI-3130CP-C-HQ Rev.2 and AOS Promon U1000). LED backlight was installed behind the column to provide good illumination of the recorded videos. Gas bubbles of diameters in the range of circa 2.5–5.5 mm were considered, which corresponds to the diameters commonly used in industrial practice.

Different procedures for determination of the bubble equivalent diameter as well as the influence of the experimental setting on the accuracy of determined results using optical shadowgraphy method were investigated and compared [3]. First, three edge detectors were compared, i.e. Otsu's binarization method [4], Laplacian of Gaussian filter [5] and Canny algorithm [6] (Fig. 1). Second, each bubble was approximated diversely – using maximum and minimum axes of the fitted ellipse or Feret diameters of the detected shape. Finally, bubble superficial and volumetric diameters were calculated and compared. In the next stage, the utility of multiple parameters of experimental setting was investigated and compared, including: the distance between the bubble rising surface and camera lens, optical zoom used (associated with bubble image resolution on the recorded images), image distortion and the use of its digital correction, the number of analyzed video frames showing each bubble during its flow [7].

Based on the research and calculations carried out, it has been proven that the most accurate results of bubble equivalent diameters with respect to experimental results are obtained if Canny algorithm is used for edge detection and Feret diameters are used to calculate volumetric bubble equivalent diameter. The results of the calculated bubble equivalent diameters vs experimental ones for the several procedures analyzed are shown in Fig. 1. Furthermore, for the studied setup, it has been proven that better accuracy is obtained if the distance between the bubble rising surface and camera is large enough and there is no optical zoom – even though the resolution of the bubble increases in the image with the increase of optical zoom and with the decrease of camera distance, the benefit from analysis of a larger number of frames concerning each bubble is the most significant and exceeds the profits derived in the reverse case.

The study sheds new light on the issue of determining the size of gas bubbles and may lead to the formulation of more accurate correlations to predict the size of bubbles flowing in industrial apparatuses in which two-phase liquid-gas bubble flows occur.

References

[1] Besagni, G., Gallazzini, L., Inzoli, F., Effect of gas sparger design on bubble column hydrodynamics using pure and binary liquid phases, *Chem. Eng. Sci.*, 2018, 176, 116–126.

[2] Di Nunno, F., Alves Pereira, F., Granata, F., de Marinis, G., Di Felice, F., Gargano, R., Miozzi, M., A shadowgraphy approach for the 3D Lagrangian description of bubbly flows, *Meas. Sci. Technol.*, 2020, 31, 105301.

[3] Luty, P., Prończuk, M., Bizon, K., Experimental verification of different approaches for the determination of gas bubble equivalent diameter from optical imaging, *Chem. Eng. Res. Des.*, 2022, 185, 210–222.

[4] Otsu, N., A threshold selection method from gray-level histograms, *IEEE Trans. Syst. Man Cybern.*, 1979, 9(1), 62–66.

[5] Gonzales, R.C., Woods, R.E., Eddins, S.L., Digital Image Processing Using MATLAB. NJ. Prentice-Hall, Englewood Cliffs, 2004.

[6] Canny, J., A computational approach to edge detection, *IEEE Trans. Pattern Anal. Mach. Intell.*, 1986, PAMI-8(6), 679–698.

[7] Luty, P., Prończuk, M., Bizon, K., Wpływ odległości kamery na wyznaczanie średnicy zastępczej pęcherza gazowego z użyciem metody cieniograficznej, Trzecie Seminarium Praktyczne Aspekty Inżynierii Chemicznej PAIC-2022, 225–237.

CARBON QUANTUM DOTS AS FREE RADICAL SCAVENGERS

Wiktoria Matyjasik*, Olga Długosz, Jolanta Pulit-Prociak, Marcin Banach

Faculty of Chemical Engineering and Technology, Cracow University of Technology, Cracow, Poland

*corresponding author: wiktoria.matyjasik@doktorant.pk.edu.pl

Carbon quantum dots (CQDs) are a relatively new class of nanomaterials, discovered in 2004, defined as zero-dimensional luminescent carbon nanostructures with crystalline core and amorphous surface, with an average size of less than 10 nm. CQDs are materials with a unique structure and size that enable customisation of chemical, physical and optical properties – these properties make them multifunctional materials with significant potential. The high potential of CQDs is related to their simplicity of preparation, low cost, ease of functionalisation, electric conductivity, low toxicity, environmental friendliness and biocompatibility. These abilities make them a material that outperforms classical semiconductor quantum dots by its functionality. The diversity and customisation possibilities make these nanomaterials applicable in many fields, both in medicine and medical analytics as bioimaging substances, drug carriers, bio-labelling, antibacterials, anticancer substances, as well as in optoelectronics or in strictly chemical applications related to, for example, photocatalysis, supercapacitors, semiconductors or optical detection [1–4].

In living organisms, 25% of the known reactions catalysed by enzymes involve oxidation reactions. Through normal aerobic metabolism, a variety of reactive oxygen species are produced, which are maintained at appropriate levels by specific enzymes that convert them to less harmful metabolites. When homeostasis is disturbed, ROS can temporarily or permanently damage proteins, lipids or nucleic acids, while a certain amount of them is necessary for the proper functioning of signalling pathways, redox processes or gene expression. Reactive oxygen species include free radicals such as singlet oxygen ($^1O_2$), hydroxyl radical ($\cdot OH$) or superoxide anion radical ($O2^{-\cdot}$), as well as non-radical molecules with high reactivity, such as hydrogen peroxide (H_2O_2) or lipid peroxides [5–8].

The properties of carbon quantum dots can be easily modified - the size and surface composition of carbon quantum dots significantly affect properties such as photoluminescence and band gap diversity. Furthermore, by modifying the composition of carbon quantum dots, it is possible to obtain carbon dots capable of inactivating reactive oxygen species (ROS) and having an antioxidant effect, as well as carbon dots with the opposite properties, related to radical generation, e.g. under the influence of radiation [1], [9–11]. In the presentation, the ability of the obtained carbon quantum dots to act as free radical scavengers or generators will be presented.

References:

[1] Xue Y., Liu C., Andrews G., Wang J., Ge Y., Recent advances in carbon quantum dots for virus detection, as well as inhibition and treatment of viral infection, *Nano Convergence*, 2022, 9(1).
[2] Gu L., Zhang J., Yang G., Tang Y., Zhang X., Huang X., Zhai W., Fodjo E.K., Kong C.., Green preparation of carbon quantum dots with wolfberry as on-off-on nanosensors for the detection of Fe3+ and L-ascorbic acid, *Food Chem*, 2022, 376, 131898.
[3] Tepliakov N.V., Kundelev E.V., Khavlyuk P.D., Xiong Y., Leonov M.Y., Zhu W., Baranov A.V., Fedorov A.V., Rogach A.L., Rukhlenko I.D., Sp2-sp3-Hybridized Atomic Domains Determine Optical Features of Carbon Dots, *ACS Nano*, 2019, 13(9), 10737–10744.
[4] Kurian M., Paul A., Recent trends in the use of green sources for carbon dot synthesis-A short review, *Carbon Trends*, 2021, 3, 32.
[5] Berg J.M., Tymoczko J.L., Gatto G.J., Stryer Jr.L., *Biochemistry*. W. H. Freeman and Company, 2019.
[6] Hornig S., Michael M., Grinyer A., Turner J., "Introduction to enzymes and their applications," *Introduction to Pharmaceutical Biotechnology, Volume 2*, Sep. 2018.

[7] Harris I.S., DeNicola G.M., The Complex Interplay between Antioxidants and ROS in Cancer, *Trends Cell Biol*, 2020, 30(6), 440–451.
[8] Perillo B., di Donato M., Pezone A., di Zazzo E., Giovannelli P., Galasso G., Castoria G., Migliaccio A., ROS in cancer therapy: the bright side of the moon, *Exp. Mol. Med.*, 2020, 52(2), 192–203.
[9] Lv A., Chen Q., Zhao Ch., Li S., Sun S., Dong J., Li Z., Lin H., Long-wavelength (red to near-infrared) emissive carbon dots: Key factors for synthesis, fluorescence mechanism, and applications in biosensing and cancer theranostics, *Chin. Chem. Lett.*, 2021, 32(12), 3653–3664.
[10] Chaudhary P., Verma A., Mishra A., Yadav D., Pal K., Yadav B.C., Kumar E.R., Thapa K.B., Mishra S., Dwivedi D.K., Preparation of carbon quantum dots using bike pollutant soot: Evaluation of structural, optical and moisture sensing properties, *Physica E Low Dimens Syst Nanostruct*, 2022, 139, 115174.
[11] Jhonsi M.A., Jhonsi M.A., "Carbon Quantum Dots for Bioimaging," *State of the Art in Nano-bioimaging*, Jun. 2018.

OXIDE NANOMATERIALS CONTAINING MNO AND CUO IN ENZYMATIC CASCADE REACTION

Julia Matysik*, Olga Długosz, Marcin Banach

Cracow University of Technology, Faculty of Chemical Engineering and Technology,
Warszawska 24, Kraków, Poland
*corresponding author: julia.matysik@doktorant.pk.edu.pl

Knowledge of nanoparticle synthesis allows designing of the obtained materials; their shape, size or surface modifications, which affect the final chemical and physical properties [1]. The creation of a nanomaterial with the desired characteristics, compatible with other particles of the catalytic system, is the basis of modern nanotechnology research. Microwave processes play an important role in the controlled synthesis of nanomaterials. Conducting or assisting the preparation of nanometric materials through the use of microwaves is an important modification of the preparation process. Thus, it is possible to control the shape and size of the nanoparticles obtained [2].

Currently, nanomaterials with enzyme catalytic characteristics (nanozymes) are rapidly developing as multifunctional nanostructured platforms, as they can be used to mimic physiological activities due to their unique physicochemical characteristics and specific structural composition [3]. Nanozymes are widely used in the biomedical, clinical, environmental and food sectors [4]. Compared to natural enzymes, nanozymes are more stable and cost-effective, and their catalytic properties can be regulated.

Natural enzymes are susceptible to environmental changes due to their limited thermostability and small operating pH range. Going beyond the typical parameters of temperature and reaction causes their denaturation and significantly weakens or hinders their enzymatic activity [5, 6]. Currently, nanozymes of the nature of enzymes from oxidoreductase groups such as superoxide dismutase (SOD), catalase (CAT), peroxidase (POD) or glutathione peroxidase (GPX) are distinguished [7].

The aim of the present study was to obtain and analyze the activity of ZnO-MnO-CuO and MnO-CuO multioxide nanomaterials. The materials were characterized with SEM, XRD and ATR to determine the composition and nature of the substances. Proteolytic tests with casein degradation were performed to investigate their activity, where the activity of the materials was 0.0422U/mg for ZnO-MnO-CuO and 0.0941U/mg for MnO-CuO. In addition, the materials were characterized in glucose decomposition reactions with simultaneous reduction of H2O2 and in the sorption and decomposition reaction of thymol blue (a phenolic dye). Antimicrobial tests (*E.Coli)* were also carried out to verify activity against microorganisms.

References

[1] Bogdan J., Jackowska-Tracz A., Zarzyńska J., Pławińska-Czarnak J., Znaczenie procesów fotokatalitycznych TiO2/UV, ZnO/UV i MgO/UV w inaktywacji czynników zakaźnych, *Med Weter*., 2015, 71, 472–479.
[2] Burda C., Chen X., Narayanan R., El-Sayed M.A., Chemistry and properties of nanocrystals of different shapes, *Chem Rev*., 2005, 105, 1025–1102.
[3] Huang Y., Ren J., Qu X., Nanozymes: Classification, Catalytic Mechanisms, Activity Regulation, and Applications, *Chem Rev.*, 2019, 119 4357–4412. https://doi.org/10.1021/acs.chemrev.8b00672.
[4] Wong E.L.S., Vuong K.Q., Chow E., Nanozymes for Environmental Pollutant Monitoring and Remediation, 2021.
[5] Wang H., Wan K., Shi X., Recent Advances in Nanozyme Research, *Advanced Materials*., 2019, 31, 1–10.
[6] Yang W., Yang X., Zhu L., Chu H., Li X., Xu W., Nanozymes: Activity origin, catalytic mechanism, and biological application, *Coord Chem Rev*., 2021, 448, 214170.
[7] M. Pietrzak, P. Ivanova, Bimetallic and multimetallic nanoparticles as nanozymes, *Sens Actuators B Chem*., 2021, 336, 129736.

INFLUENCE OF DRYING AND GRANULATION CONDITIONS ON CHARACTERISTICS OF MICRONUTRIENT CHELATE GRANULES

Bernard Michałek[1,*], Katarzyna Bizon[2], Tomasz Wilk[1]

[1]Faculty of Chemistry Adam Mickiewicz University, Uniwersytetu Poznańskiego 8, 61-614 Poznan, Poland
[2]Faculty of Chemical Engineering and Technology, Cracow University of Technology, Warszawska 24, 31-155 Kraków, Poland
*corresponding author: bm9309@st.amu.edu.pl

Fluidized-bed spray granulation (FBSG), also referred to as wet fluidization or wet granulation, is a technology that enables solutions, suspensions, or melts to be converted into coarse-grained, dust-free, and easy-to-handle granules. Generally, in spray granulation carried out in a fluidized bed, the liquid is sprayed onto a bed made of particles, fluidized by a stream of hot drying gas, which induces particle (tablets, granules) enlargement [1]. Nowadays, FBSG is widely implemented in such areas as pharmaceutical, food, agricultural and chemical industries [1-3]. Its popularity is due to the fact that through fluidized-bed granulation, critical particle or product characteristics can be achieved, such as porosity, particle size distribution, bulk density, dust content and solubility. Despite the undoubtedly huge potential of FBSG and many practical applications already implemented, the huge number of factors conditioning the entire process, and thus the quality of granules obtained, is up to now still a major problem. The most important of these include (Fig. 1) the design of the apparatus itself, the materials used, the process conditions adopted, as well as the measurement and computational procedures supporting the control of the actual process.

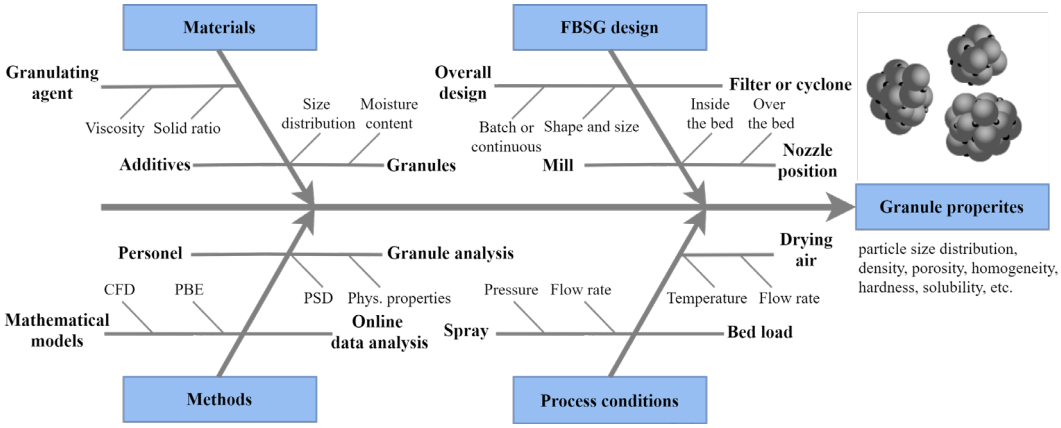

Fig. 1. Diagram indicating selected parameters and factors that may affect the properties of granules

This study provides a comprehensive overview of the influence of selected factors on the characteristics of granulated chelates. Considering that one of the factors significantly affecting the drying process and granulation itself are various additives, the effect of the addition of polyglucoside surfactants and betaines to the fertilizer solution sprayed into the fluidized bed during the production of D, L-aspartic acid, N-(1,2-dicarboxyethyl) Zn disodium salt by PPC ADOB was analyzed. In particular, the effect of surfactant addition on the evolution of the granule size distribution during the start-up of the apparatus [3] and during its continuous operation was studied. Given that, in addition to the broadly defined experimental conditions (e.g., "Materials" used, "Process conditions" or "FBSG design" in Fig. 1), different granule analysis techniques (i.e. "Methods" in Fig. 1) affect the final characteristics of the granules, e.g. their d_{50}, particle size distribution was determined using various techniques, i.e. sieve analysis, laser diffraction particle size analysis (Malvern Mastersizer® 2000) and automated image analysis (Malvern Morphologi®

G3). The latter tool also allows assessment of granule morphology, which turns out to be different for samples collected from the bed during tests conducted with and without surfactant. It turned out that the circularity of the final granules (i.e. fraction with diameters in the range of 0.2-0.9 mm) obtained with the surfactant was lower than those manufactured without it (0.81 versus 0.85). The more irregular character of granules produced with tenside is strictly related to distinctive phenomena occurring during its drying and granulation process.

Figure 2a shows how mass density distribution of granules evolves during the fluidized bed start-up in the production process of D, L-aspartic acid, N-(1,2-dicarboxyethyl) Zn disodium salt with surfactant addition. The results denoted by LD and S respectively refer to distributions determined by laser diffraction and sieve analysis. Both methods yielded similar values of diameter d_{50}, which gradually increase as the process proceeds. However, it should be emphasized that the method based on laser diffraction is indispensable for the analysis of fine fractions. Information about the fine fraction, including nuclei which can be generated internally through overspray (Fig. 2b) or the attrition process, is essential in modeling the process and predicting further evolution of the granule size distribution as well as, for controlling a stable continuous granulation process.

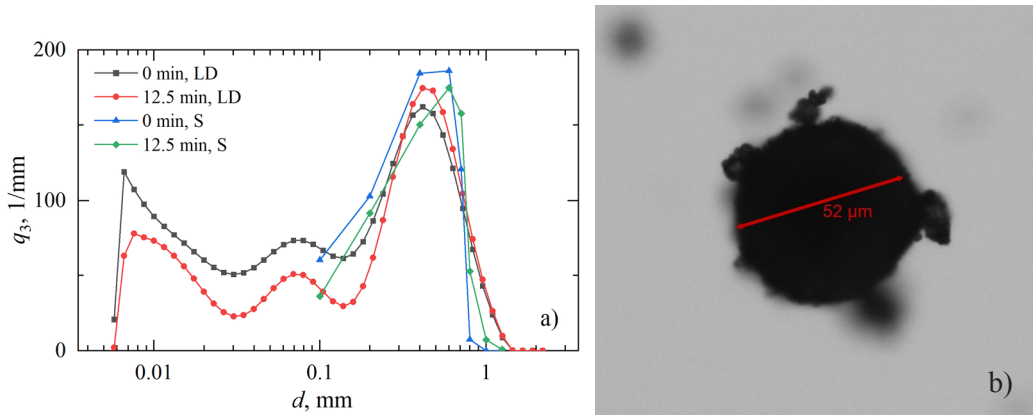

Fig. 2. Representative mass density distributions q_3 (a) for the batch process run with surfactant addition determined using laser diffraction (LD) and sieve (S) analysis, and nucleus produced internally due to overspray (b)

In addition to the influence of the properties of the fertilizer solution fed to the bed, the effect of the flow rate of selective air, which determines the withdrawal of granules from the apparatus, was analyzed on the values of d_{50}. For the production of granules of a fertilizer containing D, L-Aspartic acid, N-(1,2 dicarboxyethyl) micronutrient disodium salt, these variables were shown to be highly correlated. The obtained results indicate a directly proportional dependence of the selective air velocity on the grain size in the fluidized bed. Both during the start-up of the fluidized bed spray granulation process and after its stabilization, it is necessary to control this parameter in order to control the particle size distribution which is essential for the process.

References

[1] Grünewald G., Westhoff B., Kind M., Fluidized bed spray granulation: nucleation studies with steady-state experiments, *Dry. Technol.*, 2010, 28, 349–360.

[2] Burggraeve A., Monteyne T., Vervaet C., Remon J.P., De Beer T., Process analytical tools for monitoring, understanding, and control of pharmaceutical fluidized bed granulation: A review, *Eur. J. Pharm. Biopharm.*, 2013, 83, 2–15.

[3] Michałek B., Ochowiak M., Bizon K., Włodarczak S., Krupińska A., Matuszak M., Boroń D., Gierczyk B., Olszewski R., Effect of adding surfactants to a solution of fertilizer on the granulation process, *Energies*, 2021, 14(22), 7557.

ENHANCING MECHANICAL AND MOISTURE ABSORPTION PROPERTIES OF SILANE FUNCTIONALIZED 3D – PRINTED PEGDA WITH NOVEL PHOTOCURABLE POLYMERIC MATERIAL FORMULATIONS FOR WATER APPLICATION

Mohd Yusoff Nurul Husna[1], Chien Hwa Chong[1]*, Kean How Cheah[2], Yoke Kin Wan[1], Voon-Loong Wong[3]

[1]Department of Chemical and Environmental Engineering, Faculty of Science and Engineering, University of Nottingham Malaysia, 43500 Semenyih, Selangor, Malaysia.
[2]School of Aerospace, Faculty of Science and Engineering, University of Nottingham Ningbo China, Ningbo, Zhejiang, China.
[3]School of Engineering and Physical Sciences, Heriot-Watt University Malaysia, 62200 Putrajaya, Wilayah Persekutuan Putrajaya, Malaysia.
*corresponding author: ChienHwa.Chong@nottingham.edu.my

In this work, novel acrylate-based photosensitive resins designed for Digital light processing (DLP) were prepared to fabricate a 3D-printed monolithic structure with poly (ethylene glycol) diacrylate (PEGDA), plant-based resin that was prepared with addition of 2 different comonomers, 1,4-butanediol diacrylate (BDDA) and 1,6-hexanediol diacrylate (HDDA). The influence of comonomer concentration on the mechanical and thermal properties was systematically investigated. The 3D-printed monolithic structure was further grafted with silane coupling agent to enhance moisture absorption and hydrophobicity behavior to be applied in water environment. The result showed that PEGDA with 3wt.% of HDDA had the greatest Young's modulus, ultimate tensile strength and elongation at break. Surface grafting with a single silane agent on the 3D-printed monolithic structure was clarified to have a more balanced effect than hybrid silane coupling agent for the lowering of moisture absorption and increase of hydrophobicity without causing any cracking in the inner truss. The synergistic effect of 3D-printed monolith with the silane coupling agent was identified to be stable chemically and mechanically for practical application in water.

Keywords: biopolymer; 3D printing; silane coupling agent; mechanical properties; moisture absorption; water technology

DESIGN OF FLUIDIZED BED PHOTOREACTOR FOR ETHYLENE REMOVAL UNDER UV LIGHT

Piotr Rychtowski*, Piotr Miądlicki, Bartłomiej Prowans, Beata Tryba

West Pomeranian University of Technology in Szczecin, Department of Catalytic and Sorbent Materials Engineering, Pulaskiego 10, 70-322 Szczecin, Poland
*corresponding author: piotr.rychtowski@zut.edu.pl

Ethylene occurs in the natural environment as a gas and is a plant hormone produced by fruit and vegetables. Both positive and negative effects of ethylene have been observed in agriculture. As a positive effect, ethylene can accelerate the maturation of plants, but on the other hand it is responsible for deterioration of their physical parameters and faster spoilage [1]. The harmful effects of ethylene occur after harvesting, during transport and/or storage. There are some classical methods used to reduce the concentration of ethylene in a storage atmosphere, such as ventilation, adsorption, potassium permanganate oxidation, catalytic oxidation or exposure to ozone. More recently, photocatalytic methods are being investigated to remove ethylene from the atmosphere [2].

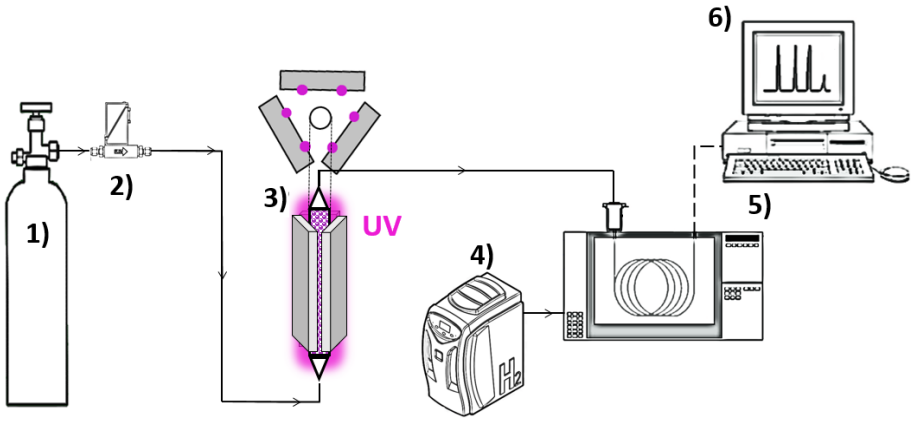

Fig. 1. Photocatalytic system for ethylene removal: 1) ethylene gas bottle, 2) flow meter, 3) fluidized bed photoreactor, 4) H_2 generator, 5) gas chromatograph, 6) PC

A photocatalytic system for the removal of ethylene gas was designed (Fig. 1), consisting of a tubular quartz reactor, filled with a photocatalytic bed and surrounded by UV lamps. Ethylene gas (50 or 200 ppm) in synthetic air flowed continuously through the reactor at different flows: from 80 to 240 ml/min. Expanded polystyrene (EPS) microspheres (>1 mm) were used as the bed filling. The EPS spheres were coated with a TiO_2 photoactive layer (Fig. 2).

Fig. 2. PS- TiO_2 optical microscope image

Commercial tubular UV lamps (72 W) were used as UV light source, as well as a self-built UV-LED system consisting of 3 panels with 16 UV LEDs mounted on each panel (total power was 115 W). Various parameters of the photocatalytic reactor were considered, such as reactor diameter, bed height, gas flow rate and type of UV light source. The smaller diameter of the quartz reactor resulted in a lower minimum fluidization speed of the gas stream. The minimum fluidization flow was calculated, using the following relationship:

$$\dot{V}_{min} = \frac{\varepsilon^3}{1-\varepsilon} \cdot \frac{\breve{g} \cdot \pi \cdot {D_R}^2 \cdot (\rho_P - \rho_L) \cdot d_p^2}{600 \cdot \eta_L} \quad (1)$$

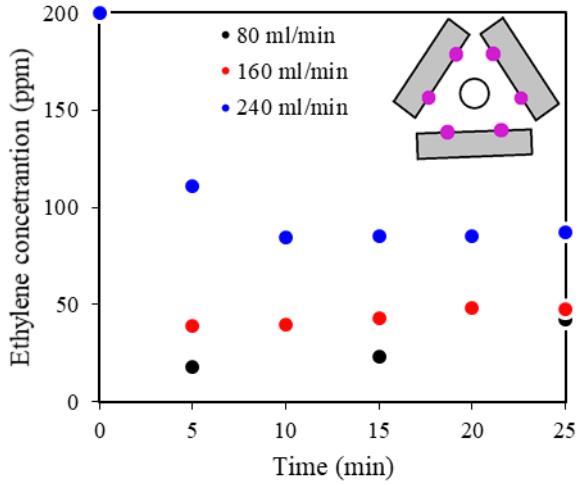

Fig. 3. Photocatalytic ethylene decomposition with the use of fluidized bed reactor and set of three UV-LED modules

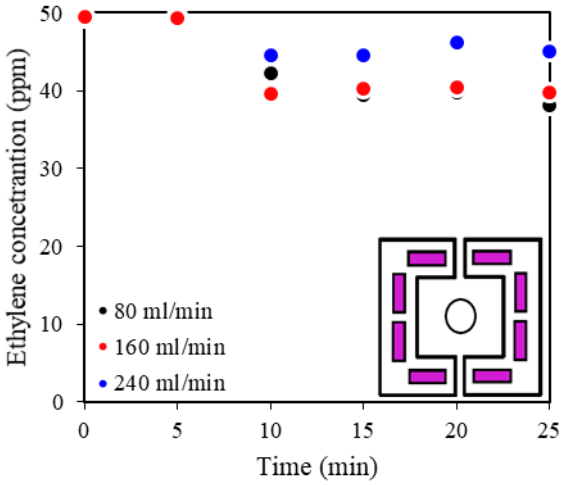

Fig. 4. Photocatalytic ethylene decomposition with the use of fluidized bed reactor and set of two UV-compact lamps

The minimum fluidization flow was independent of the height of the bed, but different gas flow velocities had to be used to achieve the same fluidization degree at different bed fill rates. It was shown that an increase in gas flow through the photocatalytic bed caused a decrease in removal efficiency. The optimal parameters for the photocatalytic reactors were determined: quartz tube diameter of 10 mm, bed height of 80 mm and ethylene gas flow rate of 160 ml/min when the fluidized bed was extended to 150 mm. The self-constructed UV-LED panels led to high ethylene decomposition efficiency. The ethylene removal efficiency of the UV-LED lamps (Fig. 3) was 27 µg/min under dry air conditions, while that of commercial UV lamps (Fig. 4) was only 2 µg/min. The power of the UV-LED lamps was 1.6 times higher than that of the commercial lamps, but the ethylene removal efficiency was 13.5 times higher.

Funding: This research was funded by the National Science Centre, Poland, grant no. 2020/39/B/ST8/01514.

[1] Zhu, Z., Zhang, Y., Shang, Y., Wen, Y., Electrospun Nanofibers Containing TiO2 for the Photocatalytic Degradation of Ethylene and Delaying Postharvest Ripening of Bananas, *Food Bioprocess Technol.*, 2019, 12, 281–287.

[2] De Chiara M.L.V., Pal S., Licciulli A., Amodio M.L., Colelli G., Photocatalytic degradation of ethylene on mesoporous TiO_2/SiO_2 nanocomposites: Effects on the ripening of mature green tomatoes, *Biosyst. Eng.*, 2015, 132, 61–70.

STRUCTURAL DIFFERENCES BETWEEN TITANIUM DIOXIDE OBTAINED VIA VARIOUS METHODS OF SYNTHESIS

Konrad S. Sobczuk*, Iwona Pełech, Piotr Staciwa, Urszula Narkiewicz

West Pomeranian University of Technology in Szczecin, Faculty of Chemical Technology and Engineering, Department of Inorganic Chemical Technology and Environmental Engineering, Pułaskiego 10, 70-322 Szczecin, Poland
*corresponding author: sk43128@zut.edu.pl

In order to study the CO_2 photoreduction process carried out in an aqueous phase, different forms of titanium dioxide (TiO_2) (consisting of anatase, rutile, and brookite) [1] were synthesized using various methods and then compared with commercially available photocatalyst P25. T-TiO_2 samples were obtained using a sol-gel method with titanium tetra-isopropoxide (TTIP) as a precursor [2]: 20 mL of TTIP were mixed with 5 mL of absolute ethanol on a magnetic stirrer. Subsequently, 50 mL of deionized water was added dropwise until total precipitation of white titania. The obtained suspension was stirred for the next 24h, then aged for 24h and dried resulting in white powder (T-TiO_2-NR-NF).

B-TiO_2 and N-TiO_2 were obtained via solvothermal reaction in an autoclave from titanium(IV) fluoride and titanium(III) chloride [3], where the molar ratio of those salts was 40:1 (B-TiO_2) and 1:40 (N-TiO_2). The phase composition of the obtained materials was studied using the X-ray diffraction method and the diffraction patterns are presented in Figure 1.

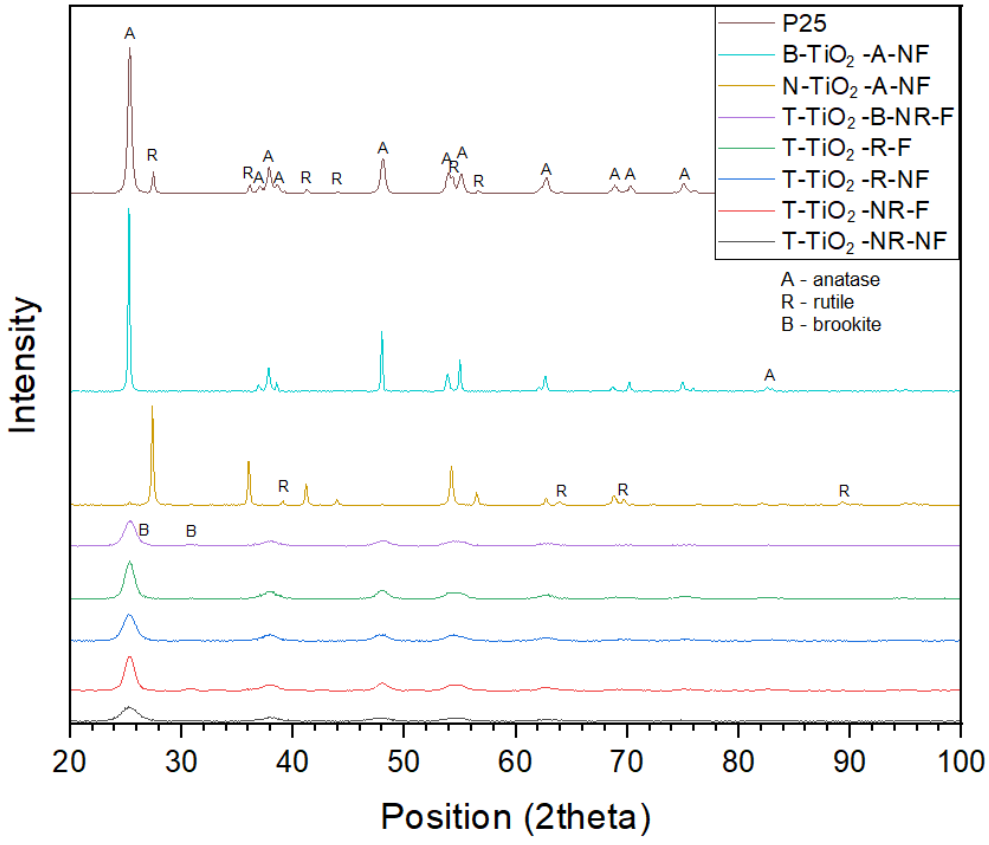

Fig. 1. XRD patterns of the selected samples

It has been found that the method of synthesis greatly affects the phase structure of the samples. Sol-gel method of synthesizing titanium oxide leads mostly to the formation of the anatase phase [2] (Fig. 1.). All T samples contained low content of brookite and no significant amount of rutile phase. B-type samples contained mostly anatase with a slight content of rutile. Alternatively, N-type samples consisted mostly of the rutile phase. In both types of samples, no significant amount of brookite phase was indicated.

Post-hydrolysis treatments like boiling (T-TiO_2-B-NR-F), the use of a microwave reactor (T-TiO_2-R-NF and T-TiO_2-R-F), and heating in a furnace at 400 °C (T-TiO_2-B-NR-F, T-TiO_2-NR-F, and T-TiO_2-R-F) did not change phase composition but affected the average size of crystallites.

Table 1. Adsorption parameters of post-hydrolysis modified T samples

Sample	BET Surface area [m^2/g]	$V_{micropores}$ [cc/g]	$V_{mesopores}$ [cc/g]	TPV [cc/g]
T-TiO_2-NR-NF	281	0.04	0.19	0.23
T-TiO_2-NR-F	117	0.01	0.22	0.23
T-TiO_2-R-NF	220	0.02	0.32	0.34
T-TiO_2-R-F	131	0.01	0.26	0.27
T-TiO_2-B-NR-F	159	0.02	0.20	0.22
P25	54	0.01	0.12	0.13

Adsorption properties of T-TiO_2 samples treated under different experimental conditions were also investigated and compared with P25. Surface properties were determined using N_2 adsorption/desorption isotherms performed on a QUADRASORB evoTM Gas Sorption automatic system (Quantachrome Instruments, Boynton Beach, FL, USA) at –196 °C [4]. Modifications in both the solvothermal reactor (R) and in the furnace (F) reduced the BET surface of the samples as compared to the non-modified sample T-TiO_2-NR-NF (Table 1.). However, treatment in a solvothermal reactor raises the calculated volume of mesopores and subsequently total pore volume (TPV) of titanium oxide samples.

A low amount of brookite (which introduces the band gap (E_g) lower than anatase to the system [5]) in T-type samples is a plausible reason why this type of obtained photocatalyst presented good photocatalytic activity in CO_2 photoreduction reaction (better than commercial P25).

Acknowledgment

The research carried out has received funding from the Norway Grants 2014-2021 via the National Centre for Research and Development under grant no. NOR/POLNORCCS/PhotoRed/0007/2019-00.

References

[1] Liu L., Zhao H., Andino J. M., Li Y., Photocatalytic CO2 Reduction with H2O on TiO2 Nanocrystals: Comparison of Anatase, Rutile, and Brookite Polymorphs and Exploration of Surface Chemistry, *ACS Catal.*, 2012, 2(8), 1817–1828.

[2] Neppolian B., Wang Q., Jung H., Choi H., Ultrasonic-assisted sol-gel method of preparation of TiO2 nano-particles: Characterization, properties, and 4-chlorophenol removal application, *Ultrason. Sonochem.*, 2008, 15(4), 649–658.

[3] Zhu Q., Peng Y., Lin L., Fan C.-M., Gao G.-Q., Wang R.-X., Xu A.-W., Stable blue TiO2−x nanoparticles for efficient visible light photocatalysts. *J. Mater. Chem. A*, 2014, 2(12), 4429.

[4] Pełech I., Staciwa P., Sibera D., Pełech R., Sobczuk K.S., Kayalar G.Y., Narkiewicz U., Cormia R., CO_2 Adsorption Study of Potassium-Based Activation of Carbon Spheres, *Molecules*, 2022, 27, 5379.

[5] Li J.-G., Ishigaki T., Sun X., Anatase, Brookite, and Rutile Nanocrystals via Redox Reactions under Mild Hydrothermal Conditions: Phase-Selective Synthesis and Physicochemical Properties, *J. Phys. Chem. C*, 2007, 111(13), 4969–4976.

INFLUENCE OF SYNTHESIS PARAMETERS ON PHYSICOCHEMICAL PROPERTIES OF IRON PIGMENTS PRODUCED FROM WASTE IRON SULFATE

Kamila Splinter*, Zofia Lendzion-Bieluń

Department of Inorganic Chemical Technology and Environment Engineering, Faculty of Chemical Technology and Engineering, West Pomeranian University of Technology in Szczecin, Piastów 42, Szczecin, 71-065, Poland,
*corresponding author: kamila.splinter@zut.edu.pl

The work presents a two-step method of iron red synthesis based on waste iron(II) sulfate, sulfate from the production of titanium dioxide by the Sulfate Process in Grupa Azoty Zakłady Chemiczne “POLICE” S.A. which was deposited 1976-2012 in a landfill.

A natural development of the existing technologies [1] is to use chemical waste and check whether the obtained products are different from those made from pure raw materials. Chemical waste that can be used for the synthesis of iron pigments in accordance with the concept of "waste to materials" is increasingly being sought. Waste iron(II) sulfate is a promising raw material for the synthesis of iron red pigments along with iron sands [2], coke from bituminous shale [3] and oily mill scale [4].

A microwave reactor was used in the work as a method of synthesis. The work investigated the influence of factors such as temperature, pressure, concentration of solutions and synthesis time on the physicochemical properties of pigments. The obtained pigments were tested with instrumental analytical methods, e.g. X-ray Diffraction, FT-IR, or BET surface area analysis. The pigments were analyzed for color as well as for oil number. Laboratory pigments were also compared with commercial pigments synthesized from pure ingredients.

Based on previous studies [5-6], the use of a microwave reactor in the synthesis of iron red reduces the temperature of the goethite-hematite phase transition from 500°C to 170°C. The formation of agglomerates of synthesized materials is reduced when the temperature of synthesis is lowered (Fig. 1). What is more, such a significant reduction in the phase transition temperature is promising from the point of view of industrial synthesis.

The results of the research showed a change in the physicochemical properties of the obtained pigments depending on the conditions of synthesis. Laboratory pigments have been found to be different from commercial pigments. The difference in properties speaks in favor of the synthesized materials.

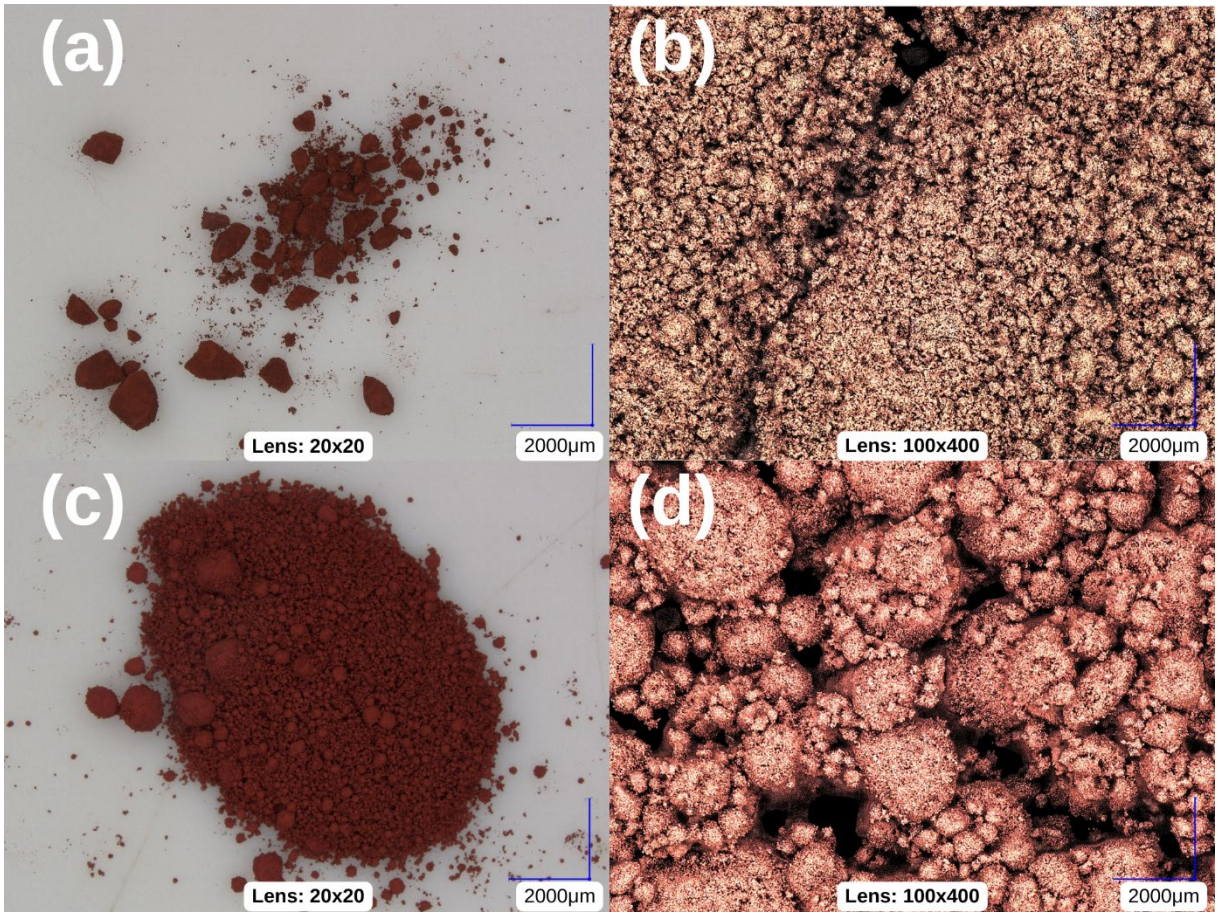

Fig 1. Microscope images of iron pigments. (a, b) laboratory material synthesized in 170°C, (c, d) commercial pigment calcinated in temperature >500°C

Acknowledgements

Part of the research was carried out under the "Najlepsi z Najlepszych 4.0" grant (MEiN/2021/182/DIR/NN4) under the Knowledge Education Development Operational Program Co-financed by the European Social Fund

References

[1] Krześla A., Hoffmann J., Zieliński S., Najlepsze Dostępne Techniki (BAT). Wytyczne dla Branży Chemicznej w Polsce, 2005.
[2] Mufti N., Atma T., Fuad A. Sutadji E., Synthesis and characterization of black, red and yellow nanoparticles pigments from the iron sand, *AIP Conf. Proc*., 2014, 1617, 4897129.
[3] Lu Y., Xu J., Wang W., Wang T., Zong I., Wang A., Synthesis of iron red hybrid pigments from oil shale semi-coke waste, *Adv. Powder Technol.*, 2020, 31, 2179-2586.
[4] Varvara D.A., Aciu C., Pica E.M., Sava C., Research on the Chemical Characterization of the Oily Mill Scale for Natural Resources Conservation, *Procedia Eng*, 2017, 181, 439-443.
[5] Splinter K., Lendzion-Bieluń Z., Otrzymywanie pigmentów żelazowych na bazie odpadowego siarczanu(VI) żelaza(II), in: *Postępy w Technologii i Inżynierii Chemicznej 2021*, Lendzion- Bieluń Z., Moszyński D. (Ed.) Szczecin: Wydawnictwo Uczelniane Zachodniopomorskiego Uniwersytetu Technologicznego w Szczecinie, 2021, 240–249.
[6] Splinter K., Lendzion-Bieluń Z., Wojciechowska A., PL437851A1, 2021.

FACILE FABRICATION OF $NI(OH)_2$ OVER NI FOAM AND THEIR CATALYTIC PERFORMANCE FOR AMMONIA ELECTROOXIDATION REACTION

Sara Sumbal*, Justyna Luczak, Marek Lieder

Politechnika Gdańska, Gdańsk, Poland
*corresponding author: sara.sumbal@pg.edu.pl

For electrochemical energy conversion and storage, ammonia is an appealing carbon free energy source. However, the sluggish kinetic rates of the ammonia electrooxidation reaction (AOR), as well as high cost and poisoning of Pt-based catalysts still remain obstacles [1]. To overcome these barriers, researchers have started to explore more earth-abundant metals. Nickel is a considerably more abundant metal on the planet, making it more economical to employ as an electrode material in electrochemical systems. Kapałka et al. reported that $Ni(OH)_2$ generated through the electrooxidation of Ni foam electrode in alkaline conditions could be used for electrooxidation of ammonia [2]. Herein, we report direct production of α-$Ni(OH)_2$ and β-$Ni(OH)_2$ on Ni foam (NF) electrodes via facile one step solvothermal synthesis method for AOR. Moreover, α-NiCu-LDH and β-NiCu-LDH/NF were prepared using the same procedure as for α-$Ni(OH)_2$/NF and β-$Ni(OH)_2$/NF, respectively by introducing Cu precursor into reactant solutions. In addition, α and β phases of $Ni(OH)_2$ were confirmed through X-ray diffraction (XRD) analysis.
To confirm the AOR activity of prepared catalysts, cyclic voltammograms (CVs) were performed. The catalytic AOR activity of α-$Ni(OH)_2$ can be observed in CVs presented in Fig. 1. Moreover, it was observed that α-NiCu-LDH and β-NiCu-LDH/NF achieved current density of 55.56 mA/cm^2 and 39.78 mA/cm^2 at 1.55 V vs RHE, which was higher than bare α-$Ni(OH)_2$ and β-$Ni(OH)_2$, respectively. Furthermore, α-NiCu-LDH seems to be the most promising electrocatalyst for AOR with least onset potential among other prepared electrocatalysts. Additionally, to get clear insights into the properties of electrocatalysts, electrochemical active surface area (ECSA) and the double layer capacitance (C_{dl}) were calculated.

In this work, the AOR activity of α-$Ni(OH)_2$ and β-$Ni(OH)_2$ was explained properly along with insights into the role played by doped Cu in both phases. Moreover, this study indicates a feasible and effective strategy to prepare highly efficient single metal and bimetallic electrocatalysts for AOR.

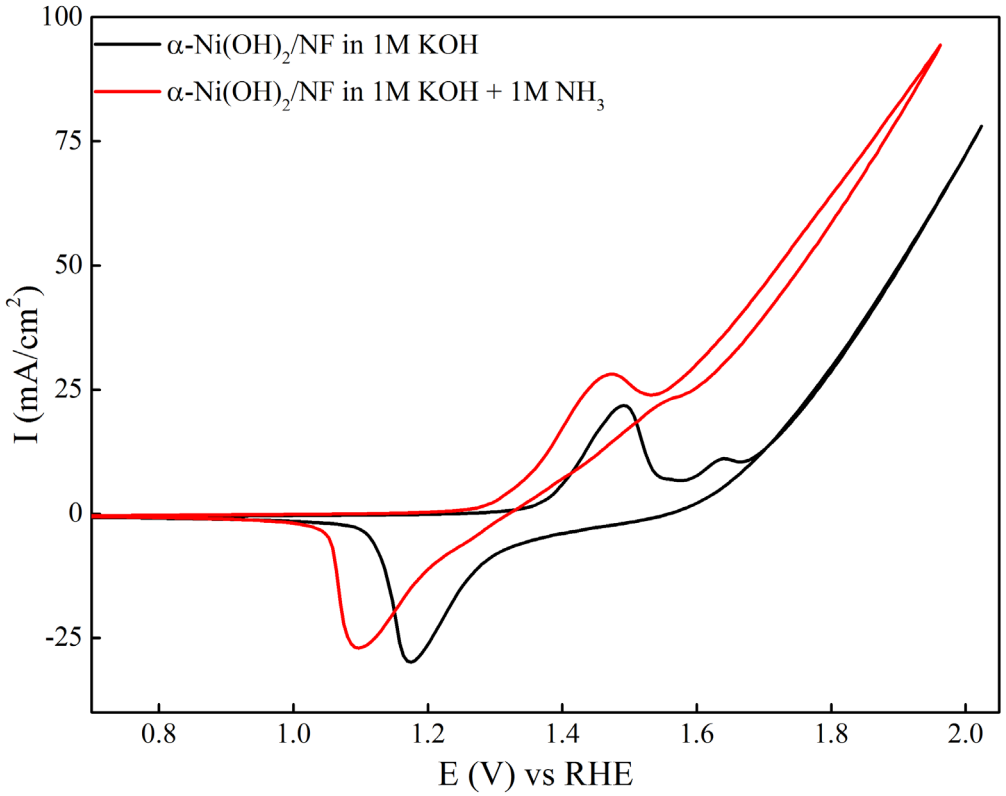

Fig. 1. Cyclic voltammograms (CVs) in 1M KOH with and without 1M NH_3

Acknowledgements
This research work was funded by NCN under program OPUS with the agreement UMO-2021/41/B/ST4/03255 and carried out at Department of Process Engineering and Chemical Technology, Gdansk University of Technology, Gdansk, Poland.

References:

[1] Xu W., Lan R., Du D., Humphreys J., Walker M., Wu Z., Wang H., Tao S., Directly growing hierarchical nickel-copper hydroxide nanowires on carbon fibre cloth for efficient electrooxidation of ammonia, *Appl. Catal. B: Environmental*, 2017, 218, 470–479.
[2] Kapałka A., Cally A., Neodo S., Comninellis C., Wächter M., Udert K. M., Electrochemical behavior of ammonia at Ni/Ni(OH)2 electrode. *Electrochem. Commun*., 2010, 12(1), 18–21.

INFLUENCE OF PROCESS PARAMETERS AND GEOMETRY OF CATALYST WIRES ON AMMONIA OXIDATION AND DEGRADATION OF CATALYST GAUZE – CFD ANALYSIS

Mariusz Tyrański[1]*, Jakub Michał Bujalski[2], Wojciech Orciuch[1], Łukasz Makowski[1]

[1]Faculty of Chemical and Process Engineering, Warsaw University of Technology, Waryńskiego 1, 00-645 Warsaw, Poland
[2]Yara International ASA, Yara Technology and Projects, 3936 Porsgrunn, Norway
*corresponding author: mariusz.tyranski.dokt@pw.edu.pl

Humanity's most pressing challenges include the constantly increasing demand for food and the ongoing degradation of the habitats of many animal species. Because of that, an increase in food production efficiency without constant increases in agricultural land is mandatory. It makes fertilisers perhaps the most crucial branch of the chemical industry. One of the critical stages, ammonia oxidation is a complex and multistep process with a surface reaction on a solid catalyst: platinum-rhodium wire gauze. However, harsh operating conditions cause the degradation of catalytic meshes during the process, negatively affecting conversion efficiency and increasing running costs.

This work concerns the influence of process and chemical properties on the efficiency of nitrogen oxide conversion and degradation of the catalyst wires using CFD analysis [1–2]. Two variants of catalyst gauze geometry were investigated in the present work. The first one was a typical construction used in the industry created based on the literature [3], while the latter was a novel version proposed by the authors. CFD methods were used to evaluate the influence of process parameters and geometry on the degradation of catalyst wire. The catalyst material was platinum and 5% rhodium alloy, and the diameter of wires forming a woven gauze was 0.06 mm, which was expected to give the highest nitrogen oxide conversion rate [4]. The concentration meshes in catalyst woven gauze were 1024 per cm^2. In this work, the stoichiometric reaction of the ammonia oxidation was defined as the wall surface reaction on a volumetric basis. The Discrete Phase Model (DPM) with turbulent dispersion was utilised to predict entrained platinum's movement and deposition using the Lagrangian frame of reference.

Complete distributions of the velocity field (Figure 1), temperature and concentration of reagents on fragments of three-layer platinum wire gauze were obtained.

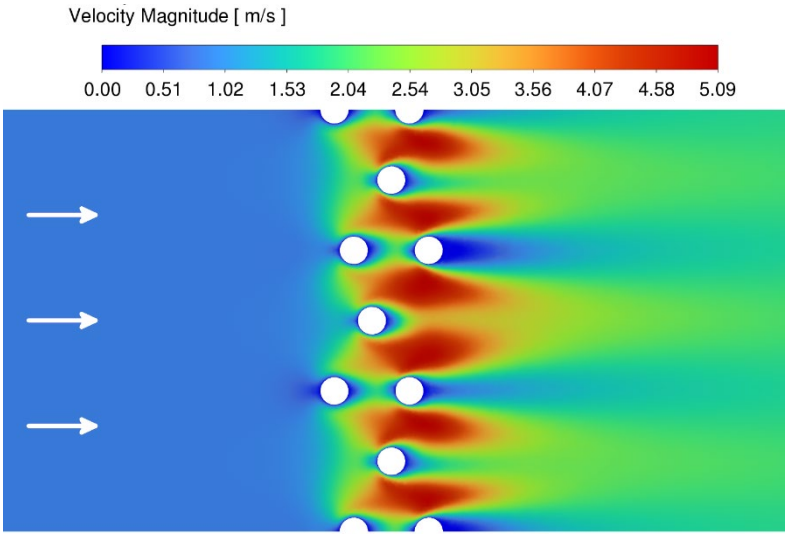

Fig. 1. Contours of mass fraction of nitrogen oxide, contact time: 0.00025s

In our calculations, we assumed that platinum particles were released from the area of the first layer of catalyst gauze with the highest surface temperature (Figure 2). For this purpose, it was decided to divide the surface of the wire into “hot” and “cold” zones.

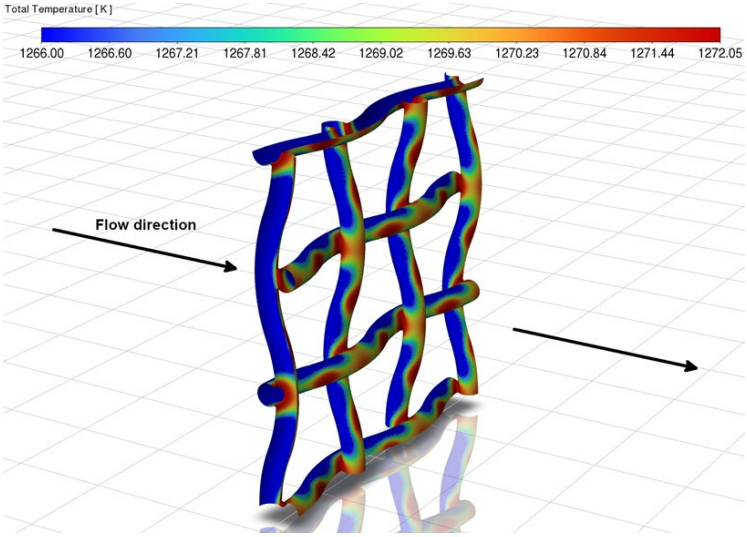

Fig. 2. Surface temperature gradient on the first layer of gauze

From obtained results, it can be observed that essential regions of the considered process are the stagnation areas behind the wires and, in the case of wire gauze, also the shadowing of successive layers by previous ones, which leads to a change in the hydrodynamic conditions close to the catalyst affecting the rate of the surface chemical reaction and the temperature distribution (Figure 3). The geometry of the preceding layer has a crucial influence on the deposition of the entrained platinum, which can reduce the amount of platinum loss.

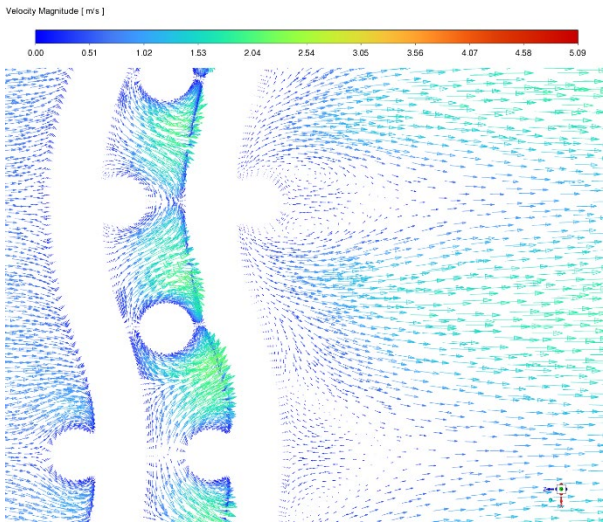

Fig. 3. Stagnation zones behind catalyst gauze, contact time: 0,00025 s

References

[1] Tyrański M., Pasik I., Bujalski J.M., Orciuch W., Makowski Ł., Computational Fluid Dynamics of Influence of Process Parameters and the Geometry of Catalyst Wires on the Ammonia Oxidation Process and Degradation of the Catalyst Gauze, *Energies*, 2022, 15, 8123.
[2] Thiemann M., Scheibler E., Wiegand K. W., Nitric acid, nitrous acid, and nitrogen oxides. *Ullmann’s encyclopedia of industrial chemistry*, 2000.
[3] Hatscher S.T., Fetzer T., Wagner E., Kneuper H.-J., Ammonia Oxidation, in: *Handbook of Heterogeneous Catalysis, 8 Volume Set, 2nd Edition* | Wiley. 2008, pp. 2575–2592.
[4] Bergene E., Tronstad O. Holmen A., Surface Areas of Pt-Rh catalyst gauzes used for ammonia, 1996.

PROLIFERATION OF NON-ADHERENT HL-60 CELLS IN WAVE 25 BIOREACTOR: INFLUENCE OF CFD-DETERMINED VALUES OF SHEAR STRESS ON BIOMASS

Kamil Wierzchowski*, Łukasz Makowski, Maciej Pilarek

Faculty of Chemical and Process Engineering, Warsaw University of Technology,
Waryńskiego 1, 00-645 Warsaw, Poland
*corresponding author: Kamil.Wierzchowski.dokt@pw.edu.pl

Disposable bioreactors with wave-induced agitation allow efficient aeration of the culture medium via oscillatory rocking movements of the polymer bag-like vessel. The rocking allows renovation of the interfacial area between the liquid and the gas phase and provides bubble-free surface aeration of the culture broth waving inside a bag-like vessel. Furthermore, the waves generated on the liquid phase surface provide homogeneity of the culture, and mixing the culture medium ingredients can be achieved. The main applications of wave-agitated disposable bioreactors are cultures of fragile plant or animal cells, aggregated cells, tissues, organs, and biomass-biomaterial structures [1]. In bioreactors with wave-assisted agitation, desirable culture conditions can be achieved at lower values of the liquid flow turbulence characterized by the Reynolds number (Re_L), in contrast to the relatively higher values of the Re_L number noted for conventional stirred bioreactor systems [2].

Computational Fluid Dynamics (CFD) is widely used to characterize both traditional and disposable bioreactors. Nevertheless, most CFD analyses describe conditions in the stirred tank bioreactors due to their similarity to chemical reactors. Nowadays, only a few papers consider the CFD application for wave-agitated bioreactor characterization, mainly to determine mixing and gas-liquid mass transfer parameters [3-5].

The aim of this study was to recognize the relationship between shear stresses and the proliferation of HL-60 cells under various wave-assisted agitation conditions (described by Re_L) in a disposable bioreactor. The influence of mixing time (t_{95}), maximum shear stress (τ_{max}), and maximum liquid velocity (v_{max}) determined with CFD simulations in ANSYS Fluent software, on HL-60 cells proliferation, i.e., cell density (X), cell viability (Z), the metabolic activity of cells (a_m) and lactate dehydrogenase activity (a_{LDH}) was identified and discussed.

The *ReadyToProcess* WAVE™ 25 bioreactor system (WAVE 25) equipped with a disposable polymer-based 2 dm^3 culture bag (Cellbag™ 2L), both manufactured by Cytiva (USA), was used for bioprocessing of non-adherent HL-60 cells. The following conditions of wave-assisted agitation were investigated: Re_L=5104 (α=6°, ω=20 min^{-1}), Re_L=10152 (α=12°, ω=20 min^{-1}), Re_L=10208 (α=6°, ω=40 min^{-1}) and Re_L=20305 (α=12°, ω=40 min^{-1}). HL-60 cells were maintained in the culture medium consisting of 89% RPMI, 10% inactivated fetal bovine serum, and 1% commercial antibiotic/antimycotic mixture. The detailed methodologies applied for determining values of X, Z, a_m, and a_{LDH} are available in the previously published reports, e.g. [2].

Values of t_{95}, τ_{max}, and v_{max} were determined based on the VOF method supported by the Eulerian multiphase model in Ansys Fluent software.

Table 1. Values of t_{95}, τ_{max}, and v_{max} determined by CFD analysis for various values of Re_L

Re_L	t_{95} [s]	τ_{max} [s^{-1}]	v_{max} [m s^{-1}]
5104	25.0	2700	0.034
10152	7.5	7500	0.075
10208	4.0	24500	0.105
20305	2.5	31200	0.130

Values of X, Z, a_m, and a_{LDH} determined experimentally for HL-60 cells cultured under various Re_L values in the WAVE 25 bioreactor system are presented in Fig 1.

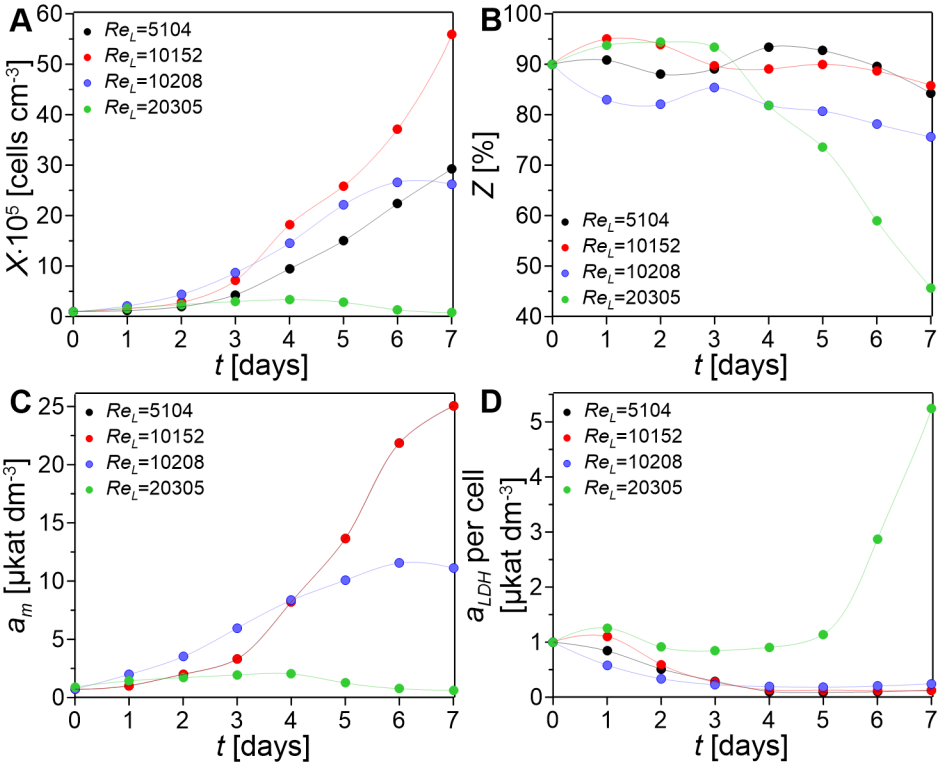

Fig. 1. Values of X (A), Z (B), a_m (C), and a_{LDH} per cell(D) determined in cultures of HL-60 cells maintained under various Re_L values in WAVE 25 bioreactor system

Based on data presented in Fig. 1, the most suitable conditions for maintaining HL-60 cells in WAVE 25 bioreactor were supported by Re_L=10152, which was proved by the highest values of X and a_m the high value of Z, and low values of a_{LDH} per cell. Such favorable conditions for HL-60 cell proliferation at Re_L=10152 can be explained by supporting satisfactory mixing conditions (described by high values of t_{95}) and by low hydrodynamic stress (rather low values of τ_{max} and v_{max}) (please see Table 1.). On the other hand, for HL-60 cells maintained at Re_L=20305, the values of X, Z, and a_m were very low, in contrast to high values of a_{LDH} per cell. This could have been caused by the negative influence of hydrodynamic conditions (described by the high value of both τ_{max} and v_{max}) (Table 1.).

In conclusion, the experimentally estimated data identifying growth (i.e., X) and physiological (i.e., Z) and metabolic (i.e., a_m and a_{LDH}) conditions of *in vitro* cultured animal non-adherent cells successfully verified the values of t_{95}, τ_{max}, and v_{max} determined numerically with CFD.

References

[1] Wierzchowski K., Kuźmińska A., Pilarek M., Intensification of chondrocytes proliferation by microcarriers and wave-induced mixing: Reynolds number influence on CP5 cells growth. *Chem. Eng. Process.*, 2021, 166, 108472.

[2] Pilarek M., Sobieszuk P., Wierzchowski K., Dąbkowska K., Impact of operating parameters on values of a volumetric mass transfer coefficient in a single-use bioreactor with wave-induced agitation. *Chem. Eng. Res. Des.*, 2018, 136, 1–10.

[3] Öncül A.A., Kalmbach A., Genzel Y., Reichl U., Thévenin D., Characterization of flow conditions in 2 L and 20 L wave bioreactors® using computational fluid dynamics. *Biotechnol. Progress,* 2010, 26, 101–110.

[4] Zhan C., Hagrot E., Brandt L., Chotteau V., Study of hydrodynamics in wave bioreactors by computational fluid dynamics reveals a resonance phenomenon. *Chem. Eng. Sci.*, 2019, 193, 53–65.

[5] Svay K., Urrea C., Shamlou P.A., Zhang H., Computational fluid dynamics analysis of mixing and gas–liquid mass transfer in wave bag bioreactor. *Biotechnol. Progress*, 2022, 36, 3049.

PURIFICATION OF VISCOUS AND THERMAL SENSITIVE PRODUCT IN ROTATING PACKED BED EQUIPMENT

Dawid Zawadzki*, Jerzy Pela, Michał Pawłowski, Andrzej Górak

Prospin sp. z o.o., Rokicińska 156, 92-412 Łódź, Poland
*corresponding author: dawid.zawadzki@rpb-prospin.com

Process intensification is one of the most important topics in contemporary chemical engineering. It can be described as a set of methods and techniques leading to improvements in process performance in terms of production efficiency, energy consumption, waste formation, equipment size [1]. High gravity (HiGee) processes are the leading examples of PI. The main idea of HiGee is to substitute gravitational force with centrifugal force [1]. An example of HiGee technology is the Rotating Packed Bed (RPB), which is a device for intensified mass transfer, first patented by Ramshaw and Mallison in 1981 [2].

RPB is a gas-liquid contact apparatus (see Figure 1), which can work both in co- and counter-current configurations. In co-current variant, the gas flows from the eye of the rotor (14) through packing to casing (7) while in the counter-current the gas flows in the opposite direction. The liquid, regardless of configuration, is sprayed in the eye of the rotor (14) on the inner area (5) of the rotating packing (1). Centrifugal force, generated by the rotation, forces the liquid through the packing (1). The liquid is collected at the bottom of the case (11). The central part of the RPB is an annular packing (1) embedded between rotor plates, whose rotation axis may be either vertical or horizontal. The lower rotor plate (2) is directly mounted on a shaft (3), while the upper plate (4) is centered by positioning elements and bolts. The distance between the rotor plates is determined by an inner support ring (5) and spacers fitted to a packing height.

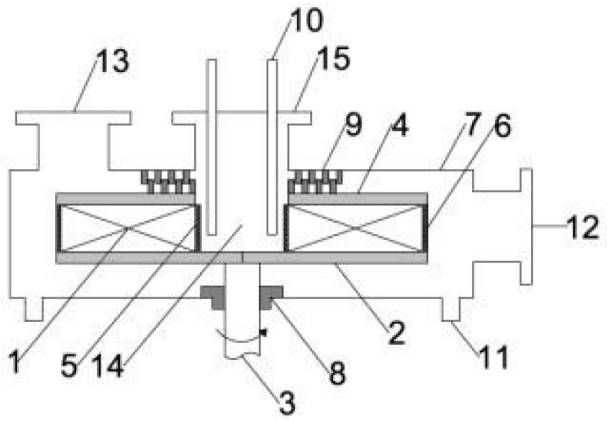

Fig. 1. Schematic drawing of vertical axis single block RPB: 1. Packing 2. Lower rotor plate 3. Shaft 4. Upper rotor plate 5. Inner support ring 6. Perforated ring 7. Casing 8. Lower seal 9. Upper seal 10. Liquid distributor 11. Liquid outlet 12. Tangential gas outlet/inlet 13. Top gas outlet/inlet 14. Eye of the rotor 15. Central gas inlet/outlet

In comparison to traditional apparatus, RPB provides increased liquid and gas throughput over 10 times, increased mass transfer coefficient up to 10 times and reduction of volume apparatus up to 10 times [3]. Substituting gravitational force with centrifugal force, which can be up to 1000 times greater, allows to use much more viscous liquid and dramatically decreases liquid residence time in apparatus. Due to its very short liquid residence time and high mass transfer coefficient, the RPB can be used as a machine for stripping thermally sensitive liquids. Over the past decades, there has been a growing interest in RPBs within academia and industry, owing to their portable nature (see Figure 2), high responsivity, good mass transfer efficiency, and compact design [3].

Fig. 2. Mobile plant delivered by Prospin as a part of the ACCSESS project

Increasing awareness and familiarity with modern Rotating Packed Bed technology is the goal of Prospin. Not only for the absorption or distillation processes but also implementing RPBs in other gas-liquid processes.

One of the potential applications of RPB is product purification by solvent evaporation in an inert gas environment. A feed mixture containing approximately 50% solvent, with a viscosity of 2500 mPas at 25 °C, was concentrated in an RPB unit. Due to the high boiling point of the solvent and the thermal sensitivity of the product, the process was carried out at a pressure of 0.1 bar. The feed was introduced at elevated temperatures between 150-200 °C. In addition, the inert stripping gas was also heated. The viscosity of the purified product was 22 000 mPas at 25 °C. This work will present the results of conducting such separation in an RPB, with focus on the product quality and separation efficiency.

References

[1] Ramshaw C., Higee' distillation-an example of process intensification, *Chem. Eng*., 1983, 13–14.
[2] Ramshaw C., Mallinson R.H., US 4,283,255, Mass transfer process, 1981. https://patents.google.com/patent/US4283255A/en.
[3] Neumann K., Gladyszewski K., Groß K., Qammar H., Wenzel D., Górak A., Skiborowski M., A guide on the industrial application of rotating packed beds, *Chem. Eng. Res. Des*., 2018, 134, 443–462.

Lectures

S6. Bioprocess and medical engineering

IN VITRO RELEASE STUDIES OF POORLY WATER-SOLUBLE COMPOUNDS USING FLOW-THROUGH CELL USP4 APPARATUS

Katarzyna Bialik-Wąs*, Paulina Sapuła

Department of Organic Chemistry and Technology, Faculty of Chemical Engineering and Technology, Cracow University of Technology, Warszawska 24, 31155 Cracow, Poland
*corresponding author: katarzyna.bialik-was@pk.edu.pl

Currently, there is a tendency for new forms of carrier-drug systems with prolonged and controlled release to be developed. However, in order to design medical or pharmaceutical devices, which have to be characterized by high quality and the assumed parameters in real conditions, it is necessary to analyze this process based on *in vitro* release (IVR) testing methods. For this purpose, extracorporeal studies are carried out, which enables determination of the release profiles of active substances using a simulated tissue-like environment. According to the United States Pharmacopeia (USP), it stands out seven typically used equipment for releasing active substances, such as basket (USP1), paddle (USP2), cylindrical reciprocating (USP3), flow (USP4), Paddle-over-Disk (USP5), cylindrical (USP6) as well as reciprocating (USP7) apparatus [1-3].

Here, we focused on the release tests of poorly water-soluble compounds (salicylic acid and fluocinolone acetonide) from a dual drug delivery system using the flow-through cell method (USP4, Erweka GmbH, Langen, Germany). The apparatus contained seven in-line flow-through diffusion cells. The membrane was placed over the support with an orifice of 1.5 cm diameter (diffusional area, 1.766 cm^2). The vertical cell was made of glass and was designed to have a volume into the donor compartment of 6.22 ml. The cells were placed in a cell warmer connected to the Erweka heater DH 2000i and the Erweka piston pump HKP 720. The piston pump transported the receptor fluid via seven channels to the flow-through cells and automatically adapted the flow rate setting. All the determinations were made in triplicate for each cell. The release studies of salicylic acid and fluocinolone acetonide were carried out using a regenerated cellulose membrane Spectra/Por®Dialysis Membrane MWCO 6-8,000 Carl Roth® Company. The assays were performed in 2% ethanol in PBS (pH = 7.40) at a temperature of 37 °C. The released concentration of active components in the acceptor medium was analyzed using UV-Vis spectroscopy (Perkin Elmer Company). Additionally, we used two possibilities for conducting the research, such as 1) open system, in which the media are passed once only through the cell with the sample and 2) closed system, in which the media are continuously cycled past the cell with the sample.

On the basis of results, we can conclude that the USP4 method may be suitable, especially for the release tests of poorly water-soluble components introduced into modern forms of drug administration, such as polymeric matrices, hydrogels, nano- and microcarriers as well as hybrid systems.

Acknowledgements
This research was financial supported by The National Centre for Research and Development — project LIDER/41/0146/L-9/17/NCBR/2018.

References

[1] Uddin R., Saffoon N., Sutradhar K.B., Dissolution and dissolution apparatus: a review, *Int. J. Cur Biomed. Phar. Res.*, 2011, 1(4), 201-207.
[2] Todaro V., Persoons T., Grove G., Healy A.M., D'Arcy D.M., Characterization and simulation of hydrodynamics in the paddle, basket and flow-through dissolution testing apparatuses-a review, *Dissolution Technol.*, 2017, 24(3), 24-36.

[3] Sievens-Figueroa L., Pandya N., Bhakay A., Keyvan G., Michniak-Kohn B., Bilgili E., Davé R.N., Using USP I and USP IV for discriminating dissolution rates of nano-and microparticle-loaded pharmaceutical strip-films, *AAPS PharmSciTech.*, 2012, 13, 1473-1482.
[4] Bialik-Wąs K., Miastkowska M., Sapuła P., Pluta K., Malina D., Chwastowski J., Barczewski M., Bio-Hybrid Hydrogels Incorporated into a System of Salicylic Acid-pH/Thermosensitive Nanocarriers Intended for Cutaneous Wound-Healing Processes, *Pharmaceutics*, 2022, 14(4), 773.
[5] Farmakopea Polska X. Urząd Rejestracji Produktów Leczniczych, Wyrobów Medycznych i Produktów Biobójczych, PTF Warszawa 2014.

BIOBASED HYDROGELS AS FUNCTIONAL PLATFORMS FOR CATALYSIS, NUTRITION AND MEDICAL APPLICATION

Karolina Labus*, Halina Maniak, Katarzyna Kołodzińska, Łukasz Radosiński

Department of Micro, Nano and Bioprocess Engineering, Faculty of Chemistry, Wrocław University of Science and Technology, Norwida 4/6, 50-373 Wrocław, Poland
*corresponding author: karolina.labus@pwr.edu.pl

Currently, the eyes of the whole world are turned towards the dizzying degeneration of the natural environment, caused mainly by the rapidly ever-increasing rate of production and consumption of various commercial products. As a result of both the industrial manufacturing processes and the worldwide use of the goods received, countless amounts of waste and pollution are generated that pose a huge threat to the environment. In particular, the chemical, nutrition and medical sectors produce millions of tons of by-products, and waste effluents contributing to the high carbon footprint [1-3]. Therefore, effective minimization of these adverse effects is crucial for regaining balance in the coexistence of mankind and nature. One of the possibilities to tackle this challenge is to leverage the achievements of bioengineering in providing sustainable, eco-friendly solutions in the production of biocatalysts and biomaterials with improved applicability.

In the current work, we present our contribution to the development of indicated bioprocess engineering approach by providing functional hydrogel-based materials dedicated to specified applications in industrial biocatalysis, modern nutrition and medicine. The following case studies are discussed: (i) enzyme immobilization using biodegradable hydrogel matrices [4, 5]; (ii) colorimetric assays based on functionalized hydrogels [6, 7]; (iii) novel plant-derived hydrogels formulations enriched with superfoods blends; and (iv) bio-based hydrogels for laparoscopic skills training.

In each of them, maximum simplification of the applied manufacturing procedures was pursued, while maintaining the highest quality and functionality of the products obtained. We used compounds of natural origin such as sodium alginate, κ-carrageenan, and gelatin from porcine skin. Crosslinking reactions were carried out under mild ionotropic or enzymatic conditions to produce hydrogel matrices. In order to achieve the desired biofunctionality, most of the tested materials were enriched with: enzymes of microbial origin (β-galactosidase from *Kluyveromyces lactis*; invertase from *Saccharomyces cerevisiae*, laccase from *Trametes versicolor*, tyrosinase from *Agaricus bisporus*), reactive chemicals (o-nitrophenyl-β-galactoside, ONPG; 2,2′-Azino-bis(3-ethylbenzothiazoline-6-sulfonic acid) diammonium salt, ABTS; L-3,4-dihydroxyphenylalanine, L-DOPA), or superfoods (matcha – *Camellia sinensis* (L.) Kuntze; maca – *Lepidium meyenii*, moringa – *Moringa oleifera*, acai – *Euterpe oleracea*, spirulina – *Arthrospira platensis*, chlorella – *Chlorella vulgaris*). In the course of detailed studies, the chemical composition of hydrogel materials (e.g. mono- or multi-components) and production conditions (e.g. reagents concentration, temperature and time of cross-linking) were carefully selected. Then, their physicochemical properties (e.g. mechanical resistance, swelling, hydrolytic degradation, susceptibility to microbial contamination) and functional potential for commercial use were determined.

The research resulted in the development of (i) immobilized biocatalysts with improved operational properties characterized by enhanced thermal, process and storage stability, (ii) highly specific detection plate tests for screening purposes in enzymology and medical diagnostics; (iii) balanced vegan food supplements with proven health-promoting properties, as well as (iv) biodegradable hydrogel inserts for professional laparoscopic training. Selected examples of products obtained are depicted in Fig. 1.

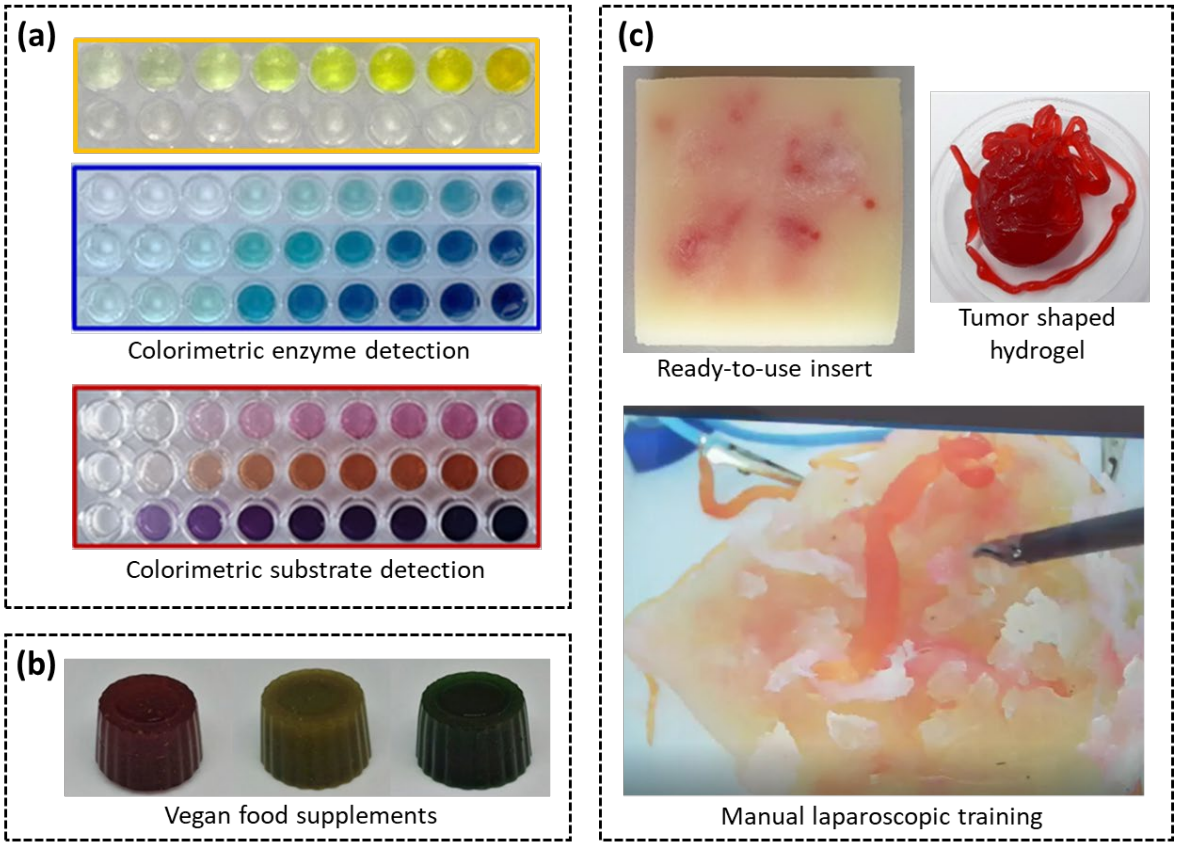

Fig. 1. Application of bio-based hydrogel platforms for development (a) colorimetric detection tests, (b) health-promoting food products, (c) biodegradable inserts for laparoscopic training

References

[1] Naidu R., Biswas B., Willett I.R., Cribb J., Singh B.K., Nathanail C.P., Coulon F., Semple, K.T., Jones, K.C., Barclay A., Aitken R.J., Chemical pollution: A growing peril and potential catastrophic risk to humanity, *Environ. Int.*, 2021, 156, 106616.
[2] Pandey A., Food wastage: Causes, impacts and solutions, *Sci. Herit. J.*, 2021, 5, 17–20.
[3] Sharma J., Joshi M., Bhatnagar A., Chaurasia A.K., Nigam S., Pharmaceutical residues: One of the significant problems in achieving 'clean water for all' and its solution, *Environ. Res.*, 2022, 215, 114219.
[4] Labus K., Wolanin K., Radosiński Ł., Comparative study on enzyme immobilization using natural hydrogel matrices - Experimental studies supported by molecular models analysis, *Catalysts*, 2020, 10, 489.
[5] Labus K., Radosiński Ł., Kotowski P., Functional Properties of Two-Component Hydrogel Systems Based on Gelatin and Polyvinyl Alcohol—Experimental Studies Supported by Computational Analysis, *Int. J. Mol. Sci.*, 2021, 22, 9909.
[6] Labus K., Effective detection of biocatalysts with specified activity by using a hydrogel-based colourimetric assay – β-galactosidase case study, *PLOS ONE*, 2018, 13(10), e0205532.
[7] Labus K., Maniak H., Colourimetric Plate Assays Based on Functionalized Gelatine Hydrogel Useful for Various Screening Purposes in Enzymology, *Int. J. Mol. Sci.*, 2023, 24, 33.

LACTOBACILLUS RHAMNOSUS FERMENTATION PROFILE IN THE PRESENCE OF UBIQUITOUS LIGNOCELLULOSIC HYDROLYSIS BY-PRODUCTS

Magdalena Lech*

Wroclaw University of Science and Technology, Faculty of Chemistry, Group of Micro, Nano and Bioprocess Engineering

*corresponding author: magdalena.lech@pwr.edu.pl

The brewery spent grain (BSG) is a lignocellulosic waste material produced in a considerable amount around the world. Strict environmental protection law requires its proper utilization. BSG can be transformed into easy-fermentable carbohydrates as a result of hydrolysis. This may be a low-cost raw material for biotechnological fermentation. However, chemical hydrolysis of lignocellulose creates also by-products which are potentially noxious to bacteria cells employed in fermentation. The influence of by-products (furfural, acetic, formic, gallic, and levulinic acid) on the lactic acid fermentation effectiveness was tested. These compounds were introduced into *Lactobacillus* cultures in various concentrations. The rate of cell growth, glucose consumption, and lactic acid production were calculated.

Inhibitors added to the cultures have a significant though diverse impact on cell growth rate, glucose consumption, and LA production. Some of them are stronger than others and even a small amount of them slows down bacterial growth and metabolism.

The most toxic effect was shown by formic acid. A limited amount of formic acid results in a significant drop in cell efficiency of LA formation and the concentration of it higher than 1.1 g/L reduces this parameter almost 27% and addition of 2.1 g/L of FA causes lack of LA formation ability.

Gallic, levulinic and acetic acid also had a negative impact on the cells, but the concentrations which reduced fermentation yield were slightly higher (greater cell tolerance of them). The concentration of these by-products should not exceed (in [g/L]): 0.7, 2.3, 0.7, respectively, to maintain the highest LA production effectiveness. Furfural has the weakest influence on LA concentration in cultures and can be even negligible.

On the other hand, furfural, acetic, levulinic and gallic acid inhibited mainly growth whereas the activity of cells remained almost unchanged. The lower cells efficiency (Fig. 1) was noticed in cultures with formic acid, where cells had a limited ability of LA formation. The LA concentrations in flasks after one day of propagation with the 2.1 g/L of appropriate inhibitor drop app. [%] 16 (F), 22 (GA), 8 (LevA), 40 (AA), and 100 (FA) in comparison to the flask without any inhibitor.

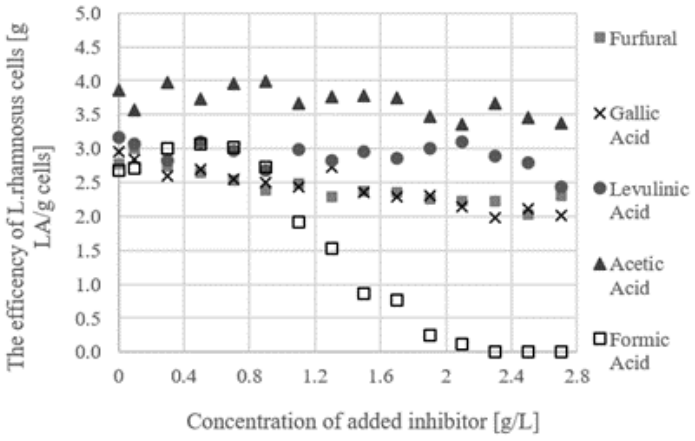

Fig. 1. The fermentation efficiency of cells in flasks with inhibitors (calculated for the 24 hours culture)

The above results are important data for BSG hydrolysis design and the application of hydrolysates for LA fermentation. Hydrolysis can be carried out in many ways (chemical, enzymatic, mixed) and under very different conditions (concentration of reagents or raw material, its fragmentation, pressure, temperature, etc.). The obtained results show that the process conditions and its design must be chosen in a way which limits the concentration of formic acid in the final product.

References

[1] Mussatto S.I., Dragone G., Roberto I.C., Brewers' spent grain: Generation, characteristics and potential applications. *J. Cereal. Sci*., 2006, 43(1), 1–14.

[2] Abdel-Rahman M.A., Tashiro Y., Sonomoto K., Lactic acid production from lignocellulose-derived sugars using lactic acid bacteria: Overview and limits. *J. Biotechnol.* [Internet]., 2011, 156(4), 286–301.

[3] Palmqvist E., Hahn-Hägerdal B., Fermentation of lignocellulosic hydrolysates. II: Inhibitors and mechanisms of inhibition. *Bioresour. Technol*., 2000, 74(1), 25–33.

[4] van der Pol E.C., Vaessen E., Weusthuis R.A., Eggink G., Identifying inhibitory effects of lignocellulosic by-products on growth of lactic acid producing micro-organisms using a rapid small-scale screening method. *Bioresour. Technol.* [Internet]., 2016, 209, 297–304.

[5] Jönsson L.J., Martín C., Pretreatment of lignocellulose: Formation of inhibitory by-products and strategies for minimizing their effects. *Bioresour. Technol*., 2016, 199, 103–12.

STATISTICAL METHODS OF DATA ANALYSIS IN OBTAINING THYME OIL- LOADED NANOEMULSIONS AS POTENIAL SKIN DISINFECTANTS

Małgorzata Miastkowska, Anna Łętocha, Alicja Michalczyk

[1]Department of Chemical Engineering and Technology, Cracow University of Technology, Cracow, Poland
[2]Lukasiewicz - Research Network-Institute of Industrial Organic Chemistry, Warsaw, Poland
*corresponding author: malgorzata.miastkowska@pk.edu.pl

Essential oils, due to their antimicrobial properties, have found wide application in the cosmetic, pharmaceutical and food industries. Due to their widespread availability, high antimicrobial effectiveness and safety, those active substances and containing them nanoemulsions can be a green alternative to commercial preparations containing nanosilver with antimicrobial properties applied to the skin [1, 2].

The aim of this study was to obtain stable thyme-oil loaded nanoemulsions and to confirm their antimicrobial and disinfecting properties.

The first stage of the work was to develop nanoemulsion recipes using the statistical design of experiment method (DOE). For this purpose, the fractional plan $3^{(K-p)}$ was selected, where K - the number of variables (parameters that change), p - always takes the value 1. In all cases, the statistical significance level was assumed to be $p < 0.05$.

Thyme oil was used as the oil phase, ECO Tween ® 80 acted as the emulsifier, and the rest of the formulation was deionized water. Ultrasonification was chosen as the method of obtaining nanoemulsions. It was checked whether the input parameters (oil concentration, emulsifier concentration, amplitude, and sonication time) had a significant impact on the output parameters (nanoemulsion particle size, polydispersity index, viscosity and stability over time). The particle size of nanoemulsions was characterized with dynamic light scattering. The chemical composition of the thyme oil was analyzed with GC-MS method. For the formulations selected on the basis of the statistical data analysis, the values of minimum inhibitory concentrations (MIC) and minimum biocidal concentrations (MBC/MFC) were determined in relation to 10 bacterial strains (e.g. *Bacillus subtilis ATCC 6633, Pseudomonas aeruginosa NCTC 6749, Moraxella catarhalis ATCC 25238, Staphylococcus aureus NCTC 4163, Staphylococcus epidermidis ATCC 49134*) and 4 strains of yeast-like fungi of the genus *Candida*. The test was performed by serial dilutions in liquid medium [3, 4]. Thyme oil was used as a control, for which the MIC and MBC/MFC values were also determined.

The results obtained from the statistical analysis showed that the concentration of the oil and emulsifier as well as sonication time had the greatest influence on the physicochemical properties of the nanoemulsion. On the basis of approximation profiles, it was concluded that the optimal concentration of the thyme oil in nanoemulsion should amount to 2%. Biological studies have shown that the nanoemulsions based on thyme oil were characterized by stronger activity against bacteria and yeast-like fungi than pure oil. The MIC values of the nanoemulsion for most of the test strains were 0.156-0.312 µg/µl, and MBC/MFC 0.312-0.625 µg/µl. For thyme oil, MIC values ranged from 1.25-2.5 µg/µl, and MBC/MFC 2.5-10 µg/µl. A weaker effect of thyme oil and nanoemulsion was found for strains of *Pseudomonas aeruginosa* and *Enterococus fecalis*, for which the MIC and MBC values were 10-> 10 µg/µl.

In the further stages of the research, the basic disinfecting effect for the above-mentioned substances was also checked. It was shown that the nanoemulsion based on 2% thyme oil after 30 minutes of contact time caused the required for disinfectants reduction of >5 log of bacterial strains (*S. aureus, Ps. aeruginosa*) and > 4 log of fungal strains (*C. albicans*). In the case of 2% of the oil, the required reduction was obtained only for *Ps. aeruginosa* (> 5 log) and *C. albicans* (> 4 log). The commercial preparation, containing Ag ions, used for comparison purposes, after 30 minutes also

caused the required reduction > 5 log test strains of bacteria (*S. aureus, Ps. aeruginosa*), but did not show the required fungicidal activity (> 4 log) against the strain of *C. albicans*.

It was found that thyme oil - based nanoemulsion showed stronger antibacterial and antifungal activity compared to pure oil. Moreover, it was characterized by disinfecting properties. However, further research is needed to confirm the safety of the obtained formulations after skin application.

References

[1] Miastkowska M., Michalczyk A., Figacz K., Sikora E., Nanoformulations as a modern form of biofungicide, *J. Environ. Health Sci. Eng*., 2020, 18(1), 119–128.

[2] Michalczyk A., Ostrowska P,. Essential oils and their components in combating fungal pathogens of animal and human skin*, J. Mycol. Med.*, 2021, 31(2), 101118.

[3] Andrews J.M., Determination of minimum 497 inhibitory concentration, *J. Antimicrob. Chemother.,* 2002; 48(1), 5–16.

[4] Cybulski J., Wiśniewska A., Kulig-Adamiak A., Dąbrowski Z., Praczyk T., Michalczyk A., Walkiewicz F., Materna K., Pernak J., Mandelate and prolinate ionic liguids: synthesis,characterization, catalytic and biological activity. *Tetrahedron Lett.*, 2011, 52(12), 1321328.

A NOVEL PROCESS OF BIOELECTROCHEMICAL SYNTHESIS AND MONITORING OF BIOSURFACTANTS

Grzegorz Pasternak*, Aleksander de Rosset, Bartosz Widera, Natalia Tyszkiewicz

Laboratory of Microbial Electrochemical Systems, Department of Process Engineering and Technology of Carbon and Polymer Materials, Faculty of Chemistry, Wroclaw University of Science and Technology, Wroclaw, Poland
*corresponding author: grzegorz.pasternak@pwr.edu.pl

In recent decades, bioelectrochemical systems (BES) have undergone significant improvements and numerous exciting applications have emerged. This technology has great potential to contribute to solving multiple global issues such as environmental contamination. There are, however, some limitations in the efficiency of treating hydrophobic wastes such as petroleum contaminants or waste cooking oil.

In our research, we aimed to couple the bioelectrochemical degradation of these substrates with *in-situ* production of biosurfactants in microbial fuel cells (MFCs) and potentiostatic – controlled BESs. Several approaches have been taken for the enrichment of microbial consortia capable of bioelectrochemical synthesis of surfactants. The microbial communities were derived from environments with various contact with hydrocarbons such as contaminated soil, municipal environments, river sediments, activated sludge, mud volcanoes, and glacier environments. In the following trials the enriched communities have undergone further, long-term adaptation in a custom-designed microbial fuel cell and potentiostatically-controlled bioelectrochemical systems. We have established a process where significant foaming, surface tension and emulsification activities were reported. Most notably, the amount of power generated by BES was highly correlated to the surface tension parameters when cooking oil and petroleum waste were degraded.

In this novel process we are able to biosynthesize surfactants in energy net positive way and to further monitor biosynthesis directly by voltage monitoring. The established electrofermentation leads to the synthesis of biosurfactants and increased bioavailability of hydrophobic substrates for their further biodegradation but may become a new approach to acquire biosurfactants for their commercial applications.

Funding: This work was supported by the Polish National Agency for Academic Exchange – Polish Returns grant (PPN/PPO/2018/1/00038) and National Science Centre (Poland) OPUS grant (2019/33/B/NZ9/02774).

References

[1] Pasternak G., de Rosset A., Rutkowski P., Horizontal microbial fuel cell system producing biosurfactants in response to current generation from waste cooking oil as a fuel, *Energy Convers. Manag.*, 281, 116807.

NEW INSTRUMENTAL CRITERION FOR EVALUATING THE POTENTIAL OF INJECTABLE SCAFFOLDS FOR BIOMEDICAL ENGINEERING APPLICATIONS

Anna Rył*, Piotr Owczarz

Department of Chemical Engineering, Lodz University of Technology,
Wolczanska 213, Lodz, Poland
*corresponding author: anna.ryl@p.lodz.pl

Due to the increasing number of traffic accidents, the development of civilization and oncological diseases, recently there has been a growing demand for modern methods of treatment and regeneration that would shorten the convalescence time and simultaneously would be minimally invasive for the patient. One of the solutions proposed by researchers are polymer drug carriers obtained with thermoinduced sol-gel phase transition, during which polymer aggregates form a spatial scaffold inside which drugs are trapped. Potential applications of hydrogels include injectable cell scaffolds, shear-sensitive drug release systems, and matrices manufactured using 3D printing techniques. When properly designed, such systems can be injected directly into the lesion, and the formation of the lattice occurs *in vivo*. Even though thermosensitive systems are often tested in many respects, their application potential in the form of minimally invasive injection is determined exclusively by the Lower Critical Solution Temperature. Simultaneously, no studies have determined the possibility of injection of these systems, as well as no studies discussed the influence of the flow through the injection needle or 3D printer nozzle on the gelation time. In addition, most researchers argue that the sole requirement to ensure injectability is to keep the system in a liquid-like sol phase. The available studies conducted with synthetic polymers, emulsions, and protein systems indicate that exposure to the shear field of colloidal systems may lead to reversible or irreversible structural changes.

The aim of the work was to propose a new criterion for assessing the application potential of injectable biomedical scaffolds, taking into account their actual application and its impact on the ability of the tested systems to form a spatial polymer network. The indirect goal was to propose a research methodology that would enable qualitative and quantitative assessment of the possibility and kinetics of gelation after injection application and thus determine the usefulness of the prepared formulations in tissue engineering.

As an experimental material, colloidal systems of chitosan (CS) with the addition of disodium β-glycerophosphate salt and water solutions of hydroxypropyl cellulose (HPC) undergoing a sol-gel phase transition under physiological conditions, i.e. temperature of 37 °C and pH in the range of 6.8-7.2, have been used. The formulations were prepared according to commonly used procedures. Instrumental injectability tests were carried out using a texture analyzer, recording the force necessary for injection using hypodermal needles in sizes 14G - 25G at the assumed syringe plunger speed of 1mm/s. The influence of the injection application on the gelation kinetics was determined based on the rheometric and turbidimetric tests preceded by shearing directly in the rheometer or injecting the sol through hypodermal needles.

Based on the dynamic glide force (DGF) values determined during instrumental injectability tests, it was found that both tested systems (CS and HPC) can be used as injectable drug carriers, while the potential is lower when sol obtained from a cellulose derivative was used. This is due to the fact that the permissible DGF forces (determined during panel tests) were exceeded when trying to use needles smaller than 22G, the use of which is recommended by European and global medical agencies. The differences between the tested formulations result mainly from the stronger shear thinning character of chitosan sols (flow index n = 0.44) than is observed in the case of those obtained from cellulose derivative (n = 0.7).

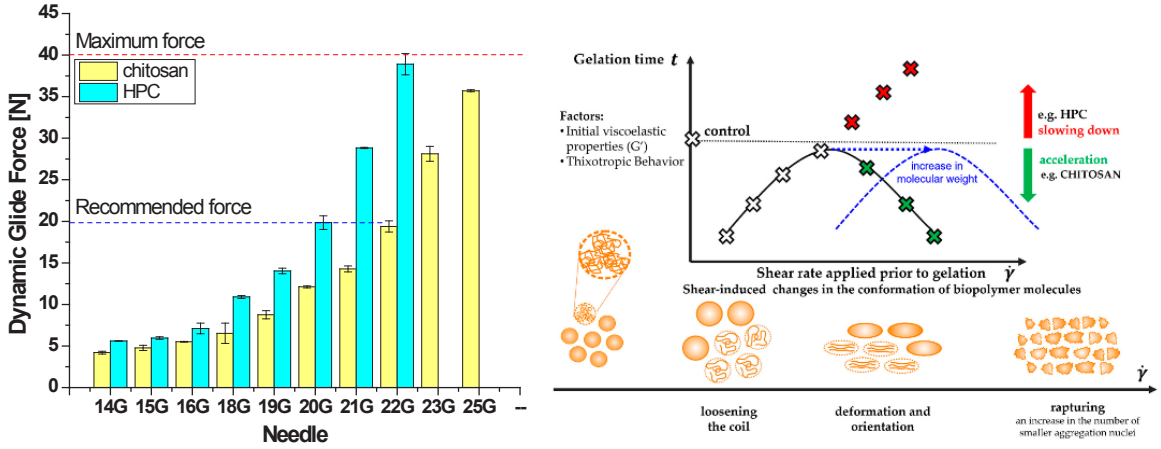

Fig. 1. Effect of injection needle size on the DGF force value for tested formulations and schematic depiction of the shear effect on the polymer coils conformation and gelation time [1]

The research on the impact of the injection application on the gelation kinetics showed that the application of low (in relation to injection) shear rates accelerated the phase transition of all investigated polymer systems due to the ordering of aggregates and easier access to the so-called junction zones. Due to the shear-thinning nature of the studied polymer systems, the observed decrease in their viscosity caused by a short-term but intense shear field caused a decrease in the mutual diffusion resistance of polymer clusters, and consequently facilitated their aggregation. With the increase of the shear rate, the phase transition time is prolonged, probably due to the progressive deformation of the aggregates in the shear field and the time needed to relax the resulting stresses. After exceeding the critical value of the shear rate (characteristic for each system), colloidal aggregates are fragmented, leading to an increase in their number with a simultaneous reduction in their size. Depending on the type of interactions between the aggregation nuclei, this phenomenon may accelerate (chitosan) or delay (HPC) the gelation process. The proposed author's methodology for determining the characteristic time of the phase transition, considering the kinetics of the polymer network formation, unequivocally confirmed the acceleration of aggregation caused by the velocity gradient (orthokinetic regime) compared to aggregation limited solely by stochastic Brownian motion (perikinetic regime).

The proposed research methodology allows to determine the potential of polymer formulations as a minimally-invasive drug carrier or cellular scaffold, according to which an attempt to use a hydroxypropyl cellulose sol is associated with difficult or even impossible manual injection when using needles smaller than 19G. Additionally, it is associated with a significant extension of the gelation time compared to the control measurements. Consequently, this may lead to undesirable spillage of the sol before it has gelled in the body. Contrary to that, injection of chitosan sol was possible even using small diameter needles (23G - 25G), and additionally, the flow through the capillary caused a significant reduction of the sol-gel phase transition time. The discussed effect of the shear field can also be observed during the flow of thermosensitive formulations in the nozzles of the 3D printer. During printing, the speed of the printer head is not as strongly limited as in the case of manual injection, and this causes the experimental medium to flow at much higher shear rates (10^3 - 10^5 s^{-1}). Thus, as a result of the flow through the nozzle of the 3D printer, similar effects of the influence of the shear field will be observed both on the structural changes of the tested systems as well as the gelation conditions.

Finally, the conducted research clearly shows that providing the liquid form of the sol is not the sole condition for ensuring their injection, and the shear field occurring during the injection has a significant impact on the conditions of formation of the spatial polymer network. Consequently, both of these criteria must be taken into account when consciously designing thermosensitive drug carriers.

References

[1] Rył, A., Owczarz, P., Influence of Injection Application on the Sol–Gel Phase Transition Conditions of Polysaccharide-Based Hydrogels, *Int. J. Mol. Sci.*, 2021, 22(24), 13208.

INTENSIFICATION OF MASS TRANSFER OF THERAPEUTIC AEROSOLS AND VACCINES IN THE NASAL CAVITY

Tomasz R. Sosnowski[1]*, Emil Florkiewicz[2]

[1]Faculty of Chemical and Process Engineering, Warsaw University of Technology, Waryńskiego 1, 00-645 Warsaw, Poland

[2]Specialized Diagnostic and Consultation Team for Allergy Problems, Bohaterów Września 61, 98-200 Sieradz, Poland

*corresponding author: tomasz.sosnowski@pw.edu.pl

It is believed that drugs sprayed in an aerosol penetrate much better into the nasal cavity than liquid that is applied in the form of large drops. Unfortunately, this is not true, as liquid particles (droplets) sprayed using standard nasal pumps with the nozzle inserted into the narrow nasal passage (nostril) are unable to expand into aerosol cloud and immediately impact the wall of the front of the nasal cavity or nasal septum [1]. This is due to the highly complex geometry of the nasal airways, Fig. 1, whose main physiological role is to effectively humidify and heat (or cool) the inhaled air. Therefore, hydrodynamic transport of liquid already deposited on the nasal surface has been proposed as a reasonable explanation for the increased penetration of sprayed drugs along the nasal geometry. This flow is caused by the action of the inhaled air on the liquid layer formed by deposited drug and depends on its rheological properties [2].

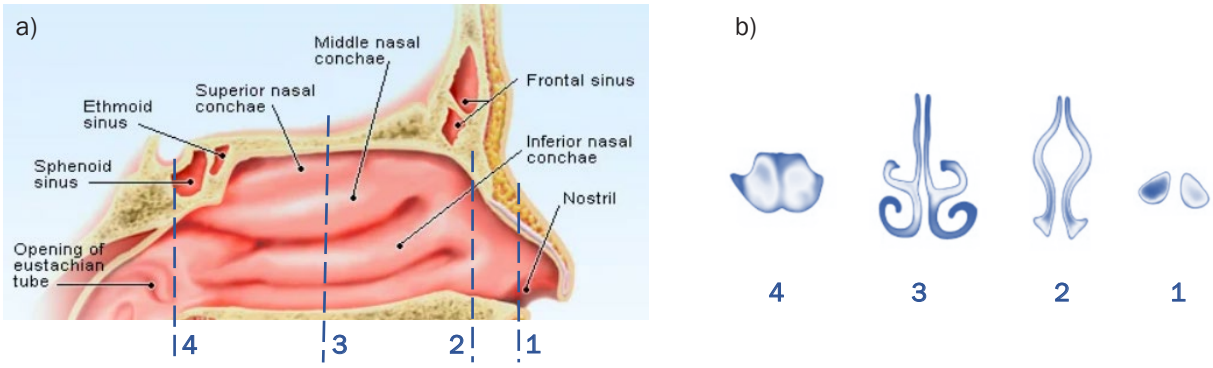

Fig. 1. a) Nasal geometry; b) cross sections of the air spaces inside the nose (based on [3] and [4])

Drugs or vaccines can also be delivered to the nose using a different type of aerosol than that containing relatively large droplets (50-60 μm on average) generated from hand-held atomizers. A finer aerosol can better penetrate the nasal airways, but it can also flow down into the throat or bronchial tree, which is not desirable and can be responsible for side effects. Since no optimal method of intranasal aerosol drug delivery has been developed to date, this study focused on the use of pressure pulsations added to aerosol generated by medical nebulizers and assessing the influence of such pulsations on the intensification of drug mass transfer in narrow nasal air spaces.

We studied pressure waves superimposed on the main aerosol stream generated by a pneumatic nebulizer (Monsun MP1, Medbryt, Poland) connected to Sidestream nebulizing vessel (Philips Respironics, USA). The particle size distribution of aerosol measured with Spraytec diffraction spectrometer (Malvern, UK) was log-normal with the median size Dv50 = 2.6 μm and geometric standard deviation GSD = 1.7. Pressure pulsations were produced by an additional device built into the nebulizer.

First, we measured the effect of pressure fluctuations on the airflow produced by the nebulizing system using a thermal mass flow meter (model 3040, TSI Inc., USA; response time <4

milliseconds). The results in Fig. 2 illustrate the measured oscillations in air flow rate. The flow visualization presented in Fig. 3b shows that these oscillations destabilize the aerosol stream emitted from the nebulizing vessel. The droplets are deflected from the main flow, so they are transported in a direction perpendicular to the flow.

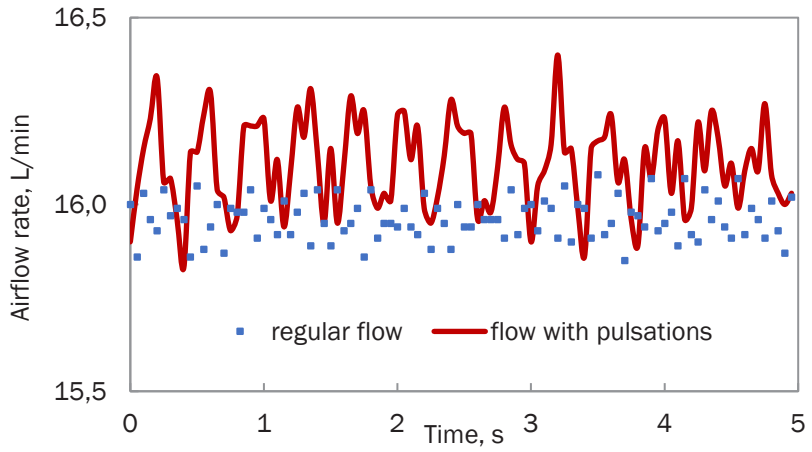

Fig. 2. Airflow rate of aerosol emitted from nebulizer with and without pressure fluctuations

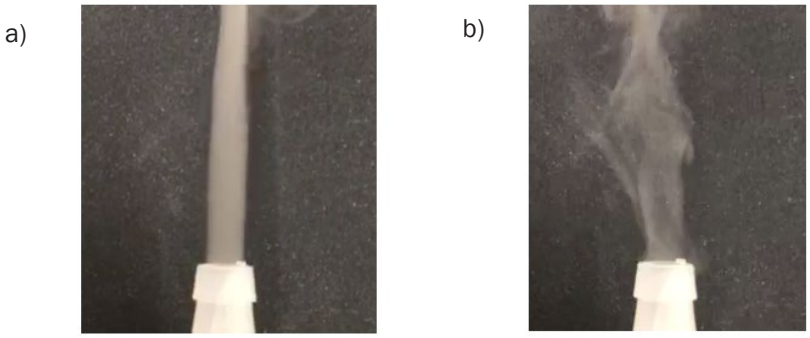

Fig. 3. A recorded frame showing the geometry of aerosol stream emitted from the nebulizer: (a) without, and (b) with pressure fluctuations

Further experiments with an anatomical cast of the human nasal cavity confirmed that pulsations allow deeper penetration and deposition of the aerosol inside the complex structure of the nose (data not shown). Therefore, the presented concept of using the pulsations of a fine aerosol delivered to the nasal cavity can be proposed as a method to improve targeted delivery of drugs or vaccines to deeper regions of this anatomical structure.

Acknowledgement:
Work supported by NCN project No. 2018/29/B/ST8/00273.

References

[1] Sosnowski T.R., Rapiejko P., Sova J., Dobrowolska K., Impact of physicochemical properties of nasal spray products on drug deposition and transport in the pediatric nasal cavity model, *Int. J. Pharm.*, 2020, 574, 118911.
[2] Sosnowski T.R., Dobrowolska K., Aerodynamically driven translocation of non-Newtonian fluids: the relevance for intranasal drug delivery, *Chem. Eng. Transact.*, 2021, 86, 1207-1212.
[3] Available at https://www.emedicinehealth.com/sinus_headache/article_em.htm (access: 13.02.2023).
[4] Inthavong K., Ma J., Shang Y., Dong J., Chetty A.S.R., Tu J., Frank-Ito D., Geometry and airflow dynamics analysis in the nasal cavity during inhalation. *Clin. Biomech.*, 2019, 66, 97-106.

DRUG CARRIERS: POLYLACTIDE LAYER COVERED ALGINATE STRUCTURES IN CONTROLLING DRUG RELEASE

Anna Trusek[1]*, Omoyemi Ajayi[1], Maciej Grabowski[1], Edward Kijak[2]

[1]Wroclaw University of Science and Technology, Wybrzeże Wyspianskiego 27, 50-370 Wroclaw, Poland
[2]Wroclaw Medical University, Krakowska 26, 50-425 Wroclaw, Poland
*corresponding author: anna.trusek@pwr.edu.pl

The study aimed to assess how the coating of hydrogel carriers affected the mass release rate of the antibiotics tested. The tested carriers are to be used, among other applications, to treat dentistry inflammation.

Hydrogel (alginate and hyaluronic acid) capsules were covered with polylactide (PLA) using Celeva Mini Coater Drier. PLA solution with a concentration of 2.5 w/v was prepared in methylene chloride. The process temperature was changed in the range 45-55°C. The solution was dosed at a speed of 4 RPM/min, air flow was 13 m/s, shaking 19 hZ, pressure at the nozzle 0.5 bar. Capsule coating was carried out for 20-50 minutes. The procedure is presented in Fig. 1.

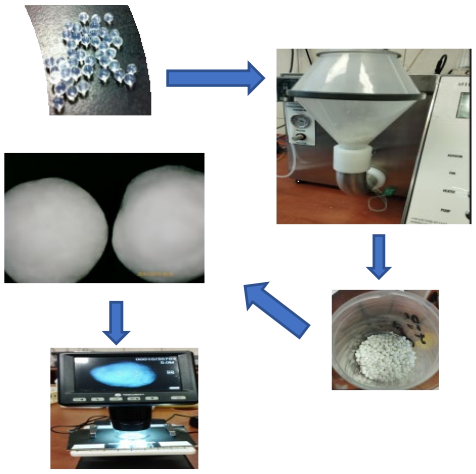

Fig. 1. The procedure of coated capsules creation

a) b)

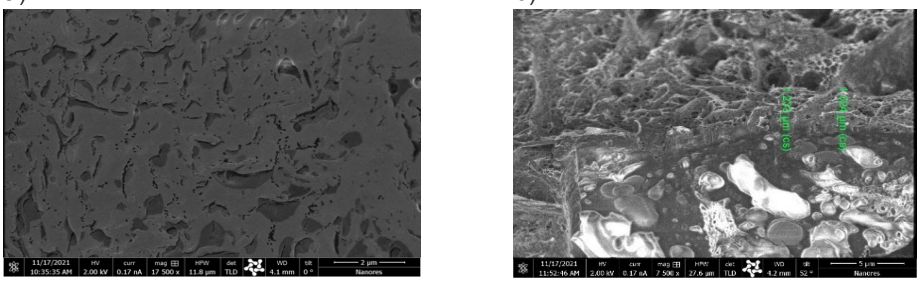

Fig. 2. Carriers covered with PLA layer SEM surface (a) and SEM/Ga-FIB section image (b)

The tested strain was *Porphyromonas gingivalis*, and the released antibiotics were amoxycillin, metronidazole and doxycycline. *Porphyromonas gingivalis* belongs to the *Bacteroidota* and is a pathogenic bacterium. It causes periodontal disease as well as disease in the upper gastrointestinal tract, respiratory track, colon, track the colon and is present at bacterial vaginosis.

Selected conditions for covering the capsules were established on 2.5% w/w polylactide, 45°C, 50 minutes. Without PLA layer, the transport was observed (an equilibrium state was reached) for a few hours independent of physical or chemical gelation – Figs. 3a and b. The cross-linking bath contained 10% w/v $CaCl_2$ and 0.05M EDC by chemical gelation and the given antibiotic with a concentration of 1g/L. The time of the mass release was much extended by PLA layer application (Fig. 3c). The mass transport can be well described by Korsmeyer-Peppas model [1].

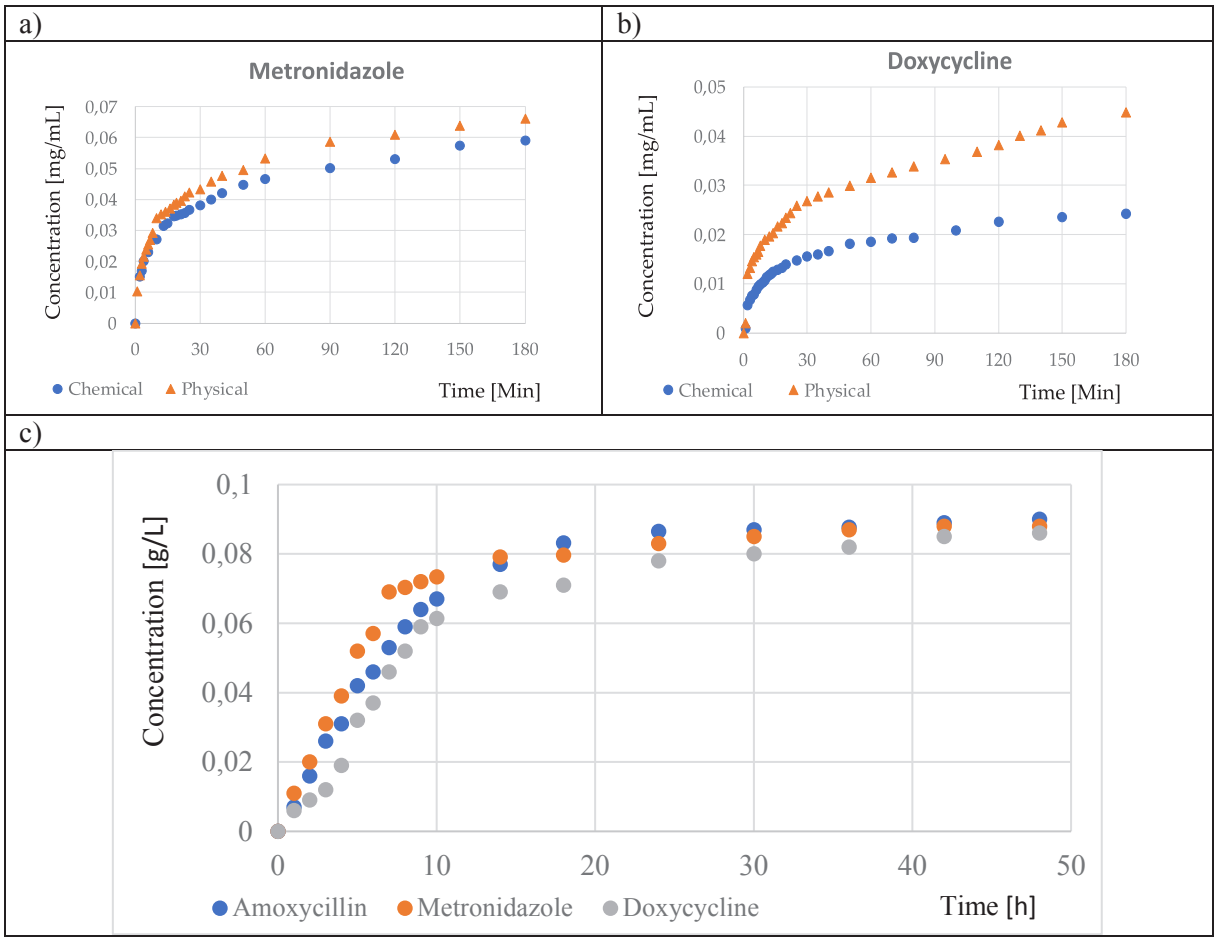

Fig. 3. Mass transport release from capsules without PLA layer (a and b) and with PLA layer (c)

Conclusion

Thanks to the polylactide layer, drug transport was prolonged 10-fold, making it possible to prepare a long-term carrier with slowed, extended release.

References

[1] Korsmeyer R.W., Peppas N.A., Effect of the morphology of hydrophilic polymeric matrices on the diffusion and release of water-soluble drugs, *J. Membr. Sci.*, 1981, 9(3), 211-227.

Lectures

S7. Green and sustainable chemical engineering

BENEFITS OF USING SACCHARIDE AND AMINO-ACID TYPE SURFACTANTS IN THE OPTIMIZED FABRICATION OF NANODETERGENTS AS STUBBORN GRAFFITI PAINT REMOVERS

Marcin Bartman[1,*], Sebastian Balicki[1], Kazimiera A. Wilk[1], Lucyna Hołysz[2]

[1]Department of Engineering and Technology of Chemical Processes, Faculty of Chemistry, Wrocław University of Science and Technology.
Wybrzeże Wyspiańskiego 27, 50-370 Wrocław, Poland
[2]Country Institute of Chemical Sciences, Faculty of Chemistry, Maria Curie-Skłodowska University, M. Curie-Skłodowska 3, 20-031 Lublin, Poland
*corresponding author: marcin.bartman@pwr.edu.pl

Property owners and managers frequently face the issue of removing undesirable graffiti. However, they frequently do not know how to clean up the graffiti without damaging the surface beneath it. It should be emphasized that it is incredibly challenging to clean painted and coated surfaces using so-called “brush on, wipe off” detergents [1, 2], including painted walls, ceramic tiles, stainless steel, aluminum, vinyl fences, signs, transparent acrylic, plastics, windows, and many others. Additionally, many factors, including the substrate’s (chemical composition, texture, porosity, hardness, etc.), the paint's (and the substrate's) aging process, and the time between applications and removals make graffiti coating removal a difficult process [3–5].

The development of a new generation of graffiti cleaning preparations that are both highly effective and non-toxic is a huge challenge for research teams. The application of a sustainable strategy to the eco-design of professional goods, with a special emphasis on the fundamentals of green chemistry, is the top priority as of right now. Therefore, the formulation of selection criteria should take into account the following: the necessity of using biodegradable raw materials, which are produced from renewable resources and are not subject to accumulation in the environment; high efficiency of cleaning the surface from graffiti while preserving all of its functional properties; as well as product safety [3]. In recent years, there has been significant progress in removing unwanted paint coatings from urban spaces or historical objects owing to the use of nanotechnological detergents [4–6]. Formulations of ecological surfactants based on saccharides or amino acids are novel nanodetergents for the removal of graffiti [4, 5], and constitute the most innovative technology in the area of colloid engineering.

The aim of the research was to obtain novel eco-removers of graffiti coatings using nanodetergents of the "brush on, wipe off" type. High-pressure homogenization (HPH) was used to produce water-in-oil nanoemulsions [4, 5] that included non-toxic and eco-friendly components such as amino-acid type surfactants (AAS) or alkyl polyglucosides (APG), esterified vegetable oils, and ethyl lactate. Optimization by design of experiments (DoE) was used to find the most effective detergents. These detergents were then used to remove graffiti coatings from sensitive surfaces like glass, aluminum, natural stone, and marble. Furthermore, several experimental studies were conducted on surface topography, wettability, free energy of the surface, and the work of water adhesion to sensitive surfaces before and after they were covered with black graffiti paint, as well as after the paint layers were removed with the eco-remover.

Using nanostructured fluids and knowledge of surface properties, one could develop efficient nanodetergents that would easily remove unwanted and stubborn contaminants from various surfaces in a fully controlled way.

References

[1] García-Florentino C., Maguregui M., Ciantelli C., Sardella A., Bonazza A., Queralt I., Carrero J.A., Natali C., Morillas H., Madariaga J.M., Arana D., Deciphering past and present atmospheric metal pollution of

urban environments: The role of black crusts formed on historical constructions. *J. Clean. Prod*., 2020, 243, 118594.
[2] Baglioni M., Poggi G., Giorgi R., Rivella P., Ogura T., Baglioni P., Selective removal of over-paintings from "Street Art" using an environmentally friendly nanostructured fluid loaded in highly retentive hydrogels, *J. Colloid Interface Sci*., 2021, 595, 187–201.
[3] Bartman M., Balicki S., Wilk K.A., Formulation of Environmentally Safe Graffiti Remover Containing Esterified Plant Oils and Sugar Surfactant. *Molecules*, 2021, 26, 4706.
[4] Bartman M., Balicki S., Hołysz L., Wilk K.A., Graffiti coating eco-remover developed for sensitive surfaces by using an optimized high-pressure homogenization process, *Colloids Surf., A Physicochem. Eng. Asp.*, 2023, 659, 130792.
[5] Bartman M., Balicki S., Hołysz L., Wilk K.A., Surface properties of graffiti coatings on sensitive surfaces concerning their removal with formulations based on the amino-acid type surfactants, *Molecules*, 2023 (in press).
[6] Baglioni M., Sekine F.H., Ogura T., Chen S.-H., Baglioni P., Nanostructured fluids for polymeric coatings removal: surfactants affect the polymer glass transition temperature. *J. Colloid Interface Sci.*, 2022, 606 124–134.

GREEN HYDROGEN PRODUCTION USING PHOTOREFORMING OF METHANOL IN FLOW SYSTEM

Karol Ćwieka[1,*], Kamil Czelej[1], Zuzanna Bojarska[1], Łukasz Werner[1], Krzysztof Wojtas[1], Dariusz Łomot[2], Juan Carlos Colmenares[2,3], Leon Gradoń[1]

[1]Faculty of Chemical and Process Engineering, Warsaw University of Technology, Ludwika Warynskiego 1, 00645, Warsaw, Poland
[2]Institute of Physical Chemistry, Polish Academy of Sciences, Kasprzaka 44/52, 01224, Warsaw
[3]Engineering Research Institute, Universidad Cooperativa de Colombia, Medellín 50031, Colombia
*corresponding author: karol.cwieka@pw.edu.pl

In present times, the main priority axis of the energy production is focused on independence from fossil fuels and decarbonization due to the pursuit of a circular economy and sustainability. The sense of sustainability means searching for effective approaches involving ecological fuels, and processes with a less possible environmental concern especially when modern civilization is experiencing global warming effect and facing issues of the climate change. Utilization of solar energy as a renewable driving force, and biomass derived compounds as renewable feedstocks for hydrogen production, as the most promising energy carrier, is highly desired as the solutions for sustainable energy generation simultaneously with value added compound production or water recultivation. The need for development of a sustainable, benign, and efficient photocatalytic production of hydrogen has been growing rapidly year after year. Solar driven production of this "fuel of the future" via photoreforming poses major challenges in terms of nano-photocatalyst design (both morphology and chemical composition) as well as the design of entire photocatalytic reactor system for enabling maximization of yield.

The literature examples reported to date demonstrate the superiority of plasmonic nano-photocatalysts over conventional ones in efficient hydrogen production that originates from the enhanced quantum efficiency in photon-to-hydrogen conversion. It is particularly governed by localized surface plasmon resonance phenomenon (LSPR), large electric field enhancement, and induced heating localized in nano-regions that can lower the activation barriers of the surface reactions. Recently, vast majority of scientific efforts are devoted to designing efficient heterogeneous systems using a single metal or dual co-catalyst loaded semiconductor (mainly TiO_2) photocatalysts that enable bandgap reduction, tuning the photooxidation pathways, improving the selectivity, and making hydrogen production form aqueous organic solutions more efficient and feasible. [1, 2]

In the presentation, we report a TiO_2/Cu nanocomposite catalyst with high activity and selectivity of hydrogen production using photoreforming of methanol solution, proven by detection of hydrogen as the only gaseous product. Usually, this transformation releases significant amounts of CO_2 and CO, so it cannot be deemed sustainable. Another undoubtful advantage of our photocatalyst is its excellent stability proven by the similar activity after 6 months. By means of extensive experimental characterization supported by theoretical calculations, we propose the reaction mechanism and the reasoning behind the behaviour of our photocatalyst in achieving zero carbon footprint hydrogen photogeneration from methanol. We link high hydrogen generation yield to a remarkable 10% apparent quantum efficiency.

Another aspect is the design of continuous flow reactors by optimization of their geometry that enables efficient harnessing of illuminous (solar) flux to fully control plasmonic photochemistry and LSPR effect at long term operation. Maintaining the nanocatalysts in operando stability, achieving the maximum possible hydrogen production yield and selectivity now constitute the main challenges for further implementation of plasmon photocatalytic flow systems dedicated to solar-tohydrogen- conversion at industrial scale. Selected results from the recent works of our

research team are also presented as the original contribution to the topic following the concept schematically illustrated in Figure 1.

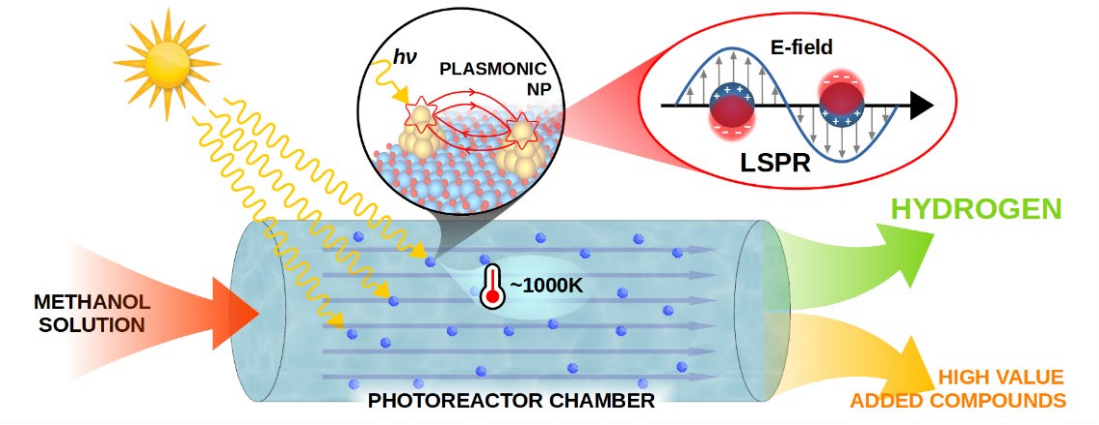

Fig. 1. Schematic illustration of the green hydrogen generation during the photoreforming of methanol solution over plasmonic nanocatalysts

Acknowledgements
The work was supported by the National Centre for Research and Development Poland in the framework of the LIDER research project (contract no. LIDER/19/0069/L 11/19/NCBR/2020).

References

[1] Czelej K., Colmenares J. C., Jabłczyńska K., Ćwieka K., Werner Ł., Gradoń L., *Catal. Today*, 2021, 380, 156.
[2] Ćwieka K., Czelej K., Colmenares J. C., Jabłczyńska K., Werner Ł., Gradoń L., *ChemCatChem*, 2021, 13, 4458.

CARBON EMISSION PINCH ANALYSIS (CEPA) FOR POLISH ENERGY GENERATION SECTOR

Grzegorz Poplewski[1,*], Melvin Ting[2], Dominic C.Y. Foo[2], Raymond R. Tan[3], Yin Ling Tan[4]

[1]Department of Chemical and Process Engineering, Rzeszow University of Technology, Rzeszow, Powstancow Warszawy 6, 35-959 Rzeszow, Poland
[2]Centre of Excellence for Green Technologies/Department Chemical and Environmental Engineering University of Nottingham Malaysia, Broga Road, 43500 Semenyih, Selangor, Malaysia
[3]Chemical Engineering Department, Gokongwei College of Engineering, De La Salle University, 2401 Taft Avenue, 0922 Manila, Philippines
[4]School of Engineering and Science, Curtin University of Technology, Sarawak Campus Malaysia, CDT 250, 98009, Miri, Sarawak, Malaysia
*corresponding author: ichgp@prz.edu.pl

In response to climate change urgency, the Paris Agreement ratified by 196 countries in 2015 has the aim to cap global warming to within 2 °C, with an effort to limit it below 1.5 °C above pre-industrial levels. Despite this effort, no sign has been observed for the deceleration of greenhouse gas (GHG) emissions in the past few years. Extreme weather incidents are reported in various parts of the world on a regular basis, which is believed to be largely associated with GHG emissions. As the main element of GHG, the global carbon dioxide (CO_2) concentration is reported to be close to 420 ppm at the beginning of 2023 [1]. Note that it is actually 20% higher than the safe planetary boundary as proposed by Rockström et al., i.e. 350 ppm [2]. Hence, serious efforts are necessary to ensure the deceleration of GHG and CO_2 emissions, in the hope that net zero emission can be reached by the middle of this century.

The European Union Emission Trading System (EU ETS) remains the main mechanism for reducing CO_2 emissions. By gradually reducing the number of emission allowances which causes an increase in their prices, the EU ETS enforces emission reduction by the large production and power plants. Note, however, that the EU ETS only covered sectors that are easiest in its modification, i.e. power and heat generation, as well as energy-intensive industrial plants. The long-term goal is for the EU to achieve climate neutrality by 2050. To achieve this important goal, the European Commission pushed through the “Fit for 55” plan, which assumes an acceleration of emission reduction to 55% by 2030 compared to 1990 levels. The “Fit for 55” plan will cover sectors such as maritime transport, aviation, building emissions and road transport [3]. The EU policy on CO_2 emissions is flexible and adapted to the current political and economic situation. The war in Eastern Europe made it necessary to change fuel sources to ensure energy security. For this reason, the “RePowerEu” plan was introduced, with the goal to end EU's dependence on Russian fossil fuels, and to tackle climate crisis. The RePowerEu plan focuses specifically on energy savings, diversification of energy supply and accelerated deployment of renewable energy.

For better planning of CO_2 emissions, various useful tools have been proposed. One among such techniques that have gained good attention is undoubtful *carbon emission pinch analysis* (CEPA). In the seminal work on CEPA by Tan & Foo [4], a graphical tool known as *energy planning pinch diagram* (EPPD) was introduced for the optimum allocation of energy sources to the demand, by taking CO_2 emission limit as the main constraint. To overcome the inaccuracy problem of EPPD, Foo *et al.* [5] developed an algebraic technique as an alternative to supplement the graphical tool. In this work, the EPPD is used to study the performance of new measures and policies set by the Polish government. It provides key insights into the system bottlenecks that may hinder decarbonisation efforts. Moreover, CEPA can identify effective decarbonisation options for the Polish power generation sector.

As an example of the application of the EPPD, the Polish power generation data in 2021 (Table 1) was used. Based on this data, the *source composite curve* was plotted (blue line in Figure 1 (a)). Next, the *demand composite curve* is plotted on the EPPD (red line in Figure 1 (a)), representing the actual energy demand and CO_2 emissions in accordance with [6]. These lines intersect as seen in the enlarged view (Figure 1(b)). In order for 2021 CO_2 emissions [6] to be met, it is necessary to shift the source composite curve to the right of the demand composite curve, by generating additional energy from renewable sources (ΔE_R = 1.1 TWh, see Figure 1(b)), or by replacing some high-emission energy sources (lignite, hard coal) with less-emission ones (e.g. natural gas).

Table 1. Polish power generation data for 2021

Energy sources	Energy generation [TWh]	CO_2 emissions [Mt]	Energy sources	Energy generation [TWh]	CO_2 emissions [Mt]
Biomass and biogas	7.8	0.0	Factory power plants	3	2.7
Hydropower	2.3	0.0	Solar energy	3.8	0.0
Wind energy	16.5	0.0	Hard coal	84	75.6
Imported electricity	0.9	0.0	Pumped storage power plants	0.8	0.9
Natural gas	15.3	6.9	Lignite	46	49.0

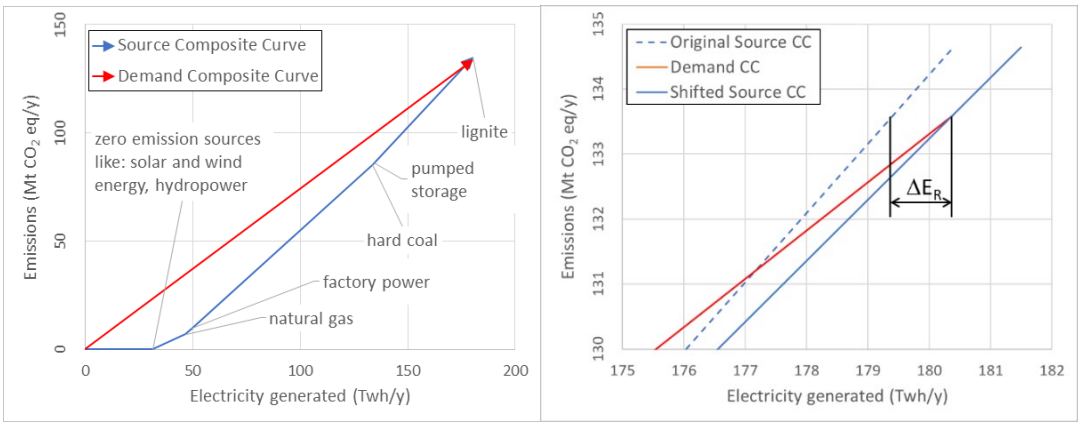

(a) (b)

Fig. 1. EPPD for 2021 (a) infeasible EPPD (b) feasible EPPD (magnification of the end of the graph)

References

[1] https://keelingcurve.ucsd.edu/.

[2] Rockström J., Steffen W., Noone K., Persson A., Chapin F.S., Lambin E.F., Lenton T.M., Scheffer M., Folke C., Schellnhuber H.J., Niykvist B., De Wit C.A., Hughes T., Van der Leeuw S., Rodhe H., Sorlin S., Snyder P.K., Constanza R., Svedin U., Falkenmark M., Karlberg L., Corell R.W., Fabry V.J., Hansen J., Walker B., Liverman D., Richardson K., Crutzen P., Foley J.A., A safe operating space for humanity, *Nature*, 2009, 461, 472–475.

[3] https://ec.europa.eu/commission/presscorner/detail/pl/qanda_21_3542.

[4] Tan, R.R. and Foo, D.C.Y., Pinch analysis approach to carbon-constrained energy sector planning, *Energy*, 2007, 32(8), 1422–1429.

[5] Foo, D.C.Y., Tan, R.R. and Ng, D.K.S., Carbon and footprint-constrained energy planning using cascade analysis technique, *Energy*, 2008, 33(10), 1480–1488.

[6] Energy Policy of Poland 2040, Warsaw 2021.

REMOVAL OF CYCLOHEXANE VAPORS FROM AIR IN BIOTRICKLING FILTERS: EFFECTS OF GAS MIXTURE COMPOSITION AND CIRCULAR ECONOMY APPROACH

Piotr Rybarczyk[1,2]*, Bartosz Szulczyński[1], Dominik Dobrzyniewski[1], Karolina Kucharska[1], Jacek Gębicki[1]

[1]Gdańsk University of Technology, Faculty of Chemistry, Department of Process Engineering and Chemical Technology, Narutowicza 11/12, 80-233 Gdańsk, Poland
[2]EkoTech Center, Gdańsk University of Technology, Narutowicza 11/12, 80-233 Gdańsk, Poland
*corresponding author: piotr.rybarczyk@pg.edu.pl

Pollution of air with volatile organic compounds (VOCs) is a serious problem for both human health and the environment. VOCs may be effectively removed from air streams using biological methods, including biotrickling filtration. Compared to conventional biofilters, biotrickling filters offer more complex process control and regulation possibilities, allowing adjustment of liquid phase pH, composition or watering frequency as well as offer longer operation times due to application of inert packing materials [1]. Biofiltration techniques are regarded as sustainable and green technologies for air purification [2]. However, their beneficiary application can be expanded by the circular economy approach through valorization of the process final products i.e. treated gas and spent trickling liquid for culturing of plants. Selection of proper plant species may allow to obtain advantageous effects of energetic biomass production, further upgrading biofilter-treated air or enhanced soil phytoremediation.

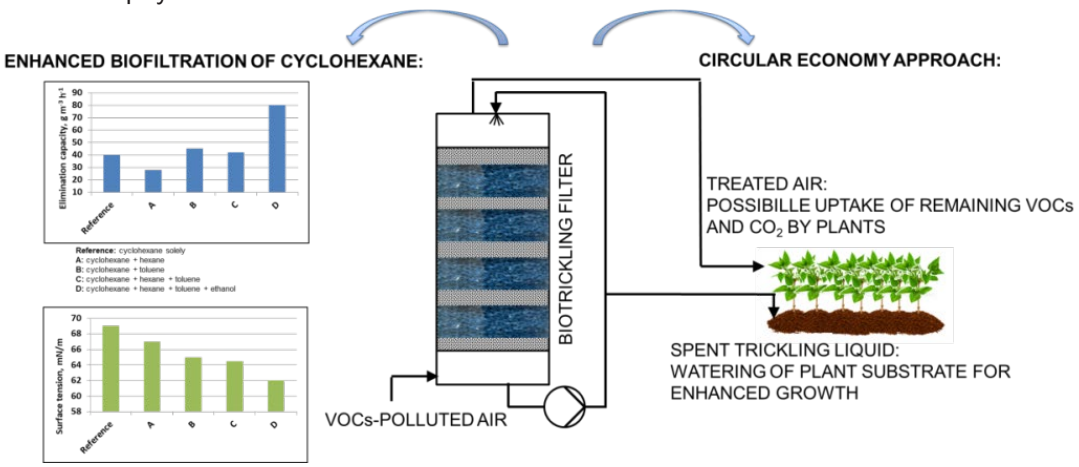

Fig. 1. Idea of enhancing biotrickling filtration of cyclohexane and coupling air biofiltration to circular economy

In this work, the results of biotrickling filtration of cyclohexane co-treated in binary, ternary and quaternary VOCs mixtures are reported, i.e. cyclohexane – hexane, cyclohexane – toluene, cyclohexane – hexane – toluene and cyclohexane – hexane – toluene – ethanol. Investigations aimed at revealing effects of cyclohexane co-treatment with other VOCs. The possibility of enhancing the process performance by tuning the gas-phase composition was checked. To the authors' best knowledge, up to date, the removal of cyclohexane from air in biofiltration processes has been rarely studied [3, 4]. The components of these mixtures differ in their affinity to water phase, represented e.g. by Henry's law constants or octanol/water partitioning coefficient, and the biofiltration performance is highly dependent on the solubility of the gas pollutants in the liquid and biofilm phases. Moreover, spent trickling liquid is applied to the culture of grass mix with the perspective of enhancing the crop yield (Figure 1).

It is evident that the more hydrophilic compound, represented by low values of dimensionless Henry's law coefficients, the higher its bioavailability and higher expected removal, compared to hydrophobic compounds. In order to enhance the removal of hydrophobic VOCs in biotrickling filters, various measures are possible, including addition of surfactants or non-aqueous liquid phase, pre-treatment operations (e.g. photooxidation), mixing hydrophobic and hydrophilic gas streams or inoculation with selected microbial species, specialized in the removal of hydrophobic VOCs [5, 6].

In this work, investigations of liquid phase of a BTF are proposed. Surface tension measurements for various investigated systems are presented in order to reveal changes of interfacial tension. The lower the surface tension, the lower the barrier for hydrophobic VOCs to reach the biofilm i.e. the bioavailability of VOCs is increased. It is assumed that the changes in surface tension of the trickling liquid will be related with the VOCs treatment and primarily, with the specialized microbial species, constituting the biofilm and the presence of protein released to the medium during cell growth. It may be that due to secretion of metabolic products of some microbes, biosurfactants may be released, which are believed to promote the removal of hydrophobic VOCs in BTFs [7].

The removal of cyclohexane from gas mixture depends on the physicochemical properties of the co-treated VOCs and the lower the hydrophobicity of the VOC, the higher the removal efficiency of cyclohexane. The performance of biotrickling filtration of cyclohexane is discussed in terms of changes of physicochemical parameters of the trickling liquid (pH, absorption of VOCs, surface tension). To the best knowledge of the authors, the evaluation of the surface tension of liquid phase for the assessment of enhanced biofiltration performance of hydrophobic VOCs is not reported in the literature. Additionally, a practical approach of utilizing a mixed natural/synthetic packing for a biotrickling filter, presenting promising performance and limited maintenance requirements is proposed. Maximum elimination capacity of 95 g m^{-3} h^{-1} for cyclohexane was reached corresponding to the total inlet loading of VOCs mixture equal to 450 g m^{-3} h^{-1}. Utilization of a spent trickling liquid for grass culturing resulted in its enhanced growth in the first 3 weeks of experiments, while further addition of liquid did not affect the plant growth as compared to the reference, suggesting a need for further optimization of both the dosing pattern and liquid composition.

Acknowledgements

Financial support of these studies from Gdańsk University of Technology by DEC-9/2022/IDUB/II.2/Sc grant under the Scandium – "Excellence Initiative – Research University" program is gratefully acknowledged.

References

[1] Rybarczyk P., Szulczyński B., Gębicki J., Hupka J., Treatment of malodorous air in biotrickling filters: A review. *Biochem. Eng. J.*, 2019, *141*, 146–162.
[2] Sarkar P., Tiwari H., Garkoti P., Neogi S., Biswas J.K., Dey A., Biofiltration as a green technology for abatement of volatile organic compounds (VOCs): A synoptic review. *An Innov. Role Biofiltration Wastewater Treat. Plants*, 2022, 477–496.
[3] Salamanca D., Dobslaw D., Engesser K.-H., Removal of cyclohexane gaseous emissions using a biotrickling filter system. *Chemosphere*, 2017, *176*, 97–107.
[4] Rybarczyk P., Marycz M., Szulczyński B., Brillowska-Dąbrowska A., Rybarczyk A., Gębicki J., Removal of cyclohexane and ethanol from air in biotrickling filters inoculated with *Candida albicans* and *Candida subhashii*. *Arch. Environ. Prot.*, 2021, *47*, 26–34.
[5] Rybarczyk P., Removal of Volatile Organic Compounds (VOCs) from Air: Focus on Biotrickling Filtration and Process Modeling. *Process.*, 2022, 10, 2531.
[6] Wu X., Lin Y., Wang Y., Yang C., Interactive effects of dual short-chain n-alkanes on removal performances and microbial responses of biotrickling filters. *Chem. Eng. J.*, 2023, *461*, 141747.
[7] He S., Ni Y., Lu L., Chai Q., Liu H., Yang C., Enhanced biodegradation of n-hexane by *Pseudomonas sp. strain NEE2. Sci. Reports*, 2019, *9*, 1–9.

DETERMINATION OF THE ENVIRONMENTAL IMPACT OF HCPV WITH PLANAR OPTICAL MICRO-TRACKING SYSTEM

Aleksandra Ziemińska-Stolarska*, Monika Pietrzak, Ireneusz Zbicinski

Faculty of Process and Environmental Engineering
Lodz University of Technology, Lodz, Poland
*corresponding author: aleksandra.zieminska-stolarska@p.lodz.pl

Limited resources of fossil fuels force transformation of the global energy supply system towards development of renewable energy resources [1]. One of the options is the application of highly concentrated photovoltaic panels (HCPV) which eliminates disadvantages of traditional solar power systems, e.g. low conversion efficiency. The concentrated photovoltaic systems offer relatively high conversion efficiency, reduction of the operation cost and elimination of toxic materials used in solar cell production. HIPERION (Hybrid Photovoltaics For Efficiency Record Using Integrated Optical Technology) HCPV module with planar optical micro-tracking system, developed in the Horizon2020 project (http://www. hiperion-project.eu/) meets the challenge of improving the efficiency of silicon panels. A unique and highly efficient solar module, capable of providing a real-time record of energy generation per m_2, between 50% and 80% has been constructed. The goal was achieved through the design of a solar photovoltaic module, based on hybrid technology where planar optical micro-tracking system concentrates sunlight on multi-junction solar cells situated on top of a conventional silicon backplane. The technology is based on a combination of optics, space-grade solar cells, and micro-tracking [2].

The paper presents Life Cycle Assessment (LCA) analysis of a new HCPV technology developed in the HIPERION project for constructional data. In the LCA calculations, the module was adopted as the functional unit. SimaPro version 9.00.49, the recent Ecoinvent database (3.8) and the IPCC 2021 GWP 100a environmental model were employed to determine the environmental load. Ecoinvent system methodology was: "allocation at point of substitution". The cradle-to-grave approach was chosen. The inventory analysis where all the material and energy flows and all the waste discharged to the environment over the whole life cycle were identified and collected from the manufacturers (primary data) to ensure reliable results. Available databases, mass and energy balances, were also used (secondary data) to complete the inventory table. The impact of the transport of raw materials was also assessed. In the interpretation phase, a review of all LCA stages in order to check the consistency with assumptions and data quality in relation to the goal and scope of the study was performed.

Examples of the LCA calculations are shown in Figs. 1 and 2 displaying simplified process tree for contribution in CO_2 eq. emissions (in kg and %) of individual materials used to manufacture the module.

Results of the calculations show that the biggest environmental load was produced with the PV cells; 99.9 kg CO_2 eq., which corresponds to 41.7 % of the total environmental load due to the large number of solar cells used in the construction. An important load is also generated by PMMA (methyl methacrylate) 38.8 kg kg CO_2 eq. (16.2%) and integrated circuits 30.8 kg CO_2 eq. (12.9%).

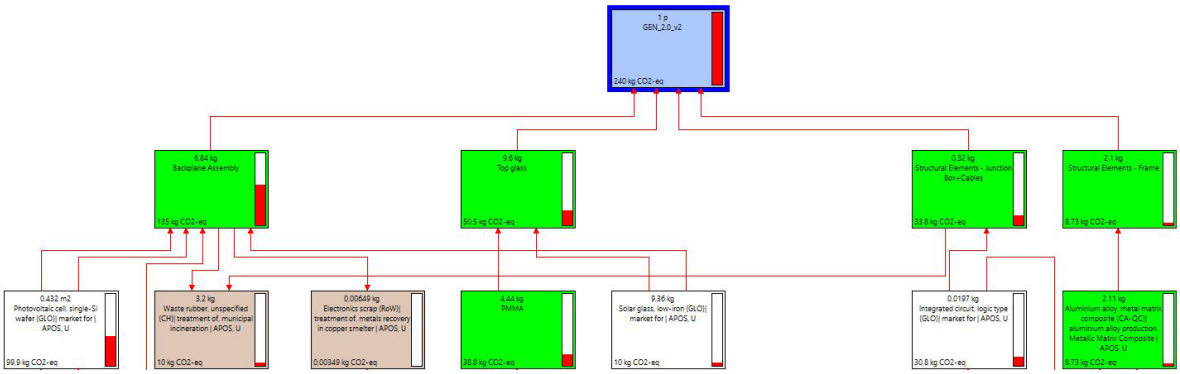

Fig. 1. Reduced process tree showing contribution in kg CO_2 eq. emission of individual materials used to manufacture the module (only elements with contribution higher than 0.5% are shown)

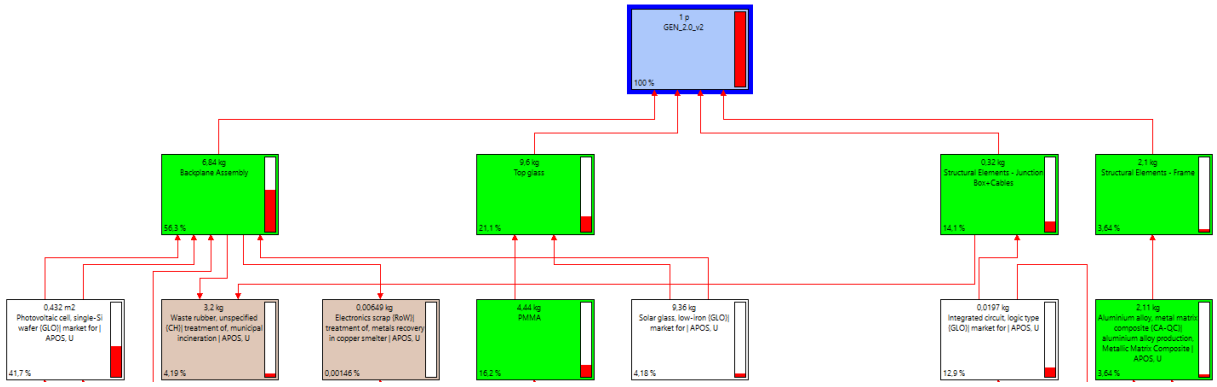

Fig. 2. Reduced process tree showing the percentage of contribution of individual materials used to manufacture the module (only elements with contribution higher than 0.5% are shown)

High efficiency of energy conversion of HCPV Hiperion panel results in low carbon footprint per kWh produced by the module which is in the range of 17–29 g CO_2-eq./kWh. The carbon footprint of the module can be reduced further with recycling and recovery of the materials which can improve the sustainability of the photovoltaic industry.

Acknowledgment

This project has received funding from the European Union's Horizon 2020 research and innovation program under Grant Agreement No. 857775.

References

[1] Holechek J.L., Geli H.M.E., Sawalhah M.N., Valdez R., A Global Assessment: Can Renewable Energy Replace Fossil Fuels by 2050? *Sustain.*, 2022, 14(8), 4792.
[2] Ziemińska-Stolarska A., Pietrzak M., Zbiciński I., Application of LCA to Determine Environmental Impact of Concentrated Photovoltaic Solar Panels—State-of-the-Art, *Energies*, 2021, 14(11).

Posters

THE INVESTIGATIONS OF MASS TRANSFER IN SIMULATED BIOMEDICAL SYSTEMS

Anna Adach-Maciejewska*, Klaudia Kopka, Małgorzata Turula, Michał Stępnik

Warsaw University of Technology, Faculty of Chemical and Process Engineering,
Waryńskiego 1, 00-645 Warsaw, Poland
*corresponding author: anna.adach@pw.edu.pl

Drug release in biomedical systems is a multi-stage, complex process, whose analysis requires the interdisciplinarity approach, which allows to incorporate physical and biochemical phenomena into mathematical models and verify them based on experimental research.

Coronary intervention (PCI) techniques use stents to cure and prevent atherosclerosis. Stents are longitudinal, mesh-shaped elements, which simulate scaffolding in the vessel, preventing coronary artery stenosis. The second generation stents, so called drug-eluting stents (DES), are covered by a thin layer containing antiproliferative drug preventing restenosis, which was once frequent complication after surgery. The percentage of drug absorbed by the blood vessel wall to the amount of the active substance diluted in flowing blood is the object of interest of scientists.

The completed experiments simulated systems where the active substance diffused from the DES stent to the artery vessel walls and simultaneously was drifted by the convection of the blood flow. The measurements were conducted in the original, custom designed experimental setup (Fig. 1). The coaxial, thin, internal hydrogel collet, containing the active substance (New Coccine, NC) simulated the „stent". The central aperture formed the cylindrical lumen with the flowing "blood" (simulated by water, flowing in a closed loop) while the external, cylindrical collet made of hydrogel (biological agar) simulated the "vessel wall".

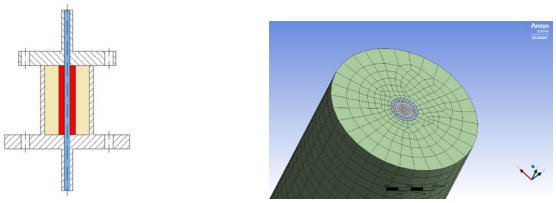

(a) (b)

Fig. 1. (a) Scheme of the experimental system [1], and
(b) numerical mesh of the system generated by Ansys Fluent [2]

Different experiments were performed to evaluate the rate of mass transfer as well as relative mass decay in the hydrogel including various flow rates, substance concentrations and diverse active substances. The rates of mass transfer calculated for these systems are in the range of N'_A=1,9·10^{-9}÷ 1,3·10^{-7} [mol/s] and are similar to the literature values. Below the exemplary percentages of New Coccine in the respective parts of the system are presented.

Table 1. The relative mass amounts in percentages of New Coccine in the subsequent parts of the system. The experiment: "stent" containing initially 0,1% [wt.] of New Coccine , the "blood" flow 30 [cm^3/min], diffusion coefficient $D_{NC,H}$= 7,5·10^{-11} [m^2/s], results after 210 minutes of measurements [1].

Percentage of New Coccine in "blood" = $m_{NC,H_2O}/m_{NC}$ [%]	42
Percentage of New Coccine in "stent" = $m_{NC,S}/m_{NC}$ [%]	21
Percentage of New Coccine in „vessel wall" = $m_{NC,H}/m_{NC}$ [%]	37

The results show that a large amount of the substance is being carried away by convection by the flowing liquid, which means that this amount of drug is not working therapeutically in the required place.

In the examined system, the distribution of the active substance between three media is considered. However, the calculated mass transfer coefficients of New Coccine to the flowing water, evaluated on the adequate correlations, proved that in this system the rate-limiting process of this drug release is diffusion in hydrogel [1]. Therefore, mathematical modeling of this process is described by the second Fick's law as the transient diffusion from thin polymer layer with adequate initial and boundary conditions, which is typical approach met in literature [3] ÷ [6]. The solution gives two analytical solutions of relative mass release from the hydrogel layer [3], [4]:

$$f(t) = \frac{m_{NC}(t)}{m_\infty} = 2\left(\frac{D_{NC,H}t}{L^2}\right)^{\frac{1}{2}}\left\{\pi^{-\frac{1}{2}} + 2\sum_{n=1}^{\infty}(-1)^n\, ierfc\frac{nL}{\sqrt{D_{NC,H}t}}\right\} \quad (1)$$

$$f(t) = \frac{m_{NC}(t)}{m_\infty} = 1 - \sum_{n=0}^{\infty}\frac{8}{(2n+1)^2\pi^2}\exp\left[\frac{-D_{NC,H}(2n+1)^2\pi^2 t}{4L^2}\right] \quad (2)$$

The above equations can be simplified, as the further modules of the sum take much smaller values and can be neglected:

- For $f(t) < 0.60$ equation (1) is simplified to the form:

$$f(t) = \frac{m_{NC}(t)}{m_\infty} = 2\left(\frac{D_{NC,H}t}{\pi L^2}\right)^{0,5} \quad (3)$$

The values of the relative weight loss of New Coccine determined by the experiments were compared with results of calculations obtained for mathematical model. The results achieved for the-in-vessel wall are quite close e.g.: 37% (experimental data) vs. 43% (calculated value).
However, the percentages of New Coccine in "stent" and in "blood" differ drastically. Further work must be done to verify the experiments and the model.

The rate of drug release can be also described as the first reaction kinetics. Following this assumption Etters [7] introduced the half-empirical model of relative mass release of a drug from a thin polymer layer (*a*, *b* and *g* are process parameters evaluated by experimental data):

$$\frac{m_{CzK}(t)}{m_\infty} = \left\{1 - \exp\left[-a\left(\frac{D_{CzK,Ag}t}{L^2}\right)^b\right]\right\}^g \quad (4)$$

Etters' semi-empirical model showed a good fit to the experimental data, which is related to its empirical nature, as this model coefficients have no clear physical interpretation.

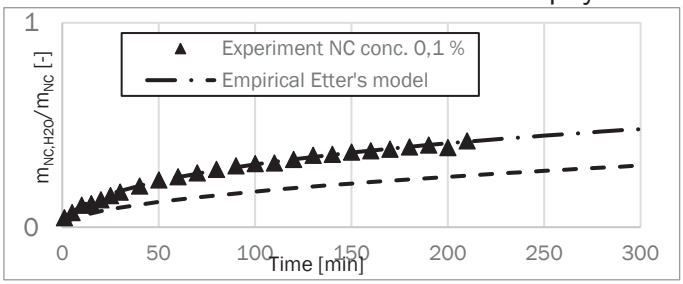

Fig. 2. Experimental data and calculated models

Further work will focus on providing complex experimental verification of diffusion models and the numerical modeling of such systems, which is already in progress (Fig. 1). These inquiries will allow to comprehensively analyze active substance release from drug eluting stents.

References

[1] Turula M., Modelowanie *układu symulującego transport substancji aktywnej z naczynia krwionośnego do krwi*, Praca Inżynierska nr 665, Politechnika Warszawska, Warszawa 2023.

[2] Stępnik M., *Modelowanie układu symulującego transport substancji aktywnej z naczynia krwionośnego do krwi*, Praca Inżynierska nr 619, Politechnika Warszawska, Warszawa 2022.

[3] Seidlitz A., Nagel S., Semmling B., Grabow N., Martin H., Senz V., Harder C., Sternberg K., Schmitz K-P., K. Kroemer H.K., Weitschies W., Examination of drug release and distribution from drug-eluting stents with a vessel-simulating flow-through cell, *Europ. J. of Pharmac. and Biopharmac.*, 2011, 78, 36-48.

[4] Guo Q., Knight P. T., Mather P. T., Tailored drug release from biodegradable stent coatings based of hybrid polyurethanes (with Supplementary data), *J. of Control. Release*, 2009, 137, 224-233.

[5] Saltzman W.M., *Drug delivery: engineering principles for drug therapy*, 1st ed. Oxford, England, Oxford University Press 2001.

[6] Siepmann F., Siepmann J., Modelling of diffusion controlled drug delivery, *J. Control. Release*, 2012, 161, 351-362.

[7] Etters J. N., Diffusion equation made easy, 1980, *Text. Chem. Color.,* 12, 140-145.

MODELING OF CARBON DIOXIDE SEPARATION FROM WET GAS MIXTURE ON ZEOLITE FIXED BED BY CYCLIC PRESSURE SWING ADSORPTION

Tomasz Aleksandrzak*, Kamila Zabielska, Elżbieta Gabruś

West Pomeranian University of Technology Szczecin, Faculty of Chemical Technology and Engineering, Department of Chemical and Process Engineering,
Piastów Ave. 42, 71-065 Szczecin, Poland
*corresponding author: Tomasz.Aleksandrzak@zut.edu.pl

Carbon dioxide is the main greenhouse gas responsible for climate change. One of the possibilities to reduce carbon dioxide emissions is its capture and storage (CCS). Among the methods of capturing and retaining CO_2 separation processes based on the adsorption of a gas stream on a fixed bed of a selected adsorbent are a common choice. Removal of carbon dioxide from the gas mixture using adsorption allows to increase air quality and reduces greenhouse gas emissions to the environment [1].

Pressure Swing Adsorption (PSA) is a cyclic column process with a fixed bed of adsorbent. The main advantages of PSA are: low investment and operating costs, short time of the cycle, long life of the adsorbent, high efficiency of the process and fixed operating costs. In order to guarantee the continuity of the separation process in adsorption plants, it is necessary to use at least two identical beds. A contaminated gas stream is introduced into the inlet of the adsorption column, in which the pressure increases, which is favorable for the adsorption of carbon dioxide from the gas mixture with nitrogen. The adsorbent bed regeneration process occurs as a result of lowering the pressure in the adsorber, which promotes the desorption of previously adsorbed carbon dioxide and its removal from the bed [1, 2]. The pressure swing adsorption process consists of the following stages: I – pressurization, II – adsorption, III – depressurization, IV – desorption [3, 4, 5], which require optimization of operating parameters, i.e. pressure, stream flows and length of time of individual stages. During the design of the adsorption installation and analysis of the effectiveness of capturing carbon dioxide from flue gases, it is necessary to develop an appropriate mathematical model. The model should include all the mechanisms of mass, heat and momentum transport relevant to the PSA process, and its postulates regarding the individual stages of the process should be consistent with an analysis of experimental data and prediction of the range of process conditions implemented in practice.

PSA process was used to remove carbon dioxide from a model gas mixture consisting of carbon dioxide, nitrogen and water vapor, as water molecules are present in real off-streams and easily adsorb on the 13X zeolite. The composition of the gas was similar to the composition of flue gas. The sources of carbon dioxide (99.995%) and nitrogen (99.999%) were pressurized gas cylinders (Messer), while the water came from the municipal water supply and was distilled before use. On the basis of previous equilibrium and kinetic studies, zeolite 13X (Hurtgral, Poland) was selected for separation of the CO_2, N_2, and H_2O gas mixture, which showed a high adsorption capacity for CO_2 (5,45 mol/kg at 2000 kPa) [2,3]. The basic physical properties of zeolite 13X are: shape - spheres, bulk density - 700 kg/m^3, adsorbent grain diameter - 3 mm. The adsorbent was packed as a fixed bed in a cylindrical apparatus with an internal diameter of 26 mm to a height of 500 mm. Experimental studies of the pressure swing adsorption process were carried out with the following process parameters: composition of the $CO_2/N_2/H_2O$ gas mixture: 15/84,98/0,02; 10/89,99/0,01; 20/79,98/0,02; adsorption process pressure 3 and 5 bar; ambient temperature 298 K; inlet gas flow rate 4.738 L/min; purge gas flow rate 180 mL/min. The composition of gas streams was measured with a mass spectrometer HPR-20 (Hiden Analytical, UK). The experimental results were presented in the form of breakthrough curves.

The mathematical model was developed for one adsorbent layer consisting of zeolite 13X. The entire model consists of partial differential equations, which relate to mass and energy, along with

transport rate and adsorption equilibrium equations. The following simplifying assumptions were made in the modeling of a non-equilibrium, non-isothermal cyclic PSA process of carbon dioxide capture from a model gas mixture. The fluid flow through the bed is described by plug flow of the gas phase with axial dispersion of mass and heat, the adsorption isotherm is described by the extended Langmuir model, there is no thermal equilibrium between the gas phase and the grains of the solid. In the model, the physical properties of the adsorbed substances and the walls of the adsorption column are independent of temperature and pressure. Moreover, temperatures and concentrations of radial gradients are negligibly small and isosteric heat of adsorption has a constant value [5].

The mathematical model was solved with the numerical method of lines (NMOL) in Matlab R2021b using solver ODE23s. The basic idea of the NMOL is to replace the spatial (boundary-value) derivatives in the partial differential equations (PDE) with algebraic approximations. Once this is done, the spatial derivatives are no longer stated explicitly in terms of the spatial independent variables. Thus, in effect, only the initial-value variable, typically the time in a physical problem, remains. In other words, with only one remaining independent variable, we have a system of ordinary differential equations (ODEs) that approximate the original PDE [5].

Mathematical modeling was based on our own measurements of equilibrium and kinetics performed on an IGA-002 apparatus (Hiden Isochema, UK) and findings from the bench-scale PSA column installation. During the adsorption stage of the PSA process, an increase in bed temperature from 293 to 314 K was observed, depending on the composition of the gas mixture. Therefore, it was reasonable to perform CO_2, N_2, H_2O gas/vapor - zeolite 13X isotherms for adsorption systems in a wide temperature range and introduce them to the PSA process model in the form of multi-temperature isotherms [2, 3]. Calculated breakthrough curves and temperature profiles were obtained while simulating CO_2 capture from a wet gas mixture on the fixed zeolite bed. The experimental data were used to verify the results of model calculations, obtaining their good agreement with real cases. Thus, the usefulness of the model for simulating the uptake of carbon dioxide from the $CO_2/N_2/H_2O$ mixture on zeolite 13X was confirmed. Detailed process modeling, simulations and optimization strategies can be a very reliable tool for both qualitative and quantitative assessment of potential adsorbents for CO_2 capture.

References

[1] Schell J., Casas N., Marx D., Mazzotti M., Precombustion CO_2 Capture by pressure swing adsorption of laboratory PSA experiments and simulations. *Ind. Eng. Chem. Res*., 2013, 52, 8311–8322.

[2] Zabielska K., Aleksandrzak T., Gabruś E., Adsorption equilibrium of carbon dioxide on zeolite 13X at high pressures, *Chem. Process Eng. - Inz. Chem. Proces*., 2018, 39(3), 309-321.

[3] Zabielska K., Aleksandrzak T., Gabruś E., Infuence of humidity on carbon dioxide adsorption on zeolite 13X, *Chem. Process Eng. - Inz. Chem. Proces*., 2020, 41(3), 197-208.

[4] Hefti M., Marx D., Joss L., Mazzotti M., Model-based process design of adsorption processes for CO_2 capture in the presence of moisture, *Energy Procedia*, 2014, 63, 2152–2159.

[5] Li S., Deng S., Zhao L., Zhao R., Lin M., Du Y., Lian Y., Mathematical modeling and numerical investigation of carbon capture by adsorption: Literature review and case study, *Appl. Energy*, 2018, 221, 437–449.

A DYNAMIC APPROACH IN EVALUATING PHYSIOLOGICAL EFFECTS OF NANOMATERIALS ON BACTERIA

Adrian Augustyniak[1, 2, 3]*, Kamila Dubrowska[1], Joanna Jabłońska[1], Natalia Gurgacz[2], Krzysztof Cendrowski[4], Beata Tokarz-Deptuła[2], Rafał Rakoczy[1]

[1] West Pomeranian University of Technology in Szczecin; Faculty of Chemical Technology and Engineering; Department of Chemical and Process Engineering; Piastów 42, 71-065 Szczecin, Poland
[2]University of Szczecin, Institute of Biology, Wąska 13, 71-415 Szczecin
[3] Technische Universität Berlin; Chair of Building Materials and Construction Chemistry; Gustav-Meyer-Allee 25, 13355 Berlin, Germany
[4] West Pomeranian University of Technology in Szczecin; Faculty of Civil and Environmental Engineering; Department of General Civil Engineering; Piastów 50a, 70-311 Szczecin, Poland
*corresponding author: adrian.augustyniak@zut.edu.pl

Nanomaterials are known for their antimicrobial activity. Therefore, they are extensively studied on microbiological models for novel applications in biotechnology, environmental protection, and medicine [1]. However, most of the tests on microorganisms are end-point methods that may ignore specific or subtle physiological changes in the studied population. Furthermore, methods such as disk diffusion or minimal inhibitory concentration assays may not be enough to obtain conclusive results [2]. Mainly carbon nanomaterials are difficult to use with any of the classic spectrophotometric methods as they considerably change the optical properties of the nanomaterial suspension. The often-used solution to this problem is the plate count method. However, this technique does not inform on possible cell agglomeration or switching to the viable but non-culturable state (VBNC). It means that only cells able to be cultured and to form a colony on a microbiological medium can be taken into account.

This study applied dynamic spectrophotometric and cytometric methods to evaluate the interaction between reference bacteria and selected nanomaterials.

The material for the study consisted of a group of reference microorganisms (*Escherichia coli* ATCC 25922, *Staphylococcus aureus* ATCC 33591, and *Pseudomonas aeruginosa* ATCC 27853) and selected nanomaterials, including metal oxide nanoparticles (Fe_3O_4, TiO_2, ZnO) and carbon nanomaterials (nanotubes and graphene oxide nanoplates). Various physiological multi-point measurements were recorded, including population growth kinetics, membrane potential, cell counts, viability, and respiration.

The dynamic approach revealed physiological changes in selected microorganisms in greater detail than end-point values [3]. Even though the populations often reached a similar state at the end of the experiment, there were discrepancies in the shape of the curves leading to this point. This method could also visualize other phenomena, such as cell agglomeration, temporary growth inhibition, and growth stimulation [4]. Resazurin assay was proven useful, particularly with carbon-based nanomaterials, where optical density could not be measured with high precision.

Dynamic methods can shed light on new dimensions of nanomaterial-bacterial interactions and improve the understanding of these processes.

References

[1] Vajtai R. (Ed.), *Springer handbook of nanomaterials*, Springer, 2013.
[2] Balouiri M., Sadiki M., Ibnsouda S.K., Methods for *in vitro* evaluating antimicrobial activity: A review., *J. Pharm. Anal.*, 2016, 6, 71–9.
[3] Augustyniak A., Cendrowski K., Grygorcewicz B., Jabłońska J., Nawrotek P., Trukawka M., Mijowska E., Popowska M., The response of Pseudomonas aeruginosa PAO1 to UV-activated titanium dioxide /silica nanotubes, *Int. J. Mol. Sci.*, 2020, 21.

[4] Augustyniak A, Jablonska J., Cendrowski K., Głowacka A., Stephan D., Mijowska E., Sikora P., Investigating the release of ZnO nanoparticles from cement mortars on microbiological models, *Appl. Nanosci.*, 2021.

Acknowledgment: This study was funded by National Science Centre Poland (Preludium 16, 2018/31/N/NZ1/03064).

SYSTEMIC APPROACH TO THE IMPLEMENTATION OF INDUSTRIAL ECOLOGY IN THE PRODUCTION OF SILVER NANOPARTICLES

Marcin Banach*, Olga Długosz, Jolanta Pulit-Prociak

Cracow University of Technology, Faculty of Chemical Engineering and Technology,
Warszawska 24, 31-155 Cracow, Poland
*corresponding author: marcin.banach@pk.edu.pl

Industrial ecology deals with the implementation of strategies to reduce the environmental impact of industry by ensuring cleaner production, with the focus not only on the environment but also on people, it is primarily about symbiosis between them [1]. In addition to reducing the consumption of energy and raw materials, which have a negative impact on the environment, it is intended to ensure quality of life and maintain profitability for trades, industry, and commerce [2]. The growing ecological trend dictates the development of obtaining nanostructures in accordance with the principles of Green Chemistry. According to industrial ecology, such a process should first and foremost reduce the use of energy and materials, as well as minimise waste generation and the use of toxic reactants as much as possible [3].

Design for the Environment (DFE) implies, among other issues, reuse, recycling and utilisation. Zero emission is mainly understood in the context of energy extraction and utilisation. It is therefore clear that, as Green Chemistry postulates, processes should be carried out as often as possible at ambient temperature and pressure. Zero liquid discharge determine the complete recycling of water, the treatment of wastewater, the elimination of the discharge of toxic compounds. It is therefore expedient to maintain the principle of Atomic Economics, to incorporate the raw material atoms into the product as much as possible. It is also important to eliminate the use of compounds with environmentally and humanly harmful properties. But what if the product itself, despite its many valuable properties, exhibits toxic properties?

The importance and many possible applications of silver nanoparticles have influenced the development of their manufacturing technology. The production of nanoparticles with specific size, stability and physicochemical properties has become significant. Growing concerns about the environmental issues of production have drawn scientific and economic attention to environmentally friendly processes that lead to reduced costs, energy and emissions. There is also a need for continuous modification of the processes used to obtain them, in order to better control properties or develop formulations that do not exhibit harmful properties towards living matter, or these properties are reduced while maintaining the functionality of the materials.

A system is a set of elements related in an organised manner. The properties of a system result from the integration of its constituent elements. In the case of technological issues, integration should start with determining the influence of process parameters on product properties and/or the process of obtaining the product (productivity, efficiency) and modelling these dependencies to predict the effects of the system and its elements.

The paper proposes the creation of a system constituting a technology for obtaining nanomaterials, using silver nanoparticles as an example, consisting of raw materially distinct but process-identical components. Each of the component processes leads to a final product in the form of silver nanoparticles, although, they are characterised by different product properties, various material and energy intensity and thus different cost intensity.

Compounds commonly used in the production of nanoparticle silver are described in the literature, including sodium borohydride and polyvinylpyrrolidone, However, the production of nanosilver using the above-mentioned compounds is associated with their negative impact on the environment. Consequently, another element of the system is based on the use of raw materials that do not endanger human health or the environment. This is a method of obtaining stable nanosilver suspensions using two synthetic substances, the use of which guarantees the reduction of metal ions and stabilisation of the resulting nanometal suspension. The requirement is the

specific physicochemical properties of the chemical compounds used, which allows the method to be treated as environmentally friendly. For this purpose, D(+)-glucose or L(+)-ascorbic acid were used as reductants, as well as gelatine, which acted as a dispersing agent. Gelatine is a natural substance whose dry matter is a mixture of proteins and peptides. Glucose is known as "biological fuel". It is the energy source of many living organisms, including bacteria and humans. Ascorbic acid has strong antioxidant properties and is an important factor in the functioning of the human body. Due to its antioxidant properties, the substance has found use as a food preservative additive. In the food industry, ascorbic acid is known by the symbol E300. However, the process does not demonstrate adequate efficiency due to the need for two additional reactants (in addition to the metal ion source) [4, 5].

Plant extracts in which compounds with stabilising-reducing properties are present can be used in processes to obtain metal nanoparticles. The study focused on the use of aqueous extracts of selected plants. The substances obtained by extraction made it possible to achieve both reducing and stabilising effects in the suspensions formed. The complexity of the composition of the plants makes it possible to state that they are a natural source of all of the above-mentioned compounds with reducing properties, i.e., ellagic, gallic, ascorbic acids and anthocyanins, as well as other compounds belonging to the groups of polyphenols, flavonoids, and tannins. The extracts obtained also contain other substances whose nature allows effective stabilisation of the resulting nanometal suspensions, and these include mucilaginous compounds, peptides and biopolymers. Aqueous extracts of dried raspberry fruit were used in this study [6].

The use of extracts enables a product with the expected properties to be achieved, but it is not advisable to use such high-quality materials in solutions that do not require this.

Stable suspensions of nanoparticles can be obtained using synthetic chemical compounds, whose physicochemical properties allow them to be used to simultaneously reduce metal ions and stabilise forming suspensions. In addition to suitable physicochemical properties, an important criterion for the selection of these compounds is the fact that they occur in the natural environment. As a result of the natural origin of the compounds used, the method can be described as pro-ecological.

It was found possible to obtain silver nanoparticles with a chemical reduction using tannic acid. Tannic acid belongs to the group of polyphenols of natural origin. It is characterised by its high antioxidant activity. The macromolecular structure of this compound allows effective size stabilisation of the resulting nanoparticles.

Industrial Ecology aims to close the product cycle. Following this approach, the final component of the system was made using an infusion of waste coffee. With such a set of methods for obtaining silver nanoparticles, the main question to be answered when embarking on their production concerns the type of final product in which the nanoparticles will be contained, in which industry or in which sphere of everyday life they will be used? Only then should the expected properties of the product be defined.

The rational use of the established properties of nanoparticles may make it possible to control and reduce the environmental impact, which, as a consequence of time and the prevalence of uncontrolled use, may become a significant problem. The most favourable solution is to use silver nanoparticles in a sustainable manner, in situations, places and products, when and where they actually perform their function and are needed. Depending on the answer to the question posed and the expected properties of the nanomaterial, a choice should be made as to how to obtain NAg from the system, which in its entirety should be considered as a single technology - eco-innovative, energy-efficient, cleaner, compatible with the principles of Green Chemistry and an Industrial Ecology strategy with Sustainability as the ultimate goal.

References

[1] Bartolucci C., Antonacci A., Arduini F., Moscone D., Fraceto L., Campos E., Attaallah R., Amine A., Zanardi C., Cubillana-Aguilera L.M., Santander J.M.P., Scognamiglio V., Green nanomaterials fostering agrifood sustainability, *TrAC Trends Anal. Chem*., 2020, 125, 115840.

[2] Abdelbasir S.M., McCourt K.M., Lee C.M., Vanegas D.C., Waste-derived nanoparticles: Synthesis approaches, environmental applications, and sustainability considerations, *Front. Chem*., 2020, 782.

[3] Rodrigues G., da Costa Sousa M.G., Rezende T.M.B., Franco O.L., Can metallic nanomaterials be green and sustainable? *Curr. Opin. Environ. Sci. Health*, 2021, 24, 100292.

[4] Babbitt C.W., Moore E.A., Sustainable nanomaterials by design. Nature nanotechnology *Nat. Nanotechnol*. 2018, 13(8), 621–623.
[5] Mohamed Fahmy H., Mahmoud Mosleh A., Abd Elghany A., Engy Shams-Eldin, Serea E.S.A., Ashour Ali S., Esmail Shalan A., Coated silver nanoparticles: synthesis, cytotoxicity, and optical properties, *RSC Adv*., 2019, 9, 20118–20136.
[6] de Souza T.A.J., Souza L.R.R., Franchi L.P., Silver nanoparticles: An integrated view of green synthesis methods, transformation in the environment, and toxicity, *Ecotoxicol. Environ. Saf*., 2019, 171, 691–700.

PHOTOREACTIVE URETHANE (METH)ACRYLATE OLIGOMERS WITH BUILT-IN DIELS-ALDER REACTION ADDUCT – SYNTHESIS AND THERMALLY REVERSIBLE MECHANISM

Paulina Bednarczyk*, Karolina Mozelewska, Joanna Klebeko, Joanna Rokicka, Małgorzata Nowak, Paula Ossowicz-Rupniewska

West Pomeranian University of Technology in Szczecin, Faculty of Chemical Technology and Engineering, Piastów 17, 70-310 Szczecin, Poland

*corresponding author: bednarczyk.pb@gmail.com

A series of UV-curable urethane (meth)acrylates was obtained by copolymerization of the Diels-Alder adduct (HODA), isophorone diisocyanate, PEG1000, and various hydroxy (meth)acrylates. The aim of the presented work was to determine the influence of the chemical structure of the introduced (meth)acrylic groups, i.e., hydroxyethyl acrylate, hydroxypropyl acrylate, hydroxyethyl methacrylate, and hydroxypropyl methacrylate, on the UV-curing process and thermally reversible mechanism of cured polymers. The chemical structure of prepolymers was characterized by FTIR and NMR spectroscopy, whereas the UV-curing process was monitored in real time using FTIR and photo-DSC. In turn, the thermally reversible mechanism was tested using an FTIR spectroscope equipped with a heating attachment, DSC and TG apparatus, as well as an optical microscope equipped with a stage with programmable heating. The result of comprehensive research on the thermally reversible mechanism of urethane (meth)acrylate oligomers with built-in Diels-Alder reaction adduct in the context of the presence of various photoreactive groups allows one to control the self-healing process of cured polymers by reducing the effective heating temperature [1]. The presented research is part of the work supported by The National Centre for Research and Development (NCBR; grant no. LIDER/16/0102/L-10/18/NCBR/2019

References

[1] Bednarczyk P., Mozelewska K., Klebeko J., Rokicka J., Ossowicz-Rupniewska P., Impact of the chemical structure of photoreactive urethane (meth)acrylates with various (meth)acrylate groups and built-in Diels–Alder reaction adducts on the UV-curing process and self-healing properties, *Polymers,* 2023, 15, 924.

EFFECT OF PARTITION WETTABILITY ON NANOPARTICLE DIFFUSION THROUGH MODEL STRUCTURES IMITATING HUMAN SKIN

Mariola M. Błaszczyk*, Jerzy P. Sęk, Aleksandra Budzyń

Lodz University of Technology, Faculty of Process and Environmental Engineering,
Wólczańska 213, 93-005 Lodz, Poland

*corresponding author: mariola.blaszczyk@p.lodz.pl

The transport of dispersion systems, especially in small, micro or nanostructures, plays a fundamental role in many fields of science and industry such as medicine, pharmaceuticals and oil extraction [1]. One of the top challenges for scientists today is the non-invasive introduction of active substances into the human body. This will make it possible to stop using outdated injection methods, which are not only sometimes painful but can also cause cross-infection, which directly threatens human life. The development of nanotechnology and the ability to create increasingly complex drug carriers at the nanoscale offers increasingly realistic prospects for meeting this challenge. However, in the absence of sufficient knowledge of the mechanisms of transport of such systems through the human skin structure, a deeper consideration of these issues is necessary.

Human skin consists of layers, which are characterized not only by different structures but also by varied lipophilicity. Due to the tight structure of keratinocytes and the laminar arrangement of lipids surrounding the cells, the most difficult layer to overcome is the outer layer of the skin - the stratum corneum. This layer in its structure consists of alternating lipid layers and aqueous layers (See Fig. 1).

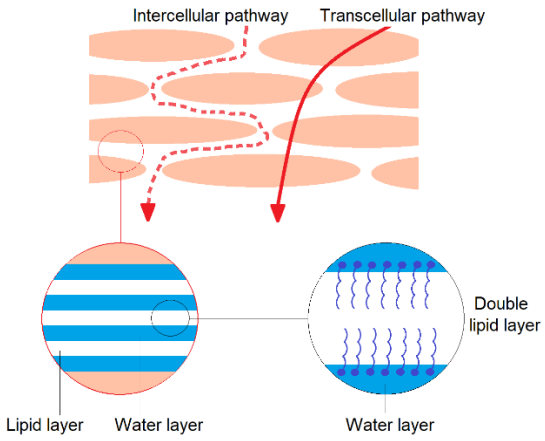

Fig. 1. Intercellular and transcellular diffusion

The farther into the skin its hydrophilicity increases. This changing wettability of the medium greatly complicates the ability to transport the introduced compounds. For this reason, active substances are often placed on or in so-called carriers and in this form are transported to selected layers of the skin [2]. The simplest carriers of active substances are nanoparticles, which provide a matrix for many types of compounds [3]. Rapid advances in nanotechnology in recent years have contributed to the possibility of creating nanoparticles with well-defined parameters adapted to medical purposes [4]. However, in order to take advantage of the potential of using nanoparticles as non-invasive drug carriers, it is not enough just to be able to produce them, but it is also necessary to know the mechanisms of their transport through the skin structure. The movement of substances through this pathway is described in the literature as diffusive transport and is characterized by Fick's first law [5]. The proportionality factor between the mass flux and the concentration gradient along the path is the diffusion coefficient. For the diffusion process of nanoparticles in liquids, the

diffusion coefficient is described by the Stokes-Einstein relationship [6]. However, nanoparticles moving in the skin, encounter skin cells on their way, which translates into the fact that transport takes place through a certain porous structure. It is generally accepted that the transport of particles through porous structures depends on the ratio of the size of these particles to the size of the pores, or in this case, the intercellular spaces (cement) [7]. That is, the smaller the diameters of the paths through which a substance can be transported, the greater the resistance and the less intense the flow. This therefore suggests that in the case of the transport of nanoparticles through dermal structures, it is the size of the intercellular spaces that has a decisive influence on their migration. However, recent experimental works indicate that some of the particles are captured (adsorbed) by the structure during transport, resulting in a significant reduction in permeability [8]. The deposition of particles in the skin layers will also depend on their hydrophilicity. There is a lack of quantitative studies in the literature on how this property of the partition surface affects the diffusion process of nanoparticles. Therefore, experimental work was undertaken to track diffusion using Franz chambers for nanoparticle suspensions through partitions with modified surfaces. Hydrophilic and hydrophobic filters with adequate parameters were used. Studies of nanoparticle diffusion over time were carried out for both single layers of partitions and several - one on top of the other. Alternating systems of hydrophilic and hydrophobic partitions in various combinations were also used. This allowed us to determine changes in the concentration of nanoparticles in solution over time for the systems studied. Therefore, it was possible to estimate the influence of surface wettability on the nanoparticle diffusion process. The quantitative results of this study can provide a basis for modeling the transport of drug nanocarriers in human skins taking into account the varying wettability.

Foundation
This research was funded by the National Science Center (Poland), within a research grant NCN Sonata 2019/35/D/ST8/01033.

References

[1] Rahman H., Hossain M.R., Ferdous T., The recent advancement of low-dimensional nanostructured materials for drug delivery and drug sensing application: A brief review, *J. Molec. Liq*., 2020, 320 A, 114427.
[2] Waghule T., Rapalli V.K., Gorantla S., Saha R.N., Dubey S.K., Puri A., Singhvi G., Nanostructured Lipid Carriers as Potential Drug Delivery Systems for Skin Disorders, *Curr. Pharm. Design*, 2020, 26(36), 4569-4579.
[3] Prow T.W., Grice J.E., Lin L.L., Faye R., Butler M., Becker W., Wurm E.M.T., Yoong C., Robertson T.A., Soyer H.P., Roberts M.S., Nanoparticles and microparticles for skin drug delivery, *Adv. Drug Deliv. Rev.*, 2011, 63(6), 470-491.
[4] McNamara K., Tofail S.A.M., Nanoparticles in biomedical applications, *Adv. Phys. X*, 2017, 2(1), 54-88.
[5] Mitragotri S., Anissimov Y.G., Bunge A.L., Frasch H.F., Guy R.H., Hadgraft J., Kasting G.B., Lane M.E., Roberts M.S., Mathematical models of skin permeability: an overview, *Int. J. Pharm*., 2011, 418(1), 115-29.
[6] Lee B.J., Cheema Y., Bader S., Duncan G.A., Shaping nanoparticle diffusion through biological barriers to drug delivery, *JCIS Open*, 2021, 4, 100025.
[7] Zeb A., Arif S.T., Malik M., Shah A., Ud Din F., Qureshi O.S., Lee E.S., Lee G.Y., Kim J.K., Potential of nanoparticulate carriers for improved drug delivery via skin, *J. Pharm. Invest.*, 2019, 49, 485–517.
[8] Błaszczyk M.M., Sęk, J.P., The New Attempt at Modeling of the Three-Dimensional Geometry of the Epidermal Skin Layer and the Diffusion Processes of Nanomolecular Drug Carriers in Such Structures, Molecules, 2023, 28, 205.

NUMERICAL SIMULATIONS OF ADSORPTION OF NANODROPLETS DURING THEIR TRANSPORT IN NARROW CHANNELS

Mariola M. Błaszczyk*, Jerzy P. Sęk, Aleksandra Budzyń

Lodz University of Technology, Faculty of Process and Environmental Engineering,
Wólczańska 213, 93-005 Lodz, Poland
*corresponding author: mariola.blaszczyk@p.lodz.pl

Nanodroplets and nanoparticles are objects from a few to a dozen or so nanometers in size. They exist commonly in the natural environment from where they can enter living organisms. They can intrude during swallowing, breathing, or directly through the skin. This path is the most interesting from the point of view of the cosmetic and pharmaceutical industry as the route of noninvasive delivery of cosmetics and medicaments to the organism without damaging the skin surface [1, 2].

The skin is the biggest organ of most mammals' bodies. In the case of humans, it weighs about ten percent of the total body mass. This cover protects the organism's interior against external impacts. It generally consists of four layers of different structure as presented in Fig. 1.

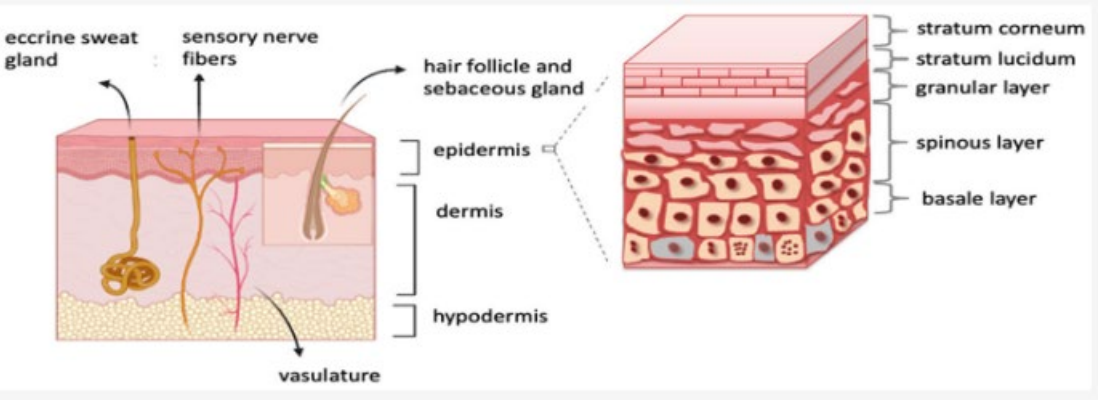

Fig. 1. The cross-section of skin

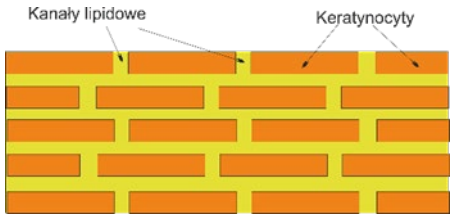

Fig. 2. Brick and mortar model of stratum corneum

The outermost of these layers is named stratum corneum. It has a thickness of about 10 to 20 micrometers and it is permanently revived. Despite this, it is the main barrier protecting the body's interior against external infections. In scientific considerations, the stratum corneum is very often presented as the brick-and-mortar model shown in Fig. 2 [3].

The vertical slits as presented in Fig. 2 have a width of about dozens of nanometers. Therefore, their size is comparable with the dimensions of transported nanobodies. In such a layout, the transport of nanobodies can be very slow or even entirely stopped into the deeper layers of skin.

This protecting effect occurs as the result of at least two processes. One is the limitation of the speed of diffusion. Nanobodies have usually dimensions comparable to the size of slits. It causes

the values of diffusion coefficients to be low, very often below 10^{-9} m^2/s. The second mechanism is the adsorption of transported material on the walls of channels. Because of the micro-sizes of the considered domain and the nanosizes of migrating nanodroplets or nanoparticles, it does not seem that any experimental technique could say what is the proportion between the number of particles transported as the result of diffusion and those which are adsorbed on the walls of the channels.

The only insight into these phenomena can be estimated on the basis of numerical simulation.

Numerical simulations of the transition of particles through the slit as the result of diffusion and adsorption on walls in the narrow channel were performed using the COMSOL Multiphysics v.6 program package. Calculations were conducted in the two-dimensional domain of the geometry presented in Fig. 3.

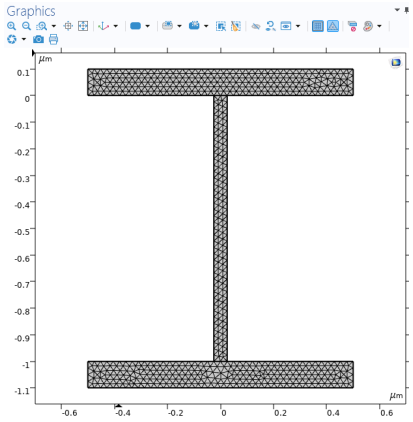

Fig. 3. Geometry of the numerical domain

The height of the vertical channel was equal to 1μm and its width was 50 nm. To the main transport zone two chambers were added as the elements of the horizontal lipid layers. Simulations were carried out assuming that the nanoelements were moving as the result of Brown forces including Stoke's viscous drag resistance. It was assumed in the simulations that the density of the liquid in which the transport occured was equal to 1000 kg/m3 and viscosity was 0.001, 0.005, 0,01, 0,02, and 0,05 Pa·s. The density of the transported material was equal to 800 kg/m3. It corresponds to the density of the oil phase in most of the real emulsions. Diameters of the migrating particles were equal to 1, 5, 10, 15, and 20 nm.

The results of this modeling work allowed to estimate how many nanodroplets will be transported along the vertical channels and how many will settle on walls as the result of adsorption. Such results allow for predicting how effective, in the sense of penetration, can a given drug, medicament, or cosmetic be when it is delivered noninvasively through the skin surface.

Funded by:

This research was funded by the National Science Center (Poland), within a research grant NCN Sonata 2019/35/D/ST8/01033.

References

[1] Zeb A., Arif S.T., Malik M., Shah A., Ud Din F., Qureshi O.S., Lee E.S., Lee G.Y., Kim J.K., Potential of nanoparticulate carriers for improved drug delivery via skin, *J. Pharm. Invest.*, 2019, 49, 485–517.

[2] Olejnik A., Semba J.A., Kulpa A., Danczak-Pazdrowska A., Dalibor Rybka J., Gornowicz-Porowska J., 3D Bioprinting in Skin Related Research: Recent Achievements and Application Perspectives. *ACS Synth. Biol.*, 2022, *11*, 26–38.

[3] Schneider M., Stracke F., Hansen S., Schaefer U., Nanoparticles and their interaction with the dermal barrier, *Dermato-Endocrinology*, 2009, 1(4), 197-206

[4] Błaszczyk M.M., Sęk, J.P., The new attempt at modeling of the three-dimensional geometry of the epidermal skin layer and the diffusion processes of nanomolecular drug carriers in such structures, *Molecules*, 2023, 28, 205.

A STUDY OF ISOTHERM EQUATIONS FOR A MIXTURE OF STRONGLY ADSORBING SPECIES

Dominika Boroń*, Katarzyna Bizon

Cracow University of Technology, Faculty of Chemical Engineering and Technology,
Warszawska 24, 31-155 Cracow, Poland

*corresponding author: dominika.boron@pk.edu.pl

There are numerous types of isotherms in the literature that can be used to describe the adsorption equilibria for pure substances, including but not limited to simple Langmuir-type equilibria or S-type isotherms. However, for multicomponent mixtures, there exist only a few equations, such as the extended Langmuir isotherm or the Sips isotherm. Typically, IAS (*Ideal Adsorption Solution*) or RAS (*Real Adsorption Solution*) methods are used to determine multicomponent equilibria [1]. It is therefore justified to propose approximation formulas for such equilibria characterized by a sufficiently small number of parameters. The aim of this study was to propose equations approximating adsorption isotherms for a mixture of two strongly adsorbing compounds.

The mixture of carbon tetrachloride and n-hexane, which adsorb on Ajax activated carbon at 303 K was analyzed in this study. In Table 1, the Thoth isotherm parameters for the analyzed adsorption system are shown. The pure substance isotherms have a typical Langmuir-type shape.

Table 1. Parameters of Toth equation for CCl_4 and n-hexane on Ajax activated carbon (T = 303 K) [2]

	CCl_4	n-hexane
q_1^*, mol/kg	7.194	5.265
b_{0i} , Pa^{-1}	0.8447	0.7801
t	0.3653	0.4092

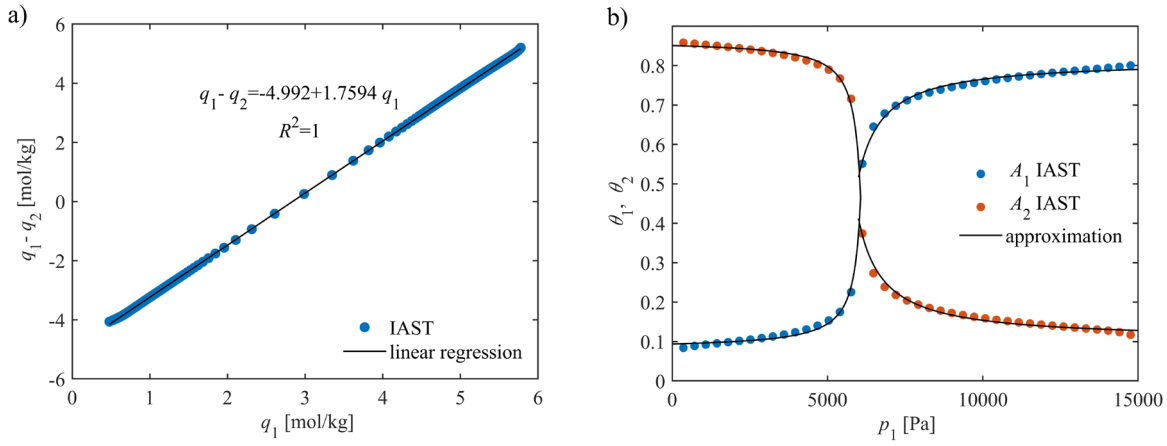

Fig. 1. (a) Linear relationship between difference q_1-q_2 and loading q_1 and (b) approximation of the isotherm in binary mixture {CCl_4-n-Heskane} on Ajax activated carbon (T = 303 K)

The IAS method was used to calculate sorption isotherms for this binary mixture. Due to the high values of adsorption affinity (b_{0i}), S-type isotherms were obtained [3]. In order to approximate the results with the appropriate equation, the S-shaped isotherm was divided into two parts, where the abscissa of its inflection point was the separation point. In addition, it was shown that there is

a linear relationship between the difference in the concentrations of the mixture components in the solid and the concentration of one of them. Thus, the following linear relationship can be written:

$$q_1 - q_2 = a_0 + a_1 q_1 \tag{1}$$

In Equation (1), the values of a_0 and a_1 can be determined using linear regression. This makes it possible to determine the concentration of the second adsorbed component from a known value for the first component. Figure 1a shows the results of using linear regression for the CCl_4–n-hexane mixture.

The following isotherm equation was proposed for n-hexane (A_2) in the first interval, i.e. for values of partial pressures lower than the abscissa of the inflection point:

$$\theta_2 = \frac{b_2 \cdot (p_2 - p_{2f})}{1 + b_1 \cdot p_1 + b_2 (p_2 - p_{2f})} + b_3 \tag{2}$$

There are only three parameters in this equation. For the second interval ($p_1 > p_{1f}$), the following equation for carbon tetrachloride (A_1) was proposed:

$$\theta_1 = \frac{b_1 \cdot (p_1 - p_{1f})}{1 + b_1 \cdot (p_1 - p_{1f}) + b_2 p_2} + b_3 \tag{3}$$

The parameters of Equations (2) and (3) were obtained separately for each interval using non-linear regression. Their values are reported in Table 2. The concentration of, respectively, CCl_4 in the first interval and n-hexane in the second one, were determined with linear regression (Equation (1)).

Table 2. Parameters of isotherm equation for mixture CCl_4 - n-hexane (T=303 K)

	$p_1 < p_{1f}$	$p_1 > p_{1f}$
b_1 , Pa^{-1}	$-1.562 \cdot 10^{-4}$	$4.181 \cdot 10^{-5}$
b_2 , Pa^{-1}	$6.904 \cdot 10^{-5}$	$-9.884 \cdot 10^{-5}$
b_3 , $\mathrm{mol/kg}$	0.5576	0.5167

The results of this procedure are illustrated in Figure 1b. The point symbols are derived from the application of the IAS method, while the solid lines are the values obtained on the basis of equilibrium approximation using Equations (2) and (3).

As can be seen in Figure 1b, the proposed method of approximating the adsorption equilibria for a mixture of two strongly adsorbing substances is sufficiently accurate. Thus, it may be used for simple engineering calculations. This procedure can be employed to determine equilibrium adsorption equations in various binary mixtures of strongly adsorbing species.

It was also shown that the S-shape of the isotherms for a binary mixture of strongly adsorbing compounds persists even when a significant amount of inert gas is added to the system.

References

[1] Do D.D., *Adsorption analysis. Equilibria and kinetics.*, London, Imperial College Press 1998.

[2] Bae J.S., Do D.D., Surface diffusion of strongly adsorbing vapors in activated carbon by a differential permeation method. *Chem. Eng. Sci.*, 2003, 58, 4403-4415.

[3] Bizon K., Boroń D., Tabiś B., Practical issues concerning two-component equilibria of strongly adsorbing species in porous solids. *Chem. Eng. Res. Des.*, 2022, 187, 290-298.

MONOLITHIC SILICA MICROREACTORS FOR SEQUENTIAL HYDROLYSIS-CONDENSATION REACTIONS

Agnieszka Ciemięga*, Katarzyna Maresz, Julita Mrowiec-Białoń
Polish Academy of Sciences, Institute of Chemical Engineering,
Bałtycka 5, 44-100 Gliwice, Poland
*corresponding author: ciemiega@iich.gliwice.pl

Continuous flow microreactors are attractive tools employed in modern technologies, designed for new molecule production in a greener and more sustainable manner. They proved to be an efficient, eco-friendly, lower-cost alternative for periodically conducted processes. In contrast to typical batch reactors, they provide efficient mixing, safety handling and facilitated control of process parameters. In the presented studies, benefits of flow microreactors were combined with the advantages of comprehensive synthesis of chemical compounds based on tandem catalysis assumptions. A tandem reaction is a complete multistep chemical synthesis of desired products from commercially available precursors. New pathways in cascade strategies require the development of tailored bifunctional heterogeneous catalysts with different catalytic functions.

Herein, the cores of microreactors were formed by a highly porous skeleton with an extended surface area modified with zirconia and propylamine active sites. Processes involving deacetalization and Knoevenagel condensation were merged to create a complex system for the synthesis of ethyl α-cyanocinnamate. The processes were performed in two variations of microreactor set-up: i) microreactor with silica core modified with mixed centres and ii) two microreactors of different catalytic features connected in series.

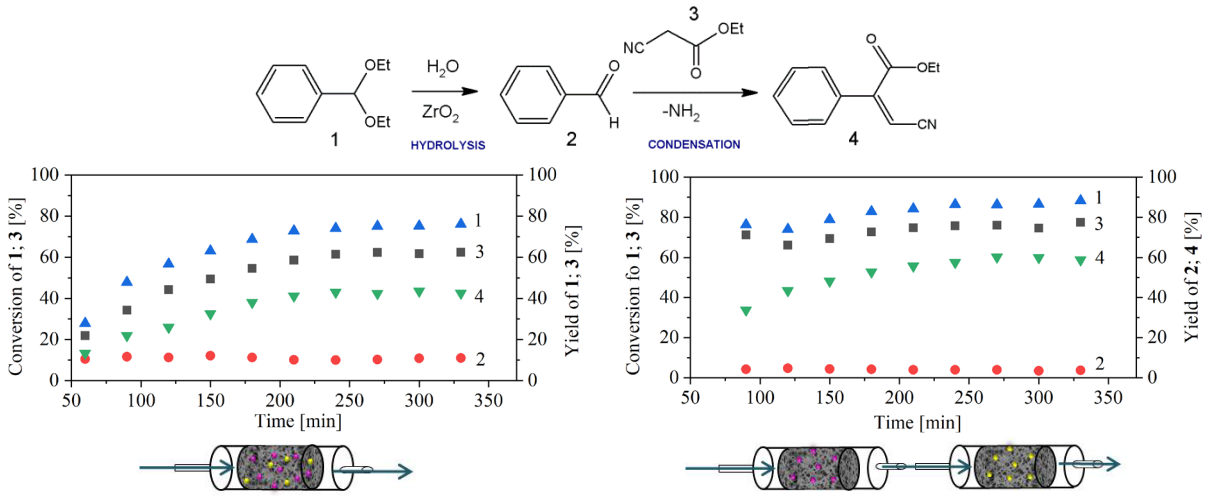

Fig. 1. Performance of bifunctional microreactor (left) and microreactors connected in series (right)

The results showed the beneficial effect of the dual modification with both acid and base sites over the single functionalization of two separated cores (Fig. 1). Microreactors of 4 cm and 1 cm were employed to probe the influence of the residence time on catalytic performance. The highest product yield was achieved in the 4cm-long microreactor (for the longest residence time) while an inverse relationship was observed for selectivity.

The application of a bifunctional microreactor in cascade synthesis is a new, perspective strategy in the area of process miniaturization.

Acknowledgements: Financial support from the Polish National Science Centre (project no. 2021/43/D/ST8/01727) is gratefully acknowledged.

HYDRODYNAMICS OF TWO- AND THREE-PHASE SYSTEMS IN AN AGITATED VESSEL WITH TWO IMPELLERS

Magdalena Cudak

West Pomeranian University of Technology, Szczecin, Faculty of Chemical Technology and Engineering, Piastów Ave. 42, 71-065 Szczecin
*corresponding author: cudak@zut.edu.pl

The manufacture of multiphase systems is an activity aimed at obtaining a homogeneous system and maintaining it for the time required for a particular process. One of the basic criteria for maintaining the proper hydrodynamic state in the agitated vessel is the appropriate selection of the configuration of the impellers on one shaft [1, 2, 3]. The study presented in this paper is aimed at determining the influence of the impeller configuration and, additionally, the impeller speed, the superficial gas velocity, the sucrose concentration in aqueous solution, and the yeast suspension concentration on the hydrodynamics of two- or three-phase systems in an agitated vessel with two impellers.

The gas hold-up and the average residence time of the bubbles were measured in an agitated vessel with a liquid height of $H = 2D$ and the internal diameters of $D = 0.288$ m. Four standard $B = 0.1T$ baffles were placed in the agitated vessel. The distance of the impellers from the bottom of the vessel was $h_L = 0.167H$ (for the lower impeller) and $h_U = 0.67H$ (for the upper impeller). Gas was introduced into liquid through a sparger of diameter $d_d = 0.7D$. The sparger was located at a distance of $e = 0.5h$ from the bottom of the agitated vessel. Different impeller configurations lower (L) – upper (U) high-speed impellers of diameter $d = 0.33D$ were used in the measurements.

The study was carried out for gas-liquid and biophase-gas-liquid systems, where the gas phase was air, the liquid phase were distilled water or an aqueous solution of sucrose ($c = 2.5\%$ mass., 5% mass.), and the biophase was a suspension of *Saccharomyces cerevisiae* yeast ($y_s = 1\%$ mass.). The measurements were conducted for the ranges of superficial gas velocity $w_{og} \in$ <3.413·10^{-3} m/s; 8.53 x 10^{-3} m/s>. The properties of the liquid were changed in the following ranges: density ρ [kg/m^3] $\in$ <1000; 1019>, surface tension σ[N/m] $\in$ <0.072; 0.086>; dynamic viscosity coefficient of the liquid phase η_l [Pas] $\in$ <1 x 10^{-3}; 1.16 x 10^{-3}>; dynamic viscosity coefficient for the biophase-liquid system was calculated from the following equation:

$$\eta_{b-l} = K \cdot \gamma^{m-1} \tag{1}$$

The research results were analyzed taking into account the influence of the type of the upper or lower impeller, impeller speed, superficial gas velocity and type of liquid in the system on the gas hold-up and the average residence time of the bubbles. The experimental results were mathematically described.

References

[1] Stręk F., *Agitation and Agitated Vessels*, Warszawa, WNT 1981 (in Polish).
[2] Kamieński J., *Agitation of Multiphase Systems*, Warszawa, WNT, 2004 (in Polish).
[3] Major-Godlewska M., Cudak M., Gas hold-up in vessel with dual impellers and different baffles, *Energies*, 2022, 15, 8685.

INTEGRATED PRODUCTION OF ETHANOL AND XYLITOL FROM CORN STRAW HYDROLYSATES – THE IMPACT OF SELECTED PROCESS PARAMETERS

Katarzyna Dąbkowska-Susfał[1,*], Jolanta Mierzejewska[2]

[1]Warsaw University of Technology, Faculty of Chemical and Process Engineering, Waryńskiego 1, 00-645 Warsaw, Poland
[2]Warsaw University of Technology, Faculty of Chemistry, Noakowskiego 3, 00-664 Warsaw, Poland
[*]corresponding author: Katarzyna.Dabkowska@pw.edu.pl

Due to the need to implement sustainable development policies, efficient methods of producing valuable products from 2nd generation raw materials (i.e. lignocellulosic plant biomass) are being sought. Examples of such biomass are wastes from agricultural production, including corn straw. They are a source of 5- and 6-carbon monosaccharides, which microbiological methods in biorefineries can process into biofuels, biodegradable polymers, and medicines. Biomass conversion into biofuels has recently been implemented in developed countries to gradually become less dependent on fossil sources. Bioethanol is particularly important to the global economy, which is growing in demand, mainly in the transportation sector. The profitability of bioethanol production can be increased by integrated production of valuable chemicals, such as xylitol, by fermentation of pentoses released from the hemicellulosic fraction of biomass [1]. Xylitol has applications in food, pharmaceutical, and material engineering and is currently produced chemically by hydrogenating xylose using Ni/Al_2O_3 as the catalyst [2]. However, the cost of the chemical process is high, mainly due to the formation of by-products and low yields.

The best natural producers of xylitol are yeast strains e.g. *Candida tropicalis* [3]. In addition, they ferment glucose to ethanol, which makes them particularly useful when using lignocellulosic waste as a raw material. The efficiency of xylitol production is affected by many factors, such as monosaccharide concentration in the medium, nitrogen source, oxygen availability, and culture conditions. Many solutions have been proposed to increase xylitol release [2], but they have not led to the development of cost-effective technology as an alternative to chemical methods.

The present work aimed to investigate the efficiency of integrated biotechnological production of ethanol and xylitol by hydrolysis and then fermentation of corn straw using *Candida tropicalis* depending on the process parameters such as nitrogen source and temperature. Unlike the studies reported, the raw material before hydrolysis was pretreated using 2% NaOH. The advantage of this method is the high degree of delignification and the recovery of cellulose and hemicelluloses. Most often in the processes of producing xylitol from lignocellulosic biomass, the first step is the acid hydrolysis of hemicellulose to xylose, accompanied by the formation of inhibitors of enzymatic hydrolysis and fermentation. Therefore, additional steps of purification of the obtained acid hydrolysates are necessary, which increases the cost of the technology and prevents its application on an industrial scale [4]. The proposed pretreatment method has no such disadvantages and makes biomass highly susceptible to enzymatic hydrolysis. Hydrolysis was conducted using Cellic CTec2 enzymatic mixture as the catalyst according to the method previously reported [5]. Obtained hydrolysates, containing glucose (32.4 g/dm^3) and xylose (12.25 g/dm^3), were subjected to fermentation using yeast extract, aminobak or ammonium sulfate as nitrogen source at 3 different temperatures (30, 35 and 40°C) at 150 rpm. Each experiment was performed in triplicate.

The results showed that the studied process conditions influenced both glucose and xylose consumption rates and amounts of ethanol and xylitol produced by yeast. The lowest fermentation efficiency was observed using ammonium sulfate. Yeast extract and aminobak led to a similar maximum ethanol concentration in the fermentation broths (ca. 12 g/L). However, the amount of produced xylitol was the highest using aminobak. The time courses of ethanol and xylitol are presented in Fig.1. It can be observed that the production of ethanol was much faster than xylose

regardless of studied process parameters. The rate of ethanol release was similar in each case although the concentration of this product decreased after ca. 10 h of fermentation. Additionally, the higher the temperature, the faster the decline. It was probably due to the utilization of ethanol by the yeast as a carbon and energy source when they thoroughly consumed glucose. Regarding xylose, its concentration in the broth was also impacted by temperature. Nevertheless, the highest productivity was obtained at 40°C for broth that showed nitrogen sources.

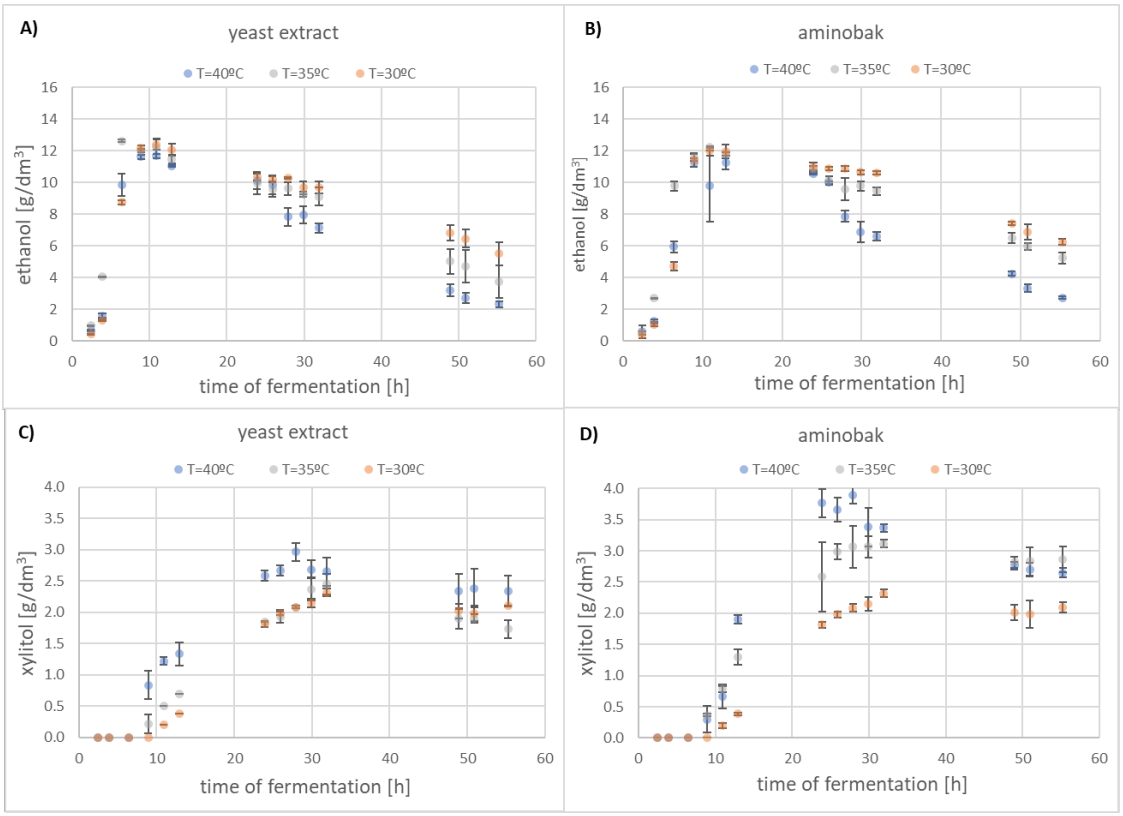

Fig. 1. Ethanol and xylitol concentrations vs fermentation time at different temperatures using yeast extract (A and C) and aminobak (B and D) as a nitrogen source

Although the efficiency of xylitol release was the highest at 40°C, at this temperature, the rate of ethanol consumption increased. Therefore, it seems to be desirable to remove ethanol from the broth after 10 h of fermentation.

The research was funded by (POB Beyond) of Warsaw University of Technology within the Excellence Initiative: Research University (IDUB) programme.

References

[1] Dionísio S.R., Santoro D.C.J., Bonan C.I.D.G., Soares L.B., Biazi L.E., Rabelo S.C., Ienczak J.L., Second-generation ethanol process for integral use of hemicellulosic and cellulosic hydrolysates from diluted sulfuric acid pretreatment of sugarcane bagasse, *Fuel*, 2021, 304, 121290.
[2] Felipe Hernández-Pérez A., Vaz de Arruda P., Sene L., Silvério da Silva S., Kumar Chandel A., Felipe M.G.A., Xylitol bioproduction: state-of-the-art, industrial paradigm shift, and opportunities for integrated biorefineries, *Crit. Rev. Biotechnol.*, 2019, 39(7), 924-943.
[3] Venkateswar Rao L., Khanna Goli J., Gentela J., Koti S., Bioconversion of lignocellulosic biomass to xylitol: An overview, *Bioresour. Technol.*, 2016, 213, 299-310.
[4] Kumar V., Krishania M., Sandhu P.P., Ahluwalia V., Gnansounou E., Sangwan R.S., Efficient detoxification of corn cob hydrolysate with ion-exchange resins for enhanced xylitol production by Candida tropicalis MTCC 6192, *Bioresour. Technol.*, 2018, 251, 416-419.
[5] Dąbkowska-Susfał, K., Efficiency of corn and poplar biomass saccharification after pretreatment with potassium hydroxide, *Ecol. Chem. Eng. S*, 2020, 27, 41-53.

GRAPHENE AS AN INNOVATIVE ADDITIVE TO GREASE WITH IMPROVED TRIBOLOGICAL PROPERTIES

Małgorzata Djas[1,2,*], Anna Matuszewska[3], Beata Borowa[3], Krystian Kowiorski[1], Piotr Wieczorek[3], Adrian Chlanda[1]

[1]Łukasiewicz Research Network – Institute of Microelectronics and Photonics, Lotników 32/46, 02-668 Warsaw, Poland
[2]Faculty of Chemical and Process Engineering, Warsaw University of Technology, Waryńskiego 1, 00-645 Warsaw, Poland
[3]Łukasiewicz Research Network – Automotive Industry Institute, Jagiellońska 55, 03-301 Warsaw, Poland
*corresponding author: malgorzata.djas@imif.lukasiewicz.gov.pl

Lubricants such as oils and greases play a key role in many industries, including in particular the automotive, transportation, chemical and food industries. The factor driving the growth of the market for these products in the world is the dynamic technological development. Lubricant manufacturers must keep up with increasingly advanced vehicles as well as innovative equipment where precision and efficient operation are crucial for their effective and profitable operation. During mechanical processes, as a result of strong friction between the surfaces, the elements of the friction node wear out and heat is generated, which reduces the work efficiency and shortens the useful life of the device. It is estimated that as much as about 23% (119 EJ) of the world's energy consumption is caused by anti-friction and regeneration of friction elements [1]. The reduction of friction contributes not only to the reduction of energy consumption, but also to fuel savings and the related financial and environmental benefits, in particular the reduction of CO_2 emissions. Enriching additives are added to oils and greases to improve their anti-wear (AW) and anti-seize (extreme pressure EP) properties. Conventional additives are mainly based on sulfur, chlorine or phosphorus compounds, which are not environmentally friendly [2, 3]. Therefore, it is necessary to undertake new research initiatives promoting activities for the development and implementation of technologies of innovative additives with improved tribological properties and reduced negative impact on the natural environment, compared to conventional agents. Nanotechnology is currently a new and intensively developed area of research in the production of lubricant additives. One of such nanoadditives may be flake graphene and its derivatives (graphene oxide, reduced graphene oxide). Graphene is a 2D material with a thickness of one carbon atom. Its application is currently the subject of many scientific studies in various areas (e.g. composites, coatings, electronics, energy storage, or medicine). One of the intensively developed and promising areas of flake graphene applications is tribology. It was found that the introduction of flake graphene as an additive to the lubricant improves its lubricating properties, reducing the coefficient of friction and surface wear. This is due to the unique properties of this material, such as the layered structure, small flake size, large specific surface area, high mechanical strength, high thermal conductivity and good lubrication.

This work proposes an innovative approach to the implementation of reduced graphene oxide (RGO) as a nanoadditive with anti-wear properties to grease. In order to obtain the best knowledge about the influence of graphene based additive on the anti-wear properties of the grease, the tests were carried out for a wide range of concentrations of RGO in the grease, amounting to 0.25-5.00 wt.%. The tests of the lubricating properties of the obtained greases with the addition of flake graphene were determined by measuring the average diameter of the wear scar. The tests were performed with the use of a four ball tester (Stanhope-SETA) at a load of 60 kgf for 60 minutes.

Figure 1 shows the results of the research on the effect of the concentration of the RGO (0.25-5.00 wt.%) on the lubricating properties of grease. It has been found that the addition of graphene flakes improves the anti-wear properties of the lubricant. The obtained data show that the

introduction of RGO to the lubricant in a small concentration of 0.25 wt.%, increases the wear of the test pieces by 24% (4.03 ± 0.27 mm) compared to the grease without additive (3.26 ± 0.28 mm).

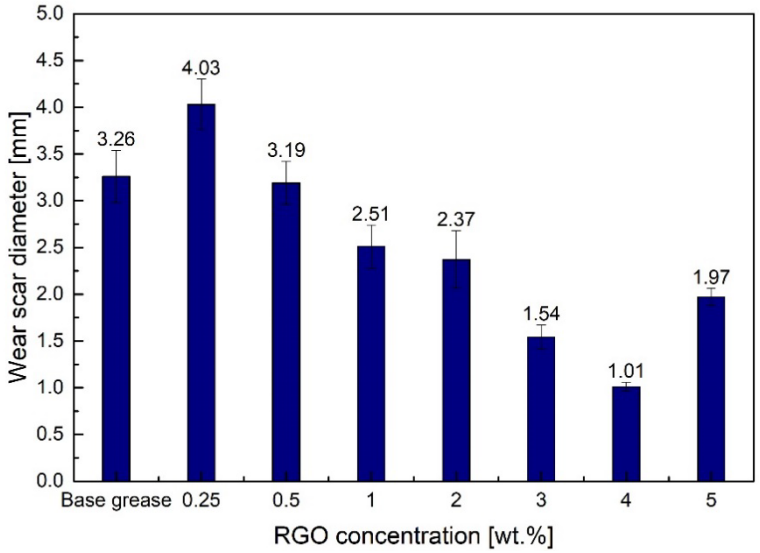

Fig. 1. Influence of RGO additive concentration on the tribological properties of a grease

However, the introduction of an RGO additive in the concentration 1.00 - 4.00 wt.% resulted in a significant improvement in lubricating properties and reduction of wear. The lowest wear was observed at 4.00 wt.% RGO concentration. Increase in RGO concentration in the lubricant from 1.00 to 4.00 wt.% reduced the average diameter of the wear scar from 2.51 ± 0.23 mm (23%) to 1.01 ± 0.05 mm (69%), respectively. Further increase of the additive content to 5.00 wt.% may increase the wear of the balls. It can be concluded that the RGO concentration 4.00 wt.% in the grease is the limit concentration, exceeding which the anti-wear properties of the grease may deteriorate. In the case of high concentrations of graphene, agglomerates form in the lubricant, which negatively affect the friction surface protection. In addition, surface activity of RGO may cause a violation of the internal structure of the lubricant and may cause reduced wear protection at low additive contents, which results in a larger wear scar diameter for concentrations in the range of 0.25-0.50 wt.% compared to pure base grease. The concentration of graphene in the lubricant is probably too low to compensate for the breakdown of the lubricant's internal network. Only higher concentrations of graphene flakes are able to cover enough of the friction surface to protect the node elements.

It has been found that the RGO tested in operation can be successfully used as a material improving the tribological properties of lubricants. The use of flake graphene in lubricants is not a thoroughly researched and explained issue. In order to further develop the application of graphene flakes as a lubricant additive, it is necessary to continue research, including in the direction of chemical modification of the flake surface, as well as explaining the mechanisms of graphene operation during friction.

This research was funded by Łukasiewicz Research Network – Institute of Microelectronics and Photonics and Łukasiewicz Research Network – Automotive Industry Institute (Statutory Research). This research was funded by National Science Centre, Poland – grant "Identification of mechanisms and investigations of flake graphene production by direct exfoliation using supercritical carbon dioxide", project number 2019/35/D/ST8/02977.

References

[1] Holmberg K., Erdemir A., Influence of tribology on global energy consumption, costs and emissions, *Friction*, 2017, 5, 263-284.
[2] Matuszewska A., Gradkowski M., Antiwear action of mineral lubricants modified by conventional and uncoventional additives, *Tribol. Lett.*, 2007, 27, 177-180.
[3] Waara P., Hannu J., Norrby T., Byheden Å., Additive influence on wear and friction performance of environmentally adapted lubricants, *Tribol. Int.*, 2001, 34, 547-556.

ANALYSIS OF RADON-222 PENETRATION INTO ROOMS IN BUILDINGS

Agnieszka Dołhańczuk-Śródka*, Daniel Janecki, Zbigniew Ziembik

University of Opole, Institute of Environmental Engineering and Biotechnology,
Kominka 6a, 45-032 Opole
*corresponding author: agna@uni.opole.pl

Radon-222 is the most common radon isotope found in nature. Its short-lived decay products account for almost half of the dose of ionizing radiation received by the inhabitants of Poland from natural sources. In 2021, exposure from natural sources in Poland accounted for 64% of the total effective dose and amounted to approx. 2.68 mSv/year, with a statistical inhabitant of Poland receiving a dose from radon and its decay products of approx. 1.20 mSv/ year [1].

Rn-222 is a colorless and odorless noble gas that occurs naturally as a decay product of the long-lived Ra-226. It has a half-life of about 3.8 days. Radon does not directly affect our body. However, short-lived derivatives of radon decay combine with aerosols in the air and enter the respiratory system during breathing, where they can cause cancer [2].

Radon in atmospheric air comes mainly from the earth's crust. As a noble gas, it easily migrates, e.g. through the soil environment, getting into the atmosphere. The average concentration of radon in the ground-level air layer in Poland depends on weather and the season and ranges from 5 to 20 Bqm^{-3} [3]. Found in the soil air of the foundation of a building, Rn-222 penetrates into the interior of the building relatively quickly, depending on its construction, and can reach high activities > 100 Bqm^{-3}. Radon enters with air sucked in from the ground through cracks in foundations, building walls, sewage manholes, leaks around sewage pipes, from building materials, etc. Due to the fact that Rn-222 relatively easily penetrates into the air at the ground surface, estimating the radon hazard associated with this phenomenon is an important part of assessing the safety of the human environment.

Forecasting the Rn-222 concentration using various mathematical models enables determination of the degree radiological risk level for future residents, and thus the use of appropriate security techniques, already at the building design stage.

The purpose of this work was to develop and verify a CFD model that can be used to analyse Rn-222 penetration from the ground and building materials into the interior of buildings. At this stage of research, this model does not yet take into account all the most important factors influencing this process.

To determine the concentrations of natural gamma radioactive isotopes (radium Ra-226, thorium Th-232 and potassium K-40) in building materials, enabling the calculation of the radioactive concentration index Rn-222, a Gamma spectrometer with a germanium detector, GC4018-F-RDC-6 -CP-5-Plus; MIRION Technologies (CANBERRA) was used. Determination of Rn-222 concentration in the soil air and in the air in the building was carried out using an AlphaGUARD DF2000 apparatus (Bertin Technologies SAS, France).

The phenomenon of radon transport and its exhalation are complex and depend on many factors. It is assumed that radon is transported from the depth of soil to the contact surface with the building. The process of radon entering the building is controlled by driving forces (concentration gradient for diffusion, pressure difference for convection and advection) and the type of material used as the foundation and insulation layer. The source of indoor radon is also the air supplied to the house through ventilation. All these factors have been taken into account in the proposed CFD model. The porosity model was used to calculate the soil air flow, and the component mass balance was used to calculate Rn-222 concentration.

Comparison of Rn-222 concentrations in the soil air and in the building room, calculated and obtained experimentally, indicates that the CFD model developed in this work can be used to model the penetration of Rn-222 into the interior of closed rooms. A good agreement between observed and calculated values was obtained. Despite the fact that modelling of this type of processes is

difficult due to many factors affecting each other, the differences between the obtained results did not exceed 30%. At the present stage, work is underway to improve the model so that it predicts results with greater accuracy.

References

[1] Annual Report, Activity of the President of the National Atomic Energy Agency and assessment of nuclear safety and radiological protection in Poland in 2021, PAA, Warszawa 2022 (in Polish).

[2] Denton G.N.W, Namazi S., Indoor Radon Levels and Lung Cancer Incidence on Guam., *Procedia Environ. Sci.,* 2013, 18, 157-166.

[3] Podstawczyńska A., Kozak K., Pawlak W., Mazur J., Seasonal and diurnal variation of outdoor radon (^{222}Rn) concentrations in urban and rural area with reference to meteorological conditions. *Nukleonika*, 2010, 55(4), 543–547.

[4] Zeilinger A., A foundational principle for quantum mechanics, *Found. Phys.*, 1999, 29(4), 631-643.

DYNAMICS OF AEROSOL GENERATION AND FLOW DURING INHALATION FOR IMPROVED IN VITRO-IN VIVO CORRELATION (IVIVC) OF PULMONARY MEDICINES

Agata Dorosz*, Arkadiusz Moskal, Tomasz R. Sosnowski

Faculty of Chemical and Process Engineering, Warsaw University of Technology,
Waryńskiego 1, 00-645 Warsaw, Poland
*corresponding author: agata.dorosz@pw.edu.pl

Aerosols are used as convenient carriers for targeted drug delivery to the lower respiratory tract [1]. The process of aerosol generation can proceed in different ways depending on the properties of the precursor. Powders are dispersed by aerodynamic forces, typically generated by the flow of inhaled air in so-called passive dry powder inhalers (DPIs) [2], whereas liquid solutions or suspensions are dispersed by atomization done with various methods, with pneumatic or ultrasonic nebulization (including vibrating mesh nebulization) being the most common. In any aerosol generation system, the mass output and size distribution of dispersed particles or droplets are influenced by the aerodynamic conditions of airflow through the inhaler [3]. By affecting the aerosol size distribution, these conditions determine the penetration and deposition of the drug inside the respiratory system, and thus - the effectiveness of inhalation therapies. Regardless of the type of inhaler, the actual behavior of the aerosol particles in the surrounding airflow field in the respiratory tree depends on the way of the inhalation maneuver.

This communication presents several variants of experimental research demonstrating the influence of airflow dynamics on the generation and transport of aerosol particles inside and outside various inhalers. This direction of research helps to improve *in vitro – in vivo correlation* (IVIVC) and bioequivalence when linking the information gained from inhaler testing to clinically assessed lung deposition [4, 5].

The experiments were done using a programmable simulator of inhalation flows (ASL 5000XL, Ingmar Medical, USA) and aerosol diffraction spectrometer (Spraytec, Malvern, UK). For powder inhalers (capsule RS01, Plastiape, Italy, and Turbospin, Ph&T, Italy) additional studies with the Next Generation Impactor NGI equipped with the mixing inlet (Copley Scientific, UK) were done.

For DPIs inhalation pattern through an inhaler is directly linked to time-dependent size distribution of aerosol particles, Fig. 1. It is seen that aerosol is released from the inhaler only during the initial phase of inhalation, when the airflow rate (and hence the energy that can be used to aerosolize the powder) is smaller than the maximum flow value during inhalation, i.e., PIFR (peak expiratory flow rate). Most powder is dispersed efficiently during the first second of the inspiratory flow, and the aerosol generated after that time contains mostly larger particles. The results show that the standard (compendial) method of the assessment of aerodynamic particle size under PIFR through an inhaler is not realistic and probably overestimates the amount of small aerosol particles released during the actual use of a DPI.

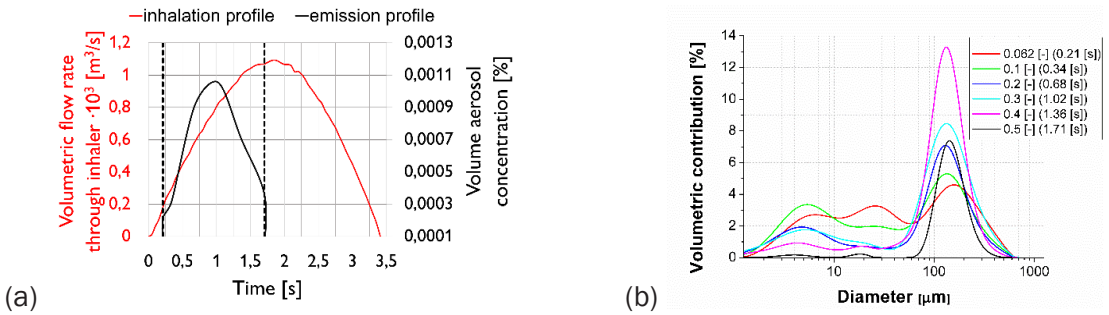

Fig. 1. (a) Dynamics of aerosol generation in RS01 DPI; (b) the evolution of particle size distribution in the aerosol emitted from the DPI

Aerosol generation in nebulizers takes place under completely different conditions. These are "active" devices, since the energy needed to atomize the liquid drug is supplied from external sources, i.e., compressed air or ultrasonic vibrations. The aerosol is generated continuously and is drawn without the need for special inhalation maneuvers. The dynamics of inhalation, however, varies from patient to patient and affects the speed at which the droplet flows through the external components of the nebulizer (mouthpiece, mask, tubings, etc.) [6, 7]. Instantaneous flow rate affects the size-dependent droplet separation in these parts of the nebulizing system. Droplets larger than 5 μm are removed from the aerosol by inertial forces, which dominate when the flow is fast (close to PIFR). On the other hand, periods characterized by low velocity allow these droplets to be carried into the respiratory tract, where they cannot reach the target region of lower airways due to complex geometric structure and obturations of the diseased lungs [8]. As the aerosol flows through the mouthpiece of the nebulizer, not only are large droplets separated, but also droplets can evaporate in contact with additional air drawn in from the environment. Both effects lead to a reduction in the size of the aerosol droplet leaving the nebulizer mouthpiece, which is usually completely ignored in the analysis of medical nebulizations. Based on both CFD calculations and experimental analysis, we have demonstrated a reduction in average droplet size caused by the above processes for a vibrating mesh nebulizer (Intec Twister Mesh, Kraków, Poland), Fig. 2.

The research presented here demonstrates the usefulness of the scientific tools offered by chemical and process engineering for solving problems related to improving drug delivery and the evaluation methods for nebulizers and other inhalers. The results of such studies also should improve the IVICV allowing to establish the more reliable relationships between inhaler testing data and the actual pulmonary deposition of inhaled medicines.

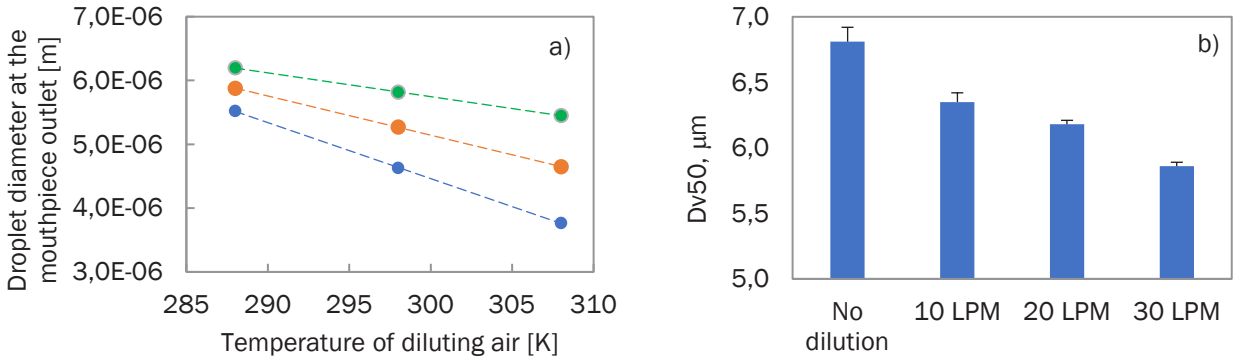

Fig. 2. (a) Calculated diameter of water droplet (initial diameter = 7 μm) at the outlet of nebulizer mouthpiece upon dilution with additional inhaled air; (b) experimental change in droplet median diameter Dv50 upon dilution of polydisperse aerosol with additional inhaled air (RH=15%) for various flow rate (in liters per minute: LPM)

Acknowledgement: Work supported by NCN project No. 2018/29/B/ST8/00273.

References

[1] Sosnowski T.R., *Chem. Eng. Sci.,* 2023, 268, 118407.
[2] Dorosz A., Żaczek M., Moskal A., *J. Aerosol Sci.,* 2021, 151, 105673.
[3] Dorosz A., Urbankowski T., Zieliński K., Michnikowski M., Krenke R., Moskal, A., *J. Aerosol Med. Pulm. Drug Deliv.* 2022, 35, 91-103.
[4] Pirożyński M., Sosnowski T.R., *Exp. Opin. Drug Deliv.*, 2016, 13, 1559-1571.
[5] Newman S.P., Chan H.-K., *Adv. Drug Deliv. Rev.,* 2020, 167, 135-147.
[6] Sosnowski T.R., Janeczek K., Grzywna K., Emeryk A., *Chem. Proc. Eng.* 47, 253-261.
[7] Mazela J., Chmura K., Kulza M., Henderson C., Gregory T.J., Moskal A., Sosnowski T.R., Florek E., Kramer L., Keszler M., *J. Aerosol Med. Pulm. Drug Deliv.* 2014, 27, 58-65.
[8] Kadota K., Matsumoto K., Uchiyama H., Tobita S., Maeda M., Maki M., Kinehara Y., Tachibana I., Sosnowski T.R., Tozuka Y., *Eur. J. Pharm. Biopharm.* 2022, 174, 10-19.

ADSORPTION BEHAVIOR OF POLAR SOLVENT AND WATER VAPORS ON SORBONORIT B4 ACTIVATED CARBON

Dorota Downarowicz*, Elżbieta Gabruś

West Pomeranian University of Technology in Szczecin, Faculty of Chemical Technology and Engineering, Piastów 42, Szczecin, Poland

*corresponding author: ddownar@zut.edu.pl

One of the environmental problems is the release of volatile organic compounds (VOCs), which are substances that have a high vapor pressure. VOCs are commonly used in both industrial applications and household chemicals as solvents and ingredients in products such as antiseptics. Activated carbon (AC) fixed-bed adsorption can be used to capture VOC vapors from waste gases [1]. However, the process may be problematic in the presence of water vapor, which also adsorbs on the adsorbent, reducing its VOC capture capacity [2, 3]. The strength of the adsorbate/adsorbent interaction depends on the properties of the adsorbate, the heterogeneity degree of the AC surface, temperature and the presence of competing adsorbates. Adsorption equilibrium data for individual adsorbate/adsorbent systems are necessary to characterize the adsorbability of air pollutants and to select the appropriate adsorbent for adsorption fixed bed processes.

The main objective of this study was to compare the adsorption behavior of water and polar VOCs, such as methyl ethyl ketone (MEK), isopropyl alcohol (IPA), n-propyl alcohol (NPA) and isobutyl alcohol (IBA) on Sorbonorit B4 (SB4) activated carbon. The adsorbent is heterogeneous [4, 5], which determines its adsorption affinity for polar adsorbate molecules that are capable of adsorbing either in the porous AC structure or on surface functional groups. The adsorption isotherm measurements were conducted using an IGA-002 intelligent gravimetric analyser (Hiden Isochema Ltd., U.K.). Figure 1 presents experimental adsorption isotherms at 293 K. The water vapor adsorption isotherm on SB4 is Type V in the IUPAC scheme, while the others are Type I. As can be seen, the adsorbent capacity for water at relative humidity RH > 40% is greater than that of VOC vapours. This effect is negligible when RH < 10%. In the range of higher RH, competitive adsorption between water and VOC molecules on activated carbon can be expected.

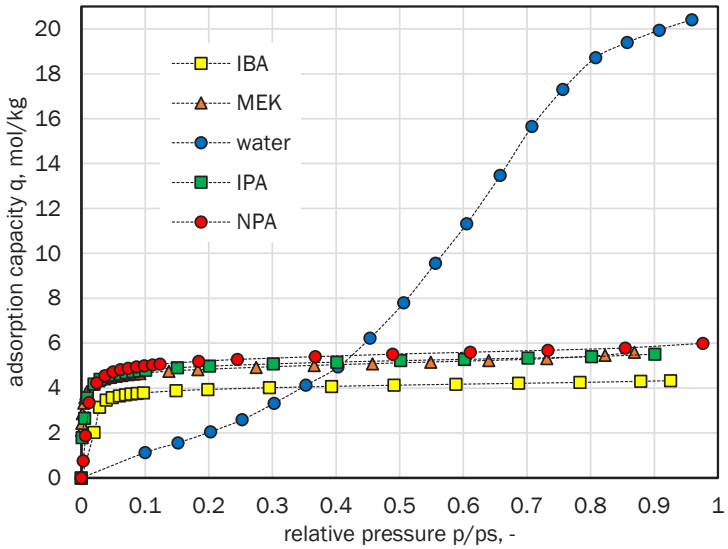

Fig. 1. Experimental isotherms for MEK, IPA, NPA, IBA and water vapor on Sorbonorit B4 at 20 °C

The adsorption equilibrium of VOCs and water vapor on activated carbon was analysed using Langmuir, Freundlich, Toth, Redlich-Peterson, Dubinin-Astakhov and Dubinin-Radushkevich

isotherms [6]. Table 1 presents values of the maximum adsorption capacity q_m and the characteristic energy E. As can be seen, SB4 shows the highest maximum adsorption capacity q_m for water vapor, while for VOC it is much lower and decreases as follows: NPA>IPA>MEK>IBA, which corresponds to the critical size of adsorbate molecules. The characteristic energy of the adsorbate-adsorbent interaction is the lowest for the system with water and increases for VOC in the order IBA<NPA<IPA<MEK, respectively. This may be caused by different adsorbate-adsorbent interactions. The isosteric heat of the adsorption (Q_{st}) was used to characterize the strength of these interactions. It was calculated based on the multi-temperature adsorption isotherms using Clausius-Clapeyron equation. The calculation revealed that the Q_{st} value depends on the amount of adsorbate which indicated that the process occurs on various types of adsorption sites with different binding energies. The Q_{st} values were lower than 80 kJ/mol, which is characteristic for physisorption [7].

Table 1. Selected parameters of VOCs and water vapor adsorption model isotherms on SB4 at 20 °C

parameter	MEK	NPA	IPA	IBA	water vapor
q_m, mol/kg	5.243	5.501	5.258	4.120	21.708
E, kJ/mol	20.198	12.359	15.696	10.565	1.745

IPA was selected as the adsorbate for the column studies. The tests were carried out in a glass adsorption column (internal diameter 0.055 m) with an SB4 fixed bed with the mass of 0.26 kg and height of 0.27 m. During the adsorption step, tests of breakthrough curves (BTCs) at ambient temperature were conducted. In the tests, a IPA-laden air stream with specific concentrations ranging from 5 to 15 g/m^3 was passed through the adsorption column until the SB4 bed was completely saturated. The experimental data analysis shows that the increase in the inlet concentration of adsorbate shortens the breakthrough and saturation times. The values of the equilibrium capacity of the adsorbent were higher than those determined from the BTCs. This suggests that equilibrium was not reached in the fixed bed process.

In BTC tests, the temperature inside the bed was measured. The obtained time-temperature profiles showed that the adsorption process was exothermic and the heat released during the adsorption process increased the temperature inside the bed. The maximum temperature increase was estimated based on the isosteric heat of adsorption, specific heat capacity of the adsorbent and the gas mixture and operating parameters [3]. The calculated values of the maximum temperature rise in the fixed bed were consistent with the relevant experimental data. At high concentrations of adsorbate in the air, the increase in bed temperature may be so large that the process cannot be treated as isothermal, which should be taken into account when designing a fixed-bed adsorber.

References

[1] Li X., Zhang L., Yang Z., Wang P., Yan Y., Ran J., Adsorption materials for volatile organic compounds (VOCs) and the key factors for VOCs adsorption process: a review, *Sep. Purif. Technol*., 2020, 235, 116213.
[2] Delage F., Pré P., Le Cloirec P., Effects of moisture on warming of activated carbon bed during VOC adsorption, *J. Environ. Eng*., 1999, 125, 1160–1167.
[3] Gabruś E., Downarowicz D., Anhydrous ethanol recovery from wet air in TSA systems – Equilibrium and column studies, *Chem. Eng. J*., 2016, 288, 321–331.
[4] Hung H.W., Lin T.F., Prediction of the adsorption capacity for volatile organic compounds onto activated carbons by the Dubinin–Radushkevich–Langmuir model, *J. Air Waste Manage. Assoc*., 2007, 57, 497–506.
[5] Downarowicz D., Aleksandrzak T., Adsorption of propanol isomer vapors on Sorbonorit B4 activated Carbon: equilibrium and spectroscopic studies, *J. Chem. Eng. Data*, 2016, 61, 3650–3658.
[6] Do D.D., *Adsorption analysis: equilibria and kinetics*, Imperial College Press, London, 1998.
[7] Patel H., Fixed bed column adsorption study: a comprehensive review, *Appl. Water Sci*., 2019, 9, 1-17.

SIMPLIFIED MODEL FOR THE FABRICATION OF SILVER NANOWIRES IN A CONTINUOUS FLOW PROCESS AND ITS EXPERIMENTAL VERIFICATION

Grzegorz Dzido[1,*], Muhammad Omer Farooq[2], Aleksandra Smolska[2]

[1] Silesian University of Technology, Department of Chemical Engineering and Process Design, Strzody 7, Gliwice, Poland
[2]Silesian University of Technology, Doctoral School, Akademicka 2A, Gliwice, Poland
[*]corresponding author: Grzegorz.Dzido@polsl.pl

The growing demand for nanomaterials is prompting the search for new production methods. While processes based on batch operations are relatively well understood, a lack of sufficient data is observed for continuous processes. The relatively small number of papers on the fabrication of silver nanowires (AgNWs) in a continuous flow process [1-4] provided the rationale for this research. This paper presents a simplified mathematical model to determine the changes in basic process parameters along the flow path through a convection-heated tubular reactor and its experimental verification due to the final conversion rate of the nanomaterial precursor. The so-called polyol synthesis, in which ethylene glycol (EG) was the reductant of the nanomaterial precursor and the solvent, was used to produce AgNWs. Obtaining a product with a high aspect ratio was possible in this process by using polyvinylpyrrolidone (PVP) and $CuCl_2$ as a stabiliser and mediating agents, respectively. A system of equations including heat balance (1-4) and reaction kinetics (5) was used to model the AgNWs production process in a tubular reactor:

$$Q = Gc_p\left(t_i - t_{in}\right), \tag{1}$$

$$Q = \alpha_{ge}\pi d l_i\left(t_w - t_i\right), \tag{2}$$

$$Q = \alpha_p \pi d_z l_i\left(t_p - t_{wz}\right), \tag{3}$$

$$Q = \left(\frac{1}{\alpha_p d_z} + \frac{1}{2\lambda_t}\ln\left(\frac{d_z}{d}\right) + \frac{1}{\alpha_{ge} d}\right)^{-1} \pi l_i\left(t_p - t_i\right), \tag{4}$$

$$C_A = C_{A0}\exp\left(-l_i\frac{k}{u}\right) = \exp\left(-l_i\frac{k_0}{u}\exp\left(-\frac{E_A}{R\left(t_i + 273\right)}\right)\right), \tag{5}$$

where: G mass flow rate, c_p heat capacity, t_{in}, t_i, t_w, t_{wz}, t_p inlet, local, internal wall, external wall and surrounding temperature, respectively, α_p, α_{ge} heat transfer coefficient to the outer wall of the reactor (α_p=25 W/m^{2}K) and inside reactor, respectively, l_i location relative to the inlet, d, d_z I.D.=0.003 m and O.D.=0.009 m, respectively, λ_t heat conductivity coefficient of reactor material, assumed to be equal λ_t=1 W/mK, C_{A0} initial concentration of AgNWs precursor ($AgNO_3$), u linear velocity, the k reaction rate constant, k_0=4600 1/s, pre-exponential factor in Arrhenius equation, E_A=54 kJ/mol the activation energy of nanoparticle formation [5], R universal gas constant.

The heat transfer coefficient, α_{ge} of the reaction side, was calculated as for a coil. Equation (5) describes the change in concentration of the silver nanowire precursor during flow through the tubular reactor, assuming a pseudo-first-order reaction model (r_A=kC_A), which is justified by the significant excess of EG over the nanomaterial precursor used. For the same reason, the heat effect of the reaction was neglected in the heat considerations, and the physical parameters of the reaction mixture were assumed as for pure EG. The effect of temperature on the reaction rate was considered using the Arrhenius equation. For given values of l_i, a system of equations (1)-(5) was

solved against the unknowns Q, t_i, t_w, t_{wz} and C_A using the MathCAD™15. Calculations were carried out for the residence times of 10, 20 and 30 min., t_{in}=27-38°C and t_p=172-183°C corresponding to the experimental conditions. Values of physical parameters were calculated at mean temperature using equations implemented in ChemCAD™. Figures 1a, 1b and 1c show examples of the calculation results, which portray the course of temperature and conversion changes during flow through the reactor.

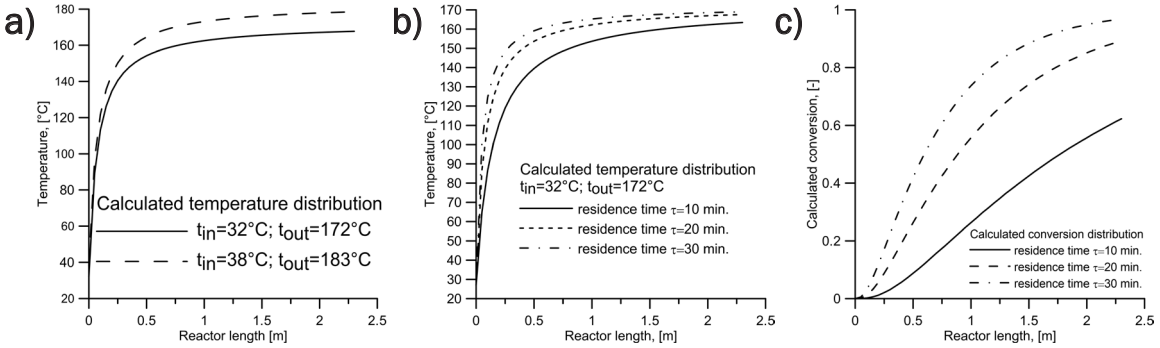

Fig. 1. Example results of calculations carried out using model (1) - (5)

Experimental verification of the model was carried out using the system shown in Fig. 2a. The reaction mixture was supplied by a syringe pump (1) to a tubular reactor (3) located inside a laboratory dryer (2) and made of a 2.310 m long silicon tube wound around a 0.054 m diameter glass tube. The reaction mixture was collected in a vessel (4), cooled, and then purified and separated by centrifugation and washing with DI water. The syntheses were carried out for C_{A0}=16.8 mM, reaction mixture composition [Ag^+]:[Cl^-]=76.5, [PVP]:[Ag^+]=3, the residence times and temperatures given above. Silver nanowire precursor's conversion was determined by measuring the concentration of Ag^+ ions with an ion-selective electrode in the post-reaction mixture. The experiments resulted in a product with average diameters of 98-160 nm and lengths of 25-45 μm. A comparison of the calculated and experimentally determined conversions shows that despite the simplified nature of the model, in most cases, the relative error does not exceed 15% (Fig. 2b).

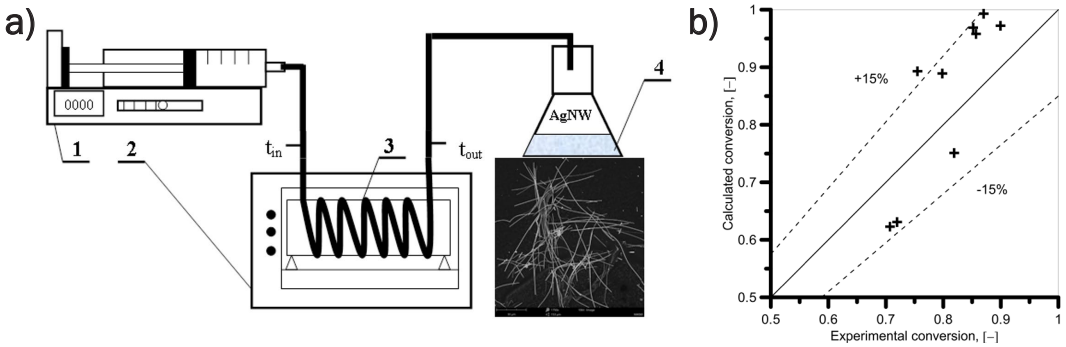

Fig. 2. Scheme of the laboratory setup (a), comparison of calculated and experimental conversion values (b)

Publication supported under the Rector's pro-quality grant. Silesian University of Technology, 04/030/RGJ22/0062.

References

[1] Yu J., Yang L., Jiang J., Dong X., Cui Z., Wang Ch., Lu Z., Scalable production of high-quality silver nanowires via continuous-flow droplet synthesis, *Nanomat.*, 2022, 12, 1018.
[2] Gottesman R., Tangy A., Oussadon I., Zitoun D., Silver nanowires and nanoparticles from a millifluidic reactor: application to metal assisted silicon etching, *New J. Chem.*, 2012, 36, 2456–2459.
[3] Espinosa N., Søndergaard R.R., Jørgensen M., Krebs F.C., Flow synthesis of silver nanowires for semitransparent solar cell electrodes: A life cycle perspective, *ChemSusChem*, 2016, 9, 893–899.
[4] Chou K.S., Hsua Ch.Y., Liu B.T., Salt-mediated polyol synthesis of silver nanowires in a continuous-flow tubular reactor, *RSC Adv.*, 2015, 5, 29872.
[5] Zhai X., Efrima S., Reduction of silver ions to a colloid by Eriochrome Black T, *J. Phys. Chem*. 1996, 100, 1779-1785.

METAL FOAMS AS CATALYST SUPPORT IN THE METHANE AFTERBURNING PROCES

Anna Gancarczyk[1,*], Joanna Profic-Paczkowska[2], Maciej Sitarz[3]

[1]Polish Academy of Sciences, Institute of Chemical Engineering, 44-100 Gliwice, Poland
[2]Jagiellonian University, Faculty of Chemistry, 30-387 Krakow, Poland,
[3]AGH University of Science and Technology, Faculty of Material Science and Ceramics, 30-059 Krakow, Poland
*corresponding author: anna.g@iich.gliwice.pl

Solid foams with open cell structure represent structured catalyst support. They offer great possibilities of combining high porosity ensuring low flow resistance with the satisfactory size of the specific surface area available for depositing a layer of catalyst. Moreover, they provide sufficiently high mass transfer coefficients. All these properties make solid foams attractive especially for fast catalytic processes, like for example catalytic combustion of methane [1].

The research focused on three Fecralloy foams (Goodfellow Cambridge Ltd., England) with a pore density of 4, 8 and 16 PPC (pore per centimeter). An image of an exemplary foam is shown in Fig. 1.

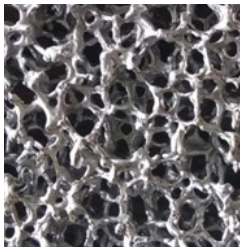

Fig. 1. Fecralloy 4 PPC foam

The transport properties of the foams have been tested and compared with packed bed and the monolith (Fig. 2). In the measuring range, the tested foams are characterized by a more intense heat transport than the monolith. As the fluid velocity increases, the values obtained for foams approach the characteristics of the packed bed.

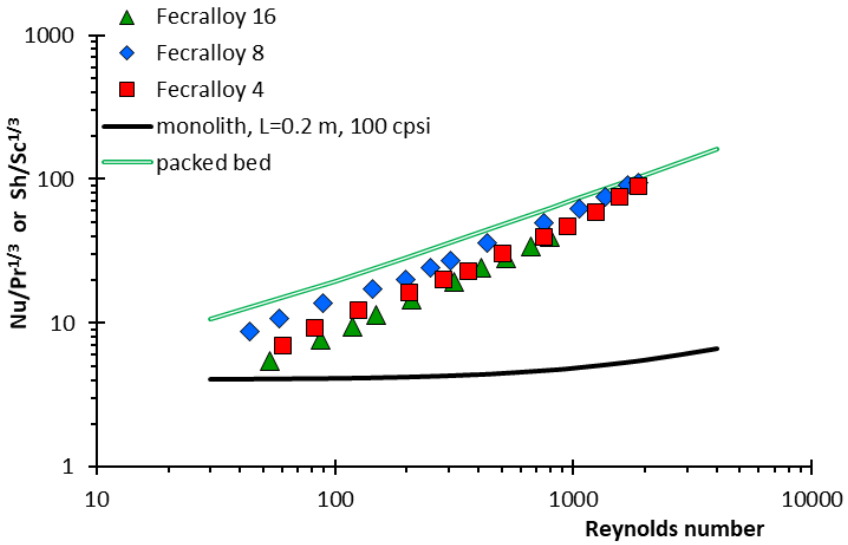

Fig. 2. Transport properties of Fecralloy foams in comparison to packed bed and monolith

The reactor packed with Fecralloy 16 PPC foam was tested in the process of catalytic methane combustion using palladium (Pd/Al_2O_3) as the catalyst (Fig. 3). As can be seen, methane conversion increases with decreasing gas velocity, and for the same gas velocity, it is higher for lower methane concentration.

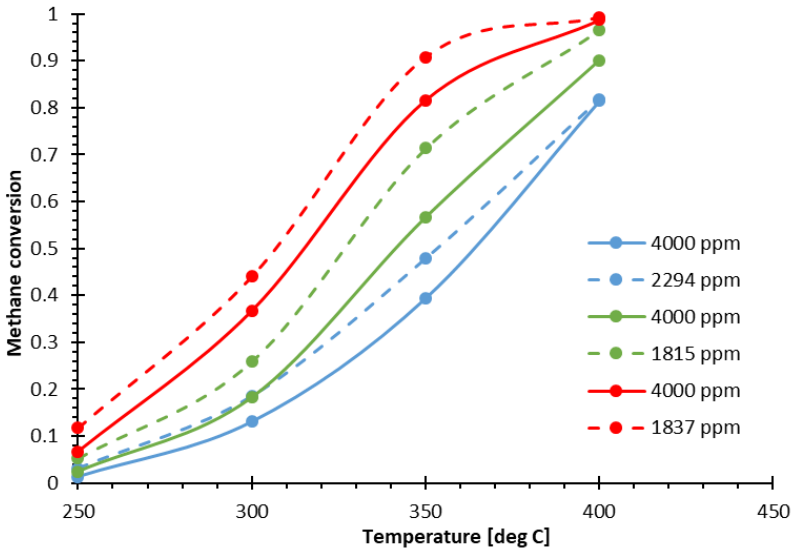

Fig. 3. Methane conversion vs. methane concentration and gas flow velocity (blue – 1000 ml/min, green – 500 ml/min, red – 200 ml/min)

Acknowledgements

This work was supported by the Polish National Science Centre (Projects No. Dec-2016/23/B/ST8/02024)

References

[1] Gancarczyk A., Sindera K., Iwaniszyn M., Piatek M., Macek W., Jodlowski P.J., Wronski S., Sitarz M., Lojewska J., Kolodziej A., Metal Foams as Novel Catalyst Support in Environmental Processes, *Catalysts*, 2019, 9(7).

[2] Rutkowska I., Marchewka J., Jelen P., Odziomek M., Korpys M., Paczkowska J., Sitarz M., Chemical and Structural Characterization of Amorphous and Crystalline Alumina Obtained by Alternative Sol-Gel Preparation Routes, *Materials,* 2021 14(7).

A SIMPLIFIED METHOD FOR DETERMINATION OF OPTIMAL FEED TEMPERATURE FOR HYDROGEN PEROXIDE DECOMPOSITION PROCESS OCCURRING IN IMMOBILIZED ENZYME FIXED-BED REACTOR

Ireneusz Grubecki*, Wirginia Tomczak

Bydgoszcz University of Science and Technology, 3 Seminaryjna, 85-326 Bydgoszcz, Poland
*corresponding author: ireneusz.grubecki@pbs.edu.pl

It is well known that fixed-bed reactors (FXBR) are important workhorses in biochemical industry because of their efficiency, low cost, and numerous construction, operation, maintenance advantages, and – from automation viewpoint – a better process control. This type of reactors is widely employed when the use of immobilized enzymes is required [1]. However, when working with immobilized enzymes convective and dispersive mass transport as well as convective and conductive energy transport in the bulk phase, mass and heat transport between the solid and fluid phase, heat transfer between the reaction mixture and the cooling (heating) agent, dispersive mass and conductive energy transport and biocatalytic conversion in the solid phase including enzyme deactivation should be taken into consideration. Thus, design and optimization of a fixed-bed reactor are not an easy task and often involve a trade-off between different conflicting objectives [2].

In order to find such a trade-off under phenomena mentioned above the use of partial differential equations models has gained an increasing importance over the past decades. Thus, there is a need to discover a simplified analysis to assess the optimal feed temperature (OFT) for the process occurring in the immobilized enzyme packed-bed bioreactor. In the present study hydrogen peroxide decomposition (HPD) occurring in the presence of immobilized *Terminox Ultra Catalase* (TUC) undergoing deactivation dependent on the substrate concentration was adopted as a model process. This optimal feed temperature has been estimated by maximizing the average substrate conversion over a given period at the fixed feed flow rate and accounting for the lower T_{min} = 293 K and the upper T_{max} =323 K temperature constraints as well as diffusional resistances expressed by the global effectiveness factor η_{eff} [3].

The general problem of searching for the OFT was already discussed previously [4]. However, it is known that in industrial applications the HPD process runs at the HP concentrations lower than 2×10^{-2} kmol·m^{-3}, so the temperature conditions may be assumed to be isothermal ones. Furthermore, to minimize the influence of the axial dispersion in the bulk phase the appropriate geometry of reactor ($D_R/d_P \geq 10$ and $L/d_P > 50$) should be considered. The length (L) and diameter (D_R) of a reactor selected in this way enable one to fulfill an assumption of plug flow. Such geometry selection makes the optimization problem solution presented in the previous work simpler.

As a result, the quantitative description in dimensionless form of the HPD course in fixed-bed bioreactor can be stated as follows:

$$\frac{\partial \bar{C}_S}{\partial \tau} + \frac{\partial \bar{C}_S}{\partial z} = -\eta_{\text{eff}} \beta_R \bar{C}_E \bar{C}_S \qquad \bar{C}_S(0,\tau) = 1 \tag{1a}$$

$$\frac{\partial \bar{C}_E}{\partial \tau} = -\eta_{\text{eff}} \beta_D \beta_R \bar{C}_E \bar{C}_S \qquad \bar{C}_E(z,0) = 1 \tag{1b}$$

where

$\bar{C}_i = C_i / C_{i0}$ $(i = E,S)$; $z = l/L$; $\tau = U_S t / \{L[\varepsilon_b + (1-\varepsilon_b)\varepsilon_p]\}$;

$\beta_D = k_D C_{S0} / (k_R a_m) \cdot [\varepsilon_b + (1-\varepsilon_b)\varepsilon_p] / [(1-\varepsilon_b)(1-\varepsilon_p)]$; $\beta_R = k_R a_m L(1-\varepsilon_b)(1-\varepsilon_p)/U_S$; $\varepsilon_b, \varepsilon_p$ denote the voidages of the bulk fluid phase and the particulate phase, respectively.

Optimization problem: The optimizing problem has been formulated as searching for the feed temperature that under a constant feed flow rate Q would provide a maximum (minimum) time-averaged HP conversion (concentration) at the reactor outlet.

Objective function:

$$\alpha_m = 1 - \bar{C}_{Sm} = 1 - \frac{1}{\tau_f}\int_0^{\tau_f} \bar{C}_S(z=1,x,T)\,\mathrm{d}x \tag{2}$$

An analytical solution of the system of equations (1) for distributions of TUC activity, $C_E(z,\tau)$, and HP concentration, $C_S(z,\tau)$ and substitution the last of them into Eq. (2), after integration, yields:

$$\bar{C}_{Sm}(T) = \frac{1}{\eta_{\mathrm{eff}}(T)\,\beta_D(T)\,\beta_R(T)\tau_f}\ln\left\{\frac{\exp[\eta_{\mathrm{eff}}(T)\cdot\beta_R(T)] + \exp[\eta_{\mathrm{eff}}(T)\cdot\beta_D(T)\beta_R(T)\cdot(\tau_f - 1)] - 1}{\exp[\eta_{\mathrm{eff}}(T)\cdot\beta_R(T)] + \exp[-\eta_{\mathrm{eff}}(T)\cdot\beta_D(T)\beta_R(T)] - 1}\right\} \tag{3}$$

Equation (3) describes the time-averaged HP concentration at the bioreactor outlet as a function of temperature, T.

In order to evaluate the feed temperature that minimizes (maximizes) the time-average HP concentration (HP conversion) the optimization procedure *fminbnd* with lower $T_{\min}$ and upper $T_{\max}$ temperatures constraints contained in MATLAB® Optimization Toolbox has been employed. A set of experimental data was determined by HP conversions obtained in a model reactor (inner diameter of $D_R = 8{\cdot}10^{-3}$ m) with a fixed-bed of commercial catalase immobilized on the surface of non-porous glass beads of diameters ranging from 4.8×10^{-4} m to 6.0×10^{-4} m (average diameter of $5.05{\cdot}10^{-4}$ m).

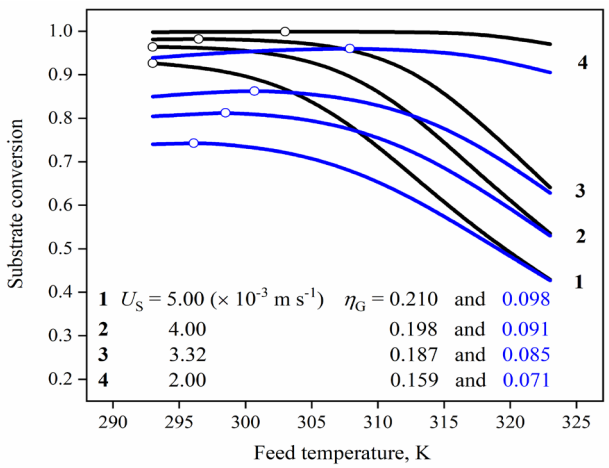

Fig. 1. Time-average HP conversion as a function of feed temperature T_{in} and superficial velocity U_S and particle diameter d_p (black lines for $d_p = 5\times10^{-4}$ m, and blue lines for $d_p = 10\times10^{-4}$m) for feed concentration equal to 5×10^{-3} kmol·m^{-3}. Open symbols represent the maximum values of time-average HP conversion.

The approach developed in this work makes it possible to evaluate the operational conditions (feed temperature and feed flow rate) at which productivity of the FXBR for hydrogen peroxide decomposed by immobilized commercial catalase achieves a maximum or the highest value.

References

[1] Rajaram M., Mariappan U.M., Visuvasam J., Meena A., Rajendran L., Lyons M.E.G., Modeling glucose isomerization in a packed- bed reactor: A complete theoretical and numerical approach, *Int. J. Electrochem. Sci.*, 2023, 18(3), 100023.

[2] Carrié M., Velly H., Ben-Chaabane F., Gabelle J.-C., Modeling fixed bed bioreactors for isopropanol and butanol production using Clostridium beijerinckii DSM 6423 immobilized on polyurethane foams, *Biochem. Eng. J.*, 2022, 180, 108355.

[3] Tai N.M., Greenfield P.F., Approximate solutions for catalyst deactivation within a particle, *Chem. Eng. J.*, 1978, 16(2), 89-100.

[4] Grubecki I., Optimal feed temperature for an immobilized enzyme fixed-bed reactor: A case study on hydrogen peroxide decomposition by commercial catalase, *Chem. Proc. Eng.*, 2018, 39(1), 39-57.

IMPACT OF UF PROCESS PARAMETERS ON THE PERFORMANCE OF POLYETHERSULFONE MEMBRANES

Marek Gryta*, Piotr Woźniak

[1]West Pomeranian University of Technology in Szczecin, Pułaskiego 10, 70-322 Szczecin, Poland
*corresponding author: marek.gryta@zut.edu.pl

The ultrafiltration (UF) membranes retain fine particles, colloidal materials, bacteria, viruses and some other pathogens. Such properties allow to produce clean water for re-use applications, e.g. water for car wash [1]. However, formation of deposits on the membrane surface (fouling phenomenon) causes a decline in the permeate flux resulting from increasing membrane resistance. The UF process parameters have a significant impact on fouling intensity [2].

In the present study, experimental investigations were performed with two polyethersulfone (PES) membranes (UE10 and UE50) manufactured by TriSep Corporation (Goleta, California, USA). These membranes are characterized by molecular weight cut-off (MWCO) equal to 10 kDa (UE10) and 100 kDa (UE50). The solutions of commercial cleaning agents applied for washing cars were used as the feed.

In the first stage of the study, a linear correlation between the water permeate flux and transmembrane pressure (TMP) was obtained (Fig. 1). Higher performance was observed for UE50 membranes since they have significantly larger pore size. Increasing the feed flow velocity (V_F) increased the flux, which indicates that the feed contained small amounts of suspension [3]. The increase of V_F leads to the increase in shear stress flow, which sweeps deposited foulants on the membrane away, reducing the fouling [2]. Although in spiral-wound modules the increase in flow velocity is limited, it can be implemented in tubular modules.

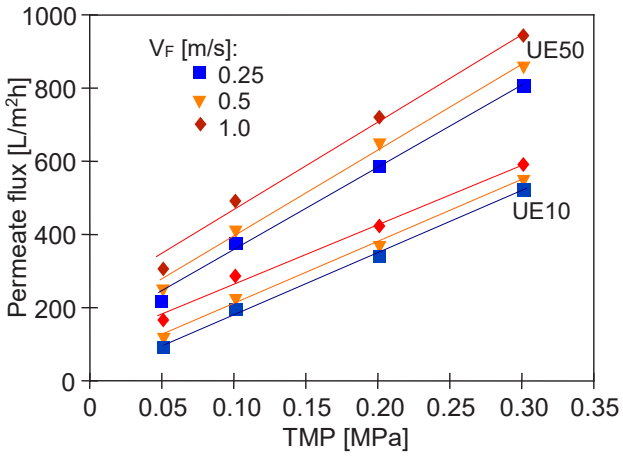

Fig. 1. The impact of TMP value and feed flow velocity on the obtained permeate flux

In the second step, the detergent solution with a turbidity of 2.1 NTU was filtered. It has been found that increasing the turbidity of the feed caused a rapid decrease in permeate flux (Fig. 2). After washing the membranes, better stability was obtained for the UE10 membranes. It can be explained by the fact that, as indicated above, the UE50 membranes have larger pores. It facilitates the penetration of impurities into the membrane and, as a result, it leads to the formation of hydraulically irreversible resistance, which makes the successful cleaning of membrane a great challenge [2].

It is well known that increasing the TMP value allows to increase UF performance. However, it can also increase the fouling intensity. This finding was confirmed by the UF studies of a solution containing a mixture of surfactant and wax (NTU=24). It was noted that during the initial stages of

filtration the permeate flux obtained for 0.3 MPa was decreased much larger compared to that observed for TMP=0.1 MPa (Fig. 3). Such a result indicates that the use of lower TMP values is more advantageous in industrial applications.

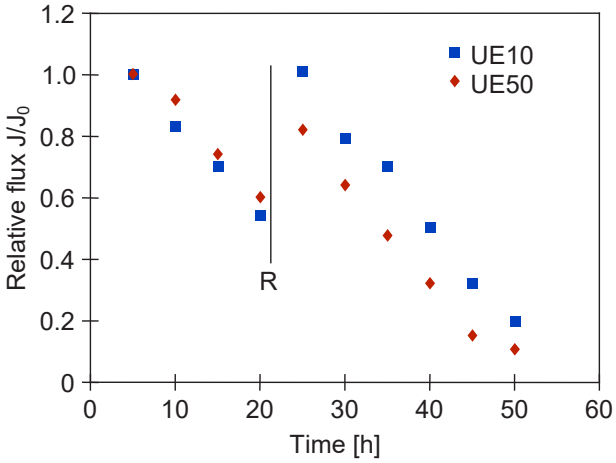

Fig. 2. Changes in the permeate flux during UF of surfactants solution (NTU =2.1). TMP=0.3 MPa, V_F=0.5 m/s. Point R - membranes rinsed with distilled water

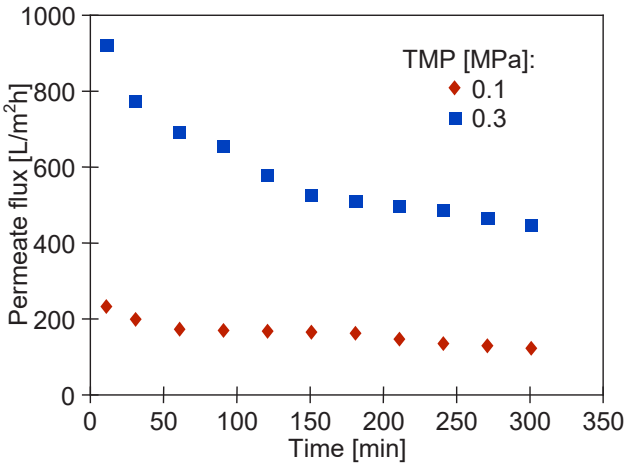

Fig. 3. Changes in the permeate flux during UF of surfactants +wax solution (NTU =24). Membrane UE50, V_F=0.5 m/s

Acknowledgements

The publication was financed from the Polish budget within a framework of the programme of the Minister of Education and Science in Poland entitled “Science for the Society”, project No. NdS/538617/2021/2022, amount of funding 352 135 PLN, total amount of funding 352 135 PLN.

References

[1] Moazzem S., Wills J., Fan L., Roddick F., Jegatheesan V., Performance of ceramic ultrafiltration and reverse osmosis membranes in treating car wash wastewater for reuse, *Environ. Sci. Pollut. Res.*, 2018, 25, 8654–8668.

[2] Chen B., Xiong X., Yao Z., Yinb N., Lowc Z.-X., Zhong Z., Integrated membrane process for wastewater treatment from production of instant tea powders, *Desalination,* 2015, 355, 147–154.

[3] Tomczak, W.; Gryta, M., Long-Term Performance of Ultrafiltration Membranes: Corrosion Fouling Aspect, *Materials*, 2023, 16, 1673.

ZIRCONIUM-BASED METAL-ORGANIC FRAMEWORKS FOR MEPHEDRONE DETOXIFICATION OR SUPERVISED WITHDRAWAL

Kornelia Hyjek[1], Grzegorz Kurowski[1], Klaudia Dymek[1], Anna Boguszewska-Czubara[2], Barbara Budzyńska[3], Olga Wronikowska-Denysiuk[3], Aleksandra Gajda[4], Witold Piskorz[5], Paweł Śliwa[1], Piotr Jeleń[6], Maciej Sitarz[6], Przemysław J. Jodłowski[1]*

[1]Cracow University of Technology, Faculty of Chemical Engineering and Technology, Warszawska 24, 31-155 Kraków, Poland
[2] Medical University of Lublin, Department of Medical Chemistry, Chodzki 4A, 20-093 Lublin, Poland
[3] Medical University of Lublin, Independent Laboratory of Behavioral Studies, Chodzki 4A, 20-093 Lublin, Poland
[4]Strata Mechanics Research Institute of the Polish Academy of Sciences, Reymonta 27, 30-059 Kraków, Poland
[5]Jagiellonian University, Faculty of Chemistry, Gronostajowa 2, 30-387 Kraków, Poland
[6]AGH University of Science and Technology, Faculty of Materials Science and Ceramics, Mickiewicza 30, 30-059 Kraków, Poland
*corresponding author: przemyslaw.jodlowski@pk.edu.pl

Metal-organic frameworks (MOFs) are classified as crystalline high-porous materials. They are characterized by high stability and very low toxicity Their specific structure, more precisely the combination of metal ions with organic ligadins, allows them to achieve large specific surface areas and high biocompatibility. Biocompatibility and high degrees of drug packing in MOF structures provide opportunities for their use in modern drug delivery systems (DDS) [1].

The phenomenon of drug addiction is one of the most widespread problems of contemporary times. Year by year there is an increase in both new psychoactive substances and the number of addicts. Among the many types of substances, it is the group of synthetic cathinones (SCs) that is the most common. This may be due to their action similar to the pharmaceutical properties of amphetamines. The main representative of this group is mephedrone (4-methylmethcathinone ,4-MMC) [2].

The focus has been on looking for substances that produce antagonistic effects to the action of SC. Typical symptoms of 4-MMC overdose are trachycardia or hypertension. The compounds currently used to counteract arrhythmia or palpitations are β-blockers. Thus, it has been shown that they can enter into combination with psychoactive compounds, causing a reduction in the side effects of their use. An example of a β-andrenergic receptor antagonist (β-blocker) is propranolol (PRO). This very popular and inexpensive drug can be used during a mephedrone overdose or to mitigate the side effects of its withdrawal. Such PRO administration would provide an innovative and completely safe system for detoxifying the body after taking the drug [3].

Safe and effective delivery of the drug is a key component of the therapy. The use of metal-organic frameworks as a carrier for PRO used during overdose of synthetic cathinones, including 4-MMC, and to minimize the side effects of its withdrawal, seems to be a modern and rational approach. The use of MOFs as a DDS promotes the gradual release of the drug, thereby reducing the side effects of drug intake. In addition, the metal-organic framework has a protective effect against drug-loaded molecules [4].

Our study involved synthesizing MOF materials, introducing the active ingredient propranolol, forming PRO@MOF composites, and then characterizing by PXRD, FTIR, RAMAN, BET, and SEM techniques to determine the crystallinity, specific surface area, morphology, and degree of drug loading. The release profiles of PRO from the composite materials into water and Simulated Body Fluid (SBF) human body solution were determined.

In addition, in vivo cytotoxicity tests were performed. The mechanism of PRO loading in the MOF network was calculated using theoretical methods - density functional theory (DFT) and molecular dynamics (MD).

The prepared PRO@MOF differed in the structure properties which clearly affected the kinetics of PRO release. The limiting effect of ions dissolved in a SBF was observed on the amount of PRO released. The inhibitory effect of SBF resulted in a gradual PRO release from PRO@MOF composites. The experimental results indicate that the prepared PRO@MOF composites may be considered as potential candidates in mephedrone detoxification or supervised withdrawal.

Acknowledgments

The work was supported by the National Science Centre, Poland, under research project "MOF-antidote: Novel detoxification materials based on metal-organic frameworks for drugs of abuse removal – syn- thesis, chemical characterization, toxicity and efficacy in in vivo and in vitro studies", no. UMO-2021/43/B/NZ7/00827.

References

[1] Kumar Gangu K., Maddila S., Babu Mukkamala S., Jonnalagadda S.B., A review on contemporary Metal–Organic Framework materials, *Inorganica Chim. Acta*, 2016, 446, 61–74.

[2] Rourke C.E.O., Subedi B., Occurrence and mass loading of synthetic opioids, synthetic cathinones, and synthetic cannabinoids in wastewater treatment plants in four U.S. Communities*, Enviromental Sci. Technol.*, 2020, 54, 6661–6670.

[3] Wagner M.J., Cranmer L.D., Loggers E.T., Pollack S.M.*,* Propranolol for the treatment of vascular sarcomas, 2018, 51–58.

[4] Bury W., Jodłowski P., Dymek K., Kurowski G., Jaśkowska J., Pander M., Wnorowska S., Targowska-Duda K., Piskorz W., Wnorowski A., Boguszewska-Czubara A., Zirconium-based Metal − Organic Frameworks as acriflavine cargos in the battle against coronaviruses. A theoretical and experimental approach, *ACS Appl. Mater. Interfaces*, 2022, 14, 28615−28627.

INFLUENCE OF DIFFUSION ON THE REACTION OF SULFURIC ACID WITH ILMENITES

Maciej Jabłoński, Krzysztof Lubkowski, Elwira K. Wróblewska*

West Pomeranian University of Technology, Faculty of Chemical Technology and Engineering, Department of Organic and Physical Chemistry, Piastów 42, 71-065 Szczecin, Poland
*corresponding author: elwira.wroblewska@zut.edu.pl

Among the inorganic pigments, the most important and widespread are titanium dioxide pigments, commonly known as titanium white [1, 2]. Due to the unique optical properties, titanium dioxide pigments are widely used in the production of coatings (paints, varnishes, lacquers), plastics, paper and in many other industrial branches [1-3].

Titanium dioxide pigments are produced with the use of two technologies: the sulphate method, where titanium dioxide is precipitated from a solution of titanyl sulphate, and the chloride method, where gaseous titanium chloride is oxidized to titanium dioxide with pure oxygen at high temperatures [1, 2]. The sulphate method has been used for the production of titanium white since 1919 [1] and this method is used to produce about 54% of the pigment worldwide.

In the production of titanium dioxide pigments with the sulphate method titanium-bearing minerals (ilmenite ores or titanium-iron slags) react with concentrated sulphuric acid [1–5]. In the technological process, the initiation of the reaction is carried out in two ways.

The first way is to mix concentrated sulfuric acid with ilmenite and then add water to the mixture. After adding water, the temperature of the reaction mixture rises as a result of the release of heat of dilution. Raising the temperature of the mixture initiates the reaction. During the reaction, thermal energy is released, which causes a further increase in temperature and acceleration of the reaction until the maximum temperature of the reaction mixture is reached. The concentration of sulfuric acid on the surface of the raw material grain is initially high, and after dilution it is reduced to the level at which the reaction is initiated. The time after which the concentration decreases is related to the process of diffusion of sulfuric acid in water and the mixing process.

The second method of initiating the reaction consists in heating the reaction mixture of sulfuric acid and ilmenite with steam. As a result of heating the mixture to the initiation temperature, water vapor condenses and thus changes the concentration of sulfuric acid. The diffusion and mixing processes also determine the concentration of sulfuric acid on the grain surface.

The rate and efficiency of the reaction are also affected by the transport of sulfuric acid to the reaction surface as well as the flow of reaction products into the solution. Since some of the reaction products go into the solution, while the rest forms a porous structure, diffusion processes may also play an important role in this case.

The aim of the research work was to explain the influence of diffusion processes on the reaction of sulfuric acid with titanium raw materials by means of laboratory experiments and using appropriate kinetic models.

Calorimetric measurements were performed in a calorimeter vessel (capacity of 0.6 dm^3), equipped with an electric heater, stirrer, temperature sensor, dispenser and safety valve. The calorimetric vessel parameters were as follows: time constant – 257.5 min, heat transfer coefficient – 0.098 $J \cdot K^{-1} \cdot s^{-1}$. The mass of ilmenite sample used in the study was about 100 g, while the mass of sulfuric acid was in the range from 200 g to 400 g, depending on the concentration of the acid.

As a result of the conducted experiments, dependencies of temperature changes and thermal power during the reaction time were obtained. In the interpretation of the experimental data, the mass and heat balance for the reaction taking place in the calorimeter were used, taking into account heat losses to the environment, the surface of the solid and the degree of conversion, which can be presented in the form of the following equations:

$$C\frac{dT}{dt} = \Delta H_r k_0 \exp\left(-\frac{E}{RT}\right) S_0 (1-\alpha)^{2/3} - G(T(t) - T_0) \quad (1)$$

$$\frac{d\alpha}{dt} = k_0 \exp\left(-\frac{E}{RT}\right) S_0 (1-\alpha)^{2/3} \quad (2)$$

The presented system of equations was solved using numerical methods for the initial conditions $T(0) = T_0$, $\alpha(0) = 0$, obtaining dependencies of changes in temperature, thermal power, degree of conversion, and interfacial surface during the reaction.

Comparison of experimental data with the proposed model for changes in temperature and thermal power during the reaction is shown in Fig. 1.

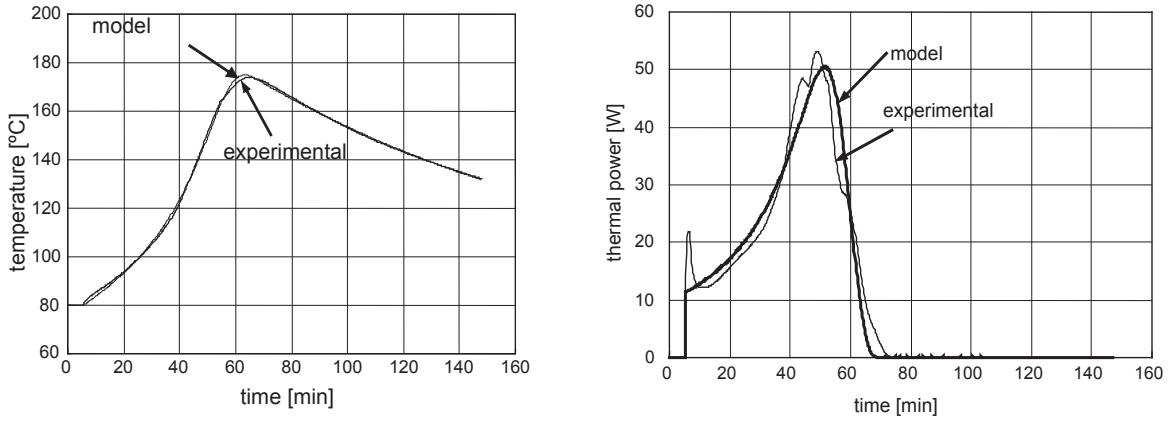

Fig. 1. Experimental and model data for temperature and thermal power changes during the reaction of sulfuric acid with ilmenites

It has been shown that in the case of the reaction of sulfuric acid with ilmenites, diffusion and mass transport processes are so fast that the reaction on the surface of the molecule has the main influence on the kinetics of the reaction. The adopted model of calculations taking into account this type of assumption shows a very good agreement with the experiment.

References

[1] Blakey, R.R., Hall, J.E., *Titanium Dioxide*, in Pigment Handbook (P.A. Lewis, Ed.), Wiley and Sons, New York, 1988.
[2] Winkler, J., *Titanium Dioxide*, Vincentz Network, Hannover, 2003.
[3] Dąbrowski, W., Tymejczyk, A., Lubkowska, A., *Właściwości i zastosowanie pigmentów dwutlenku tytanu*, Zakłady Chemiczne „Police" S.A., 2006.
[4] Gázquez M.J., Bolívar J.P., García-Tenorio R., Vaca F., Physicochemical characterization of raw materials and co-products from the titanium dioxide industry, *J. Hazard. Mater.*, 2009, 166, 1429-1440.
[5] Mantero J., Gázquez M.J., Bolívar J.P., García-Tenorio R., Vaca F., Radioactive characterization of the main materials involved in the titanium dioxide production process and their environmental radiological impact, *J. Environ. Radioact.*, 2013, 120, 26-32.

HEALTH SAFETY-ORIENTED INHIBITION OF TiO_2 PHOTOCATALYTIC ACTIVITY MAINTAINING ITS UV-SHIELDING PROPERTIES IN COSMETICS

Marcin Janczarek*, Waldemar Szaferski, Olga Scheffs, Brygida Szymańska

Poznan University of Technology, Institute of Chemical Technology and Engineering,
Berdychowo 4, 60-965 Poznan, Poland
*corresponding author: marcin.janczarek@put.poznan.pl

The efficacy and health safety of sunscreen cosmetics are the important issues in terms of the production and application of these products. Sunscreens provide protection against adverse effects of ultraviolet irradiation: UVB (280–315 nm) and UVA (315–400 nm). There is a limited list of chemicals available for use as sun protecting ingredients. Among the group of inorganic UV-filters, titanium dioxide (TiO_2) can be distinguished [1, 2]. Sunscreen products based on inorganic blockers comprise absence of skin irritation and sensitization, inertness of these additives and limited skin penetration. However, as TiO_2 is a semiconductor material, any photon with energy higher than the band gap energy (3.0–3.2 eV, corresponding to UV range of radiation) will be absorbed resulting in the formation of electron – hole pairs [3]. These charge carriers undergo a series of complex redox reactions that yield to the formation of reactive oxygen species (ROS) such as hydroxyl radicals and superoxide radicals. The presence of ROS in skin environment as a result of photocatalytic properties of titanium dioxide can cause various adverse effects, e.g., phototoxicity to skin fibroblasts and photo-oxidation of cellular DNA and RNA [4]. Therefore, the application of TiO_2 as an additive to sunscreen cosmetics should include the issue of inhibiting its photocatalytic activity.

The commercially available titanium dioxide (Aeroxide® P25) was selected to perform studies on hampering of ROS generation. Two modification strategies were applied to inhibit photocatalytic activity of P25: (a) thermal treatment in high temperatures, (b) modification with SiO_2. Photocatalytic properties were evaluated using 4-chlorophenol as a model organic compound and UV-LED (395 nm) as a light source. Figure 1 shows the results of photocatalytic activity tests for modified titanium dioxide samples in comparison with unmodified P25.

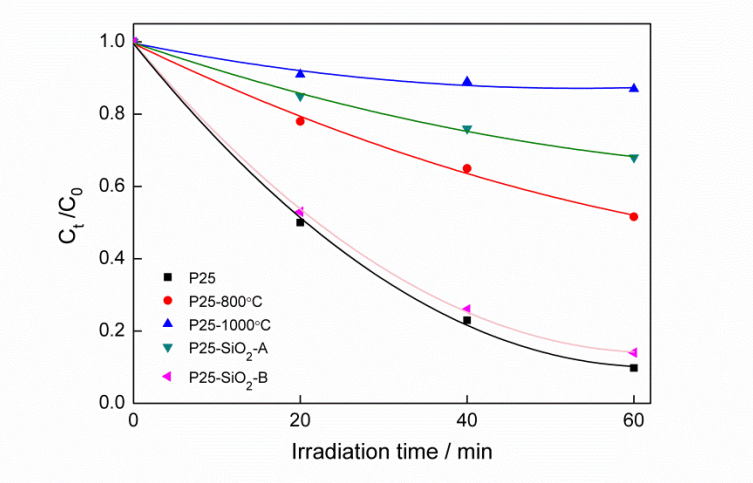

Fig. 1. Comparison of photocatalytic properties of P25 TiO_2 with modified P25-based materials. 4-chlorophenol initial concentration (C_0) was 10 mg/L

It has been found that simple modification methods such as thermal treatment and modification with SiO_2 can be efficient in inhibition of photocatalytic activity, Considering calcination of P25 above 800°C under air, only rutile phase appears, which can be a key factor for the activity inhibition. In the case of modification with SiO_2, it has been shown that this material with hydrophobic properties (SiO_2-A) is more efficient in hampering photocatalytic activity than hydrophilic silicon dioxide (SiO_2-B). Although preferred modifications should not affect UV-shielding properties, it is very important to consider the influence of particle size on UV absorption profile of modified TiO_2 materials. This detrimental effect can be observed for the sample treated at 1000°C despite the almost complete inhibition of photocatalytic activity.

References

[1] Smijs T.G., Pavel S., Titanium dioxide and zinc oxide nanoparticles in sunscreens: focus on their safety and effectiveness, *Nanotechnol. Sci. Appl.*, 2011, 4, 95-112.

[2] Serpone N., Dondi D., Albini A., Inorganic and organic UV filters: Their role and efficacy in sunscreens and suncare products, *Inorg. Chim. Acta*, 2007, 360, 794-802.

[3] Carp O., Huisman C.L., Reller A., Photoinduced reactivity of titanium dioxide, *Prog. Solid State Chem.*, 2004, 32, 33-177.

[4] Carlotti M.E., Ugazio E., Sapino S., Fenoglio I., Greco G., Fubini B., Role of particle coating in controlling skin damage photoinduced by titania nanoparticles, *Free Radical Res.*, 2009, 43, 312-322.

POLLUTANT EMISSION CHARACTERISTICS OF POLYMERS AND BIOMASS IN A BUBBLING FLUIDIZED BED REACTOR

Dawid Jankowski[1]*, Witold Żukowski[1], Gabriela Berkowicz-Płatek[1], Jan Wrona[2]

[1]Cracow University of Technology, Faculty of Chemical Engineering and Technology, Warszawska 24, 31-155, Cracow, Poland
[2] Cracow University of Technology, Faculty of Environmental and Power Engineering, Warszawska 24, 31-155, Cracow, Poland
*corresponding author: dawid.jankowski@pk.edu.pl

The paper presents the results of combustion of polymers (LDPE, HDPE, PP, PS, PET, PA, ABS and PC) and biomass (solid pine wood and beech wood, briquettes and pellets) in a bubbling fluidized bed reactor. It was determined that 850◦C is the minimum temperature at which the combustion process should be carried out. To simulate bubble chemical composition in a hot fluidized bed, FTIR analysis was performed under pyrolysis conditions. Recorded IR spectra were deconvoluted to determine the composition of fuel bubbles in the fluidized bed. Volumetric shares of gases generated during thermal decomposition of the exemplary samples are shown in Fig. 1.

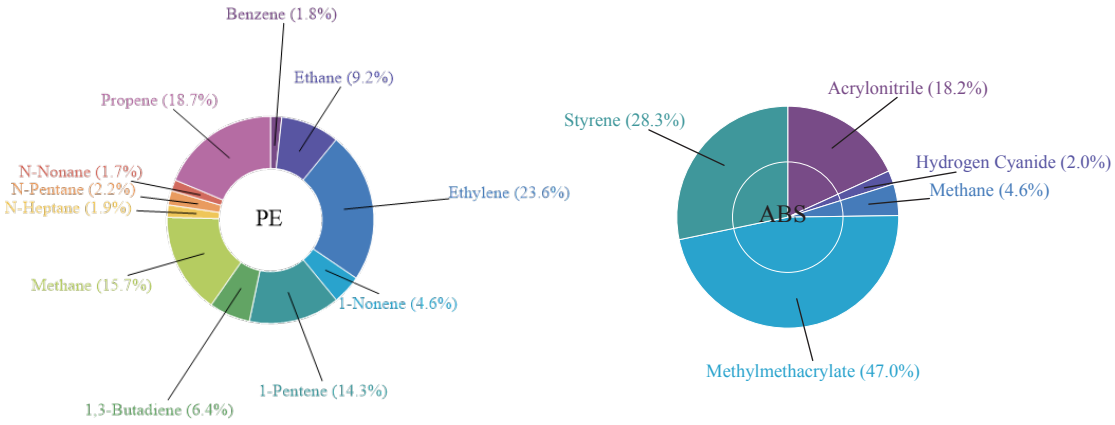

Fig. 1. Volumetric fractions of gases formed during thermal decomposition of PET and ABS in pyrolytic conditions

Due to the accidental chemical bonds breaking during thermal decomposition of polyolefins, the resulting mixture is a series of unsaturated and saturated hydrocarbons. It was shown that a uniform access to oxygen is necessary for the combustion of complex gas mixtures.

The combustion processes in a bubbling fluidized bed reactor were conducted in two ways. In the first case, samples were incinerated in autothermal conditions with a continuous supply of selected types of polymers. The study began with the warming up of the fluidized bed to an 850–950◦C range, using gaseous fuel (LPG-liquified petroleum gas). Next, the gaseous fuel supply was shut off and the bed was fluidized with air (1.66 dm^3/s). The reactor was fed with subsequent polymer fractions. In the second case, the incineration of polymer materials and biomass was conducted periodically in the co-combustion process with auxiliary, gaseous fuel. The fluidized bed temperature was kept at around 900◦C and at constant CO, CO_2 concentrations and at constant volatile organic values (VOC) in the exhaust, the periodical dosing of the material was started.

Tables 1 and 2 show emission coefficients (g/kg) of inorganic and organic pollutants in the exhaust gases. The results in Table 1 were obtained from the measurement data carried out during continuous combustion of different types of polymers in autothermal conditions. The coefficients shown in Table 2 are related to the co-combustion case. As far as the CO_2 emission index is

concerned, no significant differences were observed between these two ways of organizing the combustion processes. In the case of CO, the emission indicator during co-combustion reaches about twice the value compared to autothermal combustion.

For materials containing fuel nitrogen (PA, ABS), the nitrogen oxide concentrations in the exhaust gases exceeded almost several times the standard value. The NO_x concentrations for PA and ABS equal 1156 mg/m^3 and 889 mg/m^3 respectively, while the standard was 180 mg/m^3.

Table 1. Emission coefficients of inorganic pollutants released during polymer autothermal combustion

Sample	CO_2	CO	NO_x	HCN	VOC
	g/kg				
LDPE	2959	52	1.0	0.6	15.5
PA	1544	5	19.3	0.8	0.5
PET	2131	16	0.5	0.1	1.1
PC	2552	30	1.1	0.2	2.7
ABS	2170	26	12.6	1.9	3.9
PP	2878	48	1.7	0.7	11.4
HDPE	3023	52	0.9	0.4	12
PS	3008	73	2.2	1.5	13.6

Table 2. Emission coefficients of inorganic pollutants released during polymer co-combustion

Sample	Sample weight	CO_2	CO	NO_x	HCN	VOC
	g	g/kg				
LDPE	0.073	3058.4	93.1	n.d.	n.d.	36.0
PA	0.313	1423	27	12.8	12.1	9.39
PET	0.313	1952	50.7	n.d.	1.9	34.5
PC	0.396	2407	82	0.2	3.3	74.0
ABS	0.403	1516	90	11.5	17.3	123.1
PP	0.06	2931	60	n.d.	n.d.	75.9
HDPE	0.141	1849	206	n.d.	n.d.	267.7
PS	0.048	3352	51	n.d.	n.d.	0.00

n.d – not detected

During combustion of biomass it can be observed that only in the case of CO there is a correlation between the particle size of material introduced into the bed and the emission factor for this pollutant. It applies to solid, unprocessed materials, such as pine and beech. The absence of clear dependence of the CO emission coefficient on the mass of the particles in the case of briquets and pellets may be due to the fact they disintegrate in a fluidized bed into very fine particles from which they were made. Due to this fact the particle size of the combustible materials, briquettes or pellets, does not affect emission factors.

Combustion of polymers can be combined in a fluidized bed with biomass combustion. The use of these materials for the production of thermal energy will be beneficial from the environmental point of view because when both combustible materials are burned simultaneously it contributes to the reduction of the consumption of conventional fuels. Supporting the combustion of engineering or packaging polymers with the use of biomass does not deteriorate the emission factors because biomass emission factors are lower than those of most plastics.

CFD MODELLING OF THREE-PHASE FLUID FLOW IN A BUBBLE REACTOR WITH A SLOT GAS DISPERSER

Jolanta Jaschik[1,*], Marek Tańczyk[1], Aleksandra Janusz-Cygan[1], Daniel Janecki[2], Jan Mrozowski[3]

[1]Polish Academy of Sciences, Institute of Chemical Engineering, Bałtycka 5, Gliwice, Poland
[2]University of Opole, Institute of Environmental Engineering and Biotechnology, Kardynała Kominka 6-6a, Opole, Poland
[3]Research Network ŁUKASIEWICZ - Institute of Non-Ferrous Metals, Sowińskiego 5, Gliwice, Poland
*corresponding author: jjaschik@iich.gliwice.pl

A bubble reactor equipped with a slot gas disperser of special design for deep desulfurization of SO_2-rich gases was developed in the Institute of Non-Ferous Metals in Gliwice. Experimental studies of desulfurization process were performed in a large-scale laboratory bubble reactor (diameter 1.2 m, height 1.6 m) of 1.5 m^3 working capacity. Details of the experimental set-up, procedure and results are described in [1].

A CFD model of bubble reactor was developed to study the large-scale implementation of the process. The bubble reactor works in a three-phase system containing liquid medium, dispersed process gas and solid gypsum, that is a reaction product. For the three-phase gas-liquid-solid reactor system a three-phase flow model was developed and presented in this study. The commercial program Fluent version 2021.R2 from ANSYS was used for simulation calculations. The Eulerian multiphase model extended to three phases with standard k- ε turbulence model was used. Simulations concerning hydrodynamics in the presented bubble reactor were made for different values of operating parameters. The validation of the developed model was done by comparing the experimental and calculated values of the inlet gas pressure drop and the power of mixing. A very good agreement was found for these parameters.

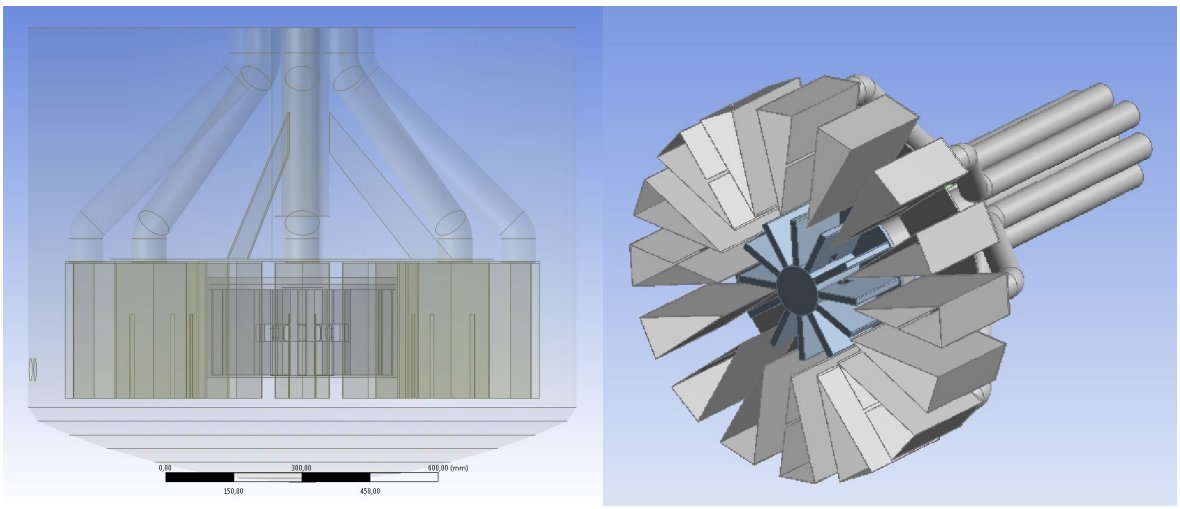

Fig. 1. Geometry of the bubble reactor of 1.5 m^3 working volume for CFD calculations; left - the marked level corresponds to H = 1 m, 1.01 m^3 slurry tank filling, right - slot gas disperser, bottom view

A detailed analysis of the hydrodynamic phenomena occurring in the various areas of the reactor was performed. This analysis confirmed good conditions for mixing of gas and liquid phases in the reactor of modelled configuration, especially in the space between the disperser blades, irrespective of the direction of stirrer rotation which must be changed during an industrial process.

This is due to the intensive, dynamic interaction of the phases and/or large area and large contact time of this interaction. Such conditions favor effective absorption of SO_2, which was found in experimental studies [1]. Some results of numerical calculations are presented in Figures 2 and 3. The turbulent Reynolds number, presented in Figure 3, for k-ε model is defined as [2]:

$$Re_t = \frac{k^2}{\varepsilon \, \mathrm{n}}$$

where k is turbulent kinetic energy, Jkg^{-1}, ε - turbulent dissipation rate, $Jkg^{-1}s^{-1}$ and ν is kinematic viscosity for the mixture, m^2s^{-1}.

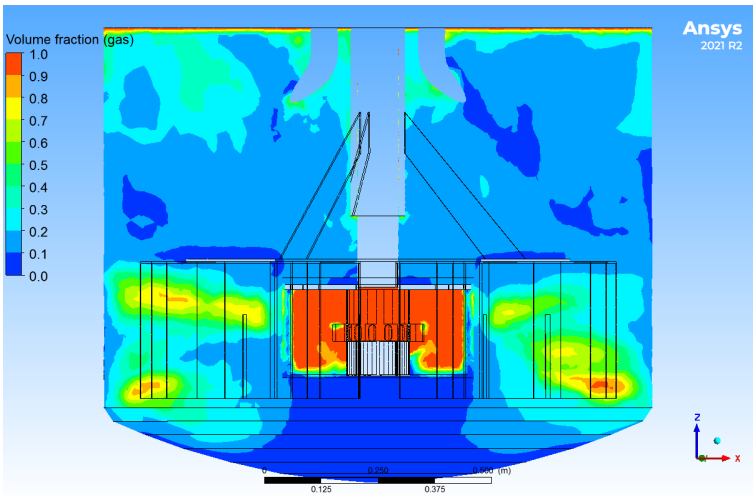

Fig. 2. Volume fraction of gas phase in the space between the disperser blades

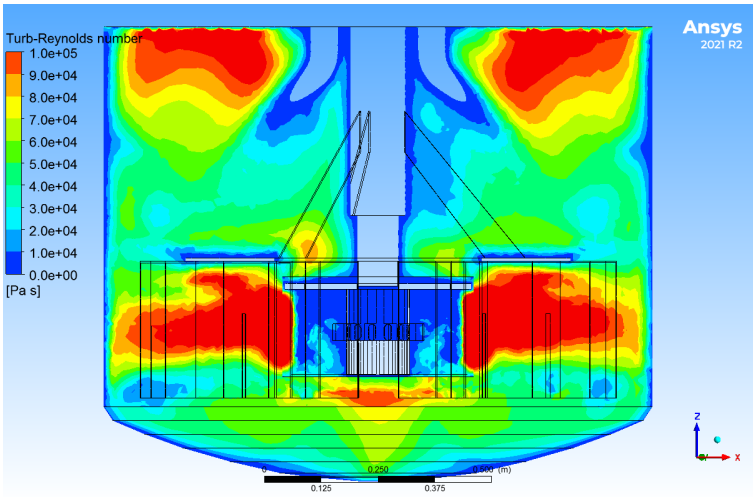

Fig. 3. Turbulent Reynolds number in the space between the disperser blades

The presented model has been used in the scaling-up process. In particular, it was used to develop the optimal reactor design leading to maximum intensification of phase contact in the bubble reactor of pilot scale.

References

[1] Mrozowski J., Jaschik J., Desulfurization of SO_2-rich gases in a bubble reactor with a special design, *Przem. Chem.*, 2021, 100(6), 585–590.

[2] Al-Rashed, M., Wójcik, J., Plewik, R., Synowiec, P., Kuś, A., Multiphase CFD modeling: Fluid dynamics aspects in scale-up of a fluidized-bed crystallizer, *Chem. Eng. Process: Process Intensif.*, 2013, 63, 7–15.

DEVELOPMENT OF THE BETA-PDF CLOSURE METHOD FOR COMPLEX REACTIONS IN A TURBULENT MIXING REGIME

Magdalena Jasińska[1*], Grzegorz Tyl[1], Jan Krzysztoforski[1], Otton Roubinek[2]

[1]Warsaw University of Technology, Faculty of Chemical and Process Engineering, Waryńskiego 1, 00-645 Warsaw, Poland
[2]Łukasiewicz – Industrial Chemistry Institute, Rydygiera 8, 01-793 Warsaw, Poland
[*]corresponding author: magdalena.jasinska@pw.edu.pl

This paper presents the effects of mixing on the course of multiple complex chemical reactions in a turbulent flow regime. Development of methods which can be applied for determination of product distribution in the mixing equipment of industrial importance is extremely necessary for the proper process design involving multiple chemical reactions. The most important factor concerns manufacturing of pure products at high reaction selectivity, so that the costs of the main product separation is the lowest. Another issue concerns designing mixing strategies that will be able to characterize mixing in the arbitrary apparatus (i.e. reactor or crystallizer). Design of such systems is possible based on the method in which homogenous test reactions are applied in conjunction with an appropriate closure scheme. This approach is the most accurate and thus is recommended by the mixing community. In this paper a new β-pdf closure method was introduced, applied, and developed in order to predict the course of a single reaction or multiple reactions of any rates. This means that the application of the introduced method allows one for correct prediction of the product distribution of complex reactions (including so-called test reactions) without any limitation in respect to reaction rate. The only condition that must be fulfilled is that a reaction is characterised as sufficiently fast relative to mixing on the molecular scale. In other words such a reaction should be regarded as sensitive to micromixing in homogenous systems.

As an example of multiple reactions two types of complex elementary reactions were considered in this work: a) the competitive-consecutive type of reaction which proceeds in accordance to the following scheme:

$$A + B \overset{k_1}{\rightarrow} R \;\&\; R + B \overset{k_2}{\rightarrow} S \qquad (1)\;\&\;(2)$$

and b) the parallel type of reaction which can be represented as:

$$A + B \overset{k_1}{\rightarrow} R \;\&\; A + C \overset{k_2}{\rightarrow} S \qquad (3)\;\&\;(4)$$

In the new approach the front of reaction is no longer fixed as the (first) reaction is not necessarily infinitely fast. In this case a reactive zone, where the reaction proceeds should be defined, and this zone is represented in the introduced scheme by continuous shift in reaction front position. In other words the reaction front is no longer fixed and is moving from value of f_{s1} to f_{s2} as shown in Figure1, with f_{si} being the universal form of reaction front position. For competitive-consecutive reactions it is defined as $f_{si} = \frac{\beta}{\nu_i + \beta}$, where $\nu_1 = 1$ and $\nu_2 = 2$ for reaction $A + \nu_i B \rightarrow Products$.

The method introduced here enables determination of the substate and product concentrations as a function of a mixture fraction, f, and eventually the average concentration of reacting species from:

$$\overline{c_i} = \int_0^1 c_i(f)\phi(f)\,df \qquad (5)$$

as well as the average reaction rate, defined by consumption of A in the first reaction (1) of the competitive-consecutive scheme as:

$$\bar{r_A} = k_1 \overline{c_A(f) c_B(f)} = \int_0^1 k_1 \, c_A(f) c_B(f) \phi(f) df \tag{6}$$

and with $\phi(f)$ being β-pdf function expressed as:

$$\phi(f) = \frac{f^{v-1}(1-f)^{w-1}}{B(v,w)} \tag{7}$$

To simulate mixing of the added reactant with the bulk the turbulent mixer model (TMM) [1, 2] has been employed in this paper.

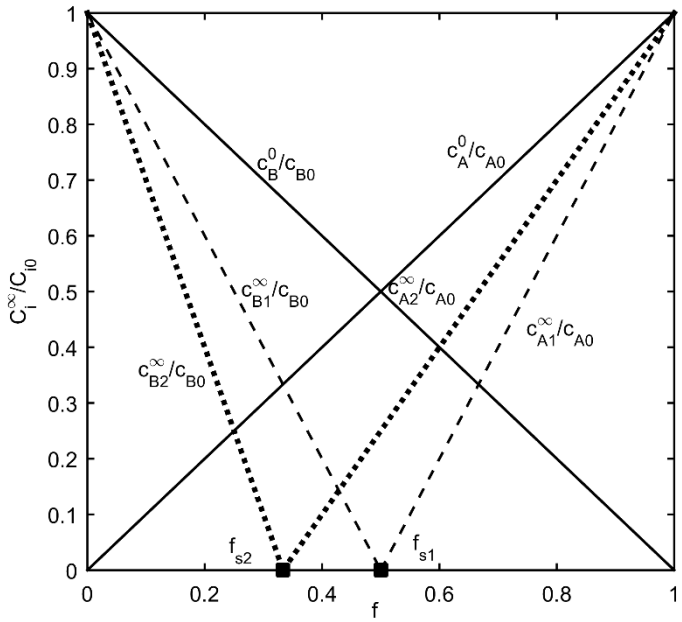

Fig. 1. Concentrations of substrates as a function of mixture fraction

The new closure represents an extension of the conditional PDF closure applied before to simple reaction schemes [1]. Existing models usually assume the first reaction to be instantaneous leaving only the second one sensitive to mixing. This assumption has been dropped in the proposed work allowing for characterization of complex interaction between chemical reactions and mixing on molecular scale.

Additionally, the introduced method of closure for complex reaction schemes has been tested using simple flows. The results of these simulations show how to fit the test reaction system to the process conditions expressed by the rate of energy dissipation (hence the total power input) and the integral scale of turbulence which corresponds to the effect of the system scale.

References

[1] Bałdyga J., Bourne J.R., *Turbulent mixing and chemical reactions*, Chichester, Wiley, 1999.
[2] Bałdyga J., Turbulent mixer model with application to homogeneous, instantaneous chemical reactions, *Chem. Eng. Sci.*, 1989, 44 (5), 1175-1182.

MICROPOROUS CARBONS FOR CO_2 ADSORPTION DERIVED FROM CITRUS PEELS

Karolina Kiełbasa*

West Pomeranian University of Technology in Szczecin, Faculty of Chemical Technology and Engineering, Department of Catalytic and Sorbent Materials Engineering,
Piastów 42, 71-065 Szczecin, Poland
*corresponding author: kkielbasa@zut.edu.pl

Herein, the raw material for preparation of carbonaceous materials was a water solution with powder citrus peels, placed in an autoclave for 12/24/48 hours at 200 °C. After hydrothermal synthesis, the sample was removed from the autoclave, rinsed with deionized water until neutral, and dried at 110 °C. After drying, the spherical material obtained from hydrothermal synthesis was activated with solid KOH for 3 hours. The material was heated at 750 °C under nitrogen flow (20 dm^3/h). The prepared carbon materials containing the decomposition products of potassium hydroxide or potassium carbonate were washed with distilled water to achieve a neutral reaction. Subsequently, the activated carbon was dried at a temperature of 110 °C for 20 h.

The characterization of the activated biocarbon samples was carried out via several instrumental techniques such as XRD, FTIR, Raman, N_2 sorption at the temperature of 77 K, and CO_2 sorption.

Activation of carbon spheres with potassium hydroxide caused production of carbon materials through mesoporous spheres to microporous carbons.

It was found that the textural properties i.e. specific surface area, total pore volume, and micropore volume decreased along with an increase in temperature of hydrothermal synthesis.

The CO_2 adsorption equal to 9 mmol/g at the temperature of 273 K and pressure of 1 bar was achieved. The CO_2 adsorption at 1 bar pressure decreased with the increase in temperature of hydrothermal synthesis.

CONDITIONS OF AERATED LIGHT SUSPENSION PRODUCTION IN STIRRED TANKS OF DIFFERENT SCALE

Anna Kiełbus-Rąpała*

West Pomeranian University of Technology in Szczecin, Department of Chemical Engineering,
Piastów 42, PL–71 065 Szczecin, Poland
*corresponding author: anna.kielbus-rapala@zut.edu.pl

Aerated light suspensions are used in many industries, e.g., petrochemical, polymerization or fermentation. In a multiphase system, it is essential to ensure the best possible contact between the phases. Generally, the production of any multiphase system is an activity leading to the appropriate homogenization of this system and maintaining this state for the time required by the process. Due to the specificity of operation, tanks with a stirrer are most often used for this purpose.

The conditions of the production of an aerated light suspension in a stirred tank depend on many factors, including geometrical parameters of the tank, type of the stirrer used, particle content and properties, and type of continuous phase. One of the important things in the production of multiphase systems is the problem of scale up or down of the apparatus. It is very difficult due to the large variety of operating parameters, as well as the properties of the system components. When reducing or enlarging the scale of the stirred tank, geometric, kinematic and dynamic similarity should be taken into account.

The aim of this research work was to analyse the conditions of the production of the aerated light suspension in two stirred tanks with different inner diameters. In this analysis the effect of gas flow rate V_G, particle concentration and type of the stirrer on the hydrodynamics of the gas-light particle-liquid system (particularly on the critical stirrer speeds n_{JDG}, required to create the system). The effect of the tank scale was also investigated.

Measurements were conducted in two transparent cylindrical tanks with the liquid height of H=T and inner diameters T_1 = 0.15m and T_2 = 0.288m (working liquid volume V_{L1} = 0.0026m^3 and V_{L2} = 0.02m^3). Four flat baffles were mounted in the tanks. To create the three-phase system single or double high-speed stirrers were used. Rushton turbine (RT) or Smith turbine (CD 6) worked as single stirrers. The set of two stirrers on the common shaft included Rushton turbine (RT) as the lower (its role was to break gas bubbles to smallest pieces and distribute them into the volume of liquid) and pitch blade turbine (PBT) as the upper one (its main task was drawing down floating particles under the surface of the liquid). All stirrers had diameter d= 0.33T.

The study was carried out in the system, where the continuous phase was aqueous solution of glucose with the concentration C equal to 10 mass %. The gas phase was air, whilst polyethylene particles of density ρ_p = 955 kg/m^3, with mean diameter d_p equal to 3.025mm and concentration X were used as the solids. All the experiments were conducted within the turbulent regime of the fluid flow in the agitated vessel. Measurements were conducted for six various gas flow rates and four different values of the solid concentration X up to 5 mass %.

The minimum stirrer speeds n_L, n_{CD} and n_{JD}, at which the characteristic flow patterns of three-phase mixture were obtained, were determined visually, observing in each concentration X and each gas stream V_G the behaviour of the dispersed phases. The value of n_{JDG} was determined analogically to Zwietering criterion for conventional suspension.

On the basis of the studies the characteristic flow patterns of the aerated light suspension in the stirred tank, including: flooding (gas flows axially towards the liquid surface), loading (dispersion of gas bubbles only in the zone from lower stirrer to the liquid surface) and complete dispersion (dispersion of gas with recirculation under the lower stirrer, bubbles are dispersed in a whole liquid volume), with the minimum stirrer speeds adequate to obtain each of them: n_L, n_{CD} and n_{JD} were determined. The results showed that there was the influence of gas flow rate, particle concentration and stirrer type on the value of n_L, n_{CD}, n_{JD}, n_{JDG} in the analysed systems.

To determine the effect of the scale, the results of the measurements conducted at a constant gas flow rate Q_{GV} [$(m^3/min)/m^3$] in both tanks were compared. All the results obtained were described mathematically.

COMPLEXATION DEGREES OF MICROELEMENT IONS BY IDHA BIODEGRADABLE CHELATOR IN FERTILIZATION ENVIRONMENT

Ewelina Klem-Marciniak*, Marcin Biegun, Krystyna Hoffmann, Józef Hoffmann

Wroclaw University of Science and Technology, Faculty of Chemistry, Department of Engineering and Technology of Chemical Processes, Wybrzeże Wyspiańskiego 27, 50-370 Wrocław, Poland
*corresponding author: ewelina.klem@pwr.edu.pl

Chelators are used in many industries. Their structure provides metal ions. Chelators are sources as carriers of microelement ions and for the production of fertilizers. Their structure affects the stabilization of microelement ions in a wide pH range and in the soil solution, which enables their use on calcareous and alkaline soils. Under such conditions, metal ions in the form of inorganic salts pass into forms inaccessible to plants [1-3].

The wide use of ligands with different chelating properties means that their high proportion is found in inland waters. The presence of these people in the environment can help eutrophicate water, remobilize heavy metals from bottom and river sediments and get them into the installation. The current research study is on the source components that comprise the biodegradation process. IDHA (imidodisuccinic acid) can be used for biodegradable chelators. Tests in static and kinetic conditions cause it to appear at the beginning of decomposition in contact with activated sludge, which prevents it from getting into water [4-6].

The aim of the work was to determine the degree of complexation of microelement ions by IDHA in the fertilization environment. The 2021 update of the Regulation of the European Parliament and of the Council 2019/1009 laid down regulations on making EU fertilising products available on the market, thanks to which various properties with chelating properties can be used in the production of micronutrient fertilizers [7]. The condition that must be met by any chelator is the complexation of the total amount of water-soluble microelement ions to a degree of at least 80%. The degree of complexation was determined using differential pulse voltammetry. The results obtained are based on the preliminary assessment of the possibility of using IDHA chelates as a component of compound fertilizers [8].

Table 1. The degree of complexation of microelement ions by IDHA in fertilizer environments at pH 5.

Microelements ions / Environment	Zinc ions	Copper ions	Manganese ions
nitrogen environment	93.63%	23.11%	88.88%
nitrogen-phosphorus environment	100%	40.75%	51.50%
nitrogen-phosphorus-potassium environment	72.24%	-	71.72%

The conclusion that IDHA chelates will most effectively supplement micronutrient deficiencies as water solutions is acceptable [8]. The addition of macronutrients makes the degree of complexation lower.

References

[1] Hoffmann J., Hoffmann K., Nawozy mikroelementowe, *Przem. Chem.*, 2006, 85:8-9, 827-830.
[2] Abadía J., Vázquez S., Rellán-Álvarez R., El-Jendoubi H., Abadía A., Álvarez-Fernández A., López-Millán A., Towards a knowledge-based correction of iron chlorosis, *Plant Phys. Biochem*., 2011, 49, 471-482.
[3] Knepper T.P., Synthetic chelating agents and compounds exhibiting complexing properties in the aquatic environment, *T. Anal. Chem.,* 2003, 22:10, 708-724.
[4] Fuerhacker M., Lorbeer G., Haberl R., Emission factors and sources of ethylenediaminetetraacetic acid in waste water—a case study, *Chemosphere*, 2003, 52, 253–257.
[5] Klem-Marciniak E., Hoffmann K., Hoffmann J., Porwoł M., Badania biodegradacji chelatorów nawozowych w środowisku wodnym w warunkach testu kinetycznego, *Przem. Chem*., 2017, 96 (11), 2253-2255.
[6] Klem-Marciniak E., Hoffmann K., Hoffmann J., The aerobic biodegradation of EDDHA and EDDHSA in water under the static test conditions*, Desal. Water Treat*., 2018, 134, 1-6.
[7] Rozporządzenie (WE) nr 2019/1009 Parlamentu Europejskiego i Rady z dnia 5 czerwca 2019 r. w sprawie nawozów.
[8] Klem-Marciniak E., Huculak-Mączka M., Marecka K.M., Hoffmann K., Hoffmann J., Chemical stability of the fertilizer chelates Fe-EDDHA and Fe-EDDHSA over time, *Molecules*, 2021, 26 (7), 1-16.

Acknowledgements

This research was founding by the Ministry of Science and Higher Education of Poland within a frame of science subsidy for 2023 which was realized in the Department of Engineering and Technology of Chemical Processes, Wrocław University of Science and Technology (No. 8211104160-K24W03D05).

IMPROVING CARBON DIOXIDE CAPTURE IN AQUEOUS AMMONIA SOLUTIONS BY FINE SiO_2 PARTICLES

Donata Konopacka-Łyskawa[1,*], Temesgen Abeto Amibo[1], Dominik Dobrzyniewski[1], Marcin Łapiński[2]

[1]Gdańsk University of Technology, Faculty of Chemistry, Department of Process Engineering and Chemical Technology, Narutowicza 11/12, 80-233 Gdańsk, Poland
[2]Gdańsk University of Technology, Faculty of Applied Physics and Mathematics, Department of Solid State Physics, Narutowicza 11/12, 80-233 Gdańsk, Poland
*corresponding author: donata.konopacka-lyskawa@pg.edu.pl

In order to reduce the emission of anthropogenic CO_2 into the atmosphere, technologies for carbon dioxide capture, sequestration, and utilization (CCS and CCU) are currently being developed. The largest share in the capture of CO_2 is made by processes that use physical or chemical absorption [1]. Various strategies are used to improve the absorption process, e.g. using amine mixture solutions, testing new compounds for CO_2 absorption, e.g. ionic liquids or newly synthesized amines, and deep-eutectic solvents [2, 3]. Recently, nanofluids have been proposed as a new type of absorbent [4]. Nanofluids consist of a base liquid and nanoparticles, and the small size of the added materials ensures high stability of dispersion produced. The results of absorption studies in nanofluids are promising and indicate that it is possible to increase the absorption rate during both physical and chemical absorption [4]. From a practical point of view, effective solvents are nanofluids obtained on the basis of chemical absorbents, which are characterized by high absorption capacity. The tested solvents containing amines and nanoparticles showed an increase in the absorption rate of several dozen percent [4]. Also, ammonia-based nanofluids may have great potential. Carbon dioxide absorption in ammonia solutions is characterized by high CO_2 absorption efficiency and capacity, low energy requirements for stripping and low heat of reaction in comparison with MEA, lower price as well as insensitivity to the presence of compounds such as COS, CS_2, or H_2S [5]. Zhang et al. [6] obtained an enhancement in the rate of CO_2 absorption in ammonia solutions with the addition of Fe_3O_4 nanoparticles, with the most favorable effect observed (increase by 14.5%) for the solution with the highest tested ammonia concentration of 4%. The cost of commercially available nanoparticles is relatively high. Therefore, in this work, colloidal SiO_2 with an average diameter of 600 nm was tested as an additive to the absorption solutions. The aim of the conducted research was: (i) to determine the rate of CO_2 absorption in dispersions obtained on the basis of aqueous solutions of ammonia and colloidal SiO_2 particles and in aqueous dispersions containing ammonia and SiO_2 microparticles; (ii) to test the influence of the presence of SiO_2 particles on ammonia desorption during the flow of the gas mixture through the absorber and (iii) to determine the most favorable concentration of fine particles in ammonia solutions for carbon dioxide capture.

CO_2 absorption was carried out in aqueous solutions of ammonia with NH_3 concentration of 0.53 mol·dm^{-3} containing SiO_2 from 0 to 0.15% by weight in the form of colloidal or microparticles. Gum arabic at 100 ppm was a dispersion stabilizer. Measurements of the rate of CO_2 absorption and NH_3 desorption were performed in the test setup described in detail in [7]. The volume of the tested absorbent was 0.250 dm^3, and the CO_2-air gas mixture ($x_{V,CO2}$=0.15) at the volume flow rate of 0.5 dm^3·min^{-1} was supplied through a glass sinter. The CO_2 and NH_3 content in the exhaust gas was analyzed using sensors and recorded in a computer. Absorption was carried out for 30 min.

Based on the obtained measurement results, the number of moles of absorbed CO_2 in the tested solutions, the rate of CO_2 absorption over time, the number of moles of desorbed ammonia during the gas flow, and the rate of ammonia desorption were determined. Fig. 1a shows the number of moles of absorbed CO_2 in the ammonia solution after 30 min as a function of SiO_2 particle concentration. The relationship between the number of moles of desorbed ammonia and

the concentration of SiO_2 colloidal and microparticles is shown in Fig. 1b. In the case of colloidal particles, their addition in the tested range (0.01%-0.15%) increased the rate of CO_2 absorption and, consequently, increased the number of moles of absorbed CO_2 by 30%. When SiO_2 microparticles were added to the ammonia solution, the rise of CO_2 absorption rate was observed for the lowest SiO_2 concentration tested, i.e. 0.01%. A higher proportion of SiO_2 microparticles did not influence significantly the amount of absorbed CO_2. NH_3 desorption was the highest from the ammonia solution without SiO_2 particles. On the other hand, the addition of both SiO_2 colloidal and microparticles reduced the escape of NH_3 from the solvent. The greatest inhibition of ammonia desorption was in the tested colloidal dispersions.

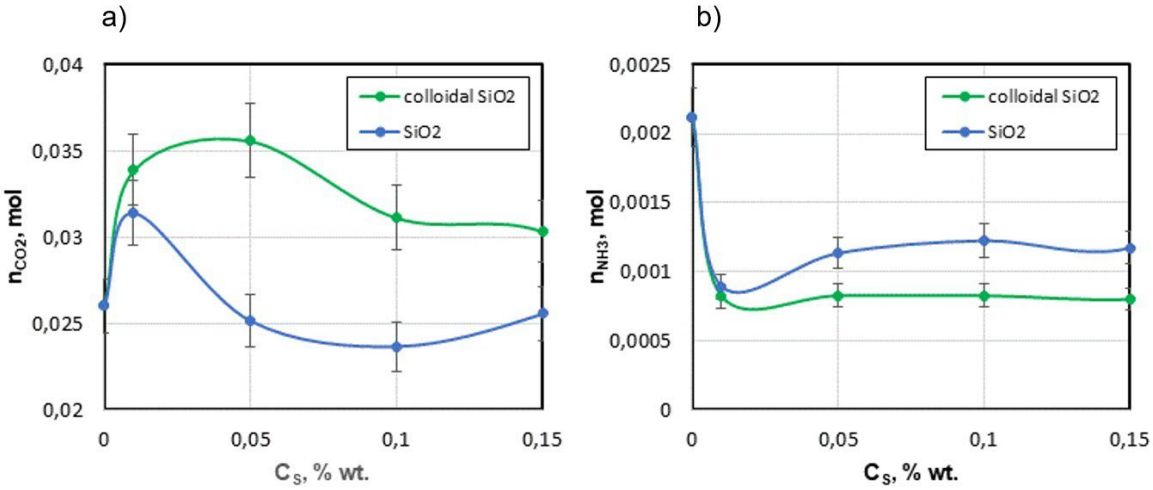

Fig. 1. Influence of the concentration of SiO_2 particles on: a) the number of moles of carbon dioxide captured; b) the number of moles of ammonia desorbed

In summary, SiO_2 colloidal particles are an effective additive to ammonia solutions used for CO_2 absorption. The calculated enhancement in absorbed CO_2 was above 30% in solvents containing 0.01% and 0.05% SiO_2. The presence of colloidal SiO_2 particles had a positive effect on the desorption of ammonia and reduced the number of moles of NH_3 stripped from the flowing gas by about 60%.

References

[1] Chao, C., Deng, Y., Dewil, R., Baeyens, J., Fan, X., Post-combustion carbon capture, *Renew. Sustain. Energy Rev.*, 2021, 138, 110490.

[2] Chai S.Y.W., Ngu L.H., How B.S., Review of carbon capture absorbents for CO_2 utilization, *Greenh. Gases Sci. Technol.*, 2022, 12(3), 394–427.

[3] Liu Y., Dai Z., Zhang Z., Zeng S., Li F., Zhang X., Nie Y., Zhang L., Zhang S., Ji X., Ionic liquids/deep eutectic solvents for CO_2 capture: Reviewing and evaluating, *Green Energy Environ.*, 2021, 6(3), 314–328.

[4] Tavakoli, A., Rahimi, K., Saghandali, F., Scott, J., Lovell, E., Nanofluid preparation, stability and performance for CO_2 absorption and desorption enhancement: A review, *J. Environ. Manage.*, 2022, 313, 114955.

[5] Borhani T. N., Wang M., Role of solvents in CO_2 capture processes: The review of selection and design methods, *Renew. Sustain. Energy Rev.*, 2019, 114, 109299.

[6] Zhang Q., Cheng C., Wu T., Xu G., Liu W., The effect of Fe_3O_4 nanoparticles on the mass transfer of CO_2 absorption into aqueous ammonia solutions, *Chem. Eng. Process. - Process Intensif.*, 2020, 154, 108002.

[7] Czaplicka, N., Dobrzyniewski, D., Dudziak, S., Jiang, C., Konopacka-Łyskawa, D., Improvement of CO_2 absorption and inhibition of NH_3 escape during $CaCO_3$ precipitation in the presence of selected alcohols and polyols, *J. CO_2 Util.*, 2022, 62, 102085.

STUDY OF MIXING PROCESS IN A NOVEL CONSTRUCTION OF A STATIC MIXER AIDED BY THE CFD SIMULATIONS

Maciej Konopacki*, Dawid Sołoducha, Tomasz Borowski, Marian Kordas, Dominik Figas, Rafał Rakoczy

West Pomeranian University of Technology in Szczecin, Faculty of Chemical Technology and Engineering, Department of Chemical and Process Engineering, Piastów 42, 71-065 Szczecin, Poland
*corresponding author: mkonopacki@zut.edu.pl

Mixing plays an important role in many branches of industry such as food processing, pharmaceutics, chemical, petrochemical, biotechnology, and others [1]. Many industrial processes are conducted under continuous regime, where flow mixers equipped with mechanical or static agitators are commonly utilized. Such devices can be easily installed into different systems and their work can be automated, which is in line with the actual world leading trends. The biggest advantage of static mixers is the lack of moving parts, which requires increased rate of maintenance, repair or replacement. Moreover, they need no power supply for the agitator like mechanical mixers, but only a pump with enough force to overcome the pressure drop created by the mixer elements [2].

This kind of mixer commonly consists of a few mixing elements (inserts) mounted inside a cylindrical tube. Briefly, inserts split streams of fluid flow, then shift their flow directions and combine them again in order to mix fluid elements. The main goal of static mixer design is to create a geometry of insert which allows to achieve high mixing efficiency with relatively small pressure drop which corresponds with the energetic cost of the system. For that reason, a detailed analysis of the hydrodynamics inside that device should be performed, ensuring that inserts work together in a proper manner. Otherwise, a wrongly designed geometry can create cyclic disturbances in mixing process or create dead-zones which can lead to expensive changes in system design or equipment replacement [6]. Therefore, design of static mixer can be aided by the Computational Fluid Dynamics (CFD) simulations. CFD basis on the solution of Navier-Stokes equations with additional transport equations which together describe fluid dynamics inside the analyzed system. This method gives an opportunity to view and study hydrodynamics, especially velocity profile distribution of fluid stream flowing through the static mixer, allowing to verify work of the proposed geometry of insert at the early stage of the prototyping process [4].

The aim of the research was to study a novel geometry of a static mixer insert which was created through rapid prototyping. The proposed geometry of insert was used to create a model of static mixer, which consists of five mixing elements. In the current study a few cases were analyzed, each for various positions of inserts. For each case a CFD analysis was performed to verify the hydrodynamics and pressure drop. Three most promising models were selected based on numerical results. These models were 3D-printed and tested in a laboratory-scale static mixer. Obtained experimental data related to the mixing efficiency and pressure drop was analyzed and discussed in relation to the available literature data of other static mixers.

References

[1] Aanjaneya K., Agrawal S., Optimization of twisted-tape element static mixers for industrially relevant setups, *Chem. Eng. Res. Des.*, 2023, 191, 426-438.
[2] Chen J., Xie S., Huang H., A novel method of utilizing static mixer to obtain mixing homogeneity of multi-species powders in laser metal deposition, *Chinese J. Aeronaut.*, 36, 423-433.
[3] Ghotli R.A., Raman A.A.A., Ibrahim S., Baroutian S., Liquid-liquid mixing in stirred vessels: a review, *Chem. Eng. Commun.*, 2013, 200, 595-627.
[4] Pujari A.R., Kumar S., Sow P.K., Fluid flow simulation on a Turritella-seashell-like geometry demonstrating its ability as static mixer for inline mixing, *Chem. Eng. Sci.*, 2022, 262, 118031.

NUMERICAL AND EXPERIMENTAL STUDY ON HYDRODYNAMICS OF A STATIC MIXER WITH A NEW MIXING INSERT

Marian Kordas*, Tomasz Borowski, Anna Story, Grzegorz Story, Mateusz Łukasiewicz, Rafał Rakoczy

West Pomeranian University of Technology in Szczecin, Department of Chemical and Process Engineering, Piastów 42, 71-065, Szczecin, Poland
*corresponding author: mkordas@zut.edu.pl

In practice, the processes of mass, momentum and energy transport are intensified by mixers. The most common type of mixer is a mechanical mixer with a rotating agitator powered by external energy source. Mechanical agitators with rotary agitators are characterized by a large variety of designs of agitators, baffles and tanks. Unfortunately, these mixers, despite many advantages, are characterized by a rather low efficiency of mass and energy transport processes carried out in them in comparison with other devices [1, 2].

Attempts are currently being made to use static mixers as an alternative to mechanical mixers in continuous processes. In the case of static mixers, the pressure difference in the line with the mixing elements is required for them to operate. However, the pressure drop generated by the mixing inserts cannot be too high, because it will decrease process effectiveness. Properly working static mixers have low energy consumption and no moving parts. The advantages of this solution are the modular structure and no need to use expensive devices. In the case of static mixers, the key element that has influence on their performance is the geometry of the mixing inserts. The number of mixing inserts used and their placement in the tube through which the mixed fluid flows is also important [3, 4].

The aim of this work was to analyze the impact of the new construction solution of the mixing insert on the hydrodynamics in a static mixer. The figure below shows three tested new insert variants. These inserts were created as a result of multiplying the developed elementary mixing module in the axis of the mounting rod.

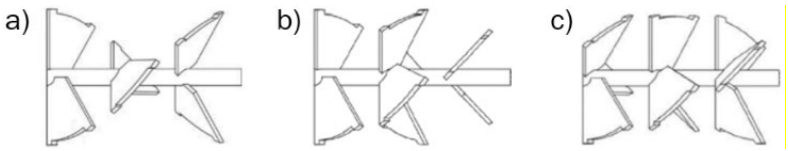

Fig. 1. Sketch of tested new geometries of mixing inserts: variant a), b), c)

The mixing inserts were grouped in packages of five and inserted into the cylindrical tube of the static mixer. Then, for the prepared mixing systems, numerical simulations were carried out which resulted in velocity magnitude distribution maps and they allowed to calculate pressure drops. Physical prototypes of inserts were also made and tested for generated pressure drop. Pressure was measured in a cylindrical tube before and after the mixing inserts which allowed to determine the pressure drop. Experimental results were similar to those obtained from numerical simulations. This allowed for an initial assessment of the suitability of the proposed new construction solution of mixing inserts.

References

[1] Zlokarnik M., *Stirring Theory and Practice*, Wiley-VCH 2001, ISBN 9783527299966.
[2] Dietrich T.R., *Microchemical Engineering in Practice*, Hoboken, Wiley 2009, ISBN 978-0-470-23956-8.
[3] Masiuk S., Rakoczy R., Kordas M., Badania podstawowe nowej konstrukcji mieszalnika statycznego, *Przem. Chem*., 2009, 88, 1019–1024.
[4] Ghanem A., Lemenand T., Della D., Hassan V., Static mixers: Mechanisms, applications, and characterization methods – A review, *Chem. Eng. Res. Des*., 2014, 92, 2, 205–228.

TRANSPORT PROPERTIES OF FRACTAL STRUCTURES IN CATALYTIC DECOMPOSITION OF HYDROGEN SULFIDE

Mateusz Korpyś[1,*], Anna Gancarczyk[1], Mikołaj Suwak[1], Maciej Sitarz[2], Joanna Profic-Paczkowska[3]

[1]Polish Academy of Sciences, Institute of Chemical Engineering, Gliwice, Poland
[2] AGH University of Science and Technology, Faculty of Materials Science and Ceramics, Kraków, Poland
[3] Jagiellonian University, Faculty of Chemistry, Kraków, Poland
*corresponding author: matkor@iich.gliwice.pl

The environmental problem of the emission of hydrogen sulfide from stationary sources is serious, especially in the case of copper mines in Poland, where the ventilation airflow is 300,000 Nm^3/h, and contains 1-100 ppm H_2S. In catalytic chemical processes, the selection of the proper catalytic support is crucial for reactor optimization. The catalyst carrier should ensure a high surface area for the catalyst layer deposition and the highest possible heat and mass transport rates combined with minimal flow resistance. Amongst the possible structured rector internals, the most commonly spread in the industry are ceramic monoliths. Indeed, monoliths have unquestionable advantages over classical fixed-bed reactors. Their long straight channels give rise to very low flow resistance in the reactor. Also, they are relatively easy to cover with the active layer. However, at the same time, they show low mass and heat transport coefficients that result in long reactors making up for it. It occurs especially for processes of fast kinetics such as combustion [1]. Therefore, carriers that will provide more favorable transport properties compared to monoliths, with slightly higher flow resistances, are still sought after. To meet the requirements stated above it was decided to design and numerically investigate a new efficient structured catalyst support that could be in the future obtained by the additive 3D manufacturing method.

According to previous studies of structured reactors and literature investigations [2, 3] fractal geometries such as Hilbert's curve and Menger's cube were selected as new catalyst supports. Figure 1 shows the investigated structures. Momentum and energy simulations were performed using the CFD package ANSYS. The aim of numerical calculation was to determine pressure drop and Nusselt number in the function of Reynolds number. Simulations were carried out for air with constant physical properties.

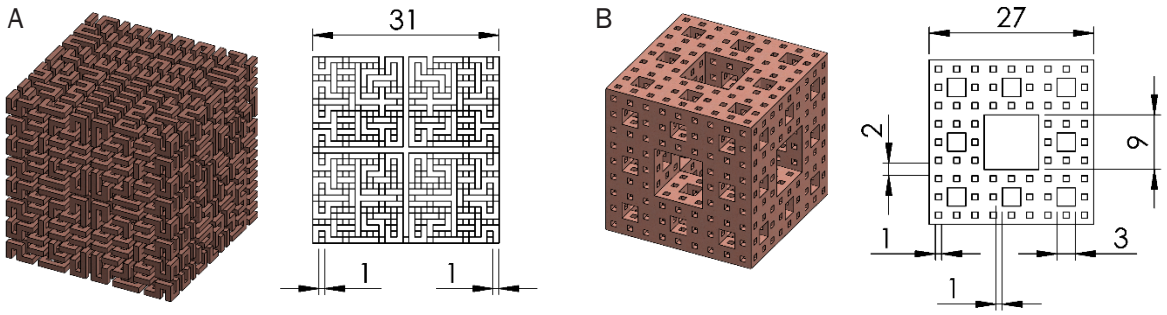

Fig. 1. Investigated catalytic supports. A) Hilbert's curve; B) Menger's cube

Acknowledgments
This work was supported by the Polish National Science Centre. Projects No. 2020/37/B/ST8/02859.

References

[1] Gancarczyk A., Iwaniszyn M., Piątek M., Korpyś M., Sindera K., Jodłowski P.J., Łojewska J., Kołodziej A., Catalytic combustion of low-concentration methane on structured catalyst supports, *Ind. Eng. Chem. Res.*, 2018, 57, 10281–10291.
[2] Iwaniszyn M., Piątek M.; Gancarczyk A., Jodłowski P. J., Łojewska J., Kołodziej A., Flow Resistance and heat transfer in short channels of metallic monoliths: experiments versus CFD, *Int. J. Heat Mass Transf.,* 2017, 109, 778–785.
[3] Bracconi M., Ambrosetti M., Maestri M., Groppi G., Tronconi E., A fundamental analysis of the influence of the geometrical properties on the effective thermal conductivity of open-cell foams, *Chem. Eng. Process. - Process Intensif.*, 2018, 129, 181–189.

COMPARISON OF METHODS FOR DETERMINING THE PARTICLE SIZE DISTRIBUTION OF SPRAY DRIED MALTODEXTRINE

Michał Krempski-Smejda[1,*], Marcin Piątkowski[1], Susana Simal[2], Paweł Wawrzyniak[1]

[1]Faculty of Process and Environmental Engineering, Lodz University of Technology, 213 Wolczanska St., 93-005 Lodz, Poland
[2] Department of Chemistry, University of the Balearic Islands, Ctra. Valldemossa, km. 7.5, 07122 Palma de Mallorca, Spain
*corresponding author: Krempski@p.lodz.pl

The vast majority of conducted technical experiments can be assigned into two fundamental approaches: white-box and black-box based methods. The first one is focused on internal process mechanisms. Due to the complexity and multitude of parameters, the experimental approach often assumes a black-box model. Depending on the input parameters, the output is observed. In this approach, based on changes in process conditions, the impact of these parameters on the product is determined. Therefore, for the black box model, it is crucial to correctly determine the parameters after the process is completed. One of such parameters widely used is analysis of particle size distribution (PSD) of obtained particles. There are many instruments for particle size distribution (PSD) measurement, each using a particular physical phenomenon to define the size. In this article a comparison of particle size distribution (PSD) obtained by measurement methods based on dynamic image analysis, static laser light scattering, and sieve analysis is presented.

Dynamic image analysis is suited for measurements of powders and granules. In this method, a stream of particles is recorded and analyzed by a camera system. Dynamic image analysis involves illuminating the particle stream from one side by a light source and recording particle images as shadow projections. During measurement particles are in motion which ensures particle separation. In the presented study the measurement was made for particles in an air stream. For each sample a minimum of 4 thousand particle images were detected. Different morphological parameters were recorded and quantitatively evaluated for detected particles. The particle size distribution was based on particles (d10, d50, d90). The results are presented in Figure 1.

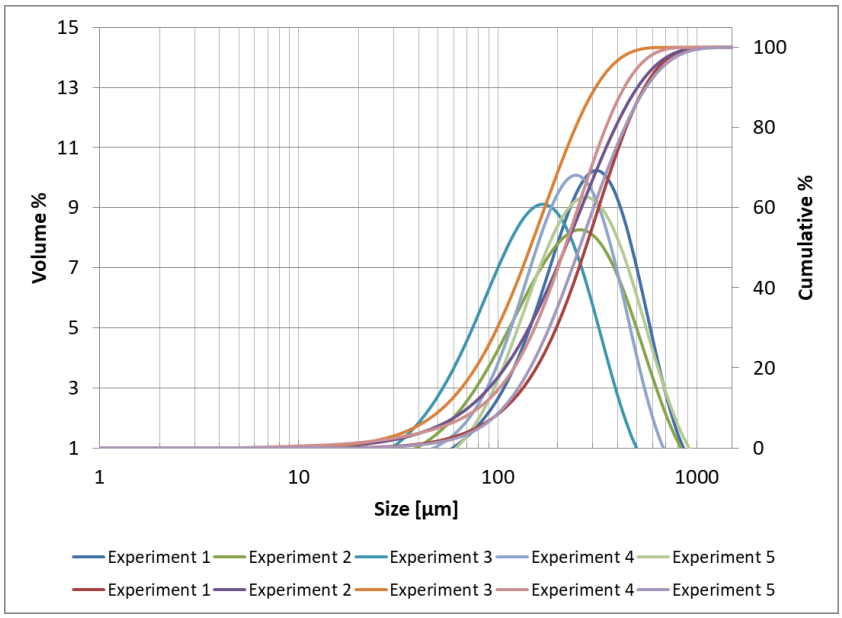

Fig. 1. Particle size distribution with cumulative curves

The second method was based on laser diffraction phenomena which occur when light interacts with particles resulting in certain angle-dependent patterns of light scattered by the particles in different directions. Scattering angle and intensity are dependent on the size of particles occurring in samples. For the static laser light scattering method three measurements were performed for each sample. The differences between measurements obtained by these methods are presented in Figure 2.

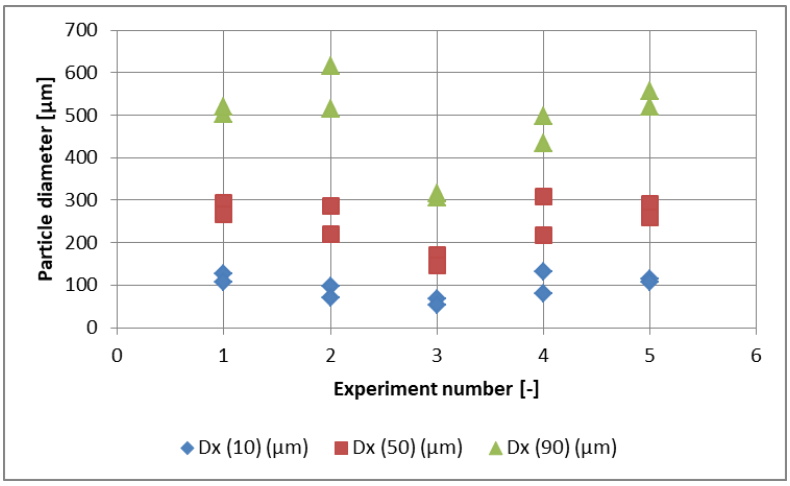

Fig. 2. Comparison of particle diameters d10, d50, d90

Both described methods were compared with a traditional method of determination of particle size distribution - sieve analysis. The sieve method enables to separate particle size fractions. In the presented study the mechanical sieving method was applied using HAVER EML DIGITAL PLUS Sieve shaker with ultrasonic sieving support AGS 35-100. 7 sieves with the following sizes of mesh: 20, 25, 32, 45, 63, 90, 125 µm were used during the tests.

The material used in the research was the product of the drying process of the 40% maltodextrin (Nowamyl S.A., Poland). Table 1 shows initial parameters of maltodextrin. The drying process was carried out in a spray tower in a counter-current mode with two pneumatic nozzles. The processes were carried out for two atomizing air intensities, three process temperatures, and three drying agent flow rates.

Table 1. Initial properties of maltodextrin used in the experiments

Parameter	Value
Form	Dried powder
Mechanical impurities	Absent
Moisture content, %	4.9
pH	6.0
Dextrose equivalent	11.74
Ash content, % dry mass	0.4%

The application of a wide range of process parameters allowed to obtain maltodextrin particles with different size distributions. At the same time, the used measuring techniques showed a similar trend of selected representative deposit diameters.

THE CONCEPT OF A MULTIPLE PARALLEL STREAM SEPARATOR (MPSS): DESIGN, CONSTRUCTION AND PRELIMINARY TESTS

Andżelika Krupińska[1]*, Sylwia Włodarczak[1]*, Magdalena Matuszak[1], Marek Ochowiak[1], Kamil Makowski[1]

[1]Poznan University of Technology, Department of Chemical Engineering and Equipment, M. Sklodowska-Curie 5, 60-965 Poznan, Poland
*corresponding authors: sylwia.wlodarczak@put.poznan.pl, andzelika.krupinska@put.poznan.pl

Human activities can have a strongly destructive impact on the environment, which in turn leads to the deterioration of peoples' living conditions. Life on our planet is dependent on water and oxygen. A person cannot survive a few minutes without oxygen, and a few days without water. Therefore, taking care of clean air and water plays a key role in human life. One of the first steps in the process of water purification is to clean it of the polluting solids that it carries with it. Solid-liquid separation is also a key stage in wastewater treatment, and is widely used in many industries, such as power industry, mining, or chemical and food industries. Despite appearances to the contrary, an extremely important stage is the initial purification of water. Separators are used for this purpose.

The purpose of this study was to design a modified vertical suspension separator, to make a laboratory-scale apparatus, and then to carry out tests using the constructed device.

The modification of the separator described elsewhere [1, 2] included the addition of partitions and shelves in the outer part of the apparatus. The proposed construction is shown in Figure 1.

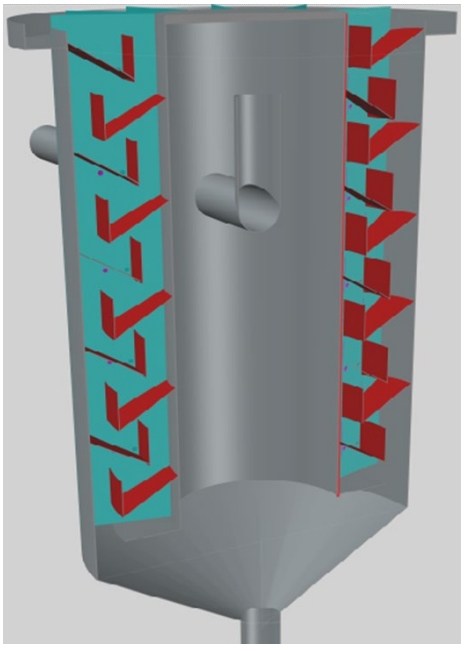

Fig. 1. The proposed modification of the apparatus

It was proposed to modify the outer part of the apparatus due to the fact that it is then possible to conduct the flocculation process constantly in this section and the simultaneous initial separation of the solid from the liquid in its inner part. Shelves will be installed in segments in order to avoid long shelves where solids could accumulate. The advantage of such a solution may be the possibility of removing a single segment, e.g. for maintenance purposes, or for regenerating an adsorbent and reassembling the shelf. The segments would be separated from each other by

partitions in order to avoid the flow of liquid around the shelves from the side. However, there is then a possibility of solids accumulating on a shelf. This is why the perforation of partitions at the height of the inside of the shelf was proposed.

In order to check whether the proposed modification can be used for the treatment of rainwater and sewage by separating the suspension (solid-liquid separation and light substances-liquid separation), tests were carried out. A volumetric flow rate of 0.1 m^3/h was used in each measurement. The test stand is shown in Figure 2.

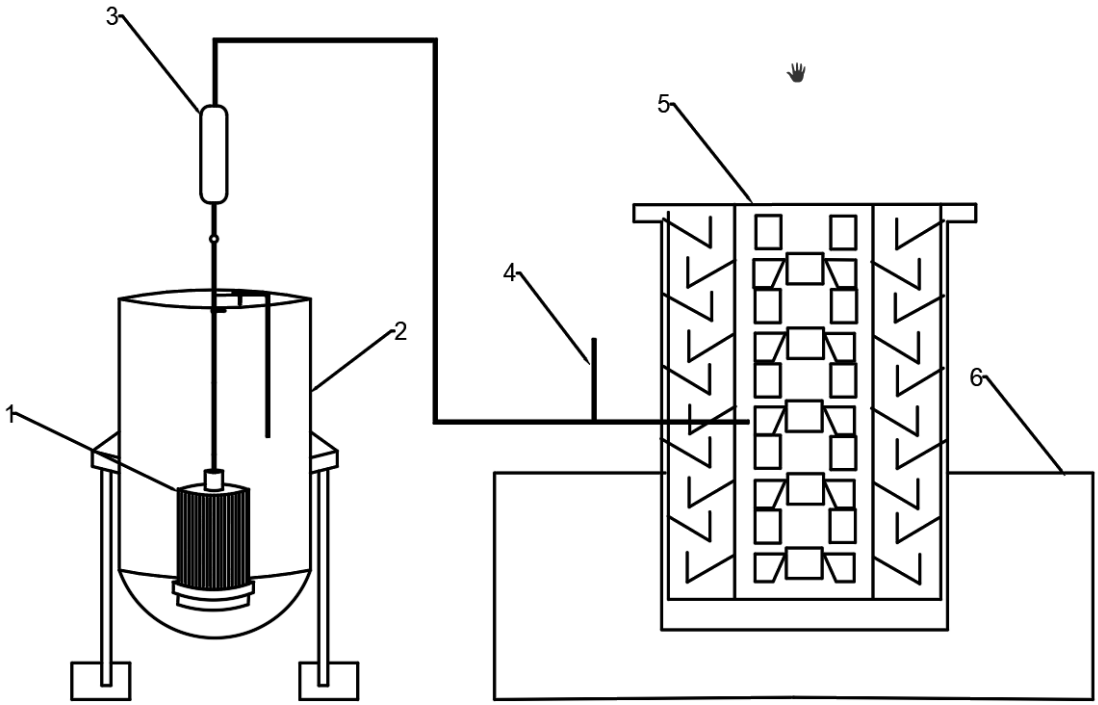

Fig. 2. Test stand; 1 –pump; 2 – liquid tank, 3 – rotameter; 4 – piping, tee pipe and dispenser; 5 –apparatus; 6 – clear liquid tank

The research material (heavy fraction) consisted of sand fractions selected with the use of sieve analysis. They had diameters of 100-150 μm and 300-400 μm. The constructed device showed a high, nearly 100%, efficiency of solid separation, and about 65% efficiency in the case of the oil fraction (η=72 mPa·s, ρ=886 kg/m^3). It should be emphasized that this efficiency decreased for smaller particles. Therefore, it is recommended to conduct further research on smaller grains, and also to perform comparative tests for a separator without shelves and partitions, as well as for a separator with a different number of shelves and a different angle of shelf inclination. It is also recommended to modify the overflow from the tank in order to be able to run tests for a longer period of the process. The modified design was less efficient in separating the oil phase from water, which could be caused by the direction of the inlet that supplies the mixture to the apparatus. In this part of the separator, the direction of water flow changes, and it is likely that oil particles are entrained together with the water.

Funding: The research was financed by the Polish Ministry of Education and Science (SBAD).

References

[1] Yao K.M., Theoretical Study of High-Rate Sedimentation, *J. Water Pollut. Control Fed.*, 1970.,42, 218–228.

[2] He Ch., Scott E., Rochfort Q., Enhancing sedimentation by improving flow conditions using parallel retrofit baffles, *J. Environ. Manage.*, 2015, 160, 1–6.

ANALYSIS OF BALL MILL EFFECTIVENESS – EXPERIMENTAL STUDY AND CFD SIMULATIONS

Radosław Krzosa[1], Łukasz Makowski[1]*, Wojciech Orciuch[1], Radosław Adamek[2]

[1]Warsaw University of Technology, Faculty of Chemical and Process Engineering, Warsaw, Poland
[2]ICHEMAD – Profarb sp. z o. o., Gliwice, Poland
*corresponding author: Lukasz.Makowski.ichip@pw.edu.pl

Titanium dioxide powders are commonly used in industry. Due to its high refractive index, this material is a white paint base. It also has photocatalytic properties. Therefore, it is used in the decomposition of organic compounds and the sterilisation process. Due to its high mechanical and chemical stability, it can be used as a coating. Combined with photocatalytic properties, it can be used to create an antimicrobial coating. Also, titanium dioxide can be used in hydrogen production reactions [1].

Due to its comprehensive application, a study on its processing is highly desired. Industrial-grade titanium dioxide consists of aggregates and agglomerates of primary particles. A final product's properties depend on the particles' structure, mostly on its size. Therefore, to obtain the desirable properties, breakage of particles must be applied. Hydrodynamic stresses can easily break agglomerates because the connection in this structure is made of weak van der Waals forces [2]. Connection in aggregates is made of solid bridges. Therefore, breakage of those structures requires more energy. To reduce the size of those particles, a unique design of devices is required. Mainly in this process, ultrasonic homogenisers and ball mills are used. Ultrasonic devices generate high-stress values but have poor performance. The ball mill breakage process can be carried out for dry powder and wet media. In this type of device, high-speed shaft rotation in a chamber causes the movement of balls. Collisions of balls cause high values of stresses that can break particles.

This work investigated the breakage of titanium dioxide particles in a ball mill. At first, the breakage mechanism of particles was investigated. Particle size distribution change in time was investigated via a Bechman&Coulter particle size analyser. Based on that, it was observed that most agglomerates are crushed in the first minutes of the breaking process. Further breakage caused the creation of a population of submicron particles and moved the aggregate population towards smaller sizes. The size range of submicron particles corresponds with the size of primary particles of titanium dioxide. Therefore, the hypothesis of the erosion mechanism of deaggregation was made. To prove that the population of submicron particles is made of primary particles of titanium dioxide, transmission electron microscopy with energy dispersive spectroscopy (TEM-EDS) was applied. This technique could identify the composition of each particle in the image.

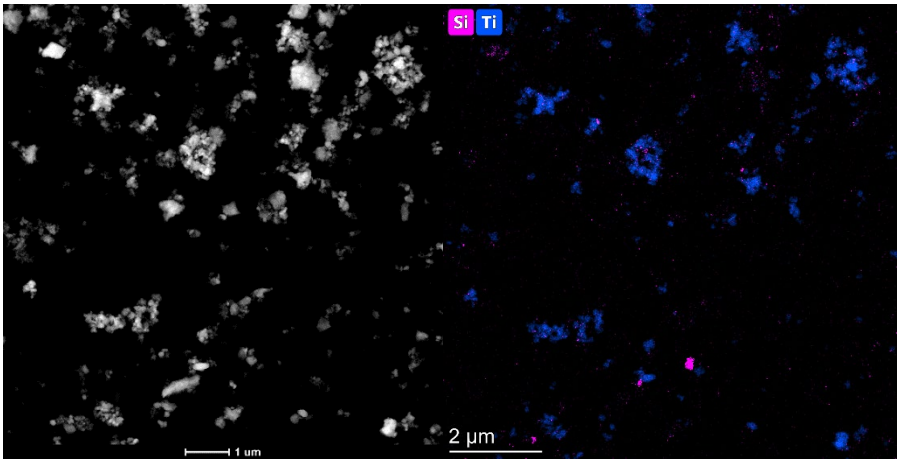

Fig. 1. TEM-EDS images of particles after milling

The influence of process parameters on the final particle size was investigated. The volume of the milling media and rotational speed was changed. Two types of milling media beads were tested. One size was in the range from 0.8 mm to 1.4 mm. The second size ranged from 0.1 mm to 0.2 mm.

In the modelling part, the Eulerian granular multiphase model was used to simulate the presence of milling beads in the mill chamber [3]. The rheology of suspension was applied via the Carreau model. Due to the high-speed rotation of shaft, turbulence k-ε model was used. Using a combination of those models allowed the reconstruction of the process. As a result, the flow pattern and the mean kinetic energy of milling beads were calculated. The stresses generated during the collisions and collision frequency were calculated based on it. Comparing the simulation result with the experiments showed that collision frequency controls the rate of size drop of TiO_2 particles.

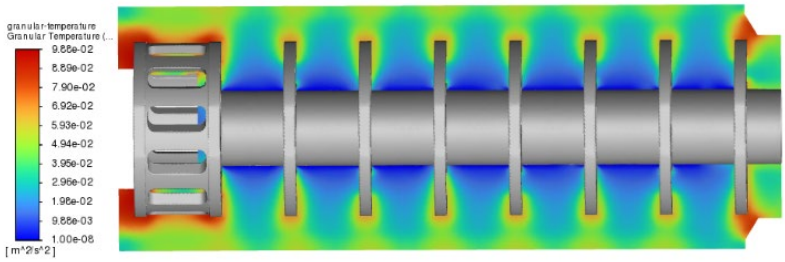

Fig. 2. Granular temperature of beads in a ball mill

References

[1] Krzosa R., Wojta, K., Golec J., Makowski Ł., Orciuch W., Adamek, R., Modelling particle deagglomeration in a batch homogeniser using full CFD and mechanistic models, *Chem. Process. Eng.-Inz. Chem. Proces.*, 2021, 42(2), 105-118.

[2] Krzosa R., Makowski Ł., Orciuch W., Adamek R., Population balance application in TiO2 particle deagglomeration process modeling. *Energies*, 2021, 14(12), 3523.

[3] Machado M.V., Santos D.A., Barrozo M.A., Duarte C.R., Experimental and numerical study of grinding media flow in a ball mill. *Chem. Eng. Technol.*, 2017, 40(10), 1835-1843.

PRODUCTION LINE FOR MULTI-INGREDIENT VEGETABLE AND FRUIT FROZEN FOOD PRODUCTS – PROCESS CONTROL, MATHEMATICAL MODELING AND OPTIMIZATION

Jan Krzysztoforski[1]*, Radosław Płotkowiak[2], Marek Henczka[1]

[1]Warsaw University of Technology, Faculty of Chemical and Process Engineering, Waryńskiego 1, 00-645 Warsaw, Poland
[2]Polski Ogród sp. z o.o, Mszczonowska 2, 02-337, Warsaw, Poland
*corresponding author: jan.krzysztoforski@pw.edu.pl

Modern production lines for manufacturing multi-ingredient vegetable and fruit frozen food products have to meet numerous technical and economic requirements, including high production capacity, smooth operation, maintaining the “cold chain” of all ingredients of the product, as well as a stable and repeatable composition of the final product – a plastic bag containing the frozen food product. In this work, the modernization of a production line in the manufacturing facility of Polski Ogród sp. z o.o., located in Skierniewice, Poland, is described, which was accompanied by the development of three tools, useful for process control, mathematical modeling and optimization.

As the first tool, a system for monitoring the composition of multi-ingredient vegetable and fruit frozen food transported along the production line was designed, constructed and launched. The system consists of 5 CCD cameras, a video recorder and a PC with software for image analysis. The software enables to estimate the current food composition at different locations at the production line, based on the color distribution in the HSV color space of the recorded video frames. The composition monitoring system controls the proper operation of the production line. It is also useful for detection of possible causes of inhomogeneous composition of the frozen food product.

As the second tool, a mathematical modeling method for heat transfer phenomena in the production line was developed. Submodels for various stages of the production process were created and used for performing numerical simulations of the considered manufacturing process. The developed method can be used to simulate gradual increase in the product temperature along the production line, depending on specific operational parameters, as well as to check various production scenarios and unusual situations for maintaining the “cold chain”.

As the third tool, a packing unit simulator was developed. The packing unit is the final apparatus, where each individual product bag is being packed with the frozen food composition, using numerous cups filled with the product, in order to obtain the desired final mass of the product bag. However, due to local inhomogeneities of the multi-ingredient product mixture, as well as the quasi-random nature of the packing process, packing results in some variations in the product composition in individual bags. The packing unit simulator enables the simulation of the packing process occurring in the packing unit, the estimation of realistic mass and composition distribution of a set of individual bags, and the development of optimum production recipes.

The modernization of the production line resulted in an increase of production capacity of the manufacturing facility, along with enhanced process stability. The three tools provided insight into the manufacturing process itself, to perform parametric analyses, to identify bottlenecks and intrinsic limitations of the production line performance, as well as to plan production strategies.

The work was financed by the European Regional Development fund in the Smart Growth Operational Programme 2014-2020, measure 1.1, submeasure 1.1.1.

References

[1] Krzysztoforski J., Boczkowski M., Załuski J., Płotkowiak, R. Henczka M., System monitorowania składu wieloskładnikowych mrożonek warzywnych i owocowych na linii produkcyjnej, *Inż. Ap. Chem*, 2018, 57, 5, 136-137.

[2] Krzysztoforski J., Załuski J., Płotkowiak, R. Henczka M., Modelowanie zjawisk wymiany ciepła w procesie produkcji wieloskładnikowych mrożonek warzywnych i owocowych, *Inż. Ap. Chem*, 2018, 57, 5, 138-139.

PRE-TREATMENT OF BIO FRACTION WASTE PRIOR TO DARK FERMENTATION

Karolina Kucharska*, Patrycja Makoś-Chełstowska, Edyta Słupek, Jacek Gębicki

Gdansk University of Technology, Faculty of Chemistry, Department of Process Engineering and Chemical Technology, 80-233 Gdansk, Poland
*corresponding author: karolina.kucharska@pg.edu.pl

Current efforts are taken to increase resource efficiency, close material loops, and improve sustainable waste and by-products management [1]. Increasing the amount of generated bio-waste streams and posing a significant environmental concern is considered in the context of circular economy to generate biofuel precursors by means of dark fermentation. Thus, efforts are made to increase resource efficiency and material circularity by networking agro-food by-products and converting them into valuable products completely exhausting the potential of the raw material [2]. The use of waste biomass containing both starch and lignocellulosic polymers for the production of biohydrogen is a process for which the simultaneous formation of value-added liquid products has been observed. Literature reports [3] and our own research [4], [5] also allow to conclude that the efficient implementation of the biohydrogen production process requires optimization of biomass pre-treatment stage. In the context of mixed waste, the so-called bio fraction, this treatment consists mainly of the saccharification of polysaccharides present in the raw material [6].

The greatest advantage of bio fraction application for biomass hydrolysates generation is the possibility of using a wide variety of substrates as input for the process. In countries, like Poland, where agro-food substrates are only available seasonally, the use of bio fraction waste can ensure constant access to the raw material used in fermentation processes [5]. However, in this case, anaerobic digestion requires optimization in terms of the average composition of applied raw material. For this purpose, substrate digestion must provide not only hydrogen-rich biogas but also nutrient and carbon rich digestate [6]. Further, the recovery of valuable nutrients from digestate is an important issue in closing the entire loop of biowaste valorisation.

Research was carried out in the field of pre-treatment of a bio fraction rich in both starch and lignocellulosic polymers prior to the definition of the key parameters and factors affecting the effectiveness of biomass digestion and further, the biohydrogen yield in the laboratory scale. Statistical methods have been employed to determine the parameters significantly affecting the results of the process. Comparison of the different process courses obtained in diversified conditions allowed to define the key parameters between biomass pre-treatment and biohydrogen production chains.

Model lignocellulosic and starch-based biomass were subjected to pre-treatment with the application of acidic compounds, i.e. sulphuric (SA) and acetic (AA) acids. The applied concentrations of acids were in the range from 2% up to 60%. The hydrolysis process (time) lasted from 1 h to 96 h and the process temperature (T) was in the range of 20–80 ^{0}C. The process has been carried with and without agitation (0 - 300 RPM). The proportion between biomass and hydrolysing agent amount (m/m) was in the range of 0.01 to 0.5 (by mass). The applied size (size) of the biomass ranged within 0,25 mm up to 4 mm. After saccharification, the hydrolysates were analysed via HPLC to determine the reducing sugars yield (sugar). Also, the concentration of value-added products was defined. Among the substances present in the hydrolysates, protein, peptides, hydroxybenzyl acid (HA), 5-HMF, furfural (FF), vanillin (V), vanillic acid (VA), formic acid (FA) and levulinic acid (LA) were found [7]. Further, the hydrolysates were introduced to dark fermentation, to determine, whether it is possible to carry out biohydrogen generation with hydrolysate based sole carbon sources. Depending on the hydrolysis parameters diversified yields of hydrogen were obtained. The development of dark fermentation with the application of acidic hydrolysates of bio waste fraction was confirmed. To define the effect of hydrolysis process parameters on the course of subsequent saccharification and dark fermentation, the data were normalised and correlogram

was prepared (Figure 1). Positive and negative correlation effects were determined according to the values presented in Figure 1.

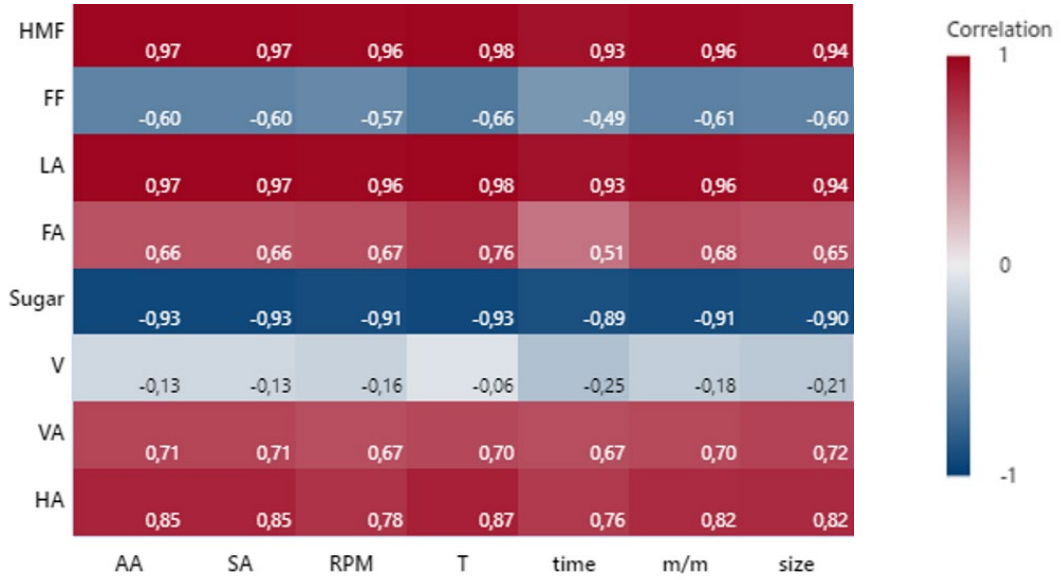

Fig. 1. Correlation between pre-treatment parameters and the saccharification product yield

The applied process parameters affected the main product yields during hydrolysis. Several products were formed in concentrations independent of the process parameters (V, VA, FA and FF), while HMF, LA, sugar, HA were obtained with strong relation to the process course. Concluding, the measurable effects of the research delivered information about the statistically important parameters for the process course, the range of experiment and the procedure allowing to manage the agro-food material via subsequent saccharification and dark fermentation.

This research was funded by the National Science Centre, Poland,under research project No. UMO-2021/41/B/ST8/02395

References

[1] Bundhoo Z.M.A., Potential of bio-hydrogen production from dark fermentation of crop residues: A review, *Int. J. Hydrogen Energy*, 2019, 44, 32, 17346–17362.
[2] Anwar Z., Gulfraz M., Irshad M., Agro-industrial lignocellulosic biomass a key to unlock the future bio-energy: A brief review, *J. Radiat. Res. Appl. Sci.*, 2014, 3, 1245–52.
[3] Faloye F.D., Gueguim Kana E.B., Schmidt S., Optimization of hybrid inoculum development techniques for biohydrogen production and preliminary scale up, *Int. J. Hydrogen Energy*, 2013, 38(27), 11765–11773.
[4] Kucharska K., Hołowacz I., Konopacka-Łyskawa D., Rybarczyk P., Kamiński M., Key issues in modeling and optimization of lignocellulosic biomass fermentative conversion to gaseous biofuels, *Renew. Energy*, 2018, 129, 384–408.
[5] Kucharska K., Łukajtis R., Słupek E., Cieśliński H., Rybarczyk P., Kamiński M., Hydrogen production from energy poplar preceded by MEA pre-treatment and enzymatic hydrolysis, *Molecules*, 2018, 23, 11, 3029.
[6] Łukajtis R., Rybarczyk P, Kucharska K, Konopacka-Łyskawa D, Słupek E, Wychodnik K, Kamiński M., Optimization of saccharification conditions of lignocellulosic biomass under alkaline pre-treatment and enzymatic hydrolysis, *Energies*, 2018, 11(4), 886.
[7] Makoś-Chełstowska P., Słupek E., Kucharska K., Kramarz A., Gębicki J., Efficient Extraction of Fermentation Inhibitors by Means of Green Hydrophobic Deep Eutectic Solvents, *Molecules*, 2022, 27, 157.

SULFUR REMOVAL FROM METHANOL FOR FUEL CELL APPLICATIONS

Michał Lewak, Robert Cherbański, Andrzej Stankiewicz, Eugeniusz Molga*

Faculty of Chemical and Process Engineering, Warsaw University of Technology,
Waryńskiego 1, 00-645 Warszawa

*corresponding author: eugeniusz.molga@pw.edu.pl

Among the different fuel cell types available, the SOFC technology is distinguished among others by fuel flexibility as all: diesel, methane, methanol, syngas, ammonia, bio-methanol, hydrogen and natural gas can be used. Besides hydrogen and methane all other fuels warrant a fuel reformer and cleaning system prior to feeding it to the stack. For SOFCs, particularly removal of sulfur contamination is crucial as the content of sulfur compounds is strictly limited by their producers to a few ppm's or even ppb's.

In this paper removal of sulfur compounds from methanol is considered, as their presence is often detected while methanol is contaminated by diesel or gasoline. Significant amounts of sulfur compounds are also present in methanol when it is obtained as a by-product in pulp production [1].

Purification of methanol by adsorption was here investigated for the following testing system: dibenzothiophene (DBT) – activated carbon (AC), where DBT was taken as a representative of contaminating sulfur compounds. An appropriate model of the adsorption column packed with activated carbon pellets was elaborated and a series of simulations was carried out.

The analysis of adsorptive purification process was carried out for the system shown in Fig. 1.

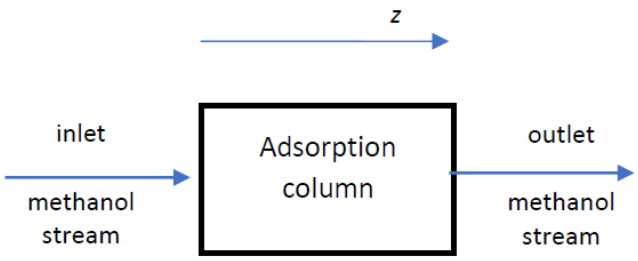

Fig. 1. Schematic diagram of the adsorption column

The following model equation describing the mass balance for DBT in the packed bed was used to determine the concentration profiles along the considered adsorption column at different time moment:

$$\varepsilon \frac{\partial c}{\partial t} = -\varepsilon\, u\, \frac{\partial c}{\partial z} + D_L \frac{\partial^2 c}{\partial z^2} - (1-\varepsilon)\, \rho_s\, \frac{\partial q}{\partial t} \tag{1}$$

where ε – is the bed porosity, u – liquid velocity and ρ_s – density of solid pellets, while c [mol/m^3] and q [mol/kg] are DBT concentrations in liquid and solid phases, respectively. Axial dispersion was also taken into account and the appropriate dispersion coefficient calculated from the following relationship [2]:

$$D_L = u\, d_s \left(\frac{\varepsilon}{\sqrt{2}\, Re\, Sc} + \frac{1}{2} \right) \tag{2}$$

Adsorption equilibrium was described with the Langmuir equation [2]:

$$q_e = \frac{q_m K_L c}{1 + K_L c} \tag{3}$$

while the adsorption kinetics with a pseudo-second order model [2]:

$$\frac{dq}{dt} = k_{2,ad}(q_e - q)^2 \quad (4)$$

The constants (K_L, q_m and $k_{2,ad}$) appearing in Equations (3 and 4) were taken from the work [2], then the presented model was implemented in the MATLAB domain and solved with the application of Danckwerts boundary conditions.

Simulation calculations were carried out to find the influence of operating conditions on purification process efficiency. For the process performed at ambient temperature the following inlet and operating conditions were examined: - inlet concentration of DBT in methanol stream, - bed porosity, - liquid velocity in the bed.

An example of the obtained results is shown in Fig. 2, where DBT concentration in methanol is shown as a function of time and location along the adsorbent bed.

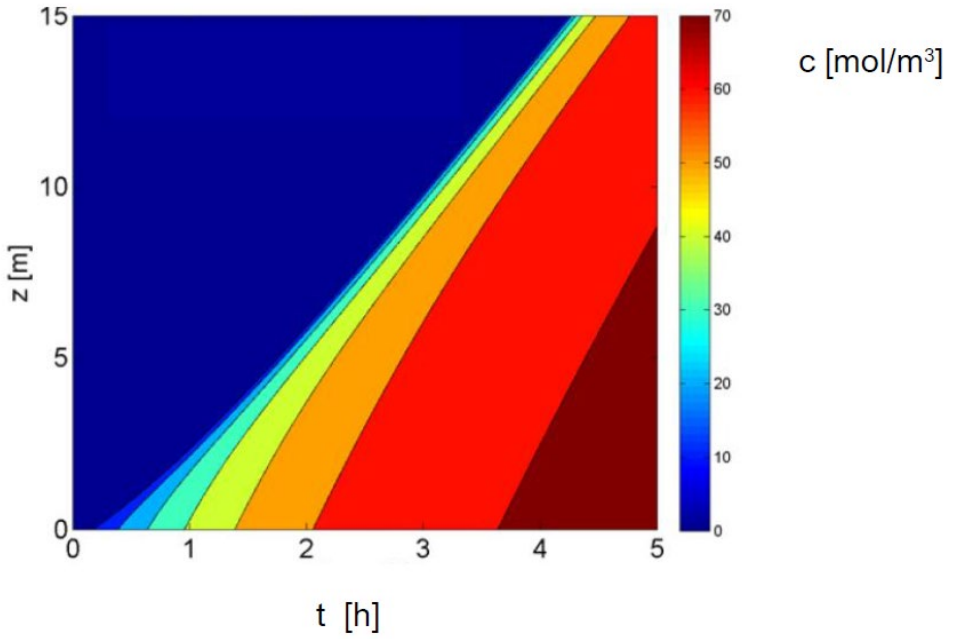

Fig. 2. DBT content in methanol as a function of time and location along the adsorption column

With data presented in Fig. 2 an operating diagram indicating the breakthrough time at chosen column dimensions and operating conditions can be constructed. Then the obtained results can be utilized for effective designing of an installation for purification of raw methanol before feeding it to the converter and further to the SOFC.

The investigated adsorptive method of sulfur removal is very promising. However, the problem of sorbent regeneration after its saturation with removed sulfur compounds remains still very relevant.

Acknowledgments

This work is part of the European Union's Horizon Europe research and innovation program "FuelSOME" under Grant Agreement No. 101069828, funded by the European Union. Views and opinions expressed are however those of the authors only and do not necessarily reflect those of the European Union. Neither the European Union nor the granting authority can be held responsible for them.

References

[1] International patent WO 2015/05370404 A1.
[2] Wen J., Han X., Lin H., Zheng Y., Chu W., A critical study on the adsorption of heterocyclic sulfur and nitrogen compounds by activated carbon: Equilibrium, kinetics and thermodynamics, *Chem. Eng. J.*, 2010, 164(1), 29–36.

CFD MODELLING EFFECT OF CATALYST ARRANGEMENT IN DRY METHANE REFORMING

Michał Lewak*, Leszek Rudniak

[1]Warsaw University of Technology, Faculty of Chemical and Process Engineering, Waryńskiego 1, Warsaw, Poland
*corresponding author: Michal.Lewak@pw.edu.pl

Online data [1] show that around three-quarters of hydrogen is produced using fossil fuels. The main substrate used in this process is purified natural gas - methane. The methane reforming process is carried out using a solid catalyst, which consists of atoms of elements such as: Ni, Pt, Rh, Ru.[2] The elements are deposited on a solid carrier such as: Al2O3, TiO2, MgO [2, 3]. There are three methods of producing hydrogen from methane. The first method is the so-called steam reforming of methane SRM, in which methane is decomposed into syngas components, i.e. hydrogen and carbon monoxide, with the help of steam. This method is quite expensive, because it requires the supply of heat associated with the transition of water into steam. The second method is dry reforming of methane DRM. This method uses carbon dioxide gas to convert methane to syngas. Both methods are characterized by a fairly large endothermic effect of the reaction, which increases the cost of syngas production. The third method is the partial oxidation of methane POX leading to the formation of syngas. The POX method, unlike the other two methods, is an exothermic process with a reaction energy of -38 kJ/mol. An important issue is the ratio of hydrogen to carbon monoxide. With the DRM method, this ratio fluctuates around unity [2]. In the POX method, it is about 2 [2] and in the SRM method, the ratio of hydrogen to carbon monoxide is 3 [2]. The ratio of syngas components is crucial due to its use in the production of methanol, ammonia or methyl ether. This work focuses on the problem of placing the catalyst in the reactor in the process of converting methane with carbon dioxide. This process is highly endothermic, therefore the arrangement of the catalyst lumps in the reactor may affect the course of the entire process of obtaining syngas. A mathematical model of forty-one surface reactions on the Ni/Al2O3 catalyst was used to describe the methane reforming process [4]. The mathematical model can be applied to both dry and steam methane reforming. The kinetic model was implemented for CFD calculations using the Chemkin format available on an internet site [5]. The five basic reactions involved in dry methane reforming are listed below:

$$CH_4 + CO_2 \leftrightarrow 2H_2 + 2CO \quad (\Delta H^0_{298K}=247 kJ/mole) \tag{1}$$

$$H_2 + CO_2 \leftrightarrow CO + H_2O \quad (\Delta H^0_{298K}=41 kJ/mole) \tag{2}$$

$$CH_4 \leftrightarrow C_{(s)} + 2H_2 \tag{3}$$

$$2CO \leftrightarrow C_{(s)} + CO_2 \tag{4}$$

$$H_2 + CO \leftrightarrow C_{(s)} + H_2O \tag{5}$$

Reactions (3–5) are catalyst deactivation reactions as carbon is deposited on the active sites of the catalyst. This makes it difficult for reagents to access the catalyst surface and thus inhibits the reforming process. The data in the literature show that there are two basic methods of counteracting this process. The first consists in conducting the process at a sufficiently high temperature, and the second in the appropriate ratio of molar streams of methane and carbon dioxide F_{nCO2}/F_{nH2} [2, 6]. Therefore, simulations were carried out for process parameters in which Reactions (3-5) did not occur. Figure 1 shows the distribution of the mole fraction of methane in the reactor cross-section with the axial arrangement of catalyst particles. The catalyst was placed on a special wire mesh, which was omitted in the geometrical model. Figure 2 shows the distribution

of the mole fraction of hydrogen in the cross-section of the converter. In the simulation, it was assumed that the reactor wall had a constant value of the temperature **Twall**.

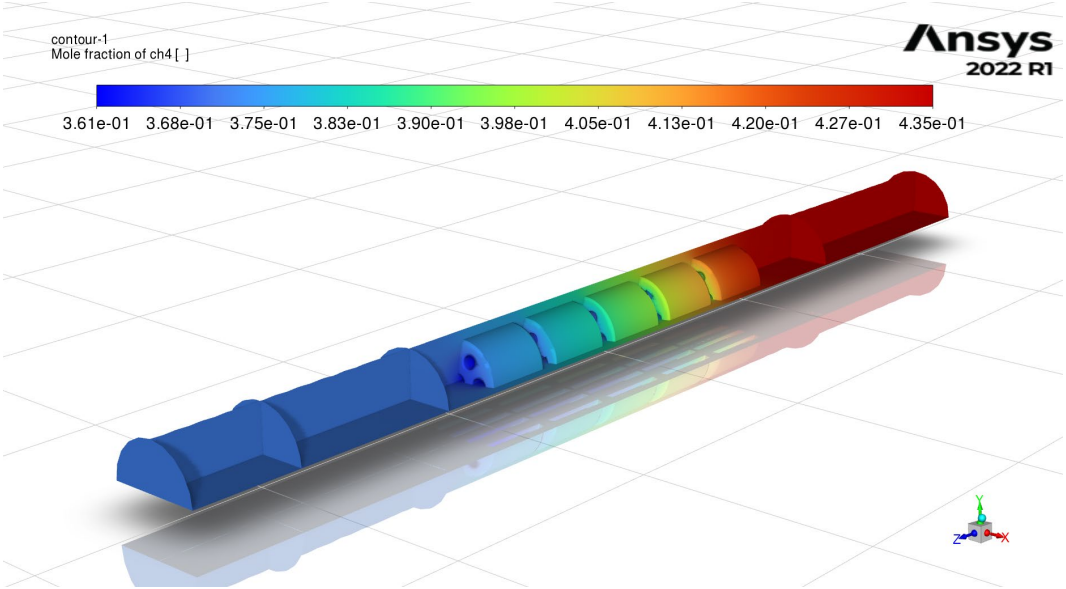

Fig. 1. The distribution of the mole fraction of CH_4 in the reactor, F_{nCO2}/F_{nCH4}=1.3;Twall=1073.15 [K]

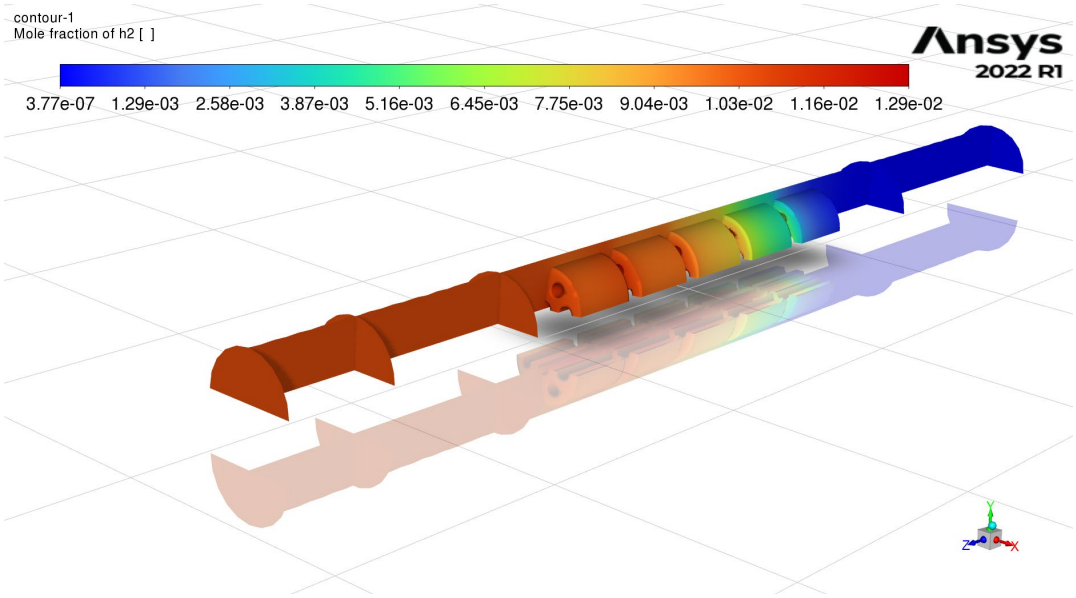

Fig. 2. The distribution of the mole fraction of H_2 in the reactor, F_{nCO2}/F_{nCH4}=1.3;Twall=1073.15 [K]

References

[1] https://www.iea.org/reports/the-future-of-hydrogen, access 14.02.2023.
[2] Shah Y.T., Gardner T.H., Dry reforming of hydrocarbon feedstocks, *Catalysis Reviews*, 2014, 56(4), 476-536.
[3] Sandoval-Diaz L.E., Schlögl R., Lunkenbein T., *Quo Vadis Dry Reforming of Methane?—A Review on Its Chemical, Environmental, and Industrial Prospects. Catalysts*, 2022, 12,465.
[4] Maier L., Schadel B., Herrera Delgado K., Tischer S., Deutschmann O., *Steam Reforming of Methane Over Nickel: Development of a Multi-Step Surface Reaction Mechanism, Top Catal*., 2011, 54, 845–858.
[5] *https://www.detchem.com/mechanisms*, access 14.02.2023.
[6] Osaki T., Horiuchi T., Suzuki K., Mori T., Suppression of carbon deposition in CO_2-reforming of methane on metal sulfide catalysts, *Catal. Letters*, 1995, 35, 39-43.

CFD INVESTIGATION ON SOLID CIRCULATION RATE IN A MODIFIED WURSTER APPARATUS FOR DRY COATING

Wojciech Ludwig[1]*, Viraj Pawar[2]

[1]Wroclaw University of Science and Technology, Department of Process Engineering and Technology of Polymer and Carbon Materials, Gdanska 7/9, 50-344, Wroclaw, Poland
[2]Wroclaw University of Science and Technology, Faculty of Chemistry, Chemical and Process Engineering, Norwida 4/6, 50-373, Wroclaw, Poland
*corresponding author: wojciech.ludwig@pwr.edu.pl

Spouted bed devices have been widely used in energy, chemical, pharmaceutical, and food industries, wherever granular materials are applied. Solid circulation rate is the most crucial parameter that affects the performance of spouted bed columns [1].

The main aim of this work was to use computational fluid dynamics (CFD) methods for calculation of the solid circulation rate for different geometric and hydrodynamic parameters in a modified Wurster apparatus for dry coating.

Fig. 1 shows the modelled device. It is made up of three cylindrical sections and a cone. All parts are equipped with a draft tube (f). A spouting gas nozzle (a) is installed at the bottom of the apparatus where particles are entrained and accelerated. The cone has two openings for loading and unloading solids. In this zone a liquid (c) and a powder (b) spraying nozzle are placed. In the upper draft tube above the nozzles the circulating solid is coated. The upper section is finished by a deflector (d), which prevents particles from being blown away from the installation.

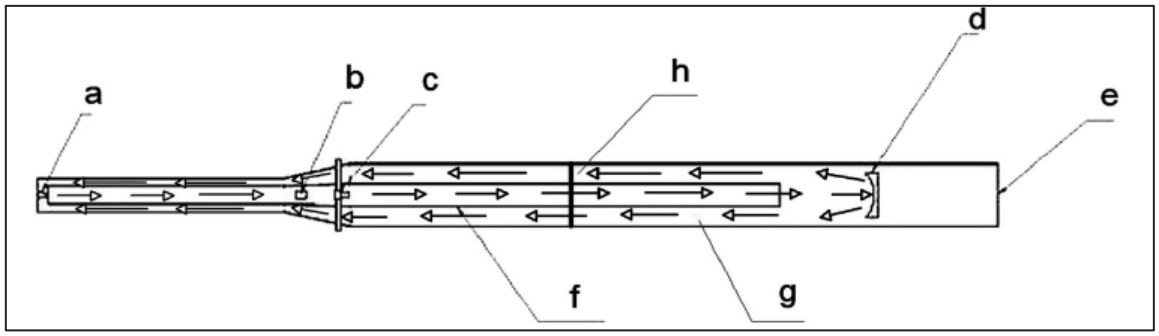

Fig. 1. Cross-section of the modelled column: a – spouting air nozzle, b – powder spraying nozzle, c – liquid spraying nozzle, d – deflector, e – air outlet, f – draft tube, g – annular zone, h - localization of simulation data reading (arrows show the direction of particle circulation) [2]

To perform simulations of the movement of both phases (air and particles) in the device, Ansys CFD package was applied. A discrete phase model (DPM) with unsteady particle tracking and phase coupling served the purpose of determining the solid circulation rate. Air (constant density of 1.22 kg/m^3, constant viscosity of $1.79 \cdot 10^{-5}$ Pa·s) and Cellets® 1000 particles (density of 1570 kg/m^3, mean diameter of 1.11 mm), respectively, were the continuous and discrete phases.

The k-ε realizable turbulence model, which provides improved predictions of turbulence in jets, described the turbulent flow of air. The stochastic tracking model predicted dispersion of particles due to turbulence in the continuous phase. Because the multiphase flow in the modelled apparatus

was quasi-stationary and the instantaneous values of the calculated parameters (particle velocity and volume fraction) in the selected cross-section (see Fig. 1) were characterized by periodical fluctuations, they had to be averaged. The solver settings and the calculation algorithm were presented in detail in the previous paper [2].

The solid circulation rate was calculated with the following formula:

$$\dot{m} = a \times A \times w \times \rho \tag{1}$$

where a is the mean volume fraction of the particles, A is the cross-section area of the upper draft tube, w is the mean velocity of the particles and ρ is the density of the particles.

At the beginning, simulations were performed for various spouting gas velocities (278-490 m/s) and solid volumes (200, 300, 400 cm^3) for the standard geometry of the apparatus. After that, the geometry configuration was altered, including the deflector distance with respect to the upper draft tube (10, 30, 60 and 120 mm), the lower draft tube radius (15, 20, 25 and 30 mm) and entrainment zone length (5, 10, 20, and 30 mm), while their effect on solid circulation rate were checked for the volume of the poured bed equal to 200 cm^3 and the minimum stable circulation velocity of the spouting gas (278 m/s).

The solid circulation rate increased slightly with the steady increase in the spouting gas velocity for a small bed volume of 200 cm^3 and reached a maximum at 370 m/s. When the capacity of the poured bed was increased to 300 and 400 cm^3, the solid circulation rate rose rapidly and linearly with the rise in the spouting gas velocity.

The solid circulation rate was greatly influenced by the distance between the draft tube outlet and the deflector. It was observed that the increase in the value of this parameter entailed an increase in solid circulation rate. As the distance increased, the effect of the deflector on the movement of the particles disappeared and they could move more freely.

The solid circulation rate augmented when the diameter of the lower draft tube was increased as it provided more area for particles to flow. However, when the radius was increased to 30 mm, this diminished the size of the annulus between the lower draft tube and the outer wall of the apparatus, which ultimately restricted the motion of particles into the draft tube and hence the solid circulation rate was decreased.

The solid circulation rate increased with the enlargement of the length of the entrainment zone. It was obvious that increasing this factor resulted in the increase in the space where particles became sucked into the draft tube and ultimately augmented the solid circulation rate.

It can be concluded that the application of the discrete phase model enabled to test the impact of the main constructional and hydrodynamics parameters on the solid circulation rate which is very difficult to determine experimentally. CFD is an efficient tool to investigate complex multiphase flow in the modified Wurster apparatus and can be applied to optimize the construction of this device in the future.

References

[1] Ar F.F., Uysal, B.Z. , Solid circulation in a liquid spout-fluid bed with multi draft tubes, *J. Chem. Technol. Biot.*, 1999, 72(2), 143-148.

[2] Ludwig W., Płuszka P., Euler-Lagrange model of particles circulation in a spout-fluid bed apparatus for dry coating, *Powder Technol.*, 2018, 328, 375-388.

CONVERSION OF GALACTOSE BASED ON LIGNOCELLULOSIC BIOMASS WITH THE PARTICIPATION OF A CATALYST BASED ON NATURAL ZEOLITE

Igor Łabaj, Marcin Piotrowski, Izabela Czekaj, Natalia Sobuś*

Tadeusz Kosciuszko Cracow University of Technology, Faculty of Chemical Engineering and Technology, Warszawska 24, 31-155 Krakow, Poland

*corresponding author: natalia.sobus@pk.edu.pl

Lignocellulosic biomass is a potential application as a renewable raw material for the production of energy, heat, fuels or chemicals [1]. Due to its diverse structure, depending on the origin and the method of modification, it can be a valuable source for obtaining chemical compounds, including carboxylic acids [2]. One of the potential possibilities is the catalytic conversion of biomass, in particular the hemicellulose fraction, to obtain levulinic acid using catalysts, including appropriately modified synthetic and natural zeolites [3, 4].

In this study, the conversion of biomass based on galactose was carried out with the use of a suitably modified natural zeolite - clinoptilolite. Catalysts with active centers - copper, were obtained using the sonication technique. Tests were also carried out to determine the optimal conditions of the catalytic process and for this purpose the one-pot method was used, where the concentration of the raw material in the aqueous solution was prepared and a previously modified natural zeolite was added. The galactose conversion process was carried out at the temperature of 250 °C for 5 h, and the identification of the obtained products was performed using HPLC-RID along with the comparison of retention times with standard substances. Table 1 presents the results along with the conversion of the raw material. The selectivities of the products relative to each other and the carbon balance were determined.

Table 1. Results of catalytic tests of galactose conversion

Catalyst	Raw material	Raw material conversion [%]	Conversion products - selectivity [%]								Carbon balance [%]
			5-HMF	LAC	FA	LA	AC	PAC	AD	PA	
CLI	Galactose	100	-	9.3	-	33.9	5.1	22.1	18.4	11.1	99.9
H-CLI	Galactose	100	-	8.1	-	34.6	3.4	18.6	20.6	14.7	99.9
Cu-H-CLI	Galactose	100	7.7	3.7	-	42.1	5.3	32.1	4.9	4.2	100.0
Co-H-CLI	Galactose	100	7.3	4.7	6.1	45.5	4.8	21.0	4.3	6.2	99.9

Acknowledgments

This work was financially supported by the National Science Centre, Poland under grant no. UMO-2021/41/N/ST5/00084

References

[1] Guragain Y.N., Vadlani P.V., Renewable Biomass Utilization: A Way Forward to Establish Sustainable Chemical and Processing Industries*, Clean Technol*., 2021, 3, 243-259.
[2] Bert Boekaerts B., Sels B.F., Catalytic advancements in carboxylic acid ketonization and its perspectives on biomass valorisation, *Appl. Catal. B: Environ.*, 2021, 283, 119607.

[3] Qazi U.Y., Javaid R., Ikhlaq A., Khoja A.H., Saleem F. A., Comprehensive Review on Zeolite Chemistry for Catalytic Conversion of Biomass/Waste into Green Fuels. *Molecules*, 2022, 27, 8578.
[4] Sobuś N., Król M., Piotrowski M., Michorczyk B., Czekaj I., Kornaus K., Trenczek-Zając A., Komarek S., Conversion of dihydroxyacetone to carboxylic acids on pretreated clinoptilolite modified with iron, copper, and cobalt, *Catal. Commun*., 2022, 171, 106509.

KINETICS OF FLUORESCENT GOLD NANOCLUSTER DEPOSITION AT SOLID/LIQUID INTERFACES

Julia Maciejewska-Prończuk[1,2]*, Paulina Żeliszewska[2], Katarzyna Matras-Postołek[1], Monika Wasilewska[2], Marta Gajewska[3], Patrycja Gnacek[2], Ditta Ungor[4], Edit Csapó[4,5], Magdalena Oćwieja[2]

[1]Cracow University of Technology, Department of Chemical and Process Engineering, Warszawska 24, 31-155 Krakow, Poland
[2]Jerzy Haber Institute of Catalysis and Surface Chemistry, Polish Academy of Sciences, Niezapominajek 8, 30-239 Krakow, Poland
[3]AGH University of Science and Technology, Academic Centre for Materials and Nanotechnology, Mickiewicza 30, 30-059 Krakow, Poland
[4]MTA-SZTE Lendület „Momentum" Noble Metal Nanostructures Research Group, University of Szeged, H-6720 Rerrich B. sqr. 1, Szeged, Hungary
[5]Interdisciplinary Excellence Center, Department of Physical Chemistry and Materials Science, University of Szeged, H-6720 Rerrich B. sqr. 1, Szeged, Hungary
*corresponding author: julia.maciejewska-pronczuk@pk.edu.pl

Fluorescent gold nanoclusters synthesized in a protein matrix attract a lot of attention in biomedical research due to their stability, high fluorescence and low toxicity [1]. It is important to note there is no literature describing examples of applications of nanoclusters in the form of layers and films deposited on solid surfaces. It can be assumed that this limitation results from the lack of available data on the methods of obtaining such materials. The aim of the research was to determine the deposition mechanism of fluorescent gold nanoclusters obtained using hen egg white lysozyme (HEWL) on a model silicon surface under convection controlled transport by applying quartz crystal microbalance (QCM) measurements and atomic force microscopy (AFM).

The initial stage of research was the synthesis of gold nanoclusters with the use of HEWL. The obtained hydrosols of nanoclusters were purified by membrane ultrafiltration. The physicochemical characterization of gold nanoclusters dispersed in hydrosols provided information on the hydrodynamic diameter, the extent of their stability and electrical properties. The isoelectric point of gold nanoclusters on HEWL matrix was determined at pH equal to 5.0. The aggregation of studied nanomaterials (increase in values of hydrodynamic diameters) was observed in the pH range of 4.0-6.0. The gold nanoclusters on protein matrices were characterized by a positive surface charge in acidic medium, while in neutral and basic medium they showed a negative surface charge. The measurements of emission spectra over a wide range of ionic strengths (0.0001 M - 0.15 M) and pH (2.0-11.0) were determined. The above data was important for the selection of conditions for the deposition of gold nanoclusters on solid surfaces.

The most important stage of the research was to determine the kinetics of nanocluster deposition using: Quartz Crystal Microbalance with energy dissipation monitoring (QCM-D), streaming potential measurements, surface imaging by AFM and scanning electron microscopy (SEM). The deposition measurements were carried out in both acidic (pH 3.5) and basic (pH 9.0) environments for ionic strengths in the range of 0.0033 M - 0.15 M. An example of the deposition kinetics of a monolayer of gold nanoclusters is shown in Fig. 1. The effect of the presence of a positively charged anchoring layer of polydiallyldimethylammonium chloride (PDDA) was investigated on the maximum degree of surface coverage by particles. Changing the pH and ionic strength had a significant effect on the maximum degree of particle surface coverage. These measurements made it possible to confirm the research hypothesis that the self-organization process of gold nanoclusters, leading to the formation of layers on the silicon surface, was controlled by electrostatic interactions. Desorption measurements showed high stability of the formed layers of gold nanoclusters. The topography of the monolayers was also measured using

AFM. The images confirmed the presence of dense and homogeneous layers. The streaming potential measurements (SP) provided information on the electrokinetic properties of the layers.

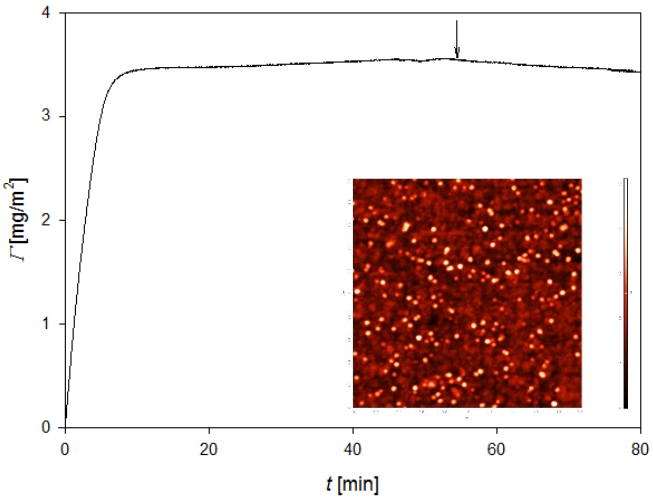

Fig. 1. Examplary QCM measurements of gold nanocluster deposition at the PDDA modified silica sensor and AFM image of the obtained monolayer (in the right corner). Measurement conditions: bulk suspension concentration c = 10 mg·L^{-1}, ionic strength I = 0.0033 M, pH = 9.0 and flow rate u = 0.00133 cm^3·s^{-1}; T = 298 K

Acknowledgments

The research presented in the presentation was financed by the National Science Center – MINIATURA research project no. 2021/05/X/ST5/00244.

References

[1] Ghosh R., Sahoo A.K., Ghosh S.S., Paul A., Chattopadhyay A., Blue-emitting copper nanoclusters synthesized in the presence of lysozyme as candidates for cell labelling, *ACS Appl. Mater. Interfaces*, 2014, 6(6), 3822-3828.

PRODUCTION OF MULTIPLE EMULSION IN A VESSEL WITH A STIRRER

Marta Major-Godlewska*

West Pomeranian University of Technology, Faculty of Chemical Technology and Engineering,
Szczecin, Piastów 42, 71-065 Szczecin, Poland
*corresponding author: mmajor@zut.edu.pl

The structure and size of droplets of the inner phase of a multiple emulsion may be influenced by the method of its production or the emulsifier used. In the preparation of multiple emulsions, Span 80, Tween 20 or Tween 80 are used as emulsifiers. It is especially worth paying attention to the use of natural emulsifiers in the production of multiple emulsion in the food, cosmetic or pharmaceutical industries. One such natural emulsifier is lecithin.

Lecithin, due to its emollient properties of the epidermis through which the proper active ingredient can penetrate, can be used in the production of multiple emulsions used in the pharmaceutical or cosmetic industries. Lecithin belongs to the group of natural, amphoteric emulsifiers [1, 2].

The aim of the research was to define the structure of the emulsion produced, including the size of the internal phase droplets and to study the rheological properties of the multiple emulsion produced using soya lecithin as the emulsifier. The tests were carried out for two different stirring times with the use of two different amounts of lecithin and two different types of stirrers.

The stirred vessel was used to produce the emulsion. Two different stirrers were used in the tests. The geometrical parameters of the vessel were: the vessel of inner diameter D = 0.1 m, the height of the liquid $H = 0.5D$ and four standard planar baffles $B = 0.1D$. The liquids used in the tests were: distilled water as water phase, refined sunflower oil produced for Jeronimo Martines Polska S.A. as the oil phase. Sudan III (producer: Eurochem BGD Sp.z o. o.) was used to color the oil. Lecithin from soya beans produced for Vemica was used as the emulsifier.

The evaluation of the structure and droplet size of the produced emulsion was performed using the diagnostic inverted microscope OPTA-TECH MW 100, with software and digital camera OPTA-TECH 5MP. The rheological measurements of multiple emulsion samples were carried out on a rheoviscometer of type RT 10 manufactured by Haake.

The influence of the stirring time, the type of stirrers used in the emulsion production and the amount of lecithin used as the emulsifier on the structure of the emulsion produced and on the size of the internal phase droplets were determined on the basis of the tests data. The results of the tests were presented in the form of images of the structures of the obtained emulsions. Droplet size and rheological properties are presented graphically. The obtained rheological data were described with appropriate models.

References

[1] Molski M., *Chemia piękna*, Warszawa, WN PWN SA, 2009.
[2] Brud W.S., Glinka R., *Technologia kosmetyków*, Łódź, Wyd. MA, 2001.

THE APPLICATION OF METABOLOMICS FOR INTERPRETATION OF ANTIOXIDANT ACTIVITY RESULTS FROM FUNGUS-RESISTANT GRAPE VARIETIES CULTIVATED IN POLAND

Magdalena Anna Malinowska[1,*], Manon Ferrier[2], Marin Pierre Gemin[2], Nathalie Guivarc'h[2], Arnaud Lanoue[2]

[1]Cracow University of Technology, Faculty of Chemical Engineering and Technology, Institute of Organic Chemistry and Technology, Warszawska 24, 31-155 Cracow, Poland
[2]EA 2106 «Biomolécules et Biotechnologie Végétales», UFR des Sciences Pharmaceutiques, Université François-Rabelais de Tours, 31 av. Monge, F37200 Tours, France
*corresponding author: Magdalena.malinowska@pk.edu.pl

The antioxidant activity of plant extracts is one of the key features determining their effectiveness in reducing free radicals and reactive oxygen species, causing oxidative stress and, consequently, the degradation of skin structures [1, 2]. There are many methods for assessing the ability of plant extracts to reduce free radical oxidants, but there is no universal and easy way to determine the mechanism of antioxidant activity for a selected raw material. Natural chemical diversity of phytochemicals in plant kingdom as well as the influence of genotype and environmental factors on their abundance makes it difficult to select plant material that is the most effective protectant against skin degradation caused by free radicals [1].

Grapevine (Vitis vinifera L.) is known for its abundance of polyphenols with high antioxidant potential including phenolic acids, anthocyanins, flavonols and stilbenoids. These classes of metabolites are present in various grape organs (canes, leaves, fruits), and their content varies depending on the grape variety, growing conditions, and the extraction method [3].

In our study, we used UPLC-DAD-MS/MS-based metabolomics to identify the most effective grape extracts and related metabolites as efficient free radical scavenging agents. A chemometric analysis of hydroalcoholic berry extracts obtained from twelve fungus-resistant grape varieties cultivated in southern Poland was carried out, followed by in vitro antioxidant activities using ORAC, ABTS, DPPH, FRAP, CUPRAC and iron chelation assays and finally the pairwise correlations between polyphenol and antioxidant activities were represented on heatmaps.

References

[1] Billet K., Unlubayir M., Munsch T., Malinowska M.A., Dugé de Bernonville T., Oudin A., Courdavault V., Besseau S., Giglioli-Guivarc'h N., Lanoue A. ACS Sustain, *Chem. Eng.*, 2021, 9(9), 3509–3517.
[2] Ferrier M., Billet K., Drouet S., Tungmunnithum D., Malinowska M.A., Marchal C., Dedet S., Giglioli-Guivarc'h N., Hano C., Lanoue A. Identifying Major Drivers of Antioxidant Activities in Complex Polyphenol Mixtures from Grape Canes, *Molecules,* 2022, 27, 4029.
[3] Malinowska M.A., Billet K., Drouet S., Munsch T., Unlubayir M., Tungmunnithum D., Giglioli-Guivarc'h N., Hano C., Lanoue A. Grape Cane Extracts as Multifunctional Rejuvenating Cosmetic Ingredient: Evaluation of Sirtuin Activity, Tyrosinase Inhibition and Bioavailability Potential, *Molecules*, 2020, *25*, 2203.

THE APPLICATION OF ROTATING MAGNETIC FIELD TO ENHANCE THE ANTIMICROBIAL ACTIVITY OF THYME AND ROSEMARY ESSENTIAL OIL

Agata Markowska-Szczupak[1]*, Paszkiewicz Oliwia[1], Wesołowska Aneta[2], Sołoducha Dawid[1], Borowski Tomasz[1], Kordas Marian[1], Rakoczy Rafał[1]

[1]West Pomeranian University of Technology in Szczecin, Department of Chemical and Process Engineering, Piastów 42, 71-065, Szczecin, Poland
[2]West Pomeranian University of Technology in Szczecin, Department of Organic and Physical Chemistry, Piastów 42, 71-065, Szczecin, Poland
*corresponding author: agata.markowska.szczupak@gmail.com

The essential oils from plants are used in cosmetics (e.g. soaps, perfumes, creams etc.), air fresheners and other products, for flavoring and adding scents to incense and household cleaning products. They are also used for aromatherapy in which healing effects are ascribed to aromatic compounds. As described in our previous work, rotating magnetic field RMF at the frequency range of 25–50 Hz in less than 100 min can be used to increase antimicrobial performance of pine oil. Therefore, the aim of this study was to identify the optimal magnetic field exposure and rosemary (REO) and thyme oil (TEO) concentrations to disturb the growth of the model gram-negative bacteria *Escherichia coli*. Both thyme *Thymus vulgaris* L. and rosemary *Rosmarinus officinalis* L. are gramineous plants that grow widely in southern Europe. For these reasons they represent the most popular essential oils used in alternative medicine. Inexpensive extraction is a relatively easy procedure [2].

Commercial REO and TEO oil was purchased from Polish company Avicenna-Oil ® W. Podlaski (Wroclaw, Poland). The individual constituents were identified by comparison of their mass spectra with those stored in the Wiley NBS75K.L and NIST/EPA/NIH (2002 version) mass spectral libraries and confirmed by comparison of their retention indices (RI) with data re-ported in NIST Chemistry WebBook. The reference strain of Gram-negative bacteria, *Escherichia coli* K12 (ATCC 25922 (*E. coli*) was tested. To examine the effect of thyme and rosemary and rotating magnetic field RMF) on antibacterial performance 1, 2 or 3 drops of oil in 50 ml of sterile saline buffer were prepared. All measurements were performed using the self-designed and constructed magnetically assisted photoreactor (MAP). The applied magnetic field had a frequency of 27 Hz. To find out the optimum levels of parameters for improving the proposed antimicrobial method, RSM based on CCD was used.

Thyme contained monoterpene phenols, including carvacrol, thymol and p-cymene, and other monoterpenes, such as α-pinene, 1,8-cineole, camphor, linalool and borneol, whereas rosemary oil comprised 1,8-cineole, camphor and α-pinene. It was shown that thyme oil in 1 drop concentration resulted in a total bacterial number reduction after 40 minutes under the rotating magnetic field. Rosemary antibacterial effect was much weaker. At the same time only 0.32 log reduction was observed. After 160 minutes the decline in germ number did not exceed 2 logs. We summarized that the rotating magnetic fields (RMF) at the frequency of 27 Hz can increase antimicrobial efficiency but the effect depends on the type of essential oil.

References

[1] Markowska-Szczupak A., Wesolowska A., Borowski T., Sołoducha D., Paszkiewicz O., Kordas M., Rakoczy R., Effect of pine essential oil and rotating magnetic field on antimicrobial performance, *Sci. Rep.,* 2022, 12, 9712.
[2] Ali B., Al-Wabel N.A., Shams, Ahamad A., Khan S.A., Anwar F., Essential oils used in aromatherapy: A systemic review, *Asian Pac. J. Trop. Biomed*., 2015, 5(8), 601-611.

ENERGY ANALYSIS OF LABORATORY WATER DESALINATION BY MEANS OF PERVAPORATION AND REVERSE OSMOSIS METHODS

Joanna Marszałek*, Izabela Gortat, Paweł Wawrzyniak

Lodz University of Technology, Faculty of Process and Environmental Engineering,
Wólczańska 215, 93-005 Łódź, Poland
*corresponding author: joanna.marszalek@p.lodz.pl

More and more countries in the world are struggling with the shortage of drinking water. Problems affect over 50% of the world's population [1]. Fresh water is only 2.6% of all water resources, of which 0.5% can be directly obtained for consumption. According to the WHO report, in the near future another 1.5 million people will have a problem with access to drinking water, including the Mediterranean countries [2].

Desalination techniques are based on thermal, membrane and alternative methods, e.g. freezing, ion exchange techniques. Commercial thermal methods include multistage flash distillation (MSF) and multiple-effect distillation (MED) [3]. These methods use energy from conventional sources and result in high energy consumption and costs. Energy consumption of desalination is defined as specific energy consumption, *SEC*, kWh/m^3.

The most widely used desalination technique in the industry is reverse osmosis (RO). Optimization of the RO process, known for 50 years in the industry, has led to the reduction of energy consumption to the level below 3 kWh/m^3 [4]. In order to reduce operating costs, existing installations are improved, optimized and combined into hybrid systems. New methods of seawater desalination are constantly being sought. A new, proposed method is pervaporation (PV) - a modern, low-pressure membrane technique, which is characterized by high quality of the obtained filtrate.

Laboratory experiments of sea water desalination by means of pervaporation and reverse osmosis and measurement of their energy consumption were carried out in the work. Earlier studies are included in reference [5]. Pervaporation and reverse osmosis experiments were performed using PV and RO laboratory equipment. The pressure on the low-pressure side of the PV membrane was 3 kPa and the transmembrane pressure in the RO was 3 MPa. PERVAP 2210, 4510 flat membranes were used for PV and AG-RO for RO experiments. In both cases, a model aqueous solution containing 0.7 and 3.5% NaCl was used. Experiments were performed at 40, 60, 80°C for PV and 40°C for RO. The feed flow rate was set to 20, 40 and 60 dm^3/h for the PV. Salt concentration in the collected samples was measured with the universal apparatus Elmetron CPC 501 using the conductometric method.

The following formulas were used to assess the desalination efficiency, giving the permeation flux (also called productivity, determining the efficiency of the process) (J_p) and the rejection factor (R) - the selectivity of the membrane.

$$J_p = \frac{m_p}{A\ t} \tag{1}$$

$$R = \left(1 - \frac{c_p}{c_F}\right) 100\% \tag{2}$$

where:
m_p, kg is a mass of the permeate obtained after time t,
A, m^2 – membrane area,
t, h – time taken to collect permeate mass,
c_p, c_F , mg/kg – concentration of salt in the permeate and feed.

The desalination process was characterized by a very high retention factor (R) of over 99% for both PV and RO. For PV, the permeate fluxes increased with the increase of the feed flow rate, the process temperature and slightly with the increase of the salt content in the feed.

To calculate the energy consumption of the process, the PV station was divided into 3 power consumption blocks: feed temperature control (thermostat), feed circulation (pressure pump) and permeate collection (vacuum pump). The RO station needed to be divided into only 2 blocks: feed temperature control (thermostat) and feed circulation (pressure pump). The trans-membrane pressure was achieved by adjusting the throttle valve. Energy consumption measurements were carried out for devices using electricity with a connected SilverCrest wattmeter.

Measurements of the energy intensity of desalination processes allowed to determine the specific energy consumption, *SEC*. The calculated *SEC* values for both laboratory PV and RO processes gave results in the range of 2÷70 MWh/m^3, which is much higher than the data obtained in industrial installations. Depending on the origin of the raw material (surface water, sea water) and desalination methods, this parameter, in industrial conditions, varies in the range of 0.4-10 kWh/m^3 [4]. An important factor in reducing energy consumption can be lowering the temperature of the thermostat, which consumes 30 to 60% of the total energy used in the PV process.

In addition, a slight increase in power consumption was observed during the PV process. This is probably related to the phenomenon of fouling, and more precisely scaling, i.e. slow deposition of salts on the membrane surface during the desalination process. There was no such phenomenon during the RO process.

The SEC and permeate flux values for laboratory desalination processes (PV and RO) and the membranes used at 40°C and various initial salt concentrations in the feed are presented in Table 1. In the case of RO we observed 2 to 17 times lower *SEC* values and 2 to 19 times higher flux values (*Jp*) compared to PV, depending on the pervaporation membrane used.

Table 1. Comparison of the *SEC* and permeate flux J_p for laboratory desalination processes (PV and RO) and membranes at 40°C and different initial salt concentration in the feed (c_0)

c_0, % mas	PV (PERVAP 4510)		PV (PERVAP 2210)		RO (Osmonics AG)	
	SEC, MWh/m^3	J_p, kg/(m^2 h)	SEC, MWh/m^3	J_p, kg/(m^2 h)	SEC, MWh/m^3	J_p, kg/(m^2 h)
0.7	22.02	1.362	6.42	4.668	2.29	24.78
3.5	67.35	1.768	9.09	5.339	3.99	14.32

Based on the experiments, the following conclusions can be drawn:

1. SEC consumption in the PV process can be controlled by using different pressures on the low-pressure side of the membrane and reducing or completely eliminating feed temperature control. This can be achieved by using waste heat or heat from renewable energy sources.
2. Due to low permeate fluxes (productivity) and the lack of pervaporation membranes dedicated to water desalination on the market, it is necessary to produce a selective pervaporation membrane for the seawater desalination process.

References

[1] Li Q., Cao B., Li P., Fabrication of high performance pervaporation desalination composite membranes by optimizing the support layer structures, *Ind. Eng. Chem. Res*., 2018, 57, 11178–11185.

[2] World Health Organization, *Water, sanitation, hygiene and health: a primer for health professionals*. (WHO/CED/PHE/WSH/19.149). Licence: CC BY-NC-SA 3.0 IGO, Geneva; 2019.

[3] Xiao G., Wang X., Wang M. Ni, F., Zhu W., Luo Z., Cen K., A review on solar stills for brine desalination, *Appl. Energy*, 2013, 103, 642–652.

[4] Nassrullah H., Anis S. F., Hashaikeh R., Nidal Hilal N., *Energy for desalination: A state-of-the-art review, Desalination*, 2020, 491, 114569.

[5] Kaminski W., Marszałek J., Tomczak E., Water desalination by pervaporation – Comparison of energy consumption. *Desalination*, 2018, 433, 89–93.

SUPERCRITICAL CO_2 TREATMENT OF CARBON SUPPORTS FOR OXYGEN REDUCTION CATALYSTS USED IN A DIRECT FORMIC ACID FUEL CELL

Marta Mazurkiewicz-Pawlicka*, Monika Jałowiecka, Joanna Kobek, Szymon Jaworowski, Piotr Cendrowski, Jan Krzysztoforski

Warsaw University of Technology, Faculty of Chemical and Process Engineering, Waryńskiego 1, 00-645 Warsaw, Poland
*corresponding author: marta.pawlicka@pw.edu.pl

Low temperature fuel cells are a promising technology that can help to solve the energy crisis. In the fuel cell the chemical energy of the fuel is changed into electrical energy due to redox reactions. On the anode side of the cell, the fuel (usually hydrogen, methanol, or formic acid) is oxidized, while on the cathode side the oxidant (air, oxygen) is reduced. In order to enhance the reactions and increase power obtained from the fuel cell different catalysts are used for the anode and cathode sides. The reaction limiting the operation of the fuel cell is oxygen reduction reaction (ORR) and the best catalyst used for it is platinum. Due to high price and scarcity of Pt current research is focused on finding a catalyst with decreased platinum content. One of the solutions is using a carbon support thanks to which the obtained Pt particles are smaller and exhibit higher activity. The second solution is preparing bimetallic catalysts where next to platinum other metals (like Fe, Co, Ni) are used.

In this study we combined both approaches, where we prepared Pt-Fe nanoparticles deposited on different carbon supports (carbon nanotubes – CNTs and reduced graphene oxide – rGO). We studied the possibility of enhancing the catalytic activity of the prepared materials by increasing the surface of the carbon support with the use of supercritical CO_2 ($scCO_2$). The results show that using $scCO_2$ has a significant effect on the catalysts deposited on rGO (an 8x increase in the catalytic activity when using $scCO_2$), while for CNTs no big differences were observed. This can be explained by the exfoliation of the reduced graphene oxide platelets and increasing the available surface for particle precipitation, while for carbon nanotubes no increase in the surface was observed. Electron microscopy pictures for Pt-Fe catalysts deposited on rGO and CNTs are presented in Fig. 1 and Fig. 2.

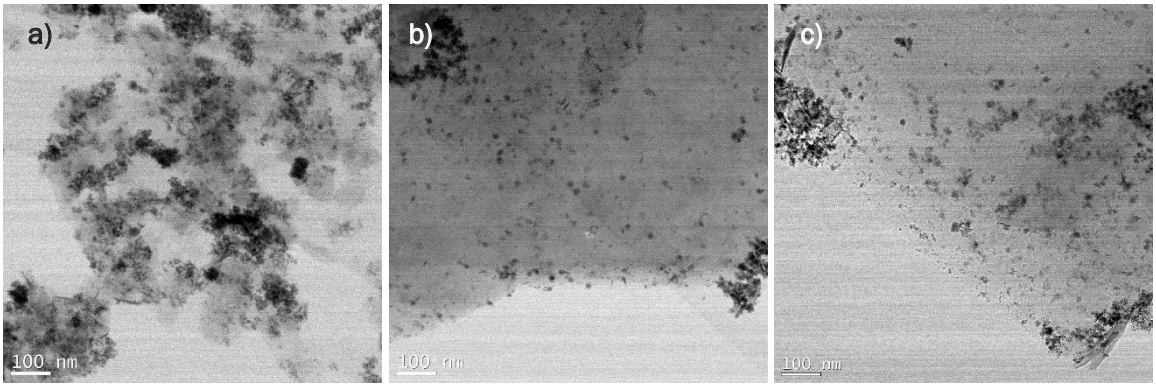

Fig. 1. Pt-Fe nanoparticles deposited on a) rGO, b) rGO treated with $scCO_2$ at 12 MPa, c) rGO treated with $scCO_2$ at 18 MPa

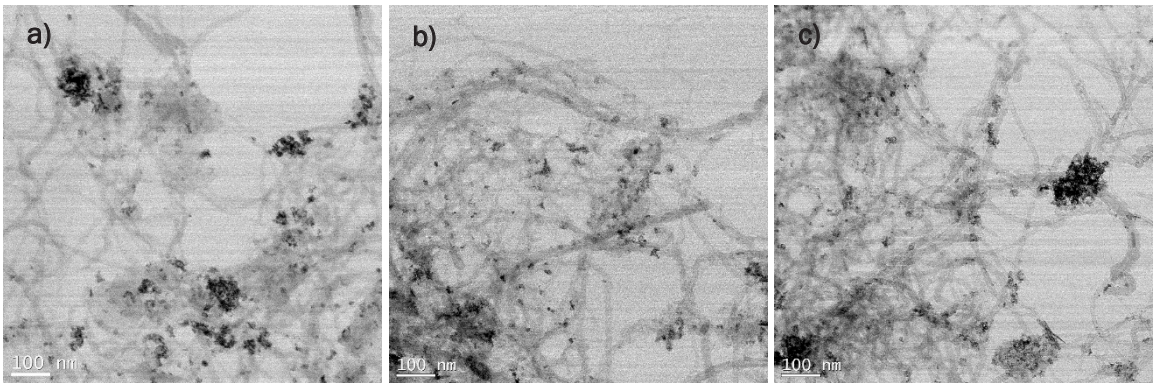

Fig. 2. Pt-Fe nanoparticles deposited on a) CNTs, b) CNTs treated with $scCO_2$ at 12 MPa, c) CNTs treated with $scCO_2$ at 18 MPa

The prepared catalysts were studied using different analytical techniques, such as thermogravimetric analysis (TGA), X-ray fluorescence spectroscopy (XRF), X-ray diffraction (XRD) and electron microscopy. The assessment of their catalytic activity was performed by testing them in a direct formic acid fuel cell (DFAFC) – results are presented in Table 1.

Table 1. Results of the catalysts' activity obtained in DFAFC

Sample	Maximum power density [mW/mg_{metal}]	Current density [mA/mg_{metal}]	Voltage [V]
Pt-Fe/rGO	4.30	13.38	0.322
Pt-Fe/rGO 12 MPa	34.05	90.58	0.376
Pt-Fe/rGO 18 MPa	19.26	64.56	0.298
Pt-Fe/CNTs	48.26	133.58	0.361
Pt-Fe/CNTs 12 MPa	39.56	98.93	0.400
Pt-Fe/CNTs 18 MPa	37.16	104.39	0.356

The study proved that using supercritical CO_2 is beneficial for catalysts used for oxygen reduction reaction deposited on reduced graphene oxide. Treatment of rGO with $scCO_2$ led to an increase of the surface available for precipitation of Pt and Fe nanoparticles. This allowed to obtain smaller particles that were uniformly dispersed on the carbon surface leading to a significant increase in the material's catalytic activity. This phenomenon was not observed in the case of carbon nanotubes, but further studies on this topic should be undertaken to explain the effect of $scCO_2$ on the properties of carbon support and the final behavior of the catalysts used for ORR.

EVALUATION OF ULTRASOUND ACTION ON THE VACUUM IMPREGNATION EFFECT IN APPLE

Dominik Mierzwa[1], Justyna Szadzińska[1,*], Elżbieta Radziejewska-Kubzdela[2], Róża Biegańska-Marecik[2]

[1]Poznan University of Technology, Division of Process Engineering, Institute of Chemical Technology and Engineering, Berdychowo 4, 60-965 Poznan, Poland

[2]Poznan University of Life Sciences, Department of Food Technology of Plant Origin, Wojska Polskiego 31, 60-624 Poznan, Poland

*corresponding author: justyna.szadzinska@put.poznan.pl

Raw materials of plant origin, such as fruit and vegetables, belong to a group of materials with low microbial stability because of very high moisture content and water activity. They are usually eaten fresh. However, in order to prevent such phenomena as darkening and food spoilage following the harvest, these materials are subjected to various processing methods, e.g., cooking, pasteurizing, freezing, canning, or drying. In addition to the limited storage period, another problem is, e.g., the surplus production of dessert apples on the domestic fruit market. One of the ideas to solve these problems may be to allocate part of the harvest to processing into food enriched with functional additives. Not only in Europe, but also worldwide, apples constitute an important part of the human diet. They are a source of carbohydrates, including fiber. In addition, apples are rich in vitamins, healthy minerals, carotenoids, and antioxidants. Therefore, the fruit can be successfully used as a good base for functional food production [1].

The enrichment of raw materials of plant origin with bioactive components already takes place in the cultivation stage or during food processing. Data from the literature show that enriching apples with bioactive ingredients is now an emerging interest. An increasing need for a healthy lifestyle, including a healthy diet, is generating consumers more and more often looking for functional foods. One method of enriching foods with valuable compounds is vacuum impregnation (VI). This operation is a relatively new method used in food product processing, invented in the 1990s. It allows any water-soluble substance to be introduced in the form of solution into the porous structure of the raw material, improving the health-promoting properties, e.g., by enriching with vitamin C. VI can be carried out as a pretreatment prior to other processing. This process is based on the replacement of native fluids located in the material tissue into a desired active ingredient under a mechanically generated pressure gradient and consists of two stages, i.e., vacuum stage (under reduced pressure) and relaxation stage (atmospheric pressure). The effectiveness of VI depends on many factors, such as vacuum pressure, temperature, duration of individual stages, and structure of raw material. One of the main properties that affects mass transfer during VI is porosity. In order to increase the volume of active porosity in plant material during VI, ultrasound can be applied. The phenomenon of acoustic cavitation - the formation, development, and implosion of cavitation bubbles in tissue liquids - increases the volume available for impregnation, and therefore improves mass (bioactive compound) transfer [2, 3].

The purpose of the research was to evaluate the ultrasound action on the vacuum impregnation of apple fruit with ascorbic acid. The effect of ultrasound was studied at various stages of VI, that is, during vacuum, relaxation, throughout the processing duration, and during the aeration period (between vacuum and relaxation). The VI processes were carried out under a vacuum of 300 mbar, in the IS-PP apparatus (INTERSONIC, Poland). During the experiment, an aqueous ternary solution of analytically pure ascorbic acid of 0.5% (w / w) citric acid of 0.5% (w/w), and sucrose of 11% (w / w) was used. The effective concentration of the solution was 12% (w/w), which is equal to the solid soluble content, as measured using a PAL-α digital refractometer (ATAGO, Japan). The temperature of the solution inside the device was measured with the Pt100 sensor and kept constant at about 25 °C using a water jacket. During each process, 3 kg of solution and 400 g

of apple cubes (15×15 mm) were used, so the ratio of the weight of raw material to the solution was 1:7.5. In the ultrasound-assisted VI processes (UVI), the ultrasonic waves at a frequency of 35 kHz, generated by piezoelectric transducers attached to the bottom of the device were used. The effective power of ultrasound was 240 W. A total of five VI processes were carried out as shown in Table 1. The result of ultrasound action on VI was evaluated based on ascorbic acid content (*AAC*) and degree of impregnation (*ID*) in the impregnated apples, as well as several quality indicators such as water activity (a_w), total color change (ΔE), and browning index (*BI*).

Table 1. Details of the VI processes

Process	Vacuum duration (min)	Relaxation duration (min)	Aeration duration (min)	Ultrasound application
VI	30	30	10	-
UVI1	30	30	10	during vacuum
UVI2	30	30	10	during relaxation
UVI3	30	30	10	during whole process
UVI4	30	30	10	during aeration

After impregnation, a significant increase in ascorbic acid content (*AAC*) was observed. The raw apple contained only 14 mg of vitamin C per 100 g (fw), whereas all impregnated samples were characterized by a content of this compound up to 140 mg per 100 g (fw), on average. Similar effects of the degree of impregnation (mass change) were also observed after all impregnation processes. The application of ultrasound during different stages of VI failed to improve notably the impregnation effect. However, despite the lack of noticeable differences between different processes, the highest *AAC* was observed after ultrasound impregnation applied during the vacuum stage (UVI1), and the lowest amount of vitamin C was found in samples impregnated with ultrasound only during the aeration stage (UVI4). Analogically as in case of impregnation effects, the changes in quality parameters between the VI and UVI samples were not very significant, as the values of the quality parameters were comparable.

On the basis of the results, it was concluded that the effect of apple impregnation does not depend on the ultrasound action, as the ultrasound-induced phenomena do not have such a strong impact on vacuum impregnation. This probably results from the fact that apple tissue is characterized by high porosity and low density as compared to other raw materials of plant origin, e.g., potato, carrot, etc. Further research is required to analyze the possible controlled change in the concentration of the bioactive compound. It is especially important in terms of functional food production with therapeutic potential.

References

[1] Hui Y.H., *Handbook of Fruits and Fruit Processing*, Oxford, Blackwell Publishing 2006.
[2] Yılmaz F.M., Bilek S.E., Ultrasound-assisted vacuum impregnation on the fortification of fresh-cut apple with calcium and black carrot phenolics, *Ultrason. Sonochem.*, 2018, 48, 509-516.
[3] Mierzwa D., Szadzińska J., Radziejewska-Kubzdela E., Biegańska-Marecik R., Ultrasound-Assisted Vacuum Impregnation as a Strategy for the Management of Potato By-Products, *Sustainability*, 2021, 13, 3437.

DEACTIVATION ENERGIES OF INULIN HYDROLYSIS BY INULINSASES

Justyna Miłek*

Bydgoszcz University of Science and Technology, Faculty of Chemical Technology and Engineering, Department of Chemical and Biochemical Engineering, Seminaryjna 3, 85-326 Bydgoszcz, Poland
*corresponding author: jmilek@pbs.edu.pl

Inulinases catalyze the hydrolysis of inulin to obtain fructose with a yield of about 90–95%. Inulin is a reserve carbohydrate in plant tubers like Jerusalem artichoke, chicory, garlic and onion, leek, rye, barley, dandelion, burdock and banana [1]. Inulinases can be divided into endo-inulinases (EC 3.2.1.7) [2] and exo-inulinases (EC 3.2.1.80) [1].
However, processes involving inulinases for industrial purposes cannot be designed and optimized without knowing the kinetic parameters of the process and thus the effect of temperature on activity of inulinases. It is necessary to determine the values of activation energy of the deactivation process E_d, activation energy E_a and optimum temperature T_opt for inulinases.

The basic equation (mathematical model) of this method is the equation describing the change in the dimensionless activity of the enzyme *a* depending on the temperature *T:*

$$a(T) = \frac{\exp\left(\frac{(T_\mathrm{opt}-T)}{RTT_\mathrm{opt}}\frac{E_\mathrm{d}\beta}{(\exp\beta-1)}\left\{1-\exp\left[-\beta\exp\left(\frac{E_\mathrm{d}(T-T_\mathrm{opt})}{RTT_\mathrm{opt}}\right)\right]\right\}\right)}{1-\exp(-\beta)} \quad (1)$$

where E_a is the activation energy for the enzymatic reaction [kJ/mol], E_d is the activation energy of the deactivation process [kJ/mol], R is the gas constant 8.315 [J/(mol · K)], and T is the absolute temperature [K], T_opt is the temperature at which inulinase shows maximum activity. The dimensionless parameter β determines the relationship:

$$\beta = k_{\mathrm{d}0}t_\mathrm{a}\exp\left(-\frac{E_\mathrm{d}}{RT_\mathrm{opt}}\right) \quad (2)$$

where $k_{\mathrm{d}0}$ is a pre-exponential factor the kinetic constant of the deactivation process of inulinase [1/min] and t_a is the reaction time of inulinase [min].
The values of parameters E_d and T_opt were determined in Sigma Plot 15.0 by a non-linear regression according to the Levenberg-Marquardt procedure, determining the minimum sum of squared errors defined by the equation

$$\mathrm{SSE}(E_\mathrm{d}, T_\mathrm{opt}, \beta) = \sum\left(a_\mathrm{exp} - a_\mathrm{cal}(E_\mathrm{d}, T_\mathrm{opt}, \beta, T_\mathrm{i})\right)^2 \quad (3)$$

where a_exp inulinase activity was determined experimentally, $a_\mathrm{cal}(E_\mathrm{d}, T_\mathrm{opt}, \beta, T_\mathrm{i})$ inulinase activity calculated from Equation (1).
The values of deactivation energy for endo-inulinases *A. niger* [1], exo-inulinases *A. niger* [3], recombinant endo-inulinases *A. niger* [2] and also recombinant exo-inulinases *A. niger* [4] are presented in Table 1. In most cases, the analyzed inulinase activities were determined with the DNS method using dinitrosalicylic acid at 540 nm, and also with the Nelson–Somogyi method [*] at 620 nm. The initial inulin concentration measured was in the range of 1–6%. In most analyzed cases, recombinant exo-inulinases have lower value of E_d, so they are less thermally stable than no-recombinant exo-inulinases [3, 4]. For measurements carried out with the Nelson–Somogyi method [in Table 1 marked with a superscript *], a higher E_d value was obtained, compared to the measurements made with the DNS method, in which the inulin hydrolysis time was the same and amounted to 30 min.

Table 1. The values of E_d and T_{opt} for inulinases

Source of inulinase	t (min)	T_{opt} (K)	E_d (kJ/mol)	Ref
Endo-inulinase				
Aspergillus niger 12	30	317.12 ± 0.83	127.78 ± 5.58	[1]
A. niger (Megazyme, Ireland)*	30	332.55 ± 0.72	142.09 ± 16.02	
Recombinant endo-inulinase				
A. niger to *Penicillium canescens* A3	5	328.91 ± 1.32	146.80 ± 20.31	[2]
A. niger CICIM F0620 in *Pichia pastoris* KM71	10	334.81 ± 1.08	250.58 ± 28.02	
Exo-inulinase				
A. niger 20 OSM	20	325.25 ± 0.41	204.63 ± 6.14	[3]
A. niger PTCC 5012	8	337.35 ± 0.70	245.62 ± 26.18	
Recombinant exo-inulinase				
A. niger CBS 513.8 to *P. pastoris*	5	318.91 ± 1.19	120.87 ± 6.18	[4]
A. niger 5012 to *E. coli* DH5	8	326.84 ± 1.15	149.40 ± 19.30	

*Nelson–Somogyi method,

The determined values of E_d, T_{opt} for inulinases depended on the origin of inulinases and conditions (reaction time, pH) of activity measurement.

The determination of E_d and T_{opt} of inulin hydrolysis by inulinase allows to conclude that:

1. The commercial endo-inulinases *A. niger* was characterised by higher values of T_{opt} as well as higher values of energy E_d than non-commercial endo-inulinases *A. niger.*
2. Recombinant exo-inulinases have lower E_d values, so they are less thermally stable than no-recombinant exo-inulinases.
3. The large differences between the energy value E_d for *A. niger* exo-inulinase are due to the different origins of the *A. niger* strains.
4. Knowledge of presented parameters for inulinases will allow the design, modeling and optimization process of inulin hydrolysis.

References

[1] Miłek J., Determination the optimum temperature and activation energies for the hydrolysis of inulin hydrolysis by endo-inulinase *Aspergillus niger*, *Chem. Process Eng.,* 2020, 41 (2), 229–236.

[2] Miłek J., Recombinant endo-inulinases: Determination the activation, deactivation energies and optimum temperatures in inulin hydrolysis, *J. Therm. Anal. Calorim.,* 2023, 148, 859–866.

[3] Miłek J., Application of the new method to determine the activation energies and optimum temperatures of inulin hydrolysis by exo-inulinases *Aspergillus niger*, *J. Therm. Anal. Calorim.,* 2022, 147, 1371–1377.

[4] Miłek J., The inulin hydrolysis by recombinant exo-inulinases: determination the optimum temperatures and activation energies, *J. Therm. Anal. Calorim.,* 2022, 147, 8061–8067.

MONOAMMONIUM PHOSPHATE FERTILIZER PRODUCTION. PART I: NUMERICAL SIMULATION OF TWO-PHASE FLOW IN TUBULAR REACTOR

Halina Murasiewicz, Barbara Zakrzewska*

West Pomeranian University of Technology, Szczecin, Faculty of Chemical Technology and Engineering, Department of Chemical and Process Engineering
Piastów 42, 71-065 Szczecin, Poland
*corresponding author: barbara.zakrzewska@zut.edu.pl

Monoammonium phosphate fertilizer (MAP) is commonly used in agriculture as an important granular fertilizer and source of phosphorus and nitrogen [1], the two main constituents, which are important for growth and development of plants. MAP is prepared by the exothermic reaction of liquid phosphoric acid (H_3PO_4) and anhydrous ammonia (NH_3) in the one-to-one ratio. The slurry product of the reaction is either solidified in a granulator (dual pipe reactor process: one located in a granulator and second in a dryer) or heat of the reaction causes evaporation of water and then solidifies MAP (single pipe reactor located in the granulator, TVA process) [2]. The 'key apparatus' in MAP plant in TVA process is a cross-pipe reactor. The literature lacks detailed information on the hydrodynamics of the two-phase flow of aqueous and vapour phase and transport mechanism that occurs in a reactor, which is important for product formulation. It is very difficult and probably impossible because of the cost to experimentally investigate hydrodynamics in a pipe reactor in any plant. However, computational fluid dynamics (CFD) can help to solve the problem since it allows to simulate turbulent flow together with the reaction in real size apparatus and provides better understanding of flow patterns, mixing behaviour and impact velocity of phosphoric acid on the product (MAP).

The study presented herein deals with the numerical simulation of turbulent flow in the tubular reactor used for MAP production. The aim of this work was to theoretically examine turbulent flow of the two-phase system consisting of gas and liquid phases, mixing process in the tubular reactor under the process conditions similar to those applied in the fertilizer manufacturing. Understanding of transport characteristics within a gas-liquid flow is of vital importance for the design, operation and optimization of such a tubular reactor. However, to the best of our knowledge, there is no comprehensive flow analysis so far of a turbulent gas-liquid system in a tubular reactor used for MAP fertilizer production.

The Eulerian–Eulerian multi-fluid model was applied for simulation of two-phase flow in the tubular reactor. The multi-fluid approach is appropriate for separated flows where both phases can be described as a continuum and it can also be applied to simulate dispersed flows when the total motion of particles is desirable rather than a single particle [3]. In this model a set of conservation equations is numerically solved for each phase and phases are treated as interpenetrating continua. Coupling between the phases is accomplished by the pressure and interphase exchange coefficients, which need to be modelled. The way coupling is handled depends upon the type of phases involved, i.e. differently for fluid-solid (granular) flow than fluid-fluid (non-granular) flow.

The solution domain, similar to that used in a fertilizer plant, investigated in this study is presented in Fig. 1, meshing with 3.3 M and 500 K tetrahedral cells. The results presented here were obtained for the fine mesh. The dimensions of the reactor are similar to those used in MAP production which is composed of two inlets, separately for ammonia (gas) and phosphoric acid (liquid) and one outlet for the product of the reaction. The diameter of the inlet was 0.07 m and 0.05 m for H_3PO_4 and ammonia, respectively. Gaseous ammonia is supplied to the reactor from the front of the reactor whereas phosphoric acid flows through side inlet as is presented in [4]. The inflow conditions were defined separately for two inlets where ammonia and phosphorous acid velocities were fixed from the annual MAP production capacity. The boundary conditions for inlet for gaseous ammonia – defined as continuous phase, were set as inlet velocity with the value of gas equal to 177.8 m/s (with a null velocity for liquid). The volume fraction of dispersed phase

corresponded to 0. Here, we consider a case that is characterized by one continuous gas phase (NH_3) that coexists with a dispersed liquid phase (H_3PO_4). It means that liquid droplets are entrained by the gas-phase since the velocity of the gaseous phase is much larger. The boundary conditions for the second inlet, where H_3PO_4 is supplied to the reactor, were fixed as *velocity inlet* with the value of velocity assumed to be 2.07 m/s and the volume fraction of dispersed phase was 1.

Figures 2 and 3 show the distribution of the volume fraction of the dispersed phase in the initial section and at the outlet of the tubular reactor, respectively. The phosphoric acid flowed into the space between the pipes in the initial section of the reactor and filled it over time. Only when it flowed beyond the outlet area of the inner tube was it entrained by ammonia, which flowed at a much greater speed. Therefore, a small volume fraction of acid was observed in the reactor axis. With the passage of time, it accumulated at the bottom of the reactor tube, where the velocities were much lower than in its axis. The presence of H_3PO_4 acid at the outlet was observed about after 0.9 s, and over time it was observed on the entire plane, but with a tendency to accumulate near the back wall of the pipe. This phenomenon can be explained by the assumed high velocity of ammonia, which entrains some of the dispersed phase droplets and, after passing through the narrowing, hits the rear wall of the reactor, and then falls by gravity towards the outlet. Excessive difference in the speed of the two streams may be the cause of this phenomenon. Therefore, the presented volume share maps show two areas of occurrence of both phases: continuous and dispersed, which may indicate strong segregation. Probably, the inclusion of the transport equations of chemical components in the calculations, taking into account the kinetics of chemical reactions, would allow to obtain a more accurate picture of the volumetric distribution of both phases and to observe the appearance of the reaction product at the reactor outlet.

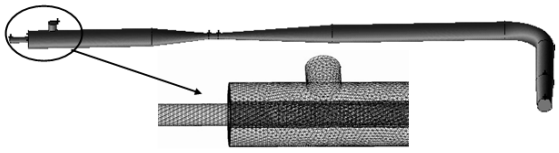

Fig. 1. Solution domain of pipe cross reactor and unstructured mesh used in the model

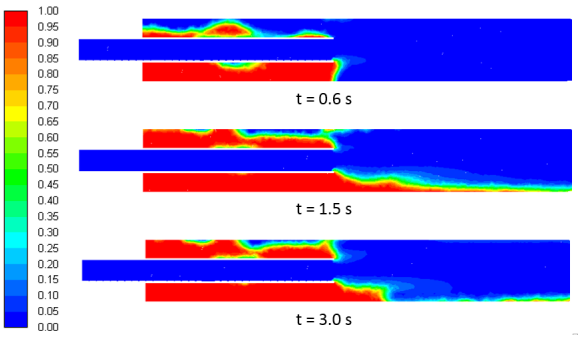

Fig. 2. Volume fraction of H_3PO_4 in the initial section of the tubular reactor for different simulation times

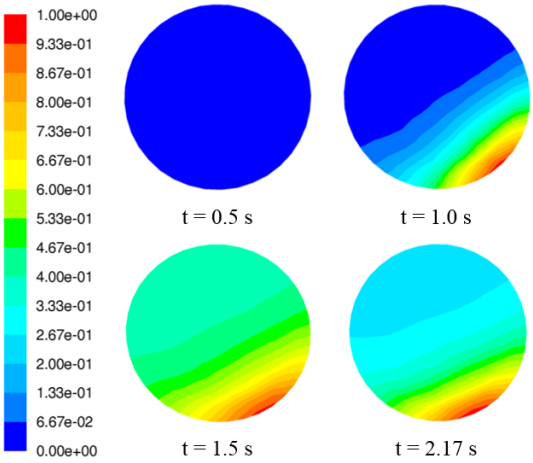

Fig. 3. Volume fraction of H_3PO_4 at the outlet of the tubular reactor for different simulation times

References

[1] Havelange S., Van Lierde N., Germeau A., Martins E., Theys T., Sonveaux M., Toussaint C., Schrödter K., Bettermann G., Staffel T., Wahl F., Klein T., Hofmann T., *Phosphoric Acid and Phosphates*, in: Ullmann's Encyclopedia of Industrial Chemistry, Wiley-VCH GmbH, 2023.

[2] Fertilizer Manual, Editors: *UN Industrial Development Organization*, Int'l Fertilizer Development Center (Eds.), 3rd edition, Springer Netherlands, 1998.

[3] Jakobsen H.A., Chemical reactor modeling: *Multiphase reactive flows*, Springer-Ferlag, Berlin, Heidelberg, 2008.

[4] Hudson J.W., Pendergrast R.A., Process for the manufacture of monoammonium phosphate, Patent US4009245A, 22.02.1977.

MICROWAVE-ASSISTED DRY REFORMING OF METHANE: HEATING EFFICIENCY OF CATALYTIC FLUIDISED BED AT 915 MHZ

Stanisław Murgrabia, Tomasz Kotkowski, Eugeniusz Molga, Andrzej Stankiewicz, Robert Cherbański*

Warsaw University of Technology, Waryńskiego 1, Warsaw, Poland
*corresponding author: robert.cherbanski@pw.edu.pl

Electrification of chemical processes can help to reduce the carbon footprint of various industries worldwide [1]. Therefore, several unconventional heating methods that proved their potential at the laboratory and pilot scales have been investigated to be widely introduced in the industry. Among different unconventional heating methods, microwave heating is especially attractive due to several unique properties including direct, volumetric and selective heating [2].

Among numerous applications of microwave heating, its use is very beneficial in catalytic reforming of methane with carbon dioxide, known as dry reforming of methane (Eq. 1) [3].

$$CH_4 + CO_2 = 2H_2 + 2CO, \quad \Delta H = 247 \ kJ/mol \tag{1}$$

Due to the strong endothermic effect of this reaction, an effective energy supply to the reaction zone is crucial for its performance. The main advantage of microwave-assisted dry reforming of methane (MADRM) is that microwaves are delivered remotely to the catalyst bed while heat is produced directly inside the catalyst grains. Such a MADRM process will be investigated within the EU TITAN project (Horizon Europe) [4]. Whereas the TITAN project aims to develop an innovative method to produce cost-competitive hydrogen with integrated carbon sequestration, this work focuses on the microwave heating efficiency of a catalytic fluidised bed. To calculate the efficiency, the heat balance of the fluidised reactor is employed. The heat balance includes all required terms of heat inflow, heat accumulation and heat outflow.

$$\dot{Q}_{MW} + \dot{Q}_{gas,in} = \dot{Q}_{acc} + \dot{Q}_{gas,out} + \dot{Q}_{loss} \tag{2}$$

where $\dot{Q}_{MW}$ is the heat generation rate due to microwaves, $\dot{Q}_{gas,in}$ is the heat inflow due to inlet gas (cold gas), $\dot{Q}_{acc}$ is the heat accumulation rate, $\dot{Q}_{gas,out}$ is the heat outflow due to outlet gas (hot gas), $\dot{Q}_{loss}$ is the heat loss through the reactor wall.

Microwaves are produced by a solid-state microwave generator operating at 915 MHz with adjustable power between several and 1500 W. The 915 MHz microwave generators are especially interesting as they have high electrical efficiency (about 80%) and high power (even 100 kW). Microwaves are delivered to a customised applicator by the WR975 waveguide. The maximum electric field intensity in the catalytic bed is obtained using a 3-stub tuner and an adjustable short. A fluidised bed reactor made of quartz glass is arranged inside the microwave applicator, perpendicularly to it. A catalyst bed inside the glass reactor fluidises in a gas stream. An infrared temperature sensor measures the temperature of a catalyst bed. Additional temperature sensors are placed in the fluidised bed reactor below and above the microwave applicator to measure the inlet and outlet gas temperatures to/from the heating zone. One fibre optic sensor is also fixed in the microwave applicator outside the glass reactor.

As this work seeks to test possible catalysts for MADRM, such materials as silicon carbide (four fractions), nickel catalyst on Al_2O_3 carrier and commercial activated carbon are examined.

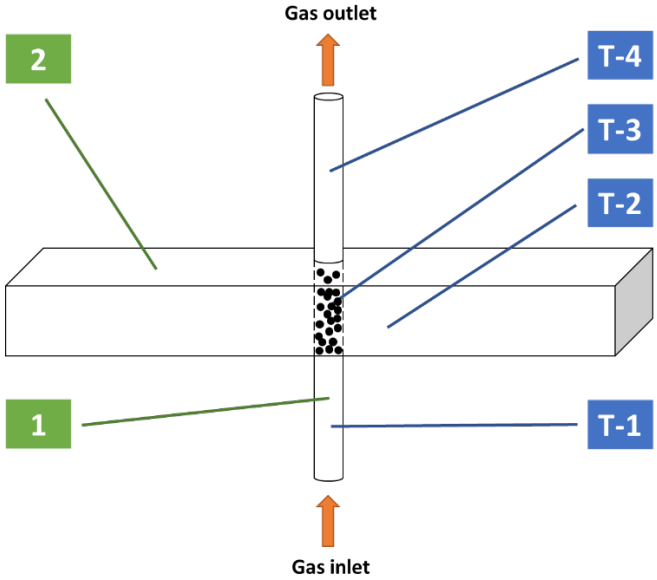

Fig. 1. Simplified scheme of the experimental setup. (1) Fluidised reactor, (2) microwave applicator, (T-1), (T-2), (T-3), (T-4) temperature sensors

Acknowledgements

Funded by the European Union. Views and opinions expressed are however those of the authors only and do not necessarily reflect those of the European Union or the European Climate, Infrastructure and Environment Executive Agency (CINEA). Neither the European Union nor the granting authority can be held responsible for them.

Funded by the European Union

titan microwave biogas cracking

References

[1] Stankiewicz A.I., Nigar H., Beyond electrolysis: Old challenges and new concepts of electricity-driven chemical reactors, *React. Chem. Eng.*, 2020, 5, 1005–1016.
[2] Cherbański R., Molga E., Intensification of desorption processes by use of microwaves-An overview of possible applications and industrial perspectives, *Chem. Eng. Process. Process. Intensif.*, 2009, 48, 48–58.
[3] Zerva C., Stefanidis G.D., Stankiewicz A.I., *Microwave-assisted Catalytic Dry Methane Reforming, in: Chemical Valorisation of Carbon Dioxide*, Stefanidis G., Stankiewicz A, (Ed.), The Royal Society of Chemistry; 2022, 429-445.
[4] European Commission. Funding & tender opportunities [Internet]. Available from: https://ec.europa.eu/info/funding-tenders/opportunities/portal/screen

HEAT EXCHANGE IN MINIATURE TRIANGULAR CHANNEL HEAT EXCHANGER

Krzysztof Neupauer*, Aleksander Pabiś

Faculty of Chemical Engineering and Technology, Cracow University of Technology,
Warszawska 24, 31-155 Kraków, Poland
*corresponding author: krzysztof.neupauer@pk.edu.pl

The results of testing a prototype of a miniature heat exchanger with sixteen triangular channels [1] are presented in this study. Each channel was 40 mm long and had an isosceles triangular cross-section with a base of 2 mm and a height of 1 mm. The channels were made in two polytetrafluoroethylene (PTFE) plates, and 0.4mm thick copper sheet heat transfer surface was inserted between the plates. The entire assembly was bolted together with six screws as shown in Fig. 1a. Each plate had two inlet and two outlet ports for the heat transfer fluid. Cold tap water and heated water with temperatures ranging from 30°C to 80°C was used in the study. The flow rate of cold water was varied from 10 to 90 dm^3/h and hot water from 10 to 60 dm^3/h. Measurements were made for counter-current and co-current flow, for an uninsulated and an insulated exchanger. A total of 458 measurement series were carried out. The heat exchanger materials were chosen to minimise heat loss to the environment due to the low thermal conductivity value of polytetrafluoroethylene amounting to 0.24 $W/(m \cdot K)$ and to reduce the thermal resistance of the exchange surface, which was made of copper with a thermal conductivity of $k \approx 380$ $W/(m \cdot K)$. Cold and hot water flow rates were measured using rotameters, while temperatures at the exchanger inlet and outlet, on its uninsulated and insulated surfaces, and in the ambient air were measured using copper-constantan thermocouples. In addition, several images were taken by means of a thermal imaging camera during operation to visualise the temperature field of the miniature heat exchanger as shown in Fig. 1b.

The measurements carried out allowed the calculation of heat transfer fluxes, logarithmic mean temperature differences and heat transfer coefficients U. The Re values ranged from 114 to 1100 on the cold water side and from 180 to 2290 on the hot water side. The U values ranged from 2500 to 6500 $W/(m^2K)$. The obtained values of the heat transfer coefficients were compared with those calculated from the empirical equations of Sieder-Tate [2], Mikheev [3], Peng and Peterson [4], Shah and London [5] and Brandner [6].

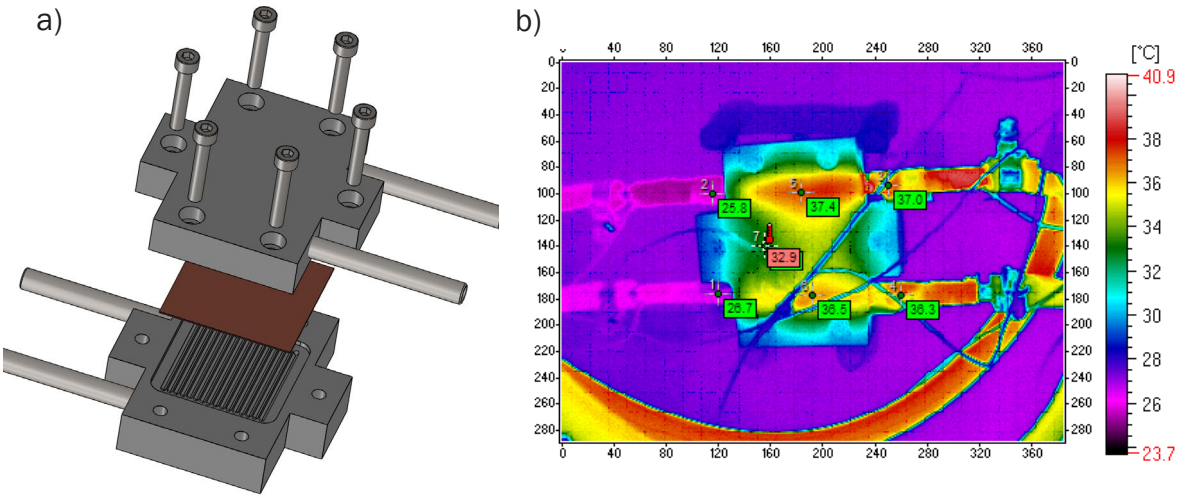

Fig. 1. View of the miniature exchanger with triangular channels (a) and thermal image of the heat exchanger in operation (b)

A series of several dozen measurements were also carried out for both counter-current and co-current flow, adjusting the cold and hot water consumption to obtain equal values of the Re number. With the knowledge of the heat transfer coefficient and the properties of the heat transfer media, an attempt was made to determine the conductive heat transfer coefficients on the cold water side h_c and the hot water side h_h.

The results were correlated in the form of the following equation:

$$Nu = C \cdot \left(Re \cdot Pr \cdot \frac{d_e}{L} \right)^n \tag{1}$$

Consequently, Equations (2) and (3) were obtained, respectively, for the counter-current and co-current flows:

$$Nu_p = 1.016 \cdot \left(Re \cdot Pr \cdot \frac{d_e}{L} \right)^{0.52} \tag{2}$$

$$Nu_w = 0.941 \cdot \left(Re \cdot Pr \cdot \frac{d_e}{L} \right)^{0.46} \tag{3}$$

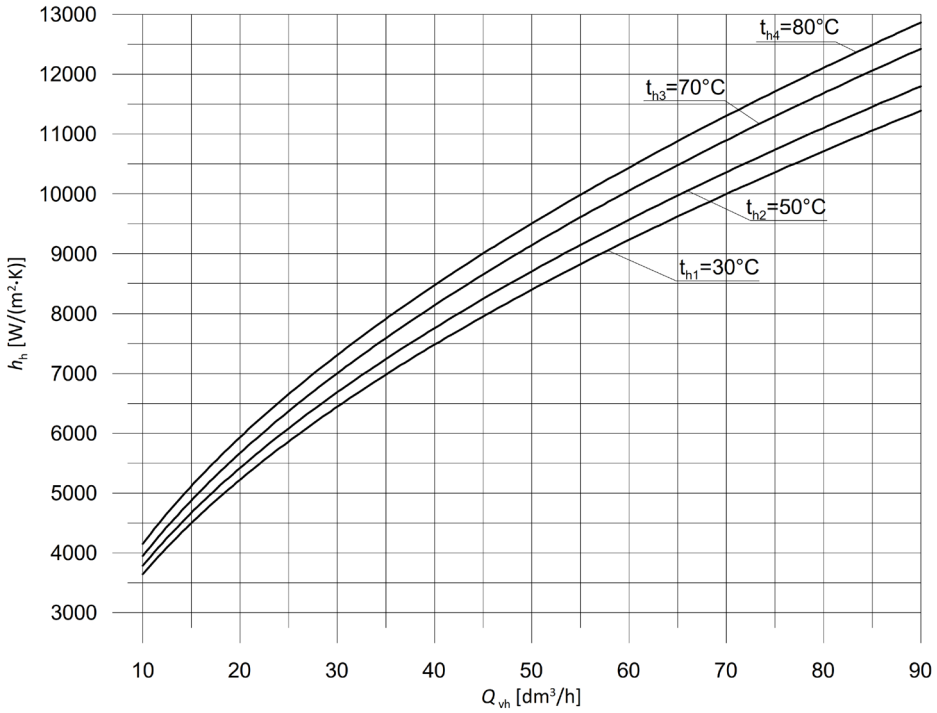

Fig. 2. Conductive heat transfer coefficient *h* as a function of flow rate and temperature (counterflow)

As shown in Fig. 2, the heat transfer coefficients calculated from Equation (2) varied from 3500 to 12860 W/(m²K). The achievement of such high heat transfer coefficients with low values of the Reynolds number confirms literature reports on the possibility of significant intensification of heat transfer by using microchannels. The fluxes of exchanged heat per unit area and volume in microchannels many times exceed the results obtained in classical heat exchangers. If the required space (area/volume) is not available, miniature heat exchangers can successfully replace traditional design solutions.

References

[1] Pabiś A., Wzór użytkowy nr 68975, Miniaturowy przeponowy wymiennik ciepła, UPRP, Warszawa, 2017
[2] Hobler T., *Ruch ciepła I wymienniki*, WNT, Warszawa 1986, 195.
[3] Staniszewski B., *Wymiana ciepła. Podstawy teoretyczne*, WNT, Warszawa, 1979, 227.
[4] Peng X.F., Peterson G.P., Convective heat transfer and flow friction for water flow in microchannel structures, *Int. J. Heat Mass Transfer*, 1996, 39, 2599-2608.
[5] Shah R.K., London A.L., *Laminar flow forced convection in ducts*, Suppl. 1, *Adv. Heat Transfer*, 1978.
[6] Brandner J.J., Benzinger W., Schygulla U., Zimmermann S., Schubert K., Metallic micro heat exchangers, *Heat Exchanger Fouling and Cleaning* VII, 2007, Vol. RP5, Article 49, 384-393.

APPLICATION OF MODIFIED METHODS FOR EXTRACTION OF HUMIC ACIDS FROM PEAT AS EFFICIENT PROCESSES IN THE PRODUCTION OF FORMULATIONS FOR AGRICULTURAL PURPOSES

Dominik Nieweś*, Kinga Marecka, Magdalena Braun-Giwerska, Marta Huculak-Mączka

Wrocław University of Science and Technology, Faculty of Chemistry, Department of Engineering and Technology of Chemical Processes, Wybrzeże Wyspiańskiego 27, 50-370 Wrocław, Poland
*corresponding author: dominik.niewes@pwr.edu.pl

Due to their chemical structure, including the presence of various functional groups, humic acids are used as soil conditioners. There are many fertilizer preparations on the market that contain humic acids. They are most often described as mixtures of traditional mineral fertilizers and humic acids, which were previously extracted from raw materials such as peat, lignite, or leonardite. However, the technology for producing fertilizer preparations with humic acids is hampered by the thermolability of these macromolecular substances. Therefore, in solid fertilizer technology, it is possible to add humic acids during processes and unit operations in which elevated temperatures are not used [1–5].

The main objective of the presented study was to develop technology for the simultaneous isolation of humic acids and their enrichment in fertilizer macronutrients. The process developed included four steps related to the decalcification of the peat, its neutralization, alkaline extraction, and the acidification of the extract to precipitate the humic acid fraction. During the study, four process variants were considered, which differed in the type of solutions used in each step, as presented in Table 1.

Table 1. Summary of the process variants

Symbol of the variant	Type of solutions for each step			
	Decalcification of peat	Peat neutralization	Alkaline extraction	Acidification of the extract
I	H_3PO_4	KOH	$NH_3 \cdot H_2O$	HNO_3
II	HNO_3	KOH	$NH_3 \cdot H_2O$	H_3PO_4
III	H_3PO_4	$NH_3 \cdot H_2O$	KOH	HNO_3
IV	HNO_3	$NH_3 \cdot H_2O$	KOH	H_3PO_4

For the intensification of isolation efficiency of humic acids from peat, ultrasound-assisted extraction (UAE) for the alkaline extraction step was implemented for each variant. Next, for the variant III, which allowed to achieve the highest efficiency of humic acid isolation, results were collected following the experimental matrix that was generated based on the fractional factorial design, where each of process parameters was coded at three levels presented in Table 2.

Table 2. Independent variable values and levels for experimental matrix design

Independent variable	Mark	Levels and values		
		-1	0	1
Extractant concentration, mol·dm^{-3}	x_A	0.1	0.3	0.5
Ultrasound intensity, W·cm^{-2}	x_B	0.2	0.3	0.4
Time, min	x_C	45	90	135
Temperature, ^{o}C	X_D	30	45	60

A statistical analysis of the results allowed to describe the dependency between the efficiency of the isolation of humic acids in the process with the use of substances that were carriers of macronutrients of fertilizers (y_{NPK}) and the four main process parameters: extractant concentration (x_A), ultrasound intensity (x_B), process time (x_C) and temperature (x_D). The influence of the process parameters on the response, after removing the statistically insignificant parts, was presented as a polynomial equation (1).

$$y_{NPK} = 34{,}10 + 7{,}75 \cdot x_A + 2{,}54 \cdot x_B + 5{,}34 \cdot x_C - 5{,}28 \cdot x_C^2 + 10{,}81 \cdot x_D + 6{,}16 \cdot x_D^2 \quad (1)$$

Acknowledgments

This research was funded by the Ministry of Science and Higher Education of Poland within a frame of science subsidy for 2023 which was realized in the Department of Engineering and Technology of Chemical Processes, Wroclaw University of Science and Technology (no. 8211104160 - K24W03D05).

References

[1] Stevenson F.J., *Humus Chemistry. Genesis. Composition. Reactions*. Second Edition. New York, John Wiley and Sons 1994.
[2] Tan K.H. *Humic matter in soil and the environment. Principles and controversies*. Boca Raton, CRC Press 2014.
[3] Orlov D.S. *Humic Substances in Soils and General Theory of Humification*. London: CRC Press 1995.
[4] Erro J., Urrutia O., Baigorri R., Fuentes M., Zamarreño A.M., Garcia-Mina J.M. Incorporation of humic-derived active molecules into compound NPK granulated fertilizers: main technical difficulties and potential solutions*, Chem. Biol. Technol. Agric*., 2016, 3, 18.
[5] Kolokassidou C., Pashalidis I., Costa C.N., Efstathiou A.M., Buckau G. Thermal stability of solid and aqueous solutions of humic acid, *Thermochim. Acta*, 2007, 454, 78–83.

THE CONCEPT OF A NEW AERODYNAMIC MULTIPHASE REACTOR FOR CATALYST INJECTION FOR A PULVERISED COAL BOILER

Marek Ochowiak[1,2]*, Zdzisław Bielecki[2,3], Andżelika Krupińska[1], Sylwia Włodarczak[1], Magdalena Matuszak[1]

[1]Poznan University of Technology, Department of Chemical Engineering and Equipment, M. Sklodowska-Curie 5, 60-965 Poznan, Poland
[2]Kuncar S.A., Pszczyńska 167C, 43-175 Wyry, Poland
[3]Silesian University of Technology, Department of Automatic Control and Robotics, Akademicka 2A, 44-100 Gliwice, Poland
*corresponding author: marek.ochowiak@put.poznan.pl

A conventional pulverized coal-fired boiler is composed of two main components: the furnace, where the burners, firing system, and combustion occur, and the convective section, which houses the heat exchanger surfaces. The walls of the boiler are typically designed to serve as the evaporator. Within the convective portion, the heat exchanger sections are arranged in a specific sequence along the flue gas pathway and have an arrangement that is typical for lignite-fired boilers.

Fuel additives enable the load related to coal combustion to be reduced, and therefore the amount of fuel that is needed to produce a unit amount of energy to also be reduced [1]. The manner in which the catalyst is fed into the dust duct is extremely important: if it is in a liquid form, the construction solution of the atomizer becomes significant. In recent years, the use of aerodynamic multiphase reactors as atomizers for generating droplets has become increasingly common. Conventional reactor-mixer designs, however, are limited by the size of the generated droplets, the maximum viscosity of the sprayed substance, and the intensity of its stream.

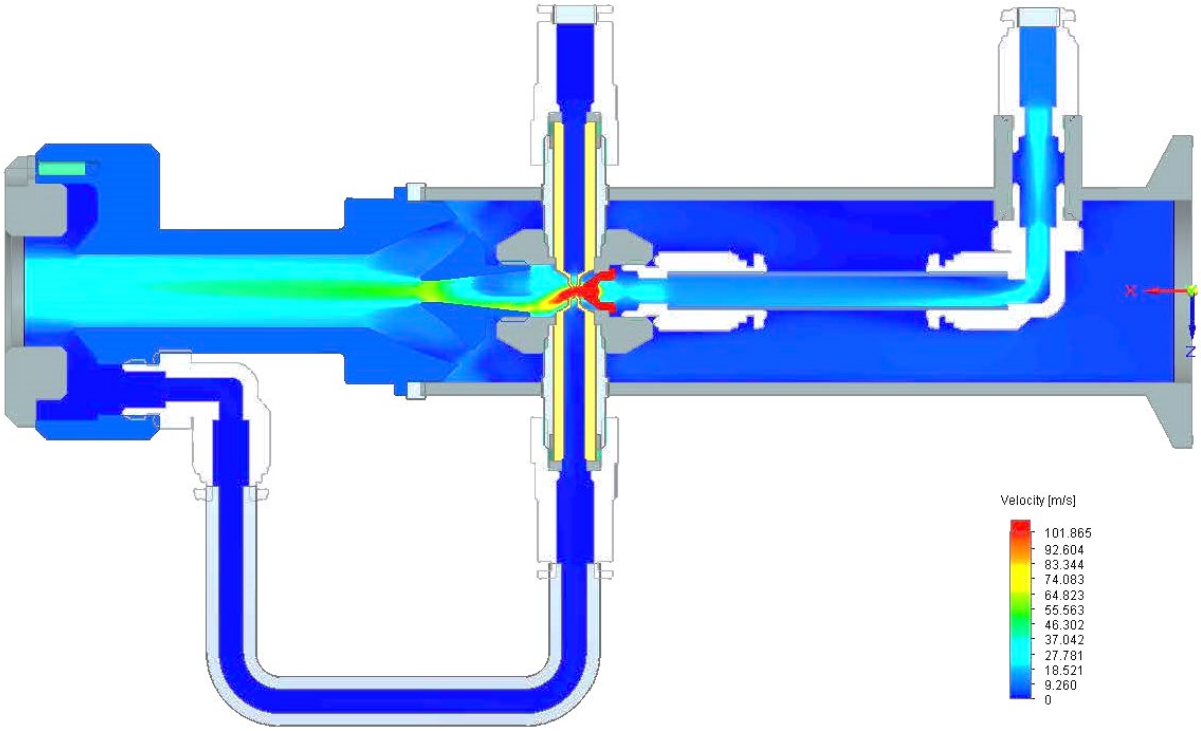

Fig. 1. The designed aerodynamic multiphase reactor with the velocity fields of the fluid flow

The purpose of this work was to design, manufacture and test (CFD and experiments) an aerodynamic multiphase reactor for feeding the catalyst in a liquid state to the dust duct. The reactor (Figure 1), as described in paper [2], should use pneumatic atomization of substances that are fed through internal nozzles. In turn, the nozzles should have diameters which are appropriate for the substance being sprayed. These nozzles must be positioned on the axis of the gas nozzle outlet, with the diameter of the chosen gas nozzle being based on the desired droplet diameter and velocity needed for atomization. When developing new designs, it is important to remember that droplets with appropriate diameters and atomization spectrums must be generated when adding a minimal amount of additional air. Moreover, the construction of an atomization device should be simplified. At a gas flow velocity of 20 m/s, the minimum droplet lifetime is 0.05 s, and the evaporation time of a 30 μm diameter droplet is approximately 1.4 s at 293 K, 0.1 s at 308 K, 0.087 s at 313 K, and 0.023 s at 373 K. When taking into consideration temperature changes along the dust duct leading to the boiler, droplets should be capable of covering the necessary distance in the aerosol [1, 3, 4]. For practical reasons, it is advisable to generate droplets with a larger diameter, such as 50 μm. This is due to the fact that flow conditions and dust duct length may affect both droplet diameter and lifetime, which is related to smaller droplets evaporating, coalescing or undergoing other transformations [1, 3, 4].

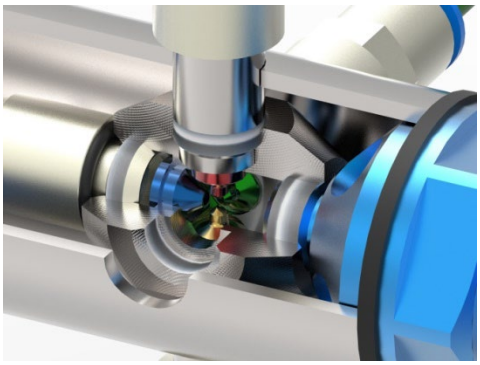

Fig. 2. The detailed visualization of liquid supply nozzles in the aerodynamic multiphase reactor

The designed aerodynamic multiphase reactor is a crucial component of the system. It utilizes a two-phase atomizing nozzle in order to produce controlled droplets of a catalyst suspension. The schematic diagram of the nozzle is shown in Figure 2, and its operation is described in detail in reference [2]. The size of generated droplets is adjustable based on process parameters and the viscosity of the catalyst suspension. The liquid supply nozzle was angled at 90° relative to the gas nozzle, with a wall cut of 30° on the opposite side of the central conduit. The diameter of the outlet was 0.5 mm. Additionally, efforts are made to minimize the introduction of additional air into the boiler [5], and to create a simple, cost-effective design.

Funding: The research was financed by the Polish Ministry of Education and Science (SBAD).

References

[1] Bielecki Z., Ochowiak M., Włodarczak S., Krupińska A., Matuszak M., Lewtak R., Dziuba J., Szajna E., Choiński D., Odziomek M., The analysis of the possibility of feeding a liquid catalyst to a coal dust channel, *Energies*, 2021, 14, 8521.
[2] Bielecki Z., Szajna E., Ochowiak M., Aerodynamic multi-phase reactor, European Patent Application, 2022.
[3] Bielecki Z., Ochowiak M., Włodarczak S., Krupińska A., Matuszak M., Jagiełło K., Dziuba J., Szajna E., Choiński D., Odziomek M., Sosnowski T.R., The optimal diameter of the droplets of a high-viscosity liquid containing solid state catalyst particles, *Energies*, 2022, 15, 3937.
[4] Ochowiak M., Bielecki Z., Bielecki M., Włodarczak S., Krupińska A., Matuszak M., Choiński D., Lewtak R., Pavlenko I., The D2-law of droplet evaporation when calculating the droplet evaporation process of liquid containing solid state catalyst particles, *Energies*, 2022, 15, 7642.
[5] Ochowiak M., Bielecki Z., Krupińska A., Matuszak M., Włodarczak S., Bielecki M., Choiński D., Smyła J., Jagiełło K., Pulverized coal-fired boilers: future directions of scientific research, *Energies,* 2023, 16, 935.

PROCESS ENGINEERING-DRIVEN CONCEPTS FOR INCREASING THERAPEUTIC EFFICACY OF DRUG DELIVERY USING NEBULIZERS

Marcin Odziomek*, Katarzyna Dobrowolska, Tomasz R. Sosnowski

Warsaw University of Technology, Faculty of Chemical and Process Engineering, Waryńskiego 1, 00-645 Warsaw, Poland
*corresponding author: marcin.odziomek@pw.edu.pl

Nebulization is a popular method of aerosol generation for delivery of medicines in the topical treatment of respiratory system diseases. The process has been demonstrated to involve several multi-scale aspects within the area of interest of chemical and process engineering [1].

In this communication, we present several types of research with different methods to improve the efficiency of drug delivery to the lower respiratory system using concepts based on engineering methods to control aerosol properties to increase the efficiency of drug deposition and expected therapeutic effects. Selected results have already been partially presented [2, 3, 4], but new data are still emerging, which are discussed here. The studies were focused on:

1. influencing the regional deposition of inhaled drugs by modifying aerosol droplet size distribution with drug adjuvants and diluting aerosol with supplemental air;
2. development of a method of drug delivery with simultaneous oxygen supplementation by nebulization of oxygen nanobubble dispersions (ONBDs);
3. using an add-on device to eliminate the fugitive emission of the drug emitted from the nebulizer.

Concept no.1 was based on altering the droplet size distribution with liquid additives that modify the liquid's viscosity (or more generally: rheological properties), surface tension and electrolytic conductivity. Each of these parameters affects the atomization process in a characteristic way depending on the type of nebulizer. Due to different atomization principles in pneumatic and vibrating mesh nebulizers, the effect of changing physiochemical parameters is not intuitive, and common relationships known, e.g., for spray nozzles, are not applicable in this case. Figure 1 shows as an example the influence of the surface tension and viscosity on the mass median aerodynamic diameter (MMAD) of aerosol droplets. The observed relationships can be explained by the two-step process of atomization and separation during generation and release of aerosol from a pneumatic nebulizer.

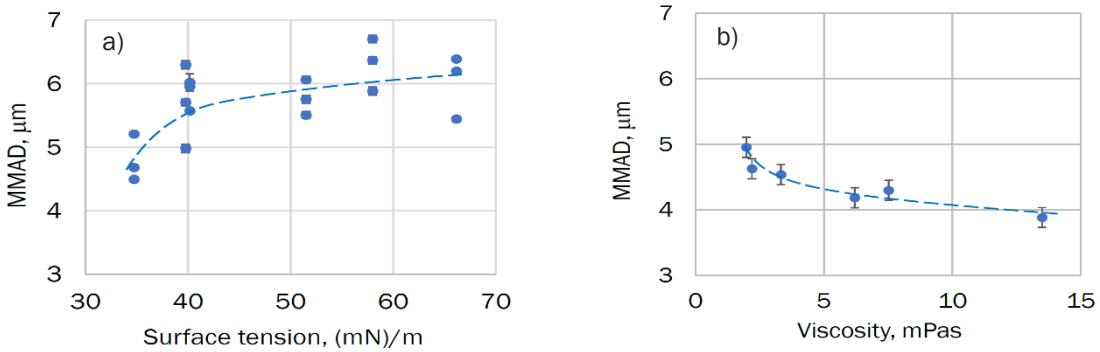

Fig. 1. The influence of (a) surface tension and (b) viscosity of atomized liquids on the mass median diameter (MMD) of aerosol droplets emitted from a pneumatic nebulizer

The second concept was verified by demonstrating measurable increased oxygen content in the aerosol generated by a medical vibrating mesh nebulizer (VMN) using ONBDs compared to the aerosol generated using ordinary liquids. Table 1 shows the comparison of oxygen content in the

aerosol directly at the outlet of VMN measured with an optical oxygen sensor. For aerosol produced from ONBDs in VMN, O_2 concentration was even up to approximately 19% higher than in the aerosol generated using water. For ONBDs after storage, this effect was decreased but still present. The results also indicate that oxygen begins to desorb from the aerosol droplets as soon as it is produced, but the aerosol is immediately inhaled by the patient. The system therefore offers the possibility of delivering an oxygen-rich aerosol without a dedicated source of this gas, allowing for the potential use of this therapy outside clinics.

Table 1. Comparison of oxygen content in the mists measured directly at the outlet of VMN for water and ONBD. Values are means ± SD, n = 3

Nebulized liquid	Vibrating Mesh Nebulizer	
	Oxygen content [mg L^{-1}]	Increase [%]
Water	8.72±0.16	N/A
ONBD - freshly prepared	10.37±0.18	18.85
ONBD - after 14 days of storage	9.43±0.18	8.16

Concept no.3 (Fig. 3) allowed to increase the aerosol emission rate per minute of inhalation (also for droplets smaller than 5 μm, which are most desirable for inhalation therapy). This could be achieved since the inhalation chamber restricted aerosol emission to the environment during exhalation, and also allowed for separation of the largest droplets by sedimentation.

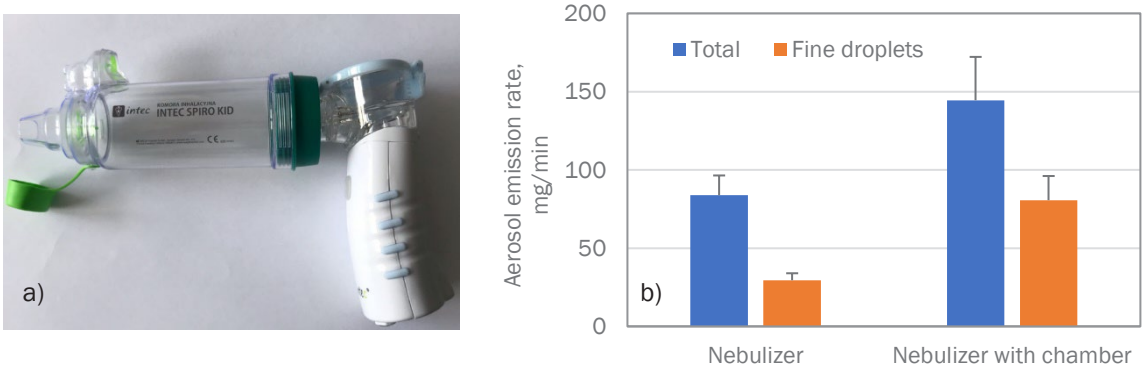

Fig. 2. (a) Vibrating mesh nebulizer with add-on inhalation chamber and (b) the increase in the mass of all and fine (smaller than 5 μm) droplets in the aerosol emitted during the inhalation phase

In conclusion, it has been shown that concepts based on process engineering knowledge can be successfully applied to medical nebulizers to enhance the ability to better treat respiratory diseases by inhalation. This area of application is particularly important in an era of widespread pulmonary diseases related to environmental pollution and epidemic threats.

Acknowledgement: Work supported by NCN project No. 2018/29/B/ST8/00273. Oxygen nanobubbles studies were done within BIOTECHMED-1 project granted by Warsaw University of Technology under the program Excellence Initiative: Research University (IDUB).

References

[1] Sosnowski T.R. *Chem. Eng. Sci.*, 2023, 268, 118407.
[2] Dobrowolska K.E., Kinowska M., Sosnowski T.R., *Nebulization of solutions containing guar gum as a viscosity modifier of natural origin*, in: Respiratory Drug Delivery 2022, Dalby R.N. et al. (Eds.), RDD Online, Richmond, 2022, Vol. 1, 541-544.
[3] Odziomek M., Ulatowski K., Dobrowolska K., Górniak I., Sobieszuk P., Sosnowski T.R., *Scientific Reports*, 2022, 12, 12455.
[4] Sosnowski T.R., Vilkotsky A.I., Emeryk A., *Vibrating mesh nebulizers with a valved inhalation chamber for increased drug delivery to the lower airways*, in: *Respiratory Drug Delivery 2022*, Dalby R.N. et al. (Eds.), RDD Online, Richmond, 2022, Vol. 1, 551-554.

SEPARATION MODELING OF NON-RACEMIC MIXTURES OF ENANTIOMERS BY ACHIRAL CHROMATOGRAPHY

Maksymilian Olbrycht[1,*], Justyna Gumieniak[2], Patrycja Mruc[1], Wojciech Piątkowski[1], Dorota Antos

[1]Rzeszów University of Technology, Department of Chemical and Process Engineering, Rzeszów, Poland
[2]Rzeszów University of Technology, Department of Chemical and Process Engineering, Stalowa Wola, Poland
*corresponding author: m.olbrycht@prz.edu.pl

Recently, more than half of the drugs currently manufactured consist of chiral ingredients. As the individual enantiomers of a drug usually differ in biological activity, most of the new drugs marketed today are single enantiomers. Chiral chromatography is considered as the most versatile technique to isolate the pure target compound from enantiomeric mixtures. However, to this moment it is usually a cost driver of the whole production process, which stems from a high price of CSPs and their limited mechanical stability [1–3].

Despite identical physico-chemical properties of enantiomers, their achiral separation is possible in many cases. This stems from asymmetric interactions of certain enantiomers in the liquid and adsorbed phases due to the formation of homo and hetero-chiral associates with different adsorption properties. The occurrence of that phenomenon, termed as self-disproportionation of enantiomers (SDE), has been evidenced in literature for a number of different chiral compounds including: sulfoxides, CF3-derivatives, amides, carboxylic acids, amino acids, dipeptides derivatives, alcohols, phenols, esters, heterocycles, etc. Yet, quantitative description of phenomena underlying achiral adsorption of SDE-phoric compounds is still incomplete [4-6].

In this study, a mechanistic model for description of retention behaviour of SDE-phoric compounds in silica-based achiral chromatography has been developed along with a procedure for fast determination of the model parameters. The model accounts for the formation of associates of chiral molecules in the adsorbed phase (Fig. 1). The ability of the model to reproduce band profiles was verified for enantiomeric mixtures of three structurally different chiral compounds.

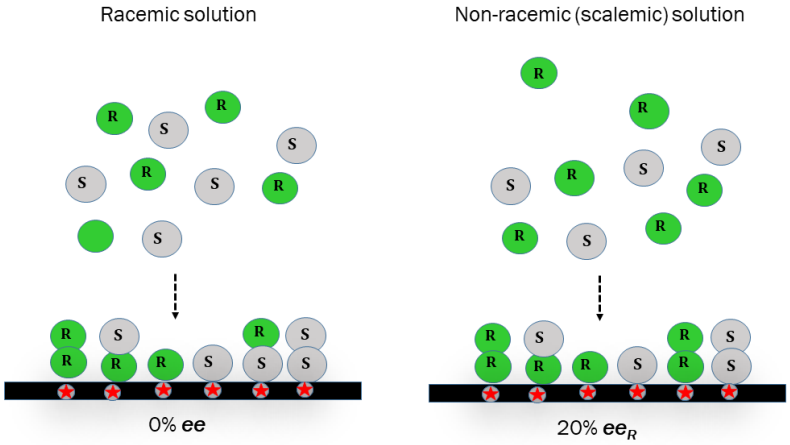

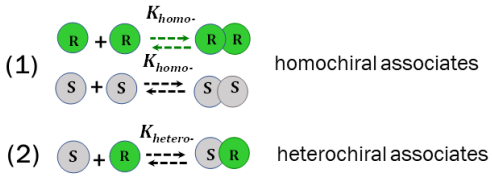

Fig. 1. Formation of associates of enantiomers on the adsorbent surface and the reaction mechanism the binary interactions

Financial support of this work by National Science Center Poland (UMO-2021/41/B/ST8/00631) is gratefully acknowledge

References

[1] *Differentiation of Enantiomers II. Topics in Current Chemistry*. Editor Volker Schurig, Springer 2013.
[2] Soloshonok V.A., Remarkable Amplification of the Self-Disproportio-nation of Enantiomers on Achiral-Phase Chromatography Columns, *Angewandte Chemie*, 2006, 118, 780-783,
[3] Soloshonok V.A., Wzorek A., Klika K.D., A question of policy: should tests for the self-disproportionation of enantiomers (SDE) be mandatory for reports involving scalemates?, *Tetrahedron: Asymmetry*, 2017, 28, 1430–1434.
[4] Olbrycht M., Gumieniak J., Mruc P., Balawejder M., Piątkowski W., Antos D., Separation of non-racemic mixtures of enantiomers by achiral chromatography, *J. Chromatogr. A*, 2023 (submited).
[5] Han J., Kitagawa O., Wzorek A., Klika K.D., Soloshonok V. A., The self-disproportionation of enantiomers (SDE): a menace or an opportunity?, *Chem. Sci*., 2018, 9, 1718–1739
[6] Han J., Wzorek A., Soloshonok V.A., Klika K.D., The self-disproportionation of enantiomers (SDE): The effect of scaling down, potential problems versus prospective applications, possible new occurrences, and unrealized opportunities?, *Electrophoresis*, 2019, 40, 1869–1880.

EXPOSURE TO A ROTATING MAGNETIC FIELD AS A METHOD OF ENHANCING THE PERMEABILITY OF ACTIVE PHARMACEUTICAL INGREDIENTS THROUGH THE SKIN

Paula Ossowicz-Rupniewska[1,*], Anna Nowak[2], Maciej Konopacki[3], Marian Kordas[3], Łukasz Kucharski[2], Rafał Rakoczy[3]

[1]West Pomeranian University of Technology in Szczecin, Faculty of Chemical Technology and Engineering, Department of Chemical Organic Technology and Polymeric Materials, Piastów 42, 71-065 Szczecin, Poland
[2]Pomeranian Medical University in Szczecin, Department of Cosmetic and Pharmaceutical Chemistry, Powstańców Wielkopolskich 72, 70-111 Szczecin, Poland
[3]West Pomeranian University of Technology in Szczecin, Faculty of Chemical Technology and Engineering, Department of Chemical and Process Engineering, Piastów 42, 71-065 Szczecin, Poland
*corresponding author: possowicz@zut.edu.pl

The topical application of drugs is one of the most important methods of delivering them to the body. It is known that the transdermal administration of a drug to induce a systemic effect has some significant advantages and, in many situations, is an advantage over the administration of oral or intravenous drugs. Among the many benefits of transdermal administration of the drug, the possibility of avoiding the first-pass effect (hepatic metabolism) and the elimination of side effects of the drug on the gastrointestinal tract deserve special attention. For this route of drug administration, a significant factor in limiting penetration is the skin barrier, which reduces the penetration efficiency and limits the absorption of the compounds. This layer is the greatest obstacle to the transport of active substances and is considered the primary barrier to the permeation of molecules. It is mainly composed of lipid substances such as ceramides, cholesterol, fatty acids, cholesterol esters, and small amounts of phospholipids [1]. Among the available and topically applied drugs, a significantly small group can passively cross the skin barrier in amounts sufficient to obtain a therapeutic effect [2].

The aim of the research was to increase the permeability of various active substances (API) through the skin using a rotating magnetic field (RMF). The study used 50 Hz RMF and various APIs. The study results of the permeability of active substances through the skin when exposed to a magnetic field and in a control sample without a magnetic field are presented.

The obtained results confirm the increased permeability of active substances and the permeation rate for the samples subjected to the magnetic field.

References

[1] Lam P.L., Gambari R., Advanced progress of microencapsulation technologies: In vivo and in vitro models for studying oral and transdermal drug deliveries, *J. Control. Release*, 2014, 178, 25–45.
[2] Haq A., Michniak-Kohn B., Effects of solvents and penetration enhancers on transdermal delivery of thymoquinone: permeability and skin deposition study, *Drug Delivery*, 2018, 25, 1943–1949.

THE EFFECT OF CONFECTIONING ON THE STRUCTURAL PROPERTIES OF COSMETIC EMULSIONS

Piotr Owczarz*, Anna Rył, Marta Masica

Department of Chemical Engineering. Lodz University of Technology,
Wolczanska 213, Lodz, Poland
*corresponding author: piotr.owczarz@p.lodz.pl

Currently, in every branch of industry, including food, pharmaceutical and cosmetics industries, there is a constant struggle for customers. Manufacturers compete in the use of various marketing campaigns, which try to encourage consumers to buy their products. On the other hand, the customer expects increasingly higher quality products that will meet their expectations at a lower price. The packaging used differs in design and execution depending on the type and purpose of the product, as well as its physico-chemical properties such as; viscosity, density or pH. The most frequently used are bottles, tubes, jars, and airless containers with various types of closures, such as pumps, flip-tops, caps, and atomizers.

As packaging for food, cosmetic and pharmaceutical emulsions, e.g. creams, ointments, pastes, etc., containers are commonly used, in which the opening for formulation application is also the opening for filling; these dosing cap openings usually have a diameter of at least ϕ= 10 mm. In this case, the packaging is filled using short nozzles with a similar diameter. During filling, the flow rate of the medium through the nozzle causes shear stresses, but due to the large cross-sectional area, their value is small. On the other hand, classic tubes with an application opening with a diameter of a few millimeters are filled through the open, non-welded back part of the tube. As a consequence, they are filled with a cosmetic, food or pharmaceutical product in the same way as bottle or jar packaging through a short nozzle with a fairly large diameter.

Another type of packaging is tubairless packaging developed and patented by PumpArt. They are delivered in the form of closed outer tubes, inside which an additional sealed reservoir has been placed – Figure 1. Between the outer tube and the flexible inner container there is an air cushion connected to the atmosphere through an opening in the outer shell. A tight inner tank fills the sterility of the packaging, the possibility of using up to 95% of the product filling it. Simultaneously, it causes the tubairless to be filled through a small hole with a diameter of up to ϕ= 6 mm, which is also a place for collecting the product. This solution, apart from purely mechanical problems resulting from the risk of damage to the inner container during the insertion of the dispenser needle, additionally generates high flow rates, and thus high values of shear rates occurring in the application nozzles. As a consequence, they may cause uncontrolled and undesirable structural changes to the product.

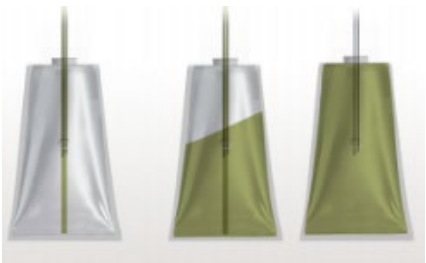

Fig. 1. Scheme of construction and filling of a tubairless

The aim of this work was to examine the impact of shear rate, with particular emphasis on very high values occurring during the packaging of cosmetic emulsion into tubairless containers, as well as to propose a research methodology that will enable to obtain results that can be analyzed

quantitatively. A commercial nourishing hand cream with 3% urea content by Seni Care and three samples of the cream with different contents of active substance in the amount of 0%, 1.5% and 4.5% prepared by the manufacturer for this project were selected for the study.

The key information for the development of the methodology of rheological research was the proposal of the emulsion pumping, measuring and dosing system and the assumptions regarding the efficiency of the dosing system at the level of 2000 pcs/h. The scheme of the proposed dosing system enabling the simultaneous filling of six containers is shown in Figure 2.

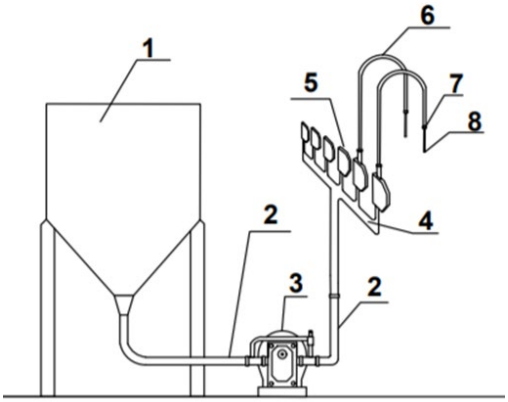

Fig. 2. Scheme of the dosing system. 1 – product tank, 2 – supply pipeline DN40, 3 – lobe pump with by-pass, 4 – distribution manifold, 5 – mass flow meter, 6 – high pressure pipe, 7 – dosing valve (cut-off), 8 – dosing needle

Based on the required capacity and geometric dimensions of the installation, the average values of the flow rate were calculated, and thus the average values of the shear rate occurring in the installation. Rheological properties of experimental emulsions were carried out using the cone-plate system of the Anton Paar rotational rheometer under isothermal conditions (20 °C, 25 °C, 30 °C, 35 °C). The tests were carried out in a wide range of shear rates from 10^{-2} to 10^{3} s^{-1}. In order to eliminate the phenomenon of slipping effect, a cone with a modified, rough surface was used. Structural properties were determined on the basis of oscillation tests carried out in analogous conditions using the same measuring system.

The impact of changes in shear rate values occurring during the packaging process on the structural properties of the tested emulsions was determined based on the three interval thixotropy test (3ITT). The essence of the test is to determine structural properties using oscillation measurements in the first interval and compare them with results obtained for the same deformation conditions obtained in the third interval. During the second interval, the sample was subjected to unidirectional shear deformations with the set time and shear rate calculated on the basis of the flow assumptions in the actual technological line. The applied shear rates were 0.1, 1, 10, 100, and 1000 s^{-1}, respectively.

Based on the conducted tests, it was found that all samples exhibited strong shear thinning behaviour; the analysis of the flow curves showed alternating thixotropy and antithixotropy phenomena during changes in the shear rate while deforming the same sample. The 3ITT tests carried out for the shear rate of 100 s^{-1} (characteristic for the transport of the product in pipelines) revealed the lack of complete structure recovery of the investigated cosmetic products after the deformation ceased. This phenomenon may have a negative impact on the product performance parameters resulting from its structural changes.

The use of higher shear rate values of 1000 s^{-1} in the second interval (characteristic for the flow through a long, small-diameter capillary, i.e. an application needle) led to the results not only of full structure recovery, but also of "strengthening" the structural properties. This proves the phenomenon of secondary homogenization of the emulsion under the influence of high shear rate values and leads to obtaining a product with the desired structural properties.

HEAT TRANSFER IN A COMPACT CROSS-FLOW MINI HEAT EXCHANGER

Mateusz Prończuk*, Aleksander Pabiś

Tadeusz Kościuszko Cracow University of Technology, Department of Chemical Engineering and Technology, Warszawska 24, 31-155 Kraków, Poland
*corresponding author: mateusz.pronczuk@pk.edu.pl

The growing popularity of mini heat exchangers can be associated with the increasing miniaturization of mass and heat exchange devices and instruments, as well as the miniaturization of electronic devices and parts. The need to dissipate large amounts of heat energy from relatively small devices requires new types of heat transfer devices. It often turns out that heat transfer in channels with hydraulic diameters of less than 3 mm cannot be described using classical equations that allow the determination of heat transfer coefficients for conventional heat exchangers, even if they have a similar structure to the analyzed mini heat exchangers. Many references state that heat transfer in channels smaller than 3 mm in diameter is characterized by high values of heat transfer coefficients [1].

A major problem in studying heat transfer in mini-channels is the inability to determine the wall temperature of the channel, since traditional temperature sensors often have a size comparable to the diameter of the channel. The inability to measure the wall temperature prevents direct experimental determination of the heat transfer coefficient for the investigated channel, only the overall heat transfer coefficient can be determined directly [2].

However, the heat transfer coefficient can be determined indirectly based on optimization methods [3]. For this purpose, it is necessary to assume a general form of equations combining heat transfer coefficients along with the operating parameters of the exchanger (such as media flow velocity and physical properties) or express them as dimensionless numbers (e.g. Reynolds number, Re, Prandtl number, Pr, Nusselt number, Nu):

$$Nu = C \cdot Re^a \cdot Pr^b \tag{1}$$

where: a, b, C – model parameters selected using optimization methods. Equation (1) must be assumed for each heat exchanger circuit. Then, using the determined heat transfer coefficients (as a function of the Nusselt number), the overall heat transfer coefficient is calculated, which can be compared with its experimental values. Using the optimization procedure, the parameters of the correlation equation (1) are determined. Here, the sum of squares of the differences between the calculated and experimentally determined overall heat transfer coefficients is taken as the objective function [3].

This paper presents the results of determining heat transfer coefficients for a cross-current mini heat exchanger described in detail in [4]. The heat exchanger consisted of two flows: the hot water flow consisted of 21 channels with a length of 30 mm and a diameter of 2 mm, while the cold water flow consisted of 19 channels with a length of 25.5 m and a diameter of 2 mm and two rectangular channels along the side of the cylindrical part with dimensions of 1 mm by 25.5 mm. A schematic drawing of the heat exchanger is shown in Fig. 1. (a). Cold water was drawn from the water mains, while hot water circulated in a closed loop and was heated using a thermostat. The flow rate of cold water was altered in the range of 10–290 dm³/h, and the initial temperature of cold water averaged 8°C. For hot water, the flow rate was altered in the range of 100–290 dm³/h, and the initial temperature of hot water was altered in the range of 40–70°C. A total of 1682 experimental points were used for the analysis, which was originally presented elsewhere [4].

Using the optimization method, the following correlation was obtained for hot water flow (21 channels with circular cross-section):

$$Nu_h = 0.4896 \cdot Re_h^{0.4205} \cdot Pr_h^{0.33} \tag{2}$$

And for cold water flow (19 channels with a circular cross-section and 2 channels with a rectangular cross-section):

$$Nu_c = 0.2519 \cdot Re_c^{0.7188} \cdot Pr_c^{0.33} \tag{3}$$

Using the obtained correlations (2) and (3), the overall heat transfer coefficients were calculated. The values of these coefficients were compared with the experimental equation presented in the paper [1]:

$$U_{calc} = 1480 + 7.42Q_{Vc} + 7.38Q_{Vh} + 1.52T_{ih} \tag{3}$$

where: Q_{Vc} i Q_{Vh} denote the flow rate of cold water and hot water, respectively, in dm³/h, and T_{ih} denotes the initial temperature of hot water in °C. The results of the comparison are shown in Fig. 1. (b) and (c).

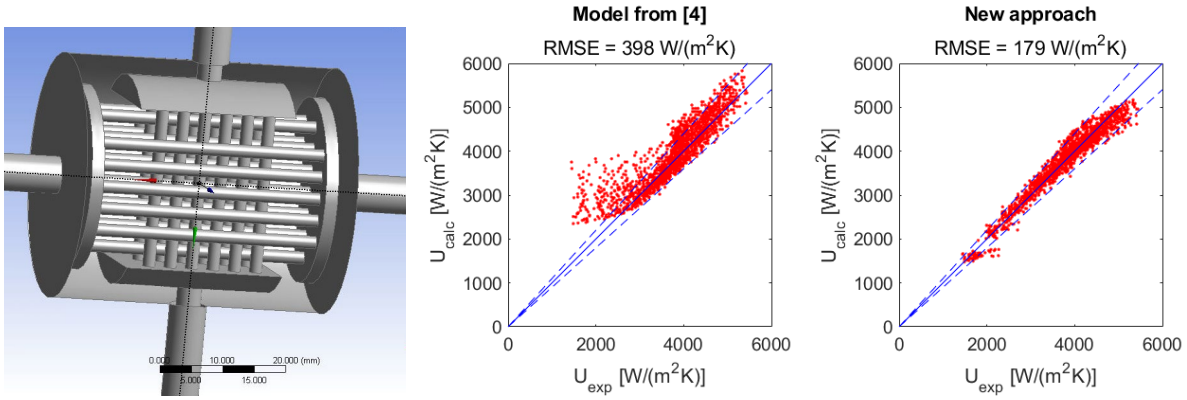

Fig. 1. (a) Schematic drawing of the investigated heat exchanger. Comparison of experimental values of overall heat transfer coefficient, U_{exp}, versus overall heat transfer coefficient, U_{calc}, calculated using: (b) experimental model from [1], (c) optimization based method. Red dots stand for experimental data, solid blue line stands for $U_{exp} = U_{calc}$ and dashed line stands for ±10% deviation from the experimental results

It can be observed that the application of the optimization method provided a significant improvement in the fit of the calculations to the experimental results as the calculated values usually do not deviate by more than ±10% from the overall heat transfer coefficients determined experimentally (Fig. 1. (c)). The greatest improvement in the quality of the fit was obtained for cases where the overall heat transfer coefficients had small values (low liquid flow rates). The root mean square error (RMSE) for the new method decreased to 179 W/(m²·K) (Fig. 1. (c)) compared to 397 W/(m²·K) for the model proposed in [4] (Fig. 1. (b)). The optimization method allowed the heat transfer coefficients to be determined with high accuracy, and the determination itself does not require knowledge of the channel wall temperature. A very good match between the calculation results and the experimental data confirms the high accuracy of the method and confirms its usefulness for studying heat transfer in mini heat exchangers.

References

[1] Morini G.L. Single–phase convective heat transfer in microchannels: A review of experimental results, *Int. J. Therm. Sci.*, 2004, 43, 631–651.

[2] Ünverdi M., Kücük H., Yılmaz M.S. Experimental investigation of heat transfer and pressure drop in a mini–channel shell and tube heat exchanger, *Heat Mass Tran.*, 2019, 55, 1271–1286.

[3] Prończuk M., Krzanowska A., Experimental Investigation of the Heat Transfer and Pressure Drop inside Tubes and the Shell of a Minichannel Shell and Tube Type Heat Exchanger, *Energies*, 2021, 14, 8563.

[4] Pabiś A., Charakterystyka pracy krzyżowo-prądowego mikrowymiennika ciepła, *Chemik*, 65, 10, 983-990.

GLUTATHIONE AS A MODIFIER OF ZINC OXIDE NANOPARTICLES TO IMPROVE TRANSPORT EFFICIENCY OF ACTIVE SUBSTANCES

Jolanta Pulit-Prociak[1,*], Olga Długosz[1], Anita Staroń[1], Paweł Staroń[1], Jarosław Chwastowski[1], Dominik Domagała[2], Krzysztof Pociecha[3], Marcin Banach[1]

[1]Cracow University of Technology, Faculty of Chemical Engineering and Technology, Warszawska 24, 31-155 Cracow, Poland
[2]University of Agriculture, Department of Human Nutrition and Dietetics, Balicka 122, 30-149 Cracow, Poland
[3]Jagiellonian University, Faculty of Pharmacy, Medyczna 9, 30-688 Cracow, Poland
[*]corresponding author: jolanta.pulit-prociak@pk.edu.pl

The aim of the study was to check whether it is possible to obtain zinc oxide nanoparticles that would have limited release of zinc ions. Released zinc ions pose a serious threat to healthy tissues. When zinc oxide nanoparticles are applied as a drug carrier, one should take into consideration that after the structure is introduced to the body, it may undergo various types of reactions. A number of compounds can be attached to their surface which may lead to changes of their physicochemical properties, for example solubility. Unprotected surface is accessible to proteins, phosphate and carbonate ions and these can easily bind to it. The released structures may penetrate into healthy cells and tissues via endocytosis and dissolve inside which may lead to the formation of zinc ions, which are harmful at higher concentrations [1, 2].

Therefore, the influence of combining zinc oxide nanoparticles with glutathione on the intensity of releasing zinc structures from the resulting conjugate was studied. The deposition of glutathione on zinc oxide nanoparticles was carried out in a microwave radiation field. A series of materials was obtained. They differed in process parameters (molar ratio of glutathione to zinc oxide, homogenization time of the reaction mixture, multiplicity of potassium hydroxide to stoichiometric amount). The reference sample contained no glutathione.

The prepared materials have been analyzed in terms of their physicochemical properties. The size of nanoparticles has been assessed with Dynamic Light Scattering method, specific surface area, pore volume and size were assessed using low-temperature nitrogen sorption. The release of zinc structures was checked via leaching processes in water as leaching medium. In in-vitro study the influence of prepared zinc oxide nanoparticles (both in basic and modified form) on cytotoxicity and proliferation of Chinese hamster ovary (CHO) cells was analyzed. Also, the obtained materials have been conjugated with tadalafil, as the active substance. Verification of bioavailability of the drug from the materials obtained was tested in in-vivo studies using Wistar rats.

It has been found out that compared to the reference sample some of the prepared materials exhibited lower rates of zinc release (Fig. 1). The size of most nanoparticles was in the range from 230 to 800 nm, which from biomedical point of view is a satisfactory result. Passive cancer therapy takes advantage of the anatomical and physiological properties of the cancer tumor. This is because it is characterized by increased vascular permeability (leaky network of blood vessels). The diameter of the fissures ranges from 100 to 800 nm, while in healthy tissues only 2–6 nm. The average size of most anticancer drugs is small and does not exceed 10 nm. Using them in an independent form would result in their diffusion into healthy and diseased tissues equally. Combining them with nanocarriers (230-800 nm) would significantly reduce or even eliminate the penetration of therapeutic substances into the structure of healthy tissues.

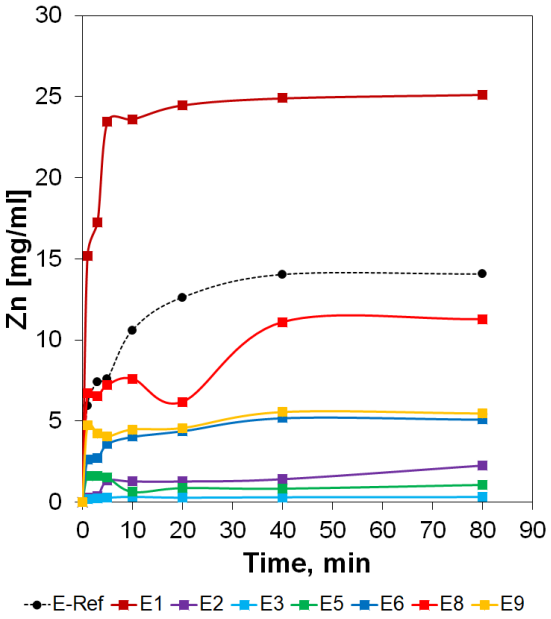

Fig. 1. Profiles of zinc releasing from the prepared materials

The modification of zinc oxide with glutathione also made the specific surface area in the material greater. All analyzed zinc oxide nanoparticles modified with glutathione induced stronger proliferation of CHO cells than in the case of using reference sample (not modified, basic ZnO). Also, they had a weaker cytotoxic effect. The bioavailability of tadalafil from the modified material was greater by almost 125% compared to the reference sample.

The results demonstrate the promising prognosis of the produced materials in light of their use as potential carriers of active substances.

References

[1] Betancourt G.R., Berlanga D.M.L., Puente U.B., Rodríguez F.O., Sánchez-Valdes S., Surface modification of ZnO nanoparticles, *Mater. Sci. Forum*, 2010, 644, 61-64.

[2] Haidar Z.S., Bio-inspired/-functional colloidal core-shell polymeric-based nanosystems: Technology promise in tissue engineering, bioimaging and nanomedicine, *Polymers*, 2010, 2, 323-352.

MATHEMATICAL MODELLING OF A HEAT EXCHANGER USED IN PRODUCTION PROCESS

Rafał Rakoczy[1,*], Piotr Jaworski[1,2]

[1]West Pomeranian University of Technology in Szczecin,
Piastów 42, 71-065 Szczecin, Poland
[2]Grupa Azoty Zakłady Chemiczne "Police" S.A., Kuźnicka 1, 72-010 Police
[*]corresponding author: rrakoczy@zut.edu.pl

The simulation of chemical engineering process is connected with the knowledge about hydrodynamics, transfer processes and chemical reactions. The residence time distribution (RTD) is one of the most informative characteristics to obtain information about chemical engineering equipment. This systematic approach allowed to establish flow patterns in various types of mixers or heat exchangers.

The RTD technique might be treated as a quantitative method to develop simple hydrodynamic models in the case of complex engineering systems. The interpretation of RTD measurements may be realized by using compartmental models which are composed of branches containing elementary ideal reactors connecting all together by the nodes. The application of a mixing model (combination of a plug flow reactor (PRF) and a continuous stirred tank reactor (CSTR) with circulation flow) to study of RTD measurements is widely presented in the relevant literature[1,2].

This study was supported by the Ministry of Education and Science, Poland [Impelenatation Doctorate Programme, granted to Piotr Jaworski].

References

[1] Buso A., Giomo M., Boaretto L. & Paratella A., New electrochemical reactor for wastewater treatment: mathematical model, *Chem. Eng. Process.*, 1997, 36, 411-418.
[2] Yianatos J.B., Bergh L.G., Díaz F., Rodríguez J., Mixing characteristics of industrial flotation equipment, *Chem. Eng. Sci.,* 2005, 60, 2273-2282.

STRUCTURAL CHANGES OF VISCOELASTIC SOLUTIONS OF ZWITTERIONIC AND ANIONIC SURFACTANT MIXTURES UNDER THE INFLUENCE OF SIMPLE SALT

Jacek Różański*, Sylwia Różańska, Patrycja Wagner, Ewelina Warmbier

Poznań University of Technology, Institute of Chemical Technology and Engineering,
Berdychowo 4, 60-965 Poznań
*corresponding author: jacek.rozanski@put.poznan.pl

Surfactants have a number of characteristic properties, among which one of the less well-known is the ability to shape the consistency of a liquid. Changes in the rheological properties of surfactant solutions are most often the result of the formation of very long micelles called wormlike micelles [1]. Although complex rheological properties are also characteristic of surfactant solutions where vesicle micelles, lamellar structures and cross-linked micelles are formed. Changes in the microstructure of micellar solutions can be caused by changes in surfactant concentration, liquid temperature, and the addition of various organic and inorganic compounds [2-5]. The aim of the research presented in this paper was to determine the relationship between the shape of the formed micelles and the molar ratio of the mixture of zwitterionic and anionic surfactants in the solution and the concentration of sodium chloride.

Solutions of cocamidopropyl betaine (zwitterionic surfactant, CAPB, PCC Exol) and sodium dodecylbenzene sulfonate (SDBS, Sigma-Aldrich) mixtures were used in the study. Changes in the rheological properties of CAPB/SDBS solutions were analyzed under the influence of sodium chloride (Chempur, Poland). Structural changes were determined in the photos of solutions taken with the CryoTEM technique and using a polarising microscope. Rheological tests were carried out using a system of parallel plates. The measuring system was connected to a Physica MCR501 rheometer (Anton Paar, Austria).

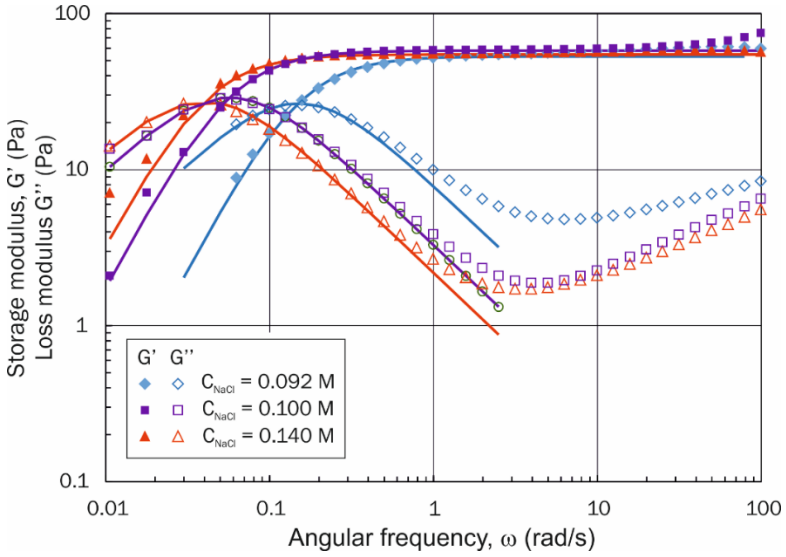

Fig. 1. Mechanical spectra for CAPB/SDBS solutions with different concentrations of NaCl

Fig. 1 presents exemplary mechanical spectra for solutions of CAPB/SDBS mixtures. Maxwell's equation was used to describe them (solid lines in Fig. 1), which means, according to the Cates theory, that, based on the results of oscillation tests, it is possible to calculate the average mesh size ξ of a micellar network. Table 1 lists the parameters of the Maxwell model (G_0 is the plateau of storage modulus, λ_M is the relaxation time), the average mesh size ξ and zero shear viscosity for CAPB/SDBS solutions with different NaCl concentrations. The values of G_0 and ξ are independent

of the sodium chloride concentration, while the zero viscosity and relaxation time are maximum at a salt concentration of 0.1 M.

Table 1. Influence of NaCl concentration on properties of CAPB/SDBS solutions

C_{NaCl} (M)	G_0 (Pa)	λ_M (s)	ξ (nm)	η_0 (Pa·s)
0.092	53.1	6.7	42.39	354.0
0.100	54.6	25.0	42.00	1365.0
0.140	57.8	17.5	41.21	1014.0

The occurrence of the maximum zero shear viscosity and relaxation time can be explained on the basis of the CryoTEM images presented in Figure 2. For CAPB/SDBS solutions with the addition of NaCl at a concentration of 0.092 M, a network of wormlike micelles can be recognized, while for the solution with the addition of 0.14 M, branched wormlike micelles were formed. The change in the structure of the fluid can be explained with the packing parameter,

$$p = v/l \cdot a \tag{1}$$

where *v* is the hydrophobic volume, *l* is the hydrophobic chain length, and *a* is the effective area per headgroup of the molecules occupied at the micellar interface. The value of parameter *p* increased with increasing salt concentration as a result of screening of the negative CAPB and SDBS groups. At high salt concentrations, the CAPB/SDBS solutions became turbid. The photos taken using a polarizing microscope showed that the turbidity of the solutions is the result of the formation of layered micelles, which confirms that the change in salt concentration leads to a change in the packing parameter.

a) b)

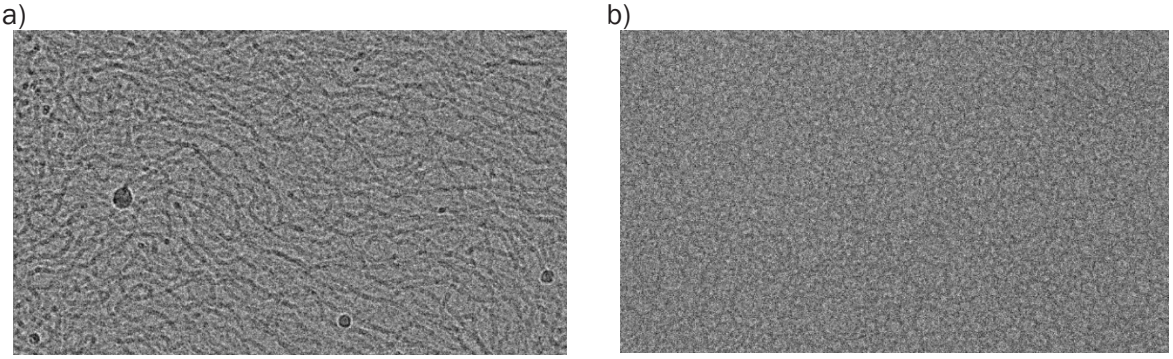

Fig. 1. CryoTEM photos of CAPB/SDBS solutions with NaCl concentration of 0.092 M (a) and 0.14 M (b)

This research was funded by the Ministry of Education and Science.

References

[1] Dreiss C.A., Wormlike micelles: where do we stand? Recent developments, linear rheology and scattering techniques, *Soft Matter*, 2007, 3(8), 956-970.
[2] Parker A., Fieber W., Viscoelasticity of anionic wormlike micelles: effects of ionic strength and small hydrophobic molecules, *Soft Matter*, 2013, 9, 1203-1213.
[3] López-Díaz D., Castillo R., The wormlike micellar solution made of a zwitterionic surfactant (TDPS) an anionic surfactant (SDS) and brine in the semidilute regime, *J. Phys. Chem. B*, 2010, 114(24), 8917-8925.
[4] Pandya N., Rajput G., Janni D. S., Subramanyam G., Ray D., Aswal V., Varade D., SLES/CMEA mixed surfactant system: effect of electrolyte on interfacial behavior and microstructures in aqueous media, *J. Mol. Liq.*, 2021, 325, 1-8.
[5] Fieber W., Scheklaukov, Kunz W., Pleines M., Benczédi D., Zemb T., Towards a general understanding of the effects of hydrophobic additives on the viscosity of surfactant solutions, *J. Mol. Liq.*, 2021, 329, 1-11.

THE STRUCTURE AND ANALITICAL STUDY OF CONDUCTING ANION RADICAL SALT [N-CH_3-2-NH_2-5-CL-*PY*](TCNQ)$_2$·CH_3CN

Tetiana Starodub*, Weronika Miśkiewicz

Jan Kochanowski University, Institute of Chemistry, 25-405 Kielce, Poland
*corresponding author: tstarodub@ujk.edu.pl

Anion radical salts (ARS) formed by TCNQ as some of the most potent π-electron acceptors attracted researchers' attention back in the mid-1960s [1, 2]. In the crystals of these salts, the TCNQ particles are stacked. The overlap of their π-orbitals gives rise to one-dimensional zone, which is partly occupied in fractional oxidation state, and this may give rise to metallic properties. Therefore, ARS TCNQ are very promising objects from the point of view of their wide applications – from phototransistors and nano-wires to biosensors in the determination of drugs or toxic substances [3, 4].

The work was devoted to the study of novel genuine organic anion-radical salt TCNQ with a cation based on 2-amin-5-chloro-pyridine:

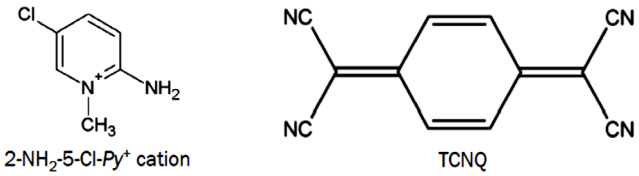

2-NH_2-5-Cl-*Py*$^+$ cation TCNQ

The unusual behaviour of TCNQ anions in the crystalline structure of [N-CH_3-2-NH_2-5-Cl-*Py*](TCNQ)$_2$·CH_3CN has been observed: the formation of $(TCNQ)_2^{2-}$ π-dimers (Fig. 1). In most cases such dimers originate between the anion radical $TCNQ^{\bullet-}$ and neutral TCNQ molecule, or σ-dimers $(TCNQ\text{-}TCNQ)^{2-}$ occur. In these $(TCNQ)_2^{2-}$ π-dimers the distance between the middle planes of anion radical is 3.24 Å. The structure of ARS [N-CH_3-2-NH_2-5-Cl-*Py*](TCNQ)$_2$ favours the formation of high conducting state of the salt [5]. In this case, ARS TCNQ with a cation based on 2-amin-5-chloro-pyridine is a promising material in electronics and biotechnologies.

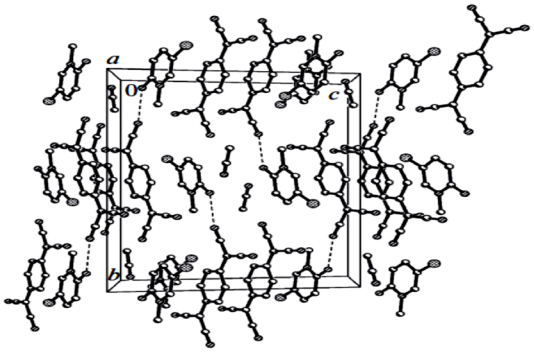

Fig. 1. Fragment of the crystalline structure of ARS [N-CH_3-2-NH_2-5-Cl-*Py*](TCNQ)$_2$

The TCNQ molecules contain in their structure active centres that help in the formation and maintenance of strong additional bonds with the molecule of biologically active substances:

In the case of ARS [N-CH_3-2-NH_2-5-Cl-*Py*](TCNQ)$_2$ charge transfer complexes (CTC) with selected drugs [Drug](TCNQ)$_x$ (X = 1, 2) are formed. The form of CTC is evidenced by the absorption spectrum of a coloured solution of this CTC obtained in the wavelength range from 500 to 900 nm (Fig. 2, 3).

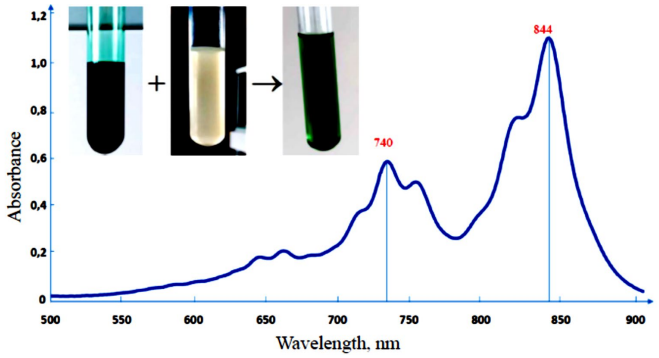

Fig. 2. Absorption spectrum of coloured CTC [Valeric acid](TCNQ). Picture in the upper left corner of the chart: ARS [N-CH_3-2-NH_2-5-Cl-*Py*](TCNQ)$_2$ solution (CH_3CN), Valeric acid solution (CH_3OH) and the final solution of CTC [Valeric acid](TCNQ)

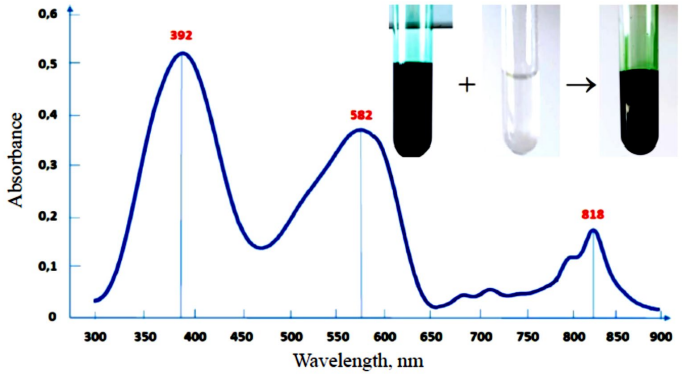

Fig. 3. Absorption spectrum of a coloured CTC [Amoxicillin](TCNQ). Picture in the upper right corner of the chart: ARS [N-CH_3-2-NH_2-5-Cl-*Py*](TCNQ)$_2$ solution (CH_3CN), Duomox 1000 solution (CH_3OH) and the final solution of CTC [Amoxicillin](TCNQ)
(Amoxicillin is the active drug substance of Duomox)

This means that a given salt can be used as an indicator of biologically active substances, for drugs, for example. In the future, we plan to study the cytotoxic properties of this salt.

References

[1] Melby L.R., Harder R.J., Hertler W.R., Mahler W., Benson R.E., Mochel W.E., Anion-Radical Derivatives and Complexes of 7,7,8,8-Tetracyanoquinodimethan, *J. Am. Chem. Soc.,* 1962, 84, 3370-3374.

[2] Melby L.R., Substituted quinodimethans: VIII. salts derived from the 7, 7, 8, 8-tetracyanoquinodimethan anion–radical and benzologues of quaternary pyrazinium cations, *Can. J. Chem.,* 1965, 43, 1448-1453.

[3] Al-Sabha T.N., Al-Karemy N.M, The use of 7,7',8,8'-tetracyanoquinodimethane for the spectrophotometric determination of some primary amines application to real water samples, *J. Analit. Met. Chem.,* 2013, 2013, 1-8.

[4] Wang C., Wu N., Jacobs D.L., Xu M., Yang X., Zang L., Discrimination of alkyl and aromatic amine vapors using TTF–TCNQ based chemiresistive sensors, *Chem. Commun.,* 2017, 53, 1132-1135.

[5] Starodub T.N., Fenske D., Fuhr O., Kazhewa O.N., Starodub V.A., The Crystal Structure of a RAS (N–CH3-2-NH2-5-Cl–Py)(TCNQ)(CH3CN) Solvate, 2020, *Crystallography reports*, 2020, 65 (2), 242-246.

MIXING POWER AND HYDRODYNAMICS FOR DIFFERENT CLEARANCES OF A FLAT BLADE TURBINE IMPELLER

Jacek Stelmach*

Lodz University of Technology, Faculty of Process and Environmental Engineering,
Wólczańska 213, 93-005 Łódź, Poland
*corresponding author: jacek.stelmach@p.lodz.pl

Rising prices of electricity encourage the search for effective systems for mechanical mixing of liquids. The literature [1] shows that the distance of the impeller from the bottom can significantly affect the mixing power. However, the energy efficiency of mixing is also influenced by the hydrodynamics in the tank. If the reduction of the mixing power is accompanied by the extension of the mixing time, the energy expenditure does not have to be reduced [2]. Our own research [3, 4] shows that changes in the height of the liquid above the impeller are accompanied by changes in the mixing power. Therefore, the purpose of this work was to determine the mixing power and velocity distributions for a flat blade turbine impeller (FBT).

The paper presents the test results of a flat blade turbine impeller (FBT) with a diameter of D = 100 mm. The tests were carried out in a tank with a diameter of T = 292 mm (T/D ≈ 3) with four standard baffles ($B = 0.1 \cdot T$). The tank was filled with water to the height of H = 300 mm ($H/T \approx 1$). The mixing power was determined on the basis of measurements of the rotational frequency of the impeller N (0.83 $s^{-1} < N < 6.67\ s^{-1}$) and the torque M. The average liquid velocities in the tank were determined using the PIV method for $N = 6\ s^{-1}$. In the tests, the impeller clearance ranged from C = 20 mm to C = 140 mm. The diagram of experimental rig is shown in Fig. 1a.

Fig. 1b shows the obtained dependence of the mixing power number Eu

$$Eu = \frac{P}{N^3 \cdot D^5 \cdot \rho} = \frac{2 \cdot \pi \cdot M}{N^2 \cdot D^5 \cdot \rho} \tag{1}$$

on the dimensionless C/D impeller clearance, also for other tests [5].

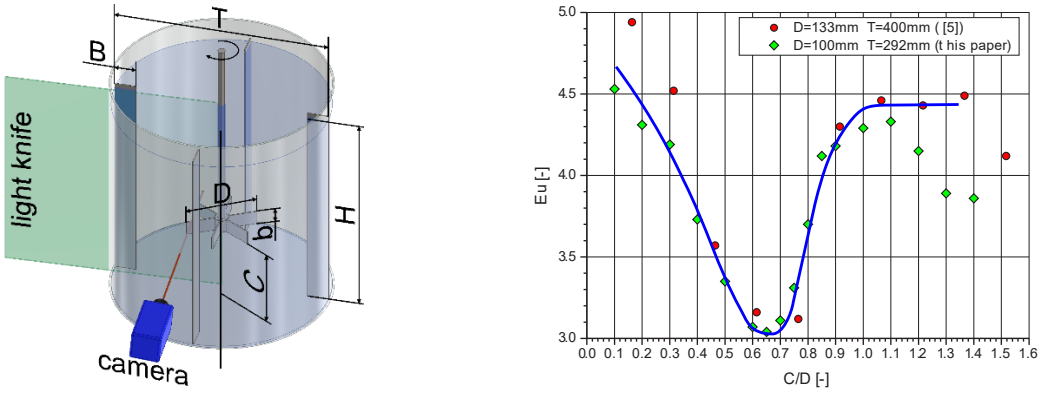

Fig. 1. Diagram of the experimental rig (a) and relationship between mixing power and clearance (b)

For $C/D \approx 1$, the power number has the value Eu = 4.4. This is a value close to that given in the literature [1, 6] for this impeller. Reducing the clearance decreases the power number. In the range from C/D = 0.6 to C/D = 0.7 the power number reaches the lowest value. Thus, from the energy point of view, this is the best distance between the impeller and the bottom of the tank.

Figure 2 presents the distributions of the average dimensionless liquid velocities in the tank:

$$U^* = \frac{U}{U_{tip}} = \frac{U}{\pi \cdot D \cdot N} \tag{2}$$

For a mid-height impeller (C/D = 1.4) there are two circulation loops as for radial flow impellers. However, axial flow of liquid through the impeller towards the top of the tank is observed (Fig. 2a). For this reason, radial flow occurs above the impeller. For clearance C/D = 1, there are still two circulation loops. However, axial flow is directed to the bottom of the tank, so radial flow occurs under the impeller (Fig. 2b). Further reduction of the clearance (C/D = 0.75) causes the lower circulation loop to disappear - the flow changes to axial, as in the case of PBT and propeller impellers (Fig. 2c). However, until C/D = 0.60, the liquid stream does not reach the bottom. Only for smaller clearances (Fig. 2d) the liquid stream is slowed down by the bottom of the tank.

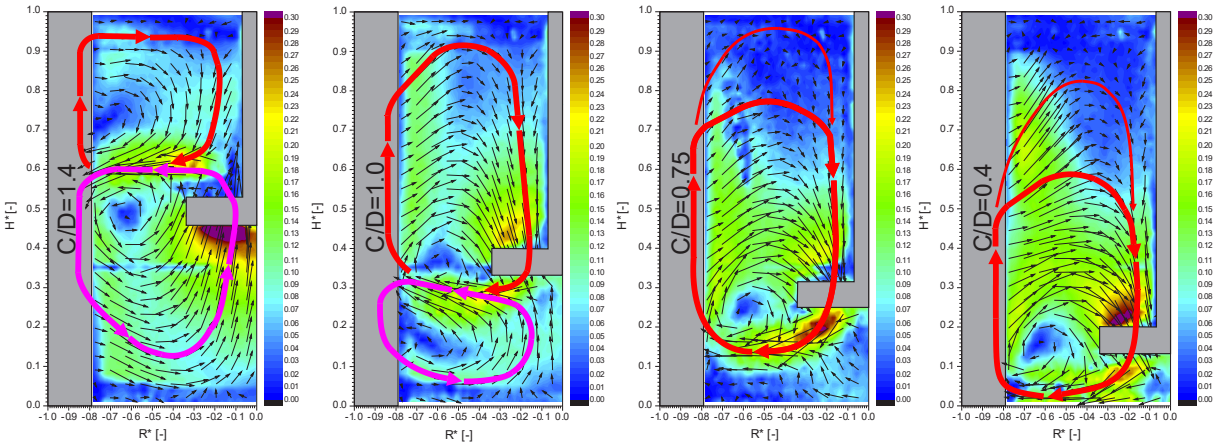

Fig. 2. Liquid circulation in the tank depending on the clearance

Comparative analysis of Figs. 1 and 2 leads to the conclusion that there is a relationship between the mixing power and the liquid flow generated by the impeller. Radial flow (with two liquid circulation loops) is more energy intensive. Reducing the clearance leads to a flow close to axial flow, which is less energy-intensive [1, 6]. However, it should be noted that typical axial flow impellers have much lower mixing powers, e.g. for a six-blade PBT mixer with a blade angle of 45° and C/D = 0.9, the power number is Eu = 1.58 [1, 6]. Therefore, the operation of FBT impellers with too small a clearance is not effective - better results will be obtained by using typical impellers generating axial flow. The minimum value of the power number is reached when the liquid stream flows towards the bottom, but it is not impeded by it. The effect of the bottom must be large, because when reducing the clearance, the mixing power increases to the value as for C/D = 1.

In the case of the tested impeller, the dimensionless clearance C/D > 0.8 ensures radial flow, and the higher the impeller is placed, the larger the lower circulation loop. A high impeller suspension (C/D > 1.3) also causes a slight (< 10%) reduction in mixing power.

Since the energy is transferred to the liquid when there is a difference in the tangential velocity of the blade and the liquid [6], a complete description of the dependence of power and hydrodynamics requires testing of this velocity component at the level of the impeller.

References

[1] Stręk F., *Mieszanie i mieszalniki*, Warszawa, WNT 1981.
[2] Stelmach J., Musoski R., Kuncewicz Cz., Jirout T., Rieger F., Efficiency of PBT impellers with different blade cross-sections, *Energies*, 2022, 15, 585.
[3] Stelmach J., Kuncewicz Cz., Rieger F., Moravec J., Jirout T., Increase of mixing power during emptying of tanks with turbine-blade impellers, *Przem. Chem.*, 2020, 99/2, 239-243 (in Polish).
[4] Rieger F., Moravec J., Stelmach J., Kuncewicz Cz., Effect of modification of the stirrer with folding blades on the increase in mixing power during emptying the tank, *Przem. Chem.*, 2021, 100/12, 1231-1235 (in Polish).
[5] Skalski M., *Investigation of the dependence of the mixing power on the distance between the impeller and the bottom of the tank*, BEng Thesis, Lodz University of Technology 2021 (in Polish).
[6] Nagata S., *Mixing. Principles and applications*, Tokyo, Kodansha Ltd. 1975.

EFFECT OF STIRRED TANK GEOMETRY ON CAVERN FORMATION IN MICROGEL FLOW

Anna Story*, Grzegorz Story

West Pomeranian University of Technology in Szczecin, Faculty of Chemical Technology and Engineering, Department of Chemical and Process Engineering,
Piastów 42, 71-065 Szczecin, Poland
*corresponding author: Anna.Story@zut.edu.pl

The term microgel is defined as a colloidal suspension of cross-linked polymer particles of 10-1000 nm or more [1], uniformly dispersed and swelling in a solvent. Because of their cross-linking, polymer particles do not dissolve in water and therefore do not form solutions. Depending on the method of synthesis, cross-linking density, or concentration, microgels can have different physicochemical properties. In addition, the level of swelling of a microgel can change due to changes in the values of external factors such as ionic strength, temperature, or pH. Due to their wide range of properties, microgels found a broad range of applications and are commonly used, among others, in pharmaceutical, food, cosmetic and biomedical industries as viscosity modifiers or dispersing and stabilizing agents. On the other hand, microgels have complex rheology, so their processing poses some challenges. For example, during the mechanical mixing of non-Newtonian shear-thinning fluids with yield stress an intensive mixing zone, called cavern [2], is generated near the rotating impeller. Outside this zone, the fluid velocity is close to zero, preventing homogenization throughout the entire volume.

In the presented study, the tested liquid was a water suspension of Carbopol 940 grade (C940) at the concentration of 0.2 wt%, neutralized with 1 M sodium hydroxide to pH = 5.1 to formulate transparent, high-viscosity hydrogel. Based on the rheological measurements of the flow curve the tested microgel was classified as yield stress shear-thinning fluid with values of Herschel-Bulkley model (Eq. 1) parameters equal to τ_y = 27.86 Pa, K = 4.62 Pas^n and n = 0.49, respectively for yield stress, consistency coefficient and flow index [3].

$$\tau = \tau_y + K\dot{\gamma}^{\mathrm{n}} \tag{1}$$

Experimental studies of the cavern formation were performed in a flat-bottomed stirred tank of a diameter T = 0.222 m, both unbaffled and baffled (four flat standard baffles), equipped with one of the two high-speed impellers, a Rushton turbine (RT) or a hydrofoil Prochem Maxflo T (PMT) impeller (Fig. 1) of a diameter D = 0.078 m. The impellers rotated over a wide range of rotational speeds, up to N = 1200 rpm. The impellers were selected to produce different, mainly radial (RT) or mainly axial (PMT) microgel circulation in the tank.

a) 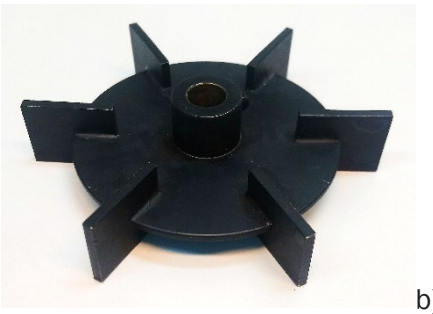 b) 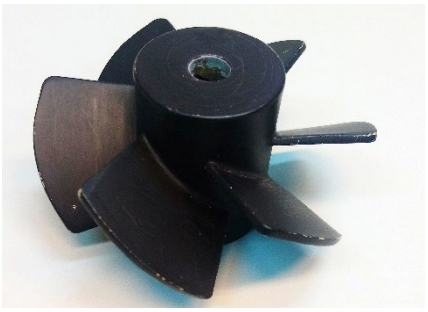

Fig. 1. Tested impellers: a) Rushton turbine; b) Prochem Maxflo T

Measurements of cavern size were performed using a planar laser-induced fluorescence (PLIF) technique. As a passive dye tracer, the tested microgel with the addition of 5 mg/l of the

rhodamine 6G was used and injected directly into the mixing fluid between the impeller blades. A detailed procedure of PLIF measurements can be found elsewhere [4].

Examples of the results obtained in PLIF measurements are presented in Figure 2, as vertical half-planes pass through the axis of the stirred tank. In the case of baffled tanks, the plane was located at an angle of 45 degrees between two adjacent baffles. The obtained results provided an analysis of the influence of several geometric and process parameters on the size of the intensive mixing zone generated in a microgel with complex rheological properties.

It was found that both the presence of baffles in the tank, the type of impeller, and its rotational speed significantly affect the diameter and height of the cavern. The presence of baffles reduces the growth of cavern diameter, but at the same time causes a greater increase in its height. Among the two impellers tested, the PMT which generates mainly axial circulation in the tank proved to be more effective.

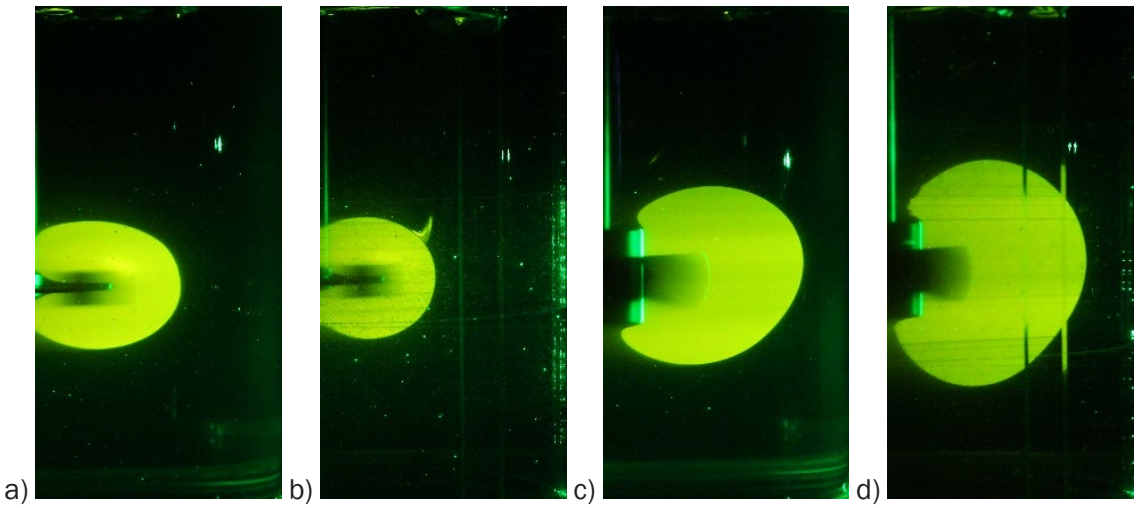

Fig. 2. Visualisation of caverns generated in a stirred tank filled with 0.2% C940, N = 360 rpm: a) RT impeller, unbaffled tank; b) RT impeller, baffled tank; c) PMT impeller, unbaffled tank; d) PMT impeller, baffled tank

References

[1] Fernandez-Nieves A, Wyss H, Mattsson J, Weitz DA. *Microgel suspensions: Fundamentals and applications*, Wiley-VCH, Weinheim 2011.
[2] Wichterle K, Wein O. Agitation of concentrated suspensions. CHISA '75, Paper B4.6, Prague 1975.
[3] Story A., Jaworski Z., Major-Godlewska M., Story G. Influence of rheological properties of stirred liquids on the axial and tangential forces in a vessel with a PMT impeller, *Chem. Eng. Res. Des.*, 2018, 138, 398-404.
[4] Story A., Jaworski Z. A new model of cavern diameter based on a validated CFD study on stirring of a highly shear-thinning fluid. *Chem. Pap.* 2017, 71, 7, 1255-1269.

COMPARATIVE STUDY OF SOLID DISSOLUTION PROCESS IN STIRRED TANK AND MAGNETICALLY ASSISTED MIXER

Grzegorz Story*, Anna Story, Marian Kordas, Rafał Rakoczy

West Pomeranian University of Technology in Szczecin, Faculty of Chemical Technology and Engineering, Department of Chemical and Process Engineering,
Piastów 42, 71-065 Szczecin, Poland
*corresponding author: Grzegorz.Story@zut.edu.pl

The process of dissolution of a solid in a liquid, which by definition denotes a heterogeneous reaction proceeding with an accompanying transition from solid to solution, is widely used in many industries, including chemical, food, pharmaceutical and biomedical industries.

Dissolution in a solid-liquid system can occur spontaneously by free diffusion. Then its driving forces are intermolecular interactions between the solute and solvent, as well as the tendency of the system to achieve maximum entropy and minimum internal energy. In industrial practice, however, the dissolution of a solid in a liquid is intensified by various methods.

One of the simplest methods to enhance the mass transfer ratio from solid to liquid is mechanical mixing using a rotating impeller [1]. Other methods which are commonly used for the intensification of the solid phase dissolution include pulsing fluid, electrical discharges, dissolution on a fixed or a fluidized bed and ultrasounds. However, researchers are still looking for new constructions of impellers or improvements to the existing systems, as well as new methods to enhance the mass transfer process. One method is the application of a rotating magnetic field [2, 3, 4]. Despite numerous articles on the effect of RMF on mass transfer, no attention has been focused on comparing this process carried out in different types of mixing equipment. Therefore, the main purpose of this paper was to study the effect of the type of mixing device on mass transfer rate, specifically on the dissolution of sodium chloride.

In the undertaken study, specially prepared cylindrical NaCl samples were dissolved in water, in two various mixing devices: a mixer assisted by a rotating magnetic field (Fig. 1), and a stirred tank equipped with a Rushton turbine.

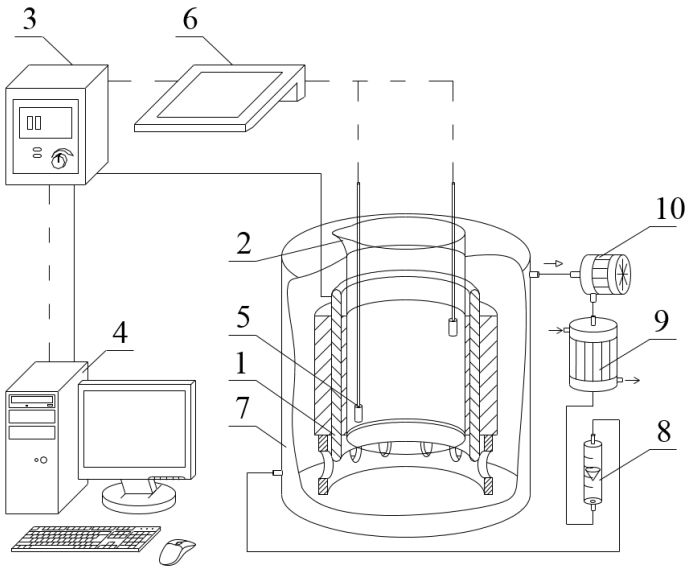

Fig. 1. The sketch of the first experimental set-up: 1 – RMF generator, 2 – glass container, 3 – a.c. transistorized inverter; 4 – computer; 5 – conductivity electrode; 6 – multifunctional computer meter; 7 – cooling jacket; 8 – rotameter; 9 – heat exchanger; 10 – oil pump

During the experiments, parameters such as the distribution of magnetic induction inside the RMF generator, the change in electrical conductivity of the solution over time, as well as the mass and diameter of the samples after a well-defined dissolution time were measured. Then, the mass transfer coefficient for two tested mixing devices was correlated by the combination of three dimensionless numbers: Sherwood, Reynolds and Schmidt.

The final comparison of the obtained results is presented in Figure 2. It was found that the values of mass transfer coefficient strongly depend on the Reynolds (*Re*) number. For the mass transfer process under the action of RMF, stronger influence was observed in the region of the lowest values of *Re*, while the mechanically agitated tank is more recommended for the turbulent region of flow. In a stirred tank, the solid-liquid mass transfer rate increases more rapidly with increasing impeller speed, compared to the increase of the same factor for the RMF device. It should be underlined that the influence of rotating magnetic field and stirred tank on the mass transfer rate was found to be equal for *Re* = 13 150.

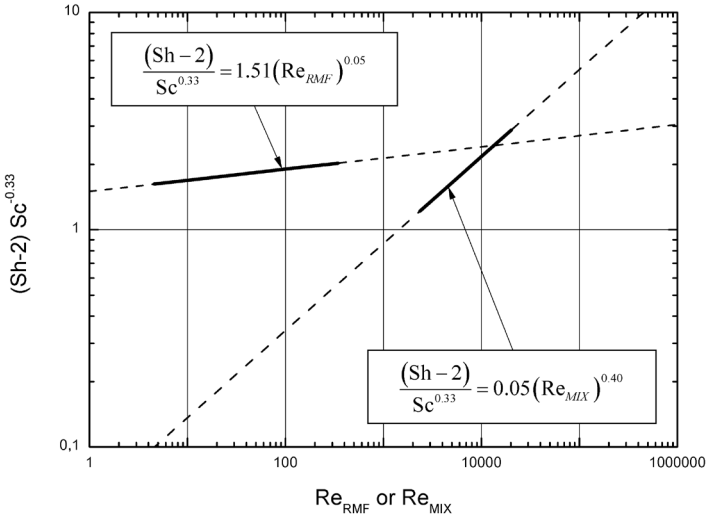

Fig. 2. Results of the mass transfer process under RMF and in a stirred tank

References

[1] Zlokarnik M. *Stirring: Theory and Practice*, Wiley-VCG Verlag GmbH, Weinheim 2001.

[2] Rakoczy R., Kordas M., Markowska-Szczupak A., Konopacki M., Augustyniak A., Jabłońska J., Paszkiewicz O., Dubrowska K., Story G., Story A., Ziętarska K., Sołoducha D., Borowski T., Roszak M., Grygorcewicz B., Dołęgowska B. Studies of a mixing process induced by a rotating magnetic field with the application of magnetic particles, *Chem. Process Eng. - Inz. Chem. Proces.*, 2021, 42, 2, 157-172.

[3] Rakoczy R. Study of effect of temperature gradient on solid dissolution process under action of transverse rotating magnetic field. *AIChE*, 2012, 58, 1030- 1039.

[4] Rakoczy R. Enhancement of solid dissolution process under the influence of rotating magnetic field. *Chem. Eng. Process.*, 2010, 49, 42–50.

ULTRASOUND-ASSISTED VACUUM IMPREGNATION OF LOW POROUS FOOD PRODUCTS: OPTIMIZATION AND QUALITY ISSUES

Justyna Szadzińska[1], Dominik Mierzwa[1,*], Elżbieta Radziejewska-Kubzdela[2], Róża Biegańska-Marecik[2]

[1]Poznań University of Technology, Institute of Chemical Technology and Engineering, Division of Process Engineering, Berdychowo 4, 60-965 Poznań, Poland
[2]Poznan University of Life Sciences, Department of Food Technology of Plant Origin, Wojska Polskiego 31, 60-624 Poznań, Poland
*corresponding author: dominik.mierzwa@put.poznan.pl

Vacuum impregnation (VI) is a process that allows the introduction of selected soluble compounds into the porous matrix of a material. The process is used in many industries. It is particularly useful in the food industry to impregnate food products with functional compounds such as vitamins, trace elements, cryoprotectants, antioxidants, browning inhibitors, prebiotics, or pH-lowering compounds. Mass exchange during vacuum impregnation occurs under the influence of a mechanically generated pressure gradient between the interior of the porous tissue and the environment. The two essential mechanisms of mass exchange are assumed to be as follows: Hydrodynamic Mechanism (HDM) and Deformation-Relaxation Phenomena (DRP). A detailed description of the vacuum impregnation process from the theoretical and practical side can be found in the works of Fito et al. [1] and Derossi et al. [2].

Since mass exchange processes during vacuum impregnation are relatively slow and may be limited to the superficial layer of material, alternative methods are sought for faster and "more complete" tissue saturation. One of the possibilities is the application of ultrasound as a mass transfer accelerator. Ultrasound is a mechanical wave that easily propagates through a liquid medium and may induce several mechanisms that enhance mass (and heat) transfer. Particularly effective, in terms of the intensification of transport processes, are the phenomena caused by the so-called unstable cavitation. In addition to cavitation, there are also other phenomena that allow to increase the rate of transport, e.g. "sponge effect". The description of the most important mechanisms and their influence on mass and heat transport was discussed by Chandrapala et al. [3].

Response Surface Methodology (RSM) is a method that allows the optimization of processes in terms of selected process parameters (factors) and responses. This method is used both in laboratory and industrial research. It has gained popularity because it allows the optimization of several parameters at the same time and determines interactions between individual factors. The use of OFAT (one-factor-at-a-time) method, during which only one parameter is changed per process, is not only more time-consuming and resource-intensive, but also does not allow to determine interactions between factors. More information on RSM can be found in the work of Sarabia and Ortiz [4].

The primary objective of this research was to find the optimal conditions for ultrasound-assisted vacuum impregnation of low porous materials. One of the most representative low porosity vegetables is, e.g., potato (*Solanum tuberosum*). For this purpose, potato bulbs were peeled and cut into cubes of 15 mm per side. Impregnation tests were carried out in an aqueous ternary solution composed of the bioactive compound – analytically pure ascorbic acid (AAC), citric acid, and sucrose. Optimization of VI was done with the use of Response Surface Methodology (RSM) in Design Expert ver. 13 software. Box-Behnken design was used with 3 factors (pressure of impregnation, stage duration and intensity of ultrasound enhancement) at 3 levels (see Table 1). On the basis of the obtained responses, impregnation processes were optimized in terms of:

- Maximization of the bioactive compound content (AAC) (R1, R2)
- Ion leakage from material (IL) minimization (R1) or maximization (R2)

- Minimization of the material hardness (H) (R1, R2)

Two optimal sets of conditions (R1 and R2) were chosen and experimentally tested.

Alteration of the optimization goal in terms of ion leakage results from the assumption that impregnated material needs to be preserved (e.g. by drying), which will be easier if its internal structure is disturbed. Structural changes in the raw material, and cell damage – cause the outflow of the cell fluids and an increase in the concentration of ions in the solution - higher IL.

Table 1. Process parameters

Factor	Box-Behnken Levels			Optimal		Reference
	-1	0	1	R1	R2	VI
pressure (mbar)	50	300	550	550	50	300
stage duration (min)	5	20	35	23	35	30
ultrasound enhancement (%)	0	50	100	100	100	0

The experimental results remain in good agreement with the predicted effects. Both optimal processes R1 and R2 were characterized by values of ascorbic acid content higher than the reference (VI) and similar to each other (no significant difference). More severe conditions in the R2 process caused significantly higher ion leakage as it was supposed. The hardness of the samples processed in R1 and R2 was similar to the raw material (no significant differences) and lower than after the reference process (VI). All these results confirm that RSM may be useful during vacuum impregnation process optimization and may predict effects with fair agreement. Analysis of other parameters, not involved in optimization, revealed a meaningful influence of ultrasound on the material being processed. The potato samples impregnated under more severe conditions (R2) were characterized by a significant color change and a visibly smaller gumminess and cohesiveness. As the last two parameters define the force and the work required to destroy the internal structure, it may be concluded that the high vacuum (lower pressure) in connection with the long ultrasound enhancement had a detrimental influence on the mechanical properties of this low porous vegetable, which in consequence led to substantial structure alteration

References

[1] Fito P., Andrés A., Chiralt A., Pardo P., Coupling of hydrodynamic mechanism and deformation-relaxation phenomena during vacuum treatments in solid porous food-liquid systems, *J. Food Eng.*, 1996, 27(3), 229–240.

[2] Derossi A., De Pilli T., Severini C., The application of vacuum impregnation techniques in food industry, in: Scientific, health and social aspects of the food industry, InTech, 2012.

[3] Chandrapala J., Oliver Ch., Kentish S., Ashokkumar M., Ultrasonics in food processing, *Ultrason. Sonochem.*, 2012, 19(5), 975–983.

[4] Sarabia L.A., Ortiz M.C., *Response Surface Methodology*, in: Comprehensive Chemometrics, Brown S.D., Tauler R., and Walczak B. (Eds.), Oxford: Elsevier 2009, 345–390.

PRODUCTION OF COSMETIC EMULSIONS BASED ON PLANT BIOCOMPONENTS

Waldemar Szaferski*, Piotr Tomasz Mitkowski, Marcin Janczarek, Weronika Ignaszak

Poznan University of Technology, Institute of Chemical Technology and Engineering,
Berdychowo 4, 60-965 Poznan, Poland
*corresponding author: waldemar.szaferski@put.poznan.pl

The paper deals with emulsions, which have found application in the production of cosmetic products, such as body lotions, face creams, biphasic micellar lotions, shampoos, facial cleansing gels and many others. Furthermore, they are widely used in pharmaceutical industry, also as microemulsions for delivering vaccines and killing microorganisms and also as preparations for accelerating the treatment of scars.

Extracts from natural plant products were used in the prepared cosmetic emulsion bases. The emulsifier was an aqueous solution of self-emulsifying base made from apricot kernel oil and soy lecithin. On the other hand, the oil phase was coconut, almond and grape seed oils. In addition, mixtures enriched with vegetable glycerin were produced.

The prepared cosmetic emulsion bases were subjected to microscopic analysis using Image-Pro Plus software. The results obtained were summarized in the form of histograms of the dependence of the values of average Sauter diameters on the concentration and type of oil phase. It has been found that for the mixture with almond oil, as the concentration of this oil phase increases, the value of the average Sauter diameter increases. For the production of emulsions with coconut oil and emulsions with grapeseed oil, the results do not allow a clear statement of the relationship between these parameters. It has also been shown that for the preparation of stable emulsions, the self-emulsifying base of apricot kernel oil performs much better. The addition of vegetable glycerin to the mixture resulted in a reduction of the average droplet diameter (Fig. 1).

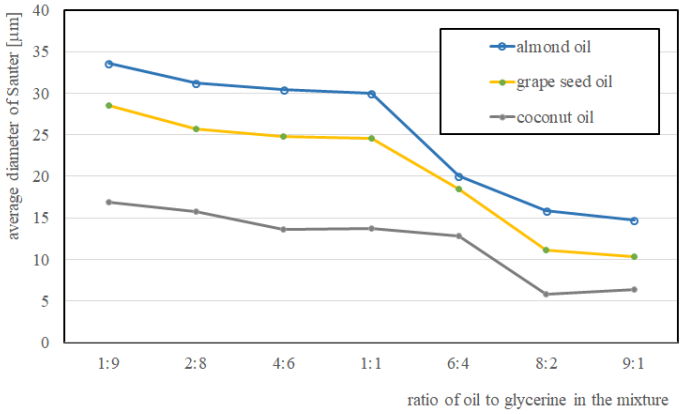

Fig. 1. Exemplary effect of the addition of vegetable glycerin in the mixture on the value of the average diameter of Sauter droplets

The samples were also visually observed for 60 days to assess their stability and possible aging processes. No tarnish was observed on the surface of the samples, indicating the formation of mold, which can lead not only to poisoning, but also to the development of allergies, respiratory diseases, liver diseases, ulcers and bleeding in the intestines. In earlier studies with other vegetable-derived oils, such a tarnish appeared after a much shorter period of time.

In conclusion, the conducted studies indicate the possibility of producing cosmetic emulsion bases based on the proposed plant biocomponents.

References

[1] Goodarzi F., Zendehboudi S.. a C*omprehensive Review on Emulsions and Emulsion Stability in Chemical and Energy Industries*. Faculty of Engineering and Applied Science, Memorial University, St. John's, NL, Canada, 2018, 282–294.
[2] Alok K. Kulshreshtha, Onkar N.Singh, G.Michael Wall. *Pharmaceutical Suspensions*. New York, 2010, 4–10.
[3] Taha A., Ahmed E., Ismaiel A., Ashokkumar M., Xu X., Pan S., Hu H., Ultrasonic emulsification: An overview on the preparation of different emulsifiers-stabilized emulsions, *Trends Food Sci. Technol.*, 2020, 105, 363-377.

USING AN ARTIFICIAL NEURAL NETWORK MODEL FOR NATURAL GAS HEAT COMBUSTION FORECASTING

Jolanta Szoplik*, Paulina Muchel

West Pomeranian University of Technology, Szczecin, Piastów 42, 71-065 Szczecin, Poland
*corresponding author: joanta.szoplik@zut.edu.pl

One parameter characterizing the quality of gaseous fuel transported by a pipeline network from the place of extraction to consumers and being the basis for the classification of gaseous fuels is the heat of combustion. Calculation of this parameter is necessary for the correct transport of gaseous fuel through the network and for balancing the network and settling gas consumers. The heat of natural gas combustion is not constant over time and depends on the composition of natural gas introduced into the national gas pipeline network transporting gas to consumers. In 2022, the main supply of the Polish gas pipeline network changed significantly (previously regasified LNG and Russian gas, and now regasified LNG and Norwegian gas), which results in the variability of the composition of natural gas at individual points of the network. A detailed analysis of the variability of natural gas composition depending on the place of origin and the load on the gas network in Poland and the possibilities of its forecasting using the MLP model was presented in [1]. It has been shown that the MLP model can be used to forecast the five most important components of natural gas depending on the selected calendar and weather factors, but the value of the forecast error of the content of a given component in the gaseous fuel depends on its component percentage in the gas mixture.

The main research hypothesis of this paper is the possibility of using the feed-forward model of the MLP 18-yi-1 neural network to forecast the heat of natural gas combustion.

The paper presents the results of natural gas heat of combustion forecasts obtained using various MLP models of the neural network. The training of the neural network models was carried out on the basis of 8760 real data items, presenting the hourly heat of natural gas combustion at one of the measurement points of this parameter in the pipeline network distributing gas in Poland. The model takes into account the influence of calendar factors (month, day of the month, day of the week and hour of the day) and weather factors (ambient temperature) on the amount of heat of natural gas combustion in a given location of the gas network. Many MLP 18-yi-1 models were trained, differing in the number of neurons in the hidden layer of the network and the activation functions of neurons in the hidden and output layers. The evaluation of the quality of the trained models and the selection of the model for forecasting the heat of natural gas combustion were made on the basis of the size of the correlation coefficient of the test set and the calculated MAPE error of the forecast. It was assumed that the best quality model is characterized by the highest correlation coefficient and the smallest MAPE forecast error. The trained MLP model can be used to forecast the value of heat of natural gas combustion at a given measurement point in the gas network for any day of the month and week, as well as ambient temperature and hour of day.

References

[1] Szoplik J., Muchel P., Using an artificial neural network model for natural gas compositions forecasting, *Energy*, 2023, 263, 126001.

LONG TERM PERFORMANCE OF SUBMERGED PHOTOCATALYTIC MEMBRANE REACTOR EQUIPPED WITH ULTRAFILTRATION MEMBRANE: TREATMENT EFFICIENCY AND FOULING STUDY

Kacper Szymański[1,*], Sylwia Mozia[1]

[1]West Pomeranian University of Technology in Szczecin, Department of Inorganic Chemical Technology and Environment Engineering, Piastów 17, 70-310 Szczecin, Poland
[*]corresponding author: kacper.szymanski@zut.edu.pl

Over the past decade an increasing number of literature reports concerning the presence of various contaminants of emerging concern (CECs) such as pharmaceuticals (PhACs) in the aquatic environment can be observed. The consumption of PhACs has significantly increased in recent years. Low efficiency of their removal during sewage treatment results in the release of numerous PhACs into aquatic environment [1]. The uncontrolled release of CECs, even at very low concentrations (ng-µg level), pose a risk to public health, affect the photosynthesis of plants and promote the development of antibiotic resistant genes. The above shows that the presence of these substances in water results in severe ecological issues [1]. Among various PhACs there is ketoprofen (2-(3-benzoylphenyl)propionic acid), which is a representative of non-steroidal anti-inflammatory drugs (NSAIDs) with analgesic and antipyretic effects. Ketoprofen was reported to create a high risk of gastrointestinal complications and potential cytotoxicity and genotoxicity at high concentrations of exposure [2].

Taking the above into consideration, there is an urgent necessity to develop efficient methods for elimination of PhACs from treated water. A promising solution to this problem is the application of photocatalytic membrane reactors (PMRs), i.e. hybrid systems coupling membrane separation and photocatalysis. The main role of a membrane in the PMR is retention of a photocatalyst, whereas during photocatalysis the organic contaminants are decomposed [2]. In the presented research a submerged photocatalytic membrane reactor (SPMR) equipped with ultrafiltration (UF) membrane (SPMR-UF) was investigated. In this configuration the treated solution is sucked through the membrane under a negative pressure and permeate is collected as a product, whereas the photocatalyst is retained by the membrane [2]. The objective of the research was the investigation on the removal of ketoprofen from water of various compositions (sea, brackish and surface water) during long term operation of the SPMR-UF system.

The composition of feed matrices applied in the experiments was described elsewhere [2]. In brief, ketoprofen (10 mg/L) was added to an appropriate solution containing inorganic salts such as $MgCl_2{\cdot}6H_2O$, $CaCl_2$, Na_2SO_4, $NaHCO_3$, KCl, NaCl and KBr in the case of sea water, $MgCl_2{\cdot}6H_2O$, $CaCl_2$, Na_2SO_4 and NaCl in the case of brackish water or humic acids (HA, 8 mgTOC/L) and inorganic salts ($MgCl_2{\cdot}6H_2O$, $CaCl_2$, $Ca(NO_3)_2{\cdot}4H_2O$, $CaCO_3$, Na_2SO_4, $NaHCO_3$, $KHCO_3$) in the case of surface water. A commercially available AEROXIDE® TiO_2 P25 (1 g/L) was used as the photocatalyst. A submerged membrane module containing 3 capillary hydrophilic UF PVDF membranes (ZeeWeed 500M (FLO), SUEZ Water Technologies & Solutions, Belgium) with the nominal pore size of 0.04 µm (according to the manufacturer) was applied. The total effective outer membrane area was 0.00615 m^2. The installation was equipped with a labyrinth flow photoreactor irradiated with 6 UVA lamps (λ_{max} =355 nm, UV radiation intensity: 150 W/m^2). The suction pressure was –0.1 bar. The air flow rate was set at 14 NL/min. The temperature of the feed in the system was equal to 20±1 °C. The process was operated in a continuous mode and permeate was continuously collected.

Fig. 1 presents a comparison of changes of ketoprofen concentration in time with reference to feed type. The fastest degradation of ketoprofen in feed (Fig. 1a) occurred in brackish water. After only 3 h of the process, the pharmaceutical was decomposed by 93%. The slowest photodecomposition took place when sea water was used. In this case, the removal of ketoprofen after 3 h amounted to 82% only. During 100 h of the SPMR-UF operation the change of

concentration of ketoprofen in feed exhibited similar trend to that in permeate for all types of matrices. This confirms that the UF membrane does not reject low molecular organic compounds and its main role in the PMR systems is confinement of photocatalyst particles in the reaction medium.

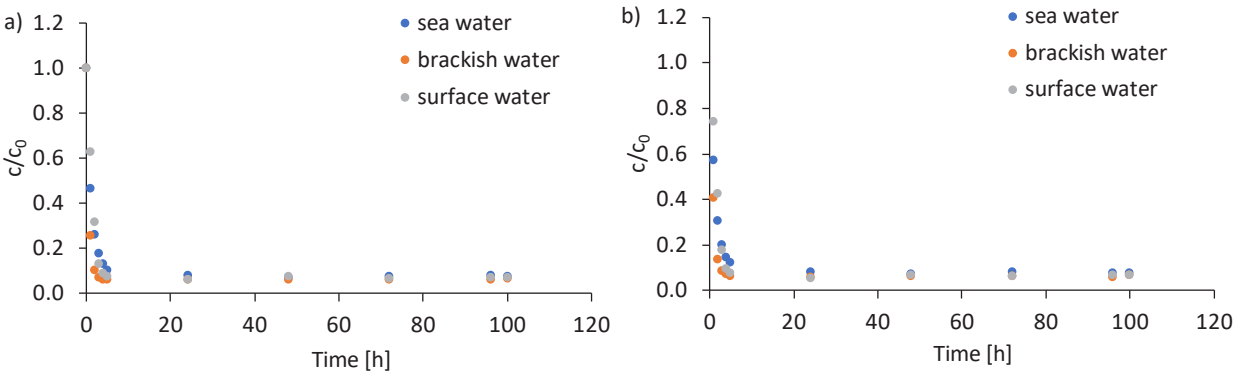

Fig. 1. Changes of ketoprofen concentration in feed (a) and permeate (b) during treatment of various feed matrices in the SPMR-UF

Another important parameter is mineralization of organic compounds present in the feed, i.e. ketoprofen in the case of sea water and brackish water, or ketoprofen and HA in the case of surface water. The total effectiveness of treatment in the SPMR is affected by adsorption, photocatalysis and membrane separation. Since adsorption of ketoprofen on TiO_2 was found to be very low, in the case of sea and brackish water this process did not play a significant role in the overall efficiency of removal of total organic carbon (TOC). In turn, for surface water, ca. 32% of TOC was removed by adsorption. Such a high adsorption rate in the overall removal of organic compounds may be related to the presence of calcium and magnesium ions, which formed bridges between humic acid molecules and photocatalyst particles [3]. After 24 h of the SPMR operation the total removal of TOC (calculated with reference to permeate composition) was 45, 53 and 58% for sea, surface and brackish water, respectively. These results could be related with the amount of salts present in the various feed matrices, which act as hydroxyl radical scavengers.

The analysis of changes of permeate flux (J) in time revealed that no noticeable membrane fouling took place when sea and brackish water were used as the feed. The permeate flux was constant during 100 h of the SPMR-UF operation. However, in the case of surface water the flux was stable until 70 h of the process, and after that time a decrease in J value was observed. That decline can be explained by deposition of humic acids and TiO_2 particles on the membrane surface which, together with the uncomplete mineralization, led to the observed deterioration of the permeate flux.

The conducted research revealed that the proposed system was effective in removal of ketoprofen from all types of water. Moreover, the application of photocatalysis allowed to conduct the process at low fouling intensity, even in the presence of HA.

Acknowledgements: This work was supported by the National Science Centre, Poland under project No. 2019/33/B/ST8/00252.

References

[1] Desbiolles F., Malleret L., Tiliacos C., Wong-Wah-Chung P., Laffont-Schwob I., Occurrence and ecotoxicological assessment of pharmaceuticals: Is there a risk for the Mediterranean aquatic environment?, *Sci. Total Environ.*, 2018, 639, 1334-1348.

[2] Szymański K., Gryta M., Darowna D., Mozia S., A new submerged photocatalytic membrane reactor based on membrane distillation for ketoprofen removal from various aqueous matrices, *Chem. Eng. J.*, 2022,435, 134872.

[3] Szymański K., Morawski A.W., Mozia S., Humic acids removal in a photocatalytic membrane reactor with a ceramic UF membrane, *Chem. Eng. J.*, 2016, 305, 19.

A STUDY OF THERMAL REGENERATION OF LOADED HYDROPHOBIC AND HYDROPHILIC ZEOLITES AFTER ADSORPTION IN THE LIQUID PHASE

Piotr Tabero[1], Elżbieta Gabruś[2,*]

[1] Department of Inorganic and Analytical Chemistry,
[2] Department of Chemical and Process Engineering,
West Pomeranian University of Technology Szczecin, Faculty of Chemical Technology and Engineering, Piastów 42, 71-065 Szczecin, Poland
*corresponding author: Elzbieta.Gabrus@zut.edu.pl

Adsorption is a technique for treating waste liquid streams with low pollutant concentrations, most often used for water treatment or liquid drying. Liquid streams are treated in a column plant that operates periodically in adsorption and thermal regeneration in a cyclic process called temperature swing adsorption (TSA). The adsorption stage usually takes place at room temperature on a fixed bed of adsorbent, such as activated carbon or zeolite. Then, the stages of thermal regeneration of the loaded bed and its cooling are carried out, usually combined with the recovery of the adsorbate. The lowest desorption temperature should be higher than the boiling point of adsorbate, and the highest one should not damage the adsorbent structure responsible for adsorption capacity. It is also important to estimate the duration of TSA steps so that the adsorption takes longer than others.

In practice, granular zeolites are usually used, prepared by mixing zeolite crystallites (diameter ~ 1 μm) with clay as a binder in the amount of 16-20%. Adsorbents prepared in this way are porous solids with both macropores and micropores. Macropores in the binder are wetted with a liquid mixture, and micropores in zeolite crystallites are capable of selective adsorption of water molecules and other compounds whose size is smaller than narrow structural cages [1]. Microporous crystalline aluminosilicates in zeolite are composed of SiO_4 and AlO_4 tetrahedra with O atoms connecting neighboring tetrahedra. As the Si/Al ratio of the framework increases, the zeolite hydrophobicity increases. Low-silica zeolites (such as 3A, 4A, 13X with Si/Al ratios of 1-3) are hydrophilic, whereas high-silica zeolites (such as ZSM-5) are hydrophobic with Si/Al ratios of 10–100 (or higher). HiSiv-3000 (HS) is essentially a pure silica ZSM-5 zeolite with the Si/Al ratio in the order of thousands. Regardless of the tendency to hydrophobicity, each granular zeolite will be saturated in the macroporous structure with a liquid mixture also containing water. Regardless of Si/Al ratio fresh zeolites contain at least 1-2% of adsorbed water.

From the economic point of view, the success of adsorption system application also depends on the possibility of carrying out an effective and low-energy regeneration of the adsorbent. This paper presents results of investigations focused on the role of water, co-adsorbed with main adsorbate in the adsorption and regeneration processes on biporous adsorbents differing in hydrophobicity. A hydrophilic isopropyl alcohol (IPA) as well as a hydrophobic ZSM-5 with the trade name HiSiv-3000 and hydrophilic 13X zeolites were selected for investigations.

For testing the efficiency of the loaded adsorbent regeneration thermogravimetric analysis (TGA) and near-infrared diffuse reflectance spectroscopy (NIR/DRS) were selected. The TGA measurements provide information on the investigated sample mass change during its heating or cooling. Its analysis enables determining the temperature range of desorption process and boundary of adsorbent thermal stability, whereas DTG curve (the first derivative of mass loss with respect to temperature) is helpful for estimating the rate of adsorbate desorption. On the other hand, NIR/DRS spectroscopy is useful for detection and identification of the adsorbed particles in the loaded adsorbent and for following their interactions during adsorption or desorption. This research also used X-ray diffraction (XRD) as this measurement technique provides valuable information on the structure of adsorbents and their changes with the increase of temperature, enabling identification of the given type of adsorbent and estimation of boundaries of their thermal stability.

Conducted investigations showed that detection and identification of IPA and water after adsorption on HS or 13X was possible using NIR/DRS spectroscopy (Fig. 1a). Moreover, the results of NIR/DRS (Fig. 1a) and DTG (Fig. 1b) investigations revealed that in all cases adsorption and desorption proceeded fast. The shifts of NIR bands in the range of 1900-2150 nm characteristic for IPA and H_2O (Fig. 1a) indicate that after adsorption on hydrophobic HS interaction between of their particles leads to formation of hydrogen bonds. Contrary to that, adsorption of IPA and water on hydrophilic 13X zeolite affects only negligible positions of bands in this range (Fig. 1a).

The analysis of regeneration tests (Fig. 1b) enabled to read out the maximum temperatures on the DTG desorption curves at 100 °C for HS-IPA. and at 170 °C for 13X-IPA (Fig.1b). The temperature of a maximum observed on the DTG curve corresponding to the maximum adsorbate release rate appeared to be the temperature ensuring the most effective regeneration of the bed. Above this temperature, the process speed decreases significantly with the consequent increase in the duration of the desorption step [1, 2]. Detection of IPA by NIR spectroscopy even during regeneration tests (100–170 °C), indicates that this adsorbate does not decompose in the temperature ranges selected for the regeneration and can be desorbed and then recovered under such conditions. The shape of HS-IPA-H_2O curve (Fig. 1b) seems to indicate that water and IPA are desorbed together in the form of dimers or more complex clusters. The three step 13X-IPA-H_2O desorption curve (80 °C, 170 °C and 280 °C) suggests desorption of loosely bonded water at the begining , next IPA and finally strongly bonded water.

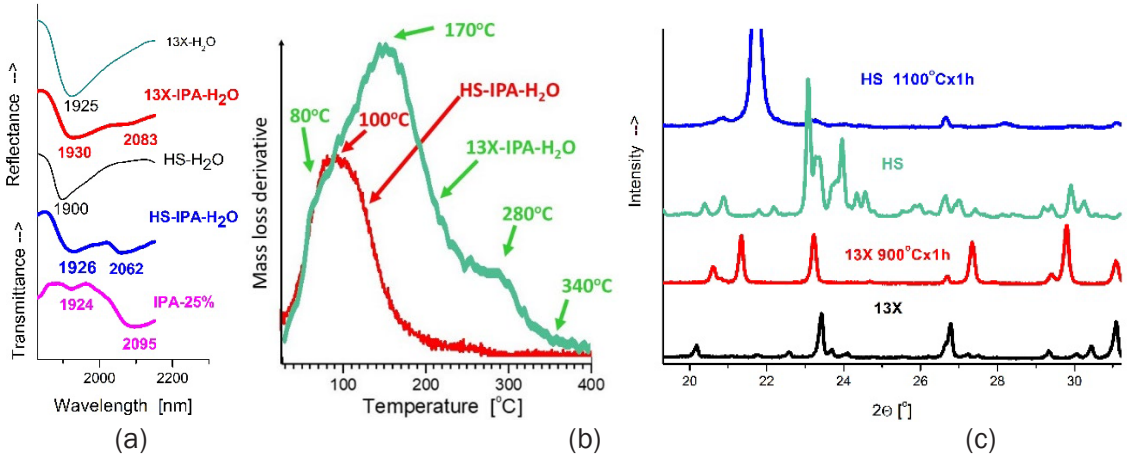

Fig. 1. (a) NIR/DRS spectra of pure IPA, 13X and HS zeolites, and these zeolites after adsorption of IPA, (b) DTG curves recorded after adsorption of IPA on 13X or HS zeolites, (c) diffraction patterns of 13X and HS zeolites and products of their heat treatment at 900 or 1100°C, respectively

At the same time, based on the results of XRD investigations (Fig. 1c) it was found that HS and 13X zeolites are stable and can be regenerated in the air at least in the temperature of 1000 °C and 800 °C, respectively. Above these temperatures HS starts to decompose to cristobalite, and 13X to nepheline.

In the light of our previous [1, 2] and current studies, it can be suggested that the maxima in the DTG curves indicate the optimal regeneration temperatures of the loaded adsorbents. Under these conditions, the process is the fastest and the duration of the stage is as short as possible. It may result in ensuring the continuity of operation of the TSA installation without increasing the number of adsorbent beds. Appropriate selection of desorption temperature conditions allows for effective regeneration of the loaded fixed bed, ensuring the stability of the adsorbate and durability of the adsorbent structure, thus leading to the optimal time and costs of process.

References

[1] Gabruś E., Nastaj J., Tabero P., Aleksandrzak T., Experimental studies on 3A and 4A zeolite molecular sieves regeneration in TSA process: Aliphatic alcohols dewatering–water desorption, *Chem. Eng. J.*, 2015, 259, 232–242.

[2] Gabruś E., Tabero P., Aleksandrzak T., A study of the thermal regeneration of carbon and zeolite adsorbents after adsorption of 1-hexene vapor, *Appl. Therm. Eng.*, 2022, 216, 119065.

DEVELOPMENT OF TECHNOLOGY FOR PRODUCING A NEW TYPE OF LIQUID FERTILIZER CONTAINING PHOSPHORUS COMPOUNDS

Agata Tarnowska[1], Magdalena Białomazur[1], Izabella Jasińska[1,*], Barbara Grzmil[2], Mirosław Karbowniczek[3], Monika Karsznia[4], Aleksandra Kostka[1], Agnieszka Kocoń[1], Anna Lubkowska[1], Kornelia Malarczyk-Matusiak[1], Magdalena Morawiec-Witczak[4], Weronika Suszka[1], Jakub Tchórzewski[1], Edyta Zielińska[1], Monika Zienkiewicz[1], Olga Żurek[1]

[1]Grupa Azoty Zakłady Chemiczne "Police" S.A., ul. Kuźnicka 1, 72-010 Police, Poland
[2]West Pomeranian University of Technology, Szczecin, Piastów 17, 70-310 Szczecin, Poland
[3]AGH University of Science and Technology in Krakow, Mickiewicza 30, 30-059 Kraków, Poland
[4]Grupa Azoty Zakłady Azotowe "Police" S.A., Tysiąclecia Państwa Polskiego 13, 24-110 Puławy, Poland
[*]corresponding author: izabella.jasinska@grupaazoty.com

Research was carried out on the development of a new technology in the form of an optimal and effective technology for purification of phosphoric (V) acid contaminated with multivalent metal cations, including cadmium ions and technology for the production of new liquid fertilizers containing phosphorus compounds with the use of purified phosphoric acid.

New technologies use phosphoric (V) acid manufactured by extraction method from raw materials of sedimentary origin. Such an acid intended for further processing into solid and liquid fertilizers or feed and food phosphates should be characterized by a certain degree of purity. The use of extractive phosphoric acid to obtain ammonium polyphosphate requires prior removal of heavy metal ions and aluminium, iron and magnesium ions, because their too high content hinders the process of acid concentration and polycondensation and contributes to the formation of so-called secondary sediment in fertilizer products [1–3].

In the course of the study, methods available only in other industrial processes and for purifying process streams other than phosphoric (V) acid were verified. So far, there has been no solution for purifying phosphoric (V) acid on an industrial scale in the fertilizer industry, and single techniques function for the purpose of purifying phosphoric acid for food use. The method for purifying phosphoric (V) acid consists of two main stages – preliminary purification and deep purification. The possibility of carrying out deep purification with the use of one of the methods selected taking into account the characteristics of the removed impurities was investigated. As part of the project, one of the possible methods was selected for use on a pilot scale: electrolytic separation of metals from post-production solutions by means of electrolysis with controlled potential [4], acid purification studies with the use of methods based on co-precipitation and ion exchange method.

As part of the work, research was carried out on concentrating extractive phosphoric (V) acid do polyphosphoric (V) acid and ammonization to obtain ammonium polyphosphate (V). Concentration of the acid to >70% by weight of P_2O_5 and polycondensation can be carried out in various ways – using vacuum concentration, electrothermal concentration and using the heat of flue gases. The choice of the method for acid concentration and polycondensation by the project team was made taking into account the availability of media and technological conditions of the process. The results obtained in the study of the influence of selected parameters on the content of various phosphorous forms in the acid confirmed that acid purity is important for the content of polyphosphates (V) in the condensation products.

As part of the research, an analysis of the durability of fertilizers based on ammonium polyphosphate (V) over time was carried out, depending on the storage conditions of prototypes of liquid fertilizers containing APP. Based on the obtained results, guidelines for storage of fertilizer solutions containing APP were developed.

The specificity of the research project required the development of a methodology and a pot study to evaluate the effectiveness of ammonium polyphosphate(V) (APP) as an alternative source

of phosphorus. The agricultural usefulness of the new liquid nitrogen-phosphorus fertilizers was tested in spring wheat, white mustard and corn crops, and their effectiveness was compared to standard fertilizers, i.e. superphosphate, ammonium phosphate and ammonium nitrate. Subsequently, field tests were carried out during two full crop growing seasons to verify the agricultural efficiency of new fertilizer products with optimal compositions, selected on the basis of results obtained in earlier phases of the study, against single nitrogen and phosphorus fertilizers. NP and NP fertilizers with additives in optimal composition and single fertilizers were tested on soil moderately rich in bioavailable forms of phosphorus. Winter rapeseed, corn, winter wheat and potato were used as test crops.

The research work also included a study of the physicochemical properties of the new fertilizer formulations developed using ammonium polyphosphate(V), which included the selection of appropriate formulations and compositions of liquid fertilizers with APP and other fertilizer components, as well as the development of methodology and microbiological studies of the soil. The microbiological studies evaluated the effect of varying nitrogen and phosphorus fertilization on the abundance and diversity of microorganisms and the activity of selected soil enzymes in the cultivation of winter rapeseed, winter wheat, potato and corn.

The obtained results of the study were used to develop a technological method for the purification of extractive phosphoric (V) acid for implementation on a pilot scale.

The work was carried out within the framework of the project POIR.01.01.01-00-0476/18. The project was co-financed by the European Union with funds from the European Regional Development Fund under the Intelligent Development Operational Program 2014-2020. The project was carried out within the framework of the National Center for Research and Development "Fast Track" competition.

References

[1] Becker P., *Phosphates and phosphoric acid*, Marcel Dekker, INC, New York 1989.
[2] Górecki H., *Przem. Chem.*, 2011, 90, 1535.
[3] Grzmil B., Kic B., Zienkiewicz M., Podolak A., *Effect of raw materials quality on the content of contaminations in raw phosphoric acid from the wet process, Przem. Chem.*, 2011, 90, 1535.
[4] Zielińska E., Białomazur M., Tarnowska A., Zienkiewicz M., Jasińska I., Łukomska A., Lach J., Wróbel K., Grzmil B., Potential-control elektrolysis as a new method for purification of extractive phosphoric acid, *Przem. Chem.*, 2021, 100/4, 333-338.

EXPERIMENTAL VALIDATION OF A CFD MODEL OF A GROUND HEAT EXCHANGER WITH SLINKY COILS

Mikołaj Teper, Robert Grzywacz*

Cracow University of Technology, Faculty of Chemical Engineering and Technology,
Warszawska 24 Cracow, Poland
*corresponding author: robert.grzywacz@pk.edu.pl

The rise in energy prices has led to an increase in the popularity of renewable energy sources, including heat pumps. The operating principles of heat pumps are relatively well understood. However, in the case of ground-source heat pumps, research related to the performance analysis and selection of ground heat exchangers as a heat source for a heating system is insufficient. Therefore, more research has been undertaken into the configuration, placement and operation of one of the more interesting ground heat exchangers, the slinky coil heat exchanger [1]. Its popularity comes from its compact design, which results in reduction of a required area and lower investment costs compared to other types of heat exchangers.

CFD modeling and simulations have been used as research tools. However, in order for such a model to be adequate, the obtained simulation results have been validated against the test results of the real heat exchanger.

The experimental stand was located in the municipality of Jordanów in the Małopolska voivodeship. The stand consisted of a horizontal ground exchanger of the slinky coil type and of hydraulic, heating and control-measuring equipment. A schematic diagram of the stand is presented in Fig. 1. The exchanger consisting of a single coil was installed in the ground at a depth of 0.5 m. In order to measure the ground temperature, four lines of temperature sensors consisting of 13 sensors per line were installed from a depth of 1 m to the ground surface. The first line was installed in the axis of the exchanger, the next two lines at opposite sides of the diameter of the coil and the last one at a distance of 4.5 m providing measurements of undisturbed ground temperature.

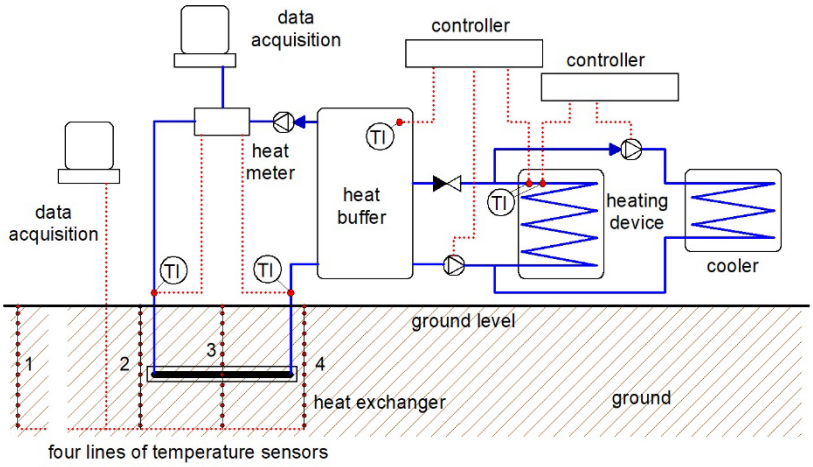

Fig. 1. Schematic diagram of the stand

The measurements were carried out between 5.12.2017 and 7.12.2017. The experiment consisted of continuously heating the ground with water at 55 °C for 72 hours. During the experiment, the following process parameters were measured: temperature in the ground and at the ground surface, temperature changes at the inlet and outlet of the exchanger and mass flux of the fluid flowing through the exchanger.

CFD modeling and simulations were carried out in the CFX Flow software, which is a part of the Ansys package. For this purpose, the geometry of the exchanger was recreated together with the surrounding soil. The measured initial temperature of the ground was used as the initial conditions. The boundary conditions of the model included the temperature of the ground surface, the temperature of the exchanger feed water, and the volume flow of the exchanger feed water.

The basis for the validation of the CFD model was a comparison of the selected temperature profiles and the heat delivered to the ground. The comparisons were made between: the temperature at the heat exchanger outlet obtained in the real process and the simulation results (Fig. 2), the measured ground temperature changes during the experiment with those obtained during simulation (Fig. 3), and the amount of heat delivered to the ground in the experiment with the value obtained in the simulation (in poster).

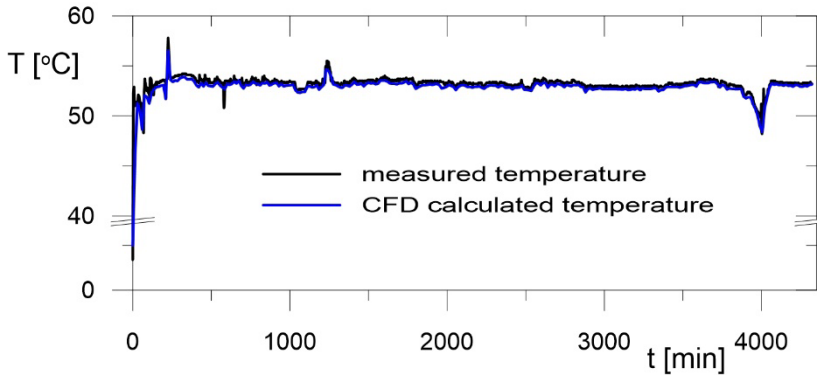

Fig. 2. Comparison of the temperature of the medium at the outlet of the heat exchanger

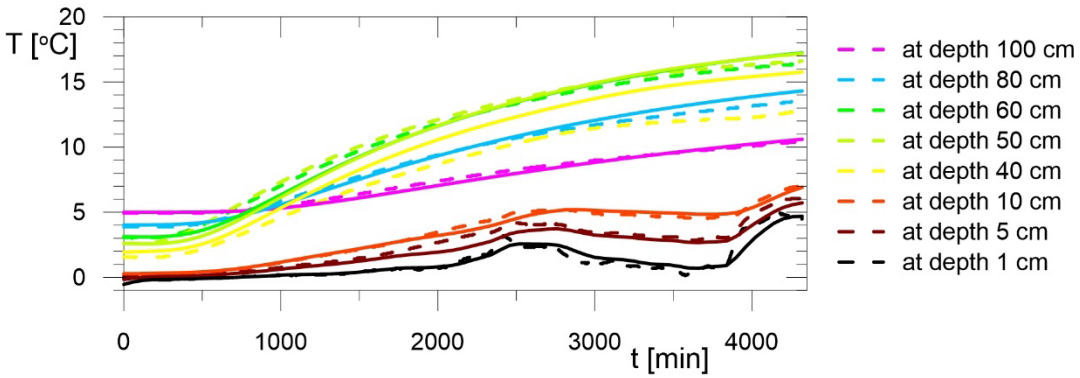

Fig. 3. Comparison of temperature changes in the ground at different depths (color-coded in the legend), on line 3 - in the axis of the heat exchanger; – – measurements, ——— CFD simulations

Analyzing the performed comparisons, the following conclusions can be formulated: 1) by using CFD modeling, the conditions and results of the ground heat exchanger operation can be realistically represented, 2) CFD modeling allows to analyze the transient states of the ground heat exchanger operation, 3) using CFD calculations it is possible to determine the temperature values at any point of the ground geometry, which can be useful for selecting operating parameters for the heat exchanger under unfavorable conditions, 4) the results of the CFD simulations allow to determine changes in the thermal power extracted from the ground and provide information for the evaluation of the temporary COP coefficient. In the authors' opinion, the validation of the CFD model using the results of the experiments on the real heat exchanger has been successful.

References

[1] Wu Y., Gan G, Verhoef A., Vidale P.L., Gonzalez R.G., Experimental measurement and numerical simulation of horizontal-coupled slinky ground source heat exchangers, *Appl. Therm. Eng.*, 2010, 30, 2574-2583.

THE APPLICATION OF HERMIA'S MODEL FOR IDENTIFICATION AND ANALYSIS OF FOULING MECHANISMS DURING PRESSURE-DRIVEN MEMBRANE PROCESSES

Wirginia Tomczak*, Ireneusz Grubecki

Bydgoszcz University of Science and Technology, Seminaryjna 3,
85-326 Bydgoszcz, Poland
*corresponding author: tomczak.wirginia@gmail.com

Presently, significant research focus is being placed on the application of membrane technology for separation of value-added products from post-fermentation solutions. However, the fouling phenomenon is a major challenge to membrane-based separation processes. Undoubtedly, it has a negative impact on process performance, especially in a long term. Indeed, it leads to a permeate flux decline and, consequently, to increased operating costs. The current knowledge on fouling demonstrates that it is a very complex issue affected by many interrelated parameters, that can be categorized into the following groups: membrane parameters, process conditions and feed characteristics [1, 2].

In the literature, it has been widely established that to determine dominant fouling mechanism during pressure-driven membrane process, the Hermia's model can be applied. The above-mentioned model is expressed by the following equation [3]:

$$\frac{d^2t}{dV^2} = k\left(\frac{dt}{dV}\right)^n \tag{1}$$

where t is the filtration process time, V is the permeate volume, k is constant and n is the characteristic exponent depending on the fouling mechanism, which includes: cake formation (n = 0), intermediate blocking (n = 1.0), standard blocking (n = 1.5) and complete blocking (n = 2.0) (Table 1).

Table 1. Fouling Mechanisms Based on the Hermia's Model

Fouling mechanism	*n*	Physical concept	Schematic diagram
Cake formation	0	Deposit formation on the membrane surface	
Intermediate blocking	1.0	Pore blocking and surface deposition	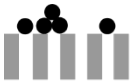
Standard blocking	1.5	Pore constriction	
Complete blocking	2.0	Pore blocking	

To the best of the authors' knowledge, the current study is the first one to present the application of the Hermia's model to identify and analyse the fouling mechanism of the microfiltration (MF), ultrafiltration (UF) and nanofiltration (NF) membranes (Table 2) used for the separation of 1,3-propanediol (1,3-PD) fermentation broths obtained via bioconversion of glycerol. For this purpose, the fitness of the experimentally obtained data with the above-presented fouling mechanisms was determined by comparing the determination coefficients (R^2), Sum of Squares Errors (SSE) and Root Mean Squared Error (RMSE).

Table 2. Characteristics of Membranes Used in the Present Study

Membrane	Manufacturer	Material	Nominal pore size [μm] or molecular weight cut-off [kDa]	Active area [m^2]
MF	TAMI Industries	ZrO_2	0.14 μm	0.0038
UF fine	TAMI Industries	TiO_2	450 Da	0.0047
NF	DOW-Filmtec	polyamide	200-300 Da	0.0150

The fermentation broths used in the present study were highly complex solutions, consisting of: 1,3-PD (the main product), mono-carboxylic acids (lactic, acetic and formic acids), dicarboxylic acid (succinic acid), ethanol as well as residue of the microbial medium and *Citrobacter freundii* bacteria. The pressure-driven membrane process was conducted under controlled operational parameters (temperature of 303 K, TMP in the range from 0.02 to 1.4 MPa). Worthy of note, prior to the NF process, the fermentation broths were pre-treated by the MF process.

It should be pointed out that the MF process allowed to eliminate colloidal particles from the feed. In turn, the UF membrane effectively retained bacteria cells. Finally, the NF process ensured complete 1,3-PD permeability and significant rejection of some broth components. Nevertheless, as expected, a significant decrease in permeate flux during the processes was noted (Fig. 1).

Results of thoroughly performed analysis using the Hermia's model have shown that various fouling mechanisms led to permeate decline. During the MF process, membrane blocking occurred in two separate phases, involving standard blocking and then, a cake layer formation. In turn, with regards to UF and NF membranes, cake formation played the major role. The above-indicated difference in the main fouling mechanisms can be attributed to differences in the pore sizes of the membranes used. Indeed, the MF membrane was characterized by the significantly larger pore size than UF and NF membranes, hence, it was more prone to internal blocking.

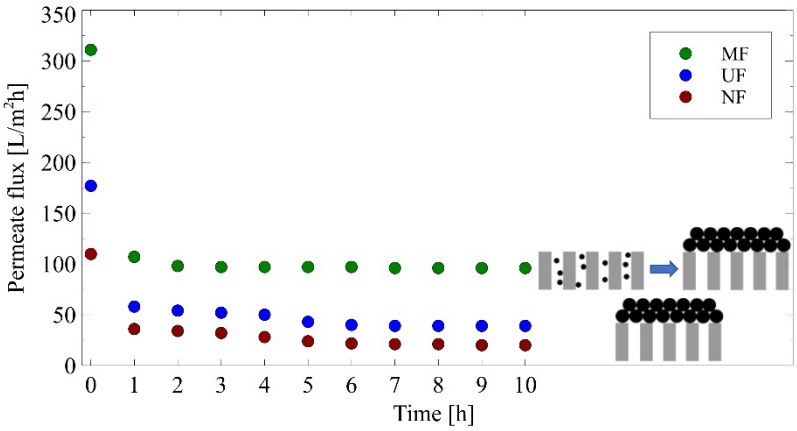

Fig. 1. Changes of permeate flux during MF, UF and NF processes. Feed: 1,3-PD fermentation broths

Results obtained in the current study have clearly demonstrated that the Hermia's model can be effectively applied for determination of the fouling mechanism during separation of fermentation broths by MF, UF and NF processes. To be complete, it should be indicated that the presented results may be used for implementation of strategies to maintain a high level of membrane process performance.

References

[1] Al-Asheh S., Bagheri M., Aidan A., Membrane bioreactor for wastewater treatment: A review, *CSCEE*, 2021, 4, 100109.
[2] Iorhemen O., Hamza R., Tay J., Membrane bioreactor (MBR) technology for wastewater treatment and reclamation: Membrane fouling, *Membranes,* 2016, 6, 33.
[3] Hermia J., Constant pressure blocking filtration laws-application to power-law non-newtonian fluids, *Trans IChemE,* 1982, 60, 183–187.

INFLUENCE OF FUNCTIONALIZED XEROGELS ON NAPHTHOQUINONES PRODUCTION AND BIOMASS PROLIFERATION IN BATCH CULTURES OF *RINDERA GRAECA* TRANSGENIC ROOTS

Kamil Wierzchowski[1], Bartosz Nowak[1], Mateusz Kawka[2], Katarzyna Sykłowska-Baranek[2], Maciej Pilarek[1,*]

[1]Warsaw University of Technology, Faculty of Chemical and Process Engineering, Waryńskiego 1, 00-645 Warsaw, Poland
[2]Medical University of Warsaw, Faculty of Pharmacy, Department of Biology and Pharmacognosy, Banacha 1, 02-097 Warsaw, Poland
*corresponding author: Maciej.Pilarek@pw.edu.pl

Pathways of secondary metabolism provide a prolific array of bioactive compounds responsible for plant adaptation to living in a given ecosystem niche. The bioactivity of extracellularly secreted plant secondary metabolites implicates the vast potential of their practical and prospective applications as pharmaceutical or cosmetic ingredients, food additives, or agricultural biochemicals [1]. Due to low concentrations of secondary metabolites typically occurring in plant biomass harvested from naturally available resources, the commercial feasibility of their industrial manufacturing is often limited [2]. However, modern biotechnological and bioengineering techniques may intensify the production efficiency of pharmaceutically relevant metabolites [3].

Nowadays, the solution for most problems related to plant biomass harvesting as feedstock for secondary metabolites production comes with *in vitro* bioprocessing of hairy roots [4]. Due to the possibility of growth in a hormone-free culture media and the specific phenotype of the transgenic roots, this specific plant biomass fits well with industrial applications and can be successfully cultured in bioreactors [5]. In the literature, much attention is dedicated to *in situ* techniques applied for bioproduct separation by the accumulation of metabolites in additional liquid phase or solid phase scaffolds [6].

The aim of this study was to investigate the influence of xerogels functionalized independently with four various chemical groups: methyl (-CH_3), hydroxyl (-OH), carboxylic (-COOH), and amine (-NH_2), on proliferation and naphthoquinones production in cultures of *Rindera graeca* transgenic roots. Biomass was maintained for 28 days in five independent systems, i.e. biomass cultured without any xerogel (as reference) and biomass cultured with disintegrated xerogels containing: -CH_3, -OH, -COOH and -NH_2 groups. The increase in fresh biomass and yield of naphthoquinones (rinderol and deoxyshikonin) per dry biomass weight was quantitatively determined.

1 g of disintegrated xerogels containing -CH_3, -OH, -COOH, or -NH_2 groups was separately placed in 250 cm^3 Erlenmeyer flasks containing 50 cm^3 of hormone-free DCR medium. Next, all systems were inoculated with 1 g of 28-day *R. graeca* transgenic roots. All cultures were incubated at 24 °C in the dark for 28 days on the oscillatory shaker at 105 rpm.

The proliferation of *R. graeca* hairy roots was identified by the fresh biomass (FB_{28}) increase values determined as:

$$FB_{28} = m_{28}\, {m_0}^{-1}\ [-] \tag{1}$$

where m_{28} is fresh biomass weight on the 28th day of culture, and m_0 is biomass inoculum weight.

The yield of naphthoquinones per dry biomass weight ($Y_{P/X}$), defined as the total mass of naphthoquinones (m_P) produced by 1.0 g of dry biomass of hairy roots, was determined as:

$$Y_{P/X} = m_p\ ({m^{DB}}_{28} - {m^{DB}}_0)^{-1}\ \ [\mu g\ g_{DW}{}^{-1}] \tag{2}$$

where $m^{DB}{}_{28}$ is the dry biomass weight on the 28th day of culture, and $m^{DB}{}_0$ is the dry biomass weight of the inoculum.

The values of FB_{28} determined for *R. graeca* hairy roots proliferated with functionalized xerogels containing various chemical groups are compared in Fig. 1A. The highest value of FB_{28} was noted for the culture supported with xerogel containing -CH_3 groups. Also, the FB_{28} value determined for the xerogel containing -OH groups was higher than the FB_{28} value noted for reference culture. For disintegrated xerogels containing -COOH and -NH_2 groups, the FB_{28} values were smaller than 1, which indicates dying of transgenic roots in these culture systems.

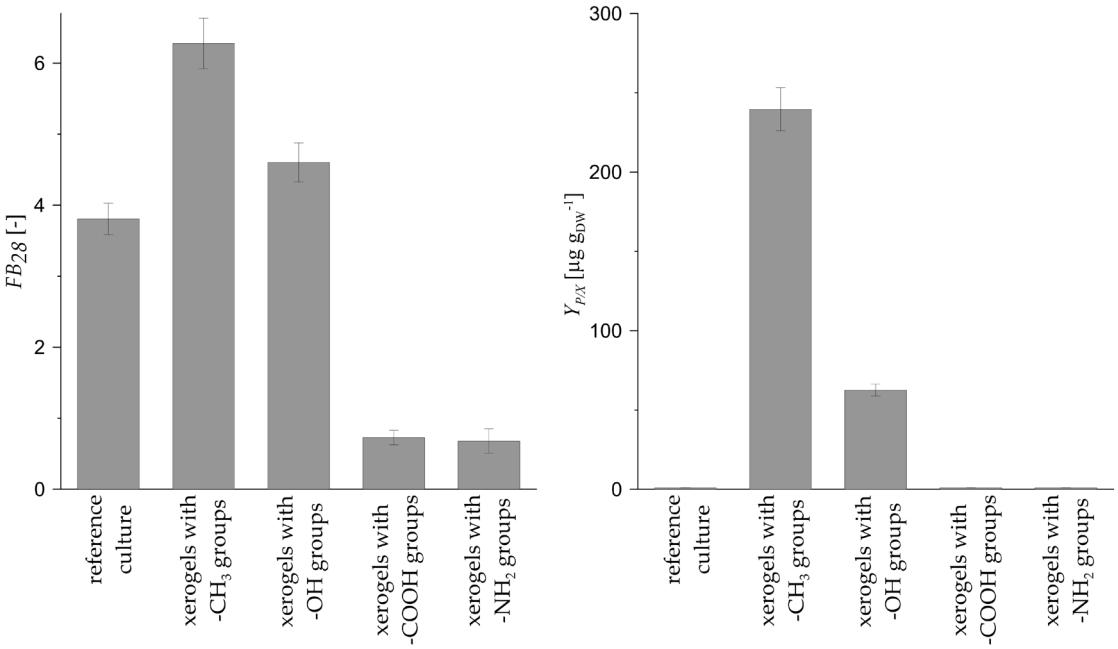

Fig. 1. The values of FB_{28} (A) and $Y_{P/X}$ (B) characterized *in vitro* proliferation of *R. graeca* hairy roots in the reference system and systems supported with disintegrated functionalized xerogels

The highest value of $Y_{P/X}$ (Fig. 1B.) was noted for the system supported with disintegrated xerogel functionalized with -CH_3 groups, and in extracts obtained from this xerogel, both rinderol and deoxyshikonin were observed. In the case of the disintegrated xerogel containing -OH groups, only rinderol was detected in extracts, and the $Y_{P/X}$ value for this xerogel was 3.5 times smaller than the $Y_{P/X}$ value for disintegrated xerogel containing -CH_3 groups. According to the lack of naphthoquinones detection for the reference system and disintegrated xerogels containing -COOH and -NH_2 groups, values of $Y_{P/X}$ were equal to 0 µg g_{DW}^{-1}.

In conclusion, the supporting culture system with disintegrated functionalized xerogel containing -CH_3 groups provided the most suitable conditions to promote biomass proliferation and naphthoquinones production by *R. graeca* transgenic roots. This effect is probably caused by high biocompatibility of xerogel functionalized with -CH_3 groups and its affinity to naphthoquinones.

References

[1] Guerriero G., et al., Production of plant secondary metabolites: examples, tips and suggestions for biotechnologists, *Genes*, 2018, 9, 309.
[2] Murthy H.N., et al., Production of secondary metabolites from cell and organ cultures: strategies and approaches for biomass improvement and metabolite accumulation, *Plant Cell Tissue Organ Cult.*, 2014, 118, 1–16.
[3] Sarsaiya S., et al., Bioengineering tools for the production of pharmaceuticals: current perspective and future outlook, *Bioengineered*, 2019, 10, 469–492.
[4] Espinosa-Leal C.A., et al., In vitro plant tissue culture: means for production of biological active compounds, *Planta*, 2018, 248, 1–18.
[5] Wierzchowski K., et al., Selective impact of MTMS-based xerogel morphology on boosted proliferation and enhanced naphthoquinone production in cultures of *Rindera Graeca* transgenic roots, *Int. J. Mol. Sci.*, 2022, 23, 13669.
[6] Nowak B., et al., MTMS-based aerogel constructs for immobilization of plant hairy roots: effects on proliferation of *Rindera Graeca* biomass and extracellular secretion of naphthoquinones, *J. Funct. Biomater.* 2021, 12, 19.

MICROWAVE REGENERATION OF CARBONACEOUS ADSORBENT IN CYLINDRICAL COLUMN WITH AXIAL EMITTER OF WAVES: EXPERIMENTAL STUDY AND SIMULATION

Konrad Witkiewicz*

West Pomeranian University of Technology in Szczecin, Department of Chemical Engineering and Environmental Protection Processes, Piastów 42, 71-065 Szczecin, Poland
*corresponding author: konrad.witkiewicz@zut.edu.pl

The use of microwave heating in adsorption processes is still limited to small size applicators. Placing an electromagnetic wave emitter in the axis of a cylindrical applicator allows to use metal adsorption columns and to enlarge the scale of the apparatus in the axial direction. However, the depth of microwave penetration into the adsorbent bed defines the final size of the apparatus. In the case of carbonaceous adsorbents, the energy of waves with a frequency of 2.45 GHz is dissipated at a depth of several centimeters. The configuration of the column with an axial emitter can still be used in the regeneration of adsorption filters, ACF (activated carbon fiber) cartridges or batteries of filters.

The subject of this experimental and theoretical research was the microwave regeneration of a carbonaceous adsorbent bed (0.1 m high) in a cylindrical column with an internal diameter of 0.047 m and a height of 0.25 m (Fig. 1). The space between the antenna and the column wall was filled with granulated activated carbon BPL 4x6 (Calgon Carbon Corporation, USA). In the adsorption-desorption cycles of the TSA (Temperature Swing Adsorption) process, a polar compound - propan-2-ol and a nonpolar - toluene were used as VOC (Volatile Organic compound).

Before the actual adsorption-regeneration tests, the characteristics of the internal heat source capacity were determined using the calorimetric method in the applied range of magnetron current settings. During desorption, a small stream of nitrogen (0.1 - 0.2 m^3/h) was directed to the column through the upper inlet, in the opposite direction to the flow of the air-VOC mixture in the adsorption step.

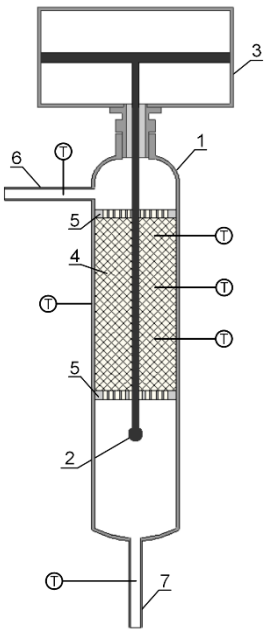

Fig. 1. Scheme of the adsorption column: 1 – cylindrical column, 2 – emitter, 3 – waveguide, 4 – adsorbent bed, 5 – Teflon, perforated shelves, 6 – inlet, 7 – outlet

The bed temperature was measured at three heights using fluoro-optic probes (Luxtron, USA). The gas temperature was recorded at the inlet and outlet of the column and the concentration of the component in the gas phase in the outlet stream was chromatographically determined.

A two-dimensional mathematical model of microwave desorption was formulated, assuming LDF (Linear Driving Force) approximation for the mass transport rate in the solid phase. The adsorption equilibrium of toluene and propan-2-ol on BPL activated carbon was described by the multi-temperature Toth isotherm equation. The term of the volumetric heat source in the energy balance equation was estimated for cylindrical geometry according to the Lambert-Beer law for microwave power decay in the material. The superposition of the emitted wave, the wave reflected from the column wall and the wave reflected from the emitter were taken into account. The effective values of dielectric parameters were calculated for the adsorbent loaded with a specific VOC concentration at a given temperature.

The mathematical model, taking into account the appropriate initial and boundary conditions, was solved using the numerical method of lines. Concentration and temperature breakthrough curves were obtained for a given value of electric field strength, flux density and washing gas temperature.

In the carbonaceous adsorbent bed, the radial damping effect of the wave caused a more than five-fold decrease in the value of the electric field strength at the column wall. The desorption process was most efficient for the propan-2-ol–activated carbon BPL system. In this case, high concentrations of the component in the gas phase at the outlet from the column, at high bed temperatures were observed. The desorption of toluene from BPL activated carbon was still feasible because heat was generated in the adsorbent throughout the process. It was not as intense as in the case of the propan-2-ol–BPL system, but effective enough to remove the compound from the bed.

The effects of the axial and radial distribution of the electric field strength correlated well with the measured and simulated temperature distribution in the adsorbent bed. For both studied adsorption systems, the mathematical model reproduced with quite good accuracy the course of concentration and temperature breakthrough curves as well as changes in the average concentration of the component in the solid phase during microwave regeneration of the adsorbent.

TESTING THE EFFECT OF NEW CONSTRUCTIONS OF SWIRL INSERTS ON SPRAY PARAMETERS

Sylwia Włodarczak[1], Daniel Janecki[2]*, Bartosz Czajkowski[1], Adam Szmyt[1], Andżelika Krupińska[1], Magdalena Matuszak[1], Marek Ochowiak[1]

[1]Poznan University of Technology, Department of Chemical Engineering and Equipment, M. Skłodowska-Curie 5, 60-965 Poznan, Poland
[2]University of Opole, Institute of Environmental Engineering and Biotechnology, 45-032 Opole
*corresponding authors: zecjan@uni.opole.pl; sylwia.wlodarczak@put.poznan.pl

Atomizers are some of the most important elements in many industrial processes. The construction of an atomizer has a direct impact on its effectiveness and efficiency. Over the last few decades, there have been significant changes in their design, which have improved their performance and reliability. The modifications include the dimensions of the outlet [1], the ratio of the diameter of the atomizer's chamber to the diameter of the outlet, the ratio of the length of the outlet to its diameter [2], and the number, geometry and shape of the inserts [3, 4]. Development regarding this matter will continue in order to meet the growing demands of the market.

The purpose of swirl inserts in atomizers is to increase energy and to homogenize the sprayed medium. These inserts create micro-turbulences that break up the liquid into smaller droplets, in turn allowing for better distribution of the medium at the spraying point. The shape and positioning of the swirl inserts vary with regards to the model of the atomizer and the type of medium to be sprayed. Depending on the individual needs and requirements of a given application, inserts can also have different sizes and configurations.

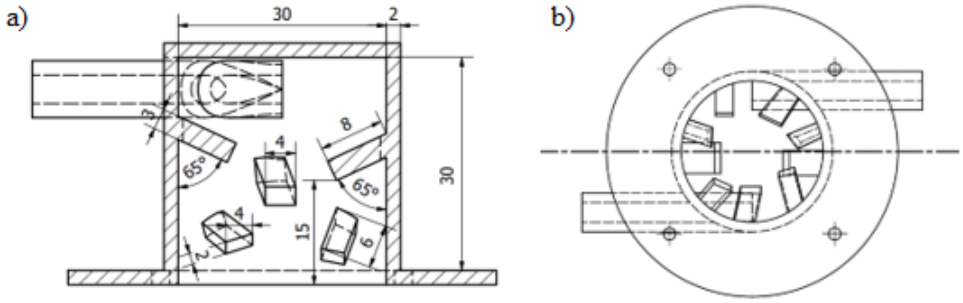

Fig. 1. The chamber of an atomizer with insert set No. 1: a) cross-section, b) bottom view

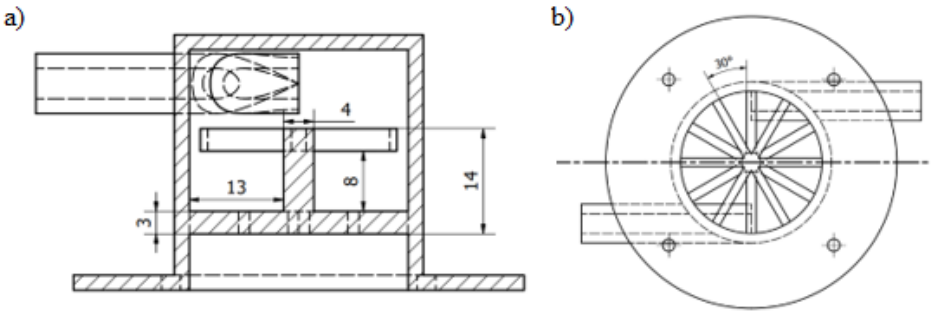

Fig. 2. The chamber of an atomizer with insert set No. 2: a) cross-section, b) bottom view

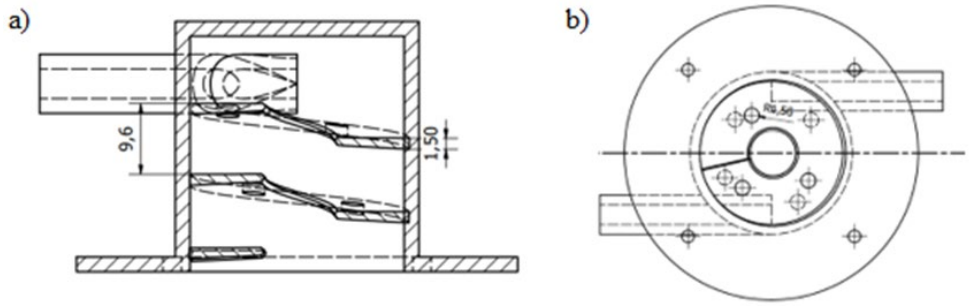

Fig. 3. The chamber of an atomizer with insert set No. 3: a) cross-section, b) bottom view

The aim of the research was to analyze the impact of the presence of the insert, as well as its construction, on flow resistance and spray angle. Pressure-swirl atomizers with a conical bottom and a cylindrical outlet with a diameter of $d_0 = 2{,}5 \cdot 10^{-3}$ m w er e des igned. The gen eral construction and dimensions of the atomizers were the same in each case. They only differed in terms of the shape of the swirl insert. Three different insert designs were used, as shown in Figures 1-3. Tests were carried out for the volumetric flow rate of tap water $\dot{V}_w$ ranging from $2{,}78 \cdot 10^{-6}$ $\left[\frac{\mathrm{m}^3}{\mathrm{s}}\right]$ to $2{,}78 \cdot 10^{-5}$ $\left[\frac{\mathrm{m}^3}{\mathrm{s}}\right]$, and the volumetric flow rate of air $\dot{V}_a$ ranging from $1{,}39 \cdot 10^{-4}$ $\left[\frac{\mathrm{m}^3}{\mathrm{s}}\right]$ to $5{,}56 \cdot 10^{-4}$ $\left[\frac{\mathrm{m}^3}{\mathrm{s}}\right]$ in a temperature of 20°C.

Pressure drops for atomizers with an insert are greater than in the case of empty atomizers. With an increase in the volumetric flow rate of liquid and gas, there is also an increase in pressure drops. The highest values of pressure drops in atomizers with inserts were obtained for the atomizer with insert set No. 1, while the smallest pressure drops were obtained for the atomizer with insert set No. 3. The pressure drops for the atomizer with insert set No. 2 were lower than for the atomizer with insert set No. 1, but higher than those obtained by the atomizer with insert set No. 3. For example, for $\dot{V}_w = 2{,}78 \cdot 10^{-5}$ $\left[\frac{\mathrm{m}^3}{\mathrm{s}}\right]$ and $\dot{V}_a$ = $4{,}17 \cdot 10^{-4}$ $\left[\frac{\mathrm{m}^3}{\mathrm{s}}\right]$, the following pressure drops were obtained: $\Delta P = 110000$ Pa (empty atomizer), $\Delta P = 116000$ Pa (atomizer with insert set No. 1), $\Delta P = 114000$ Pa (atomizer with filling No. 2), $\Delta P = 111000$ Pa (atomizer with insert set No. 3). The largest spray angles were obtained for the atomizer with insert set No. 2, with the largest value being approx. θ = 40º. It was achieved for the gas flow rate of $\dot{V}_g = 2{,}78 \cdot 10^{-4}$ $\left[\frac{m^3}{s}\right]$.

The atomizer with insert set No. 1 had slightly smaller spray angles than the atomizer with insert set No. 2. The spray angles of the atomizer with insert set No.3 were the smallest out of all the atomizers with the inserts. The smallest values of the spray angle were obtained for the empty atomizer. When analyzing the obtained results, it can be concluded that there are slight differences in the values of pressure drops and spray angles when using particular types of inserts. The most favorable atomization results, i.e. the largest angles, were obtained for the atomizer with insert set No. 2.

Funding: The research was financed by the Polish Ministry of Education and Science (SBAD).

References

[1] Cui J., Lai H., Li J., Ma Y., Visualization of internal flow and the effect of orifice geometry on the characteristics of spray and flow field in pressure-swirl atomizers, *Appl. Therm. Eng.,* 2017, 127, 812–822.
[2] Aminjan K.K., Heidari M., Rahmanivahid P., Study of spiral path angle in pressure-swirl atomizer with spiral path, *Arch. Appl. Mech.,* 2021, 91, 33–46.
[3] Nonnenmacher, S., Piesche, M., Design of hollow cone pressure swirl nozzles to atomize newtonian fluids. *Chem. Eng. Sci.*, 2000, 55, 4339–4348.
[4] Rashad M., Yong H., Zekun Z., Effect of geometric parameters on spray characteristics of pressure swirl atomizers, *Int. J. Hydrog. Energy*, 2016, 41, 15790–15799.

AXIAL THRUST IN A VESSEL WITH UNSTEADY ROTATING AXIAL IMPELLER

Szymon Woziwodzki*

Poznan University of Technology, Department of Chemical Engineering and Equipment, Poznan, Poland
*corresponding author: szymon.woziwodzki@put.poznan.pl

Unsteady mixing is one of the methods to improve mixing in an unbaffled vessel. It could be conducted in several ways, e.g. as circumferential motion of impeller [1, 2] or unsteady rotation of the impeller [3, 4]. The studies carried out so far focused on mixing of Newtonian or non-Newtonian fluids and gas-liquid systems. Results indicate that unsteady mixing decreases mixing time in viscous systems, increases shear rate in impeller region and increases mass transfer.

Roy and Acharya [5] performed simulation analysis (LES method) of unsteady mixing and showed that for radial impeller an increase in axial flow was observed. Explanation of this effect is related to a jet-stream which during deceleration of the impeller weakens radial stream and enhances axial orientation of the mainstream. Results obtained by Tezura et al. [6] also show increase of axial mixing in the region below the impeller. The increase in axial mixing and pumping capacity is approximately 13% for unsteady forward-reverse mixing and between 3% and 56% for unsteady mixing with constant direction of rotation. It suggests that unsteady mixing could be used to improve solid-liquid mixing by enhancing axial flow specially for radial impellers. There is no data for axial impellers. That in why the aim of this work was to evaluate axial flow in a stirred vessel by investigation of axial thrust using the method proposed by Fort et al. [7]. The axial thrust was determined by the gravimetric method. It usually is presented as an axial thrust number *Th* or momentum number *Mo*.

$$Th = Mo = \frac{F_a}{N^2 D^4 \rho} \tag{1}$$

where F_a is axial force. Momentum number is independent of Reynolds number and Keulegan-Carpenter number ($KC=f/N_{max}$) if $Re>10000$ and $KC>15$.

Experiments were performed in an unbaffled vessel with unsteady rotating impellers. The characteristic of unsteady motion was triangular [8] as described by Eq. (1).

$$N = \frac{8}{\pi^2} N_{max} \left(sin(2\pi f t) - \frac{1}{9} sin(6\pi f t) + \frac{1}{25} sin(10\pi f t) \right) \tag{2}$$

As unsteady motion the triangle characteristic of impeller speed was used for period about 4, 6 and 8 s and oscillation frequency f=0.115Hz, 0.23 Hz and 0.46 Hz. Three various impellers, mounted axially, were used: A315, SC-3, HE-3. Diameter of impellers *D* to vessel diameter *T* was *T/D*=3.
Figure 1 shows the relationship between the Mo number and the KC number for all impellers tested. Based on the literature data, the value of the momentum number Mo was determined for the A315, HE-3 and SC-3 impellers during steady-state mixing. For the A315 impeller, the momentum number was Mo = 0.804 [9], for the HE-3 impeller Mo = 0.343–0.358 [10], and for the SC-3 impeller Mo = 0.426 [11].

Table 1. Comparison of Mo values for unsteady and standard mixing

Impeller	Unsteady mixing		Standard mixing	
	Mo	*Fl*	*Mo*	*Fl*
A315	1.106	0.88	0.804 [9]	0.74 [9]
HE-3	0.550	0.620	0.343-0.358 [10]	0.41 [10]
SC-3	0.429	0.548	0.426 [11]	0.353-0.546 [11]

The test results indicate that during unsteady mixing, an increase in the value of the axial force is observed. Table 1 presents *Mo* values for unsteady and standard mixing.

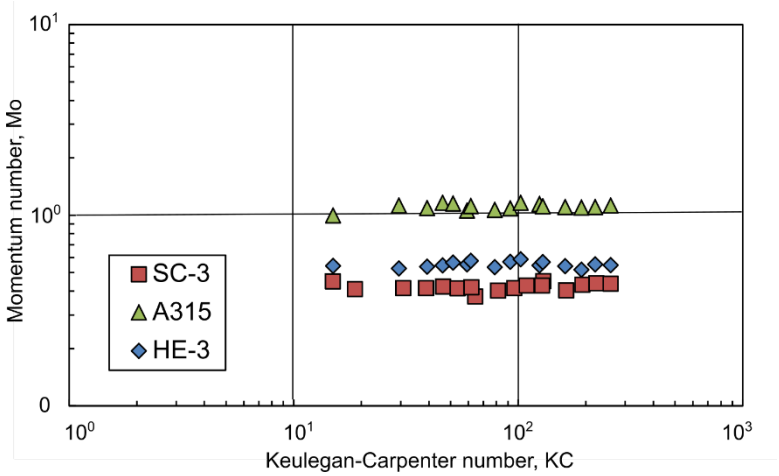

Fig. 1. Relation between momentum number Mo and Keulegan-Carpenter number KC

For unsteady mixing, an increase in the axial force is observed. The largest increase in the axial force was noted for the A315 and HE-3 impellers. In the case of the A315 impeller, the axial force is greater by 35-55%, while for the HE-3, its increase ranges from 53% to 54%. Using Eq. (3) flow number *Fl* ($Fl=Q/ND^3$) was calculated for all impellers and compared with flow number for standard, unidirectional mixing (Table 1). Results indicate an increase in flow number for unsteady mixing. For A315 impeller flow number increased about 50%, while for HE-3 about 34% and SC-3 about 6%.

Results of this research show that unsteady mixing is a good alternative to standard mixing. Increase in axial mixing and pumping capacity is observed in comparison to standard mixing. It suggests it can be used in mixing of solid-liquid systems but further investigations are needed.

Acknowledgement: This research was founded by Ministry of Education and Science

References

[1] Wójtowicz R., Flow pattern and power consumption in a vibromixer, *Chem. Eng. Sci.*, 2017, 172, 622–635.
[2] Komoda Y., Tomimasu F., Hidema R., Suzuki H., Frequency analysis of torque variation of a rotationally reciprocating impeller using Newtonian and viscoelastic fluids, *Chem. Eng. Res. Des.*, 2019, 142, 327–335.
[3] Frankiewicz S., Woziwodzki S., Gas Hold-Up and Mass Transfer in a Vessel with an Unsteady Rotating Concave Blade Impeller, *Energies*, 2022, 15(1), 346–15.
[4] Yoshida M., Kimura A., Yoneyama A., Tezura S., Design and operation of unbaffled vessels agitated with an unsteadily forward–reverse rotating impeller handling solid–liquid dispersions, Asia-Pac. *J. Chem. Eng*. 2012, 7(4), 572–580.
[5] Roy S., Acharya S., Perturbed turbulent stirred tank flows with amplitude and mode-shape variations, *Chem. Eng. Sci.*, 2011, 66, 5703–5722.
[6] Tezura S., Kimura A., Yoshida M., Yamagiwa K., Ohkawa A., Agitation requirements for complete solid suspension in an unbaffled agitated vessel with an unsteadily forward-reverse rotating impeller, *J. Chem. Technol. Biotechnol.*, 2007, 82(7), 672–680.
[7] Fořt I., Seichter P., Pešl L., Axial thrust of axial flow impellers, *Chem. Eng. Res. Des.*, 2013, 91(5), 789–794.
[8] Woziwodzki S., Unsteady mixing characteristics in a vessel with forward-reverse rotating impeller, *Chem. Eng. Tech.*, 2011, 34(5), 767–774.
[9] Bakker A., Hydrodynamics of stirred gas-liquid dispersions, Technische Univesiteit Delft, Delft 1992.
[10] Coker A.K., Ludwig's applied process design for chemical petrochemical plants, Elsevier, Amsterdam 2007.
[11] Michalak T., Projekt i badania modelowe mieszadła SC-3, Politechnika Poznańska, Poznań 2015.

A NEW TYPE OF LIQUID FERTILIZER CONTAINING FUNCTIONAL ADDITIVES

Monika Zienkiewicz, Magdalena Białomazur, Krzysztof Czachór, Dariusz Dojss, Beata Furmańczyk, Izabella Jasińska*, Piotr Jaworski, Anna Kaleta, Jadwiga Kaniecka, Kornelia Malarczyk-Matusiak, Piotr Masztalerz, Krzysztof Sokołowski, Aleksandra Wasilewska, Edyta Zielińska

Grupa Azoty Zakłady Chemiczne "Police" S.A., ul. Kuźnicka 1, 72-010 Police, Poland
*corresponding author: izabella.jasinska@grupaazoty.com

Research is being conducted to develop a technology for the production of new liquid fertilizers containing nitrogen compounds enriched with functional mineral and microbiological additives. The subject of the research is a response to the challenge of developing liquid fertilizers, which, as a supplement to the offer of granulated products of Grupa Azoty Zakłady Chemiczne "Police" S.A., will be used for foliar or soil feeding of plants exposed to physiological stress. The innovative composition of functional additives of the solution will make it possible to fill the identified technological gaps in the field of products increasing plant productivity and their resistance to adverse environmental conditions.

In the course of the research, the methods of producing the base fertilizer formula containing, apart from nitrogen compounds, silicon compounds and selected microelements were verified. Substances that are carriers of elements desirable from the agricultural point of view were selected. Technological parameters of the fertilizer solution production process were examined, including rheological parameters and physical form (turbidity) depending on the percentage of additives. The project analysed the chemical and physical stability of the prototypes over time under simulated different storage conditions (including temperature, insolation). Based on the obtained results, guidelines for the storage of new fertilizer solutions were developed.

As part of the work, research was carried out on the selection and methods of introducing microbiological components to the base fertilizer solution with mineral additives. The results of this part of the research in the project will make it possible to determine the impact of individual fertilizer components and their content on the effectiveness of microbiological additives and the selection of the most effective fertilizer composition.

Within the scope of project research, work was also carried out on the use of urease-inhibiting additives in the production of fertilizers, their stability during storage of fertilizer prototypes and the possibility of obtaining pro-environmental functionality in the form of reducing gaseous emissions of nitrogen derivatives. The research was carried out both in strictly controlled incubation conditions (laboratory), as well as in the scale of agricultural experiment on objects with specific soil conditions in maize cultivation.

The specificity of the research project required the development of a methodology and conducting agricultural tests to assess the effectiveness of new nitrogen fertilizers with functional additives. Agricultural usefulness of new, liquid fertilizers is tested during three full growing seasons in the cultivation of winter wheat, rape, corn and selected horticultural plants. The effectiveness of application of new products is compared with the results obtained using standard agricultural practice. Field tests are conducted to determine the content of individual components in new fertilizing products, selected on the basis of the results obtained in the earlier stages of research, in order to obtain optimal agricultural effects. An important element of this part of the work is the study of the impact of the use of new fertilizers on the physical parameters of plants, which determine their condition in situations of exposure to unfavourable meteorological phenomena (droughts, heavy downpours) or to threats from pathogens and pests.

The obtained research results will be used in the work on refining the technology for producing new liquid fertilizers with functional additives on a pilot scale.

The work was carried out within the framework of the project POIR.01.01.01-00-1313/20. The project was co-financed by the European Union with funds from the European Regional Development Fund under the Intelligent Development Operational Program 2014-2020. The project was carried out within the framework of the National Center for Research and Development "Fast Track" competition.

Posters

Doctoral students' posters

MODELING AND OPTIMISATION OF THE PROCESS OF CONCENTRATING AN AQUEOUS SOLUTION OF PECTIN BY FORWARD OSMOSIS (FO)

Adam Andrzejewski*, Mateusz Szczygiełda, Krystyna Prochaska

Poznan University of Technology, Institute of Chemical Technology and Engineering,
Berdychowo 4, 60-965 Poznan, Poland
*corresponding author: adam.andrzejewski@put.poznan.pl

The search for functional polymers in the natural environment is one of the global trends nowadays. Pectin belongs to the group of these compounds and is used in industry due to its emulating and thickening properties. On the industrial scale, pectin is recovered from apple pomace, which is a waste from the production of concentrated apple juice. Separation of pectin from plant tissues is complicated but not impossible. Currently used technology is a multi-stage procedure including evaporation methods to concentrate the extract obtained from the apple pomace. Such techniques are considered to be the most emissive and energy-demanding, which opposes the global environmental law rules [1].

An alternative to thermal concentration techniques may be the use of membrane separation methods, in particular forward osmosis techniques (FO). In FO, solvent transport is caused by the difference in the osmotic pressures of solutions on both sides of the semi-permeable membrane. Two solutions are involved in the FO process: a feed solution (FS), which is concentrated, and a draw solution (DS), which is diluted [2].

Based on the previous study it was claimed that the aqueous pectin solution can be effectively concentrated using the FO technique [3]. However, the process still needs investigation of the best process condition to reveal its application potential.

The aim of the study was to prepare a mathematical description of the process of concentration of an aqueous pectin solution by FO. The model was used to determine optimal process conditions. 49 processes of one-component pectin solution concentration using FO were conducted. Experiments were planned according to Box-Behnken experimental design for 5 factors, each on 3 levels [4]. Selected independent variables are presented in Table 1.

Table 1. Considered process parameters

Factor	Process parameter	Unit	Noncoded values of a factor level		
			-1	0	1
A	type of salt in DS	-	$CaCl_2$	NaCl	$MgCl_2$
B	media flow rate	$[dm^3 \cdot h^{-1}]$	20	25	30
C	initial volume of DS	$[cm^3]$	100	300	500
D	initial concentration of pectin in FS	$[g \cdot dm^{-3}]$	1	2	3
E	initial concentration of salt in DS	$[mol \cdot dm^{-3}]$	2	3	4

The proposed mathematical model consisted of a system of algebraic equations determined by fitting the full quadratic equation to experimental data using the multiple linear regression method (MLR). The dependent variables were water flux transported through the membrane (J_w), reverse salt flux (RSF) and FS concentration factor (CF) after the concentration process. The equations included linear, interaction and quadratic terms of each independent variable. In order to reduce the complexity of the mathematical model, not statistically significant terms were removed according to the results of the analysis of variance (ANOVA) (p-value<0.001). The value of the adjusted coefficient of determination for each equation was greater than 0.99.

Optimization of the model of the FO process was performed based on the desirability function method which allows to combine multiple equations into one function.

Global optimal conditions assuming values of all weights equal to 1 were determined. The best conditions of pectin solution concentration using FO are: NaCl as a salt in DS (factor A), the media flow rate equal to 30 $dm^3 \cdot h^{-1}$ (factor B), the initial volume of DS equal to 100 cm^3 (factor C), the initial concentration of pectin in FS equal to 1 $g \cdot dm^{-3}$ and the initial salt concentration equal to 2.92 $mol \cdot dm^{-3}$. The overall desirability was 0.999.

The optimisation results were experimentally validated. The differences between the experimental and simulated values were noticeable and statistically significant (p-value = 0.05) for water flux (J_{wk}) and FS concentration factor (CF) (Fig. 1). However, in the case of reverse salt flux (RSF), despite the apparent difference between the experimental value and the calculated value, the difference was not statistically significant (p-value = 0.05) due to the high variance of the RSF values. The probable reason for the observed differences between experimental and simulated results is the location of the optimal point, which takes extreme values for all the factors B, C and D. The characteristic property of the Box-Behnken experimental design is the lack of corner points, i.e. there are no experiments conducted for extreme values of many factors at once.

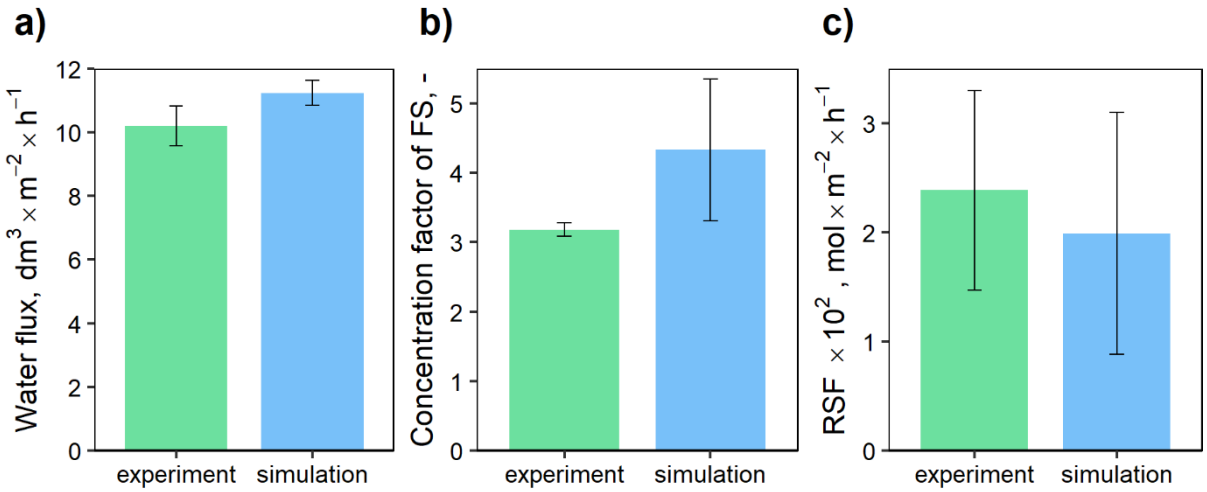

Fig. 1. The comparison of experimental and simulation values of the concentration process of aqueous pectin solution using FO in the optimal process condition: a) water flux, b) concentration factor of FS, c) reverse salt flux

To sum up, it is possible to propose the mathematical description of the aqueous pectin solution concentration process by the FO technique based on experimental data. Moreover, the fit of the model is satisfactory. However, the model does not explain the process well at extreme parameter values.

Acknowledgement: This work was financially supported by the National Science Centre, Poland (Grant no. 2021/41/N/ST8/03166).

References

[1] Mohnen D., Pectin structure and biosynthesis, *Curr. Opin. Plant Biol.*, 2008, 11, 266–277.
[2] Cath T.Y., Childress A.E., Elimelech M., Forward osmosis: Principles, applications, and recent developments, *J. Memb. Sci.*, 2006, 281,70–87.
[3] Andrzejewski A., Krajewska M., Nowak-Grzebyta J., Szczygiełda M., Stachowska E., Prochaska K., Concentration of pectin solution: Forward osmosis performance and fouling analysis, *J. Memb. Sci.*, 2022, 653, 120503.
[4] Box G., Hunter S.J., Hunter W.G., *Statistics for Experimenters: Design, Innovation, and Discovery*, John Wiley & Sons, Inc., Hoboken, NJ, 2005.

EXPERIMENTAL AND NUMERICAL ANALYSIS OF HYDRODYNAMICS IN MODIFIED INTERNAL LOOP AIRLIFT COLUMN

Tomasz Borowski*, Dawid Sołoducha, Marian Kordas, Rafał Rakoczy

Department of Chemical and Process Engineering, Pomeranian University of Technology in Szczecin, Piastów Ave. 42, 71-065, Szczecin, Poland
*corresponding author: tomasz.borowski@zut.edu.pl

Airlift columns are commonly used bioreactors owing to their specific design, which allows gas circulation and pneumatic agitation that is safer for microorganisms due to lower shear stress compared to standard bioreactors with mechanical stirrers. Over the years, researchers have developed various airlift experimental systems for different operating conditions and purposes, with common construction features such as two sections: a riser and a downcomer. These sections differ in the number of divisions, geometrical shape modifications, gas separators, and spargers [1].

In this study, modified internal loop airlift column hydrodynamics was characterized by introducing additional mixing elements to intensify the mixing process in the downcomer section. Experiments were conducted by injecting a tracer into the water-air system at different superficial air velocities in the riser section. Changes in electrical conductivity of the solution were registered by three conductivity probes located at the bottom, middle, and top of the reactor below the stagnant liquid level. The collected data was processed to obtain hydrodynamic parameters such as mixing time, mean circulation time, and mean liquid circulation velocity. The mixing time was obtained using the RMS variance method defined for the 95% mixing time, while the mean circulation time was obtained from tracer response curves averaged for the three probes. The third parameter was calculated based on the relation between the length of circulation loop and mean circulation time [2]. CFD simulations using the Eulerian model were conducted to obtain water velocity magnitude maps and vectors inside the apparatus. The discrete phase modelling was used to obtain paths of inert tracer that showed the circulation loops in the modelled column.

References

[1] Zhang T., We C., Ren Y., Feng C., Wu H., Advances inf airlift reactors: modified design and optimization of operation conditions, *Rev. Chem. Eng.,* 2016, 33(2).
[2] Lechowska J., Kordas M., Konopacki M., Fijałkowski K., Drozd R., Rakoczy R., Hydrodynamic studies in magnetically assisted external-loop airlift reactor, *J. Chem. Eng.*, 2019, 362, 298-309.

DEGRADATION OF CARBAMAZEPINE (CBZ) BY MAGNETICALLY MODIFIED TERNARY HETEROCOMPOSITE COMBINED WITH SR-(AOP)

Elvana Cako, Anna Zielinska-Jurek

Department of Processing Engineering and Chemical Technology, Gdansk University of Technology, Gdańsk, Poland,
*corresponding authors: elvana.cako@pg.edu.pl, annjurek@pg.edu.pl

Photocatalysis as a complementary method for commonly accepted biodegradation processes is successfully used in solar driven reactions such as water detoxification, degradation of pollutants from aqueous phase, CO_2 reduction, water splitting, and organic synthesis. Graphitic carbon nitride (g-C_3N_4) has gained interest in the field of photocatalysis due to its suitable band gap, low cost, non-toxicity and good stability, whereas 2D TiO_2 possesses a developed surface area. Hence, both semiconductors can be combined to complement their properties and to overcome their drawbacks like high recombination rate of photogenerated charges and UV light absorption. Furthermore, to improve separation of photocatalyst nanoparticles from wastewater after a complete water purification process, hybridization of semiconductor with spinel zinc ferrite allows efficient separation of photocatalyst nanoparticles from post-process suspension. Additionally, carbon-based materials and ferrites are known to effectively activate persulfate in SR-AOPs, and subsequently generate sulfate radicals ($SO_4^{\bullet -}$) and hydroxyl radicals ($HO^{\bullet}$).

In this regard, the aim of the present study was the synthesis and characterization of magnetically modified heterocomposite of spinel zinc ferrite ($ZnFe_2O_4$) modified with carbon nitride (g-C_3N_4) and 2D TiO_2 assisted by sulfate radical based advanced oxidation process (SR-AOP) for efficient degradation of carbamazepine (CBZ).

The obtained photocatalysts were characterized using DR/UV-Vis, XRD, FTIR, XPS, SEM/TEM, BET analysis, electrochemical analysis. Magnetic properties were analyzed using a SQUID magnetometer. Microscopy analysis confirmed the successful formation of ternary heterocomposite, which was applied in the degradation of carbamazepine under simulated solar light. Total removal of carbamazepine was achieved within 120 min of irradiation time, while an enhanced photocatalytic degradation of pollutant was observed for a combined system of ternary heterocomposite and (SR-AOP), where 100% degradation was achieved within 60 min of irradiation. Moreover, total organic carbon analysis confirmed that the combined system of persulfate (PS) and heterocomposite, yielded higher percentage of carbamazepine (CBZ) mineralization. Additionally, the remarkable magnetic recovery of spinel ferrite modified heterocomposite ensured the environmentally friendly and economic benefits of the fabricated 2D TiO_2/g-C_3N_4/$ZnFe_2O4$ photocatalyst.

Acknowledgment

The research was financially supported by Polish National Science Centre (Grant No. NCN 2021/43/B/ST5/02983).

PSEUDOMONAS AERUGINOSA CONTACTED WITH GRAPHENE OXIDE OR MAGNETITE

Kamila Dubrowska[1,*], Joanna Jabłońska[1], Adrian Augustyniak[1,2], Rafał Rakoczy[1]

[1] Faculty of Chemical Technology and Engineering, Department of Chemical and Process Engineering, West Pomeranian University of Technology, Szczecin, Piastow Ave. 42, 71-065 Szczecin, Poland
[2] Chair of Building Materials and Construction Chemistry, Technische Universität Berlin, Gustav-Meyer-Allee 25, 13355 Berlin, Germany
*corresponding author: kamila.dubrowska@zut.edu.pl

Pseudomonas aeruginosa is a bacterium with high biotechnological potential as a producer of many valuable metabolites, including rhamnolipids, pyocyanin and alginate [1]. Nevertheless, *P. aeruginosa* is considered to be a pathogen and often causes nosocomial infections [2]. On the other hand, the use of nanomaterials is growing annually, making nanotechnology one of the most intensively developing sciences [3-5]. Among many adaptations of nanomaterials, studying their effects on bacteria mainly focuses on antimicrobial effects [6-8]. However, some works have shown that the interaction between sublethal concentrations of nanostructures may have a stimulatory effect on bacteria [9-10]. In the case of *P. aeruginosa* this has implications in both, biotechnology, and medicine. Therefore, investigating the effects (stimulatory or inhibitory) of nanomaterials on pseudomonads is desired.

The study aimed to determine basic physiological effects such as changes in optical density and respiration of *P. aeruginosa* contacted with iron oxide nanoparticles (magnetite) or graphene oxide (GO).

In the study, *P. aeruginosa* DSM 1128 (ATCC 9027) was used as the reference microorganism. Tested nanomaterials included graphene oxide and iron (II) iron (III) oxide nanoparticles that were obtained commercially. To determine the influence of selected nanoparticles on *P. aeruginosa*, a 24h toxicity test was carried out. Briefly, two-fold dilutions of selected nanomaterials (resulting in the experimental concentration range of 15.625 – 1000 µg/mL) were used and compared to the control (with deionized sterile water). Next, two times concentrated Tryptic Soy Broth (TSB) (inoculated in a ratio 1:500 with an overnight culture of *P. aeruginosa*) was added in a 1:1 ratio. The optical density of the bacterial cultures (OD) was measured (λ = 600 nm) at 0h, 6h, 12h, and 24h. After the 24-h toxicity test, the respiration of the cultures was tested. Therefore, 10% resazurin (v/v) was added to the culture and measured after 4h (wavelength λ_{ex} = 520 nm and λ_{em} = 590 nm).

Depending on the material used and the concentration, significant changes in OD were observed. The biggest increases in OD readings were observed for GO concentration of 1000 µg/mL at 6h, 12h, and 24h. For magnetite, the change reached its maximum in samples containing 500 µg/mL at 6h of the experiment, where the highest reduction of reading was observed.

Even though toxicity towards *P. aeruginosa* was detected in some cases, nanomaterials could, in specific conditions, stimulate the viability of these bacteria. The results indicated that the physiological response of *P. aeruginosa* to the studied nanomaterials can be variable depending on the nanomaterial type and concentration. The growth stimulation can indicate the potential application of these nanostructures in biomass production. Nevertheless, further tests should be focused on the expression of virulence factors during observed phenomena.

References

[1] Palleroni N.J., *Pseudomonas" in Bergey's Manual of Systematics of Archaea and Bacteria*, Wiley, 2015, pp. 1–1.

[2] Rosenthal V. D., Al-Abdely H.M., El-Kholy A.A., AlKhawaja A.A.A., Leblebicioglu H., Mehta Y., Rai V., Viet Hung N., et al., International Nosocomial Infection Control Consortium report, data summary of 50 countries for 2010-2015: Device-associated module, *Am. J. Infect. Control*, 2016, 44(12), 1495–1504.
[3] Zhao L., Lu L., Wang A., Zhang H., Huang M., Wu H., Xing B., Wang Z., Ji R.., Nano-Biotechnology in Agriculture: Use of Nanomaterials to Promote Plant Growth and Stress Tolerance, *J Agric Food Chem*, 2020, 68, 7, 1935–1947.
[4] Makabenta J.M.V., Nabawy A., Li C.H., Schmidt-Malan S., Patel R., Rotello V.M., Nanomaterial-based therapeutics for antibiotic-resistant bacterial infections, *Nature Rev. Microbiol.*, 2020, 19(1), 23–36.
[5] Fytianos G., Rahdar A., Kyzas G.Z., Nanomaterials in Cosmetics: Recent Updates, Nanomaterials, 2020, 10(5), 979.
[6] Veerapandian M., Zhang L., Krishnamoorthy K., Yun K., Surface activation of graphene oxide nanosheets by ultraviolet irradiation for highly efficient anti-bacterial, *Nanotechnology*, 2013, 24(39), 395706.
[7] Khan F., Kang M.-G., Jo D.-M., Chandika P., Jung W.-K., Kang H.W., Kim Y.-M., Phloroglucinol-Gold and -Zinc Oxide Nanoparticles: Antibiofilm and Antivirulence Activities towards Pseudomonas aeruginosa PAO1, *Mar Drug*s, 2021, 19(11), 601.
[8] Kang S., Herzberg M., Rodrigues D. F., Elimelech M., Antibacterial effects of carbon nanotubes: Size does matter!, *Langmuir*, 2008, 24(13), 6409–6413.
[9] Augustyniak A., Dubrowska K., Jabłońska J., Cendrowski K., Wróbel R.J., Piz M., Filipek E., Rakoczy R., Basic physiology of Pseudomonas aeruginosa contacted with carbon nanocomposites, *Appl. Nanosci.*, 2022, 12(6), 1917–1927.
[10] Augustyniak A., Sikora P., Jabłońska J., Cendrowski K., John E., Stephan D., Mijowska E., The effects of calcium–silicate–hydrate (C–S–H) seeds on reference microorganisms, *Appl. Nanosci.*, 2020, 10(12), 4855–4867.

A STUDY ON AJUGA REPTANS EXTRACTS AS POTENTIAL COSMETIC RAW MATERIALS

Anna Dziki, Magdalena Malinowska, Elżbieta Sikora

Department of Organic Chemistry and Technology, Faculty of Chemical Engineering and Technology, Cracow University of Technology, Warszawska 24, 31-155 Kraków, Poland
*corresponding author: anna.dziki@doktorant.pk.edu.pl

Ajuga reptans L. (bugle) extracts are rich sources of active substances. Most often, the herb of the plant is used as raw material to obtain the extracts. Among others, ecdysteroids, triterpenes, sterols, diterpenes, iridoids, and flavonoids have been identified as *Ajuga r.* bioactive compounds providing anti-oxidant, anti-microbial, and anti-inflammatory activity [1, 2].

In our work, a comparative study of the antioxidant activity of ethanolic extracts obtained from the herb and roots of the bugle was carried out using the DPPH, FRAP and ABTS assays. The Folin-Ciocalteu method was used to determine the total polyphenols content. Based on the obtained results, the root extract was selected and used as an active ingredient to prepare a series of cosmetic products: O/W emulsion, W/O emulsion, face wash gel and eye serum [3, 4]. Physicochemical, microbiological and application properties were evaluated for the obtained formulations. AramoTS skin analyzer was applied to determine the influence on skin condition of volunteers testing the prepared products.

The obtained results confirmed that *Ajuga reptans* extracts exhibit significant antioxidant activity and that the formulas containing *Ajuga reptans* root extract showed the positive effect on the skin condition: causing an improvement in the degree of skin hydration and elasticity, reducing skin pore size and skin hyperpigmentation, and reducing the depth of wrinkles.

References

[1] Ono M., Furusawa C., Ozono T., Oda K., Yasuda S., Okawa M., Kinjo J., Ikeda, T., Miyashita H., Yoshimitsu H., Nohara T., Four new iridoid glucosides from Ajuga reptans, *Chem. Pharm. Bull*., 2011, 59, 1065–1068.
[2] Toiu A., Vlase L., Gheldiu A.M., Vodnar D., Oniga I., Evaluation of the antioxidant and antibacterial potential of bioactive compounds from Ajuga reptans extracts. *Farmacia*, 2017, 65, 351–355.
[3] Patent application no. P.439965, Kompozycja kosmetyczna w postaci emulsji odżywczej do stosowania na skórę. Submitted: 21.12.2021.
[4] Patent application no. P.439959, Kompozycja kosmetyczna w postaci emulsji nawilżającej do stosowania na skórę. Submitted: 21.12.2021.

PRELIMINARY STUDIES ON THE OXIDATION OF GERANIOL ON VERMICULITE

Sylwia Gajewska*, Agnieszka Wróblewska*

West Pomeranian University of Technology in Szczecin, Faculty of Chemical Technology and Engineering, Department of Catalytic and Sorbent Materials Engineering, Piastów Ave. 42, 71-065 Szczecin, Poland

*corresponding author: gs54727@zut.edu.pl, agnieszka.wroblewska@zut.edu.pl

Geraniol is a chemical compound belonging to monoterpenes with a light yellow color and oily consistency. It has a characteristic rose fragrance. Geraniol is an aromatic raw material used in the perfumery and cosmetics industry as a component of floral compositions. It also has bactericidal and fungicidal properties. This compound is obtained both from natural resources, such as Pelargonium graveolens and Pelargonium zonale, as well as by chemical synthesis.

Vermiculite is a natural, hydrated magnesium aluminosilicate that is widely used in the chemical industry. This heterogeneous, porous material is used as an environmentally friendly catalyst in chemical processes such as oxidation and isomerization. It has a yellow-brown color, and it is characterized by a lack of odor and a high melting point of more than 1300 °C. This mineral occurs naturally in Australia, Asia (China), Africa (South Africa) and in the United States (South Carolina). In addition, it occurs in Lower Silesia (Poland) but in small quantities. Vermiculite contains the largest amounts of such chemical compounds as: silicon oxide (IV), aluminum oxide (III) and magnesium oxide.

A preliminary study was conducted on the effect of temperature and reaction time on the oxidation of geraniol on vermiculite. The oxidation reaction was carried out using oxygen as an oxidant. The temperature was varied from 80 to 110 °C, and the reaction time from 60 to 300 min. The catalyst content in the reaction mixture was 1 wt%. The composition of the post-reaction mixtures was determined using gas chromatography (GC). The main products of geraniol oxidation were citral and monoepoxide. The highest obtained selectivity of transformation to citral was 11 mol%, and to monoepoxide 9 mol%, while the conversion of geraniol was 24 mol% (temperature 90 °C and reaction time 5h).

THE SYNERGISTIC PROCESS OF PHOTOCATALYSIS COUPLED WITH PMS ACTIVATION USING NOVEL TIO_2/MXENE/$MNFE_2O_4$ MAGNETIC COMPOSITE TOWARDS EFFECTIVE REMOVAL OF PHARMACEUTICALS

Anna Grzegórska, Anna Zielińska-Jurek

Department of Process Engineering and Chemical Technology, Faculty of Chemistry, Gdańsk University of Technology, G. Narutowicza 11/12, 80-233 Gdańsk, Poland
*corresponding authors: anna.grzegorska@pg.edu.pl, annjurek@pg.edu.pl

Over the last decades, world population growth, climate changes, industrialization, and destruction of the environment have contributed to an increase in water demands. Moreover, anthropogenic activity leads to high aquatic environment contamination with emerging contaminants from the group of endocrine-disrupting compounds, personal care products and pharmaceuticals, which cannot be efficiently degraded in traditional wastewater treatment plants. The presence of some pharmaceuticals in wastewater can influence human health, as they can be persistent in the environment and potentially affect aquatic life. For this reason, it is important to monitor and manage the release of pharmaceutically active compounds into the environment. The concentrations of ibuprofen and carbamazepine, being among the most frequently detected drugs in wastewater treatment plant effluents, range from ng/dm^3 to tens µg/dm^3. In the Baltic Sea region, CBZ was detected in more than 60% of reported water samples. In the MWWTP effluents with the maximum concentration of about 9 µg/dm^3, while up to 5000 µg/dm^3 in river water, and 0.08 µg/dm^3 in Baltic Sea water [1].

Among AOP, photocatalysis attracts considerable interest. This process is considered to be an environmentally friendly, highly efficient, and low-cost method, which can be used to remove pollutants from water and air [2]. Moreover, the synergistic effect may be obtained by enhancement of the photocatalytic process with peroxymonosulfate activation. Compared with hydroxyl radical (1.8–2.8 V), the sulfate radical ($\bullet SO_4^-$) has a close or even higher redox potential of 2.5–3.1 V (vs. NHE). Moreover, sulfate radical has a higher selectivity and a longer half-life (30–40 µs) and could be activated in a wider pH range (pH of 2–8) than $\bullet OH$ radicals [3].

Combining TiO_2, a commonly used photocatalytic material, with carbon materials led to improved charge carrier mobility, which is one of the major limitations during photocatalytic processes. MXenes are materials consisting of transition metal carbides, nitrides, or carbonitrides, characterized by hydrophilic surface, good electrical conductivity, and chemical stability, which were discovered in 2011. The general formula of MXenes is $M_{n+1}X_nT_x$ (n = 1–4), where M is a transition metal, X represents carbon or nitrogen, and T_x refers to surface terminations (-F,-O,-OH). A novel and promising direction is using MXenes in photocatalysis. MXenes may act as co-catalysts, enhancing the adsorption of the pollutants on the surface, photocatalyst stability, and increasing the light absorption range. Significantly, *in situ* oxidation of MXene $Ti_3C_2T_x$ led to the formation of TiO_2/Ti_3C_2 composite with intimate contact providing effective charge carrier separation [4].

Therefore, in this study, we proposed a novel heterojunction of TiO_2/MXene/$MnFe_2O_4$ and application to the photocatalytic degradation of PACs mixture - ibuprofen and carbamazepine under simulated solar light irradiation. Furthermore, the photocatalytic process was combined with PMS activation. $Ti_3C_2T_x$ has been used as a Ti precursor for anatase/rutile TiO_2 formation and as the co-catalyst. In this system, the dual role of $MnFe_2O_4$ - the magnetic part providing easy separation after the process and activation of PMS, to produce $\bullet SO_4^-$ was evaluated. The stability and reusability of the system were investigated in photocatalytic recycling experiments. Furthermore, trapping experiments with scavengers were performed to determine the major reactive species participating in the processes with TiO_2/MXene/$MnFe_2O_4$.

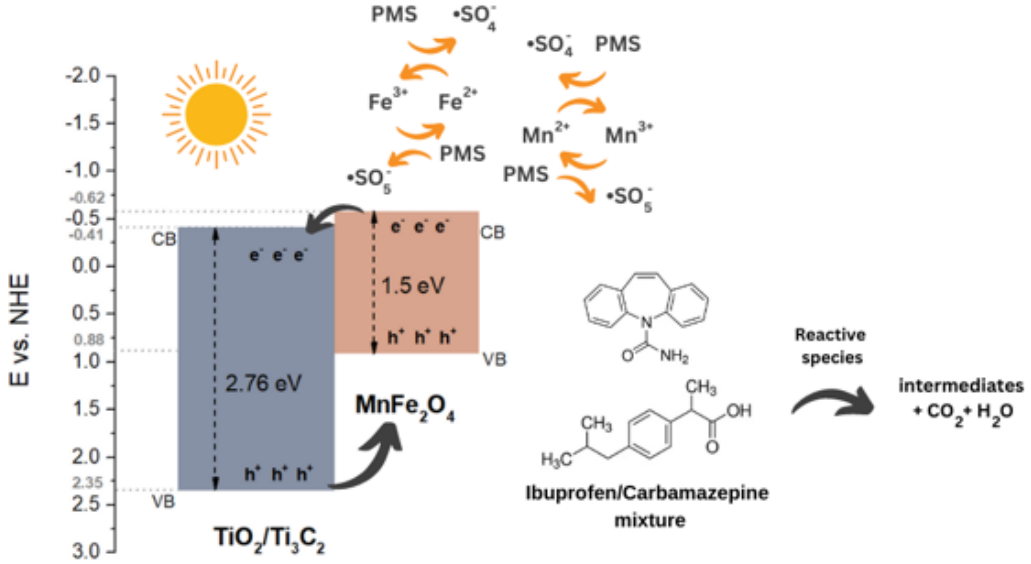

Fig. 1. The possible mechanism of IBP/CBZ mixture degradation with $TiO_2/Ti_3C_2/5\%MnFe_2O_4$

The obtained results confirmed that the ternary magnetic composites $TiO_2/Ti_3C_2/MnFe_2O_4$ were successfully fabricated and applied for the removal of pharmaceuticals - carbamazepine and ibuprofen mixture with nearly 100% removal within 60 minutes. It was concluded that $TiO_2/Ti_3C_2/MnFe_2O_4$ composite, due to the incorporation of magnetic nanoparticles, may be easily recovered from the reaction mixture after the process by an external magnetic field. Furthermore, the synergistic effect of the combination of $TiO_2/Ti_3C_2/5\%MnFe_2O_4$ with PMS activation (0.25 mM) to produce highly active $\bullet SO_4^-$ radicals under simulated solar light was confirmed with superior removal of CBZ - 100% within 20 minutes and IBP - 100% within 10 minutes. Moreover, $TiO_2/Ti_3C_2/5\%MnFe_2O_4$/PMS combined system showed excellent stability and recyclability confirmed by four subsequent photocatalytic cycles as well as XRD and FTIR analysis of fresh and re-used photocatalyst. Based on the trapping experiment with scavengers, we concluded that the $\bullet SO_4^-$ and $\bullet O_2^-$ radicals were the main species responsible for CBZ degradation, while $\bullet SO_4^-$ and h^+ were responsible for IBP degradation. Furthermore, the Mott-Schottky analysis was implemented to determine the materials' conduction band position and the valence band position according to the bandgap value. On this basis, the possible mechanism of IBP and CBZ degradation was proposed, as shown in Fig. 1. Photoexcited electrons in CB of $MnFe_2O_4$ may be transferred to CB TiO_2/Ti_3C_2 due to the higher potential of conduction band edge. On the contrary, the holes in the VB of TiO_2/Ti_3C_2 are transferred to the VB of $MnFe_2O_4$. Thus, the recombination of photogenerated electron–hole pairs is suppressed.

Acknowledgment

The research was financially supported by Polish National Science Centre (Grant No. NCN 2021/43/B/ST5/02983).

References

[1] UNESCO and HELCOM. 2017. Pharmaceuticals in the aquatic environment of the Baltic Sea region – A status report. UNESCO Emerging Pollutants in Water Series – No. 1, UNESCO Publishing, Paris.
[2] Xu Y.-J., Promises and Challenges in Photocatalysis, *Frontiers in Catalysis*, 2021, 1.
[3] Antoniou M.G., de la Cruz A.A., Dionysiou D.D., Degradation of microcystin-LR using sulfate radicals generated through photolysis, thermolysis and e− transfer mechanisms, *Appl Catal B.,* 2010, 96, 290–298.
[4] Grzegórska A., Głuchowski P., Karczewski J., Ryl J., Wysocka I., Siuzdak K., Trykowski G., Grochowska K., Zielińska-Jurek A., Enhanced photocatalytic activity of accordion-like layered Ti3C2 (MXene) coupled with Fe-modified decahedral anatase particles exposing {1 0 1} and {0 0 1} facets, *Chemical Eng. J.* 2021, 426, 130801.

OXIDATION OF ALPHA-PINENE OVER NATURAL MINERALS – COMPARSION OF ACTIVITY

Jadwiga Grzeszczak*, Agnieszka Wróblewska*

Department of Catalytic and Sorbent Materials Engineering, Faculty of Chemical Technology and Engineering, West Pomeranian University of Technology in Szczecin, Piastów Ave. 42, 71-065 Szczecin, Poland
*corresponding author: jadwiga.tolpa@zut.edu.pl, agnieszka.wroblewska@zut.edu.pl

The aim of this study was to compare the catalytic activity of natural minerals such as: halloysite, clinoptilolite, vermiculite and sepiolite in the oxidation of alpha-pinene with oxygen. The process was carried out in a three-neck spherical flask with a capacity of 25 cm^3. The flask was equipped with a reflux condenser, a magnetic stirrer and a glass babbler for oxygen delivery. Approximately 10 g of alpha-pinene (purity 98%, Sigma-Aldrich) and 0.01 g of catalyst (0.1 wt% in relation to alpha-pinene) were introduced into the flask, and oxygen was fed from a cylinder at a rate of 40 mL/min, which was adjusted with a flow meter. The flask was placed in an oil bath heated to 95 °C. The contents of the flask were stirred with a magnetic stirrer at an intensity of 500 rpm. The oxidation was carried out for 4 hours, and the reaction mixture was collected into an Eppendorf tube after 4 hours in an amount of about 1 cm^3. Then, samples of the reaction mixture, which had previously been separated from the catalyst using a laboratory centrifuge, were diluted with acetone in a weight ratio of 1:4. The oxygen derivatives of alpha-pinene were identified with the GC method (gas chromatography method) and with the application of FID detector. Catalytic activity of the tested catalysts was determined on the basis of mass balances, according to which the main functions describing the process were determined: conversion of α-pinene and selectivities of: alpha-pinene oxide, campholenic aldehyde, verbenol, verbenone, pinocarveol, myrtenal, myrtenol, carveol, carvone, and pinanediol.

Figure 1 shows the activity of the tested catalysts in the oxidation of alpha-pinene. Vermiculite proved to be the most active, considering the selectivity to alpha-pinene oxide and the conversion of alpha-pinene. After a reaction time of 4 hours, the following selectivity values for the main products were obtained: alpha-pinene oxide 21 mol%, verbenol 16 mol%, verbenone 12 mol%, and alpha-pinene conversion was 34 mol%. Similar catalytic activity was visible for sepiolite (selectivities of the main products amounted to: alpha-pinene oxide 19 mol%, verbenol 17 mol%, verbenone 13 mol%, and conversion of alpha-pinene 28 mol%). The highest selectivity value for verbenol (20 mol%) was obtained over halloysite.

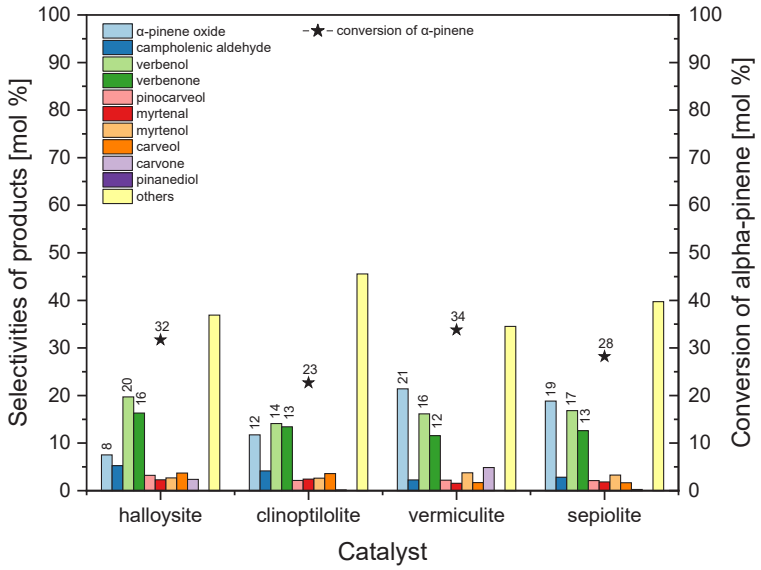

Fig. 1. Conversion of alpha-pinene and selectivities of appropriate products over natural minerals (temperature 95 °C, catalyst amount in reaction mixture 0.1 wt%, and reaction time 4 h)

Natural minerals such as halloysite, clinoptilolite, vermiculite and sepiolite proved to be excellent catalysts for alpha-pinene oxidation. The oxygen derivatives of alpha-pinene obtained in this process have very important applications in medicine, cosmetics and in the food industry.

The use of low temperature (95 °C), trace amount of catalyst (0.1 wt%), and short reaction time (4h), makes this unconventional method cost-effective and economical. The method developed by our team is environmentally friendly, as we use compounds of natural origin, such as alpha-pinene extracted from biomass and natural minerals found in sedimentary and volcanic rocks. In addition, we do not use a solvent in this method, and we use oxygen as the oxidant, which makes this method environmentally safe (there is no need to separate the products from the solvent).

We plan to continue our research. In the next stage, it will be necessary to study the effects of temperature, the amount of the catalyst and the reaction time on alpha-pinene conversion and selectivities of appropriate products, and to characterize the catalysts by instrumental methods such as: UV-Vis, FTIR, EDXRF, XRD, SEM, and by the nitrogen sorption method at 77 K.

THE MODULATION OF PSEUDOMONAS AERUGINOSA PHYSIOLOGY USING DIFFERENT TYPES OF ELECTROMAGNETIC FIELD

Joanna Jabłońska[1,*], Kamila Dubrowska[1], Adrian Augustyniak[1,2,3], Marian Kordas[1], Rafał Rakoczy[1]

[1] Department of Chemical and Process Engineering, Faculty of Chemical Technology and Engineering, West Pomeranian University of Technology in Szczecin, Szczecin, Poland
[2] Chair of Building Materials and Construction Chemistry, Technische Universität Berlin, Berlin, Germany
[3] Institute of Biology, University of Szczecin, Szczecin, Poland
*corresponding author: joanna_jablonska@zut.edu.pl

Electromagnetic fields (EMFs) are more and more often applied in bioprocesses to boost biomass or metabolite production [1, 2]. *Pseudomonas aeruginosa* is an exemplary microorganism that can be used as a producer strain. It was previously reported that the static electromagnetic field (SEMF) with the magnetic induction of 200 mT could stimulate pyocyanin and rhamnolipid production by *P. aeruginosa* [3]. Nevertheless, the growth of this bacterium was only reported as inhibited while exposed to a rotating electromagnetic field (REMF), and pyocyanin production was never assessed in this particular type of electromagnetic field. Therefore, this research aimed to examine the influence of different types of electromagnetic fields (rotating and static) on the growth rate, viability, and pyocyanin production.

The strain employed in the research was *P. aeruginosa* ATCC 27853, cultivated in King's A broth dedicated to pyocyanin production. Cultures were incubated at 37°C in magnetically-assisted reactors. The tested types of EMFs were SEMF with the magnetic induction of -17.37 mT and REMF with 24.32 mT (frequency equal to 5 Hz) and 42.64 mT (50 Hz). The growth rate was calculated using the Gompertz equation [4], viability was assessed by resazurin reduction, and pyocyanin concentration with the chloroform/HCl extraction method. EMF exposure times tested were 2, 6, and 12 hours, while the full culture lasted 48 hours. Moreover, different volumes of the culture (5 and 50 mL) were tested.

The growth rate of *P. aeruginosa* was significantly stimulated while exposed to SMF and slightly increased under 50 Hz RMF. Moreover, exposure to RMF of 5 Hz resulted in the highest pyocyanin production. However, this result did not differ significantly from the control. These data show that the use of different types of EMFs can result in different effects observed in the culture. Our study emphasizes the finding that EMFs can be used as bioprocess stimulators for population growth and pyocyanin production. Nevertheless, every setup needs optimized exposure time, culture volume EMF type, and magnetic induction [5].

This study was supported by the National Science Centre, Poland (PRELUDIUM 20, Project No. 2021/41/N/ST8/01094, granted to Joanna Jabłońska and OPUS 16, Project No. UMO-2018/31/B/ST8/03170, granted to Rafał Rakoczy).

References

[1] Jabłońska J., Augustyniak A., Dubrowska K., Rakoczy R., The two faces of pyocyanin - why and how to steer its production? *World J. Microbiol. Biotechnol.*, 2023, 39(4), 103.
[2] Jabłońska J., Dubrowska K., Gliźniewicz M., Paszkiewicz O., Augustyniak A., Grygorcewicz B., Konopacki M., Markowska-Szczupak A., Kordas M., Dołęgowska B., Rakoczy R., The use of the electromagnetic field in microbial process bioengineering, *Adv. Appl. Microbiol.*, 2022, 121, 27–72.
[3] Raouia H., Hamida B., Khadidja A., Ahmed L., Abdelwaheb C., Effect of static magnetic field (200 mT) on biofilm formation in Pseudomonas aeruginosa, *Arch. Microbiology*, 2020, 202(1), 77–83.

[4] Winsor C. P., The Gompertz Curve as a Growth Curve, *Proc. Natl. Acad. Sci*., 1932, 18, 1–8.
[5] Jabłońska J., Dubrowska K., Augustyniak A., Kordas M., Rakoczy R., Application of Magnetically Assisted Reactors for Modulation of Growth and Pyocyanin Production by Pseudomonas aeruginosa, *Front. Bioeng. Biotechnol*., 2022, 10. https://doi.org/10.3389/fbioe.2022.795871.

STUDIES OF ADSORPTION KINETICS BY STATIC AND DYNAMIC METHODS

Maciej Jabłoński, Alicja Dzienisz*, Elwira Wróblewska, Krzysztof Lubkowski

Department of Organic and Physical Chemistry, West Pomeranian University of Technology, Szczecin, Piastów 42, 71-065 Szczecin, Poland
*corresponding author: alicja.soltys@zut.edu.pl

An adsorption isotherm is the information indicating the interaction of an adsorbent and an adsorbate. Using adsorbates with different properties, it is possible to determine the type of interaction between adsorbate molecules and the surface of an adsorbent [1].

In the adsorption process, adsorption kinetics is an important element. The rate of concentration change during adsorption is a function of temperature and concentration of substrates and products. When the adsorption process is concerned, a substrate is a chemical compound in the gas phase, whereas a product is the same chemical compound adsorbed on the surface of a sorbent.

It can be assumed for the gas phase that the concentration of a chemical compound does not change during the whole adsorption process. Thus, it can be concluded that the adsorption of a substrate proceeds according to the zero-order kinetic equation. If the process follows a zero-order kinetics, it means that the process proceeds at a constant rate. The zero-order process rate for the adsorption of a substrate is a constant value equal to the reaction rate constant. The reaction is of zero order when its rate is not determined by its chemistry, but by another process independent of the concentration of the reactants, e.g. diffusion in a heterophase system.

In the case of a phase adsorbed in the adsorption process, the content of the substance in the surface layer will change over time until the state of equilibrium is reached in relation to the concentration of a given substance in the gas phase. In this case, we will use other kinetic equations to describe the kinetics.

Kinetic equations applied in thermal analysis (where thermal transformation processes of various types of chemical substances are studied) were used to describe the obtained results of kinetic measurements. The reactions studied in the thermal analysis are classified as gas-solid heterophase systems. The adsorption process can be classified as this type of system.

An important group of kinetic models are models describing the phenomenon of nucleation.

Another group of kinetic models are models describing reactions in which the phenomenon of transport to and from the reaction zone occurs. The process that determines the reaction rate is most often the diffusion process.

The presented kinetic equations were used to describe the adsorption process of organic compounds on zeolite and activated carbon. As a result of the analysis, it turned out that the best description of the adsorption kinetics process is given by the kinetic equation, which is used to describe the kinetics of the first-order reaction.

The graphs in Figs. 1 and 2 show the results of the kinetics of the adsorption of isopropanol on zeolite by the dynamic method and of acetone on activated carbon by the static method in comparison with the kinetic model of the first-order reaction.

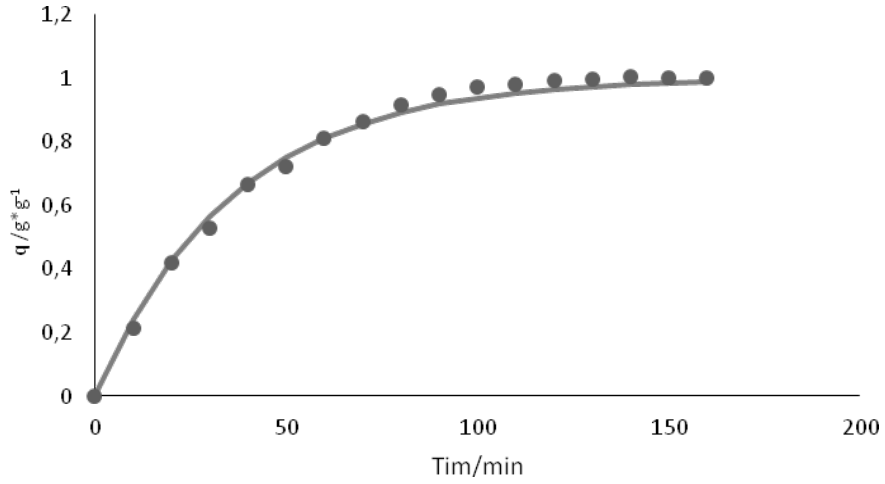

Fig. 1. Adsorption kinetics of isopropanol with a concentration of p/p0 -=0.0588 on zeolite (dynamic method)

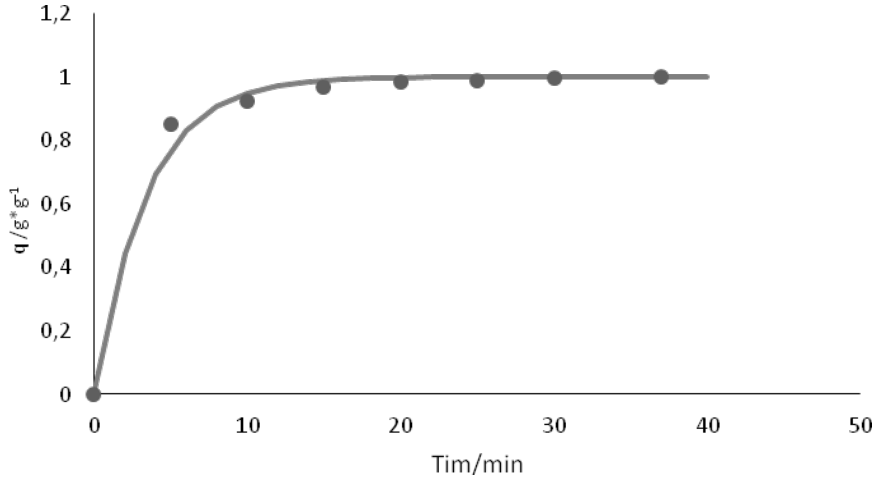

Fig. 2. Kinetics of acetone adsorption on activated carbon N under static conditions at 20°C, equilibrium p/p0 = 0.0374

References:

[1] Paderewski M.L., *Adsorption processes in chemical engineering (in Polish)*, WNT, Warsaw 1999.

BINDING BEHAVIOR OF CONVERTED DRUGS INTO AMINO ACID-BASED IONIC LIQUIDS WITH BOVINE SERUM ALBUMIN

Joanna Klebeko[1,*], Paula Ossowicz-Rupniewska[1], Ewa Janus[1], Maya Guncheva[2]

[1]West Pomeranian University of Technology in Szczecin, Faculty of Chemical Technology and Engineering, Department of Chemical Organic Technology and Polymeric Materials, Piastów Ave. 42, 71-065 Szczecin, Poland
[2]Bulgarian Academy of Sciences, Institute of Organic Chemistry with Centre of Phytochemistry, Acad. G. Bonchev Bl. 9, 1113 Sofia, Bulgaria
*corresponding author: joanna.klebeko@zut.edu.pl

Nonsteroidal anti-inflammatory drugs (NSAIDs) are the most commonly prescribed and used medications for fever, pain relief, and the reduction of inflammation. However, the low solubility of these drugs in water is the limiting factor in their bioavailability. It requires high dosages to reach a therapeutic concentration in the blood system. The current interest of the pharmaceutical industry is aimed at improving the physicochemical properties of pharmaceutical ingredients with the aim of better water solubility, dosage reduction, and improving the onset of action and safety profile [1, 2].

In recent years, many studies have shown that converting conventional drugs into ionic liquids based on active pharmaceutical ingredients (API-ILs) could be a successful strategy to solve some of the problems associated with low bioavailability and side effects, or even provide an alternative route of administration of the classic drug. Furthermore, the synthesis of API-ILs also allows to modify the physicochemical properties such as molecular weight, melting point temperatures, thermal stability, and partition coefficient by selecting proper counterions [3–5].

Here we present the synthesis and physicochemical characterization of a series of L-valine ethyl ester-based ionic liquids containing anions of selected acids from the NSAIDs group: ibuprofen, naproxen, ketoprofen, and salicylic acid. The L-amino acid ester was chosen as the counterion for the studied API due to its low toxicity, biocompatibility, and high hydrophilicity to synthesize derivatives with higher solubility from natural components. Moreover, the pharmacokinetic and pharmacodynamic profile of the obtained compounds was determined by assessing the thermodynamics of the process of binding compounds with bovine serum albumin (BSA).

References

[1] Lou Y., Zhu J., Carboxylic Acid Nonsteroidal Anti-Inflammatory Drugs (NSAIDs), in: C. Lamberth, J. Dinges (Eds.), Bioactive Carboxylic Compound Classes: Pharmaceuticals and Agrochemicals, Wiley-VCH Verlag GmbH & Co. KGaA, Weinheim, Germany, 2016, 221–236.
[2] Bindu S., Mazumder S., Bandyopadhyay U., Non-steroidal anti-inflammatory drugs (NSAIDs) and organ damage: A current perspective, *Biochem. Pharmacol*., 2020, 180, 114147.
[3] Handa, M., Almalki, W.H., Shukla, R., Afzal, O., Altamimi, A.S.A., Beg, S., Rahman, M., Active Pharmaceutical Ingredients (APIs) in Ionic Liquids: An Effective Approach for API Physiochemical Parameter Optimization, *Drug Discov. Today*, 2022, 27, 2415–2424.
[4] Bharate, S.S., Carboxylic Acid Counterions in FDA-Approved Pharmaceutical Salts, *Pharm. Res*., 2021, 38, 1307–1326.
[5] Adawiyah N., Moniruzzaman M., Hawatulaila S., Goto M., Ionic Liquids as a Potential Tool for Drug Delivery Systems, *Med. Chem. Commun*., 2016, 7, 1881–1897.

THE ANTIMICROBIAL ACTIVITY OF PLANT EXTRACTS

Magdalena Korol[1,2,*], Elżbieta Sikora[2]

[1]Grupa Azoty Zakłady Azotowe "Puławy" S.A., Tysiąclecia Państwa Polskiego 13
24-100 Puławy, Poland
[2]Cracow University of Technology, Warszawska 24, 31-155 Cracow, Poland
[*]corresponding author: Magdalena.Korol@grupaazoty.com

The use of plants for medicinal purposes has been known for hundreds of years. This is possible due to the fact that plants are rich in bioactive compounds with a wide spectrum of activity. The most important of these bioactive substances are alkaloids, flavonoids, terpenoids, steroids, tannins, and saponins [1]. Approximately 20% of known plants have been used in pharmaceutical or cosmetic applications [2].

Many plants contain active compounds with antimicrobial activity [3]. The ability of the plant origin products to inhibit increase or kill the microorganisms depends on their chemical composition. The parameters of an extraction process are the main factors influencing the concentration of active substances and as an effect the antimicrobial efficiency of the extracts [4]. Table 1 shows antimicrobial activity of some medicinal plants against selected pathogenic microorganisms.

Table 1. Effect of plant extracts

Activity	Plant extract	Chemical composition of the extract
antibacterial activity	apple pomace extract [5]	rutin, catechin, epicatechin, phloridzin, phloretin, chlorogenic acid, quercetin glycosides [6]
	oregano extract [7]	chlorogenic acid, epicatechin, caffeic acid, p-coumaric acid, ferrulic acid, benzoic acid, rosemary acid, myricetin, resveratrol, quercetin, carnosol, curcumin
antiviral activity	Rutaceae [8]	alkaloids: β-carbolines, furanoquinolines, camptothecin, atropine, caffeine, indolizidines swainsonine, castanospermine, colchicines, vinblastine
antifungal activity	Curcuma amada (mango ginger) [9]	β-Myrcene, epicurzeronone, squalene, α-acaridial, β-pinene, aromadandrene

References

[1] Wulandari L., Retnaningtyas Y., Lukman N., Lukman H., Analysis of Flavonoid in Medicinal Plant Extract Using Infrared Spectroscopy and Chemometrics, *J. Anal. Methods Chem.*, 2016, 4696803.
[2] Naczk M., Shahidi F., Phenolics in cereals, fruits and vegetables: Occurrence, extraction and analysis, *J. Pharm. Biomed. Anal.,* 2006, 41, 1523-1542.

[3] Egamberdieva D., Jabborova D., Babich S., Antimicrobial activities of herbal plants from Uzbekistan against human pathogenic microbes, *Environ.l Sustainability*, 2021, 4, 87–94.
[4] Arulmozhi P., Vijayakumar S., Kumar T., Phytochemical analysis and antimicrobial activity of some medicinal plants against selected pathogenic microorganisms, *Microb. Pathog.*, 2018, 123, 219-226.
[5] Zhang T., Wei X., Miao Z., Hassan H., Song Y., Fan M., Screening for antioxidant and antibacterial activities of phenolics from Golden Delicious apple pomace, *Chem. Cent. J.*, 2016, 10,47, PMC4970275.
[6] Cao X., Wang C., Pei H., Sun B., Separation and identification of polyphenols in apple pomace by high-speed counter-current chromatography and high-performance liquid chromatography coupled with mass spectrometry, *J. Chromatogr. A.*, 2009, 1216, 4268–4274.
[7] Hać-Szymańczuk E, Cegiełka A, Karkos M, Gniewosz M, Piwowarek K., Evaluation of antioxidant and antimicrobial activity of oregano (Origanum vulgare L.) preparations during storage of low-pressure mechanically separated meat (BAADER meat) from chickens, *Food Sci. Biotechnol*., 2018, 28(2), 449-457.
[8] Jassim, S.A.A., Naji, M.A., Novel antiviral agents: a medicinal plant perspective, *J. Appl. Microbiol.*, 2003, 95, 412-427.
[9] Policegoudra R.S., Vairale M.G., Chattopadhyay P., Shivaswamy R., Aradhya S.M., Raju P.S., Bioactive constituents of Curcuma amada (mango ginger) rhizomes and their antifungal activity against human skin pathogens, *J. Herb. Med*., 2020, 21, 100331.

ENHANCED PHOTOCATALYTIC NAPROXEN DEGRADATION UNDER VISIBLE LIGHT BY Cu_2O ANCHORED ON MULTIFACETED MONOCLINIC $BiVO_4$ PHOTOCATALYST

Marta Kowalkińska*, Anna Zielińska-Jurek*

Department of Process Engineering and Chemical Technology, Gdansk University of Technology, Gabriela Narutowicza 11/12, 80-233 Gdansk, Poland
*corresponding authors: marta.kowalkinska@pg.edu.pl, annjurek@pg.edu.pl

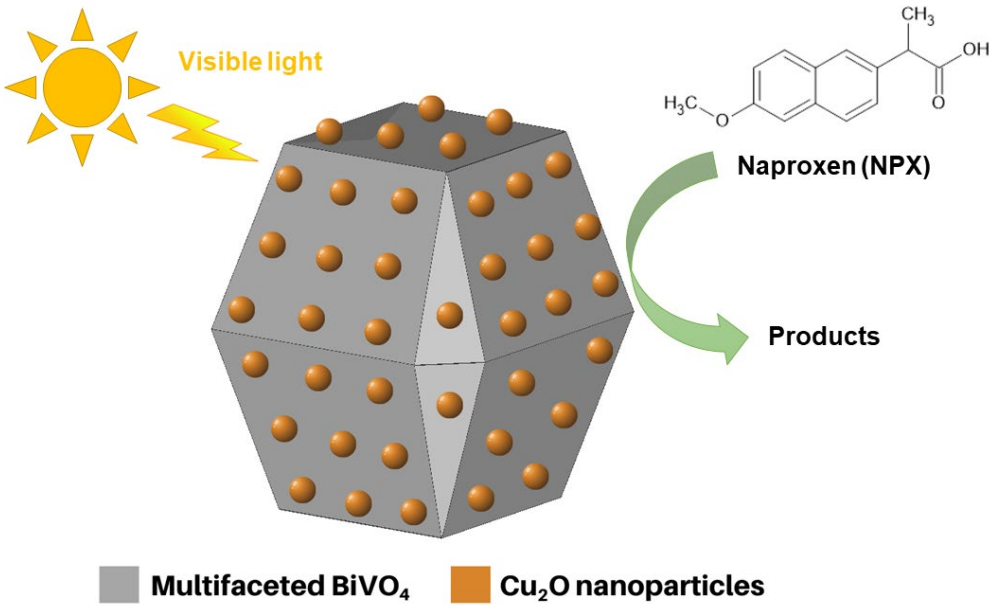

Fig. 1. Schematic illustration of $Cu_2O/BiVO_4$ photocatalyst

In recent years, due to the rapid development of medicine, more and more pharmaceuticals and personal care products (PPCP) have been introduced into the pharmaceutical market. However, the widespread use of medication has led to its excessive introduction into ground and surface waters. The effluents may contain persistent and toxic organic compounds, which are not susceptible to wastewater treatment using conventional methods [1]. One of the most frequently detected pharmaceutical compounds in Poland is naproxen (NPX), which is a popular pain killer available without prescription. It was found that naproxen can accumulate in the tissues of aquatic organisms and enter the food chain, potentially affecting human health through consumption of contaminated seafood. Therefore, efficient and more advanced degradation technologies of NPX and other PPCPs are highly desirable.

Among water treatment technologies, heterogeneous photocatalysis is worthy of attention because this process, in the presence of semiconductors, allows the degradation of trace amounts of persistent organic pollutants from water under illumination. Especially, the visible-light active photocatalysts allow the use of less energy-consuming light sources in photocatalytic reactions. Among studied oxide photocatalysts, monoclinic-scheelite bismuth orthovanadate ($BiVO_4$) is a promising material with the potential to play a significant role in solving environmental problems. $BiVO_4$ can be activated under visible light (above 420 nm). Therefore, this semiconductor is promising for future technological advancements. However, so far, the fast charge carrier recombination of photogenerated electron–hole pairs has impeded the improvement of its photocatalytic activity [2]. Therefore, different methods have been adopted to improve the charge

carrier separation efficiency and hinder the recombination process. One of the promising approaches is interface design and crystal facet engineering because the preferred surface localization of photogenerated holes and electrons depends on the photocatalyst exposed crystal facets [3, 4].

In this regard, in the present study, we present a dual approach to enhancing NPX degradation in the photocatalytic process. Firstly, we demonstrated multifaceted $BiVO_4$, in which the construction of facet homojunction improved photocatalytic naproxen degradation under visible light. Moreover, to enhance charge transport, copper(i) oxide (Cu_2O) was deposited onto the $BiVO_4$ surface to create a p-n heterojunction. The assembly of Cu_2O nanoparticles significantly promoted the photocatalytic performance of $Cu_2O/BiVO_4$ photocatalyst due to the existence of an internal electric field.

Acknowledgment

The research was financially supported by Polish National Science Centre (Grant No. NCN 2021/43/B/ST5/02983).

References

[1] Yang Y., Ok Y.S., Kim K.H., Kwon E.E., Tsang Y.F., Occurrences and removal of pharmaceuticals and personal care products (PPCPs) in drinking water and water/sewage treatment plants: A review, *Sci. Total Environ.*, 2017, 596–597, 303–320.

[2] Chen S., Huang D., Xu P., Gong X., Xue W., Lei L., Deng R., Li J., Li Z., Facet-Engineered Surface and Interface Design of Monoclinic Scheelite Bismuth Vanadate for Enhanced Photocatalytic Performance, *ACS Catal.*, 2020, 10, 1024-1059.

[3] Kowalkińska M., Dudziak S., Karczewski J., Ryl J., Trykowski G., Zielińska-Jurek A., Facet effect of TiO_2 nanostructures from $TiOF_2$ and their photocatalytic activity, *Chem. Eng. J.*, 2021, 404, 126493.

[4] Dudziak S., Kowalkińska M., Karczewski J., Pisarek M., Gouveia J.D., Gomes J. R.B., Zielińska-Jurek, A., Surface and Trapping Energies as Predictors for the Photocatalytic Degradation of Aromatic Organic Pollutants, *J. Phys. Chem. C*, 2022, 126(35), 14859-14877.

STUDIES ON THE KINETICS OF PHOTOTELOMERIZATION OF ACRYLATE-STYRENE SYSTEMS INITIATED WITH TETRABROMOMETHANE AND RADICAL PHOTOINITIATORS

Agata Kraśkiewicz*, Agnieszka Kowalczyk

West Pomeranian University of Technology in Szczecin, Faculty of Chemical Technology and Engineering, Department of Chemical Organic Technology and Polymeric Materials, Pułaskiego 10, 70-332 Szczecin, Poland
*corresponding author: agata.kraskiewicz@zut.edu.pl

The development of effective methods for the synthesis of functionalized polymers (or oligomers) is an important task for scientists. In this context, it is worth mentioning radical telomerization, a chain reaction between a telogen (also called a chain transfer agent; a molecule with an easily radically cleavable bond) and one or more polymerizable compounds (taxogens/monomers; exhibiting ethylenic unsaturation) that leads to the formation of polymers or oligomers with well-defined end-groups (telomers). The functionality of end-groups of the polymer chain depends on the chemical structure of telogens. This class of compounds includes organic molecules containing an active center bound to the carbon atom (i.e., carboxylic acids, alcohols, amines) and halogen, sulfur, silicon, or phosphorus compounds [1].

Several initiation methods of the telomerization reaction are known, e.g., using thermal initiators (organic peroxides, hydroperoxides, azo compounds), UV radiation, γ radiation, or redox processes involving metal ions with variable valences. Thermal initiators are the most commonly tested. Nevertheless, there are also reports of UV-telomerization [2]. It is noteworthy that ultraviolet technology has attracted considerable interest in polymer science lately. Its attractiveness results mainly from the possibility of achieving high reaction rates and low energy consumption [3].

Photoinitiated telomerization is a complex reaction, and various factors can affect its course. First of all, the selection of the photoinitiator is of great importance. Generally, photoinitiators are classified as cleavage (type I) and H-abstraction-type (type II) initiators. Numerous compounds with different absorbance characteristics, stability, and reactivity are available. The type of photoinitiator largely affects the rate of reaction, because it plays a major role in the production of the reactive species [4]. Moreover, the rate of telomer synthesis depends on the structure of telogens. An example of a highly effective chain transfer agent is tetrabromomethane, which is also an easily accessible and cheap compound [1, 5].

This study presented the influence of commercially available type I photoinitiators (acylphospine oxides and hydroxyketones) on the phototelomerizaion process of selected monomers (i.e., butyl acrylate, acrylic acid, and styrene) in the presence of tetrabromomethane (as telogen). The study of process kinetics was carried out using the photo DSC method. The reaction rate, monomer conversion, and photoinitiation index were determined. It was stated that bis(2,4,6-trimethylbenzoyl)-phenylphosphineoxide was the most efficient photoinitiator in the described cotelomerization reaction.

References

[1] Starks C.M., *Free Radical Telomerization*, Academic Press, New York, USA, 1974.
[2] Boutevin B., From Telomerization to Living Radical Polymerization, *J. Polym. Sci. A Polym. Chem.,* 2000, 38, 3235–3243.
[3] Shao J., Huang Y., Fan Q., Visible light initiating systems for photopolymerization: status, development and challenges, *Polym. Chem.,* 2014, 5, 4195–4210.
[4] Yagci Y., Jockusch S., Turro N.J., Photoinitiated polymerization: Advances, challenges and opportunities, *Macromolecules,* 2010, 43, 15, 6245–6260.
[5] Kumar S., Shah T.A., Punniyamurthy T., Recent advances in the application of tetrabromomethane in organic synthesis, *Org. Chem. Front.,* 2021,8, 4288-4314.

EPOXIDATION OF 1,5,9-CYCLODODECATRIENE WITH HYDROGEN PEROXIDE ON TI-SBA-15 CATALYST MODIFIED WITH WG-12 ACTIVATED CARBON

Marcin Kujbida[1]*, Grzegorz Lewandowski[2], Agnieszka Wróblewska[1]*

[1] West Pomeranian University of Technology in Szczecin, Faculty of Chemical Technology and Engineering, Department of Catalytic and Sorbent Materials Engineering, Pulaskiego 10, 70-322 Szczecin, Poland
[2] West Pomeranian University of Technology in Szczecin, Faculty of Chemical Technology and Engineering, Department of Organic Chemical Technology and Polymer Materials Engineering, Pulaskiego 10, 70-322 Szczecin, Poland
*corresponding authors: marcin.kujbida@zut.edu.pl, agnieszka.wroblewska@zut.edu.pl

The epoxidation process of 1,5,9-cyclododecatriene (CDT) leads to 1,2-epoxy-5,9-cyclododecadiene (ECDD). ECDD, due to its structure, finds many applications. This compound is used as a component of cross-linked polymers used for batteries [1-4], cross-linked acrylic rubbers [5], capacitors [6], and coatings [7, 8]. Moreover, ECDD can potentially become a raw material in the preparation of cyclododecanone and decanedicarboxylic acid (DDA) [9].

Until the authors began their research on the production of ECDD on heterogeneous catalysts, there were only a very limited number of literature reports on this subject [10-13]. We have carried out an in-depth study on conducting this process on Ti-MCM-41 [9], W-SBA-15 [14], and Ti-SBA-15 [15] catalysts. Our previous studies have shown that the studied process carried out on Ti-containing catalysts suffers from a low reaction rate expressed in terms of the CDT conversion change as a function of time. On the Ti-SBA-15 catalyst, the maximum of CDT conversion was equal to 30 mol% after 4 h of carrying out the process at 90°C [15]. The catalyst containing tungsten as the active center was significantly more active [14]. The maximum conversion of CDT was equal to 36 mol% after only 30 min of conducting the process at 60°C. Using Ti-SBA-15 under the same conditions resulted in CDT conversion equal to only about 4 mol%.

The purpose of this research was to develop a preparation method of Ti-SBA-15 catalyst modified with WG-12 activated carbon and to study its activity in the process of epoxidation of 1,5,9-cyclododecatriene. Also, an attempt was made to prepare a W-SBA-15-WG12 catalyst, but UV-Vis analysis showed the absence of W atoms embedded in the structure of the obtained material.

To study the activity of the prepared catalyst in the epoxidation of 1,5,9-cyclododecatriene, a series of experiments was performed with *Statistica* software. In the optimization the central composite design, non-factorial, surface response methodology was used. Temperature (50–70°C), time (30–60 min), catalyst content (0.05–0.13 g/mmol CDT), solvent amount (1–2 g/mmol CDT), and H_2O_2 amount (0.5–1.5 mmol/mmol CDT) were selected as the independent variables.

From the conducted experiments, it was found that the highest CDT conversion of 28 mol% (selectivity of transformation to ECDD amounted to 74 mol%) was obtained by the running the process with the following values of the independent variables: temperature 70°C, time 60 min, catalyst content 0.1290 g/mmol CDT, solvent amount 1.9935 g/mmol CDT and H_2O_2 amount 1.50 mmol/mmol CDT.

We found that Ti-SBA-15-WG12 catalyst was more active in CDT epoxidation with hydrogen peroxide than unmodified Ti-SBA-15, but less active than W-SBA-15.

References

[1] Toyoda Y., Sasaki T., Separator for secondary cell, US 009941497B2, 2018.
[2] Tabuchi M., Miura K., Miyashiro H., Bobayashi Y., Positive electrode and nonaqueous electrolyte secondary battery, US 20160006075A1, 2016.

[3] Fukumine M., Yamamoto N., Composition for electrochemical device electrode, electrode for electrochemical device, and method of producing composition for electrochemical device electrode, US 20180301744A1, 2018.
[4] Akiike J., Slurry for lithium ion secondary battery porous film, production method therefor, separator for lithium ion secondary battery, and lithium ion secondary battery, US 20160013465A1, 2016.
[5] Emori N., Ogawa T., Arakawa T., Cross-linked rubber product, US 20180030216A1, 2018.
[6] Matsubayashi S., Suzuki K., Conductive polymer solution, capacitor, and method for producing the capacitor, US 20180334577A1, 2018.
[7] Fujiki H., Suzuki T., Conductive composition, conductive composition production method, anti-static resin composition and antistatic resin film, US 20150348671A1, 2015.
[8] Komoriya H., Suzuki K., Tanaka T., Kitamoto T., Shiota M., Shimada R., Tanaka K., Antibacterial agent, substrate surface treatment method using the same, antibacterial agent composition, and substrate surface treatment method using the same, US 009204652B2, 2015.
[9] Wróblewska A., Kujbida M., Lewandowski G., Kamińska A., Koren Z.C., Michalkiewicz B., Epoxidation of 1,5,9-Cyclododecatriene with Hydrogen Peroxide over Ti-MCM-41 Catalyst, *Catalysts*, 2021, 11(11), 1402.
[10] Lin K., Lebedev O.I., Vana Tendeloo G., Jacobs P.A., Pescarmona P.P., Titanosilicate beads with hierarchical porosity: Synthesis and application as epoxidation catalysts, *Chem. A Eur. J.*, 2010, 16(45), 13509–13518.
[11] Zhang S., Jiang Y., Li S., Xu X., Lin K., Synthesis of bimodal mesoporous titanosilicate beads and their application as green epoxidation catalyst, *Appl. Catal. A Gen.*, 2015, 490, 57–64.
[12] Li X., Xu X., He Y., Jiang Y., Teng Y., Wang Q., Lin K., Titanium-containing desilicated MCM-41 with bimodal pore system as green epoxidation catalyst, *Mater Lett*, 2015, 146, 84–86.
[13] Cheng W., Jiang Y., Xu X., Wang Y., Lin K., Pescarmona P.P., Easily recoverable titanosilicate zeolite beads with hierarchical porosity: Preparation and application as oxidation catalysts, *J. Catal.*, 2016, 333, 139–148.
[14] Kujbida M., Wróblewska A., Lewandowski G., Miądlicki P., Michalkiewicz B., W-SBA-15 as an Effective Catalyst for the Epoxidation of 1,5,9-Cyclododecatriene, *Molecules*, 2022, 27(24), 8769.
[15] Kujbida M., Wróblewska A., Lewandowski G., Bosacka M., Koren Z.C., Michalkiewicz B., Effect of surface hydrophobization on the 1,5,9-cyclododecatriene epoxidation process with hydrogen peroxide on silanized Ti-SBA-15 catalyst, *J. Ind. Eng. Chem.*, 2023.

UNKNOWN PROPERTIES AND POTENTIAL APPLICATION OF Sm_5VO_{10}

Kamil Kwiatkowski*, Mateusz Piz, Elżbieta Filipek

[1]Department of Inorganic and Analytical Chemistry, Faculty of Chemical Technology and Engineering, West Pomeranian University of Technology, Szczecin,
Piastów 42, 71-065 Szczecin, Poland
*corresponding author: kamil.kwiatkowski@zut.edu.pl

Compounds that are formed in multi-component systems of various metal oxides, belonging to the group of oxosalts, constitute a large group of ceramic inorganic compounds that are practical in many fields of science and industry [1–3].

In recent years, an intensification of research has been observed, both basic and technological, conducted in order to obtain new functional materials and/or modify the properties of currently used materials. Researchers are particularly interested in materials whose components are little-known chemical compounds or solid solutions containing rare earth elements (*REE*).

Due to electron occupancy of f-orbitals, these elements exhibit a number of interesting properties, thanks to which they have been used in catalysis, ceramic materials, or electronics and optoelectronics [4]. The areas of application of rare earth elements and their compounds are shown in Figure 1.

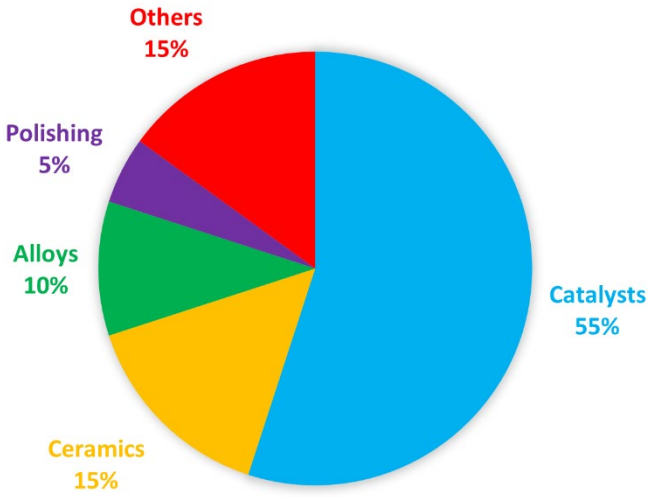

Fig. 1. Field of applications of REE and their compounds

In the scope of this work, a compound of the formula Sm_5VO_{10} was synthesized with a high-temperature method. So far, the compound has only been mentioned in the literature [5] but its various physicochemical properties are unknown.

The obtained phase (Sm_5VO_{10}) was investigated using: X-ray powder diffraction (XRD), differential thermal analysis with simultaneous thermogravimetry (DTA-TG), ultraviolet–visible diffuse reflectance spectroscopy (UV-VIS-DRS), Fourier–transform infrared spectroscopy (FTIR), laser diffraction spectrometry (LDS) and scanning electron microscopy with energy dispersive X-ray analysis (SEM-EDX).

Synthesis of Sm_5VO_{10} compound was carried out in the air atmosphere, from metal oxides i.e. vanadium(V) oxide and samarium(III) oxide mixed in molar ratio 1:5 (Equation 1), and also from separately obtained samarium(III) orthovanadate [6] and Sm_2O_3, in a molar ratio 1:2 (Equation 2).

$$5\ Sm_2O_{3(s)} + V_2O_{5(s)} = 2\ Sm_5VO_{10(s)} \quad (1)$$

$$2\ SmVO_{4(s)} + 4\ Sm_2O_{3(s)} = 2\ Sm_5VO_{10(s)} \quad (2)$$

Synthesis from the oxides was conducted in six stages in the temperature range from 600 to 1350 °C, and from $SmVO_4$ and Sm_2O_3 was carried out in four stages in the temperature range from 1000 to 1350 °C. After each step of heating, the phase composition of the samples was analysed with XRD.

Diffraction patterns obtained after the last heating of both samples were identical, which leads to the conclusion, that pentasamarium(III) vanadate(V) is forming not only from the oxides, but also in the reaction between samarium(III) orthovanadate and Sm_2O_3. Diffractogram of monophase sample that contained Sm_5VO_{10} was indexed, by using POWDER software [7]. The best obtained solution was then refined in the REFINEMENT program of DHN/PDS package. This part of investigation allows us to claim that pentasamarium(III) vanadate(V) crystallizes in a monoclinic system. Unit cell parameters have been calculated.

Results of LDS, DTA–TG and XRD analysis proved, that microcrystalline compound Sm_5VO_{10} is thermally stable up to at least 1450 °C. After reaching this temperature it decomposes to another samarium(III) vanadate and samarium(III) oxide, according to Equation (3).

$$2\ Sm_5VO_{10(s)} = Sm_2O_{3(s)} + Sm_8V_2O_{17(s)} \quad (3)$$

Additionally, FTIR analysis results showed that the structure of Sm_5VO_{10} is built from VO_6 and SmO_8 polyhedrons, connected with each other.

Moreover, it was claimed that Sm_5VO_{10} belongs to electrical semiconductors, with an energy gap value around 3 eV. This value was estimated using Kubelka–Munk method [8].

Obtained results of the investigation tentatively indicate that Sm_5VO_{10} can be applied as a photocatalyst of various reactions, such as water purification processes.

Investigation and experiments that will allow to find possible applications of described samarium(III) vanadate(V) are still in progress.

References

[1] Rasouli Jamnani S., Milani Moghaddam H., Leonardi S.G., Donato N., Neri G., Synthesis and characterisation of Sm_2O_3 nanorods for application as a novel CO gas sensor, *Appl. Surf. Sci.,* 2019, 487, 793–800.

[2] Rahimi-Nasrabadi M., Pourmortazavi S.M., Aghazadeh M., Ganjali M.R., Karimi M.S., Novrouzi P., Samarium carbonate and samarium oxide; synthesis, characterization and evolution of the photo-catalytic behaviour, *J. Mat. Sci.: Mater. Electron.*, 2017, 28, 5574–5583.

[3] Fernández-Osorio A., Redón R., Medina-Pérez J., Pedroza-Montero M., Acosta M., Photoluminescence and Thermoluminescence Properties of Nanophosphors, $YVO_4:Eu^{3+}$ and $YVO_4:Eu^{3+}:Dy^{3+}$, *J. Clust. Sci.*, 2022, 33, 653–664.

[4] Balaram V., Rare earth elements: A review of applications, occurrence, exploration, analysis, recycling and environmental impact, *Geoscience Frontiers,* 2019, 10, 1285–1303.

[5] Kitayama K., Katsura T., Phase equilibria in Sm_2O_3–V_2O_3–V_2O_5 system at 1200°C, *Bull. Chem. Soc. Jpn.,* 1977, 50(4), 889–894.

[6] Denisova L.T.,Kargin Y.F., Chumilina L.G., Denisov V.M., Istomin S.A., Heat capacity and thermodynamic properties of the $SmVO_4$ orthovanadate in the range 369–1020 K, *Inorg. Mater.*, 2015, 51 (6), 675–679.

[7] Taupin D., A powder-diagram automatic-indexing routine, *J. Appl. Cryst.*, 1973, 6, 380–385.

[8] Kubelka P., Munk F., Ein Betrag zur Optik der Farbenstriche, *Z. Tech. Phys.*, 1931, 12, 593–601.

AUTOMATIC DISHWASHER DETERGENTS FOR CONSUMER USE

Damian Lisowski[1,2]*, Elżbieta Sikora[2]

[1]Zakład Chemii Gospodarczej "Pollena-Astra" Sp. z o. o., Herburtów 34, 37-700 Przemyśl, Poland
[2]Politechnika Krakowska im. Tadeusza Kościuszki, Warszawska 24, 31-155 Kraków, Poland
*corresponding author: damian.lisowski@doktorant.pk.edu.pl

The combination of automatic dishwashers with suitable cleaning products allows the effective cleaning of soiled dishes, kitchen utensils and containers used for serving and preparing meals. High-quality washing products also protect the dishes and the dishwasher itself from chemical corrosion. Currently, consumers expect products that are effective, but also safe for their health and the environment.

In this presentation, based on a market review and available literature, the common forms of dishwasher products and their intended use were discussed. Particular attention was paid to the composition of preparations for washing dishes in automatic dishwashers. In addition to surfactants, dispersants and sequestrants, the following groups of auxiliary ingredients were presented:

- bleaches and their activators,
- enzymes,
- corrosion inhibitors,
- builders,
- fragrances, dyes and preservatives.

Furthermore, current market trends, examples of innovative solutions and development forecasts for the area of detergents for automatic dishwashers in Poland were discussed.

Keywords: Household chemicals, surfactants, dishwasher detergent, automatic dishwashing.

References

[1] Piskiewicz L., Radziukiewicz M., Zasoby dóbr trwałych w gospodarstwach domowych, *Wiadomości statystyczne*, 2018, 10 (689), 37–55.
[2] Główny Urząd Statystyczny, Budżety gospodarstw domowych w 2021 r., Warszawa 2022.
[3] International Association for Soaps, Detergents and Maintenance Products, ACTIVITY & SUSTAINABILITY REPORT 2021–22.
[4] IKW-AK automatic dishwashing detergents, Methods for ascertaining the cleaning Performance of dishwasher detergents, SÖFW-Journal, 125. Jahrgang , 1999, 11, 52–59.
[5] Zieliński R., *Surfaktanty. Budowa, właściwości, zastosowania,* Wydanie drugie zmienione. Wydawnictwo Uniwersytetu Ekonomicznego w Poznaniu, Poznań 2013.
[6] Ogonowski J., Tomaszkiewicz – Potępa A., *Związki powierzchniowo czynne. Podręcznik dla studentów wyższych szkół technicznych,* Politechnika Krakowska im. Tadeusza Kościuszki, Kraków 1999.
[7] Przondo J., *Związki powierzchniowo czynne i ich zastosowanie w produktach chemii gospodarczej,* Wydawnictwo Politechniki Radomskiej, Radom 2007.
[8] Banach M., Makara A., Trójpolifosforan sodu rozwiązanie dla środków czystości, Czasopismo Techniczne Chemia, Wydawnictwo Politechniki Krakowskiej, 2010, 10, 107.
[9] Rozporządzenie Parlamentu Europejskiego i Rady (UE) NR 259/2012 z dnia 14 marca 2012 r. zmieniające rozporządzenie (WE) nr 648/2004 w odniesieniu do stosowania fosforanów i innych związków fosforu w detergentach dla konsumentów przeznaczonych do prania i detergentach dla konsumentów przeznaczonych do automatycznych zmywarek do naczyń, Dz. Urz. UE L 94, 16.
[10] https://www.basf.com/pl/pl/media/news-releases/2015/10/2015-10-21.html, dostęp 31 stycznia 2023.

[11] EP 2494019 (2018)
[12] EP 1711589 (2014)
[13] EP 2788465 B1 (2016)
[14] Mathews J., Wzrost znaczenia aktywnych wybielaczy nadtlenkowych we współczesnych recepturach detergentów, *Chemia i biznes, rynek kosmetyczny i chemii gospodarczej*, 2019, 4, s. 100-104.
[15] EP 0549272 A1 (1992)
[16] https://www.weylchem.com/products/weylcleanr-mntacn , dostęp 31 stycznia 2023
[17] Pat. USA 4714562 (1987)
[18] https://biosolutions.novozymes.com/en/dish/automatic-dishwash, dostęp 28 stycznia 2023
[19] Naganthran A., Masomian M., Noor Zaliha R., Abd. Rahman R., Mohd Shukuri M. A., Mohd Nooh H., *Molecules*, 2017, 22, 1577
[20] Rozporządzenie Parlamentu Europejskiego i Rady (UE) nr 1272/2008 z dnia 16 grudnia 2008 r. w sprawie klasyfikacji, oznakowania i pakowania substancji i mieszanin, zmieniające i uchylające dyrektywy 67/548/EWG i 1999/45/WE oraz zmieniające rozporządzenie (WE) nr 1907/2006, Dz. Urz. UE L 353, 1.
[21] Rozporządzenie (UE) nr 648/2004 Parlamentu Europejskiego i Rady z dnia 31 marca 2004 r. w sprawie detergentów, Dz.Urz. L 104, 1.
[22] EP 3135180 (2016)
[23] EP 2850990 (2015)

FORMULATION AND STATISTICAL OPTIMIZATION OF ALGINATE MICROSPHERES FOR PROBIOTIC ENCAPSULATION

Anna Łętocha[1,*], Alicja Michalczyk[2], Małgorzata Miastkowska[1], Elżbieta Sikora[1]

[1]Faculty of Chemical Engineering and Technology, Department of Organic Chemistry and Technology, Cracow University of Technology, 31-155 Krakow, Poland
[2]Lukasiewicz - Research Network-Institute of Industrial Organic Chemistry, 03-236 Warsaw, Poland
*corresponding author: anna.letocha@doktorant.pk.edu.pl

The process of obtaining alginate microspheres (AMs) with emulsification method was optimized by applying statistical analysis software (Statistica®, StatSoft Inc.). Ten batches of microspheres were prepared using the fractional plan $3^{(K-p)}$, where K is the number of variables and p always takes the value 1. AMs were obtained with two different methods: ultrasonic homogenization (UH) process and rotor-stator mechanical homogenization (MH). The amount of a cross-linking agent ($CaCl_2$), calcium chloride rate addition, and the sonication amplitude (in the case of the ultrasound method) or the speed of rotor rotation (in the case of MH) were selected as formulation variables (Fig. 1.).

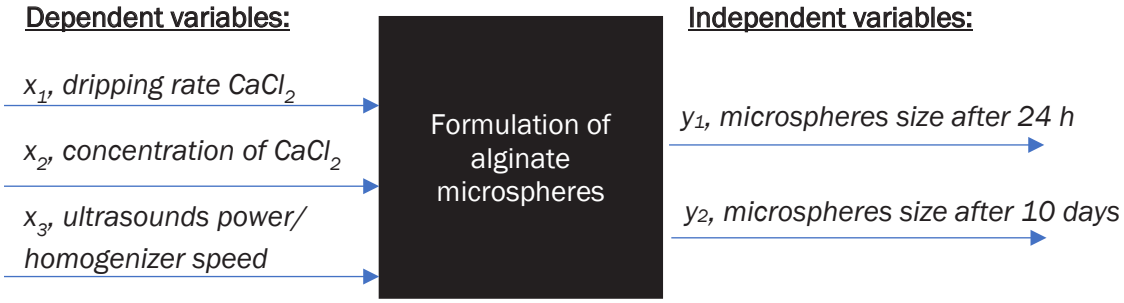

Fig. 1. Schematic description of the optimization process

All the batches were evaluated in terms of stability and size of alginate microspheres. Approximation profiles were developed. Multiple linear regression was applied to confirm significant effect of each variable. As a result of the conducted research, stable alginate microspheres with sizes ranging from 10 to 30 micrometers were obtained (Fig. 2.).

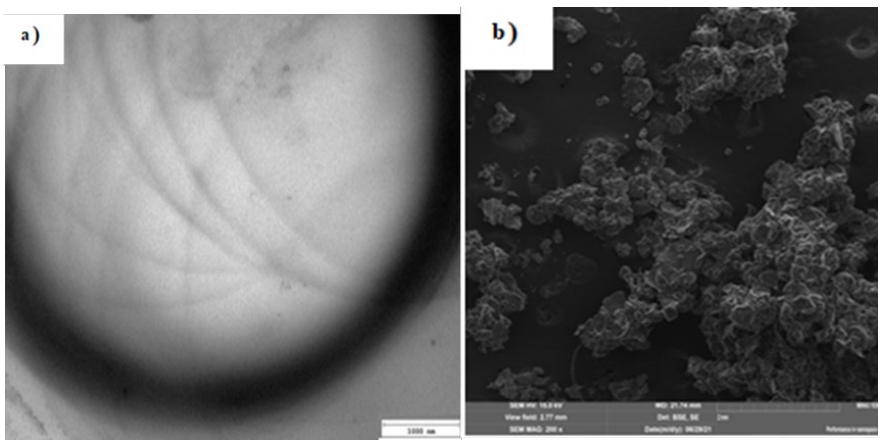

Fig. 2. a) TEM of the alginate shell, b) SEM of structure of microspheres

The obtained results showed that the quality of AMs was mainly affected by the concentration and the rate of calcium chloride addition into the system. Therefore, the role of calcium ions in the mechanisms of shell structuring was discussed. *Lactobacillus casei* bacteria were encapsulated into the batches found to be optimum. The high efficiency of bacteria encapsulation (72-94% depending on the form) and their viability over time were obtained. The model developed in the study can be effectively utilized to achieve AMs formulations.

MULTIPLE EMULSIONS AS CARRIERS FOR TOPICAL DELIVERY OF ANTI-INFLAMMATORY DRUGS

Agnieszka Markowska-Radomska, Patryk Skowroński, Ewa Dłuska*

Warsaw University of Technology, Faculty of Chemical and Process Engineering, Waryńskiego 1, 00-645 Warsaw
*corresponding author: Ewa.Dluska@pw.edu.pl

The common side effect of radiotherapy and chemotherapy are skin lesions (pain, skin irritation, itchiness, dryness, swelling, redness). A number of factors influence the intensity of side effects experienced during cancer treatment. Among them are the total radiation/drug dose, the size of a single doses, and the area of skin exposed to radiation. In this paper, multiple emulsions were developed and evaluated as carriers of non-steroidal anti-inflammatory drugs (NSAID) as an effective formulation for the topical administration and treating skin lesions following anti-cancer therapy.

The paper proposes multiple emulsions of W1/O/W2 (water in oil in water) type as carriers for effective encapsulation and delivery of diclofenac and ketoprofen. Multiple emulsions are complex structured systems ("drops in drops"). The functional structure of the W1/O/W2 emulsion enables the incorporation of one or more drugs (lipophilic and hydrophilic), enhancement of stability and bioavailability of encapsulated substances, prevention of interactions between substances, as well as with the external environment, and drug release in a controlled manner.

The multiple emulsions were prepared by a one-step method in a continuous Couette-Taylor flow (CTF) contactor [1, 2]. The emulsions were prepared using Span 83, Tween 80, Pluronic P-123, poloxamer 407 as surfactants, sodium alginate and sodium carboxymethylcellulose as viscosity modifiers. The membrane phase of emulsions was soybean oil. The liquid flow rates in the CTF contactor for emulsions D1-D4 were: the internal phase 20 cm^3/min, membrane phase 40 cm^3/min, external phase 60 cm^3/min. The rotational frequencies of the internal cylinder in the CTF contactor were: (D1: 1166 RPM; D2: 925 RPM; D3; 1264 RPM, D4: 976 RPM). The W1/O/W2 emulsions were evaluated for their characteristics (drops size, drop size distribution, volume packing fraction), encapsulation efficiency, stability (37ºC and 24ºC), and rheology (Rheolab QC, Anton Paar). Also, the in vitro NPLS release process was investigated in a simulated skin environment. In order to assess the effectiveness of emulsion formulations, the in-vitro therapeutic effect for K21 fibroblast cell line irradiated (Crosslinker CL-1000) with UV doses (15 J/m^2) was evaluated (similar biological impact on cells as a commonly used in radiotherapy dose of ionizing radiation of 2 Gy [3, 4]). For this purpose, cytotoxicity tests were conducted using the presto blue reagent - relative fluorescence was measured (at the wavelength of 535/590 nm, DTX880 Multimode Detector, Beckman Coulter). Cell viability was measured after 24, 48, and 72 h of incubation.

Stable multiple emulsions with diclofenac and ketoprofen were obtained. The NSAID drugs were encapsulated in the internal droplets of emulsion. For all emulsions, high encapsulation efficiency (over 90%) and high volume packing fraction of internal droplets (0.54 - 0.96) were obtained. All emulsions displayed properties of shear-thinning fluids. In addition, due to the presence of a polymer (CMC-Na) with adhesive properties, high emulsion stability was achieved. The release study of encapsulated substance confirmed the possibility of modifying release rates. It was found that the releasing process can be controlled through the composition, structure, and physicochemical parameters of emulsions. Moreover, an increase in cell viability was observed after incubating the human fibroblast (K21 cell line) with an emulsion-based carrier of diclofenac/ketoprofen. Examples of the results are presented in Figure 1 and Table 1.

These results showed that the multiple emulsion-based formulations may be appropriate carriers for the topical delivery of NSAID drugs.

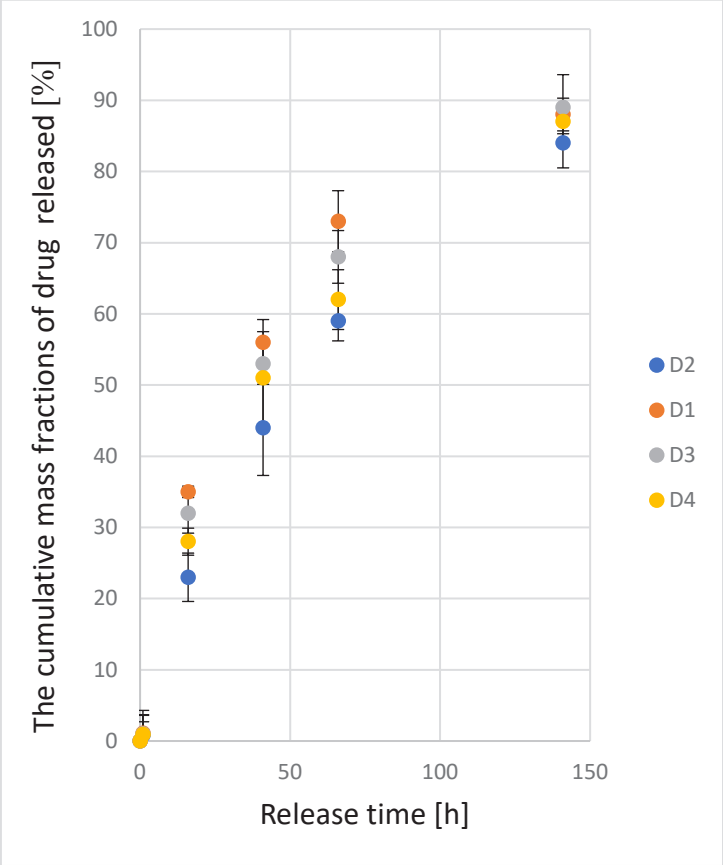

Fig. 1. Time-dependent cumulative mass fractions of the anti-inflammatory drug (diclofenac) released from multiple emulsions D1-D4 prepared in the CTF contactor

Table 1. The viability of K21 cells after irradiation (UV doses of 15 J/m^2) and treatment with drug encapsulated in multiple emulsion

time [h]	cell viability [%]		
	Control (non-treated cells)		Emulsion D1 with diclofenac
24	43	increase to →	76
48	24	increase to →	88
72	7	increase to →	95

Acknowledgements: Research was funded by (POB Biotechnology and Biomedical Engineering) of Warsaw University of Technology within the Excellence Initiative: Research University (IDUB) programme (project BIOTECHMED-2).

References

[1] Dluska E., Markowska-Radomska A., Metera A., Rudniak L., Kosicki K., *AIChEJ.*, 2022, 68(2), 17501.
[2] Dluska E., Markowska-Radomska A., Skowronski P., *Polimery*, 2022, 67(7-8), 346–354.
[3] Pan Y., Zhang Q., Atsaves V., Yang H., Claret F. X., *Oncogene*. 2013, 32(22), 2756–2766.
[4] Castle K.D., Kirsch D.G., *Cancer Research*, 2019, 79(22), 5685–5692.

INFLUENCE OF MOBILE PHASE ON SEPARATION OF ENANTIOMERS OF METHYL P-TOLYL SULFOXIDE

Patrycja Mruc[1]*, Maksymilian Olbrycht[2], Dorota Antos[2]

[1]Doctoral School of Engineering and Technical Sciences at the Rzeszów University of Technology, Rzeszów, Poland
[2]Department of Chemical and Process Engineering, Rzeszów University of Technology, Rzeszów, Poland
*corresponding author: d579@stud.prz.edu.pl

Nowadays, single enantiomers are used in many areas of industry, including food, agrochemistry and pharmaceutical industries. In the latter case, the optical purity of enantiomers is required as it determines their biological activity. To isolate a single enantiomer from enantiomeric mixtures, chiral chromatography (CCh) is typically used. However, the high price of chiral stationary phases is a stimulus for development of more economical and efficient methods for separation of enantiomers. For this reason, attempts are being made to partly replace CCh with achiral chromatography (ACh) [1, 2]. The latter exploits plain silica adsorbent, which is cheap and mechanically stable.

The mechanism of enantiomer separation on ACh is based on the phenomenon termed as self-disproportionation of enantiomers (SDE). It is characteristic of many chiral compounds, such as sulfoxides, amides, alcohols, esters, etc. The essence of SDE is that molecules of enantiomers form homo- and heterochiral associations in the liquid and adsorbed phases. The associates of enantiomers have different adsorption properties, which is the reason for their different retention properties [3].

ACh allows isolation of a single enantiomer from a non-racemic mixture that is enriched with the target enantiomer. In order to obtain complete resolution, it is necessary to combine ACh with CCh. In this way, we can reduce costs by reducing the involvement of CCh in the overall process [4]. The essence of the economic coupled process is to find proper conditions and parameters for ACh, such as composition of the mobile phase.

In this study, we demonstrated the influence of mobile phase composition on the effectiveness of ACh separation of enantiomers of a model compound that is methyl p-tolyl sulfoxide. The mobile phase was composed of apolar and polar solvents, i.e., tert-butyl methyl ether (MTBE) and ethanol with different volume ratios (Fig. 1A). The results of the studies indicated that the selectivity of enantiomer ACh separation was determined by the composition of solvents used as the mobile phase. As those solvents were present in high concentrations, nonideality of their adsorption behaviour was unavoidable. Interactions between adsorbed molecules of enantiomers and polar solvent are competitive against interactions between adsorbed molecules of the enantiomers, thus they suppress the SDE effect. Hence, pure MTBE as the mobile phase allowed good resolution of enantiomers, but at the expense of a very long elution time. An addition of polar ethanol to the mobile phase accelerated elution of enantiomers, but the recovery of the target enantiomer was significantly reduced.

Therefore, we applied a gradient of the elution strength of the mobile phase, which started with pure MTBE and ended with a mixture of MTBE and ethanol (95/5 (v/v)) (Fig. 1B). This provided significant improvement in the recovery of a single enantiomer compared with isocratic elution (Fig. 1 and Table 1). A dynamic model was used to optimize the flowrate and gradient shape.

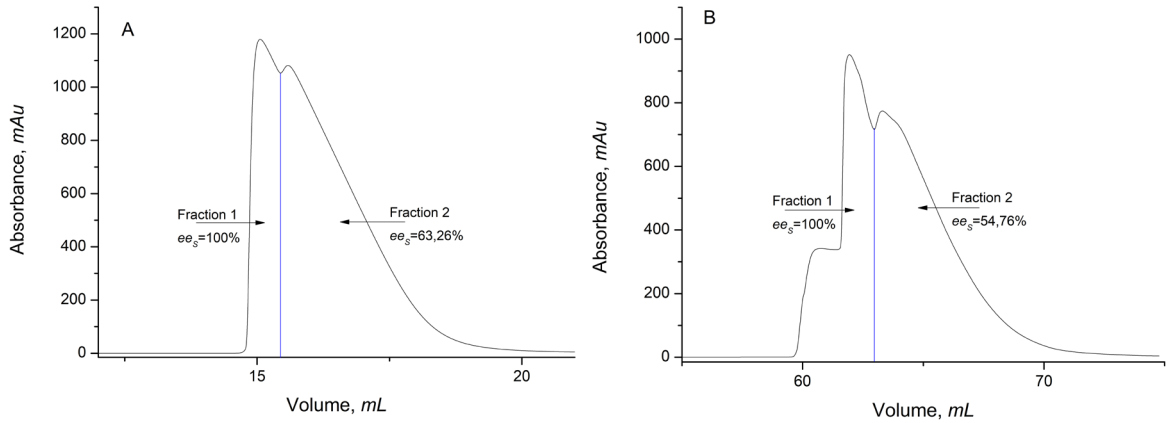

Fig. 1. Chromatogram of methyl p-tolyl sulfoxide eluted with the mobile phase (A) isocratic with MTBE/ethanol (95/5 (v/v)), (B) with a step gradient: MTBE (0 to 27 min), MTBE/ethanol (95/5 (v/v)) (27 to 37 min). The concentration of the sample: 40 g L^{-1} with enantiomeric excess, ee_S=50%, the injection volume: 60 µL, flowrate: 1 mL min^{-1} for (A), 2 mL/min for (B), detection wavelength: 280 nm. Fraction 1 contained a single S-enantiomer. Fraction 2 contains a mixture of both enantiomers

Table 1. Comparison of recovery of S-enantiomer of methyl p-tolyl sulfoxide

Elution mode	Isocratic elution	Gradient elution
Recovery of S-enantiomer [%]	32,93	73,73

References

[1] Bridgman P.W., *Dimensional Analysis*, New York, AMS Press 1978.
[2] Ghanem A., Wang C., Enantioselective separation of racemates using CHIRALPAK IG amylose-based chiral stationary phase under normal standard, non-standard and reversed phase high performance liquid chromatography, *J. Chromatogr. A*, 2018, 1532, 89–97.
[3] Han J., Kitagawa O., Wzorek A., Klika K.D., Soloshonok V.A., The self-disproportionation of enantiomers (SDE):a menace or an opportunity?, *Chem. Sci.,* 2018, 9, 1718–1739.
[4] Nakamura T., Tateishi K., Tsukagoshi S., Hashimoto S. Watanabe S., Soloshonok V.A., Luis Aceña J., Kitagawa O., Self-disproportionation of enantiomers of non-racemic chiral amine derivatives through achiral chromatography, *Tetrahedron*, 2012, 68, 21.

CATIONIC AND RADICAL PHOTOCURING OF EPOXY ACRYLATE OLIGOMERS

Małgorzata Nowak, Karolina Mozelewska, Paulina Bednarczyk*

West Pomeranian University of Technology in Szczecin, Faculty of Chemical Technology and Engineering, Piastów Ave. 17, 70-310 Szczecin, Poland
*corresponding author: bednarczyk.pb@gmail.com

In this work, epoxy acrylate resin (EA) based on industrial-grade bisphenol A-based epoxy resin (Ep6) and acrylic acid (AA) has been synthesized in order to develop a hybrid resin comprising both epoxide group and reactive, therminal unsaturation. The obtained epoxy acrylate prepolymer was employed to formulate photocurable coating compositions containing, besides the EA binder, also cationic or radical photoinitiators. Hence, when cationic photoinitiators were applied, polyether-type polymer chains with pending acrylate groups were formed. In the case of free radical polymerization, epoxy acrylates certainly formed a polyacrylate backbone with pending epoxy groups. Owing to the presence of both epoxy and double carbon-carbon pendant groups, the reaction product exhibits photocrosslinking via two distinct mechanisms: (i) cationic ring-opening polymerization and (ii) free radical polymerization. Therefore, photopolymerization behavior of synthetized hybrid resin with various photoinitiators was determined via photo-differential scanning calorimetry (photo-DSC) and real-time infrared spectroscopy (RT-IR) methods. The properties of cured coatings were investigated. The performance of the following photoinitiators was tested in cationic photopolymerization. Diaryliodonium cations or triarylsulfonium cations, and the following photoinitiators were used to induce free radical photopolymerization: hydroxyketones, acylphosphine oxides, and their mixtures [1]. The presented research is part of the work supported by The National Centre for Research and Development (NCBR; grant no. LIDER/16/0102/L-10/18/NCBR/2019).

References

[1] Bednarczyk P., Mozelewska K., Nowak M., Czech Z., *Materials,* 2021, 14, 4150.

PVOH FILM AS AN ALTERNATIVE TO PLASTICS MADE OF PE AND HDPE IN THE PROCESS OF ECODESIGNING SUSTAINABLE DETERGENT PRODUCT

Bibianna Nowak[1,*], Elżbieta Sikora[2]

[1]Lakma Strefa Sp. z o.o., Gajowa 7, 43-254 Warszowice, Poland
[2]Tadeusz Kosciuszko Cracow University of Technology, Warszawska 24, 31-155 Kraków, Poland
*corresponding author: bibianna.nowak@doktorant.pk.edu.pl

Increased awareness and expectations on the part of consumers of cleaning and washing products, as well as many initiatives to change legislation by the EU contribute to changes not only in the formulation of products, but also in the method of product application. The dynamic development of washing agents in the form of measured doses in a film casing made of polyvinyl alcohol (-PVOH) enable rational use of the product, limiting the overdosing of the detergent. The concept of concentrating the washing mixture and enclosing it in a film made of polyvinyl alcohol significantly reduces water consumption in production processes in accordance with the "water less" trend and the number of introduced plastics. The PVOH film, which gives the possibility of storing, protecting, transporting, delivering and presenting the product, is an interesting alternative to plastics made of PE and HDPE.

The presentation is a literature review of the composition, properties and production process of polyvinyl alcohol film. The relationship between the chemical composition of the film and its water-soluble and mechanical properties will be discussed. Particular attention will be paid to the biodegradability of PVOH film as a potential source of microplastics present in aquatic ecosystems. The literature review shows that both the mechanical properties and the biodegradability of PVOH film create opportunities to extend its use in the eco-design process of sustainable detergent products for cleaning and caring for hard surfaces.

References

[1] https://eur-lex.europa.eu/legal-content/PL/TXT/?uri=CELEX:52022DC0140, dostęp 3 luty 2023.
[2] https://www.eea.europa.eu/data-and-maps/figures/demand-for-common-plastics-in, dostęp 3 luty 2023.
[3] https://eur-lex.europa.eu/legal-content/PL/TXT/PDF/?uri=CELEX:32004R0648&qid=1675455295867&from=PL, dostęp 3 luty 2023.
[4] https://www.grandviewresearch.com/industry-analysis/polyvinyl-alcohol-films-industry, dostęp 3 luty 2023.
[5] J.Pielichowski, A. Puszyński, *Technologia tworzyw sztucznych*, Wydawnictwo Naukowo-Techniczne, Warszawa 1992.
[6] https://ec.europa.eu/transparency/comitology-register/screen/documents/083921/1/consult?lang=en, dostęp 4 luty 2023.
[7] EP 3443030, (2022).
[8] EP 3274398 , (2021).
[9] EP 2529002, (2017).
[10] WO 2018/081494.
[11] Pat.USA 2017/0259975 (2017).
[12] WO 2016/061025.
[13] WO 2016/160116.
[14] Pat. EP 3 178 912 (2015).
[15] EP 2204334 (2012).
[16] PL/EP 1745097 (2005).
[17] Pat. EP 4 015 567 (2020) Monosol water soluble films, water soluble unit dose articles.

[18] Vandermeulen G.W.M, Boarino A., Klok H.-A., Biodegradation of water soluble and water- dispersible polymers for agricultural, consumer and industrial applications- Challenges and opportunities for sustainable materials solution, *J. Polym. Sci*., 2022.
[19] Byrne D., Boeije G., Croft I., Hütmann G., Luijkx G., Meier F., Parulekar Y., Stijntjes G., Biodegradability of Polyvinyl Alcohol Based Film Used for Liquid Detergent Capsules, *Environ. Chem*., 2021.
[20] Pająk J., Ziemski M., Nowak B., Poli(alkohol winylowy)-biodegradowalne tworzywo winylowe, *Chemik*, 2010, 64, 7-8, 525–530.
[21] Chiellini E., Cotti A., D'Antone S., Solaro R., *Biodegradation of Poly (Vinyl Alcohol) based material*, Elsevier Science Ltd, 2003.

EFFECTIVENESS OF PHOTOCATALYTIC DISINFECTION CONDUCTED IN A NEW HYBRID PHOTOREACTOR

Oliwia Paszkiewicz[1]*, Marian Kordas[1], Rafał Rakoczy[1], Ewa Kowalska[2], Agata Markowska-Szczupak[1]*

[1] Department of Chemical and Process Engineering, Faculty of Chemical Technology and Engineering, West Pomeranian University of Technology in Szczecin, Piastow Ave. 42, 71-065 Szczecin, Poland.

[2] Faculty of Chemistry, Jagiellonian University, Gronostajowa 2, 30-387 Krakow, Poland
*corresponding authors: oliwia.paszkiewicz@zut.edu.pl (O.P), agata.markowska@zut.edu.pl (A.M.S.)

The development of new methods for various processes often involves the need for new, specially designed apparatus. Due to the ever-increasing problem with dwindling drinking water supplies, modern methods of water purification are under investigation. Recently, advanced oxidation processes (AOPs) have become mainstream as a method of water disinfection. One of the advanced oxidation processes is photocatalysis, which has not been used in industry, despite its high application potential. The photocatalytic process is initiated by electromagnetic radiation with an energy equal or greater than the energy of the band gap. Among the most used UV light sources are high-pressure irradiators, which are characterized by a high price, and thus increase the cost of conducting such a process. However, photocatalysis can also be carried out using light from the visible range, for example, emitted by LEDs, after appropriate modification of the photocatalyst [1, 2]. Another simple physical method is water purification using a magnetic field. In water, moving through magnetizers, there is a change in the configuration of the present ions, which consequently affects their solubility, as well as a change in zeta potential [3]. Studies suggest the effect of the magnetic field on changing the surface charges of water, which increases the coagulation and precipitation of particles of substances accumulated in the treated water stream [3]. The bactericidal effect of photocatalysis is a widely studied topic. The effect of magnetic fields on the bacteriostatic properties of various substances has also been proven in scientific works [4, 5]. Combining these two methods is a promising way to develop a new method for disinfecting water.

The aim of the research was to create a new design of a photoreactor with a rotating magnetic field generator and determine the efficiency of the process using certain parameters.

Two reference strains of bacteria Gram-negative *Escherichia coli* K12 (ATCC 29425) and Gram-positive *Staphylococcus epidermidis* (ATCC 49461) and metal-modified titania photocatalysts (0.5Pt@HomoP25, 2.0Ag@HomoP25, 2.0Au@HomoP25) and commercial KRONOClean7000 were used. The influence of photocatalyst, light, rotating magnetic field (RMF) and synergistic effect of light and RMF on the effectiveness of the disinfection process were determined. Experiments were performed in a self-designed and constructed photoreactor with a rotating magnetic field generator. Light-emitting diodes (LEDs) emitting radiation in the visible range were used as the light source. The concentration of photocatalyst was 0.1 $g \cdot dm^{-3}$. RMF in the frequency of 5, 25 and 50 Hz was applied. Each experiment lasted 3 hours and samples were taken in 0, 1 and 3 hours of the process. A series of decimal dilutions were made, and the diluted solutions were plated on solid media appropriate for the type of bacteria. The inculcated plates were incubated at a temperature of 37 °C for 24 h. Then visible colonies were counted. The results obtained were used to develop artificial neural network models in Statistica 13.3, through which the effect of the various process conditions on the efficiency of water disinfection was determined. A control experiment under dark conditions was also performed.

The results indicate that the photocatalytic disinfection of water is positively influenced by rotating magnetic fields. It was found that the duration of the process was the decisive factor in the efficiency of the process. The applied frequency of the magnetic field also influenced disinfection

efficiency. The best disinfection performance was obtained for the 2.0Ag@HomoP25 photocatalyst when using light and a magnetic field at 25 Hz, in the removal of Gram-positive *S. epidermidis*, and when using light and a magnetic field at 5 Hz for Gram-negative *E. coli*. In both cases, the full disinfection effect was achieved after 3 h of running the process.

The authors are grateful for the financial support of the National Science Center within the Preludium-20 project (Grant No. 2021/41/N/ST8/00482).

References:

[1] Tallósy S.P., Janovák L., Ménesi J., Nagy E., Juhász Á., Dékány, I., LED-Light Activated Antibacterial Surfaces Using Silver-Modified TiO embedded in Polymer Matrix, *J. Adv. Oxid. Technol.*, 2014, 17, 9–16.
[2] Ochoa Rodríguez P.A., Casuscelli S.G., Elías V.R., Eimer G.A., LED Visible-Light Activated Mesoporous TiO2: A Better Understanding about Carbon Role in the Photocatalytic Performance of Solid, *Catal. Today*, 2021, 372, 198–210.
[3] Vaskina I., Roi I., Plyatsuk L., Vaskin R., Yakhnenko O., Study of the Magnetic Water Treatment Mechanism, *J. Ecol. Eng*, 2020, 21, 251–260.
[4] Jabłońska J., Dubrowska K., Gliźniewicz M., Paszkiewicz O. Augustyniak A., Grygorcewicz B., Konopacki M., Markowska-Szczupak A., Kordas M., Dołęgowska B., Rakoczy R., The Use of the Electromagnetic Field in Microbial Process Bioengineering, *Adv. Appl. Microbiol.*, 2022, 121, 27–72.
[5] Markowska-Szczupak A., Wesołowska A., Borowski T., Sołoducha D., Paszkiewicz O., Kordas M., Rakoczy R., Effect of Pine Essential Oil and Rotating Magnetic Field on Antimicrobial Performance, *Sci. Rep.*, 2022, 12, 1–9.

FLUORESCENT CARBON DOTS OBTAINED FROM GLUCOSE AT DIFFERENT PH SOLUTIONS

Anna Piasek*, Jolanta Pulit-Prociak, Marcin Banach

[1]Faculty of Chemical Engineering and Technology, Department of Chemical Technology and Environmental Analytics, Cracow University of Technology, Warszawska 24, 31-155 Cracow, Poland

*corresponding author: anna.piasek@doktorant.pk.edu.pl

Carbon dots (CDs) are a category of modern material that has great potential for applications. They are easy to modify and synthesize, and their fluorescent properties can be exploited in many ways. CDs can be obtained synthetically, from natural compounds or waste [1]. They can be of good benefit in the detection of compounds in the early detection of diseases through fluorescence quenching [2], as drug targeting or cell and tumor imaging. In addition to medical applications, CDs can be used as sensors in water purification methods, optoelectronics, or energy storage [3, 4].

The aim of the study was to synthesize carbon quantum dots from glucose for biomedical applications. Such a nanomaterial has fluorescent properties that can be widely used in medicine and environmental protection for the detection of selected chemical compounds. The synthesis was carried out in a microwave reactor using a top-down method with prior homogenization of the mixture. The influence of the pH of the environment, the temperature of the process, and the presence of the monopotassium phosphate reagent as a dehydrating agent was studied on the properties of the obtained product. The use of an additional reagent yielded interesting results in the work of Z. Xu et al. and Yoshinaga et. al. [5, 6]. 0.01M HCl was used as an acidic solvent, neutral - deionized water, and alkalic solvent - 0.01M NaOH. The glucose concentration was 0.01 mol/L, and the process time was 30 min for each synthesis. Detailed parameters of the samples are shown in Table 1. To separate smaller particles from the suspension, the mixture was filtered through a 0.45 μm pore filter. CDs were analyzed with a Rayleigh UV-vis spectrophotometer, a Tecan's spectrofluorometer and a Malvern's DLS analyzer.

Table 1. Variable parameters used in the syntheses performed

Sample	Process temperature, °C	pH	Molar ratio KH_2PO_4/Glucose
1	180	2,14	0
2	220	7,17	0
3	200	12,2	0
4	220	2,14	5
5	200	7,17	5
6	180	12,2	5
7	200	2,14	10
8	180	7,17	10
9	220	12,2	10

Figure 1 shows the PL spectrum for glucose CDs showing the intensity of fluorescence emission of CDs. These properties can be enhanced by modifying the surface of the nanomaterial.

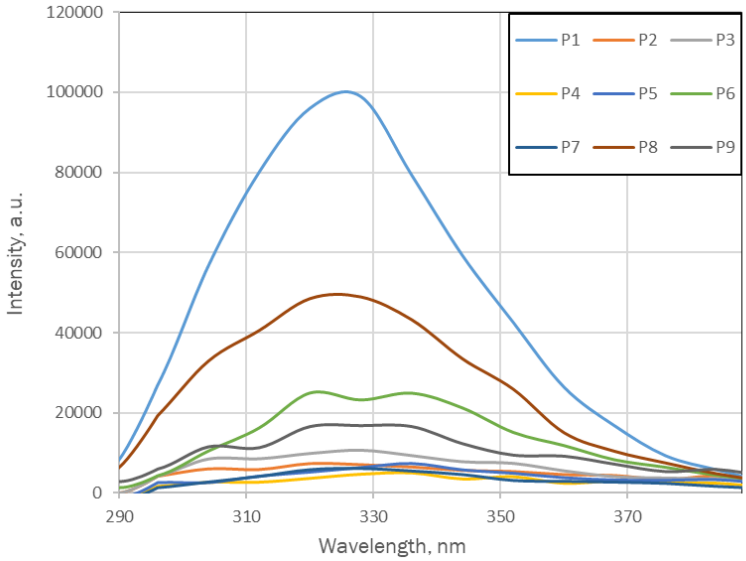

Fig. 1. PL spectrum of glucose CDs at 256 nm excitation wavelength

In the syntheses carried out, CDs with different fluorescence intensities were obtained. The best results were achieved using water as the solvent. The obtained CDs had sizes as small as 1 to 35 nm. The additional modification of CDs to enhance the fluorescence effect will make this product have great potential for application in medicine, not only as a biodetector.

References

[1] Ayiloor Rajesh G., John V.L., Pookunnath Santhosh A., Krishnan Nair Ambika A., Thavarool Puthiyedath V., Carbon Dots from Natural Sources for Biomedical Applications, *Part. Part. Syst. Charact.*, 2022, 39, 9, 1–23.

[2] Ji C., Zhou Y., Leblanc R.M., Peng Z., "Recent Developments of Carbon Dots in Biosensing: A Review, *ACS Sens.*, 2020, 5(9), 2724–2741.

[3] Liu J., Li R., Yang B., Carbon Dots: A New Type of Carbon-Based Nanomaterial with Wide Applications, *ACS Cent. Sci.*, 2020, 6(12), 2179–2195.

[4] Bag P., Maurya R.K., Dadwal A., Sarkar M., Chawla P.A., Narang R.K., Kumar B., Recent Development in Synthesis of Carbon Dots from Natural Resources and Their Applications in Biomedicine and Multi-Sensing Platform, *ChemistrySelect*, 2021, 6(11), 2774–2789.

[5] Xu Z., Wang C., Jiang K., Lin H., Huang Y., Zhang C., Microwave-Assisted Rapid Synthesis of Amphibious Yellow Fluorescent Carbon Dots as a Colorimetric Nanosensor for Cr(VI), *Part. Part. Syst. Charact.*, 2015, 32(12), 1058–1062.

[6] Yoshinaga T., Iso Y., Isobe T., Particulate, Structural, and Optical Properties of D-Glucose-Derived Carbon Dots Synthesized by Microwave-Assisted Hydrothermal Treatment, *ECS J. Solid State Sci. Technol.*, 2018, 7(1), R3034–R3039.

SOLAR LIGHT ACTIVE C,N,S-MODIFIED TiO_2-BASED PHOTOCATALYSTS FOR REMOVAL OF KETOPROFEN FROM WATER

Aleksandra Piątkowska*, Sylwia Mozia*

[1]Department of Inorganic Chemical Technology and Environment Engineering, Faculty of Chemical Technology and Engineering, West Pomeranian University of Technology in Szczecin, Pułaskiego 10, 70-322 Szczecin, Poland
*corresponding authors: aleksandra.piatkowska@zut.edu.pl, sylwia.mozia@zut.edu.pl

Currently, the world is struggling with many environmental problems. One of the major challenges is water quality. Constantly increasing production and consumption of medicinal products contributes to the growth in the amount of organic pollutants in the aquatic environment [1]. It was proved that the efficiency of conventional water and wastewater treatment processes is low in terms of removal of pharmaceuticals. Nevertheless, photocatalysis with the use of TiO_2 [2] is an effective method of decomposition and mineralization of many organic compounds, including drugs, However, this photocatalyst has one main drawback, which is high band gap energy and thus the need for activation with UV radiation. Hence, the research on the modification of TiO_2 aimed at increasing photocatalytic activity in visible light has become widespread. One of the approaches to extend the absorption range to visible light is incorporation of non-metals. Among them, C, N and S are very promising elements [2, 3]. The co-modification of TiO_2 with three non-metals: C, N and S is considered to combine the advantages of each single non-metal modification. The mentioned benefits include: (i) formation of new impurity levels (C 2p, N 2p, S 2p) above the valence band of TiO_2 and therefore, reduction of the excitation energy to the visible light range, (ii) development of carbonaceous species, acting like photosensitizers and (iii) formation of sulfate ions on the TiO_2 surface promoting the trapping of photo-induced electrons [3, 4].

In the present research a crude TiO_2 produced by sulfate technology was used as TiO_2 and S precursor. Moreover, the application of ammonium formate (AFT) as a novel modifier being the C and N source is proposed for the very first time. The main objective of this research was the investigation on the influence of the AFT dose on the solar light photoactivity of novel C, N,S-modified TiO_2-based photocatalysts. In particular, the impact on the efficiency of decomposition and mineralization of a model pollutant, ketoprofen (KPF), was examined. The crude TiO_2 was supplied by the Grupa Azoty Zakłady Chemiczne "Police" S.A. (Poland). The photocatalysts were prepared using a mechanochemical approach based on wet ball-milling followed by calcination in the air atmosphere. The crude TiO_2, precalcined at 600 °C, was mixed with AFT at the TiO_2:N weight ratios of 9:1, 8:2, 7:3, 6:4 and 5:5 and ball-milled in the presence of water for 1 h. The photocatalysts were marked as P600-AFT-9:1, P600-AFT-8:2, P600-AFT-7:3, P600-AFT-6:4 and P600-AFT-5:5, respectively. The obtained suspension was subsequently dried at 50 °C and calcined for 1 h at 600 °C. Additionally, a referential material (P600-M-600) was synthesized according to the above procedure, but without AFT addition. Moreover, P25 and the crude TiO_2 were employed for comparison purposes. The photocatalytic activity of the photocatalysts was investigated towards KPF (10 mg/L) decomposition under simulated solar light. A 150 W light bulb (Daylight Basking Spot, Exo Terra) was used as a radiation source with the intensity of ca. 1250 W/m^2 in the wavelength range of 300–2800 nm and ca. 0.4 W/m^2 in the wavelength range of UV-A and UV-B. The KPF concentration was measured using high performance liquid chromatograph (HPLC, Shimadzu, Japan), while total organic carbon (TOC) content was determined with a “multi N/C 2000” analyzer (Analytik Jena, Germany).

The influence of the AFT dose on the solar light photocatalytic activity of the photocatalysts is presented in Fig. 1. As shown, regardless the TiO_2:N ratio, the applied C,N,S-modification was proved to enhance photoactivity compared to the referential photocatalysts. The best performance was observed for P600-AFT-7:3.

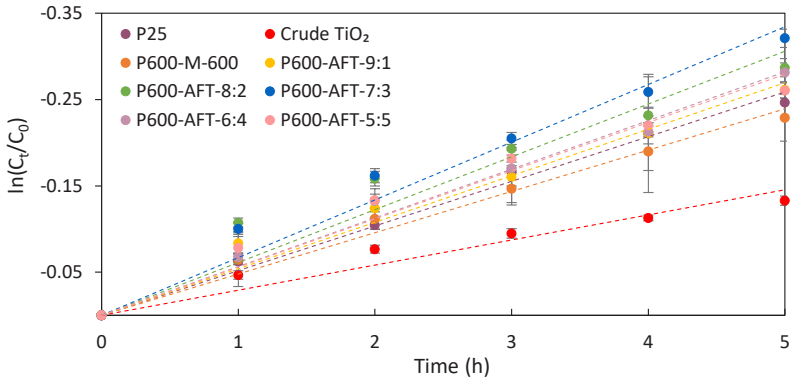

Fig. 1. Influence of AFT dose on the photocatalytic activity of the referential and C,N,S-modified photocatalysts during 5 h of irradiation with simulated solar light

The efficiency of KPF decomposition and mineralization in the presence of the C,N,S-modified and the referential photocatalysts was compared after 24 h of photocatalysis (Fig. 2). All the modified photocatalysts exhibited superior performance compared to the referential photocatalysts. The KPF decomposition efficiency was increasing with the rising AFT dose, gaining the highest value of 74% for P600-AFT-7:3. Then, the decomposition efficiency started to decrease with the further increase in the AFT dose. Moreover, all the C,N,S-modified photocatalysts displayed higher mineralization efficiency than the crude TiO_2 and P600-M-600. However, only P600-AFT-9:1, P600-AFT-8:2 and P600-AFT-7:3 revealed improved photoactivity compared to P25 in terms of mineralization. The highest mineralization efficiency of 35% was reached in the presence of P600-AFT-7:3.

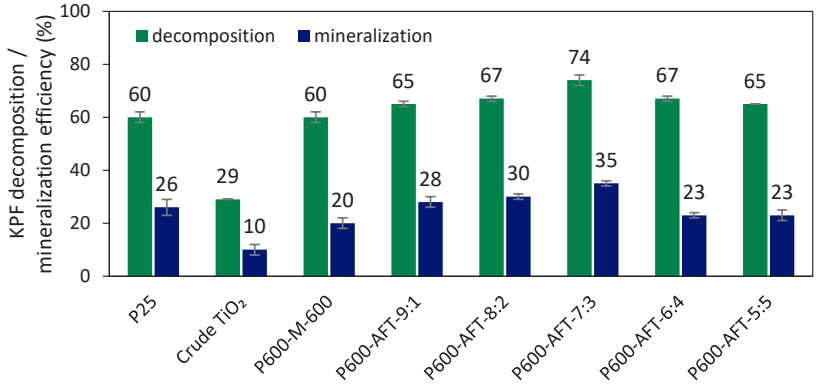

Fig. 2. Effect of AFT dose on the efficiency of KPF decomposition and mineralization in the presence of the referential and C,N,S-modified photocatalysts after 24 h of simulated solar light irradiation

It was proved that C,N,S-modification of TiO_2 with the application of AFT as C and N source enhanced photocatalytic activity under the simulated solar light. The highest KPF decomposition and mineralization efficiency of 74 and 35%, respectively was achieved for P600-AFT-7:3.

Acknowledgements: This work was supported by the National Science Centre, Poland under project No. 2019/33/B/ST8/00252.

References

[1] Adeleye A.S., Xue J., Zhao Y., Taylor A.A., Zenobio J.E., Sun Y., Han Z., Salawu O.A., Zhu Y., Abundance, fate, and effects of pharmaceuticals and personal care products in aquatic environments, *J. Hazard. Mater.*, 2022, 424, 127284.

[2] Paumo H.K., Dalhatou S., Katata-Seru L.M., Kamdem B.P., Tijani J.O., Vishwanathan V., Kane A., Bahadur I., TiO_2 assisted photocatalysts for degradation of emerging organic pollutants in water and wastewater, *J. Mol. Liq.*, 2021, 331, 115458.

[3] Piątkowska A., Janus M., Szymański K., Mozia S., C-,N- and S-Doped TiO_2 Photocatalysts: A Review, *Catalysts*, 2021, 11, 144.

[4] Sushma C., Kumar S.G., C-N-S tridoping into TiO_2 matrix for photocatalytic applications: Observations, speculations and contradictions in the codoping process, *Inorg. Chem. Front.*, 2017, 4, 1250-1267.

CHEMICAL ENGINEERING ISSUES IN THE DESIGN OF PRESSURE SENSITIVE PAINTS FOR SPECIAL APPLICATIONS

Maciej Pilch*, Dawid Kiesiewicz, Paweł Jamróz, Małgorzata Noworyta, Joanna Ortyl, Roman Popielarz

Cracow University of Technology, Faculty of Chemical Engineering and Technology, Warszawska 24, 31-155 Kraków, Poland
*corresponding author: maciej.pilch@doktorant.pk.edu.pl

This paper presents two computational models describing the behavior of OQ-PSP (Oxygen Quenching Pressure Sensitive Paints) and SQ-PSP (Solvent Quenching Pressure Sensitive Paints) coatings in aerodynamic conditions and the results of empirical spectroscopic tests of selected PSP systems. An OQ-PSP computational model was prepared using the relationships for diffusive mass transfer inside the coating and Fick's 2nd law, while the Stern-Volmer equation was used to describe the relationship between the luminescence intensity of the coating and the concentration of quencher (oxygen), the same as for collisional quenching luminescence. An SQ-PSP computational model was prepared on the basis of the Stern-Volmer equation for solvent quenching of luminescence, as well as the Eyring dependence of quenching rate constant on the free molecule enthalpy change and the dependence of free molecule enthalpy on the pressure in the system. [1]

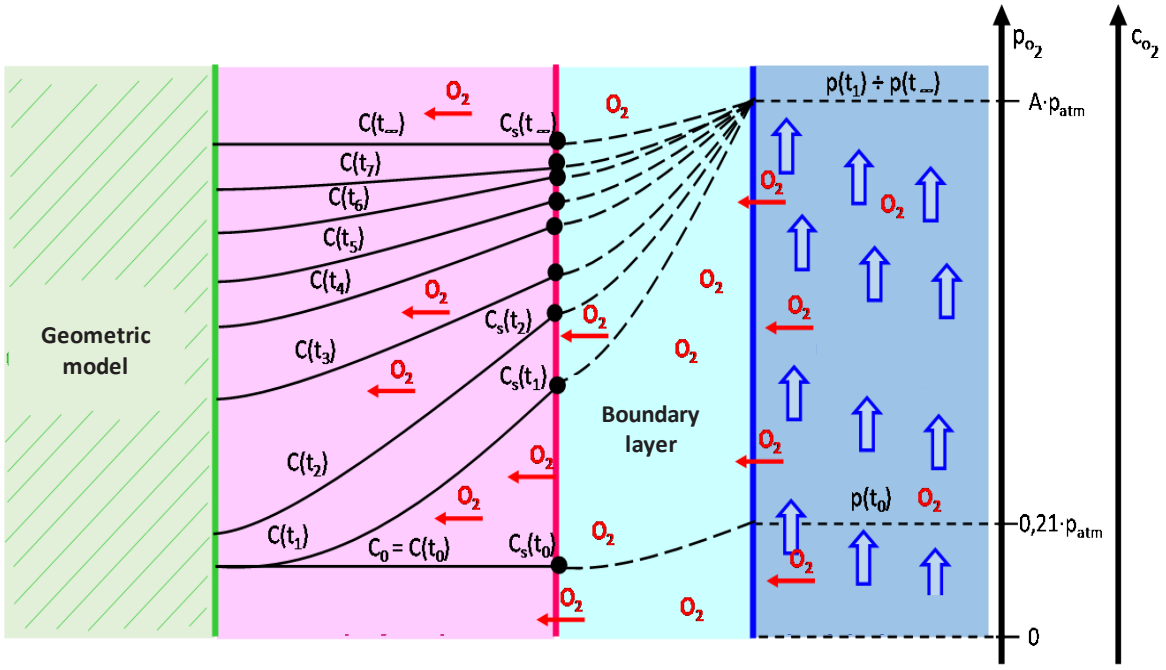

Fig. 1. Diagram of mass transfer phenomena in OQ-PSP systems in aerodynamic conditions, where: t – measurement time (t_0 = 0 s and $t_1 < t_2 < t_3 < \ldots < t_7 < t_\infty$); C(t) – molar concentration of oxygen in the PSP coating at time t; Cs(t) – molar concentration of oxygen on the surface of the PSP coating at time t; p(t) – partial pressure of oxygen in the surroundings of PSP coating at time t

Based on the solved computational models, the predicted process parameters of the OQ-PSP and SQ-PSP systems were compared with the parameters determined as a result of experimental tests and literature data. One of the main parameters characterizing OQ-PSP systems is their response time (t_R), Comparison of the computational dependence and semi-empirical literature dependence

of the response time of the OQ-PSP system on the thickness of the coating based on poly(butyl methacrylate) and platinum octaethylporphyrin luminescent sensor is shown in Figure 2 [2–3].

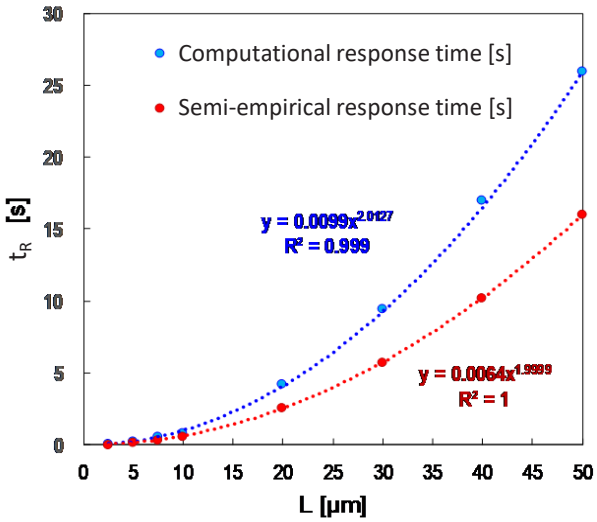

Fig. 2. The dependence of response time (tR) of OQ-PSP coating based on poly(butyl methacrylate) on its thickness (L), according to the computational dependence and semi-empirical literature equation

As can be seen in Figure 1, the relationship determined using the developed computational model and the semi-empirical literature model coincide for the coating thickness up to about 10µm. However, for thicker coatings, these relationships differ significantly. Similar observations were made for the dependence of the coating luminescence intensity on the pressure determined using the proposed computational models and experimental data. This allows us to conclude that the proposed computational models are true only for coatings with small thicknesses (up to several micrometers). It can be hypothesized that for coatings of greater thickness, additional phenomena may occur, such as deformation of the coating under pressure, which may affect the spectroscopic response of the luminescent sensor.

Acknowledgments

The research were implemented within the framework of the project titled: Designing, obtaining, and testing the application properties of a new type of PSP and TSP coatings as part of the construction of innovative systems for mapping the distribution of thermodynamic state parameters on the surfaces of real objects, for the needs of the high technology industry, funded by the Ministry of Science and Higher Education (Grant No: DI2018 000848).

The research (work) was carried out as part of the project "ROAD TO EXCELLENCE - a comprehensive university support programme" implemented under the Operational Programme Knowledge Education Development 2014-2020 co-financed by the European Social Fund; agreement no. POWR.03.05.00-00-Z214/18

References

[1] Pilch, M., Ortyl, J., Popielarz, R., Quantitative interpretation of the response of Solvent-Quenched Pressure Sensitive Paints (SQ-PSPs) to pressure, *Measurement*, 2021, 177, 109233.

[2] Obata M., Asato R., Hirohara S., Mitsuo K., Effect of polymer matrix on the performance of pressure-sensitive paint comprising 5,10,15,20-tetrakis(pentafluorophenyl)-porphinato platinum(II) and poly(1,1,1,3,3,3-hexafluoroisopropyl-co-tert-butyl methacrylates), *J. Appl. Polym. Sci.*, 2016, 133, 1–10.

[3] Tropea C., Yarin A.L., Foss J.F., *Springer Handbook of Experimental Fluid Mechanics*, Heidelberg, Springer-Verlag 2007.

EFFECT OF SYNTHESIS PARAMETERS AND STRUCTURE MORPHOLOGY ON AMBIENT PRESSURE DRIED MTMS-BASED GEL POROSITY

Aleksandra M. Pisarek*, Bartosz Nowak, Nina H. Borzęcka, Jakub M. Gac

Faculty of Chemical and Process Engineering, Warsaw University of Technology, Waryńskiego 1, 00-645 Warsaw, Poland
*corresponding author: aleksandra.pisarek2.dokt@pw.edu.pl

Aerogels are materials showing the potential to revolutionize a wide range of technology and science fields. Owing to their excellent properties, such as high porosity, low density, high specific surface area and low thermal conductivity, they can be used as insulation (thermal and acoustic), catalyst and active substances carriers, energy adsorbers or even stardust collectors [1-3]. However, the practical application of aerogels is limited by one of their crucial preparation steps – the drying process [2-3].

Production of aerogels is based on a sol-gel synthesis, in which the final product – gel – is obtained from a dispersed system (sol). To obtain an aerogel from a wet gel, the liquid present in the material pores must be replaced by a gas without skeleton damage [2-3]. This process is difficult due to the very brittle framework structure of the solid phase. Samuel K. Kistler (inventor of aerogels) solved the problem of structure deformation by using supercritical drying (SCD) [2-3]. However, SCD requires high pressure, thus making the preparation process energy-consuming and expensive. Therefore, a competing method was developed – ambient pressure drying (APD), which remains more affordable, as no dedicated apparatus is required [2-3]. Nevertheless, proper APD utilisation demands to define parameters affecting structure deformation during the drying process. This will allow the optimization of a much cheaper and safer drying method – APD, to obtain aerogels with the most satisfactory properties.

The presented research was carried out to understand the influence of the initial synthesis chemical composition on the sample morphology, porosity and volume shrinkage during the drying process. The selection of the initial synthesis chemical compositions was based on a ternary system – precursor, solvent and antisolvent components. In the presented studies methyltrimethoxysilane (MTMS) was used as the precursor, methanol – as the solvent, and water - as the antisolvent. As the synthesis procedure, the two-step, acid-base, sol-gel method was used. The first step – hydrolysis – was carried out in the presence of oxalic acid as the catalyst. The second - consisting of the condensation reaction between previously hydrolysed particles - was carried out in the presence of ammonium hydroxide. The concentration of catalysts in the solution was constant. After gel formation, solvent exchange for pure methanol was performed three times every 24h (at room temperature). After that samples were dried at 60^{o}C at ambient pressure.

The characterization of the samples aimed to designate the initial composition and gel microstructure effect on gel volume shrinkage. The scanning electron microscope (SEM) observation allowed for the obtained morphologies to be classified as one of the four distinguished by K. Nakanishi and K. Kanamori types of structures [4] – particle aggregates, co-continuous, nanoporous and isolated pores. Porosity and volumetric shrinkage were calculated based on dimensional and gravimetric measurements (gels and aerogels).

Analysis of wet gel porosity in the ternary system allowed to determine the relationship between the porosity and the initial synthesis mixture composition. It was found that the gel porosity value decreases linearly with precursor concentration (Figure 1A). No effect of the water-to-solvent ratio on wet gel density/porosity was observed.

The solvent/antisolvent effect has a visible influence on the volume shrinkage, as shown in Figure 1B. Volume shrinkage value increases with the increasing methanol-to-precursor ratio and decreases with the increasing water-to-precursor ratio. Therefore, the highest volume shrinkage exhibits gels from a high methanol and a low water content in a reactive mixture.

The characterized structure types occurrence on the Gibbs ternary plot allowed to determine the course of binode – inside which gelation occurs throughout the volume – and spinode, which separates areas characterized by different mechanisms of microscopic phase separation (nucleation and growth vs spinodal decomposition) [5]. The course of the binode, spinode and the occurrence of individual morphologies are shown in Figure 1C.

A comparison of the influence of initial synthesis mixture composition on volume shrinkage (Figure 1B) and on the morphology (Figure 1C) shows that the highest volume shrinkage occurs for the nanoporous structure type. This is because this type has the smallest pore size – and thus the highest capillary pressure, which results in the structure collapse during drying.

Two factors are responsible for the final aerogel porosity (shown in Figure 1C). Wet gel porosity is directly correlated with precursor concentration in the initial mixture. In addition, aerogel porosity depends indirectly on the methanol-to-water ratio as this decides about aerogel morphology – and hence affects volume shrinkage. In conclusion – the highest aerogel porosity values occurred for the lowest precursor concentration and the structure with the largest pore size (particle aggregate type of structure).

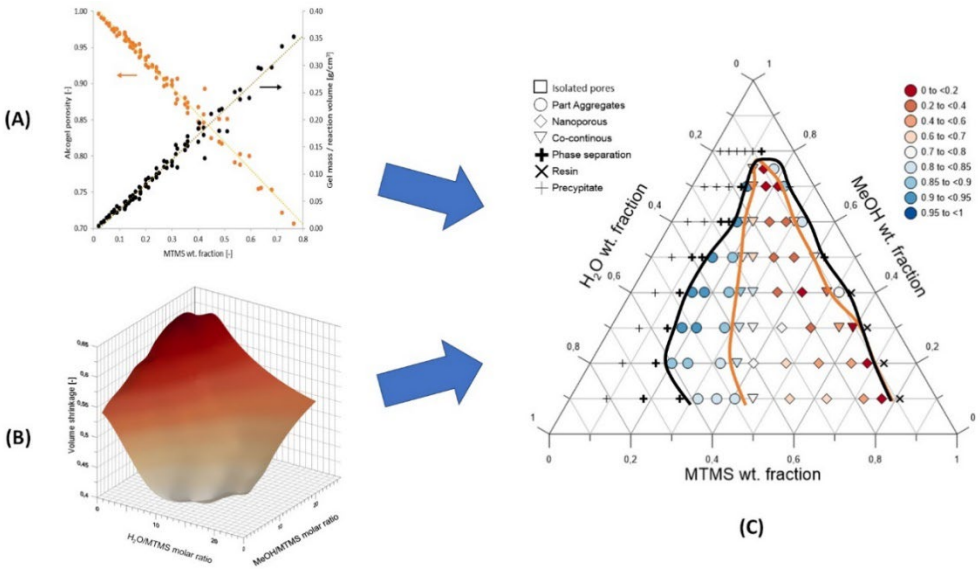

Fig. 1. Influence of reaction mixture composition on alcogel porosity (A), on volume shrinkage (B) and on morphology, binode (black curve), spinode (orange curve) and porosity (C) of MTMS-based aerogels dried in ambient pressure

The results of the presented research allow to identify the parameters that determine the final porosity of organosilica aerogel obtained with the use of a much cheaper and safer drying method – APD. This analysis gives a planning tool for syntheses of APD-aerogels with the most desirable properties (high porosity value and low volume shrinkage).

Acknowledgement

The research was funded by the Polish National Science Centre (NCN) under the PRELUDIUM BIS programme, grant no. 2021/43/O/ST8/01586

References

[1] Schmidt M., Schwertfeger F., Applications for silica aerogel products, *J. Non. Cryst. Solids*, 1998, 225.
[2] Pierre A.C., Pajonk G.M., Chemistry of Aerogels and Their Applications, *Chem. Rev.*, 2002, 102.
[3] Gurav J.L., Jung I.K, Park H.H., Kang E.S., Nadargi D.Y., Silica Aerogel: Synthesis and Applications, *J. of Nanomaterials*, 2010.
[4] Nakanishi K., Kanamori K., Organic-inorganic hybrid poly(silsesquioxane) monoliths with controlled macro- and mesopores, *J. Mater. Chem.*, 2005, 15.
[5] Kaji H., Nakanishi K., Soga N., Polymerization-Induced Phase Separation in Silica Sol-Gel Systems Containing Formamide, *J. Sol-Gel Sci. Technol.*, 1993, 1.

REMODELLING OF CALCIUM PHOSPHATE TO HYDROXYAPATITE IN A BATCH REACTOR

Kornel Prystupiuk*, Joanna Latocha, Artur Małolepszy, Michał Wojasiński, Paweł Sobieszuk

Warsaw University of Technology, Faculty of Chemical and Process Engineering,
Waryńskiego 1, 00-645 Warsaw, Poland
*corresponding author: kornel.prystupiuk.dokt@pw.edu.pl

Hydroxyapatite (HAp) is the most desirable and one of the most studied forms of calcium phosphate. It is found in human bones and teeth. HAp has the lowest solubility in aqueous media of all forms of calcium phosphate. Moreover, it has many properties of a promising biomaterial. There are many methods of HAp synthesis, but precipitation is the most popular and straightforward method. Here, we discuss precipitation/remodelling, where calcium precursor and phosphate precursor are mixed in a solution. Transition forms of various calcium phosphates precipitate instantaneously, and HAp is obtained by remodelling over time in a controlled environment.

In this work, we present the analysis of which transition forms of calcium phosphate occurred after a specific synthesis time in a batch reactor and which morphology they had when, instantaneously after initial precipitation, a constant dosage of aqueous ammonia solution raised the pH of the mixture. The temperature of the process was kept constant at 40 and 80 °C. In the experimental part of this work, we carried out 12 hydroxyapatite syntheses at a set temperature in a batch reactor using the precipitation/remodelling process with the continuous addition of ammonia solution for increasing the pH over time up to about 10 [1]. The syntheses were performed for 0, 1, 2, 3, 4, 5, 6, 7, 8, 16, 20, and 24 h. The samples were processed by repetitive centrifugation, drying, and ground before comprehensive analysis. Moreover, we collected samples of the aqueous phase from the reactor for analysis. The product quality was determined with Fourier-transform infrared spectroscopy (FTIR) and x-ray fluorescence spectrometry (XRF); the morphology of particles was studied by scanning electron microscopy (SEM).

FTIR spectra indicate that the samples obtained through synthesis at 40 and 80 °C initially had water, hydrophosphate- and hydroxyapatite-specific bonds in their structures. XRF shows that the molar ratio of calcium to phosphorus increased from about 1.00 to about 1.67 over the reaction time in both cases, indicating that the final product was HAp remodelled from previously occurring other forms of calcium phosphate. SEM images show that morphologies of HAp particles obtained at 40 and 80 °C are different. At 40 °C at the beginning, particles have an irregular structure (dominated by agglomerates made up of spherical particles). During remodelling, calcium phosphates start taking the form of plates. However, as time passes, the particles take on an increasingly irregular structure - inclusions in sphere form appear on the plates. Only after 16 hours does the visible form of the plates reappear, and after 24 h, particles become fully developed and free of inclusions. At 80 °C at the beginning, particles also have an irregular structure, but after 1 h, remodelled calcium phosphates take the form of rod-shaped particles. This morphology persists until the end of remodelling. Moreover, the presented results were referenced and compared with a concentration of calcium ions in the water phase. Then based on this comparison and using the calcium ion concentration measurement results in the aqueous phase, we determined the kinetics of HAp precipitation at 40 and 80 °C.

Knowing the occurrence of a given morphology depending on specific synthesis conditions makes it possible to design the precise production of HAp with desired morphology as needed, for example, as an admixture in 3D printing or as particles used in drug delivery systems. Further control of HAp particle morphology utilising a concentration of calcium ions in the water phase could make it easier to control the process under industrial conditions.

References

[1] Latocha J., Wojasiński M., Janowska O., Chojnacka U., Gierlotka S., Ciach T., Sobieszuk P., Morphology-controlled precipitation/remodeling of plate and rod-shaped hydroxyapatite nanoparticles, *AIChE J.*, 2022, 68(12), e17897.

SEPARATION OF MONOCLONAL ANTIBODY CHARGE VARIANTS BY PEG-AIDED PRECIPITATION AND IEX CHROMATOGRAPHY

Tomasz Rumanek[1,*], Patrycja Zimoch[1], Michał Kołodziej[2], Wojciech Piątkowski[2], Dorota Antos[2]

[1]Doctoral School of Engineering and Technical Sciences at the Rzeszow University of Technology, Rzeszow, Poland
[2]Department of Chemical and Process Engineering, Rzeszów University of Technology, Rzeszow, Poland
*corresponding author: d522@stud.prz.edu.pl

Microheterogeneity of monoclonal antibodies (mAbs) can impact their activity and stability. Formation of charge variants is considered to be the most important source of microheterogeneity. The charge variants are classified according to their isoelectric point and termed as: “acidic” (*a*ν), “main”(*m*ν) and “basic” (*b*ν). The *a*ν and *b*ν species differ in biological activity from the *m*ν species. However, *a*ν are often reported to have reduced potency compared to the remaining variants. Controlling the content of the *a*ν species is often of major importance for the production process and regulatory (EMA - European Medicines Agency) approval of therapeutic proteins. Therefore, seclusion of *a*ν from the mAb pool is a common polishing step in downstream mAbs processing.

In this study, we have developed two different techniques for reducing the content of *a*ν in mAbs downstream pools: polyethylene glycol (PEG)-aided selective precipitation and preparative ion exchange chromatography (IEX). We indicated that the presence of PEG favoured precipitation of *a*ν from the mAbs pool, which resulted in the reduction of *a*ν content in the supernatant that was the product of the process. The precipitate enriched with *a*ν was the process waste. The precipitation yield was influenced by the variant composition in the mAbs feed solutions, the concentration of the precipitant and the protein and the ionic strength of the solutions. The process was quantified using the developed model consisting of mass balance equations and the pareto relationship between yield and *a*ν content. in the supernatant [1]. The IEX process was performed by overloading the column with the protein and its elution in the pH step gradient. The column overload caused the protein mass to split into two parts: the flowthrough fraction eluted at dead time of the column and the bound fraction eluted with the pH gradient. The flowthrough fraction, which was the target product of the process, was depleted with with *a*ν, whereas the bond fraction, which was the process waste was enriched with *a*ν [2].

Both PEG-aided precipitation and IEX were coupled in different configurations (Fig. 1). The coupled process allowed improvement of the operation throughput, which may provide a benefit in reduction of manufacturing costs compared with the stand-alone separations, especially with the chromatography process.

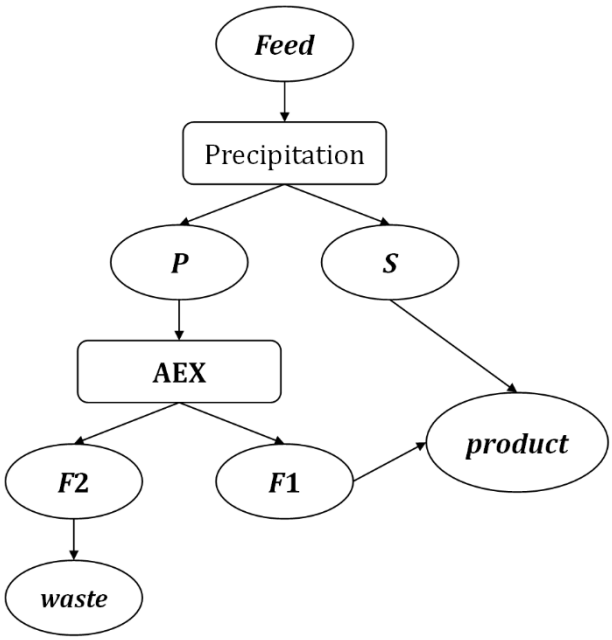

Fig. 1. Scheme of coupled processes of the PEG-aided precipitation and IEX

Acknowledgments

Financial support of this study by Narodowe Centrum Nauki (UMO-2018/31/N/ST/02538) is gratefully acknowledged. We also acknowledge Polpharma Biologics, Gdańsk, Poland for the supplement of biological material.

References

[1] Rumanek T., Kołodziej M., Piątkowski W., Antos D., Preferential precipitation of acidic variants from monoclonal antibody pools, *Biotechnol. Bioeng.*, 2023, 120, 114-124.

[2] Baran K., Zimoch P., Stańczak A., Piątkowski W., Antos D., Separation of charge variants of a monoclonal antibody by overloaded ion exchange chromatography, *J. Chromatogr. A*, 2021, 1658, 462607.

REUSE OF AVOCADO SEEDS AS PROMISING SORPTION MATERIAL

Joanna Siemak*, Beata Michalkiewicz

West Pomeranian University of Technology in Szczecin, Faculty of Chemical Technology and Engineering, Department of Catalytic and Sorbent Materials Engineering, Piastów 42, 71-065 Szczecin, Poland
*corresponding author: sj54728@zut.edu.pl

Considering sustainable development and trying to reduce the negative impact of human activity, new methods and sources are sought to save the natural environment. There is an emphasis on reducing emissions and the number of greenhouse gases in the atmosphere to combat climate change. One of them is carbon dioxide whose anthropogenic emissions have caused a significant impact on the global climate [1].

Up to date, avocado seeds considered as agricultural residues have been used successfully as an effective adsorbent only in the removal of contaminants from aqueous solutions, for example, fluorine ions, phenol or Cr(VI) ions from aqueous solutions [2]–[4].

In this work, we reported avocado seeds as carbon precursor for CO_2 sorbents for the first time. A new strategy method combining solvothermal carbonization with thermal KOH activation was used. As a result, desired ultramicroporous activated carbons were developed with uniform ultramicropores (~0.50 nm) and with the enhancement of CO_2 adsorption.

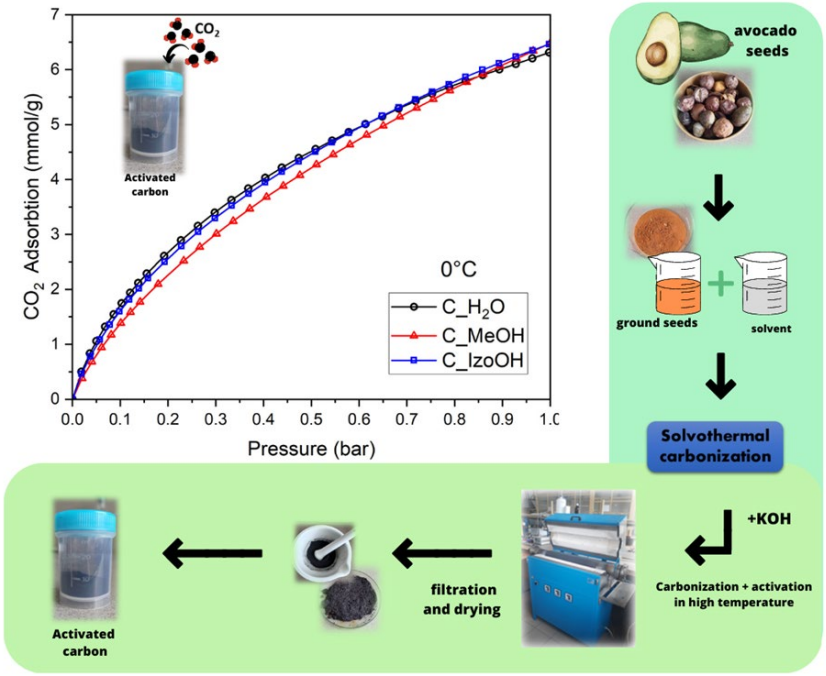

Fig. 1. Activated carbon production scheme and CO_2 adsorption

Figure 1 shows the process of obtaining activated carbon taking into account the various activities at specific stages. Firstly, dried avocado seeds were fine powdered. Solvothermal carbonizations of avocado seed in three different liquids (water, methanol and isopropyl alcohol) were performed in a stainless-steel autoclave lined with Teflon. The resulting chars were washed with deionized water and dried. Then, they were mixed with a saturated KOH solution. The dried

mixtures were placed in a tubular furnace and heated to 850°C under nitrogen flow for one hour. Then samples were washed with deionized water until neutral pH was achieved. In the end, the samples were dried. The activated carbons with excellent textural properties (pore volume, micropore volume, and specific surface area) were successfully synthesized.

Fig. 1 shows CO_2 adsorption isotherms at the temperature of 0oC. All the isotherms were similar. The highest CO_2 adsorption at 1 bar and 0°C (6.47 mmol/g) was achieved for activated carbons produced using methanol and isopropanol. When water was applied, adsorption was slightly lower, namely 6.31 mmol/g. CO_2 adsorption at 20°C ranged from 4.13 to 4.35 mmol/g depending on the solvent used. The adsorption values were very heigh compared to those presented by other researchers.

According to the conducted study, seeds can be used as a promising reagent for the production of CO_2-adsorbing carbon materials, helping to reduce the amount of it from mixtures of gasses. This shows that biomass residues as avocado seeds can be reapplied for useful purposes to counteract the anthropological effects on the environment.

References

[1] Zhang J., Yin R., Shao Q., Zhu T., Huang X., Oxygen Vacancies in Amorphous InO x Nanoribbons Enhance CO_2 Adsorption and Activation for CO 2 Electroreduction, *Angew. Chemie - Int. Ed.*, 2019, 58(17), 5609–5613.

[2] Salomón-Negrete M. Á., Reynel-Ávila H.E., Mendoza-Castillo D.I., Bonilla-Petriciolet A., Duran-Valle C.J., Water defluoridation with avocado-based adsorbents: Synthesis, physicochemical characterization and thermodynamic studies, *J. Mol. Liq.*, 2018, 254, 188–197.

[3] Rodrigues L. A., da Silva M.L.C.P., Alvarez-Mendes M.O., Coutinho A.R., Thim G.P., Phenol removal from aqueous solution by activated carbon produced from avocado kernel seeds, *Chem. Eng. J.*, 2011, 174(1), 49–57.

[4] Bhaumik M., Choi H.J., Seopela M.P., McCrindle R.I., Maity A., Highly Effective Removal of Toxic Cr(VI) from Wastewater Using Sulfuric Acid-Modified Avocado Seed, *Ind. Eng. Chem. Res.*, 2014, 53(3), 1214–1224.

HEAT AND MOMENTUM TRANSFER OF STREAMLINED CATALYTIC CARRIERS

Katarzyna Sindera[1]*, Mateusz Korpyś[1], Marzena Iwaniszyn[1], Anna Gancarczyk[1], Mikołaj Suwak[1], Andrzej Kołodziej[1,2]

[1]Institute of Chemical Engineering, Polish Academy of Sciences, Bałtycka 5, 44-100 Gliwice, Poland

[2]Faculty of Civil Engineering and Architecture, Opole University of Technology, Katowicka 48, 45-061 Opole, Poland

*corresponding author: katarzyna.sindera@iich.gliwice.pl

Research is focused on new streamlined catalytic carriers which are similar to the short-channel structures (short monoliths) displaying beneficial transport-flow properties [1]. The innovativeness of the geometry design is in forming the walls of the channels similar to airfoil, as shown in Fig. 1.

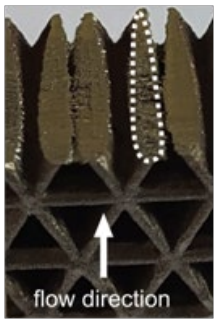

Fig. 1. Cross-section of the tested structure; the airfoil profile is marked with dashed line

Nine structures differing in length (3, 6 or 12 mm) and in the shape of the cross-section of the channels (square, hexagonal or triangular) were designed. The structures were 3D printed from 316 steel using the SLM (Selective Laser Melting) technique. The transport and flow properties of the structures were experimentally studied and the results are shown in Figs. 2 and 3. For comparison, the plots also include characteristics of a packed bed (consisting of spherical grains of 3 mm diameter [2, 3]) and monolith (50 cpsi, L = 0.2 [4]).

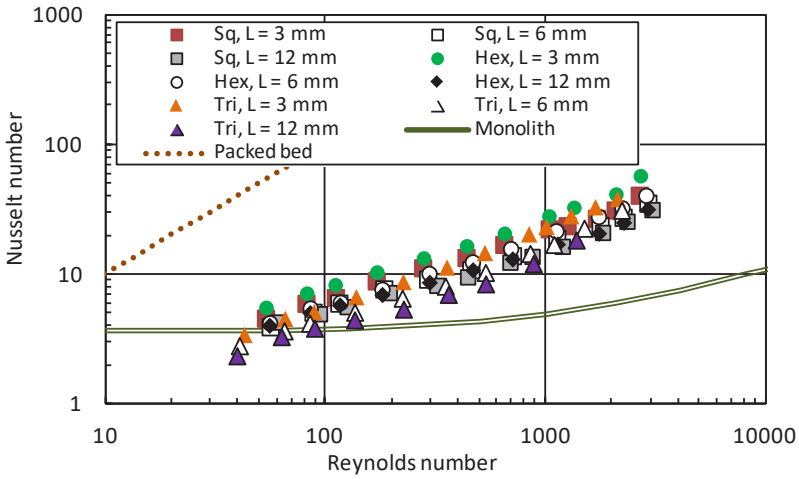

Fig. 2. Nusselt number vs. Reynolds number ("Sq" refers to square, "Hex" to hexagonal and "Tri" to triangular cross-section channels)

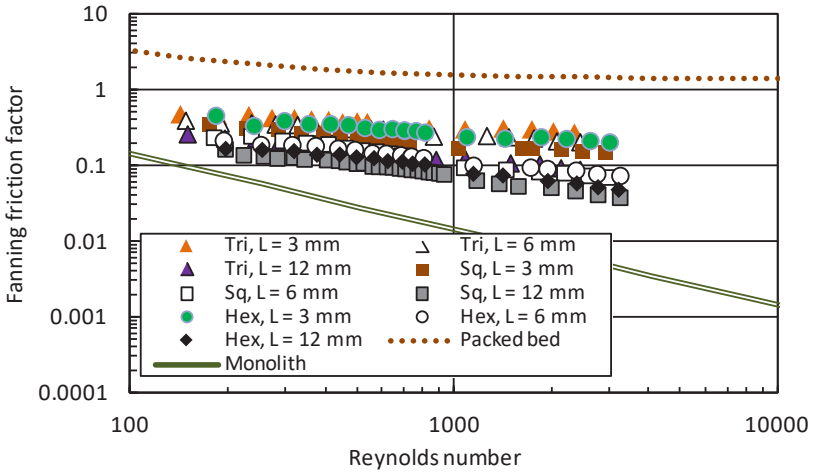

Fig. 3. Fanning friction factor vs. Reynolds number

Structures with hexagonal channels indicate the highest Nusselt numbers, while the lowest friction factors were obtained for structures with square channels. The shorter the channel length, the more enhanced heat transfer and the higher flow resistance. Nevertheless, the tested structures are characterized by intensified transport properties compared to the monolith in the majority of the measured velocity range. This intensification is accompanied by an increase in flow resistance.

Acknowledgements: this work was supported by the Polish National Science Centre (Project No., DEC-016/21/B/ST8/00496).

References

[1] Kolodziej A., Lojewska J., Ochonska J., Lojewski T., Short-channel structured reactor: Experiments versus previous theoretical design, *Chem. Eng. Process.*, 2011, 50(8), 869-876.
[2] Wakao N., Kaguei S., Funazkri T., Effect of fluid dispersion coefficients on particle-to-fluid heat-transfer coefficients in packed-beds - correlation of nusselt numbers, *Chem. Eng. Sci.*, 1979, 34(3) 325-336.
[3] Ergun S., Fluid flow through packed columns, *Chem. Eng. Prog.*, 1952, 48(2), 89-94.
[4] Hawthorn R.D., Afterburner catalysis-effects of heat and mass transfer between gas and catalyst surface, *AIChE Symp. Ser.*, 1974, 428-438.

STARCH-CHITOSAN FILMS PLASTICIZED WITH DEEP EUTECTIC SOLVENT

Dorota Skowrońska*, Katarzyna Wilpiszewska

West Pomeranian University of Technology in Szczecin, Faculty of Chemical Technology and Engineering, Department of Chemical Organic Technology and Polymeric Materials, Pułaskiego 10, 70-322 Szczecin, Poland

*corresponding author: dorota.skowronska@zut.edu.pl

The use of biopolymers in the production of plastics makes it possible to obtain biodegradable, non-toxic materials from renewable sources. Along with cellulose and chitin, starch is one of the most common polysaccharides in nature. The extended network of inter- and intramolecular hydrogen bonds results in a high melting point. Decreasing the temperature of phase transitions can be achieved by using low-molecular-weight substances - plasticizers - that can form hydrogen bonds with starch. The most commonly used starch plasticizers are glycerol, urea, sugars, and others. Recently, the use of deep eutectic solvents as starch plasticizers was tested [1,2]. Another polysaccharide popular for its antimicrobial properties is chitosan (a derivative of chitin).

Deep eutectic solvents (DES) are a relatively new group of solvents. They are mixtures of a hydrogen bond donor (e.g. polyols, amines, carboxylic acids) and a hydrogen bond acceptor (quaternary ammonium salt). When components are mixed in appropriate molar ratios, there is a 'deep' drop in the system's melting temperature (T_m). The T_m of the mixture is significantly lower than the melting points of the individual substances. DESs exhibit properties similar to ionic liquids, but their preparation is simpler [3, 4].

Thermoplastic starches have been successfully obtained using deep eutectic solvents, e.g. a mixture of choline chloride with glycerol or urea [5]. There are also reports on DESs obtained from choline chloride and lactic, malonic, and citric acid used for the preparation of chitosan films [6-8]. Films with antimicrobial properties based on *kudzu* starch and chitosan were obtained using malic acid (to dissolve the chitosan) and plasticizer (glycerol) [9].

In this work, films based on potato starch and chitosan were obtained. The deep eutectic solvent (CM, based on malic acid and choline chloride) had two functions: chitosan solvent and polysaccharide plasticizer. The deep eutectic solvent was prepared by stirring choline chloride and malic acid (molar ratio 1:1) at 80°C to obtain a homogeneous liquid. Polysaccharide films were obtained with the casting method. Starch (S), chitosan (C), deep eutectic solvent, and water were mixed with a mechanical stirrer, in the water bath for 30 minutes. The systems were poured into Petri dishes and dried at 50°C for 24 hours. Before testing, all films were conditioned in a climate chamber at least for 24 hours. The physicochemical properties of the films (tensile strength, moisture absorption, roughness) were determined. Moreover, thermal analysis (DSC) and infrared spectroscopy (FTIR-ATR) were performed.

Table 1. The composition of the samples

Sample acronym	Composition of the samples without water [wt%]		
	Starch	Chitosan	Plasticizer
F_SC(05)_CM	66.5	3.5	30.0
F_SC(10)_CM	63.0	7.0	30.0
F_SC(20)_CM	56.0	14.0	30.0
F_SC(30) CM	49.0	21.0	30.0
F_SC(50)_CM	35.0	35.0	30.0

References

[1] Ebnesajjad S., *Starch: Major Sources, Properties and Applications as Thermoplastic Materials*, In Handbook of Biopolymers and Biodegradable Plastics: Properties, Processing and Applications, Elsevier, 2013, 129–152.

[2] Montilla-Buitrago C.E., Gómez-López R.A., Solanilla-Duque J.F., Serna-Cock L., Villada-Castillo H.S., Effect of Plasticizers on Properties, Retrogradation, and Processing of Extrusion-Obtained Thermoplastic Starch: A Review, *Starch – Stärke,* 2021, *73*, 2100060.

[3] Hansen B.B., Spittle S., Chen B., Poe D., Zhang Y., Klein J.M., Horton A., Adhikari L., Zelovich T., Doherty B.W., et al., Deep Eutectic Solvents: A Review of Fundamentals and Applications, *Chem. Rev*., 2021, 121, 1232–1285.

[4] Płotka-Wasylka J., de la Guardia M., Andruch V., Vilková M., Deep eutectic solvents vs ionic liquids: Similarities and differences, *Microchem. J.*, 2020, 159, 105539.

[5] Skowrońska D., Wilpiszewska K., Deep Eutectic Solvents for Starch Treatment, *Polymers* (Basel) 2022, 14, 220.

[6] Almeida C. M. R., Magalhães J. M. C. S., Souza H. K. S., Gonçalves M. P., The role of choline chloride-based deep eutectic solvent and curcumin on chitosan films properties, *Food Hydrocoll*, 2018, 81, 456–466.

[7] Jakubowska E., Gierszewska M., Nowaczyk J., Olewnik-Kruszkowska E., Physicochemical and storage properties of chitosan-based films plasticized with deep eutectic solvent, *Food Hydrocoll*, 2020, 108, 106007.

[8] Smirnov M.A., Nikolaeva A.L., Bobrova N.V., Vorobiov V.K., Smirnov A.V., Lahderanta E., Sokolova M.P., Self-healing films based on chitosan containing citric acid/choline chloride deep eutectic solvent, *Polym Test*, 2021, 97, 107156.

[9] Zhong Y., Song X., Li Y., Antimicrobial, physical and mechanical properties of kudzu starch–chitosan composite films as a function of acid solvent types, *Carbohydr. Polym*., 2021, 84(1), 335–342.

DEEP EUTECTIC SOLVENTS AS GREEN ABSORBENTS FOR ENRICHMENT OF FERMENTATION GAS

Edyta Słupek*, Patrycja Makoś-Chełstowska, Karolina Kucharska, Jacek Gębicki

Department of Process Engineering and Chemical Technology, Faculty of Chemistry, Gdansk University of Technology, 80-233 Gdansk, Poland
*corresponding author: edyta.slupek@pg.edu.pl

The lack of strategic management of by-products and organic waste formed in the agro-food industry sector has been noticeable over the past decade, as it has contributed to increased interest in organic matter as an alternative raw material for biofuel generation [1] [2]. The use of organic matter is an essential element of sustainable development, which allows increased energy security and thus reduces the dependence of the economy in countries on energy carriers and fuel imports.

Increasingly, hybrid microbial systems, which involve a combination of alcohol or dark fermentation and photo-fermentation processes, are being used to produce biofuels such as biohydrogen [3]. Simultaneous biorefining processes allow to increase production profits and the amount of bioenergy. In the first stage of dark fermentation, carbohydrates are converted to biohydrogen and organic acids, whereas alcohol fermentation leads to ethanol formulation. The post-processing leachate from both processes contains simple organic compounds, which could be exploited as a batch for the subsequent photo-fermentation process. The total biofuel yield obtained during the realization of the hybrid system depends on the sole carbon source supplied to microorganisms [4]. However, to our knowledge, even low ethanol concentrations in the batch for photo-fermentation can expose disinfecting properties for microbial consortia, resulting in a reduced yield of biohydrogen in photo-fermentation when compared with non-ethanol batches.

In this study, new green absorbents for the separation of ethanol (EtOH) from organic acids, such as formic acid (FA), acetic acid (AA), and propionic acid (PA), which occur in post-fermentation leachates from dark fermentation and alcohol fermentation, were proposed. The authors evaluated the absorption capacity of four deep eutectic solvents (DESs) obtained by combining terpenes such as menthol (M), thymol (Th), eugenol (E), and α-carvone (α-C) with furfural (FF). The FF used for DES formation was obtained from the detoxification of hydrolysates formed during the pre-treatment of agri-food biomass. All the DESs were prepared at a molar ratio of 1:1. The basic physicochemical properties, including density, viscosity, and surface tension, were studied in the temperature range of 20–50 °C. In addition, the chemical structures of the DES were characterized.

The absorption capacity of DES and the vapor-liquid partition coefficients (K) were determined for ethanol and selected organic acids. K was calculated using Equation (1):

$$K = \frac{C_g}{C_L} \tag{1}$$

which describes the partitioning between the vapor (C_g) and liquid (C_L) phases according to a thermodynamically controlled equilibrium constant. K values were measured using static headspace gas chromatography (SH-GC). The DESs samples were thermostated for 24h at 25 and 50 °C. The effect of temperature changes on the solubility of EtOH in the individual DES was determined in the tested range. The absorption process aims to transfer EtOH, FA, AA, and PA from the gas to the DES phase by intense contact of the polluted stream with the DES. Mass transfer depends mainly on the partition coefficient. In this study, EtOH was shown to have a significantly higher affinity for all DES than FA, AA, or PA (Figure 1). The K values obtained for EtOH were significantly lower than those obtained for organic acids. The partition coefficient values were respectively 0.0027 to 0.0064 and increased in proportion to the solubility of EtOH in the hydrogen bond acceptor (HBA). Additionally, studies have indicated that lowering the temperature had a

beneficial effect on the absorption of EtOH and other organic acids. However, increasing the temperature favorably affects the intended process of separation of ethanol from organic acids, as the affinity of EtOH for DES decreases only slightly, in contrast to organic acids.

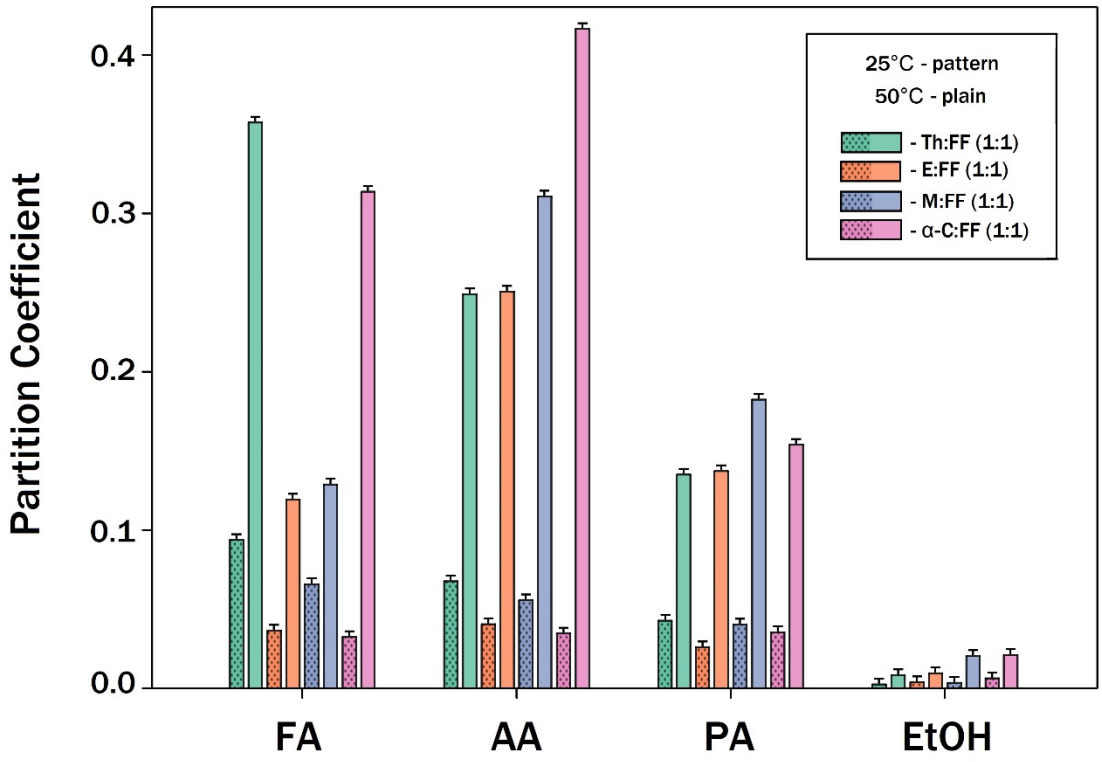

Fig. 1. Partitioning coefficients of EtOH, FA, AA, PA in DES in temperatures 25 and 50°C

This research was funded by the National Science Centre, Poland, under research project No. UMO-2021/41/B/ST8/02395

References

[1] Marone A., Izzo G., Mentuccia L., Massini G., Paganin P., Rosa S., Varrone C., Signorini A.,, Vegetable waste as substrate and source of suitable microflora for bio-hydrogen production," *Renew. Energy*, 2014, 68, 6–13.

[2] Seifert K., Zagrodnik R., Stodolny M., Łaniecki M., Biohydrogen production from chewing gum manufacturing residue in a two-step process of dark fermentation and photofermentation, *Renew. Energy*, 2018, 122, 526–532.

[3] Policastro G., Giugliano M., Luongo V., Napolitano R., Fabbricino M., Enhancing photo fermentative hydrogen production using ethanol rich dark fermentation effluents, *Int. J. Hydrogen Energy*, 2022, 47(1), 117–126.

[4] Wang B.N., Yang C.F., Lee C.M., The factors influencing direct photohydrogen production and anaerobic fermentation hydrogen production combination bioreactors, *Int. J. Hydrogen Energy*, 2011, 36(21), 14069–14077.

MIXING TIME ANALYSIS IN RECIPROCATING MIXER DEVICE

Dawid Sołoducha*[1], Tomasz Borowski[1], Marian Kordas[1], Daniel Musik[2], Krzysztof Wójcik[2], Małgorzata Sekuła-Wybańska[2], Rafał Rakoczy[1]

[1]Department of Chemical and Process Engineering, Pomeranian University of Technology in Szczecin, Piastów Ave. 42, 71-065, Szczecin, Poland
[2]ESC Global sp. z o.o., Słoneczny Sad 4F, 72-002 Dołuje, Poland
*corresponding author: dawid_soloducha@zut.edu.pl

In industrial practice, mixing process is one of the most common processes. We can find its application in many industries like chemical industry, food industry and many others. Mixing is usually carried out in an apparatus consisting of a tank with proper volume of fluid and a mechanical stirrer [1]. As studies show almost 95% of industrial applications of mixing processes are carried out in apparatus built as mentioned earlier [2], but this type of mixer does not suit well every case that we may encounter in engineering practice. It is why a new design of mixing device must be developed. In response to the demand, other types of mixing apparatus, such as static and reciprocating mixers appeared.

In this study, mixing time was used to analyse and compare five different variants of reciprocating agitator plate geometry.

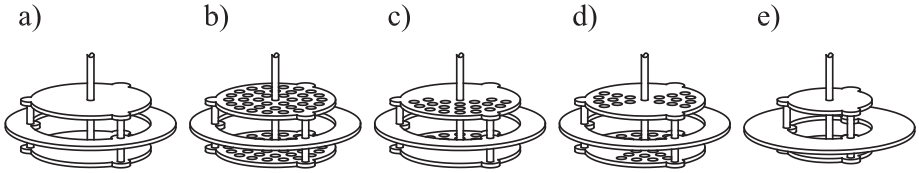

Fig. 1. Analysed geometries

The geometries differed in terms of perforation ratio and the size of reciprocating agitator plates, as illustrated in Figure 1.

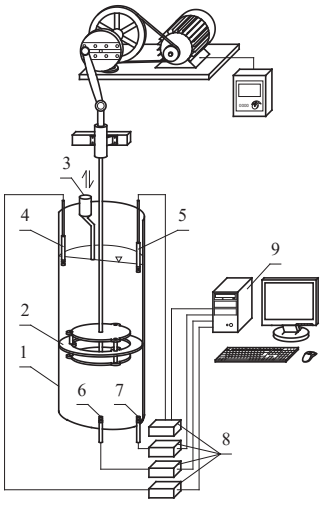

Fig. 2. Experimental setup, 1- tank; 2- stirrer; 3- tracer dosing place, 4,5,6,7 - EPP-1t conductivity probe; 8- CX-601 multifunction device; 9- computer

To obtain results, measurements of homogenization time for every variant were made. Data was obtained through tracer studies (brine was used as a tracer) carried out using a conductivity probe (EPP-1t) and a cx-601 multifunction device. The above-mentioned data allowed us to determine the mixing time using t95 method [2] according to Equation (1)

$$log\sigma^2 = log\left\{\frac{1}{4}[(G'_{n1} - 1)^2 + (G'_{n2} - 1)^2 + (G'_{n3} - 1)^2 + (G'_{n4} - 1)^2]\right\} \quad (1)$$

Where:
σ – change value,
n – measuring probe number,
G'_{nx} – normalized probe response.

To obtain results, measurements of homogenization time were taken for each variant. Data was obtained through tracer studies using brine as the tracer. Tracer studies were conducted using a conductivity probe (EPP-1t) and a CX-601 multifunction device. The data allowed us to determine the mixing time using the t_{95} method [2], according to Equation (1).

$$\Theta = f\left(Re_{p-z}\right) \rightarrow \left(\frac{t_{95} \cdot v}{D^2}\right) = \left(\frac{(4 \cdot A \cdot f) \cdot d_z}{v}\right) \quad (2)$$

Where:
Re_{p-z} – Reynolds number for reciprocating mixer [-]
A –amplitude [m]
f – frequency [Hz]
d_z – equivalent diameter of the stirrer [m]
v – kinematic fluid viscosity [m^2*s^{-1}]
t_{95} – mixing time [s]
D – tank diameter [m].

This operation made it possible to make the mixing time dependent on the turbulence and to compare different geometries of the agitator.
Obtained results allowed to conclude that the values of mixing time for the strongly perforated variants of the stirrer plate were much higher than in the case of solid plates for low turbulence in the apparatus

References

[1] Foukrach M., Bouzit M.,, Ameur H., Kamla Y., Effect of Agitator's Types on the Hydrodynamic Flow in an Agitated Tank., *Chin. J. Mech. Eng*., 2020, 33, 37.
[2] Barabash V.M., Abiev R.S., Kulov N.N., Theory and Practice of Mixing: A Review, *Theor. Found. Chem. Eng.*, 2018, 52(4), 473–487.
[3] Brown D.A.R., Jones P.N., Middletone J.C., Papadopulos G., Arik E.B., *Experimental Methods*, Handbook of Industrial Mixing, John Wiley & Sons, Ltd, 2003, pp. 145–256.

HALLOYSITE AS POTENTIALLY HIGH-ENTROPY MATERIAL FOR ADVANCED SEPARATION PROCESSES

Michał Stor, Kamil Czelej, Andrzej Krasiński*, Leon Gradoń

Faculty of Chemical and Process Engineering, Warsaw University of Technology,
Waryńskiego 1, 00-645 Warsaw, Poland

*corresponding author: andrzej.krasinski@pw.edu.pl

The properties of functional materials can be characterized according to various criteria, depending on their intended use. One of them is the value of configurational entropy, S, defined by Boltzmann as $S = k \cdot \ln W$, where k - Boltzmann constant and W is the number of real microstates corresponding to a given macrostate [1]. Entropic materials are those for which $S > 1.61\ R$, where R is the gas constant [2]. The search for material structures for separation processes, e.g. sorption, is aimed at creating nanostructured porous materials, e.g. zeolites, MOFs, nanoporous sponges and others [3]. The difference in the sorption entropy of the states of a porous structure controls the free energy of the system. It is the driving force behind the process. It can be controlled by changing the local porosity of the system. The distortions in the structure that arise in the material processing are a source of frustration (controlled use of chaotic events) that affects ion deposition, [4]. The essence of the second law of thermodynamics using the concepts and definitions of macroscopic quantities does not facilitate the analysis of phenomena occurring on a molecular scale where the tools of statistical physics are the basis. In particular, this applies to the understanding of the concept of entropy associated with the state of disorder, loss of information, or the arrow of time. Shannon [5] points out that entropy is formally identical to information, and Gell-Mann [6] argues that entropy should be seen as a measure of the lack of information. These concepts facilitate the approach to understanding the properties and designing of high-entropic materials with a given functionality, i.e. defined differences in the entropic states of the structure for the process under consideration. Increasing the entropy difference of states enhances the efficiency of the process. Another factor affecting separation is the chemical composition of the surface. This assumption inspired our research.

Halloysite is an interesting, cheap, and available raw material for creating high-entropic structures. It is one of the clay minerals that exhibits properties typical for this type of natural material – good mechanical strength, relatively large pore volumes, high surface area, and chemical inertness. The halloysite belongs to the kaolin-group minerals. The general formula can be expressed as $Al_2Si_2O_5(OH)_4 \cdot 2H_2O$ in hydrated form. The crystal structure of halloysite is defined as a two-layer structure formed by a corner-sharing $[SiO_4]$ tetrahedral layer and an edge-sharing $[AlO_6]$ octahedral layer [7, 8]. Halloysite, due to its original layered structure and chemical structure, is susceptible to the possibility of delamination and reaching high values of specific surface area. The aim of the work was to study the sorption properties and biological activity of the raw and modified material. Our preliminary theoretical considerations confirm the potential possibility of obtaining the expected results.

The atomic scale ab initio calculations revealed a significant difference in adsorption energy between the external siloxane surface, and cross-sectional interlayer surface, resulting in adsorption anisotropy. A low energy barrier facilitates the interlayer migration of heavy metals into the halloysite interior significantly increasing its sorption capacity. Thus, the experiments confirmed the theoretical prediction, which indicated a high sorption potential of halloysite towards heavy metals.

The elemental composition of raw halloysite along with purified material was performed using X-ray fluorescence spectrometer. The morphology of the halloysite samples was investigated using scanning electron microscopy imaging with energy dispersive an X-ray (EDX). The specific surface

area was determined by fitting to BET isotherm for the nitrogen adsorption-desorption process (3Flex, Micromeritics, USA).

Solutions known for their etching properties (strong, oxidizing acids and alkali) were chosen for the experiments to alter the halloysite microstructure. The primary goal of this modification was to improve sorption by increasing specific surface area and changing morphology (i.e. contributions of micropores in the structure).

The adsorption properties of the material i.e. raw and modified halloysite particles were evaluated in a batch stationary system. Magnetic stirring of the sorbent suspension was involved, and all tests were conducted at room temperature. A precisely defined amount of sorbent (mass per volume of water contaminated with heavy metal ions) was prepared in beakers. The initial concentration of contaminants in water, the mass of sorbent particles per volume of water, and process time were determined based on the preliminary research results carried out in the past.

Table 1. Comparison of parameters for raw and modified halloysite

Halloysite type	BET specific surface area [m^2/g]	Contribution of pores with diameter in range 0-3 nm [%]	Content of mineral contamination* [%]	Max. sorption capacity of Pb^{2+} ions [mg/g]
Raw	32.25	4.40	11.17	1.03
Modified	162.3	17.30	4.21	24.32

* content of metal impurities determined based on SEM-EDX analysis

Results presented in Table 1 contain a comparison of chosen structural parameters relevant for the adsorption process. It can be noticed that proper etching of the halloysite leads to a significant increase of the specific surface area and thus improves sorption capacity of lead ions from aqueous solution. Etching process affects the sample morphology, but also its chemical composition by removing the mineral contamination, which can potentially cease the transport of ions in the interlayer area of multi-walled halloysite nanotubes (HNT). Antibacterial properties of the samples depend on the amount of oxidizing additions in the structures (i.e. titanium dioxide, ferric oxide). Inhibition of microorganism growth significantly relates to the contribution of particular additions. Hence, untreated halloysite is still very effective for the inhibition of bacterial growth (bacteriostaticity).

Conducted experiments confirmed potential applications in water purification technologies as a new, functional material with adsorption properties, especially in terms of heavy metal ion separations. Additional treatment enhances surface morphology and structure of the mineral. The confirmed antibacterial effects of halloysite make it suitable to consider it to be an efficient material for various water treatment applications.

Acknowledgements

This work was supported by the Polish National Centre for Research and Development, grant no. TECHMATSTRATEG-III/0005/2019-00

References

[1] Ben-Naim A., *Entropy Demistified*, Word Scientific Publ. Com., London, 2016.
[2] Zong Y., *High-Entropy Materials*, Springer Nature, Singapore, 2019.
[3] Legrand U., Castillo Sánchez J.R., Boudreault R., Meunier J.L., Girard Lauriault P.L., Tavares J.R., Fundamental thermodynamic properties of sorbents for atmospheric water capture, *Chem. Eng. J.*, 2022, 431(2), 134058.
[4] Lee S.Y., Gradoń L., Janeczko S., Iskandar F., Okuyama K., Formation of highly ordered nanostructures by drying micrometer colloidal droplets, *ACS Nano*, 2010, 4, 4717–4724.
[5] Shannon C.E. The mathematical theory of communication, *Bell System Tech. Journal*,1948,27, 379,623
[6] Gell-Mann M. *The Quark and the Jaguar,* Abacus Book, London, 1994.
[7] Filice S., Bongiorno C., Libertino S., Compagnini G., Gradoń L., Iannazzo D., La Magna A., Scalese S., Structural Characterization and Adsorption Properties of Dunino Raw Halloysite Mineral for Dye Removal from Water, *Materials*, 2021, 14, 3676.
[8] Zhao Y., Abdullayev E., Vasiliev A., Lvov Y., Halloysite nanotubule clay for efficient water purification, *Colloid Interf. Sci.*, 2013, 406, 121–129.

PHOTOCATALYTIC ACTIVATION OF PEROXYMONOSULFATE BY CARBONIZED POLYPYRROLE@$CoFe_2O_4$/TiO_2 MAGNETIC PHOTOCATALYSTS FOR EFFICIENT IBUPROFEN DEGRADATION

Agnieszka Sulowska*, Agnieszka Fiszka Borzyszkowska, Anna Zielińska-Jurek*

Department of Process Engineering and Chemical Technology, Faculty of Chemistry, Gdańsk University of Technology, Narutowicza 11/12, 80-233 Gdańsk, Poland
*corresponding authors: agnieszka.sulowska@pg.edu.pl, annjurek@pg.edu.pl

The presence of pharmaceuticals and personal care products (PPCPs) in the environment is of increasing importance because of their documented effects on wildlife, ecosystems, and humans. Ibuprofen (IBP) is one of the most commonly used painkillers and anti-inflammatory drugs. Studies conducted in many countries around the world have shown the presence of ibuprofen in both surface waters and treated wastewater [1].

Among various AOP processes, photocatalysis utilizing sunlight is considered a promising technology for energy production and environmental remediation. The separation of photogenerated charges and utilization of sunlight are key factors that influence photodegradation efficiency. In contrast, peroxymonosulfate (PMS)-based AOP technology has become a convenient and effective method for the removal of persistent organic pollutants owing to its strong oxidative ability and mild reaction conditions [2]. Many methods or materials (semiconductors, transition metal ions, metal oxides, and non-metallic carbon materials) can be used to activate PMS [2]. Some of these methods, such as ultrasonication, UV irradiation, and electrochemical oxidation, are limited by the high energy consumption and complexity of the operation system. Transition metal-based and carbon-based catalysts are considered promising for environmental remediation because of their low cost, low toxicity, high catalytic efficiency, and magnetic recovery. Carbonization of N-containing aromatic polymers, e.g. polypyrrole, is a promising route to obtain N-doped carbon materials with low cost [3]. Additionally, the presence of spinel cobalt ferrite in the hybrid photocatalyst allowed for its easy magnetic separation from an aqueous pharmaceutical solution.

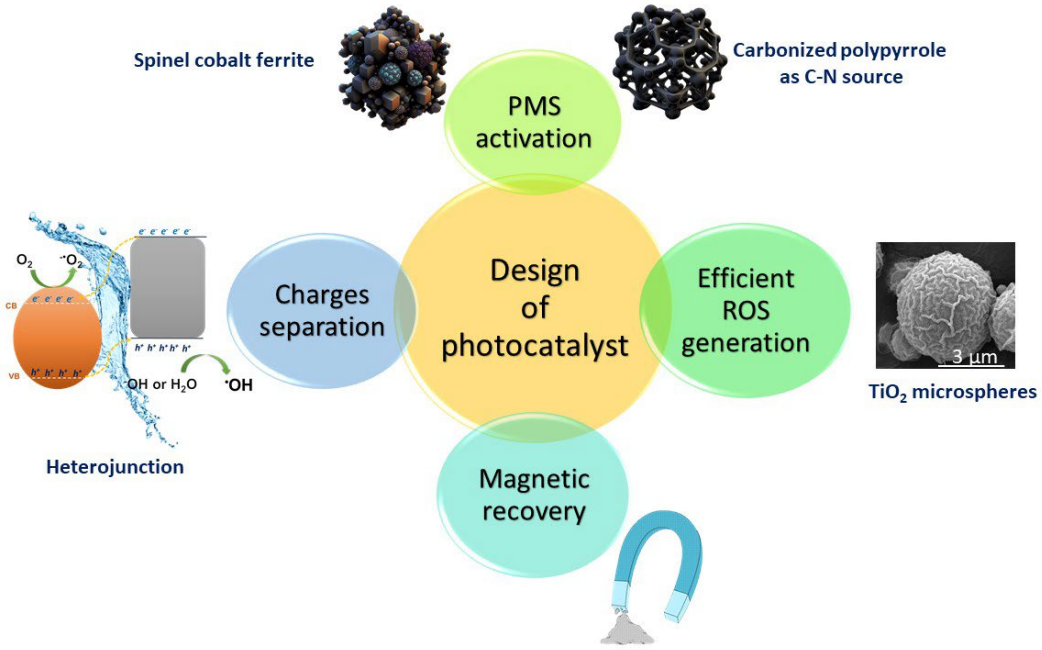

Fig. 1. Main challenges in designing photocatalysts for PPCP degradation

In this regard, the main aim of the present study was preparation of carbonized polypyrrole@$CoFe_2O_4$/TiO_2 magnetic photocatalyst for efficient ibuprofen degradation in the conjunction with PMS under simulated solar light. Fig. 1 presents the main challenges in designing photocatalysts for PPCP degradation, which were considered in this work. PMS can produce in-situ highly reactive sulfate radical ($SO_4^{\bullet -}$) and other ROSs (e.g., •OH) that can oxidize and decompose organic pollutants. In this work, both carbonized N-doped polymer and cobalt ferrite activated PMS [2,3]. The properties of the as-prepared photocatalysts were tested using X-ray diffraction (XRD), X-ray photoelectron spectroscopy (XPS), scanning electron microscopy (SEM), Fourier transform infrared spectroscopy (FTIR), specific surface area (BET) measurements, photoluminescence spectroscopy (PL), and diffuse reflectance spectroscopy (DRS). The effects of PMS concentration (1-10 mM), and solution pH (3-9) on the degradation of ibuprofen in aqueous solution with the PMS/light system were studied in detail. Carbonized polypyrrole@$CoFe_2O_4$/TiO_2 magnetic particles revealed improved ibuprofen degradation, which reached 70 % of ibuprofen mineralization after 60 min in PMS/UV-Vis light system.

Acknowledgments

This research was financially supported by the Polish National Science Centre (grant no. NCN 2018/30/E/ST5/00845).

References

[1] Santos J.L., Aparicio I., Callejón M., Alonso E., Occurrence of pharmaceutically active compounds during 1-year period in wastewaters from four wastewater treatment plants in Seville (Spain), *J. Hazard. Mater.*, 2009, 164, 1509–1516.

[2] Wang J., Wang S., Activation of persulfate (PS) and peroxymonosulfate (PMS) and application for the degradation of emerging contaminants, *Chem. Eng. J.*, 2018, 334, 1502–1517

[3] Hu P., Su H., Chen Z., Yu C., Li Q., Zhou B., Alvarez P.J.J., Selective Degradation of Organic Pollutants Using an Efficient Metal-Free Catalyst Derived from Carbonized Polypyrrole via Peroxymonosulfate Activation, *Environ. Sci. Technol.*, 2017, 51(19), 11288–11296

SURFACE ENGINEERING OF ANTIMICROBIAL DECORATED MICROPARTICLES

Weronika Szczęsna[1]*, Łukasz Lamch[1], Ewa Zboińska[2], Kazimiera A. Wilk[1]

[1]Department of Engineering and Technology of Chemical Processes, Faculty of Chemistry, Wrocław University of Science and Technology, Wybrzeże Wyspiańskiego 27, 50-370 Wrocław, Poland
[2]Department of Organic and Medicinal Chemistry, Faculty of Chemistry, Wrocław University of Science and Technology, Wybrzeże Wyspiańskiego 27, 50-370 Wrocław, Poland
*corresponding author: weronika.szczesna@pwr.edu.pl

The design of multifunctional carrier systems delivering various therapeutic drugs has attracted a considerable interest in scientific investigations. [1] Surface functionalization of microcarriers with various functional groups gives an opportunity to develop a variety of multipurpose systems. The effective strategy of microparticle surface engineering is the layer-by-layer (LbL) self-assembly technique that allows to design multilayered microcarriers with functional coatings. [2, 3] The design of new polyelectrolytes (PEs) bearing different antimicrobial moieties as building blocks for the construction of LbL microcapsules is a highly efficient approach to develop functional materials with antimicrobial features.

The main goal of the present work was to fabricate hydrogel microparticles functionalized with antimicrobial PEs and loaded with resveratrol (RES) as a chemotherapeutic agent. Thus, poly(diallyldimethylammonium chloride) (PDADMAC) was decorated with different percent degrees of substitution (n) of an antimicrobial agent such as thymol (THYM). The synthesis of functionalized PDADMAC was carried out using selective demethylation of PDADMAC followed by requaternization using THYM derivatives. We fabricated RES-loaded microcapsules composed of alginate (ALG) or chitosan (CHIT) core and LbL coatings consisting of the prepared PDADMAC derivatives as an outer layer with antimicrobial function. The structure of prepared PEs was characterized with ^{1}H NMR and FTIR analysis. The particle size and morphology of the microparticles were characterized with SEM. The encapsulation efficiency of RES and its release profile from the microcarriers were studied using UV-Vis spectrophotometry. The antimicrobial properties of decorated PDADMAC and coated microparticles were assessed against *Escherichia coli* and *Staphylococcus aureus* using broth microdilution method. The design and use of new advanced functionalized polyelectrolytes as outer coatings of carriers allowed the formation of microcapsules with desirable antimicrobial function. The constructed multipurpose systems with the controlled manner release of bioactive agent could be a promising tool in drug delivery technology.

Acknowledgements: This work has been supported by National Science Centre, Poland within the PRELUDIUM 21 program (2022/45/N/ST4/01308) and by a statutory activity subsidy from the Polish Ministry of Science and Higher Education for the Faculty of Chemistry of the Wrocław University of Science and Technology.

References

[1] Duan S., Wu R., Xiong Y., Ren H., Lei C., Zhao Y., Zhang X., Xu F., Multifunctional antimicrobial materials: From rational design to biomedical applications, *Prog. Mater. Sci.,* 2022, 125, 100887.
[2] Szczesna W., Tsirigotis-Maniecka M., Lamch Ł., Szyk-Warszynska L., Zboinska E., Warszynski P., Wilk K.A., Multilayered Curcumin-Loaded Hydrogel Microcarriers with Antimicrobial Function, *Molecules,* 2022, 27, 1415.
[3] Belbekhouchea S., Bousserrhineb N., Alphonseb V., Carbonnier B., From beta-cyclodextrin polyelectrolyte to layer-by-layer self-assembly microcapsules: From inhibition of bacterial growth to bactericidal effect, *Food Hydrocoll.,* 2019, 95, 219–227.

PROLIFERATION OF *RINDERA GRAECA* TRANSGENIC ROOTS ON 3D-PRINTED POLY(LACTIC ACID)-BASED SCAFFOLDS

Kamil Wierzchowski[1,*], Rafał Podgórski[1], Piotr Kowalczyk[1], Mateusz Kawka[2], Katarzyna Sykłowska-Baranek[2], Tomasz Ciach[1], Maciej Pilarek[1]

[1]Faculty of Chemical and Process Engineering, Warsaw University of Technology, Waryńskiego 1, 00-645 Warsaw, Poland
[2]Department of Biology and Pharmacognosy, Faculty of Pharmacy, Medical University of Warsaw, Banacha 1, 02-097 Warsaw, Poland
*corresponding author: Kamil.Wierzchowski.dokt@pw.edu.pl

Nowadays, up to 75% of small-molecule anticancer drugs originate from natural plant-derived products. In the modern pharmaceutical industry, plants are used as renewable feedstock for potential anticancer drug agent production [1]. The application of *in vitro* techniques for transgenic (i.e., hairy) root cultures provides the possibility to maintain plant biomass with plentiful options for parameter optimization and to exceed natural productivity observed in wild plants. Furthermore, the *in vitro* cultures of plant biomass provide significant advantages against conventional methods, overcoming limitations imposed by native metabolism pathways, environmental factors, or legal issues [2]. Systems for plant cells and tissues *in vitro* cultures also allow precise control of culture microenvironment, influencing biomass growth and the yielding of secondary metabolites [3]. In plants, secondary metabolites play an important role in defense against bacterial or fungal infections and adaptation to a constantly changing environment. They are biosynthesized *de novo* in response to various biotic and abiotic stress factors, and this phenomenon might be applied to stimulate the production of plant-derived metabolites in cultures of plant biomass [4].

Biomass immobilization is a practical technique recognized as a high-potential solution for scaling up *in vitro* cultures of hairy roots. Such a technique provides a suitable microenvironment for plant biomass propagation by protecting fragile transgenic roots from shear forces caused by the agitation of the culture system [5]. Also, the immobilization of plant biomass enhances the productivity of valuable metabolites. Due to metabolic pathway characteristics, hairy roots are characterized by enhanced growth kinetics and intensified production of secondary metabolites with altered phytochemical profiles [6].

The aim of this study was to investigate proliferation of *Ringera graeca* transgenic roots *in vitro* cultured on 3D-printed scaffolds made of poly(lactic acid) (PLA). Transgenic roots were maintained for 28-days in 6 independent systems, i.e. (i) non-immobilized biomass (as reference), and as biomass immobilized on PLA constructs varied in morphology: (ii) solid scaffold, (iii) solid scaffold with 3mm gaps, (iv) scaffold with 60-degree mesh, (v) scaffold with 90-degree mesh and (vi) disintegrated PLA. For each system, the increase of fresh biomass was qualitatively determined.

The scaffolds made of PLA (φ = 4 cm, 0.3 cm of thickness) were separately placed in 250 cm^3 Erlenmeyer flasks containing 50 cm^3 of hormone-free DCR medium. Next, 1 g of 28-day *R. graeca* transgenic roots were poured onto the upper surface of the tested constructs. All culture systems were incubated at 24°C in dark conditions for 28 days on the oscillatory shaker at 105 rpm.

The proliferation of *R. graeca* hairy roots was identified by the fresh biomass (FB_{28}) increase values determined with:

$$FB_{28} = m_{28}\, m_0{}^{-1}\ [-] \tag{1}$$

where m_{28} is fresh biomass weight on the 28th day of culture, and m_0 is biomass inoculum weight.

The values of specific growth rate (μ), which characterize the *R. graeca* roots growth rate in studied systems, were determined according to the following equation:

$$\mu = (\ln m_{28} - \ln m_0)\ (\Delta t)^{-1}\ [h^{-1}] \tag{2}$$

where Δt is the time of culture.

The values of FB_{28} noted for *R. graeca* hairy roots proliferated on scaffolds made of PLA after 28 days of culture are compared in Fig. 1A. The highest value of FB_{28} was observed for the PLA scaffold with 90-degree mesh. However, almost the same FB_{28} value was noticed for the PLA scaffold with 60-degree mesh and the disintegrated scaffold. For other integrated PLA constructs, the FB_{28} value was similar to the values obtained for the reference system.

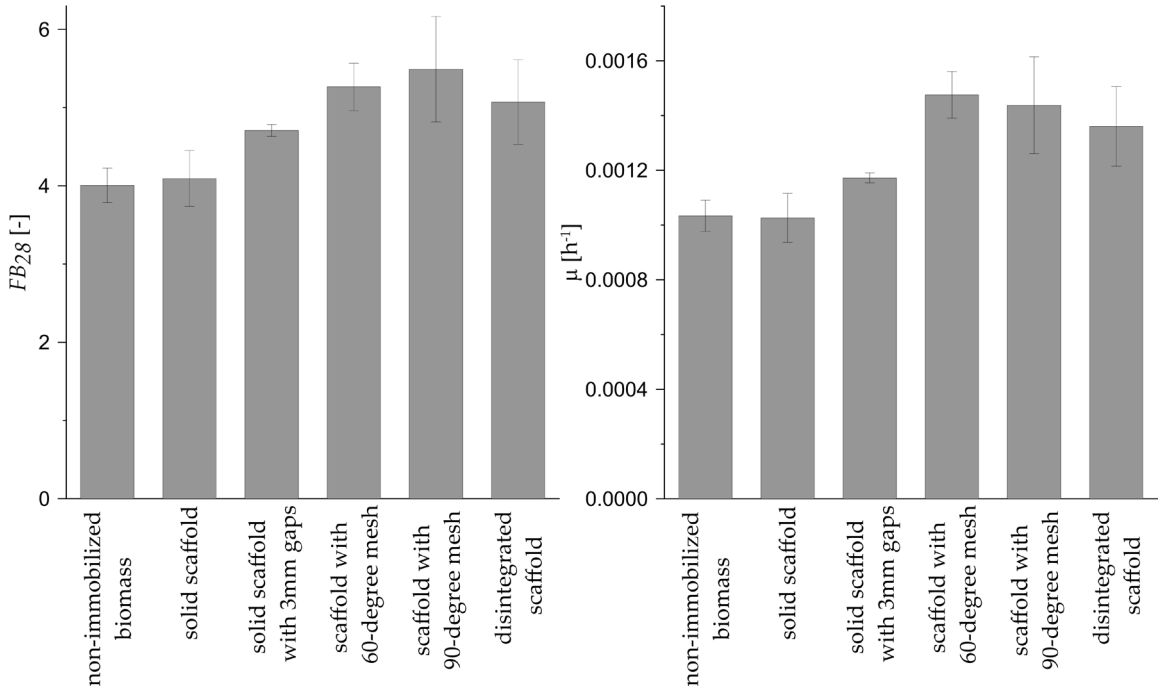

Fig. 1. The values of FB_{28} (**A**) and μ (**B**) characterize *in vitro* proliferation of *R. graeca* hairy roots cultured in the reference system and on scaffolds made of PLA

In the case of μ values (Fig. 1B.), the highest value of this parameter was noticed for the PLA scaffold with 60-degree mesh, but those values were almost the same as those obtained for the PLA scaffold with 90-degree mesh and the disintegrated PLA. For both solid PLA constructs, the μ values were at the same level as the value for the reference system.

In conclusion, both PLA scaffolds with mesh and the disintegrated PLA scaffold promote the proliferation of *R. greaca* transgenic roots. This may be caused by the mechanical protection properties of meshed constructs inside those transgenic roots which can elongate under favorable conditions without significant impact of shear forces destroying their fragile structure.

Funding: This research was funded by National Science Centre (NCN), Poland, grant no. 2021/41/N/ST8/00958.

References

[1] Seca A., Pinto D., Plant secondary metabolites as anticancer agents: successes in clinical trials and therapeutic application, *Int. J. Mol. Sci.*, 2018, 19, 263.
[2] Espinosa-Leal C.A., Puente-Garza C.A., García-Lara S., In vitro plant tissue culture: means for production of biological active compounds, *Planta*, 2018, 248, 1–18.
[3] Guerriero G., Berni R., Muñoz-Sanchez J., Apone F., Abdel-Salam E.M., Qahtan A.A., Alatar A.A., Cantini C., Cai G., Hausman J.-F., Siddiqui K.S., Hernández-Sotomayor S.M.T., Faisal M., Production of plant secondary metabolites: examples, tips and suggestions for biotechnologists, *Genes* 2018, 9, 309.
[4] Sarsaiya S., Shi J., Chen J., Bioengineering tools for the production of pharmaceuticals: current perspective and future outlook, *Bioengineered* 2019, 10, 469–492.
[5] Nowak B., Kawka M., Wierzchowski K., Sykłowska-Baranek K., Pilarek M., MTMS-based aerogel constructs for immobilization of plant hairy roots: effects on proliferation of *Rindera Graeca* biomass and extracellular secretion of naphthoquinones, *J. Funct. Biomater.* 2021, 12, 19.
[6] Wierzchowski K., Nowak B., Kawka M., Więckowicz P., Dąbkowska-Susfał K., et al., Selective impact of MTMS-based xerogel morphology on boosted proliferation and enhanced naphthoquinone production in cultures of *Rindera Graeca* transgenic roots, *Int. J. Mol. Sci.* 2022, 23, 13669.

THE INFLUENCE OF BIOINK RHEOLOGICAL PROPERTIES ON MECHANICAL PROPERTIES OF PRODUCTS

Aleksandra Wojciechowska*, Beata Butruk-Raszeja

Warsaw University of Technology, Faculty of Chemical and Process Engineering, Waryńskiego 1, 00-645 Warsaw, Poland
*corresponding author: Aleksandra.Wojciechowska2.dokt@pw.edu.pl

Cardiovascular diseases are a very important issue due to their high mortality rate. They are one of the most common causes of death worldwide. Nowadays, they are mainly treated with native vein or artery segment transplantation, which is not always possible. Due to that fact, we need to design artificial vessels. Currently, synthetic materials can be successfully used as vascular prostheses when the graft diameter exceeds 6 mm [1]. However, there is still a problem with manufacturing functional small-diameter vascular prostheses due to formation of blood clots which can cause vessel occlusion.

One of the methods which can solve this problem is bioprinting. This method allows to create designed constructs that can mimic native tissue. It is realized by usage of biocompatible materials with all the advantages of classical 3D printing. The advantage of this method is the ability to control process parameters and therefore the structure and properties of designed components. This process is extremely precise and repeatable which makes it easy to implement it in biological applications [2]. Using bioprinters we can design products which can have complex microarchitecture, including layer composition, porosity and morphology of printed components. What is also important, bioprinting makes it possible to use living cells suspended in bioink. All these advantages make this process promising for use in the manufacturing of vascular prostheses.

Bioink, which is to be used in bioprinting, has to be biocompatible, i.e. it needs to have low cytotoxicity, no inflammatory response and allow transport of substrates to and from cells. Because bioink needs to be extruded from the printing head, it needs to have proper viscosity in conditions of pressure and temperature which are not destructive to the cells. On the other hand, bioinks need to be cross-linked to preserve the shape of product. That is why it is important to use the appropriate cross-linking method specific to the composition of the chosen bioink [3]. In case of artificial blood vessels, mechanical strength of the product should be high enough to withstand pressure induced by the blood flow. These are the key conditions to be met in production of vascular prostheses.

In this work, we decided to study the influence of bioink viscosity on the mechanical strength of the product and compare it with polymer constructs. As bioinks we used alginate, methacrylated alginate and collagen bioinks, each in four different concentrations, obtaining twelve different bioink compositions. We examined viscosity of hydrogels with rotational rheometer. Then we chose bioprinting process parameters for each bioink and polymer. All constructs were printed using Bio X bioprinter (CellInk, Sweden). In the case of polymers, we have used the thermoplastic head, to achieve higher temperatures needed to melt them. Because of their biocompatibility we focused on investigations on different polyurethane types. As those are the first studies of bioprinting of these products, we decided to print square-shaped constructs. To better compare the mechanical properties, all of printed constructs had the same dimensions for each bioink composition. Eventually, we examined mechanical strength and porosity for all printed constructs using for example scanning electron microscopy.

These studies helped us in further selection of bioinks for vascular prosthesis bioprinting. The viscosity and mechanical strength are the key parameters in this process. Therefore, it is necessary to use only those materials which can be successfully extruded using typical bioprinters and for which the printed products are able to withstand the conditions typically connected with blood flow. Even though it was not analyzed in this study, it is possible that polymer scaffolds are needed in some printing strategies to provide the mechanical support for the bioprinted structure. Therefore,

it is important to know if all types of polyurethanes are printable to be used as such scaffolds and how it affects the properties of whole structures.

Funding:

The work was supported by the National Science Centre, Poland (grant no. UMO-2020/39/I/ST5/01131).

References

[1] Xiangkui R., Yakai F., Jintang G., Haixia W., Qian L., Jing Y., Xuefang H., Juan L., Nan M., Wenzhong L., Surface modification and endothelialization of biomaterials as potential scaffolds for vascular tissue engineering applications, *Chem. Soc. Rev.,* 2015, 44(15), 5680–5742.

[2] Sundaramurthi, D., Rauf, S., Hauser, C., 3D bioprinting technology for regenerative medicine applications., *Int. J. Bioprint*., 2016, 2(2), 9—26.

[3] Decante G., Costa J.B., Silva-Correia J., Collins M.N., Reis R.L., Oliveira J.M., Engineering bioinks for 3D bioprinting, *Biofabrication*, 2021, 13, 032001

MEMBRANE BIOFOULING CAUSED BY *BACILLUS CEREUS* BACTERIA

Piotr Woźniak*, Marek Gryta

West Pomeranian University of Technology in Szczecin, Pułaskiego 10, 70-322 Szczecin, Poland
*corresponding author: Piotr.Wozniak@zut.edu.pl

The presence of microorganisms inside the membrane installation causes membrane biofouling. It is the result of deposition and growth of microorganisms on membrane surfaces. Biofouling is regarded as not only the attachment/growth of microbial cells but also as the adsorption of organic matter produced by microorganisms, such as soluble microbial products and extracellular polymeric substances (EPS) [1, 2]. It is generally accepted that polysaccharides and proteins are the major components of EPS which show high adhesion ability to the presence of both hydrophilic and hydrophobic sites.

Chemical disinfection has been proposed to control biofouling during membrane processes. However, bacteria embedded in a biofilm are more resistant to biocides than the same bacteria in a dispersed state [3]. Thus, some bacteria survive disinfection, and water systems usually cannot be kept sterile over a long period. Moreover, dead biomass provides nutrients and suitable surfaces for further growth of cells imported with raw water and simulates regrowth of incompletely killed biofilm organisms.

In the examined case, the ultrafiltration installation was washed with solutions of phosphoric acid (0.5%), alkaline membrane cleaner P3 Ultrasil 11 (pH = 10.8), 75% propanol alcohol solution and then rinsed with DI water several times. A polyethersulfone (PES) membrane was assembled in the installation and stabilized with DI water at a pressure of 3 bar. After a few days, a significant drop in the permeate flux was observed. As shown by SEM studies, this finding was caused by biofouling (Fig. 1).

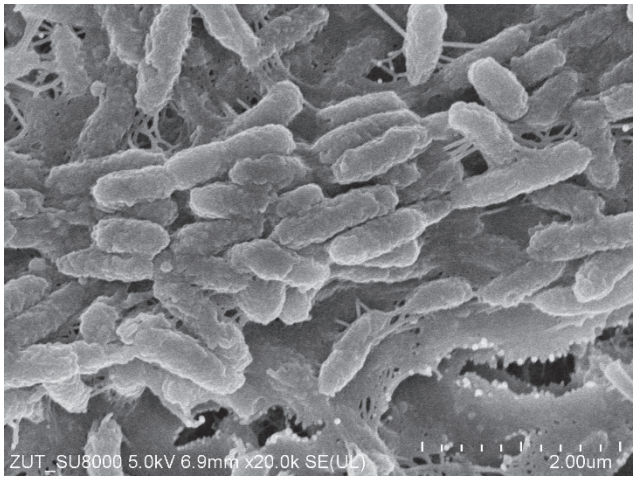

Fig. 1. SEM image of PES membrane covered by organic deposit with bacteria cells

Microbial identification was performed with mass spectrometry using a MALDI Biotyper®(MBT) instrument from Bruker (Bruker Daltonik GmbH, Bremen, Germany). Bacterial species were determined by comparing the mass spectrum of the microorganism under study with IVD's MBT mass spectra reference library of 4194 species.

In addition to the dominant bacterium (*Bacillus cereus* - Fig. 2), several other types were detected, such as *Acidovorax temperans*, *Chryseobacterium gambini*, *Stenotrophomonas maltophilia*, *Pseudomonas aeruginosa* and *Ochrobactrum anthropic*.

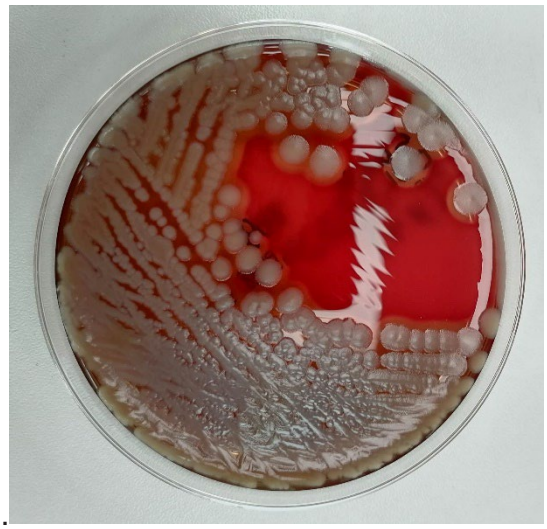

Fig. 2. *Bacillus cereus* bacterial colony growth in the Columbia LAB-AGAR™ Base medium

Bacillus cereus is a well-known foodborne pathogen capable of causing two types of gastrointestinal diseases and emesis. These bacteria multiply very quickly and show resistance to chemicals and elevated temperatures [3]. Therefore, limiting membrane biofouling caused by the above-mentioned bacteria is extremely difficult.

Acknowledgements

The publication was financed from the Polish budget within a framework of the programme of the Minister of Education and Science in Poland entitled “Science for the Society”, project No. NdS/538617/2021/2022, amount of funding 352 135 PLN, total amount of funding 352 135 PLN.

SCIENCE FOR THE SOCIETY

References

[1] Wang Z., Ma J., Tang Ch., Kimura K., Wang Q., Han X., Membrane cleaning in membrane bioreactors: A review, *J. Membr. Sci.,* 2014, 468, 276–307.

[2] Matin A., Khan Z., Zaidi S.M.J., Boyce M.C., Biofouling in reverse osmosis membranes for seawater desalination: Phenomena and prevention, *Desalination*, 2011, 128, 1–16.

[3] Huang Y., Flint S.H., Palmer J.S., *Bacillus cereus* spores and toxins – The potential role of biofilms, *Food Microbiology*, 2020, 90, 103493.

Posters

Students' posters

CONJUGATES OF AMINO ACID ALKYL ESTERS AND IBUPROFEN AS AN ALTERNATIVE TO THE COMMONLY USED DRUG – IBUPROFEN

Karolina Bilska, Paula Ossowicz-Rupniewska*

West Pomeranian University of Technology in Szczecin, Faculty of Chemical Technology and Engineering, Department of Chemical Organic Technology and Polymeric Materials, Piastów 42, 71-065 Szczecin, Poland

*corresponding author: possowicz@zut.edu.pl

Ibuprofen, or (RS)-2-[4-(2-methylpropyl)phenyl]propanoic acid, is one of the most commonly used drugs in the group of non-steroidal anti-inflammatory drugs. This drug has a wide spectrum of action: analgesic, anti-inflammatory, and antipyretic. Although it can be considered relatively safe, especially with long-term use, it can cause many side effects, particularly those affecting the gastrointestinal tract and the cardiovascular system or kidneys [1]. In addition, ibuprofen is characterised by poor solubility in water, which reduces the permeability of the active substance through biological membranes [2, 3].

New NSAID derivatives with improved solubility and increased bioavailability are sought. Modifications of NSAIDs are also intended to increase the drug's plasma half-life. Preparations belonging to this group of drugs have a negative effect on the digestive tract; they can cause damage to the gastric mucosa. Designing new NSAID derivatives is aimed at minimising side effects in the digestive system [4, 5]. Most drugs are administered orally or enterally. One way to reduce gastrointestinal side effects is to develop transdermal drug delivery systems [6].

As a result of the research, ibuprofen derivatives were obtained in the form of conjugates with amino acid alkyl esters with potential pharmacological use. These compounds were obtained as a result of the reaction of the amino acid alkyl ester hydrochloride with ibuprofen (reaction scheme – Figure 1).

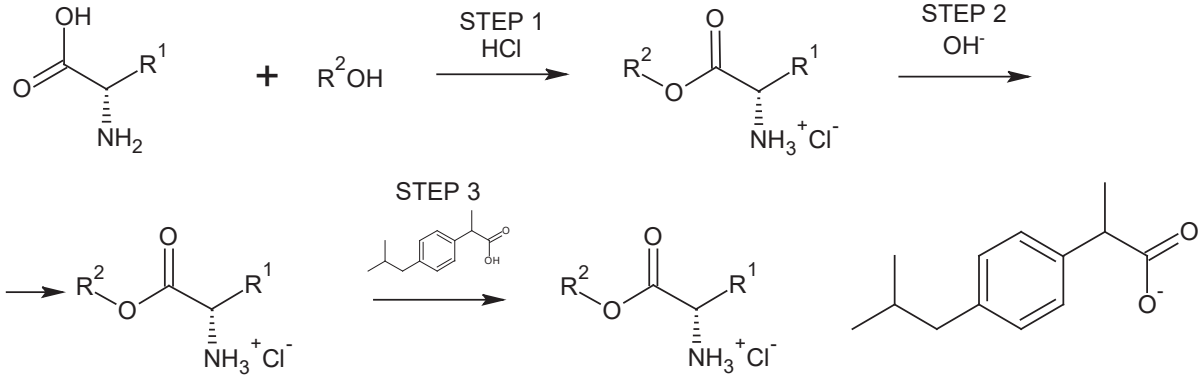

Fig. 1. Reaction scheme for the preparation of amino acid ester ibuprofenates

The obtained products were identified using nuclear magnetic resonance spectroscopy (1H-NMR, 13C-NMR) and infrared spectroscopy (FTIR/ATR). Physicochemical properties such as rotation of polarised light, thermal stability, melting points, water solubility, and lipophilicity were determined. In addition, the biodegradability, skin permeability, and skin accumulation of the obtained conjugates were determined. The modification of non-steroidal anti-inflammatory drugs, in the form of an amino acid alkyl ester salt is aimed at increasing the solubility and permeability through biological membranes. The transformation of non-steroidal anti-inflammatory drugs from the acid form to the amino acid salt form is also intended to reduce the occurrence of side effects on the digestive system and the phenomenon of polymorphism.

This research was funded by National Centre for Research and Development (project no. LIDER/53/0225/L-11/19/NCBR/2020).

References

[1] Wongrakpanich S., Wongrakpanich A., Melhado K., Rangaswami J., A Comprehensive Review of Non-Steroidal Anti-Inflammatory Drug Use in The Elderly, *Aging and Disease*, 2018, 9, 143–150.
[2] Janus E., Ossowicz P., Klebeko J., Nowak A., Duchnik W., Kucharski Ł., Klimowicz A., Enhancement of ibuprofen solubility and skin permeation by conjugation with l-valine alkyl esters, *RSC Advances*, 2020, 10(13) 7570–7584.
[3] Ossowicz-Rupniewska P., Klebeko J., Świątek E., Bilska K., Nowak A., Duchnik W., Kucharski Ł., Struk Ł., Wenelska K., Klimowicz A., Janus E., Influence of the Type of Amino Acid on the Permeability and Properties of Ibuprofenates of Isopropyl Amino Acid Esters*, Int. J. Mol. Sci.*, 2022, 23(8), 4158–4184.
[4] Perković I., Rajić Džolić Z., Zorc B., A convenient synthesis of new NSAID esters containing amino acid, urea and amide moieties, *Acta Pharm.*, 2013, 63, 409–418.
[5] Elsaman T., Ali M., Nonsteroidal Anti-Inflammatory Drugs (NSAIDs) Derivatives with Anti-Cancer Activity, *Am. J. Res. Commun.*, 2016, 4.
[6] Alkilani A., McCrudden M., Donnelly R., Transdermal Drug Delivery: Innovative Pharmaceutical Developments Based on Disruption of the Barrier Properties of the stratum corneum, *Pharmaceutics*, 2015, 7, 438–470.

INTERCALATING COMPOUNDS IN PRODUCTION OF FLAKE GRAPHENE VIA DIRECT EXOLIATION IN SUPERCRITICAL CARBON DIOXIDE

Małgorzata Djas[1,2]*, Marek Henczka[2], Przemysław Rakowski[1]

[1]Łukasiewicz Research Network – Institute of Microelectronics and Photonics, Lotników Ave. 32/46, 02-668 Warsaw, Poland
[2]Faculty of Chemical and Process Engineering, Warsaw University of Technology, Waryńskiego 1, 00-645 Warsaw, Poland
*corresponding author: malgorzata.djas@imif.lukasiewicz.gov.pl

Graphene is a material that finds applications within multiple branches of most versatile industries thanks to its outstanding properties both electrical [1] and mechanical [2]. However, methods of producing high-quality graphene with high yield are not yet fully developed. One way of producing flake graphene is direct exfoliation of graphite. This process can be conducted in organic solvents like N-methylpyrrolidone (NMP), N,N-dimethylacetamide (DMA), γ-butyrolactone (GBL) and 1,3-dimethyl-2-imidazolidinone (DMEU) [3], but also in supercritical fluids like methanol, water or carbon dioxide [4]. Supercritical carbon dioxide ($scCO_2$) is the most promising solvent due to its relatively low critical parameters, environmental friendliness and physicochemical properties (low surface tension, high diffusivity, low kinematic viscosity). The scheme of graphene production using direct exfoliation in $scCO_2$ is shown in Fig. 1. In the considered process, $scCO_2$ acts not only as a solvent but also as an intercalating compound furthermore improving the efficiency of graphite exfoliation.

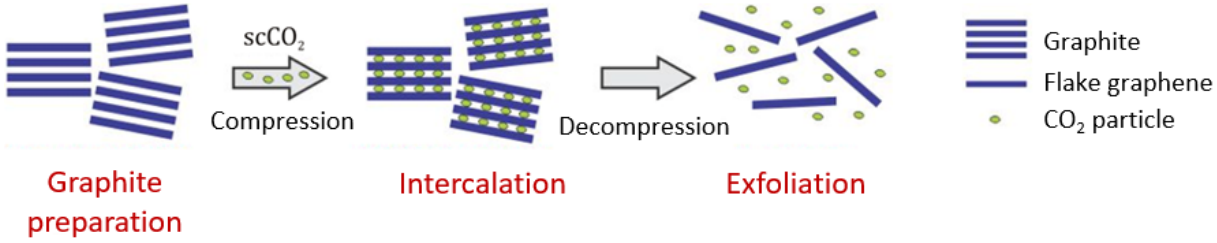

Fig. 1. Steps of flake graphene production from graphite using $scCO_2$

Although graphene production using $scCO_2$ has many advantages, there are areas that are in dire need of improvement. Graphene production yield is low and the ultrasonication process takes multiple hours to complete. In this work, in order to improve the efficiency of graphite exfoliation, the addition of external intercalating compounds in the method of direct graphite exfoliation in $scCO_2$ coupled with ultrasounds (US) was investigated. The intercalation stage was conducted directly before exfoliation via ultrasounds in $scCO_2$ in the same apparatus as the main process. As intercalating substances 2-naphthol and vanillin were used. The exfoliation process was also carried out with the addition of cosolvent – ethyl alcohol. The investigation of flake graphene production using $scCO_2$ was conducted using the experimental system shown in Fig. 2.

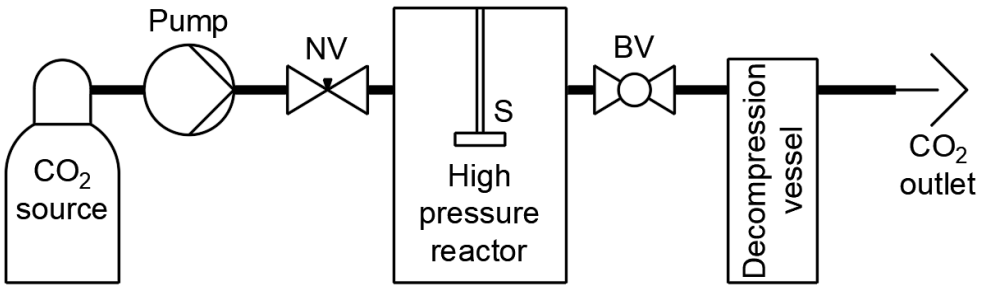

Fig. 2. Scheme of experimental system (NV – needle valve, BV – ball valve, S – sonotrode)

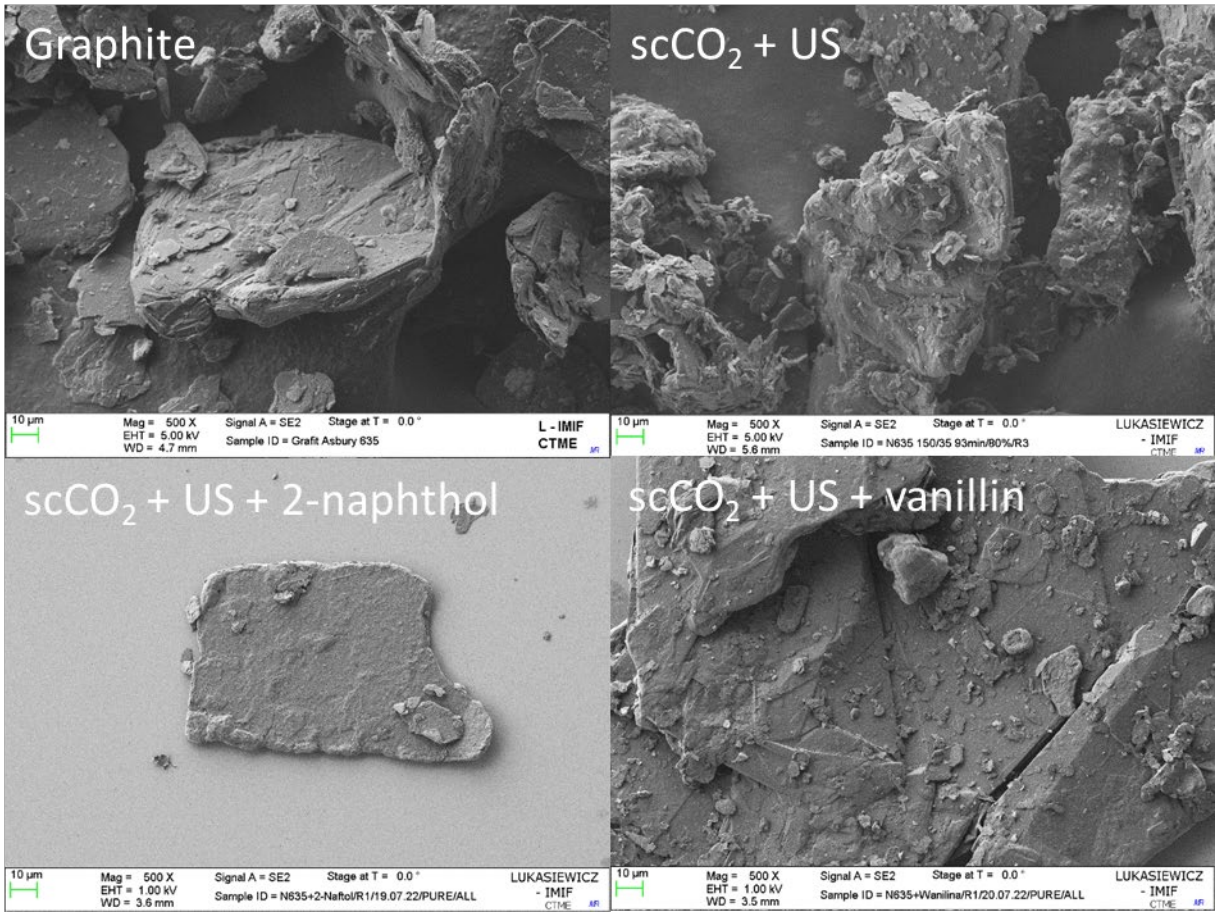

Fig. 3. SEM images of graphene material at magnitude 500 X

In Fig. 3 scanning electron microscope (SEM) images of the obtained material — multilayer graphene are presented. The results, based on Raman spectroscopy, indicate more efficient exfoliation when, as intercalating compound, vanillin was used than in the case of 2-naphthol. When intercalation was coupled with ethyl alcohol as the cosolvent, exfoliation was more efficient with the addition of 2-naphthol than vanillin. Cosolvent influence in the process of exfoliation is not straightforward as shown by results.

The research was funded by National Science Centre, Poland – grant "Identification of mechanisms and investigations of flake graphene production by direct exfoliation using supercritical carbon dioxide", project number 2019/35/D/ST8/02977.

References

[1] Sang M., Shin J., Kim K., Yu K.J., Electronic and Thermal Properties of Graphene and Recent Advances in Graphene Based Electronics Applications, *Nanomaterials,* 2019, 9(3), 374.
[2] Papageorgiou D.G., Kinloch I.A., Young R.J., Mechanical properties of graphene and graphene-based nanocomposites, *Prog. Mater. Sci.,* 2017, 90, 75–127.
[3] Hernandez Y., Nicolosi V., Lotya M., Blighe F.M., Sun Z., De S., McGovern I.T., Holland B., Byrne M., Gun'Ko Y.K., Boland J. J., Niraj P., Duesberg G., Krishnamurthy S., Goodhue R., Hutchison J., Scardaci V., Ferrari A.C., Coleman J.N., High-yield production of graphene by liquid-phase exfoliation of graphite, *Nature Nanotech.,* 2008, 3(9), 563–568.
[4] Gao H., Hu G., Graphene production via supercritical fluids, *RSC Adv.,* 2016, 6(12), 10132–10143.

INFLUENCE OF RAW MATERIAL TYPE ON EFFICIENCY OF FLAKE GRAPHENE PRODUCTION BY DIRECT EXFOLIATION USING SUPERCRITICAL CO_2

Marek Henczka[1], Małgorzata Djas[1,2,*], Izabela Bilicka[1]

[1]Faculty of Chemical and Process Engineering, Warsaw University of Technology, Waryńskiego 1, 00-645 Warsaw, Poland
[2]Łukasiewicz Research Network – Institute of Microelectronics and Photonics, Lotników 32/46, 02-668 Warsaw, Poland
*corresponding author: malgorzata.djas@imif.lukasiewicz.gov.pl

The aim of this study was to investigate the effect of the type of raw material – graphite on the efficiency of graphene production by direct exfoliation using supercritical carbon dioxide. In the process, supercritical CO_2 acts as a solvent, an intercalating agent and an agent for the separation of carbon layers in graphite. The use of supercritical CO_2 allows the elimination of organic solvents, dangerous to the environment and human health, used in the classical direct exfoliation method. In addition, CO_2 has relatively low critical parameters (T = 31.1°C and P = 7.4 MPa), is non-toxic and non-flammable, and upon expansion transforms into a gaseous state leaving no impurities in the final product.

In the experiments, natural graphite and expanded graphite were used as the starting material for flake graphene production. The direct exfoliation process using supercritical CO_2 was carried out with simultaneous ultrasonication. The experimental system for flake graphene production using $scCO_2$ is shown in Fig. 1. The following material characterization techniques were used to determine the efficiency of the investigated flake graphene production method: scanning electron microscopy (SEM) and Raman spectroscopy.

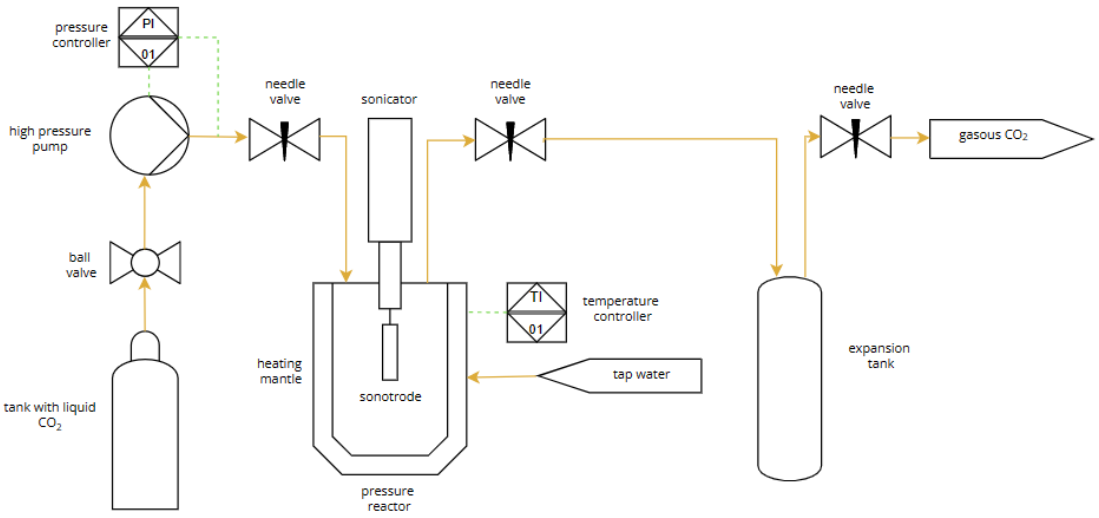

Fig. 1. Scheme of the experimental system for the flake graphene production using $scCO_2$

Figures 2 and 3 present SEM images of starting materials and materials after exfoliation. The experimental results showed that a higher efficiency of flake graphene production was obtained by using expanded graphite compared to natural graphite. Natural graphite is characterized by a structure of closely packed carbon layers, and as a result, CO_2 molecules find it more difficult to penetrate the spaces between the carbon layers. Expanded graphite has far greater interlayer spaces, into which the carbon dioxide molecules penetrate more easily, thus facilitating the delamination process compared to natural graphite. It was found that the exfoliation of expanded graphite in supercritical CO_2 results in the formation of graphene nanoplatelets.

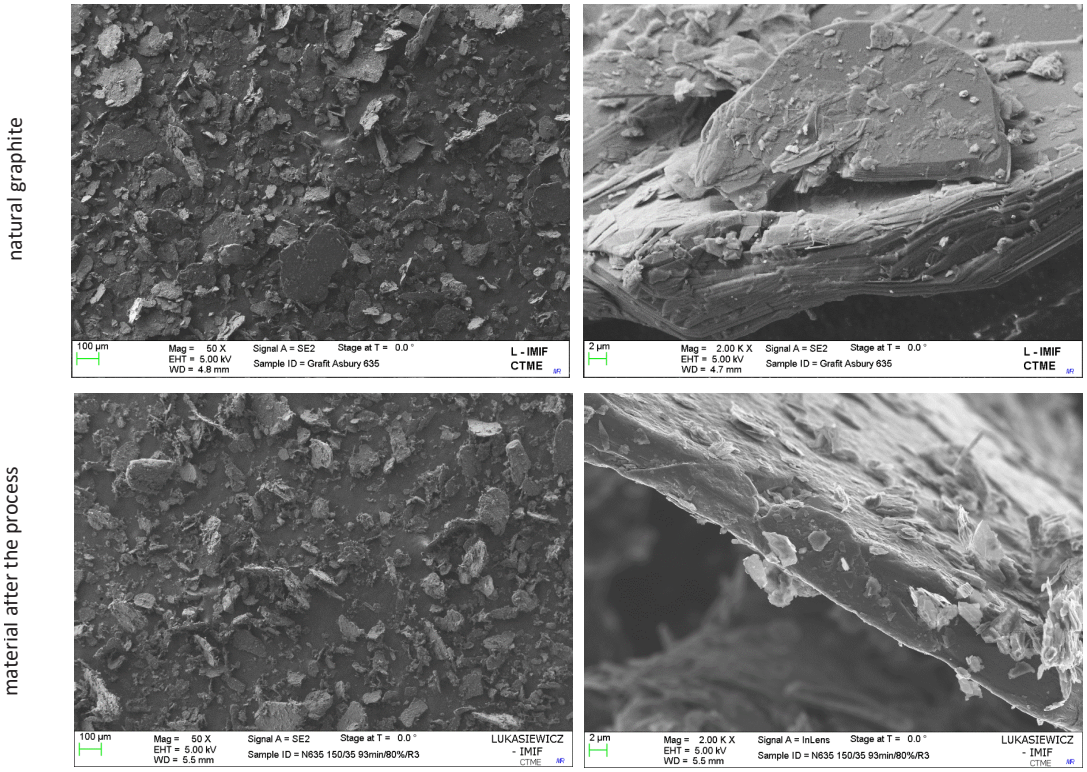

Fig. 2. SEM images of natural graphite and material after the exfoliation process

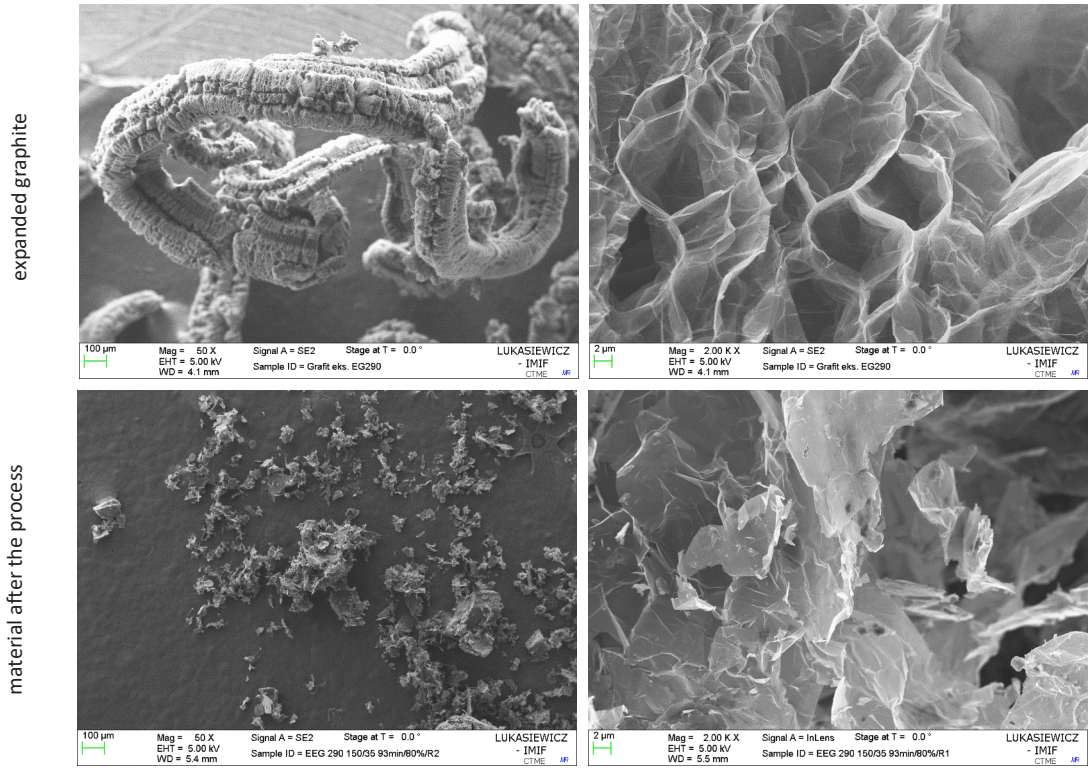

Fig. 3. SEM images of expanded graphite and material after the exfoliation process

The research was funded by National Science Centre, Poland – grant "Identification of mechanisms and investigations of flake graphene production by direct exfoliation using supercritical carbon dioxide", project number 2019/35/D/ST8/02977.

PREPARATION AND PRO-ENVIRONMENTAL APPLICATIONS OF SiO_2-Fe_XO_Y-Fe CATALYTIC SYSTEM

Gabriela Hodacka*, Olga Długosz, Marcin Banach

Faculty of Chemical Engineering and Technology, Cracow University of Technology,
Warszawska 24, 31-155 Cracow (Poland)
*corresponding author: gabriela.hodacka@student.pk.edu.pl

The thriving industrial and service sectors are providing us with ever-improving development of available technologies, but they also bring with them negative effects in the form of environmental pollution. In order to reduce the adverse environmental impact of the uncontrolled development of polluting industries, catalytic systems based on nanomaterials characterized by sorptive and catalytic properties are used to support the remediation process.

This paper presents a methodology for obtaining catalytic systems based on microsilica, iron oxide structures and iron nanoparticles, and verifies their applications in environmental purification processes and prevention of environmental pollution under model conditions. The obtained catalytic systems were characterized by physicochemical analyses, which confirmed the presence of speciated forms of iron and their catalytic properties. The first of the systems (SiO_2-Fe) was obtained according to the scheme in Figure 1. The core in all three systems is microsilica, while the role of the coating is played by iron nanoparticles, the surface of which was functionalized by using an extract obtained in the Soxhlet apparatus from apple peels-rich in polyphenolic compounds, responsible for the reducing and stabilizing properties of the system.

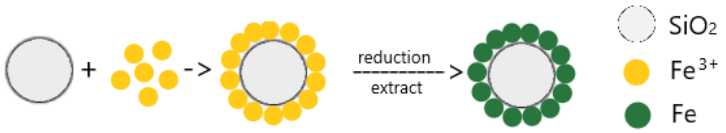

Fig. 1. Schematic of the preparation of catalytic system 1 in the form of SiO_2-Fe

The second catalytic system (Figure 2) is based on microsilica onto which Fe_2O_3 nanoparticles, synthesized using a microwave reactor have been deposited.

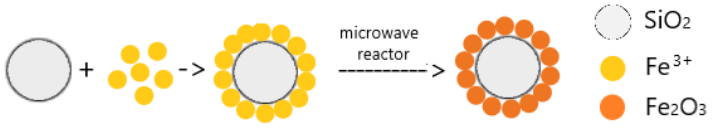

Fig. 2. Schematic of the preparation of catalytic system 2 in the form of SiO_2-Fe_2O_3

The engineering for obtaining the third catalytic system (Figure 3) was based on the structure of system 2- Fe_2O_3 onto which Fe was applied in an analogous manner to system 1.

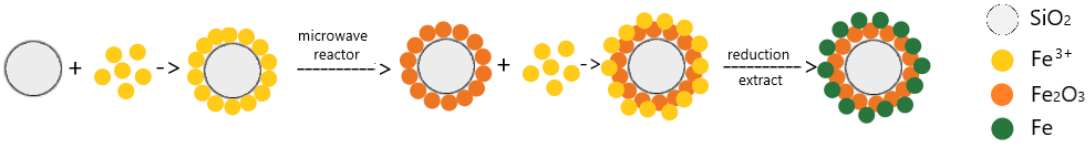

Fig. 3. Schematic of the preparation of catalytic system 3 in the form of SiO_2-Fe_2O_3-Fe

The performance of the obtained systems was verified under model conditions-catalytic reactions, in the process of thermal oxidation of soot. In this work, three by-products of incomplete combustion of fuels were used in the form of: carbonizate obtained by pyrolysis of rubber granules, technical soot- type N550 and furnace soot. In order to determine the best conditions for soot oxidation, a series of experiments was carried out with varying parameters for running the process, i.e. temperature, contact time: soot-catalytic system and % catalyst content. It was shown that catalytic systems based on speciation forms of iron nanoparticles and iron oxides exhibit catalytic properties in soot oxidation by lowering oxidation temperature and reducing contact time: catalyst-soot.

BORON- AND BOROPHENE-BASED ANTI-CORROSION COATING OF MAGNESIUM ALLOY USED IN BIOMEDICAL APPLICATIONS

Vladyslav Lavruk*, Krzysztof Sielicki, Karolina Wenelska, Ewa Mijowska

West Pomeranian University of Technology in Szczecin, Piastów Ave. 45, 70-310 Szczecin, Poland
*corresponding author: lavruk_vladyslav@zut.edu.pl

Borophene is a relatively recently discovered compound made up of boron atoms, which align into a 2D lattice - similar to graphene. Since its discovery in 2015, numerous studies have been carried out to find practical applications of this new material in different fields [1,2]. Boron atoms are a common dopant for anticorrosion coating of iron alloys [3]. Therefore, it becomes natural to investigate borophene and its anti-corrosion properties. This work aimed to investigate the anticorrosion behaviour of borophene-polymer (BP) composite under conditions mimicking highly oxidative human body environment. As a reference, the bulk boron-polymer (bBP) coating was investigated. BP and bBP composites were prepared by dispersing boron and borophene in the solution of poly(lactic acid) (PLA) with a further coating of Mg AZ91 alloy disk (Ø 14 mm) via spin coating. The parameters such as borophene and PLA concentrations, rotation speed and coating thickness were optimised. Moreover, the scanning electron microscopy (SEM) analysis was conducted both before (to control the layer homogeneity and possible defects detection) and after the electrochemically induced corrosion test (to observe the corrosion effects and coating condition). An electrochemical corrosion test was conducted via a three-electrode system, where only coated surface was exposed to the electrolyte (3.5 % NaCl). The electrochemical test revealed that BP coating surpasses bBP through a decrease of corrosion current density (I_{corr}) in the passivation region. Further analysis composed from the Tafel plot, electrochemical impedance spectroscopy (EIS), Raman spectroscopy and X-ray diffraction (XRD) revealed the possible corrosion mechanism and anticorrosion properties of borophene.

References:

[1] Ranjan P., Lee J.M., Kumar P., Vinu A., Borophene: New Sensation in Flatland, *Adv. Mater.*, 2020, 32,2000531.
[2] Liu T., Chen Y., Wang H., Zhang M., Yuan L., Zhang C., Li-Decorated β12-Borophene as Potential Candidates for Hydrogen Storage: A First-Principle Study, *Mater.*, 2017, 10, 1399.
[3] Koga G.Y., Otani L.B., Silva A.M.B., Roche V., Nogueira R.P., Jorge A.M., Bolfarini C., Kiminami C.S., Botta W.J.., Characterization and Corrosion Resistance of Boron-Containing-Austenitic Stainless Steels Produced by Rapid Solidification Techniques, *Mater.*, 2018, 11, 2189.

SILICONE-TYPE IONIC SURFACTANTS WITH REACTIVE FUNCTION FOR SURFACE HYDROPHOBIZATION

Ksenia Narożniak*, Łukasz Lamch

Department of Engineering and technology of Chemical Process, Faculty of Chemistry, Wrocław University of Science and Technology, Wybrzeże Wyspiańskiego 27, 50-370 Wrocław, POLAND
*corresponding author: narozniakk@gmail.com

Surface hydrophobization is an emerging problem, especially when a very thin and transparent layer is needed for light sources, solar panels and (photo)catalysts. Moreover, the obtained layer may be easily washed out by organic solvents or even water when it is not sufficiently anchored to the surface. On the other hand, a thin and resistant hydrophobic layer may significantly reduce unwanted processes connected with oxidation of metal or organic surfaces leading to e.g. corrosion or chemical degradation. Therefore, silicone surfactants are known for their exceptional performance properties, especially in the field of ultra low surface tension (i.e. below ca. 20 mN/m), excellent emulsifying action as well as controlled adsorption at specific interfaces and surfaces [1-4]. That is why the mentioned compounds will gain attention especially in the fields of surface hydrophobization from aqueous and solvent-borne systems as well as stimuli responsive surfaces, where traditional surfactants exhibit inferior performance.

The aforementioned issue may be solved by the development of reactive silicone surfactants capable of anchoring to the surface followed by polymerization to form a thin, insoluble layer [2]. In contrast to insufficiently hydrophobic hydrocarbon-based surfactants and hardly biodegradable perfluorocarbon derivatives the abovementioned silicone surfactants may constitute a good compromise between appropriate water-repelling action, reactivity and environmental reasons [4]. Due to unique self-assembly properties of amphiphilic compounds, the deposition of surfactants at the particular surfaces, e.g. glass, metal or polymer, may constitute spontaneous process characterized by very low energy demand [5]. The adsorbed surfactant molecules may bond to the surface by formation of either covalent or ionic bonds with appropriate groups present on the surface, e.g. hydroxyl or carboxylic acid ones. If surfactant molecules comprise polymerizable groups, the formed layer may be sufficiently bonded to the surface (step-by-step reactions with surface moieties) and cross-linked (post-deposition surface polymerization) to provide appropriate durability. Taking into account the most common and easily tunable polymerizable group, i.e. a double carbon bond, we utilized it as the reactive moiety for our surfactants. In order to study usefulness of positively and negatively charged substances toward adsorption at specific surfaces e.g. glass and metal two groups: cationic and anionic surfactants have been developed (see Fig. 1.).

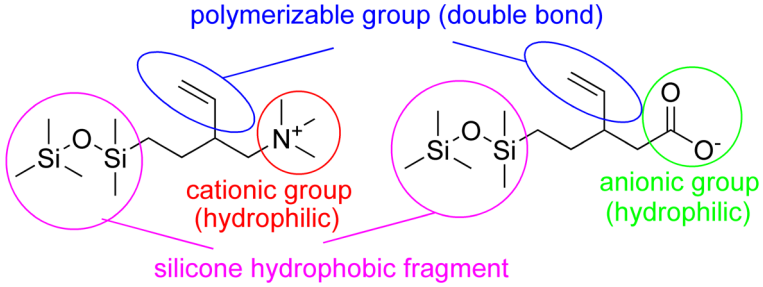

Fig. 1. Scheme of the designed and synthesized surfactants

The theoretical considerations indicate that cationic surfactants will be preferably adsorbed at negatively charged surfaces (e.g. glass), while anionic ones – at positively charged surfaces (e.g. metals), followed by formation of ionic bonds (see Fig. 2.) [5, 6]. On the other hand, the

opposite behavior may also occur due to formation of reversible ester bonds between carboxylate groups in hydrophilic fragments of surfactant molecules and surface hydroxyl moieties (see Fig. 2.).

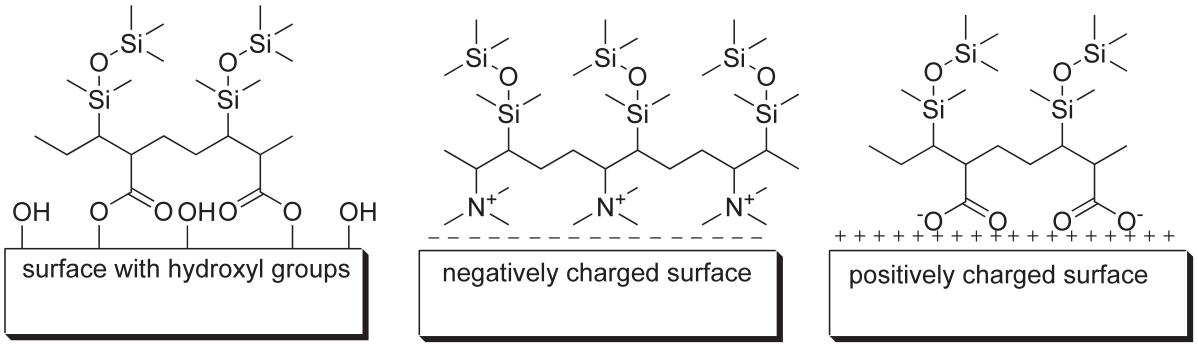

Fig. 2. Schematic representation of polymerized silicone surfactants on surface with hydroxyl groups (left), negatively charged surface (middle) and positively charged surface (right)

The main aim of our studies was to develop and optimize synthetic routes and deposition methodologies for ionic surfactants with reactive groups as well as carefully analyze obtained hydrophobized surfaces. The structure of the obtained reactive surfactants was confirmed with NMR spectroscopy, while the hydrophobic surfaces were analyzed utilizing applicable methods, e.g. contact angle, impendency and calorimetric measurements, X-ray photoelectron spectroscopy with ion sputtering and thermogravimetry. The expected outcome comprises fully scalable methodology for easy and reproducible surface hydrophobization toward sufficient water repellency and corrosion inhibition.

The performed studies enabled to obtain compounds with appropriate adsorption characteristics from both organic and aqueous solutions. Furthermore, polymerization on the surface can be performed in various conditions due to moderation of the double bond characteristics. Both cationic and anionic surfactants exhibited selective and permanent adsorption on glass and metal as a result of reactions with surface moieties or ionic interactions. The outcome of the studies constitutes a significant weakening of the wettability which may lead to metal corrosion resistance or achieving water-repellent glass. The performed careful analyses enabled to identify the crucial steps significantly affecting the performance properties of the studied surfactants and surfaces.

Acknowledgements

This work and participation in conference have been supported by National Science Center Poland via the SONATA programme grant ("Reactive silicone surfactants for interface hydrophobization – process analytical technology (PAT)", No 2021/43/D/ST8/01992).

References

[1] Hill R.M., *Silicone surfactants - new developments*, *Current Opinion in Colloid & Interface*, 2002, 7, 255–261.
[2] Lamch Ł., Pucek A., Kulbacka J., Chudy M., Jastrzębska E., Tokarska K., Bułka M., Brzózka Z., Wilk K.A., *Recent progress in the engineering of multifunctional colloidal nanoparticles for enhanced photodynamic therapy and bioimaging*, *Adv. Colloid Interface Sci.,* 2018, 261, 62–81.
[3] Zhang X.D., Macosko C.W., Davis H.T., Nikolov A.D., Wasan D.T., *Role of Silicone Surfactant in Flexible Polyurethane Foam*, *J. Colloid Interface Sci.,* 1999, 215, 270–279.
[4] Czajka A., Hazell G., Eastoe J., *Surfactants at the Design Limit*, *Langmuir*, 2015, 31, 8205−8217.
[5] Rosen M.J., *Surfactants and Interfacial Phenomena*, New Jersey, John Wiley & Sons 2004.
[6] Zieliński R., *Surfaktanty budowa właściwości zastosowania*, Poznań, Wydawnictwo UEP 2021.

PEROXYMONOSULFATE-ASSISTED PHOTOCATALYTIC DEGRADATION OF ARTIFICIAL SWEETENERS IN WATER

Jakub Smoliński, Anna Zielińska-Jurek*

Department of Process Engineering and Chemical Technology, Faculty of Chemistry, Gdańsk University of Technology, Narutowicza 11/12, 80-233 Gdańsk, Poland
*corresponding author: annjurek@pg.edu.pl

Progressive pollution of the aquatic environment related to the presence of emerging contaminants results from their resistant nature towards conventional wastewater treatment processes. Artificial sweeteners used as sugar substitutes, commonly added to beverages, personal care products, dental creams and pharmaceuticals, are not readily metabolized in our body and may be excreted into the environment as a mixture of the parent compound and its metabolites. Therefore, residues of artificial sweeteners have been detected in the most diverse aquatic environments, being recognized as emerging contaminants [1]. Especially aspartame, potassium acesulfame, sodium saccharin and sodium cyclamate have been reported as the most persistent sweeteners [2].

In this regard, in the present study, a combination of the photocatalytic process with peroxymonosulfate (PMS) activation was proposed for efficient photocatalytic degradation of aspartame, potassium acesulfame, sodium saccharin, and sodium cyclamate - a mixture of artificial sweeteners frequently present in wastewater and surface waters worldwide.

TiO_2 nanosheets with exposed {0 0 1} facets were synthesized using the fluorine-free lyophilization technique as a green concept for synthesis and used for the photodegradation of artificial sweeteners under simulated solar light. The synergetic effect of photocatalysis with the sulfate radical-based process was investigated. In comparison to hydroxyl radicals, sulfate radicals ($^{\bullet}SO_4^-$) possess a higher redox potential of 2.6–3.1 V_{NHE} and selectivity, longer half-life (30–40 μs), and are more suitable for organic pollutant degradation regardless of operating conditions (activity in a broader pH range).

It was found that the mixture of studied artificial sweeteners containing 20 mg/L of each compound was practically not susceptible to photolysis within 60 minutes of irradiation under simulated solar light. In the presence of 2D titanium (IV) oxide, the artificial sweeteners were degraded entirely in less than 30 min, whereas the addition of 0.5 mM of peroxymonosulfate resulted in complete mineralization after 5 minutes of the degradation process.

Acknowledgment

The research was financially supported by the Gdańsk University of Technology within the RADIUM program (grant nr 15/RADIUM/2022.)

References

[1] Yang Y.Y., Zhao J.-L., Liu Y.-S., Liu W.-R., Zhang Q.-Q., Yao L., Hu L.-X., ZhangJ.-N., Jiang Y.-X., Ying G.-G., Pharmaceuticals and personal care products (PPCPs) and artificial sweeteners (ASs) in surface and ground waters and their application as indication of wastewater contamination, *Sci. Total Environ.,* 2018, 616–617, 816–823.

[2] Ab Qayoom Naik, Tabassum Zafar, Vinoy Kumar Shrivastava, Environmental impact of the presence, distribution, and use of artificial sweeteners as emerging sources of pollution, *J. Environ. Public Health,* 2021, Article ID 6624569.

SUNFLOWER SEED SHELL-DERIVED AMORPHOUS CARBON-BASED SUPERCAPACITORS

Sudoł Jakub*, Matlak Adam, Sielicki Krzysztof, Wenelska Karolina, Mijowska Ewa

West Pomeranian University of Technology, Szczecin Faculty of Chemical Technology and Engineering, Department of Nanomaterials Physicochemistry,
Piastów Ave. 42, 71-065 Szczecin, Poland

*corresponding author: sj54671@zut.edu.pl

With recent development of new energy sources and electrical transportation technologies, there has been an increasing need for more efficient, cheaper, and environmentally friendly energy storage such as biomaterial-derived supercapacitors.

Sunflower (*Helianthus annuus L.*) seed shells are a cheap and common biowaste with little to none use outside of animal food supplementation but have interesting structural traits including high natural porosity and primarily consisting of cellulose fibres, which are favourable from an electrochemical standpoint. Therefore, they were chosen to produce highly potential porous carbon as electrodes for symmetrical supercapacitors.

Shells were dried, carbonized in 5 different temperatures ranging from 500 to 900°C and subsequently activated using molten KOH.

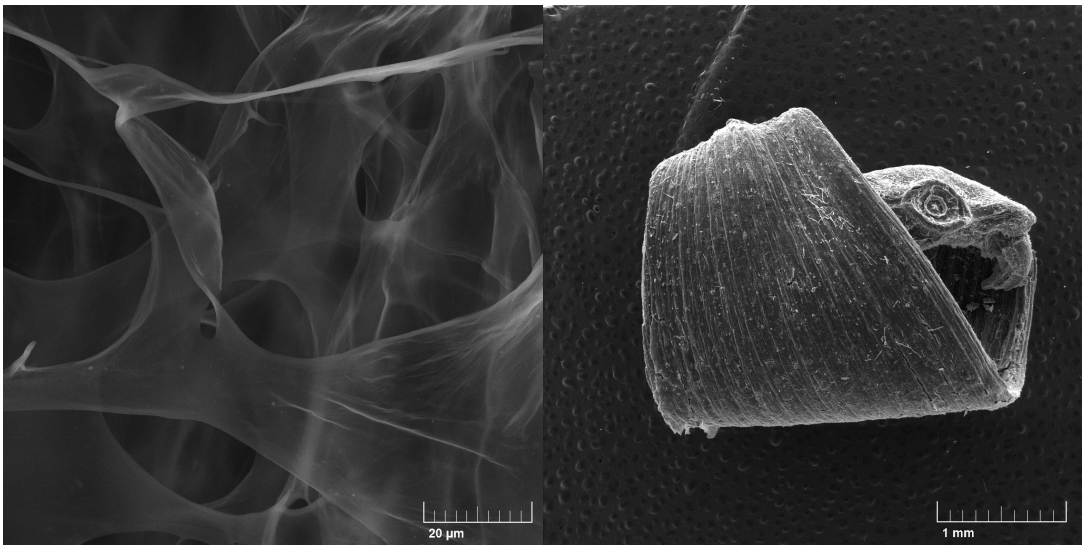

Fig. 1. SEM images of carbonized sunflower seed shell

Acquired biomaterial has been characterized with high specific surface by nitrogen adsorption analysis with sample carbonized in 500°C having the highest one: 2530m^2/g. Material was then analyzed with Raman spectroscopy to determine the graphitization level and FT-IR spectroscopy to identify functional groups within the carbon structure. The carbonized shells were also analyzed for impurities by thermogravimetric analysis and X-ray powder diffraction to identify main contaminants. The results showed that materials carbonized at higher temperatures had better overall purity.

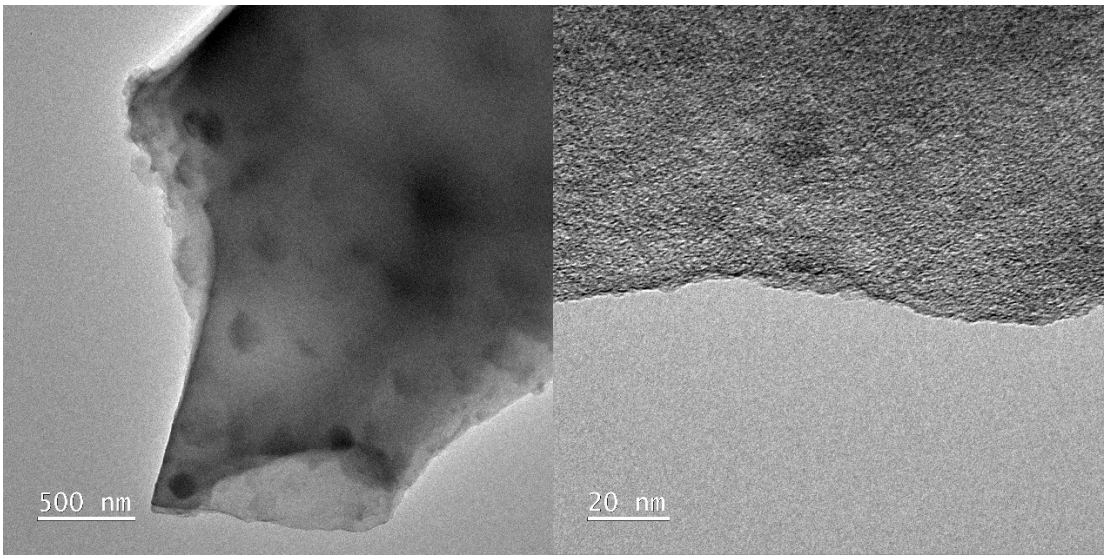

Fig. 2. TEM images of porous carbon carbonized at 800°C

The final step of physicochemical analysis was to examine the material's morphology using transmission electron microscopy (TEM) and scanning electron microscopy (SEM). Electrodes were then assembled with PVDF (polyvinylidene fluoride) as the binder and tested for their electrochemical properties using variable scan speed cyclic voltammetry (CV), galvanostatic charge/discharge (GCD) cycling, and electrochemical impedance spectroscopy (EIS).

okichip24.zut.edu.pl

Ćwiczenia z obszaru inżynierii procesowej z wykorzystaniem instalacji szkoleniowych GUNT

- Mechaniczna inżynieria procesowa
- Termiczna inżynieria procesowa
- Chemiczna inżynieria procesowa
- Biologiczna inżynieria procesowa
- Przykładowe instalacje

Więcej informacji na www.gunt.de

G.U.N.T. Gerätebau GmbH
Hanskampring 15 - 17
22885 Barsbüttel
Niemcy

+49 40 67 08 54 - 0
sales@gunt.de
www.gunt.de

MIKROPRZEPŁYWY I MIKROOBRAZOWANIE

Eurotek International

Nieinwazyjna eksperymentalna mechanika płynów

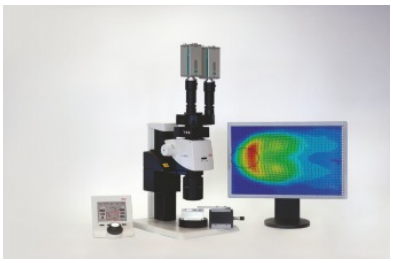

Pomiary przepływu µPIV

Planarne pomiary 2 i 3 składowych wektorów prędkości przepływu płynów.

Powiększenie do 57 razy

Pomiary stężenia µLIF

Planarne pomiary rozkładu stężenia lub temperatury w cieczach.

Powiększenie do 57 razy

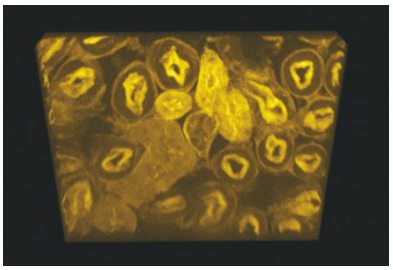

Mapy widmowe

Mapy widmowe: 2D i 3D charakterystyki przestrzenno-widmowe takich sygnałów jak: fotoluminescencja, Raman, CARS i wielu pochodnych: stężenia, mikrostruktury itp.

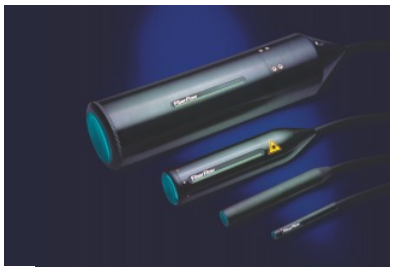

Pomiary przepływu µLDA

Punktowe pomiary 1, 2 i 3 składowych wektora prędkości i fluktuacji przepływu płyno z pełną statystyką

Eurotek International

Eurotek International Sp. z o. o
Ul Skrzetuskiego 6
02-726 Warszawa

eurotek.com.pl
eurotek@eurotek.com.pl

DANTEC DYNAMICS

ESC GLOBAL

LABORATORIUM
ANALIZ
FIZYKOCHEMICZNYCH

Zakres działalności laboratorium:

- Podstawowe parametry wody
- Analiza TOC w osadach kamień kotłowy
- Analiza TOC w wodzie
- Analiza pierwiastków w wodzie przemysłowej i surowej
- Analiza pierwiastków w osadzie kamień kotłowy
- Sprawność złożona jonowymiennego

Najwyższy standard badań

Precyzja i dokładność

Wykwalifikowany personel

Nowoczesna aparatura

Posiadamy wdrożony system zarządzania zgodny z wymaganiami normy PN-EN ISO/IEC 17025, potwierdzony certyfikatem akredytacji laboratorium badawczego nr AB 1752, wydanym przez Polskie Centrum Akredytacji.

Kontakt:
ESC GLOBAL SP. Z O.O.
ul. Słoneczny Sad 4F, 72-002 Dołuje
Tel.: (91) 43 40 158 wew. 32
lab©escglobal.co.uk

www.escglobal.pl

CEMIS TECH

WYŁĄCZNY AUTORYZOWANY PRZEDSTAWICIEL HANDLOWY I SERWISOWY W POLSCE, ŚWIATOWYCH PRODUCENTÓW APARATURY LABORATORYJNEJ – TELEDYNE ISCO INC., CEM CORPORATION, SYRRIS LTD, MANTECH INC., SOAPY-EUROPE LTD, ZEULAB, THALESNANO INC.

W szerokiej ofercie naszej firmy znajdą Państwo między innymi:

Systemy chromatograficzne firmy TELEDYNE ISCO Inc.

Urządzenia laboratoryjne firmy CEM Corporation:

- reaktory mikrofalowe
- syntezatory peptydów
- mineralizatory mikrofalowe
- piece muflowe
- analizatory składu

Reaktory i pompy strzykawkowe firmy SYRRIS Ltd.

Analizatory elektrochemiczne firmy MANTECH Inc.

Zmywarki laboratoryjne firmy GETINGE

Inteligentne urządzenia do mycia rąk firmy SOAPY-EUROPE Ltd.

Komory rękawicowe firmy JACOMEX

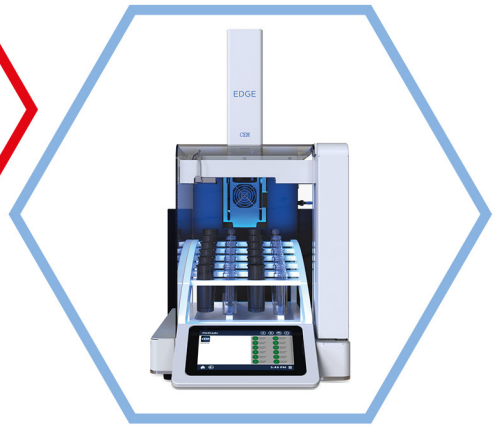

Serdecznie zachęcamy do kontaktu. Nasi specjaliści pomogą w wyborze urządzeń i dostosują ofertę do Państwa wymagań aplikacyjnych.

Zapraszamy również do korzystania z usług autoryzowanego serwisu.

CEMIS - TECH Sp. z o.o.
ul. Rydygiera 8/24 lok. 1015
01-793 Warszawa

tel. +48 22 412 49 13

www.cemis.tech

cemis@cemis.tech